

Realistic Large Break LOCA Methodology for Pressurized Water Reactors

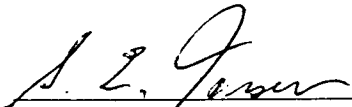
August 2001

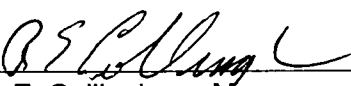


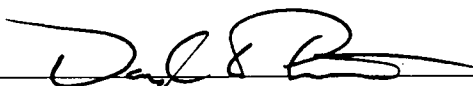
**Realistic Large Break LOCA Methodology for
Pressurized Water Reactors**

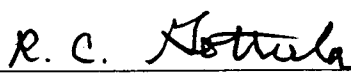
Prepared:  8/22/01
L. D. O'Dell, Manager
U.S. and Far East Research & Technology
Date

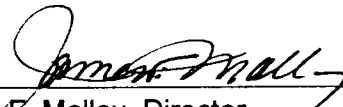
Concurred:  8/22/01
R. P. Martin, Engineer
Safety Analysis Methods
Date

Concurred:  8/22/01
S. E. Jensen, Team Leader
Safety Analysis Methods
Date

Approved:  8/22/01
R. E. Collingham, Manager
BWR Reload Engineering & Methods Development
Date

Approved:  8/22/01
D. W. Pruitt, Manager
Safety Analysis Methods
Date

Approved:  8/22/01
R. C. Gottula, Manager
PWR Safety Analysis
Date

Approved:  8/22/01
J. F. Mallay, Director
Regulatory Affairs
Date

**U.S. Nuclear Regulatory Commission
Report Disclaimer**

Important Notice Regarding the Contents and Use of This Document

Please Read Carefully

This technical report was derived through research and development programs sponsored by Framatome ANP Richland, Inc. It is being submitted by Framatome ANP Richland, Inc. to the U.S. Nuclear Regulatory Commission as part of a technical contribution to facilitate safety analyses by licensees of the U.S. Nuclear Regulatory Commission which utilize Framatome ANP Richland, Inc. fabricated reload fuel or technical services provided by Framatome ANP Richland, Inc. for light water power reactors and it is true and correct to the best of Framatome ANP Richland, Inc.'s knowledge, information, and belief. The information contained herein may be used by the U.S. Nuclear Regulatory Commission in its review of this report and, under the terms of the respective agreements, by licensees or applicants before the U.S. Nuclear Regulatory Commission which are customers of Framatome ANP Richland, Inc. in their demonstration of compliance with the U.S. Nuclear Regulatory Commission's regulations.

Framatome ANP Richland, Inc.'s warranties and representations concerning the subject matter of this document are those set forth in the agreement between Framatome ANP Richland, Inc. and the Customer pursuant to which this document is issued. Accordingly, except as otherwise expressly provided in such agreement, neither Framatome ANP Richland, Inc. nor any person acting on its behalf:

- a. makes any warranty, or representation, express or implied, with respect to the accuracy, completeness, or usefulness of the information contained in this document, or that the use of any information, apparatus, method, or process disclosed in this document will not infringe privately owned rights;

or

- b. assumes any liabilities with respect to the use of, or for damages resulting from the use of, any information, apparatus, method, or process disclosed in this document.

Nature of Changes

Item	Page	Description and Justification
1.	All	This is a new document.

Contents

1.0	Introduction	1-1
2.0	Methodology Roadmap	2-1
2.1	Requirements and Code Capabilities	2-1
2.2	Assessment and Ranging of Parameters	2-3
2.3	Sensitivity and Uncertainty Analysis.....	2-4
3.0	Requirements and Capabilities	3-1
3.1	Scenario Specification (CSAU Step 1)	3-1
3.2	Nuclear Power Plant Selection (CSAU Step 2)	3-4
3.3	Phenomena Identification and Ranking (CSAU Step 3)	3-5
3.4	Frozen Code Version Selection (CSAU Step 4)	3-10
3.4.1	RODEX3A.....	3-12
3.4.2	S-RELAP5	3-14
3.4.3	New Product Support.....	3-16
3.5	Code Documentation (CSAU Step 5).....	3-17
3.6	Determination of Code Applicability (CSAU Step 6)	3-18
3.6.1	Field Equations	3-18
3.6.2	Closure Equations.....	3-19
3.6.3	Code Numerics	3-19
3.6.4	Structure and Nodalization	3-19
4.0	Assessment and Ranging of Parameters.....	4-1
4.1	Establishment of Assessment Matrix (CSAU Step 7)	4-1
4.1.1	PIRT Considerations	4-2
4.1.2	Nodalization Considerations.....	4-4
4.1.3	Scaling Considerations	4-4
4.1.4	Compensating Errors	4-4
4.1.5	Summary	4-4
4.2	Nuclear Power Plant Nodalization Definition (CSAU Step 8).....	4-5
4.2.1	Nodalization Methodology	4-6
4.2.2	Numerical Considerations	4-8
4.2.3	Loop Model	4-9
4.2.3.1	Hot Leg	4-9
4.2.3.2	Steam Generator	4-10
4.2.3.3	Pump Suction	4-11
4.2.3.4	Reactor Coolant Pump.....	4-11
4.2.3.5	Cold Leg and Break	4-11
4.2.3.6	ECCS.....	4-12
4.2.3.7	Pressurizer.....	4-13
4.2.4	Reactor Vessel Model	4-13
4.2.4.1	Downcomer.....	4-13
4.2.4.2	Lower Vessel	4-15
4.2.4.3	Core, Core Bypass, and Fuel.....	4-16
4.2.4.4	Upper Plenum/Upper Head.....	4-17

4.2.5	Containment Model	4-18
4.2.6	Plant Model Summary	4-18
4.3	Definition of Code and Experimental Accuracy (CSAU Step 9)	4-19
4.3.1	Separate Effects Tests (SET).....	4-20
4.3.1.1	THTF Heat Transfer	4-20
4.3.1.2	THTF Level Swell.....	4-21
4.3.1.3	GE Level Swell	4-22
4.3.1.4	FRIGG2	4-23
4.3.1.5	Bennett Tube	4-24
4.3.1.6	FLECHT and FLECHT SEASET	4-24
4.3.1.7	PDTF/SMART Tests	4-29
4.3.1.8	Marviken Tests	4-31
4.3.1.9	Westinghouse/EPRI 1/3 Scale Tests	4-32
4.3.1.10	FRA-ANP CCFL Tests	4-35
4.3.1.11	UPTF Tests.....	4-37
4.3.1.11.1	UPTF Tests 6 and 7	4-38
4.3.1.11.2	UPTF Test 8.....	4-40
4.3.1.11.3	UPTF Tests 10 and 29	4-41
4.3.1.11.4	UPTF Tests 10 and 12	4-43
4.3.1.11.5	UPTF Test 11	4-45
4.3.1.12	CCTF Tests	4-47
4.3.1.13	SCTF Tests.....	4-54
4.3.1.14	ACHILLES Tests.....	4-58
4.3.1.15	Multi-Dimensional Flow Testing	4-61
4.3.1.15.1	Summary.....	4-62
4.3.1.15.2	Test Descriptions.....	4-62
4.3.1.15.3	Input Description	4-63
4.3.1.15.4	Results	4-63
4.3.1.15.5	Conclusions.....	4-64
4.3.2	Integral Effects Tests (IET).....	4-64
4.3.2.1	LOFT Assessments	4-65
4.3.2.1.1	LOFT Facility	4-65
4.3.2.1.2	LOFT Test Descriptions.....	4-68
4.3.2.1.3	LOFT Assessment Summary.....	4-69
4.3.2.1.4	LOFT L2-3 Assessment.....	4-70
4.3.2.1.5	LOFT Test L2-5 Assessment.....	4-73
4.3.2.1.6	LOFT LP-02-6 Assessment	4-75
4.3.2.1.7	LOFT Test LP-LB-1 Assessment.....	4-77
4.3.2.2	Semiscale Tests	4-80
4.3.2.2.1	Semiscale Facilities.....	4-80
4.3.2.2.2	Semiscale Test Descriptions	4-82
4.3.2.2.3	Test S-06-3 Assessment	4-84
4.3.2.2.4	Test S-07-1 Assessment	4-84
4.3.3	Methodology Treatment of PIRT Phenomena	4-85
4.3.3.1	PIRT Phenomena Not Treated Statistically	4-85
4.3.3.1.1	Core 3-D Flow and Void Distributions	4-85
4.3.3.1.2	Liquid Entrainment in Core	4-86
4.3.3.1.3	Core Flow Reversal/Stagnation	4-87

	4.3.3.1.4	Upper Plenum Liquid Entrainment/de-entrainment	4-88
	4.3.3.1.5	Counter Current Flow Limit (CCFL)	4-88
	4.3.3.1.6	Hot Leg Entrainment/de- entrainment	4-89
	4.3.3.1.7	Two Phase Pump Degradation	4-90
	4.3.3.1.8	Pump Differential Pressure Loss	4-90
	4.3.3.1.9	Non-Condensable Transport.....	4-91
	4.3.3.1.10	Downcomer Entrainment	4-91
	4.3.3.1.11	Downcomer Liquid Level Oscillations	4-91
	4.3.3.1.12	Lower Plenum Sweepout.....	4-92
4.3.3.2		PIRT Phenomena Treated Statistically.....	4-92
	4.3.3.2.1	Stored Energy	4-93
	4.3.3.2.2	Oxidation	4-93
	4.3.3.2.3	Decay Heat	4-94
	4.3.3.2.4	Departure from Nucleate Boiling.....	4-96
	4.3.3.2.5	Core Post-CHF Heat Transfer	4-96
	4.3.3.2.6	Tmin	4-97
	4.3.3.2.7	Break Flow	4-97
	4.3.3.2.8	Steam Binding	4-98
	4.3.3.2.9	Cold Leg Condensation	4-99
	4.3.3.2.10	Accumulator Discharge	4-99
	4.3.3.2.11	Reactor Vessel Hot Walls	4-100
	4.3.3.2.12	Containment Pressure.....	4-100
4.3.4		Evaluation of Code Biases	4-100
	4.3.4.1	Evaluation of Biases with CCTF.....	4-101
	4.3.4.1.1	Summary and Conclusions.....	4-101
	4.3.4.1.2	Test 54	4-101
	4.3.4.1.3	Test 62	4-102
	4.3.4.1.4	Test 67	4-103
	4.3.4.1.5	Test 68.....	4-103
	4.3.4.1.6	Conclusion Regarding Bias Evaluation in CCTF	4-104
	4.3.4.2	Evaluation of Biases with LOFT	4-104
	4.3.4.2.1	Summary and Conclusions.....	4-105
	4.3.4.2.2	LOFT Test LP-LB-1	4-105
	4.3.4.2.3	LOFT Test LP-02-6	4-106
	4.3.4.2.4	LOFT Test L2-5.....	4-107
	4.3.4.2.5	LOFT Test L2-3.....	4-108
	4.3.4.2.6	Conclusions.....	4-109
	4.3.4.3	Evaluation of Biases with Semiscale.....	4-109
	4.3.4.3.1	Summary and Conclusions.....	4-109
	4.3.4.3.2	Semiscale Test S-06-3	4-109
	4.3.4.3.3	Semiscale Test S-07-1	4-110
	4.3.4.3.4	Conclusions.....	4-110
	4.3.4.4	Conclusions from Bias Evaluation.....	4-111

4.4	Determination of Effect of Scale (CSAU Step 10)	4-111
4.4.1	Test Scaling	4-111
4.4.1.1	Blowdown	4-112
4.4.1.2	Refill	4-112
4.4.1.3	Reflood	4-113
4.4.2	Code Scaling	4-113
4.4.2.1	Post-CHF and Reflood Heat Transfer	4-114
4.4.2.2	Scaling from Tests	4-117
4.4.2.2.1	Film Boiling Heat Transfer	4-117
4.4.2.2.2	Core Entrainment	4-118
4.4.2.2.3	Critical Flow at Break	4-119
4.4.2.2.4	Carry-over to Steam Generator	4-119
4.4.2.2.5	Pump Scaling	4-120
4.4.2.2.6	Cold Leg Condensation	4-120
4.4.2.2.7	Bypass of Downcomer by ECC Water and Lower Plenum Sweep-Out	4-121
4.4.2.2.8	Loop Oscillations	4-122
5.0	Sensitivity and Uncertainty Analysis	5-1
5.1	Determination of Effect of Reactor Input Parameters and State (CSAU Step 11)	5-1
5.1.1	Determining Important Process Parameters	5-1
5.1.2	Role of Sensitivity Studies	5-2
5.1.3	Quantifying Statistical Quantities	5-3
5.1.3.1	General	5-3
5.1.3.2	Treatment of Time in Cycle	5-4
5.1.3.3	Treatment of Axial and Radial Power Shapes	5-5
5.1.4	Supporting Ranges Without Data	5-7
5.1.5	Reporting of Treatment of Process Parameters	5-7
5.2	Performance of NPP Sensitivity Calculations (CSAU Step 12)	5-7
5.2.1	Statistical Approach	5-7
5.2.2	Application of Methodology	5-11
5.2.3	New RLBLOCA Analyses	5-12
5.2.4	Ranging Uncertainty	5-12
5.2.5	Parameter Initialization	5-13
5.2.6	Calculation Order	5-13
5.2.7	Subsequent RLBLOCA Analyses	5-13
5.3	Determination of combined Bias and Uncertainty (CSAU Step 13)	5-14
5.4	Determination of Total Uncertainty (CSAU Step 14)	5-17
6.0	References	6-1
Appendix A	Overview of Base Case and Sensitivity Studies	A-1
A.1	Base Case Analyses Description	A-1
A.2	LBLOCA Calculation and Event Description	A-2
A.3	Sensitivity Studies Overview	A-4

Appendix B	Conservatism.....	B-1
B.1	Analysis for Fresh Fuel Assemblies Only	B-1
B.2	Analysis without Clad Swelling and Rupture	B-2
B.3	Radial Power Distributions	B-3
B.4	Pump Two-Phase Degradation	B-5
Appendix C	Time Step Sensitivity	C-1

Tables

3.1	Approximate Values of Key Large Break LOCA Plant Analysis Parameters.....	3-20
3.2	Appendix K Large Break LOCA Approximate Sequence of Events Timing	3-21
3.3	Preliminary Process Identification and Ranking Table (PIRT) for PWR Large Break Loss-of-Coolant Accident	3-22
3.4	Final Process Identification and Ranking Table (PIRT) for PWR Large Break Loss-of-Coolant Accident	3-24
3.5	Frozen Code Versions Used in the Methodology Development	3-26
3.6	Field Equations/Models in S-RELAP5.....	3-27
3.7	Phenomena/Processes in S-RELAP5.....	3-28
3.8	Component Modeling Requirements for PWR.....	3-31
4.1	Parameters Perturbed for PIRT Sensitivity Studies.....	4-124
4.2	Assessment Matrix	4-127
4.3	Assessment Matrix Tests and Phenomena Addressed.....	4-128
4.4	Large Break LOCA Nodalization.....	4-130
4.5	PDF SMART Tests Chosen for S-RELAP5 Verification and Validation.....	4-131
4.6	Comparison of Effluent Temperature for the Plant-Consistent Model, Westinghouse/EPRI	4-132
4.7	Test Phase Parameters for Test 10 Run 081.....	4-133
4.8	Test Phase Parameters for Test 29 Run 212/211	4-133
4.9	Calculated Water Downflow Rates for the 0.3 MPa Test Series	4-134
4.10	Calculated Water Downflow Rates for the 1.5 MPa Test Series	4-135
4.11	CCTF Test Conditions	4-136
4.12	Summary Comparison of Measured and Calculated PCT, CCTF Tests 54, 62, 67, and 68	4-136
4.13	Test Data for SCTF-II Tests Modeled	4-137

Figures

2.1	Code Scaling, Applicability, and Uncertainty Methodology Flow Chart	2-6
4.1	PCT Signature for 3- and 4-Loop NPP Base Case	4-147
4.2	PIRT Sensitivity Histogram	4-148
4.3	Loop Nodalization for NPP	4-149
4.4	Reactor Vessel Nodalization for NPP	4-150
4.5	CE 2x4 and Westinghouse 3- and 4-Loop Plant Vessel Downcomer Configurations	4-151
4.6	NPP Core Nodalization – Axial Plane	4-152
4.7	NPP Core Nodalization – Cross-Sectional Plane	4-153
4.8	NPP Upper Plenum Nodalization – Axial Plane	4-154
4.9	NPP Upper Plenum Nodalization – Cross-Sectional Plane	4-155
4.10	NPP Emergency Core Cooling System Nodalization	4-156
4.11	Double-Ended Guillotine Break Nodalization	4-157
4.12	Double-Ended Split Break Nodalization	4-157
4.13	Comparison of Calculated HTC to Measured HTC, ORNL THTF	4-158
4.14	Frequency Distribution for Scale Factor for HTC, ORNL THTF	4-159
4.15	Bounding Distribution for HTC Scaling, ORNL THTF	4-160
4.16	Comparisons of Void Profiles, ORNL THTF Test 3.09.10j	4-161
4.17	Comparison of Void Profiles, ORNL THTF Test 3.09.10 m	4-162
4.18	Comparison of Void Profiles, ORNL THTF Test 3.09.10dd	4-163
4.19	Void Profiles at 40 Seconds for the 1 ft GE Test 1004-3	4-164
4.20	Void Profiles at 100 Seconds for the 1 ft GE Test 1004-3	4-165
4.21	Comparison of Calculated and Measured Void Fraction, Frigg-2 Test 313007	4-166
4.22	Comparison of Calculated and Measured Void Fraction, Frigg-2 Test 313014	4-167
4.23	Comparison of Calculated and Measured Void Fraction, Frigg-2 Test 313016	4-168
4.24	Comparison of Calculated and Measured Void Fraction, Frigg-2 Test 313020	4-169
4.25	Comparison of Calculated and Measured Void Fraction, Frigg-2 Test 313060	4-170
4.26	Comparison of Calculated and Measured Void Fraction, Frigg-2 Test 313010	4-171

4.27	Comparison of Calculated and Measured Void Fraction, Frigg-2 Test 313013	4-172
4.28	Comparison of Calculated and Measured Void Fraction, Frigg-2 Test 313017	4-173
4.29	Comparison of Calculated and Measured Void Fraction, Frigg-2 Test 313019	4-174
4.30	Comparison of Calculated and Measured Void Fraction, Frigg-2 Test 313030	4-175
4.31	Comparison of Calculated and Measured Void Fraction at the Same Location for all 27 FRIGG Tests	4-176
4.32	Wall Temperature Profiles, Bennett Heated Tube Test 5358	4-177
4.33	Wall Temperature Profiles, Bennett Heated Tube Test 5379	4-178
4.34	Maximum Clad Temperature at All Measured Elevations, FLECHT SEASET Test 31805	4-179
4.35	Maximum Clad Temperature at All Measured Elevations, FLECHT SEASET Test 31504	4-180
4.36	Maximum Clad Temperature at All Measured Elevations, FLECHT SEASET Test 31203	4-181
4.37	Maximum Clad Temperature at All Measured Elevations, FLECHT SEASET Test 31302	4-182
4.38	Maximum Clad Temperature at All Measured Elevations, FLECHT SEASET Test 31701	4-183
4.39	Maximum Clad Temperature at All Measured Elevations, FLECHT SEASET Test 34209	4-184
4.40	Maximum Clad Temperature at All Measured Elevations, FLECHT SEASET Test 32013	4-185
4.41	Maximum Clad Temperature at All Measured Elevations, FLECHT Skewed Test 13609.....	4-186
4.42	Maximum Clad Temperature at All Measured Elevations, FLECHT Skewed Test 13914.....	4-187
4.43	Steam Temperatures Calculated at 75.6 in and Measured at 72 in, FLECHT SEASET Test 31805.....	4-188
4.44	Steam Temperatures Calculated at 75.6 in and Measured at 72 in, FLECHT SEASET Test 31504.....	4-189
4.45	Steam Temperatures Calculated at 75.6 in and Measured at 72 in, FLECHT SEASET Test 31203.....	4-190
4.46	Steam Temperatures Calculated at 75.6 in and Measured at 72 in, FLECHT SEASET Test 31302.....	4-191
4.47	Steam Temperatures Calculated at 75.6 in and Measured at 72 in, FLECHT SEASET Test 31701.....	4-192

4.48	Steam Temperatures Calculated at 75.6 in and Measured at 72 in, FLECHT SEASET Test 34209.....	4-193
4.49	Steam Temperatures Calculated at 75.6 in and Measured at 72 in, FLECHT SEASET Test 32013.....	4-194
4.50	Steam Temperatures Calculated at 82.8 in and Measured at 84 in, FLECHT Skewed Test 13609.....	4-195
4.51	Steam Temperatures Calculated at 82.8 in and Measured at 84 in, FLECHT Skewed Test 13914.....	4-196
4.52	Comparison of Calculated and Measured Heat Transfer Coefficient, FLECHT SEASET Test 31805.....	4-197
4.53	Comparison of Calculated and Measured Heat Transfer Coefficient, FLECHT SEASET Test 31504.....	4-198
4.54	Comparison of Calculated and Measured Heat Transfer Coefficient, FLECHT SEASET Test 31203.....	4-199
4.55	Comparison of Calculated and Measured Heat Transfer Coefficient, FLECHT SEASET Test 31302.....	4-200
4.56	Comparison of Calculated and Measured Heat Transfer Coefficient, FLECHT SEASET Test 31701.....	4-201
4.57	Comparison of Calculated and Measured Heat Transfer Coefficient, FLECHT SEASET Test 34209.....	4-202
4.58	Comparison of Calculated and Measured Heat Transfer Coefficient, FLECHT SEASET Test 32013.....	4-203
4.59	Comparison of Calculated and Measured Heat Transfer Coefficient, FLECHT Skewed Test 13609.....	4-204
4.60	Comparison of Calculated and Measured Heat Transfer Coefficient, FLECHT Skewed Test 13914.....	4-205
4.61	Accumulated Water Mass in the Test Section, FLECHT SEASET Test 31805.....	4-206
4.62	Accumulated Water Mass in the Test Section, FLECHT SEASET Test 31504.....	4-207
4.63	Accumulated Water Mass in the Test Section, FLECHT SEASET Test 31203.....	4-208
4.64	Accumulated Water Mass in the Test Section, FLECHT SEASET Test 31302.....	4-209
4.65	Accumulated Water Mass in the Test Section, FLECHT SEASET Test 31701.....	4-210
4.66	Accumulated Water Mass in the Test Section, FLECHT SEASET Test 34209.....	4-211
4.67	Accumulated Water Mass in the Test Section, FLECHT SEASET Test 32013.....	4-212

4.68	Accumulated Water Mass in the Test Section, FLECHT Skewed Test 13609	4-213
4.69	Accumulated Water Mass in the Test Section, FLECHT Skewed Test 13914	4-214
4.70	Total Liquid Carryover From Test Assembly, FLECHT SEASET Test 31805	4-215
4.71	Total Liquid Carryover From Test Assembly, FLECHT SEASET Test 31203	4-216
4.72	Total Liquid Carryover From Test Assembly, FLECHT SEASET Test 34209	4-217
4.73	Total Liquid Carryover From Test Assembly, FLECHT SEASET Test 32013	4-218
4.74	Total Liquid Carryover From Test Assembly, FLECHT Skewed Test 13609	4-219
4.75	Total Liquid Carryover From Test Assembly, FLECHT Skewed Test 13914	4-220
4.76	Average Rod Quench Time, FLECHT SEASET Test 31805	4-221
4.77	Average Rod Quench Time, FLECHT SEASET Test 31203	4-222
4.78	Average Rod Quench Time, FLECHT SEASET Test 31302	4-223
4.79	Average Rod Quench Time, FLECHT SEASET Test 31701	4-224
4.80	Average Rod Quench Time, FLECHT SEASET Test 34209	4-225
4.81	Average Rod Quench Time, FLECHT SEASET Test 32013	4-226
4.82	Calculated Rod Surface Temperatures at 79 in for the 20-Volume Test Section Cases With Various Time-Step Sizes, FLECHT SEASET Test 31504	4-227
4.83	Calculated Rod Surface Temperatures at 79 in for the 40-Volume Test Section Cases With Various Time-Step Sizes, FLECHT SEASET Test 31504	4-228
4.84	Maximum Cladding Temperatures vs. Axial Elevation, FLECHT SEASET Test 31504	4-229
4.85	Comparison of Predicted PCT and Measured Data, PDTF SMART	4-230
4.86	MCT vs. Elevation Comparison to Data for 4-in/s-Flooding-Rate Test, PDTF SMART	4-231
4.87	MCT vs. Elevation Comparison to Data for 2-in/s-Flooding-Rate Test, PDTF SMART	4-232
4.88	MCT vs. Elevation Comparison to Data for 1-in/s-Flooding-Rate Test, PDTF SMART	4-233
4.89	MCT vs. Elevation Comparison to Data for Variable-Flooding-Rate Test, PDTF SMART	4-234

4.90	Comparison of Break Mass Flow Rates, Marviken Test 2.....	4-235
4.91	Comparison of Break Mass Flow Rates, Marviken Test 6.....	4-236
4.92	Comparison of Break Mass Flow Rates, Marviken Test 8.....	4-237
4.93	Comparison of Break Mass Flow Rates, Marviken Test 16.....	4-238
4.94	Comparison of Break Mass Flow Rates, Marviken Test 17.....	4-239
4.95	Comparison of Break Mass Flow Rates, Marviken Test 20.....	4-240
4.96	Comparison of Break Mass Flow Rates, Marviken Test 22.....	4-241
4.97	Comparison of Break Mass Flow Rates, Marviken Test 24.....	4-242
4.98	Comparison of Break Mass Flow Rates, Marviken Test 25.....	4-243
4.99	Comparison of Calculated and Measured Mass Fluxes (All Nine Marviken Tests).....	4-244
4.100	Break Flow Uncertainty, Marviken Tests.....	4-245
4.101	Comparison of Calculated and Measured Effluent Temperature for the Plant-Specific Model, Westinghouse/EPRI.....	4-246
4.102	Cumulative Distribution Plots for CONMAS, Westinghouse/EPRI.....	4-247
4.103	Comparison Between Mini-Loop CCFL Data of a Westinghouse 17 x 17 UTP and Bankoff.....	4-248
4.104	Comparison Between Mini-Loop CCFL Data of a Westinghouse 15 x 15 UTP and Bankoff.....	4-249
4.105	Comparison Between Mini-Loop CCFL Data of a Combustion Engineering 14 x 14 UTP and Bankoff.....	4-250
4.106	Lower Plenum Liquid Level Comparison UPTF Test 6 – Run 131.....	4-251
4.107	Lower Plenum Liquid Level Comparison UPTF Test 6 – Run 132.....	4-252
4.108	Lower Plenum Liquid Level Comparison UPTF Test 6 – Run 133.....	4-253
4.109	Lower Plenum Liquid Level Comparison UPTF Test 6 – Run 135.....	4-254
4.110	Lower Plenum Liquid Level Comparison UPTF Test 6 – Run 136.....	4-255
4.111	Lower Plenum Liquid Level Comparison UPTF Test 7 – Run 203.....	4-256
4.112	UPTF Data/S-RELAP5 Cold Leg Temperature Comparison, UPTF Test 8 Run 111.....	4-257
4.113	UPTF Data/S-RELAP5 Flow Regime Comparison, UPTF Test 8 Run 111.....	4-258
4.114	UPTF Data/S-RELAP5 Cold Leg Temperature Comparison, UPTF Test 8 Run 112.....	4-259
4.115	UPTF Data/S-RELAP5 Flow Regime Comparison, UPTF Test 8 Run 112.....	4-260
4.116	Countercurrent Flow of Steam and Water UPTF Test 10 Run 081.....	4-261
4.117	Countercurrent Flow of Steam and Water UPTF Test 29 Run 212/211.....	4-262
4.118	Carryover to Steam Generators Test 10 Run 081 Beyond 150 sec.....	4-263

4.119	Cumulative Water Carryover to Steam Generators Test 29 Run 212/211	4-264
4.120	Counter Current Flow of Steam and Water, UPTF Test 10, Run 080.....	4-265
4.121	Upper Plenum Pressure Comparison Test 10, Run 080	4-266
4.122	Calculated Downflow Comparison UPTF Test 10, Run 080 (m=1.0, c=1.8).....	4-267
4.123	Counter Current Flow of Steam and Water, UPTF Test 12, Run 014.....	4-268
4.124	Upper Plenum Pressure Comparison UPTF Test 12, Run 014	4-269
4.125	Calculated Downflow Comparison UPTF Test 12, Run 014 (m=1.0, c=1.8).....	4-270
4.126	Steam and Water Injection Rates for UPTF Test 11 1.5 MPa Series	4-271
4.127	Steam and Water Injection Rates for UPTF Test 11 0.3 MPa Series	4-272
4.128	Comparison of UPTF Test 11 Data with S-RELAP5 Calculations	4-273
4.129	Comparison of Peak Surface Temperatures vs. Elevation for High Power Bundles, CCTF Test Run 54.....	4-274
4.130	Comparison of Peak Surface Temperatures vs. Elevation for High Power Bundles, CCTF Test Run 62.....	4-275
4.131	Comparison of Peak Surface Temperatures vs. Elevation for High Power Bundles for Test Run 67	4-276
4.132	Comparison of Peak Surface Temperatures vs. Elevation for High Power Bundles, CCTF Test Run 68.....	4-277
4.133	Temperature Comparison at 1.905 m, SCTF S2-17	4-278
4.134	Temperature Comparison at 1.905 m, SCTF S2-18	4-279
4.135	Thermocouple Variation Range at the PCT Elevation, ACHILLES ISP 25	4-280
4.136	Nitrogen Insurge Impact at 1.08 m, ACHILLES ISP 25	4-281
4.137	Nitrogen Insurge Impact at 1.81 m, ACHILLES ISP 25	4-282
4.138	Nitrogen Insurge Impact at 2.13 m, ACHILLES ISP 25	4-283
4.139	Nitrogen Insurge Impact at 2.33 m, ACHILLES ISP 25	4-284
4.140	Nitrogen Insurge Impact at 2.65 m, ACHILLES ISP 25	4-285
4.141	Nitrogen Insurge Impact at 3.18 m, ACHILLES ISP 25	4-286
4.142	Axial Velocities at 32.5 Inches, Asymmetric Flow - Test 1	4-287
4.143	Axial Flow Fractions for Asymmetric Flow - Test 1	4-288
4.144	Axial Velocities at 32.5 Inches, for Asymmetric Flow - Test 2	4-289
4.145	Axial Flow Fractions for Asymmetric Flow – Test 2.....	4-290
4.146	Axial Velocities at 32.5 Inches, for Asymmetric Flow - Test 3	4-291
4.147	Comparison of S-RELAP5 with Design Codes for Asymmetric Flow - Test 1	4-292
4.148	Comparison of PCTs Versus Core Elevations LOFT Test L2-3 with S-RELAP5.....	4-293

4.149	Comparison of PCTs Versus Core Elevations LOFT Test L2-5 with S-RELAP5.....	4-294
4.150	LOFT Test LP-02-6 Comparison of PCTs Versus Core Elevations.....	4-295
4.151	LOFT Test LP-LB-1 Comparison of PCTs Versus Core Elevations.....	4-296
4.152	Assessment of Semiscale LBLOCA Test S-06-3, PCTs	4-297
4.153	Assessment of Semiscale LBLOCA Test S-07-1, PCTs versus Elevation.....	4-298
4.154	Upper Plenum Level, UPTF Test 10, Run 081.....	4-299
4.155	Upper Plenum Level, UPTF Test 29 Run 212/211	4-300
4.156	Liquid Level in Upper Plenum CCTF Test 54.....	4-301
4.157	Liquid Level in Upper Plenum CCTF Test 62.....	4-302
4.158	Liquid Level in Upper Plenum CCTF Test 67.....	4-303
4.159	Liquid Level in Upper Plenum CCTF Test 68.....	4-304
4.160	Upper Plenum Levels for FLECHT-SEASET Test 31805.....	4-305
4.161	Upper Plenum Levels for FLECHT-SEASET Test 31203.....	4-306
4.162	Upper Plenum Levels for FLECHT-SEASET Test 31302.....	4-307
4.163	Upper Plenum Levels for FLECHT-SEASET Test 31701.....	4-308
4.164	Comparison of Liquid Carryover for CCTF Test 54	4-309
4.165	Comparison of Liquid Carryover for CCTF Test 62.....	4-310
4.166	Comparison of Liquid Carryover for CCTF Test 67	4-311
4.167	Comparison of Liquid Carryover for CCTF Test 68.....	4-312
4.168	Level in Broken Loop Catch Tank - UPTF Test 081.....	4-313
4.169	Level in Intact Loop Catch Tank - UPTF Test 081	4-314
4.170	Level in Broken Loop Catch Tank - UPTF Test 212.....	4-315
4.171	Level in Intact Loop Catch Tank - UPTF Test 212	4-316
4.172	Level in Separator Tank for FLECHT-SEASET Tests 31805	4-317
4.173	Level in Separator Drain Tank for FLECHT-SEASET Tests 31805.....	4-318
4.174	Level in Separator Tank for FLECHT-SEASET Tests 31203	4-319
4.175	Level in Separator Drain Tank for FLECHT-SEASET Tests 31203.....	4-320
4.176	Level in Separator Tank for FLECHT-SEASET Tests 31302	4-321
4.177	Level in Separator Drain Tank for FLECHT-SEASET Tests 31302.....	4-322
4.178	Level in Separator Tank for FLECHT-SEASET Tests 31701	4-323
4.179	Level in Separator Drain Tank for FLECHT-SEASET Tests 31701.....	4-324
4.180	CCTF TEST 54 Temperatures at Measured PCT Node.....	4-325
4.181	CCTF TEST 54 Temperatures Near Calculated PCT Node.....	4-326

4.182	CCTF TEST 54 PCT Profile.....	4-327
4.183	CCTF TEST 62 Temperatures at Measured PCT Node.....	4-328
4.184	CCTF TEST 62 Temperatures Near Calculated PCT Node	4-329
4.185	CCTF TEST 62 PCT Profile.....	4-330
4.186	CCTF TEST 67 Temperatures at Measured PCT Node.....	4-331
4.187	CCTF TEST 67 Temperatures Near Calculated PCT Node	4-332
4.188	CCTF TEST 67 PCT Profile.....	4-333
4.189	CCTF TEST 68 Temperatures at Measured PCT Node.....	4-334
4.190	CCTF TEST 68 Temperatures Near Calculated PCT Node	4-335
4.191	CCTF TEST 68 PCT Profile.....	4-336
4.192	CCTF TEST 68 Intact Loop Cold Leg Void Fraction	4-337
4.193	LOFT LP-LB-1 Temperatures at Measured PCT Node	4-338
4.194	LOFT LP-LB-1 PCT Profile.....	4-339
4.195	LOFT LP-02-6 Temperatures at Measured PCT Node	4-340
4.196	LOFT LP-02-6 PCT Profile	4-341
4.197	LOFT L2-5 Temperatures at Measured PCT Node	4-342
4.198	LOFT L2-5 PCT Profile.....	4-343
4.199	LOFT L2-3 Temperatures at Measured PCT Node	4-344
4.200	LOFT L2-3 Temperatures at Calculated PCT Node	4-345
4.201	LOFT L2-3 PCT Profile.....	4-346
4.202	Semiscale S-06-3 Temperatures at Measured PCT Node	4-347
4.203	Semiscale S-06-3 Temperatures at Calculated PCT Node	4-348
4.204	Semiscale S-06-3 PCT Profile	4-349
4.205	Semiscale S-07-1 Temperatures at Measured PCT Node	4-350
4.206	Semiscale S-07-1 Temperatures at Calculated PCT Node	4-351
4.207	Semiscale S-07-1 PCT Profile	4-352
4.208	Sleicher-Rouse HTC for Steam Compared to Data	4-353
5.1	Calculation Framework.....	5-28
5.2	[.....].....	5-29
5.3	[.....].....	5-30
5.4	[.....].....	5-31
5.5	[.....].....	5-32
5.6	[.....].....	5-33

5.7	[]	5-34
5.8	[]	5-35
5.9	[]	5-36
5.10	[]	5-37
5.11	[]	5-38
5.12	[]	5-39
5.13	[]	5-40
5.14	[]	5-41
5.15	[]	5-42
5.16	[]	5-43
5.17	[]	5-44
5.18	[]	5-45
5.19	[]	5-46
5.20	[]	5-47
5.21	[]	5-48
5.22	[]	5-49
5.23	[]	5-50
5.24	[]	5-51
5.25	[]	5-52
5.26	[]	5-53
5.27	[]	5-54
5.28	[]	5-55

Nomenclature

Acronym	Definition
ACC	accumulator core coolant
ANP	advanced nuclear products
ANS	American Nuclear Society
ASME	American Society of Mechanical Engineers
BHL	beginning of heated length
BLCL	broken loop cold leg
BLHL	broken loop hot leg
BOCREC	bottom of core recovery
BST	blowdown suppression tank
BWR	boiling water reactor
CCFL	countercurrent flow limiting
CCTF	Cylindrical Core Test Facility
CFR	Code of Federal Regulations
CHF	critical heat flux
CONMAS	interfacial condensation heat transfer coefficient multiplier
CSAU	Code Scaling, Applicability, and Uncertainty
DEG	double-ended guillotine
DIW	deionized water tank
DMS	document management system
DNB	departure from nucleate boiling
ECC	emergency core cooling
ECCS	emergency core cooling system
EDR	Experimental Data Report
EHL	end of heated length
EPRI	Electric Power Research Institute
FCTF	Full Core Test Facility
FIINVS	post-CHF inverted slug regime
FIMIST	post-CHF mist flow regime
FLECHT	Full Length Emergency Cooling Heat Transfer
FLOREG	flow regime
HEM	homogeneous equilibrium model
HPI	high pressure injection
HPIS	high pressure injection system
HTP	high thermal performance
ICAP	International Code Assessment Program
IET	Integral Effects Tests

ILCL	intact loop cold leg
ILHL	intact loop hot leg
INEEL	Idaho National Environmental Engineering Laboratory (formerly INEL)
INEL	Idaho National Engineering Laboratory
JAERI	Japan Atomic Energy Research Institute
KWU	Kraftwerk Union (SPC), now Framatome ANP GmbH
LANL	Los Alamos National Laboratory
LBLOCA	large break loss-of-coolant accident
LHGR	linear heat generation rate
LOCA	loss-of-coolant accident
LOCE	loss-of-coolant experiment
LOFT	Loss of Fluid Test
LPCI	low pressure coolant injection
LPIS	low pressure injection system
MCT	maximum clad temperature
MLHGR	maximum linear heat generation rate
MSIV	main steam isolation valve
NAI	Numerical Applications, Inc.
NPP	nuclear power plant
NRC	United States Nuclear Regulatory Commission
OECD	Organization of Economic Cooperation and Development
ORNL	Oak Ridge National Laboratory
PCP	primary coolant pump
PCS	primary coolant system
PCT	peak cladding temperature
PDTF	Product Development Test Facility
PFM	pipe flow meter
PIRT	Process Identification and Ranking Table
PLC	programmable logic controllers
PWR	pressurized water reactor
QLR	Quick Look Report
QOBV	quick-opening blowdown valve
RABS	reflood assisted bypass system
RABV	reflood assisted bypass valve
RLBLOCA	realistic large break loss-of-coolant accident
SBLOCA	small break loss-of-coolant accident
SCTF	Slab Core Test Facility
SDR	Software Development Record
SEASET	System Effects And Separate Effects Tests

SET	Separate Effects Tests
SMART	SMall Array Reflood Test
SPC	Siemens Power Corporation
S/W	steam/water
THTF	Thermal-Hydraulic Test Facility
TMDPJUN	time-dependent junction
TMDPVOL	time-dependent volume
UCSP	upper core support plate
UPTF	Upper Plenum Test Facility
USNRC	United States Nuclear Regulatory Commission
UTP	upper tie plate
W/EPRI	Westinghouse/Electric Power Research Institute

1.0 Introduction

This report describes the Framatome ANP (FRA-ANP) methodology developed for the realistic evaluation of a large break loss-of-coolant accident (LBLOCA) for pressurized water reactors (PWRs). The methodology complies with the revised LOCA emergency core cooling system (ECCS) rule as issued by the U.S. Nuclear Regulatory Commission (NRC) in 1988 (Reference 1). This rule allows the use of realistic LOCA evaluation models in place of the prescribed conservative evaluation models as specified by 10 CFR 50 Appendix K, provided that it can be established with a high probability that the criteria of 10 CFR 50.46 are not violated.

The basis for the revised rule is a large body of research performed after the 1975 LOCA ECCS rule was implemented, which shows that the prescribed Appendix K analysis methods are unnecessarily conservative. A compendium of ECCS research (Reference 2) was issued that references the relevant thermal-hydraulic research.

The revised rule requires that an acceptable realistic LOCA ECCS evaluation model have sufficient supporting justification to show that the analytical technique realistically describes the behavior of the reactor system during a LOCA. It is expected that the analytical technique will, to the extent practicable, utilize realistic methods and be based upon applicable experimental data.

The amended rule also requires that the uncertainty of the calculation be estimated and accounted for when comparing the results of the calculation to the temperature limits and other criteria of 10 CFR 50.46. The realistic evaluation model will retain a degree of conservatism consistent with the quantified uncertainty of the calculation.

The final rule does not prescribe the analytical methods or uncertainty techniques to be used. However, a Regulatory Guide (Reference 3) was issued to provide guidance for realistic LOCA analyses. The NRC also independently developed and demonstrated the code scaling, applicability and uncertainty (CSAU) methodology (Reference 4) for quantifying uncertainties in realistic codes. The 95th percentile of the probability distribution is accepted (Reference 3) as providing the level of conservatism required by the rule.

The purpose of this report is to provide a description of the FRA-ANP realistic PWR LBLOCA methodology and demonstrate its application to representative nuclear power plants. The

methodology documentation is provided in a format consistent with that outlined in the "CSAU Evaluation Methodology," which specifies that a roadmap be provided for the methodology followed by a detailed discussion. Each of the steps outlined in CSAU is addressed in both the roadmap section (Section 2) and the detailed description section (Section 3, 4, and 5).

As outlined in CSAU the development of this methodology relies on the code documentation. The models and correlations document provides the information to demonstrate the applicability of the codes to the chosen event scenario and Nuclear Power Plant (NPP) types through the use of the phenomena identification and ranking table (PIRT) process. The PIRT identifies the models and correlations in the code for which biases and uncertainties would have to be generated or conservatisms demonstrated.

Finally, the results of the code assessments reported in the verification and validation report (EMF-2102, Reference 5) provides the information required to define how each of the important PIRT phenomena are treated in the uncertainty analysis. This treatment ranges from simply acknowledging that the code is conservative and accepting that conservatism to the definition of a bias and uncertainty, including their distribution, which are required to treat the PIRT phenomena statistically.

2.0 Methodology Roadmap

This section provides an overview of the methodology and points to the detailed discussion of the individual CSAU steps that follow. The CSAU approach to realistic LOCA analysis is diagrammed in Figure 2.1. The CSAU procedure has three major elements:

- Requirements and Code Capabilities (Section 3.0)
- Assessment and Ranging of Parameters (Section 4.0)
- Sensitivity and Uncertainty Analysis (Section 5.0)

FRA-ANP's realistic LBLOCA evaluation methodology is defined and documented consistent with the CSAU procedure as shown in the following three sections. FRA-ANP's CSAU-compliant procedure for PWRs is applicable to Westinghouse (W) 3-loop and 4-loop designs and to Combustion Engineering (CE) 2x4 designs.

2.1 Requirements and Code Capabilities

The requirements and code capabilities discussion identifies and compares scenario-modeling requirements with code capabilities to determine the code's applicability to the particular scenario and to identify potential limitations. This is accomplished through the performance of the following six CSAU steps:

- Scenario Specification (Section 3.1)
- Nuclear Power Plant Selection (Section 3.2)
- Phenomena Identification and Ranking (Section 3.3)
- Frozen Code Version Selection (Section 3.4)
- Provision of Complete Code Documentation (Section 3.5)
- Determination of Code Applicability (Section 3.6)

The scenario being addressed in this report is the LBLOCA. The licensing criteria for this event are:

- The calculated peak cladding temperature (PCT) shall not exceed 2200°F.
- The maximum calculated cladding oxidation shall nowhere exceed 0.17 times the total cladding thickness before oxidation.
- The maximum calculated hydrogen generation from the chemical reaction of the cladding with water or steam shall not exceed 0.01 times the hypothetical amount that would be generated if all of the metal in the cladding cylinders surrounding the fuel, excluding the cladding surrounding the plenum volume, were to react.

- The calculated changes in core geometry shall be such that the core remains amenable to cooling.
- The calculated core temperature shall be maintained at an acceptably low value and decay heat shall be removed for the extended period of time required by the long-lived radioactivity remaining in the core.

These licensing criteria, with the primary focus on the PCT, will be used as the figure-of-merit upon which decisions will be made with respect to the acceptability of the methodology. The PCT is chosen as the primary criteria because all the other criteria are, to some extent, dependent upon or related to it.

The selected NPP types to which the methodology is to be applicable includes those PWRs with U-tube type steam generators and ECCS injection into the cold legs. Provided with the methodology is a sample problem for a (W) 4-loop PWR and a licensing analysis for a (W) 3-loop PWR. The methodology is also applicable to (CE) 2x4 plants (see end of Section 2.0).

A PIRT has been prepared for the LBLOCA and the NPP types. This initial PIRT was developed by FRA-ANP from a combination of published PIRTs (Reference 2), reviews by external experts, and a peer review conducted by FRA-ANP personnel and external experts. The PIRT that resulted from this process is provided in Table 3.4.

The codes selected for the performance of the realistic LBLOCA analysis include the RODEX3A fuel rod code (References 6, 7, and 8) and the S-RELAP5 system code (References 5, 9, 10, and 11). Frozen versions for each of these codes were selected and used to perform the analyses presented in this report. Documents were developed for each of the codes to address the models and correlations used, and include a users manual, an assessment report, and user guidelines to execute the methodology (References 12 and 13). Verification was also performed to confirm that the models reported in the documentation are the models actually contained in the code (Reference 5). In addition, the ICECON code (References 14 and 15) has been incorporated into the S-RELAP5 code, where ICECON subroutines provide the required containment boundary conditions.

The final step in the requirements and code capabilities element is to demonstrate that the code is applicable to the chosen scenario and NPP types. This objective is accomplished by comparing the important scenario phenomena from the PIRT and the selected NPP modeling requirements with the capabilities of the chosen codes. The results of this comparison

demonstrate that the chosen codes are applicable to the LBLOCA and NPP types, as shown in Section 3.6.

2.2 ***Assessment and Ranging of Parameters***

The assessment and ranging of parameters element is used to quantify the uncertainties and biases that are to be addressed in the analysis of the chosen scenario with the chosen codes.

This element includes four steps:

- Establishment of Assessment Matrix (Section 4.1)
- NPP Nodalization Definition (Section 4.2)
- Definition of Code and Experimental Accuracy (Section 4.3)
- Determination of Effect of Scale (Section 4.4)

Implementing this element requires a series of iterations among the several steps. An examination of the PIRT (Table 3.4, Section 3.3) reveals that a large number of potentially important phenomena must be addressed. That is, those phenomena ranked 5 or higher. Assessing so many phenomena would not be manageable. Thus, the following four-step process was used to reduce the number of phenomena to be addressed.

First, the NPP nodalization was defined using the following steps:

- A trial nodalization was developed based on internal FRA-ANP experience using RELAP5 codes.
- A limited number of calculations were performed.
- The NPP nodalization was then adjusted until reasonable trends, based on engineering judgement, were obtained in the results.
- A limited number of experimental assessments was selected and modeled with the nodalization.
- The nodalization was again adjusted until reasonable trends were observed in both the NPP analyses and in the assessment calculations.

A peer review was conducted using internal and external experts, to evaluate the proposed NPP nodalization and the results produced. The peer review concluded that the nodalization of the upper plenum required more detail. This change resulted in a repeat of the above process until a nodalization was obtained that addressed all the issues identified in the peer review.

Second, each of the potentially important phenomena was paired with a parameter in the code that could be varied. Third, a possible range of uncertainty for each of the potentially important

phenomena and the associated parameters that could be varied in the analysis were defined. The uncertainty ranges defined were based on a review of available literature.

Fourth, the nodalization and the identified uncertainty ranges were used to perform sensitivity calculations. Based on the results of these sensitivity studies, the dominant phenomena were identified (Table 4.1, Section 4.1) and an assessment matrix was developed to assess these phenomena (Table 4.3, Section 4.1). In addition, various assessments were chosen to be part of the assessment matrix in order to demonstrate the scalability of the code.

Using the assessment matrix, which includes separate effects (SET) and integral effects tests (IET), each of the assessment test facilities was modeled with S-RELAP5 incorporating the nodalization defined above. The initial results of the assessment calculations required additional modification of both the code and the nodalization. A complete rerun of the PIRT sensitivity calculations and a re-evaluation of the assessment matrix were performed based on the changes made. Once this iterative process had been completed, the final NPP nodalization, assessment matrix, and assessment calculations were produced.

Completion of the assessment calculations provided the uncertainties for use in the plant analyses and also provided the basis for the demonstration of code scalability. The treatment of uncertainties is described and quantified in Section 4.3. The scalability of the code is demonstrated in Section 4.4.

2.3 ***Sensitivity and Uncertainty Analysis***

The sensitivity and uncertainty analysis element combines the code and model uncertainties and the plant specific contributors to obtain a total uncertainty and to provide a basis for making an acceptability statement with respect to the established safety criteria. The following steps are included in this CSAU element:

- Determination of the Effect of Reactor Input Parameters and State (Section 5.1)
- Performance of NPP Sensitivity Calculations (Section 5.2)
- Determination of Combined Bias and Uncertainty (Section 5.3)
- Determination of Total Uncertainty (Section 5.4)

The NPP input parameters and possible operating states were reviewed to determine the applicable input parameters and state. This review identified a list of inputs that might impact

the realistic LBLOCA event. Actual NPP operating conditions and typical technical specifications were assessed to identify allowed operating conditions. Sensitivity studies were performed using the selected NPP model to determine those parameters that impact the realistic LBLOCA event. For the most important parameters additional plant data were obtained, where available, so that actual operational data distributions could be determined.

[

] The identification of the parameters and the results of the parameter studies are provided in Tables 5.1-5.4 and Section 5.1.

The methodology for determination of the combined biases and uncertainties and the development of a final statement of probability for the limiting criteria are addressed in Section 5.2. To perform these last two CSAU steps, [

]

[

] A licensing analysis for a 3-loop (W) designed plant is provided in Reference 16. Section 5.4 provides the final statement of overall conformance to the licensing criteria.

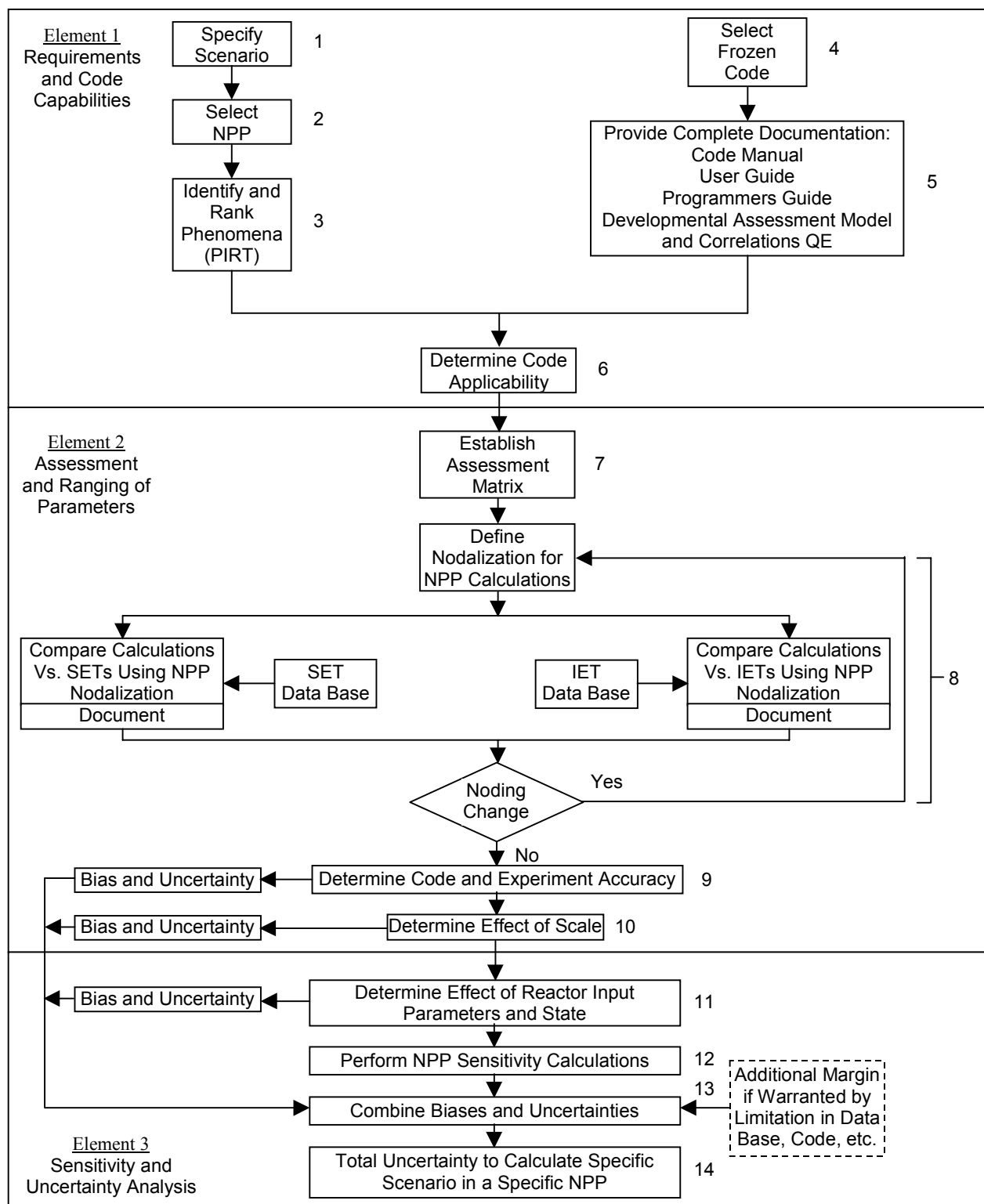


Figure 2.1 Code Scaling, Applicability, and Uncertainty Methodology Flow Chart

3.0 Requirements and Capabilities

The objective of the first element of the CSAU methodology is to establish the analysis requirements and to demonstrate that the chosen codes can address these requirements. The important phenomena are determined from the event scenario and NPP types and documented in the PIRT. The ability of the codes to address the important phenomena must then be demonstrated. Documents must be developed that contain sufficient detail to permit the code models to be correlated with the important PIRT phenomena.

3.1 Scenario Specification (CSAU Step 1)

This report describes methodology for the realistic evaluation of LBLOCAs. The Standard Review Plan (SRP) (Reference 17), Event 15.6.5, defines a LOCA. LOCAs are defined in SRP Event 15.6.5 as follows:

"Loss-of-coolant accidents (LOCA) are postulated accidents that would result from the loss of reactor coolant, at a rate in excess of the capability of the normal reactor coolant makeup system, from piping breaks in the reactor coolant pressure boundary. The piping breaks are postulated to occur at various locations and include a spectrum of break sizes, up to a maximum pipe break equivalent in size to the double-ended rupture of the largest pipe in the reactor coolant pressure boundary. Loss of significant quantities of reactor coolant would prevent heat removal from the reactor core, unless the water is replenished."

PWRs are required to be equipped with an ECCS that satisfies the requirements of 10 CFR Part 50, Section 50.46 (Reference 1).

The LBLOCA event is classified as a Postulated Accident and a Condition IV event (Reference 17). This event is not expected to occur during the lifetime of the plant but is designated a design basis accident. The specific acceptance criteria for performance of the ECCS are:

- The calculated PCT shall not exceed 2200°F.
- The maximum calculated cladding oxidation shall nowhere exceed 0.17 times the total cladding thickness before oxidation.
- The maximum calculated hydrogen generation from the chemical reaction of the cladding and water or steam shall not exceed 0.01 times the hypothetical amount that would be generated if all of the metal in the cladding cylinders surrounding the fuel, excluding the cladding surrounding the plenum volume, were to react.

- The calculated changes in core geometry shall be such that the core remains amenable to cooling.
- The calculated core temperature shall be maintained at an acceptably low value and decay heat shall be removed for the extended period of time required by the long-lived radioactivity remaining in the core.
- The radiological consequences of the most severe LOCA are within the guidelines of 10 CFR 100.
- The TMI Action Plan requirements have been met. (The TMI Action Plan requirements are more specifically related to the Small Break LOCA (SBLOCA) event.)

The methodology described here is shown to be in compliance with the first four criteria above. These criteria, with a primary focus on the PCT, will be used as the figure-of-merit upon which decisions are made with respect to the acceptability of the methodology. The PCT is chosen as the primary criterion because to some extent all the other criteria are dependent upon or related to it.

A hypothetical LOCA is initiated by an instantaneous rupture of a reactor coolant system (RCS) pipe ranging in cross-sectional area up to and including that of the largest pipe in the RCS. A spectrum of breaks for both double-ended guillotine and split break types is analyzed. The spectrum includes double-ended guillotine breaks ranging in size from one to two times the cross sectional area of the largest RCS pipe. The split break spectrum is analyzed for longitudinal split areas ranging in size from the largest small break size (10% of the cross sectional area) to one times the full cross-sectional area of the largest RCS pipe. For a LBLOCA, the most limiting break typically occurs in a cold leg pipe between the pump discharge and the vessel.

Offsite power availability must also be considered in the analysis. If loss-of-offsite power is assumed to occur coincident with the LOCA initiation, RCS pump coastdown will occur with the loss-of-offsite power. For short periods of time following the break and up to about 5 to 8 seconds into the transient, the pump head may be sufficient to maintain positive flow through the core, which can provide significant cooling of the fuel. Due to loss-of-offsite power, an additional time delay for startup of the diesel generators and safety injection system (SIS) pumps must also be accounted for in the analysis. The worst single failure is identified and applied in the analysis. The worse single failure is typically the loss of one low head safety injection (LHSI) pump or the loss of a diesel generator.

A LBLOCA event is typically described in three phases: (1) blowdown, (2) refill, and (3) reflood. The blowdown phase is defined as the time period from initiation of the break until flow from the accumulators or safety injection tanks begins. This definition is somewhat different than the traditional definition of blowdown which extends the blowdown until the RCS pressure approaches containment pressure. The blowdown phase typically lasts about 12 to 25 seconds, depending on the break size. The refill phase lasts from the end of blowdown until fluid from the ECCS has filled the downcomer and lower plenum up to the bottom of the heated length of the fuel. The reflood phase lasts from the end of refill until the core temperatures are reduced.

Following the instantaneous pipe break, the blowdown phase is characterized by a sudden depressurization from operating pressure down to the saturation pressure of the hot leg fluid. An immediate flow reversal and stagnation occurs in the core due to flow out the break which causes the fuel rods to pass through critical heat flux (CHF), usually within 1 second following the break. Following this initial rapid depressurization, the RCS depressurizes at a more gradual rate with the reactor coolant being expelled primarily by vaporization.

A reactor trip signal occurs when either the pressurizer low-pressure trip setpoint or containment vessel high-pressure trip setpoint is reached. However, reactor trip and scram are conservatively neglected in this LOCA methodology, and reactor shutdown is accomplished initially by moderator feedback and maintained by the boron content of the ECCS water. A SIS initiation signal is also actuated when the high containment pressure setpoint is reached.

When the system pressure falls below the accumulator pressure, flow from the accumulator is injected into the cold legs ending the blowdown period and initiating the refill period. Once the system pressure falls below the respective shutoff heads of the high head safety injection (HHSI) pumps and the LHSI pumps and the system startup time delays are met, SIS flows begin injection into the RCS. While some of the ECCS flow bypasses the core and goes directly out the break, the downcomer and lower plenum gradually refill until the liquid level reaches the bottom of the core. During this refill period, heat is primarily transferred from the hotter fuel rods to cooler fuel rods and structures by radiative heat transfer.

Once the lower plenum is refilled to the bottom of the fuel rod heated length, refill ends and the reflood phase begins. The ECCS fluid flowing into the downcomer provides the driving head to move coolant through the core. As the mixture level moves up the core, steam is generated and liquid is entrained. As this entrained liquid passes into the steam generators, and

vaporizes, steam binding may occur, reducing the core reflood rates. However, the fuel rods are eventually cooled and quenched by radiation and convective heat transfer as the quench front moves up the core.

3.2 ***Nuclear Power Plant Selection (CSAU Step 2)***

The selected NPP types to which the methodology is to be applied includes those PWRs with U-tube type steam generators and ECCS injection into the cold leg. This includes W 3- and 4-loop plants and CE 2x4 plants. These three NPP types have very similar hot and cold legs, pressurizers, steam generators, and vessels. The largest difference among the NPP types is the number of hot and cold legs and steam generators. However, experience in the performance of Appendix K large break LOCA analyses for the three NPPs has shown that all three types behave similarly.

All three NPP types have inverted U-tube steam generators, a pressurizer connected to the hot leg, and ECCS injection into the cold legs. The steam generators for all three plant types can all be modeled with a downcomer, boiler, plenum, dryer/separator, and steam dome region. In addition, the main and auxiliary feedwater enters the steam generators in the downcomer for all three-plant types. The pressurizers are essentially the same and can be modeled with axial nodes, associated heat structures, heaters, sprays, and a surge line connected to a hot leg. The plant nodalization for a loop is described in detail in Reference 12 and illustrated in Figure 4.3.

The configuration of the vessels for all three-plant types is also essentially the same and can be modeled in the code with the same major divisions and nodalization schemes. The coolant enters the vessel through the inlet nozzles and flows into the downcomer. In the downcomer a small fraction of the flow leaks into the upper head but the majority of the flow goes down the downcomer into the lower head/plenum region. From here the majority of the flow goes up through the active core with some flow bypassing the core through the baffle and guide tubes. From the core the flow enters the upper plenum and exits the vessel through the hot leg nozzles.

The principal difference in the vessel between the W and CE plants is in the connection between the downcomer and the lower plenum/head. In the CE plants there may be a flow skirt that is intended to force part of the flow to pass through the lower head before going into the

lower plenum region. The NPP model of the lower plenum to be used for both the W and CE plant types has been nodalized to address this vessel configuration difference. The plant nodalization for the vessel is described in detail in Reference 12 and illustrated in Figure 4.4.

As indicated above the principle difference between these NPP types is in the number of hot and cold legs and steam generators. The W 3-loop NPP has 3 hot legs, 3 cold legs and 3 steam generators. The W 4-loop NPP has 4 hot legs, 4 cold legs, and 4 steam generators. The CE 2x4 plant has 2 hot legs, 4 cold legs and 2 steam generators.

A typical vessel loop configuration for the three NPP types is shown in Figure 4.5. This figure shows the location of the cold legs (arrows pointing into vessel) and hot legs (arrows pointing out of vessel) for the three NPP types. Since the hot legs pass through the vessel downcomer region into the upper plenum they essentially provide a flow path blockage at the elevation of the hot and cold legs in all three NPP types. As illustrated in this figure the flow paths for the W 4-loop and the CE 2x4 plants are very similar in relation to the hot and cold legs.

To further demonstrate that these three NPP types are very similar and respond in essentially the same manner, approximate values for some of the important NPP parameters are provided in Table 3.1 and a sequence of events from a typical Appendix K analysis is provided in Table 3.2. As illustrated in Table 3.1 the biggest difference in the important NPP parameters is in the pressure of the accumulators for the W plants and the safety injection tanks (SITs) in the CE plants. The impact of this difference is shown in the sequence of events given in Table 3.2 where the SIT flow initiation is delayed in the CE plants until the pressure in the cold legs drops below the SIT pressure. Taking into account this delay in the SIT delivery, the sequence of events is very similar for the three NPP types.

Provided with the methodology is a sample problem for a W 4-loop PWR NPP. A licensing analysis for a W 3-loop PWR has also been completed and will be submitted on a plant specific basis.

3.3 ***Phenomena Identification and Ranking (CSAU Step 3)***

A key step in the CSAU process is to identify and rank the important phenomena that must be addressed in analyzing a LBLOCA. This step is performed by experts who are knowledgeable of LBLOCA phenomena and who define the important phases of the LBLOCA scenario and identify phenomena that could be important during each phase of the transient. Based on their

knowledge, the experts then rank the phenomena as to their relative importance during each phase of the LOCA transient. The result is a PIRT which ranks the relative importance of the phenomena for each component and phase of the LOCA. The PIRT provides the basis for: (1) determining code applicability (does the code properly model the important phenomena), (2) establishing the assessment matrix (identifying test data that contain the appropriate phenomena during each accident phase), and (3) identifying phenomena parameters to be ranged and quantified for evaluating uncertainties.

A PIRT for a W 4-loop PWR LBLOCA is presented in the Compendium (Reference 2). Table 3.3 provides an initial PIRT which was developed from the Compendium by averaging the ranking of the experts and the ranking developed by the analytical hierarchy process (AHP) and rounding up when necessary. Each phenomena is given a ranking, where importance is proportional to the numerical value (e.g., 9 = extreme importance, 1 = least importance). The ranking indicates the important phenomena that should be simulated by a realistic LBLOCA evaluation model.

Using Table 3.3 as the starting point, the following process was followed to generate a final PIRT for use in the FRA-ANP CSAU process. The initial PIRT was reviewed by three experts, who offered recommendations for the addition or deletion of phenomena from the PIRT and revisions to the ranking of the phenomena. Following this review, a peer review was held with the three experts and four additional FRA-ANP personnel to derive a final PIRT that incorporated the input from all seven participants. This PIRT is provided in Table 3.4.

To ensure a coherent peer review process, a set of definitions were agreed upon:

1. Blowdown: The blowdown phase of the LOCA is defined as the time period from initiation of the break until flow from the accumulators or safety injection tanks begins. This definition is somewhat different from the traditional definition of blowdown which continues until the RCS pressure approaches containment pressure.
2. Refill: The refill phase of the LOCA begins when the accumulators or flooding tanks begin injecting and continues until the mixture level in the vessel refills the lower plenum and begins to flow into the core.

3. Reflood: The reflood phase of the transient begins when the lower plenum fills and ECC begins flowing into the bottom of the core and continues until the temperature transient throughout the core has been terminated. At this time the LOCA stored energy and decay heat are being removed and the LOCA has been reduced to an issue of maintaining long term cooling.
4. Post-CHF Heat Transfer: Defined according to the transient phase. For blowdown it is the high pressure, high mass flux, low vapor superheat film boiling. During refill, it is a combination of dispersed flow film boiling and natural convection to single-phase vapor. During reflood, it is dispersed flow film boiling.
5. Reflood Heat Transfer: Defined only for the reflood phase as convection to single phase steam, wall to fluid radiation, film boiling, and transition boiling. Thus, includes effects of precursory cooling and quenching.
6. Rewet: Defined according to transient phase. For blowdown this is the quenching (either bottom-up or top-down) associated with high heat transfer rates near the quench front during periods of high liquid flows. For refill and reflood, limit this to top-down quenching due to falling liquid films.

With the above definitions as the basis, the following changes were made to the PIRT for the LBLOCA during the peer review process:

1. []
[]
]
[]
]
2. []
[]
]

4. []

[

]

[

]

5. []

[

]

[

]

[

]

6. []

[

]

7. []

[

]

8. []

[

]

[

]

[

]

9. []
[]
[]
10. []
[]
[]
[]
[]
11. []
[]
[]
[]
[]
12. []
[]
[]
[]
13. []
[]
[]

These results are all shown in the final PIRT given in Table 3.4. This PIRT was used in the demonstration of code applicability and as the basis for performing sensitivity studies and determining the code assessment matrix.

3.4 **Frozen Code Version Selection (CSAU Step 4)**

The codes selected for use in the realistic LBLOCA methodology include RODEX3A (References 6, 7, and 8) and S-RELAP5 (References 5, 9, 10, and 11). RODEX3A is a best

estimate fuel rod code which has been approved for use in the performance of realistic LBLOCA (RLBLOCA) analyses (Reference 6). The S-RELAP5 code is a RELAP5 based thermal hydraulic system code for performing LBLOCA analyses. The ICECON code (References 14 and 15) has been incorporated into the S-RELAP5 code to provide the required containment boundary conditions for the LBLOCA analysis. ICECON was developed to predict the long-term behavior of PWR nuclear plant containment systems.

The frozen versions of these codes used in the development of this methodology are defined in Table 3.5. The interpretation of the version designation is described below for the S-RELAP5 code version, UJUL00:

- U signifies that the code is a USE code version which means it has been verified, validated, and documented in conformance with FRA-ANP's quality assurance program. It also indicates that the code has been stored in FRA-ANP's code management system (CMS) where it can be read but not modified and is automatically archived.
- JUL00 is the month and year in which the code version was built and placed in CMS.

Two USE versions of the S-RELAP5 code were used in the development of this methodology, UJUL00 and UMAR01. The differences between these two code versions reflect the addition of the final set of multiplication parameters for use in the uncertainty analysis in UMAR01 and the correction of problems found in the verification of the RODEX3A incorporation into S-RELAP5. The verification of the RODEX3A incorporation into S-RELAP5 occurred late in the methodology development process. During this verification process, several problems were identified and corrected.

In addition, two point releases have been made for the UMAR01 use code versions. These point releases dealt only with the application of the multipliers used in the uncertainty analysis. Consistent with the CSAU definition of a frozen code, these changes do not constitute a code change.

Since a large number of the assessments had already been completed it was decided that only those assessments which actually used RODEX3A would be rerun and the software development record for UMAR01 would document that assessments performed with electrical heater rods were unaffected by the changes to the RODEX3A implementation. The assessments that used electrical heater rods and had already been completed would not be rerun with UMAR01 and would continue to rely on the UJUL00 analyses. On the other hand the

LOFT analyses which used nuclear fuel rods had to be rerun with UMAR01. In addition, all the final plant analyses were run with the UMAR01 code version. Thus, while two code versions of S-RELAP5 have been used in the methodology development, it has been demonstrated that no change in results would occur if everything was rerun with the final UMAR01 code version.

3.4.1 RODEX3A

Key to a realistic LBLOCA analysis is the model used for calculating fuel rod performance. In particular the initial operating temperature of the fuel pellets (stored energy) and the internal fuel rod gas pressure are significant parameters that affect the calculated peak cladding temperature (PCT). These parameters are functions of fuel exposure and power history.

FRA-ANP developed the realistic fuel rod mechanical response model RODEX3A, which provides exposure dependent initial fuel conditions for the realistic LOCA evaluation model. Further, to assure compatibility and consistency between the RODEX3A initial fuel conditions and the initial and transient conditions calculated by S-RELAP5, the appropriate fuel models from RODEX3A were incorporated into S-RELAP5.

The model features included in RODEX3A are:

- A coolant subchannel model to compute the coolant state and cladding surface temperature.
- A model to compute the radial temperature distribution in a fuel rod and adjust the porosity contribution to the fuel thermal conductivity.
- A model to compute gap conductance.
- A model to compute internal rod pressure.
- Models to compute grain size, and fission gas release and redistribution in the fuel microstructure.
- A model to compute pellet-cladding interaction forces.
- Models to compute cladding creep and growth.
- Models to compute cladding oxidation and hydriding.
- A model to calculate elastic response of the cladding.
- A fuel "segment mechanics" model to compute fuel pellet creep, dish filling, cracking, deformations, and mechanical response.
- Models to compute pellet densification, swelling, and hot pressing.
- A pellet flexibility model.
- Material properties models.

- A model to compute the radial dependence of the heat generation.
- Models to calculate the axially dependent exposure and fluence distribution.

To perform a LOCA analysis with the FRA-ANP RLBLOCA evaluation model, RODEX3A calculations are first performed to calculate initial condition inputs for all fuel rods modeled in S-RELAP5. Inputs to RODEX3A describe:

- The cladding geometry, composition and creep coefficients.
- The pellet geometry, composition, density, grain size and open porosity.
- The axial and radial nodalization of the fuel rod.
- The fuel plenum volume(s) and plenum spring(s).
- The initial fuel rod pressure and gas composition.
- The S-RELAP5 axial nodalizations and geometry indices.
- The time dependent power, coolant pressure, and coolant inlet temperature histories.

For each burnup of interest, an electronic transfer of RODEX3A data to S-RELAP5 is made. This transfer includes information needed to describe the exposed state of the fuel and accelerates the convergence of the S-RELAP5 steady state solution. It also ensures that the RODEX3A and S-RELAP5 fuel geometries are identical. The RODEX3A data describe the fuel state at the reference fuel temperature (usually 70 F) and zero power. A steady state S-RELAP5 calculation is required to initialize the S-RELAP5 calculation at the power of interest. The data transferred from RODEX3A to S-RELAP5 include:

- The date and time when the RODEX3A calculation was performed to provide traceability.
- The gas constant, the moles of gas in the fuel rod, the initial internal fuel rod pressure, and the gas coefficients (which are dependent upon the gas composition) which are used to calculate the rod internal pressure and the gap thermal conductivity and viscosity.
- The S-RELAP5 geometry index, the RODEX3A pellet, and cladding node radii. The S-RELAP5 and RODEX3A radial nodalizations must to be identical.
- The fuel rod plenum lengths and initial temperature(s), and the plenum spring constant(s) which are used to compute the fuel rod plenum gas temperature(s) and the internal fuel rod pressure.
- The fluence, and the cladding flexibility and yield stress coefficients which are used to compute pellet-cladding contact pressures and changes in the gap width resulting from the "trapped stack" effect.
- The cladding axial/radial elastic deflection coefficients which are used to compute the elastic deformations in the cladding.

- The axial strain distribution resulting from irradiation induced cladding creep and growth which are used to compute the fuel plenum volume and rod internal pressure.
- The pellet composition, the pellet dish volumes, the axial/radial burnup distribution, the axial/radial porosity distribution, and oxygen to fuel ratios. The porosity distribution depends upon the initial pellet density and the amount of pellet densification and swelling with exposure. These data are used to compute pellet thermal properties and the internal rod pressure.
- The exposure dependent radial displacements due to fuel migration, pellet creep, pellet densification, pellet swelling and clad creep which are used to compute the gap dimension, gap thermal properties, gap volume, and rod internal pressure.
- The axial/radial distribution of power (i.e., the flux depression profile) which are used to compute the power distribution in the fuel rod and hence the temperature distribution.
- The initial clad oxide layer thickness which are used to compute cladding temperatures and the amount of energy deposited in the cladding due to the reaction of zirconium with steam (i.e., oxygen).
- The axial/radial temperature distribution, the fuel/cladding slip ratio, and the axial force distribution which are used to help speed the convergence of the S-RELAP5 steady state calculation. These values change with time.

RODEX3 (Reference 6) has been approved for use in providing input to the RLBLOCA analysis under certain conditions. These conditions have been addressed in the methodology and are discussed in Section 4.3. Following the approval of RODEX3, the code was modified to provide the required input to the S-RELAP5 code. At that time the code was renamed to RODEX3A (References 7 and 8). The RODEX3A code provides equivalent results on all benchmarks used for the approved RODEX3 code.

3.4.2 S-RELAP5

S-RELAP5 is an FRA-ANP-modified version of RELAP5/MOD2 (Reference 18) which incorporates the computer portability aspects of RELAP5/MOD3 (Reference 19) and modifications to the constitutive package to provide congruency with literature correlations and to improve the simulation of key large break LOCA experiments. The field equations are basically in the same form as RELAP5/MOD2 with the addition of full two-dimensional momentum equations. This two-dimensional capability is only applied to the downcomer, core and upper plenum regions in the RLBLOCA methodology, but can be applied anywhere in the reactor system through input. The S-RELAP5 code structure was modified to be essentially the same as RELAP5/MOD3. The coding for reactor kinetics, control systems, and trip systems was also replaced by that from RELAP5/MOD3.

The following list summarizes the major modifications and improvements incorporated into S-RELAP5 relative to RELAP5/MOD2:

- **Multi-dimensional Capability.** Full two-dimensional treatment was added to the hydrodynamic field equations.
- **Energy Equations.** The energy equations were modified to better conserve energies transported into and out of a control volume.
- **Numerical Solution of Hydrodynamic Field Equations.** The reduction of the hydrodynamic finite-difference equations to a pressure equation is obtained analytically in S-RELAP5.
- **State of Steam-Noncondensable Mixture.** The state relations were modified to correctly simulate the accumulator depressurization and to prevent code failures during the period of accumulator ECC water injection.
- **Hydrodynamic Constitutive Models.** Significant modifications and enhancements were made to the interphase friction and interphase mass transfer models.
- **Choked Flow.** The computation of the equation of state at the choked plane was modified.
- **Counter-Current Flow Limiting.** A Bankoff form correlation was implemented, which can be reduced to either a Wallis type or Kutateladze type CCFL correlation.
- **Component Models.** A revised two-phase pump degradation model based on EPRI data was implemented.
- **Fuel Model.** Initial fuel conditions are supplied by the realistic fuel performance code, RODEX3A. To be consistent, the fuel deformation and conductivity models from RODEX3A were included in S-RELAP5.
- **Containment Back Pressure.** Capability to interface with a concurrent calculation of containment back pressure using the ICECON code was added.

FRA-ANP performed sensitivity calculations to evaluate the effects of containment back pressure. The results showed that the RLBLOCA model significantly reduces the sensitivity of calculated PCT to containment back pressure, relative to the current Appendix K based ECCS evaluation models, but does not eliminate these effects. A conservatively low (atmospheric) containment back pressure yields an increased PCT. However, varying time dependent containment pressures within a band of a few psi gave little difference in calculated PCTs. Thus, based on these results, FRA-ANP concluded that a containment back pressure calculation which provides a reasonable approximation for the time dependent back pressure is desirable for a RLBLOCA evaluation model.

The conversion from RELAP5/MOD2 includes the capability to interface external calculations with S-RELAP5. With this interface, a containment pressure calculation using a different code can be run concurrently with S-RELAP5. Break flows and enthalpies are transferred to the

containment code, which continuously feeds back calculated pressure and temperature through S-RELAP5 time dependent volumes. The choice for the containment code to use with the RLBLOCA evaluation model is ICECON (References 14 and 15), which is based on CONTEMPT LT-022 (Reference 20). ICECON was originally approved for calculating a conservative containment back pressure under Appendix K rules, but it can be used with realistic input and, with only minor modifications, to give an approximate realistic back pressure calculation. [

]

3.4.3 New Product Support

While it is understood that model enhancements and code improvements are specifically forbidden after a code has been declared frozen, updates supporting the treatment of uncertainty are allowed under the CSAU framework. Circumstances that could lead to code changes include:

- Minor plant design changes (which could introduce other uncertainty parameters)
- New fuel rod or assembly design (such as a new cladding alloy)
- Expanded thermal-hydraulic database
- Uncertainty analysis refinement (e.g., alternative probability distribution function) or error correction

Because of these possibilities, FRA-ANP distinguishes "Code Development" and "Code Maintenance" as distinct activities. Code development encompasses all the activities required to define a "frozen code" version prescribed by the CSAU methodology. This process includes model development, code implementation, developmental assessment, documentation, etc. Code maintenance includes incremental code updates or "point releases" where it is demonstrated that the change has not invalidated the fully qualified software baseline. The qualification of production use codes requires extensive validation through a suite of test cases. Simply stated, any code update that prevents the reproduction of test suite results supporting the baseline or "frozen" code version requires that a full code qualification be performed.

As a nuclear fuel vendor, FRA-ANP continually develops new fuel rod and fuel assembly designs. To support these new designs, upgrades to LOCA methodologies need to be made. Currently, FRA-ANP uses the approved fuel performance code RODEX3A, which supports fuel currently being supplied to customers who own Westinghouse and Combustion Engineering PWRs. As new designs are developed, new models and often new computer codes are developed to model the fuel performance. Even though new or modified fuel performance codes are developed and approved^{*}, the fuel performance code changes will not invalidate the qualification of a "frozen" code. These changes will expand the application of the methodology.

Expansion of the FRA-ANP methodology, which require code updates that do not require requalification of the methodology, will be reported through supplemental documentation or document revision. This documentation will include a statement of application, models and correlations, developmental assessment, a programmer's guide supplement, and user's manual and guidelines.

3.5 **Code Documentation (CSAU Step 5)**

The documentation for the codes used in the development of this methodology is provided in References 6, 7 and 8 for the RODEX3A code, in References 5, 9, 10, and 11 for the S-RELAP5 code, and References 14 and 15 for the ICECON code. This documentation describes the models and correlations used in the codes, defines the code inputs, and provides a description of the code structure. These documents have been verified against the actual coding to ensure that the documentation and coding are consistent (Reference 5).

The code validation is provided in Reference 5, which compares the code predictions to measured data in a number of SET facilities and IET facilities. In addition, the guidelines that will govern the application of the realistic LBLOCA is provided in References 12 and 13. Reference 12 describes how to develop the S-RELAP5 input for the NPP model and Reference 13 describes how to perform the actual analysis.

* For LOCA analyses, this fuel performance information, including fuel and clad material properties, fuel deformation related to burnup, and gap thermal properties, are used as parameters in estimating initial stored energy.

3.6 ***Determination of Code Applicability (CSAU Step 6)***

The objective of the determination and code applicability element of CSAU is to demonstrate that the selected codes are capable of modeling the chosen event for all NPP types. This is accomplished by comparing the event and important phenomena identified in the PIRT with the models and correlations documents for the selected codes. Four attributes are needed to make this comparison:

- Field equations that address global processes.
- Closure (constitutive) equations which support the conservation equations by modeling specific phenomena or processes.
- Code numerics that demonstrate that the code can efficiently and reliably perform the required calculations.
- Structure and nodalization, which address the ability of the code to model the NPP geometry and components and to provide an accurate prediction of the NPP response.

These four attributes are discussed in the following sections.

3.6.1 Field Equations

The field equations (conservation of mass, momentum, and energy) must possess the capability of simulating each of the distinct phases (blowdown, refill, and reflood) of a LBLOCA. During the refill and reflood phases, counter-current flow occurs at various locations in the RCS, and subcooled liquid coexists with superheated steam in parts of the reactor core. Therefore, for realistic analyses the field equations should be non-homogeneous (unequal velocity for each phase) and non-equilibrium (unequal temperature for each phase). The presence of nitrogen in the accumulator requires an additional field equation to model and track the movement of a noncondensable gas.

The S-RELAP5 field equations evaluation against their ability to model all important PIRT phenomena (Table 3.4). The results of this evaluation are summarized in Table 3.6. Additional requirements shown in the table are multi-dimensionality, separation due to gravity, and interphase exchange terms. As indicated in Table 3.6, the S-RELAP5 code has the required field equations to address the important LBLOCA phenomena.

3.6.2 Closure Equations

Closure equations (constitutive models and correlations) are required to support the basic field equations. These closure equations are essential for modeling the processes and phenomena given in the PIRT (Table 3.4). The S-RELAP5 constitutive models and correlations are presented in Reference 9. The verification and validation of the code models and correlations are given in Reference 5. The two documents together demonstrate that the S-RELAP5 code adequately simulates LBLOCA events with a high level of confidence.

The capability of the S-RELAP5 code closure equations to meet the requirements of the PIRT (Table 3.4) is summarized in Table 3.7. The closure equations address wall friction, interphase friction, mass transfer (interphase heat transfer), wall-to-fluid heat transfer, form-losses, and similar functions. The various models require flow regime maps, boiling curves, state relationships, and fluid and material properties for completeness. As indicated in Table 3.7, the S-RELAP5 code has the required closure equations to address the important LBLOCA phenomena.

3.6.3 Code Numerics

The numerical solutions contained in S-RELAP5 has been extensively demonstrated in numerous assessments reported in the literature. These numerics have been improved in S-RELAP5 as described in Section 3.4.2 and in Reference 9. The adequacy of the S-RELAP5 specific numerics has been demonstrated in the performance of the assessments reported in Reference 5 and summarized in Section 4.3. In addition, the adequacy of the numerics has also been demonstrated in the performance of the many sensitivity analyses reported in Section 4.1 and by the time step sensitivity analysis reported in Appendix C.

3.6.4 Structure and Nodalization

To properly model a NPP, a code must be able to adequately model the important components and control systems of the NPP with respect to the chosen accident scenario. The S-RELAP5 code has the ability, as indicated in Table 3.8, to model all the major components and associated control systems of the plant. The modeling of each of the NPP components is discussed in detail in Reference 12 and summarized in Section 4.2. Section 4.2 also describes the studies that were performed to determine the final plant nodalization.

**Table 3.1 Approximate Values of Key Large Break LOCA Plant
Analysis Parameters**

Plant Parameter	<u>W</u> 3-loop	<u>W</u> 4-loop	CE 2x4
Power, MWt	2700	3400	2700
RCS Flow Rate, gpm	275,000	290,000	350,000
Reactor Vessel Volume, ft ³	3600	4950	4500
Primary Coolant Volume, ft ³	9400	12,000	11,000
Core Inlet Temperature, F	545	545	550
Pressurizer Pressure, psia	2250	2250	2250
Pressurizer Liquid Volume, ft ³	750	1100	800
Accumulators/ SIT Water Volume, ft ³	1000	1000	1150
Accumulators/ SIT Water Temperature, F	120	120	120
Accumulators/ SIT Pressure, psia	640	630	230
Containment Volume, ft ³	2,300,000	2,600,000	2,500,000

**Table 3.2 Appendix K Large Break LOCA Approximate Sequence of
Events Timing**

Event	<u>W</u> 3-loop, sec	<u>W</u> 4-loop, sec	CE 2x4, sec
Analysis Initiated	0.00	0.00	0.00
Break Opened	0.05	0.05	0.05
Safety Injection Signal	0.7 to 1.4	0.6 to 1.0	0.7 to 1.0
Broken Loop Accumulator/ SIT Flow Initiated	1 to 3	2 to 7	9 to 10
Intact Loop Accumulator/ SIT Flow Initiated	10 to 15	15 to 18	14 to 16
End of Bypass/Beginning of Refill	15 to 25	20 to 25	15 to 20
Broken Loop Accumulator/ SIT Empties	25 to 35	40 to 50	50 to 60
Beginning of Reflood	25 to 45	30 to 45	30 to 35
Fuel Cladding Rupture	35 to 50	55 to 70	40 to 50
Intact Accumulator/ SIT Empties	32 to 46	45 to 55	50 to 65
PCT Occurred	80 to 135	70 to 235	135 to 155

**Table 3.3 Preliminary Process Identification and Ranking Table
(PIRT) for PWR Large Break Loss-of-Coolant Accident**

Component	Phenomenon	Avg. Ranking		
		BD	RFL	RFD
Fuel Rod	Stored energy	9	2	2
	Oxidation	-	1	8
	Decay heat	2	1	8
	Gap conductance	3	1	7
Core	DNB	6	2	2
	Post CHF	6	8	4
	Rewet	8	7	1
	Reflow HT plus quench	-	-	9
	Nucleate Boiling	4	2	2
	One-phase vapor natural convection	-	6	4
	3-D flow	1	3	8
	Void distribution, generation	4	6	8
	Entrainment/de-entrainment	2	3	6
	Flow reversal, stagnation	3	1	1
Upper Plenum	Entrainment/de-entrainment	1	1	9
	Phase separation	2	1	2
	Countercurrent flow (drain/fallback)	1	2	6
	Two-phase convection	2	1	5
Hot Leg	Entrainment/de-entrainment	1	1	9
	Flow reversal, stagnation	2	1	-
	Void distribution, generation	1	1	4
	Two-phase convection	2	2	3
Pressurizer	Early quench	7	-	-
	Critical flow in surge line	7	-	-
	Flashing, steam expansion	7	2	2
Steam Generator	Steam binding	-	2	9
	Delta-p, form losses	2	2	2

**Table 3.3 Preliminary Process Identification and Ranking Table (PIRT) for PWR
Large Break Loss-of-Coolant Accident (Continued)**

Component	Phenomenon	Avg. Ranking		
		BD	RFL	RFD
Pump	Two-phase	9	5	-
	Differential pressure form loss	3	3	8
Cold Leg, Accumulator	Condensation, oscillations	2	9	5
	Noncondensable gas	-	1	9
	HPI mixing	-	3	2
Downcomer	Entrainment/de-entrainment	2	8	2
	Condensation	-	9	2
	Hot wall	-	5	5
	3-D	2	8	2
	Countercurrent, slug, non-equilibrium flow	1	8	2
	Flashing	1	-	-
	Liquid level oscillations	-	3	7
	Two-phase convection	2	3	2
	Saturated nucleate boiling	1	2	2
Lower Plenum	Sweep-out	2	7	5
	Hot wall	1	7	6
	Multi-dimensional effects	1	2	7
Break	Critical flow	9	7	1
	Flashing	3	2	1
	Containment pressure	2	4	2
Loop	Two-phase differential pressure	7	7	6
	Oscillations	-	7	9
	Flow split	7	7	2

Notes

1. BD is blowdown; RFL is refill; RFD is reflood
2. A ranking of 9 is most important; a ranking of 1 is least important
3. A ranking of "-" means that the phenomenon does not occur in the indicated phase of the transient

**Table 3.4 Final Process Identification and Ranking Table (PIRT)
for PWR Large Break Loss-of-Coolant Accident**



**Table 3.4 Final Process Identification and Ranking Table (PIRT)
for PWR Large Break Loss-of-Coolant Accident (*Continued*)**

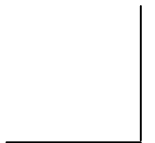


**Table 3.5 Frozen Code Versions Used in the Methodology
Development**

Code	Version	Function
S-RELAP5	UJUL00	Predict fuel, core, and system performance during transient event including containment response
	UMAR01	
RODEX3A	UJUN00	Predict fuel performance during steady state and transient operation

Table 3.6 Field Equations/Models in S-RELAP5

Scenario and PIRT Requirements	S-RELAP5 Model Existence	Field Equations/Model
Non-equilibrium two-phase flow	Yes	Six equation unequal velocity, unequal temperature
Non-condensable gas flow	Yes	Gas mass balance in vapor flow field
Solute tracking for boron	Yes	Solute mass balance liquid flow field
Multidimensional flow capability	Yes	2-D components available as required
Separation due to gravity	Yes	Gravity pressure differential in flow field equations
Interphase exchange terms	Yes	Mass and energy transfer between phases, vaporization and condensation

Table 3.7 Phenomena/Processes in S-RELAP5

Table 3.7 Phenomena/Processes in S-RELAP5 (*Continued*)

Table 3.7 Phenomena/Processes in S-RELAP5 (*Continued*)

Table 3.8 Component Modeling Requirements for PWR

Required Component	Component Model Existence	Code Component
Pressure Vessel	Yes	1-D and 2-D components: model upper head, upper plenum, core, lower plenum, downcomer, structure, flow paths, elevations, resistances, volumes Heat structures: model vessel walls, internal structures, fuel rods
Hot Leg	Yes	Pipes, volumes, and junctions: model flow areas, lengths, volumes, resistances, elevations Heat structures: model pipe walls
Steam Generator	Yes	Separators, pipes, volumes and junctions: model flow areas, volumes, lengths, resistances, elevations, flow paths, phase separation, recirculation, feedwater, steam flow Heat structures: model generator walls, heat exchange between the primary and secondary system.
Pumps	Yes	Pump: models homologous curves, degradation, flow areas, volumes, losses, suction and discharge flow
Cold Leg	Yes	Pipes, volumes, and junctions: model flow areas, volumes, lengths, resistances, elevations, branches Heat structures: model pipe walls
Pressurizer	Yes	Pipe: models volumes, flow areas, phase separation, lengths, resistances, elevations Heat structures: model vessel walls and heater
Surge Line	Yes	Pipe and junctions: models volumes, flow areas, lengths, resistances, elevations, choked flow Heat structures: model pipe walls

Table 3.8 Component Modeling Requirements for PWR (Continued)

Required Component	Component Model Existence	Code Component
Accumulators	Yes	Pipes and junctions: model volumes, flow areas, lengths, elevations, nitrogen, discharge of ECC water and noncondensable gas Heat structures: model accumulator walls
ECC Systems	Yes	Pipes, volumes, and junctions: model flow rates, pressure dependence, volumes, flow areas, lengths, resistances, elevations Heat structures: model pipe walls
Valves	Yes	Valve: models areas, control
Pressure Boundary	Yes	ICECON and junctions: model pressure boundary, break flow, containment volume

4.0 **Assessment and Ranging of Parameters**

The assessment and ranging of parameters element establishes the assessment matrix to be used in defining the NPP nodalization, quantifying the code accuracy, and demonstrating any code or model scaling effects.

4.1 ***Establishment of Assessment Matrix (CSAU Step 7)***

The following four considerations must be taken into account in establishing the assessment matrix. The first consideration is the important phenomena identified in the PIRT process described in Section 3.3 (CSAU step 3) and presented in Table 3.4. The assessment matrix must include experiments that address the important phenomena, defined as those phenomena ranked 5 or higher in Table 3.4. The selected experiments must have taken sufficient data to determine the code accuracy, including bias and uncertainty, for the important phenomena.

The second consideration is that of NPP nodalization. Here experiments must be selected that are representative of the types of NPPs being addressed and cover the identified phases of the selected scenario. Thus, for this application, experiments must be selected that are representative of W 3 and 4-loop plants and CE 2x4 plants. The experiments also should cover one or all of the LBLOCA phases identified in Section 3.1 (CSAU step 1); blowdown, refill, and reflood.

The third consideration is to demonstrate that the code and NPP nodalization have the ability to scale from experiments of different sizes to the full size NPP for which analyses will be performed. Generally this is done by selecting a number of assessments in facilities of different scale and demonstrating that the code and NPP nodalization is capable of consistently predicting the experimental data from all the experiments.

The final consideration is with respect to compensating errors in the code. Because it is extremely difficult, if not impossible, to demonstrate that a code does not contain compensating errors, it should be demonstrated that the compensating errors will not produce erroneous results for the selected scenario and NPP being analyzed. Thus, an attempt must be made to select experiments that cover the range of each important phenomenon observed in the NPP analyses. Analysis of these experiments will demonstrate that, even if the code contains compensating errors, the code as currently configured still is capable of reliably predicting the selected scenario in the selected NPP.

4.1.1 PIRT Considerations

The PIRT presented in Table 3.4 provides a qualitative expression of what is perceived to be the degree of importance of key phenomena present in a LBLOCA. Given the limitations of resources (time, human, and computational) and the incompleteness of the LBLOCA database, not all of the moderately to highly ranked phenomena can be treated as uncertainty parameters. Nonetheless, all these phenomena must be accounted for either statistically or in a bounding application. A bounding application has a major drawback in that the methodology is penalized for not applying a rigorous model. Minimizing this penalty clearly is valuable in making the methodology viable for broad application. Conversely, to treat a parameter statistically, test data must be available so the statistics can be quantified. Clearly, such tests must be included in the assessment matrix.

To optimize the choice of which parameters to treat statistically and which parameters to bound, a large set of PIRT and plant sensitivities studies (~72 calculations/set) was performed to quantify the importance of each moderately to highly ranked phenomenon along with key plant operational parameters. The first column of Table 4.1 lists the moderate and high ranked PIRT phenomena cross referenced to a description of one or more calculations performed in the sensitivity studies. These studies were performed with the 3- and 4-loop sample problems. (Note: Appendix A contains an overview of all documented plant sensitivity studies performed during the development of this methodology.)

While the chronology of the 3- and 4-loop base cases is well described in Table 3.2, some aspects of the LBLOCA model were modified to improve the usefulness of the results (additional discussion on base cases is given in Appendix A, Section A.2). The primary changes in the baseline 3- and 4-loop LBLOCA analyses used in the PIRT sensitivity studies were designed to accentuate PCT sensitivity. This was done by skewing the power profile towards the top of the core and raising core and decay power in such a manner that predicted PCTs approached regulatory limits (2000 F – 2200 F). These modifications enhance the late reflood PCT in such a way that both the 3- and 4-loop models show both an early and late reflood peak. Preceding these sensitivities, a break spectrum was performed to identify the worst break size. This was also used to bias the sensitivity studies. Fuel metal-water reaction and nitrogen transport from the accumulators were removed from the model. These two phenomena have been shown to contribute nonlinear PCT sensitivities that might disguise the sensitivity of the studied

parameters. Figure 4.1 shows the PCT signatures from the 3- and 4-loop sample problems. The integrity of the baseline calculations is built on the rigorous approach to nodalization, which emphasized demonstration of the moderately and highly rank PIRT phenomena as presented in Section 3.3.

In addition to the two baseline studies, two more sets of sensitivities were performed for the 3-loop sample problem at nominal power conditions. The difference between these two sets was whether accumulator nitrogen was allowed into the RCS or valved out. These studies were done to ensure that dominant phenomena, whose influence may diminish at higher temperatures, were considered in this methodology.

For the parameters used in performing the PIRT sensitivities (column 2, Table 4.1), best estimate or conservative parameter range limits were identified. These range limits were derived from expert experience, literature review, or physical bounds. Each sensitivity calculation perturbed the baseline model by modifying the key parameters that drove a particular phenomenon to a range limit. The changes in PCT (Δ PCT) during blowdown, early reflood, and late reflood from the baseline calculation were recorded for each study.

Interpretation of the results of over 250 calculations involved the tabulation and ranking by the magnitude of the Δ PCTs. The degree of sensitivity on PCT for a particular study was classified as either low, medium, or high. The high classification is based on the regulatory definition of "significant change" (i.e., > 50 F). [

] (Appendix C presents a confirmation study examining code variability from a set of 14 time-step sensitivities.)

The bulk of the sensitivity studies confirmed the important PIRT phenomena; however, a few parameters did show only weak sensitivity. Column 3 of Table 4.1 presents the conclusions from these results. For most of the PIRT phenomena, assessment against test program results is indicated. In some cases published uncertainty is available. Phenomena not demonstrating significant LBLOCA PCT sensitivity also are identified in column 3 of Table 4.1. For those PIRT phenomena demonstrating significant LBLOCA PCT, a database is identified, based on test

facility and or plant data, for validating a specific model or quantifying the phenomenon uncertainty.

4.1.2 Nodalization Considerations

Given the extensive experimental facility database developed from the PIRT considerations, only one additional test facility was identified strictly to address nodalization effects. That test facility was the Slab Core Test Facility (SCTF), where specific assessments were performed to address radial nodalization with variations in radial power distributions. However, in the selection of the specific tests to be analyzed in each facility, nodalization was a consideration.

4.1.3 Scaling Considerations

Within the test facility database developed to support the PIRT considerations are facilities that span a scaling range of 1:1500 to 1:1. In addition, some specific tests were performed as a counterpart to tests performed in other facilities. Where data were available, these tests have been added to the assessment matrix.

4.1.4 Compensating Errors

The issue of compensating errors arises primarily from the use of correlations and closure relations in the code. The interaction of the various correlations and closure relations can be such that an error in one of these models is compensated for by an error in another model. These compensating errors can result in the code being able to predict specific tests but incapable of predicting other tests. For the LBLOCA, only those compensating errors which could function in one manner in the assessments and in an entirely different manner in the LBLOCA are a concern. Thus, the assessment matrix must include tests that can be scaled up and that cover the range of the LBLOCA PIRT phenomena. The compensating error issue is addressed in the test matrix through the FLECHT, FLECHT-SEASET, SCTF, CCTF, and THTF for the core phenomena and UPTF for most of the other major reactor coolant system components.

4.1.5 Summary

Given these four considerations, the assessment matrix described in Table 4.2 and Table 4.3 was developed. Table 4.2 lists the test facilities and makes the association between the

selected facilities and the identified parameter groups. The actual tests analyzed from each test facility are provided in Table 4.3, along with the associated phenomena being examined.

4.2 ***Nuclear Power Plant Nodalization Definition (CSAU Step 8)***

Reference 4 ("Quantifying Reactor Safety Margins") makes the following statements regarding nodalization:

"The plant model must be nodalized finely enough to represent both the important phenomena and design characteristics of the NPP but coarsely enough to remain economical."

"Thus, the preferred path is to establish a standard NPP nodalization for the subsequent analysis. This minimizes or removes nodalization, and the freedom to manipulate noding, as a contributor to uncertainty."

"Therefore, a nodalization selection procedure defines the minimum noding needed to capture the important phenomena. This procedure starts with analyst experience in previous code assessment and application studies and any documented nodalization studies. Next, nodalization studies are performed during the simulation of separate- and integral-effects code data comparisons. Finally, an iterative process using the NPP model is employed to determine sufficiency of the NPP model nodalization."

Given these general recommendations, the goal of a nodalization methodology is to optimize somewhat independent priorities. These include preserving dominant phenomena, minimizing code uncertainty, conforming to design characteristics, and minimizing computational expense. The guidelines developed for the FRA-ANP RLBLOCA methodology (Reference 12, EMF-2054) are quantitatively explicit wherever possible to remove nodalization as a contributor to uncertainty. Because not all plants of the same type are identical, the guidelines provide rules for deriving the appropriate nodalization. This strategy serves both to remove nodalization as a contributor to uncertainty and to define a method for automating the generation of input for a RLBLOCA analysis.

As described by Step 8 of the CSAU process, "NPP Nodalization Definition," this task is iterative. To minimize the degree of iteration, the baseline nodalization definition originated from user experience with earlier manifestations of S-RELAP5 (i.e., for SBLOCA Reference 21), and RELAP5 (References 22 and 23). The current nodalization has been refined using results from sensitivity studies performed with the current frozen S-RELAP5 code version and its predecessors. Because the nodalization requirements are strictly applied, uncertainty associated with nodalization becomes part of the studies to determine the statistics of key uncertainty parameters. If the results of one or more assessments brought into question the

validity of a particular nodalization, additional studies were performed. For RLBLOCA applications, these guidelines have been developed and refined by sensitivity studies (Appendix A) and/or assessments or they have been constrained to a best fit for a complex structural configuration. Table 4.4 summarizes the guidelines for hydraulic nodalization based on this approach.

The derived input prescription defines the standardized nodalization scheme, specifies a logical numbering system, and recommends key parameter inputs for the S-RELAP5 input model. Details of noding have been determined from experience with simulation of integral- and separate-effects tests (Reference 5) that result in a technically and economically sound nodalization scheme for simulating LBLOCA in a PWR. Assessment calculations of the FLECHT/SEASET reflood experiments provided data for the axial nodalization of the core region. Studies of the Cylindrical Core Test Facility (CCTF) and SCTF were used to identify two-dimensional modeling techniques for the downcomer and core. Analyses of the LOFT and Semiscale experiments gave information on describing the primary coolant loops, reactor coolant pumps, reactor vessel, and steam generators with S-RELAP5. Assessments of Upper Plenum Test Facility (UPTF) tests also were used to identify two-dimensional modeling techniques and provide useful plant information, including experimental data on full-scale downcomer fluid behavior during the blowdown, refill, and reflood phases of a LBLOCA.

Column 1 of Table 4.4 defines a particular NPP component or coolant system region and the S-RELAP5 components generally used for its simulation. Column 2 lists the important phenomena associated with the component as evaluated through the PIRT process (Section 3.3). Column 3 defines the number of cells required, based on user experience and assessment calculations, to provide adequate detail. The source or bases for the selections are given in Column 4.

4.2.1 Nodalization Methodology

The necessary conditions for a satisfactory nodalization methodology are to discriminate key structural characteristics, to obtain reasonable steady-state agreement with plant data, to preserve first order accuracy of dominant phenomena, and to minimize PCT sensitivity to nodalization. The ability of the code and associated nodalization to describe key structural components is addressed in Section 3.6.4, where it is demonstrated that the code is capable of modeling the key components. Obtaining reasonable steady-state results is implicitly aided by

adhering to strict conformance to structural design characteristics (e.g., elevations and volumes). Obtaining reasonable results also is aided by the use of system-initialization control systems.

The most challenging of the necessary conditions is the task to preserve dominant phenomena. A computer code's ability to capture LBLOCA phenomena cannot separate the contributions of the applicable phenomenological models and nodalization. While it was stated that strict adherence to nodalization transfers the burden of code uncertainty to the uncertainty analysis of key LBLOCA parameters, every effort was made to provide a nodalization scheme that minimizes this nodalization uncertainty.

Experience indicates that S-RELAP5 plant models of W 3- and 4-loop PWRs and CE 2x4 loop PWRs will require between 200 and 500 volume component nodes, junction flow paths, and heat structures. The following figures show the modeling techniques.

Figure 4.3, Loop Nodalization

Figure 4.4, Reactor Vessel Nodalization

Figure 4.5, CE 2x4 and Westinghouse 3- and 4-Loop Plant Vessel Downcomer Configuration

Figure 4.6, Core Nodalization - Axial Plane

Figure 4.7, Core Nodalization - Cross-Sectional Plane

Figure 4.8, Upper Plenum Nodalization - Axial Plane

Figure 4.9, Upper Plenum Nodalization - Cross-Sectional Plane

Figure 4.10, Emergency Core Cooling System Nodalization

Figure 4.11, Double-Ended Guillotine Break Nodalization

Figure 4.12, Double-Ended Split Break Nodalization

The following sections discuss the nodalization of each major plant component in the context of the PIRT (as presented in Section 3.3) and describes the evolution of the nodalization schemes.

The nodalization methodology has been derived for LBLOCA. The application of the developed guidelines may not capture expected phenomena or may exhibit unacceptable variability for calculations other than LBLOCA.

4.2.2 Numerical Considerations

The nodalization of a particular model translates into a computational array used to solve the mass, momentum, and energy equations; thus, numerical constraints also must be considered in the sizing and configuration of component volumes. In general, competing criteria exist for defining nodalization. The primary numerical issues of concern are accuracy, numerical stability, and code variability. While optimizing all three is necessary to have useable results, some code variability can be tolerated as long as it is reasonably defined (Appendix C). However, numerical stability must be assured before performing any production calculations to assess accuracy through code/data comparisons.

In general, the RELAP5 series of codes has inherited a solid foundation with regard to numerical stability, as discussed in Reference 9. However, nodalization and time step decisions both can influence numerical stability. It is generally understood that numerical solutions are well behaved if the number of mesh points is sufficiently small. Such small nodes will require equally small time steps to satisfy the Courant stability requirement, leading to long uneconomical code execution times. Conversely, it has been shown that modeling interfacial drag contributes to the stability of coarser mesh models for two-phase flow codes, such as RELAP5 (Reference 24). While this stabilizing condition created by modeling interfacial drag actually works to destabilize the solution for very small mesh sizes, it also supports the coarser mesh models required for economical code execution times. As a result, considering strictly hydraulic phenomena, spatial mesh configuration is not a high concern for numerical stability.

For code accuracy, mesh sizing does become more important for heated surfaces. Steep temperature gradients will influence the adjacent fluid conditions. For this reason, smaller mesh sizes are used on heated surfaces to capture expected phenomena.

The final figure-of-merit for quantifying code variability can come from calculations of hot rod PCT. For a set of equivalent input models, differing only in time step (constrained to be less than the Courant limit), comparisons of PCT traces can be used to evaluate expected code variability. By using this approach, nodalization decisions can be made in an effort to minimize the impact of code variability.

In summary, the iteration process for defining a nodalization methodology included decisions to change a component nodalization based on the analysis of either assessments (integral- and

separate-effects) or plant sensitivity studies. These calculational results were generally used to confirm the adequacy of a chosen nodalization scheme; however, sensitivity studies also were performed to quantify the impact on peak clad temperature. In some instances, the effect of a trial nodalization scheme produced unacceptable variability in PCT results.

4.2.3 Loop Model

The loop includes those components outside the reactor vessel, including the pressurizer and ECCS. For W and CE PWRs supported by this methodology, all loops are modeled individually (i.e., the unbroken loops are not lumped into a single combined loop). Each loop models the hot-leg piping, steam generator primary and secondary fluid volume and heat transfer, pump suction piping, and pump discharge cold-leg piping. Each loop also contains modeling of the accumulator and high- and low-pressure injection ECCSs. The nodalization scheme is presented in Figure 4.3 for a sample loop with the pressurizer.

The following are key features and assumptions for the reactor coolant loops.

- []
- []
- The nodalization detail for the coolant loops, pressurizer, and primary and secondary sides of the steam generators was selected to give consistent results without increasing running time because of excessive nodalization
- []

Assessment of loop nodalization comes from various facility test programs, including SCTF, CCTF, LOFT, Semiscale, and, to a lesser extent, UPTF. In addition, the W/EPRI 1/3 Scale Steam/Water tests, a separate-effects test examining ECC mixing in the cold leg, also is a useful assessment. Acceptance of nodalization schemes was based on the general agreement in code/data comparisons for pressures, differential pressures, mass flow rates, and heat structure temperatures.

4.2.3.1 Hot Leg

The hot leg connects the reactor vessel to the steam generator inlet plenum. []

]

[

] The entrainment of droplets from the reactor vessel will enhance the effect of steam binding, which will inhibit reflood. Code-to-data comparisons of tests performed on the CCTF show that S-RELAP5 overpredicts the entrainment phenomenon from the upper plenum to the hot legs. This is considered acceptable given that over-entrainment will have a conservative influence on PCT and that the relative importance of entrainment in the hot legs is moderate.

4.2.3.2 Steam Generator

The steam generator nodalization scheme is essentially identical to the traditional approach used by other large thermal-hydraulic codes such as TRAC and RELAP5 (References 4 and 23). [

]

The dominant phenomena of importance are the steady-state heat balance and steam binding during reflood. Heat balance is ensured by the use of control systems controlling feed and steam flow depending on liquid level and recirculation ratio. Plant sensitivity studies examining steam generator performance during a LBLOCA have shown that all the liquid that gets carried into the steam generator vaporizes. This is the expected result; hence, this nodalization scheme is considered acceptable.

4.2.3.3 Pump Suction

[

]

4.2.3.4 Reactor Coolant Pump

The pump is a component model, meaning that the pump physics is independent of nodalization; hence, the primary objective of the nodalization scheme is to ensure consistency with the structural characteristics. [

]

4.2.3.5 Cold Leg and Break

The cold leg extends from the RCS pump discharge to and including the reactor vessel inlet nozzle. [

]

[

] The break model is either a double-ended guillotine or a double-ended split. The difference is break size and whether a flow path is modeled across the break. An investigation into code variability showed that the defined break configuration

reduces code variability associated with water property calculations. [

]

Condensation driven by the cold ECCS water coming in contact with steam is the primary phenomenological concern that may be influenced by nodalization. The parameter has been identified as one of the key uncertainty parameters for RLBLOCA; hence, any nodalization dependence is absorbed within the assessment that quantifies this uncertainty.

4.2.3.6 ECCS

The ECCS includes models for the accumulator and the piping connecting it to the RCS with sufficient detail to allow the code to accurately predict coolant flow splits for low-pressure injection flows. Figure 4.10 shows a typical nodalization for the ECCS of a three-loop plant. The dominant component in the ECCS is the accumulators. [

]

The dominant phenomena of importance are the accumulator discharge and the noncondensable gas transport following accumulator discharge. Activity in the accumulator lines can be characterized as a period of single-phase incompressible flow (accumulator water discharge) followed by a brief period of single-phase compressible flow (nitrogen gas) before a two-phase mixture (water-nitrogen) from the accumulator and the low pressure injection system. Accumulator discharge and LPSI flow are governed by Bernoulli physics for incompressible, single phase flows. Noncondensable gases will transport from the accumulator to the RCS by gas expansion and pressure forces. However, as the partial pressure at the ECCS-to-cold-leg junction drops with increasing noncondensable quality, flow will choke for a time and the upstream conditions will become independent of the downstream conditions. For this reason, the important phenomenon, rate of flow into the RCS, is dominated by the choked flow

phenomenon and any special treatment of the compressible flow problem will have a negligible effect on the outcome of the transient.

4.2.3.7 Pressurizer

The pressurizer vessel is modeled with [

] The dominant phenomena of interest are early quench and critical flow in the surgeline. Neither phenomenon will show much sensitivity to nodalization because the surgeline remains choked during the period in which these concerns are important (blowdown).

4.2.4 Reactor Vessel Model

The key components of the reactor vessel are the downcomer, lower head and plenum, core, and upper head and plenum. The nodalization is presented in Figure 4.4. The key features and assumptions for the reactor vessel are as follows:

- []
- []
- []
- []

4.2.4.1 Downcomer

The reactor downcomer is modeled for the RLBLOCA analysis using [

]

For asymmetric cold and hot leg connections to the reactor vessel, the only practical nodalization option is [

]

The dominant downcomer LBLOCA phenomena (condensation, hot wall effects, multi-dimensional flow, CCFL, and entrainment) affect the refill period. These phenomena primarily influence the duration of ECCS bypass. With the exception of multidimensional flow, sensitivity of these phenomena to downcomer nodalization is not expected (condensation and hot wall effects are selected uncertainty parameters). The collective sensitivity of these phenomena was evaluated by varying the azimuthal node sizes in the UPTF input model. The UPTF model for the sensitivity study was simplified by neglecting heat structures; hence, the influence of the hot wall phenomena cannot be determined from this assessment.

The UPTF Test 6 experiments investigated the countercurrent flow of steam and ECC water in the downcomer during the end-of-blowdown and the refill phases of a four-loop PWR LOCA. Test 6 consisted of five separate quasi-steady runs with essentially the same boundary conditions, but with different core steam flows ranging from 100 to 440 kg/s. Run 136 was the lowest steam flow case of the Test 6 series. The ECC water in Test 6 was injected into each of the three intact loops at the same flow rate.

[

] The conclusions from this study were that the lower plenum refill is relatively insensitive to downcomer nodalization for uniform ECC water injection into all intact loops. Both the base and sensitivity calculations showed conservative results when compared to measured data. Additionally, the base case model results with heat structures actually increased the conservative bias in the lower plenum refill.

A similar study was performed for the 3-loop plant model. The trial nodalization doubled the number of azimuthal sectors from [

] This configuration reduced the amount of ECC bypass, which resulted in a less severe transient.

In conclusion, the downcomer model described in Reference 12 was found to provide the best representation of the expected downcomer phenomena.

4.2.4.2 Lower Vessel

The lower vessel includes all volumes [

- []
 - []
 - []
-]
- []

The dominant LBLOCA phenomenon of importance that possibly is influenced by nodalization is liquid sweep-out, although this phenomenon is expected to have only a moderate influence on transient PCT. Because some multidimensional flow is to be expected, [

]

Considering that the UPTF facility is a full scale facility, the conservative bias demonstrated in the UPTF Test 6 assessment is expected to translate into a conservative bias for the sweep-out phenomenon in plant calculations.

4.2.4.3 Core, Core Bypass, and Fuel

The core region extends from the bottom of the active core to the top of the upper core support plate. [

]

The most important contributor to nodalization sensitivity is expected to be the core nodalization because it directly affects the liquid distribution in the core. The key phenomena of importance influenced by nodalization are the convective heat transfer modes, entrainment/deentrainment, multi-dimensional flow, stored energy, oxidation, core power and decay heat. Since the heat transfer modes, entrainment/de-entrainment, core power, decay heat and stored energy phenomena are treated statistically, only the multidimensional flow phenomenon is relevant for nodalization.

Axial core nodalization studies using the 3-loop plant model showed significant variability with coarse models. Given the expense of moving to a finer nodalization, the axial nodalization was defined in the range of [

] These node lengths are the smallest defined for the S-RELAP5 plant model; hence, they will define the Courant limit. [

]

Radial core nodalization studies using the SCTF assessment model has shown that the four radial ring model provides essentially the same results as on the 8 ring model. The [

]

[

]

[

] This configuration was used to give better resolution to the axial power profile. The radial widths used to describe the internals of the fuel rod are on a scale to finely resolve temperature gradients (Reference 12).

4.2.4.4 Upper Plenum/Upper Head

The upper plenum region extends from the top of the upper core support plate to the core support ledge in the vessel wall (the bottom of the upper head wall). [

]

The dominant phenomena of importance are entrainment/deentrainment, fallback (CCFL), and upper head temperature. The entrainment phenomenon is considered in the same manner as it was for the hot legs and the upper head temperature is treated statistically. Nodalization sensitivity to fallback was investigated through sensitivity studies. [

] This configuration captures the preference for fallback to colder assemblies as demonstrated in a 3-loop model test problem. The CCTF assessments were performed with

the multi-dimensional upper plenum. The results from these assessments showed general conservatism to liquid fallback.

In many plants, flow asymmetry into the upper plenum can exist. Flow can travel either directly into the upper plenum or through a support column or mixer vane and then into the middle of the upper plenum. [

] This configuration is necessary to bound the possibility of having the hot assembly under a standpipe. The standpipe will restrict liquid fallback from the upper plenum into the core relative to an open hole. [

]

4.2.5 Containment Model

Nodalization of the containment for the RLBLOCA is defined in a separate input file from the normal S-RELAP5 input. The containment model input is equivalent to the input used for the ICECON code (Reference 14), which is the FRA-ANP proprietary version of the CONTEMPT code (Reference 20). Appended to the S-RELAP5 input file is a description of the link between the S-RELAP5 input and the ICECON input. [

] S-RELAP5 drives the containment calculations with mass flow and enthalpy and the ICECON subroutines return containment pressure and temperature to update the S-RELAP5 time-dependent volumes.

The dominant phenomenon of interest related to the containment model is containment pressure. Containment pressure is treated statistically in this RLBLOCA methodology by ranging the containment volume from the best-estimate value to maximum possible free volume. Because the ICECON models provide only pressure and temperature for S-RELAP5, a simple model is adequate. This model is one volume representing the containment space surrounding the reactor vessel.

4.2.6 Plant Model Summary

The nodalization described in this section has been developed by applying the approach described in Reference 4. This nodalization development methodology was an iterative approach. The base nodalization originated through experience gained by RELAP5 users at the

Idaho National Engineering Laboratory and by ANF-RELAP and S-RELAP5 users at FRA-ANP. Nodalization has been refined from both plant and code assessment tests which, to the extent possible used the same nodalization. These studies were performed to examine the sensitivity of PCT and dominant phenomena to nodalization. Test results were used to justify any nodalization changes.

The final product of the nodalization methodology is a guideline (Reference 12) that when strictly followed defines how a CE 2x4 and W 3- or 4-loop plant should be modeled for S-RELAP5 calculations. While the uncertainty associated with nodalization is minimal, it will be included in the uncertainties determined for key LBLOCA parameters, because the NPP nodalization has been used in determining those uncertainties. Nonetheless, every attempt was made to develop a nodalization with a minimal uncertainty before any uncertainty analysis was performed.

4.3 Definition of Code and Experimental Accuracy (CSAU Step 9)

This section provides the evaluation of the code assessments reported in Reference 5 with respect to the RLBLOCA methodology. The code assessments from Reference 5 applicable to the RLBLOCA methodology are those discussed in Section 4.1 and listed in the assessment matrix Tables 4.2 and 4.3. These assessments were chosen to address the important PIRT phenomena identified in Table 3.4. The cross correlation between assessments and PIRT phenomena is provided in Table 4.3. In addition, some assessments were chosen to address issues of code scalability. These assessments and the discussion with respect to scalability are provided in Section 4.4.

One purpose of the assessments is to determine S-RELAP5's capability to predict the important phenomena in the large-scale PWR systems. Section 4.2 discusses appropriate nodalization to represent the PWR system components. For the assessment results to apply to the large-scale PWRs, nodalization used in the assessments must be consistent with the large-scale plant nodalization in the regions where the phenomena are being assessed. As far as possible, FRA-ANP used the plant nodalization described in Section 4.2 and the S-RELAP5 input guidelines (Reference 12) to derive assessment nodalizations which are consistent with the PWR application nodalization. However, unique features of the small-scale facilities sometimes require deviations from the guidelines. The detailed nodalizations for the experimental facility assessments are given for each assessment in Reference 5. For the most part, the assessment

nodalizations are consistent with the plant application, and where deviations have been made, the reasons for the deviations and the effects on results are discussed.

4.3.1 Separate Effects Tests (SET)

Separate effects tests from 15 different facilities have been used to assess the capabilities of the S-RELAP5 and RODEX3A codes to predict LOCA and transient phenomena. The detailed results comparing calculations against measured test data are given in the S-RELAP5 code verification and validation report, Reference 5. The S-RELAP5 code is used in multiple methodologies; therefore, it is appropriate that the code validation assessments are included as part of the code documentation. However, the SET assessments in Reference 5 also provide the information to assess code capability for the RLBLOCA methodology. Detailed results from Reference 5 will not be repeated in this report. Instead the appropriate information will be extracted and summarized with respect to the LBLOCA phenomena addressed. Table 4.3 shows the SET facilities, the tests that were selected, and the phenomena from the PIRT to be addressed. The following sections follow the format of Table 4.3 in providing the results of the assessments in order of the listed facilities.

4.3.1.1 THTF Heat Transfer

The Oak Ridge National Laboratory (ORNL) thermal-hydraulic test facility (THTF) was used to perform numerous heat transfer tests using full-length electrically heated fuel rod simulators. The facility, tests, and assessments are detailed in Section 3.1.2 of Reference 5. The assessment tests consisted of 22 steady-state film boiling tests, three transient boiloff tests, and two sets of reflood tests (11 tests).

The purpose of the assessments using the steady-state tests were to get optimum values of the bias for the CHF correlation and for the post-CHF heat transfer correlation. [

]

The ratio of the measured heat transfer coefficient (HTC) to the calculated HTC (from S-RELAP5) was evaluated statistically (see Figure 4.13). The frequency plot, Figure 4.14, showed the ratio to be non-normal, with a downward skew. The ratio was fit using a conservatively bounding normal distribution. This distribution is slightly conservative with respect to the distribution of measured scaling factors, as shown in Figure 4.15, and the

uncertainty in the post-dryout HTC for S-RELAP5 can be represented by []

The range of HTC bias variation was then applied to three sets of transient data: one in blowdown and two in reflood. The range of variation determined in the steady-state analysis was sufficient to allow the predictions by S-RELAP5 to bound the measured data for the blowdown cases and for nearly half the reflood cases. With one exception, for the other reflood cases, the S-RELAP5 predictions for quenching were conservatively slow. [The one case in which the prediction was not slow was the lowest reflood case.] The temperatures predicted by S-RELAP5 for all the other cases in that test series bounded the measured temperatures. The underprediction of the quench time for the one case is quite anomalous and, because of the very low flow rate, could well be an artifact of the boundary conditions.

For the second set of reflood tests, S-RELAP5 somewhat overpredicted the quench time. Overall the results of the transient test predictions by S-RELAP5 are acceptable. In the bulk of the cases, the uncertainties for the HTC bias were sufficient to make the data and the predictions agree. For those reflood cases that had data outside the predicted range, the predictions by S-RELAP5 were conservative.

The CHF bias is applied for RLBLOCA calculations, and the statistical information on heat transfer is used to derive the uncertainty multipliers on heat transfer presented in Section 4.3.3.2.

4.3.1.2 THTF Level Swell

Calculations for the three ORNL THTF Level Swell Tests, 3.09.10j, 3.09.10m, and 3.09.10dd, were carried out with S-RELAP5. Section 3.1.3 of Reference 5 presents the details of these assessments. Comparisons of calculated and measured void fractions for the three tests are shown in Figures 4.16 through 4.18, along with results using RELAP5/MOD3.2. The void fractions calculated by S-RELAP5 are slightly lower than the data in two cases and are very close to the data in the third, Test 3.09.10j. The mixture level lies between the pre-CHF and post-CHF regions. Both the data and the calculations show that the post-CHF region has a void fraction of 1 (single-phase steam) or nearly 1. Such a condition is typical of the core during a SBLOCA.

For S-RELAP5 calculations, the flow regime below the mixture level belongs to slug flow. Therefore, the purpose of this assessment was to validate the constitutive models of the slug flow in the reactor core. The subcooled boiling model is responsible for the starting point of measurable void fraction. The interphase heat transfer model takes care of the vapor generation from heat input to the fluid. The interphase friction correlations for the slug flow determine the void profile in the pre-CHF region.

The small differences between the calculated and measured void fractions indicate that the interphase correlations apply. The agreement is particularly good for Test 3.09.10j, which has the lowest pressure (609 psi) among the three tests. For the two higher pressure cases, Test 3.09.10m (1009 psi) and Test 3.09.10dd (1173 psi), the calculated void fractions are slightly lower than the data. This indicates that the interphase friction is computed somewhat lower than it should be at high pressures. The lower interphase friction tends to result in a longer dryout period and, therefore, higher clad temperatures for a SBLOCA.

4.3.1.3 GE Level Swell

The GE Level Swell Test, 1004-3, is essentially a small break blowdown of a vertical vessel 14 ft high by 1 ft in diameter. The vessel was initially pressurized to 1011 psi and filled with saturated water up to the 10.4 ft elevation. The void fraction distribution was measured axially in the test. This assessment provides a test of the two-fluid interphase models in predicting the flow regimes and void fraction distributions that occur under depressurization conditions. Section 3.6 of Reference 5 gives the detailed assessment results of the GE level swell test.

The purpose of this assessment was to validate some of the interphase heat transfer submodels. The key model affecting these assessments is the interphase friction for the bubbly and slug flows. Comparisons of measured versus calculated void fraction distributions are made at two transient times, 40 and 100 seconds. Figures 4.19 and 4.20 show the S-RELAP5 calculated void fraction results along with data and RELAP5/MOD 3.2 results. Results from S-RELAP5 compare well with the data. The void fractions calculated by S-RELAP5 are within the range of experimental uncertainty, providing excellent agreement. The calculated flow regimes are bubbly flow below the void fraction of 0.25; slug flow from the void fraction of 0.25 up to the two-phase mixture level position, which occurs at around the void fraction of 0.3 to 0.6; and annular-mist flow (very close to single-phase steam) above the mixture level. The results

indicate that, for this slow transient condition, the two-fluid interphase friction model implemented in S-RELAP5 is applicable.

The jump of void fraction from ~ 0.4 to ~ 0.99 within neighboring volumes distinctly defines the location of a two-phase mixture level. The interphase friction models for slug flow, vertical stratification, and annular-mist flow work in harmony to produce a smooth, but sharp transition from a low void fraction region to a very high void fraction (close to 1) region.

In a non-equilibrium code such as S-RELAP5, the phase exchange (vapor generation) process during blowdown is calculated through the use of an interphase heat transfer model. The calculated liquid and vapor (steam) temperatures are close to the saturation temperature. This shows that the interphase heat transfer submodels described in Section 3.4 of the code manual (Reference 9), particularly those for the metastable state conditions, are appropriate and adequate for treating the depressurization phenomena.

4.3.1.4 FRIGG2

The FRIGG2 void distribution experiments were performed in the Caps Loop Facility in the late 1960s. The test section had 36 heated rods and was designed to give a full-scale simulation of a boiling channel for the Marviken reactor. There are 27 axial void distribution tests. The void distribution was measured by the multi-beam gamma method. Section 3.10 of Reference 5 describes the FRIGG2 assessments.

The assessments were run to validate the S-RELAP5 subcooled boiling model and interphase friction model for pre-CHF flow regimes. The tests are steady state and the axial void distribution data are well-suited for the purpose. Calculations of all 27 tests were carried out.

Calculations of the 27 FRIGG2 axial void distribution tests produced good to excellent code-data comparisons, as shown in Figures 4.21 through 4.30. In the plot of calculated versus measured void fraction shown in Figure 4.31, the points are scattered around and close to the diagonal line. The mean of 170 points of calculation over measurement is 0.98 and the standard deviation is 0.096. The results confirm the applicability of the S-RELAP5 interphase friction model for the pre-CHF flow regimes, particularly the slug flow, for the core geometry.

4.3.1.5 Bennett Tube

The Bennett Heated Tube Tests were conducted by the UKAEA Research Group to measure the dry-out [or critical heat flux (CHF)] location and the surface temperature profiles in the region beyond the dry-out point. Calculations for Test Case 5358 and Test Case 5379 were performed. The main purpose of the assessment is to evaluate the applicability of the Biasi CHF correlation. Post-CHF heat transfer also was examined. The detailed assessment results are given in Section 3.2 of Reference 5.

Two Bennett heated tube tests were assessed, a low-flow test (5358) and a high-flow test (5379). As shown in Figures 4.32 and 4.33, the calculated CHF positions agree well with the data for these two cases. For the low-mass-flux case, the wall temperatures in the film boiling region are well predicted. The calculated temperature rise immediately after the CHF is not as high as the measured temperature. For the case of high mass flux, the calculated wall temperature stays rather flat in the post-CHF region and is higher than the data in the top-end region. For the low-mass-flux case, the calculated temperature continues to rise in the post-CHF region and catches up with the data. The mass flux for the high-flow case is well outside the LBLOCA conditions. In conclusion, the results of this assessment validate the S-RELAP5 correlations for predicting CHF and dry-out.

4.3.1.6 FLECHT and FLECHT SEASET

Full Length Emergency Cooling Heat Transfer - System Effects And Separate Effects (FLECHT SEASET) Tests and Full Length Emergency Cooling Heat Transfer (FLECHT) Low-Flooding-Rate Skewed Tests (Skewed) have been widely used to assess system codes. The S-RELAP5 assessments for these facilities are given in Section 3.3 of Reference 5.

The purpose of these assessments was to evaluate the S-RELAP5 code heat transfer and hydrodynamics. In addition, core axial nodalization studies were performed to validate NPP nodalization. The FLECHT SEASET facility used the W 17 x 17 geometry for the reference fuel design; the FLECHT facility used the W 15 x 15 geometry for the reference fuel design. The forced reflood separate-effect tests are with injection or flooding rates that are very demanding for simulations with the realistic system codes. The FRA-ANP selected the FLECHT SEASET tests 31504, 31701, 31302, 31203, 31805, 32013, and 34209, and FLECHT Skewed Tests 13609 and 13914 to validate the reflood modeling capability of S-RELAP5 for the RLBLOCA

methodology. For LBLOCA reflood, the selection covers the whole range of pressure, subcooling, and flooding rate, and includes cosine and skewed axial power profiles.

The important parameters for assessing the code calculation against the measured data are:

- PCT
- Cladding surface temperature history
- Steam temperatures
- Heat transfer coefficients
- Differential pressures
- Mass inventory
- Liquid carryover
- Rod quench time.

The PCT is one of the required criteria for LBLOCA licensing. PCT is the maximum value of all cladding temperatures. With the power specified, the cladding surface temperatures at various elevations depend on the heat transfer rates from the surface to the fluid. The fluid conditions, including the steam temperature and void distribution, determine the heat transfer rates. The differential pressures indirectly measure void distribution under low-flow conditions. The total mass in the test section indicates how much of the injection water stays in the test section to cool the rods and how much is entrained out. The liquid carryover is the amount of liquid entrained out of the test section and is closely related to the mass inventory. The rod quench time depends strongly on the transition boiling correlation used in the code. Information about the eight parameters listed provides a basis for understanding the computed results compared with the measured data.

Conclusions from the FLECHT-SEASET and FLECHT Skewed assessments in terms of the important parameters are provided in the following paragraphs.

Peak Cladding Temperature

Figures 4.34 through 4.42 show the calculated maximum surface temperatures and the measured temperature data at various elevations in the simulated fuel assemblies for the various tests. The S-RELAP5 calculated PCT is in good agreement with or acceptably higher than the measured data. The calculated maximum clad temperature being generally higher than the measured data at all elevations. The calculated maximum clad temperature more

closely matches the measured data below the test section mid-plane. However, the calculated maximum clad temperatures generally are much more conservative above the test section mid-plane. The conservatism above the test section mid-plane is exaggerated even more when the axial power profile is top peaked. The calculated maximum clad temperature conservatism generally increases with decreasing reflood rate, decreasing system pressure, or increasing inlet subcooling

Rod Surface Temperatures

The calculated temperature at a specified elevation has been compared with the measured temperature near the same elevation. The quench times are calculated well at the lower elevations for all tests and at all elevations for the lower flooding rate tests.

The calculated rod surface temperature during the temperature rise portion of the test compares well with the measured data. However, the quenching time is calculated late for the highest reflood rate test, Test 31701. The quenching time is progressively earlier for the tests with lower reflood rates until, at the lowest reflood rate, S-RELAP5 calculates a quenching time that is too early. S-RELAP5 has calculated good agreement of the complete transient at the 78 in elevation for the three intermediate reflood rate tests.

S-RELAP5 calculated rod surface temperatures are in good agreement for the complete transient at all elevations for the high system pressure test, Test 32013, and for elevations below 90 in for the low pressure test, Test 34209. For Test 34209, at elevations at or above 90 in, the rod surface temperature is significantly overpredicted.

For the FLECHT Skewed tests, S-RELAP5 tends to predict a higher maximum clad temperature at all elevations and tends to predict late turnaround. In the low subcooling test, Test 13914, S-RELAP5 tends to predict a late quench time. In the high subcooling test, Test 13609, S-RELAP5 tends to predict an earlier quench time at or below an elevation of 82.8 in.

For FLECHT SEASET Test 31504, the PCT occurs in the region above, but close to, the mid-plane of the test section. The calculated rod surface temperature in the temperature rise period is in good agreement with the measured data.

Steam Temperatures

Steam temperature is one of the important parameters in determining the heat transfer rate during the temperature rise period. Figures 4.43 through 4.51 show the calculated and measured steam temperatures for the FLECHT and FLECHT-SEASET tests. The calculated steam temperature generally is lower than the measured steam temperature for the FLECHT-SEASET tests and higher than measured steam temperature for the FLECHT skewed tests.

Differential Pressures

Differential pressure is an indirect measurement of void distribution, which is an important property for calculating the heat transfer rate. The calculated differential pressures are somewhat higher than the measured data in the period between 200 and 300 seconds for the three lower reflood tests. S-RELAP5 calculates excess liquid accumulation within the region between the 72 and 84in elevations during this period. This happens after the PCT has occurred and thus has no effect on PCT.

Heat Transfer Coefficient

The heat transfer coefficient normally is defined with respect to phase or saturation temperature, depending on the heat transfer mode. This definition is used in S-RELAP5 and the other codes in the RELAP5 series. The heat transfer coefficient data usually are deduced from the heat transfer measurements with reference to the saturation temperature. Good agreement between the calculated and measured data is observed for the dispersed-film-boiling heat transfer regime (before time = 200 s) leading to a good calculation of the PCT. Figures 4.52 through 4.60 show calculated versus measured heat transfer coefficients for the tests.

Mass Inventory

The calculated water mass accumulation generally is less than measured. Most of the mass accumulation occurs early in the transient as the lower half of the test section is filled. Once the water accumulation reaches the high power mid-plane region of the test bundle, the water accumulation becomes a balance between injected water entering and entrained and evaporated water leaving. Figures 4.61 through 4.69 compare calculated versus measured liquid mass inventory.

Liquid Carryover

The calculated carryover generally is greater than the liquid carryover derived from the measured carryover tank level, as shown in Figures 4.70 through 4.75 for the FLECHT-SEASET tests. This is consistent with the lower calculated mass levels in the test bundle and would indicate that S-RELAP5 is overpredicting the entrainment in the bundle.

Rod Quench Time

The calculated quench time generally is greater than the mean quench time derived from measured rod thermocouple data at high elevations in the FLECHT-SEASET test assembly. The magnitude of the delay generally increases with increasing elevation in the test assembly. These trends do not hold true for the lowest (Test 31805) and highest (Test 31701) reflood rate tests. Quench time comparisons are given in Figures 4.76 through 4.81.

Summary

Data comparisons for the eight key parameters were made for all tests calculated. The agreement is good, with S-RELAP5 generally calculating peak cladding temperature (PCT) in agreement with or higher than the measured data. These data will be used to derive the heat transfer parameter multipliers shown later in this section.

Sensitivity Studies

Timestep and nodalization sensitivity studies also were performed using FLECHT SEASET Test 31504 to demonstrate the solution convergence of the S-RELAP5 treatment of the reflood transient. FLECHT SEASET Test 31504 was chosen because it is a demanding low flooding rate (0.97 in/s) [2.46 cm/s] test. High-flooding-rate tests are known to be easier for the advanced system codes to simulate because of early temperature turnover and no sharp discontinuities in the void distribution.

The timestep and nodalization sensitivity studies showed that calculated rod surface temperatures are not sensitive to timestep sizes, particularly in the temperature rise period. The calculated results had some small variations with the node sizes, noticeably in the quench period. The local maximum cladding temperatures (as a function of elevation) computed with different node sizes and different time-step sizes are clustered in an extremely narrow band.

This band is much narrower than the corresponding measured data band. Also, the calculation points are distributed in the high-temperature outer envelope of the measured data.

Figures 4.82 through 4.84 show results from the nodalization and time step calculations.

[

]

4.3.1.7 PDTF/SMART Tests

The Product Development Test Facility (PDTF) Small Array Reflood Test (SMART) tests were performed by FRA-ANP to show that the high thermal performance (HTP)-type (FRA-ANP-type) spacer was thermodynamically equivalent to the FOCUS™ (mixing vane)-type spacer with respect to reflood and PCT. The data from these tests provides simulations of FRA-ANP prototypic fuel rods under LOCA reflood conditions. Therefore, FRA-ANP used the data from the SMART to perform verification and validation assessments on the S-RELAP5 thermal-hydraulic simulation code in support of FRA-ANP's RLBLOCA methodology. The tests are similar to the FLECHT-SEASET tests and assess the same phenomena, except that they were performed in a FRA-ANP facility and used hardware prototypic of FRA-ANP 15 x 15 fuel. The assessments also examined the effects of spacer modeling on reflood phenomena. The details of the assessments are reported in Section 3.4 of Reference 5.

The test assemblies were 6 x 6, full-height, simulated PWR assemblies. The rod diameter and pitch were characteristic of FRA-ANP's 15 x 15 PWR fuel design. The test assembly had a uniform radial power distribution and a chopped cosine axial power distribution. The tests simulated five different flooding conditions. Of the five flooding rate conditions, four were constant-flooding-rate tests and one was a variable-flooding-rate test. The constant-flooding-rate tests had flooding rates of 0.6, 1, 2, and 4 in/s. The variable-flooding-rate tests started at 8 in/s and ramped rapidly to a constant 1-in/s flooding rate. The 0.6-in/s tests were terminated prematurely; therefore, they were eliminated for the verification and validation of S-RELAP5.

* FOCUS is a trademark of Framatome ANP.

Four tests were chosen to evaluate S-RELAP5's ability to predict maximum clad temperature (MCT) at individual elevations and overall PCT. The four tests that were explicitly modeled are listed in Table 4.5.

The current methodology for RLBLOCA does not explicitly model spacers in the core. These assessments are being performed to evaluate the acceptability of this methodology. Therefore, in addition to evaluating the performance of S-RELAP5 with the current spacer-free modeling, a model that incorporates spacer volumes also was created and evaluated. This additional model only addresses the reduction in flow area through the spacer.

Figure 4.85 shows the PCT for each test as predicted by the S-RELAP5 models with and without spacer volumes, as well as the PDTF SMART test data. As can be seen, the simulations without spacer volumes, but with appropriate junction loss coefficients, predict a PCT within the range of the data (excellent agreement) for each flooding condition except for the 4-in/s case. For this test, the prediction is 34 °F (19 °C) below the range of the data. This is not a significant difference (good agreement). The model without spacer volumes represents the current Realistic LBLOCA methodology. The predictions of differential pressure across the test assembly and rod surface temperature versus time for the model without spacer volumes also were found to be adequate when compared to test data.

The effect of spacer heat transfer enhancement can be seen when comparing measured maximum clad temperatures for the 2 peak power nodes at the axial center of the assembly for tests KH02B and KH03B (the 4-in/s flooding rate for test KH01B is large enough such that spacer heat transfer enhancement is not as important). These 2 nodes have identical power peaking and, since they are adjacent nodes, they should see similar heat transfer environments. However, the upper peak power node spans a spacer. Comparison of measured maximum clad temperature data at these nodes shows a temperature differential between the two locations (72 in versus 77 in) of about 110°F (43°C). Therefore, this is the inferred spacer benefit from the measured data.

The model without spacer volumes predicted a more conservative PCT than the model with spacer volumes for every case. Also, the predictions of differential pressure across the test assembly and rod surface temperature versus time showed the simulation predictions to be in

good agreement with each other. Generally, the model without spacers predicted higher rod surface temperatures and a smaller total pressure drop than the model with spacer volumes.

Figures 4.86 through 4.89 show the predicted PCT and the maximum clad temperature (MCT) at each nodal elevation compared to the available data for each test. These figures show that the predicted PCTs and MCTs generally are within the range of the data. Also, it can be seen that while the model with spacer volumes generally predicts lower MCTs and does a better job of predicting rod surface temperature in the vicinity of the spacers, generally little difference is apparent between predictions at locations away from spacers. Because of the enhanced heat transfer associated with the spacer, PCT does not occur at the spacer location. Therefore, the superior ability of the model with spacer volumes to predict rod surface temperatures at spacer locations is unimportant with respect to this key analysis parameter.

In conclusion, this analysis shows that the S-RELAP5 code can adequately predict the reflood thermal-hydraulic behavior for the PDTF SMART reflood tests. Also, the analysis shows that the current methodology, which does not include the flow area restrictions associated with spacer volumes in the core, is an equivalent or conservative model compared to a model that includes spacer volumes.

4.3.1.8 Marviken Tests

The Marviken Test Facility and test data are well documented. The facility has four main parts: a full-scale boiling water reactor (BWR) vessel, a discharge pipe attached to the bottom of the vessel, a test nozzle connected to the downstream end of the discharge pipe, and a rupture disk assembly attached to the downstream end of the nozzle. Nozzles of various length-to-diameter ratios are used in the tests.

The assessment of the Marviken full-scale critical flow tests was performed to provide the uncertainty information for the S-RELAP5 critical flow model to support the S-RELAP5 RLBLOCA project. The Marviken full-scale critical flow test data were used in the CSAU methodology (Reference 4) to determine the critical flow multipliers and uncertainties for the break flow model. The Marviken test data also are widely used in assessing critical flow models for various system codes.

Nine Marviken tests were selected for the assessments based on the availability of electronic data. The test numbers for the nine tests are: 2, 6, 8, 16, 17, 20, 22, 24 and 25. Test 24 has

been used to assess the RELAP5 critical flow model beginning with RELAP5/MOD1 and Test 22 has been used to assess RELAP5/MOD2 and RELAP5/MOD3. The break flow data are assumed to be accurate, (i.e., uncertainties of data are ignored, when the uncertainties of the S-RELAP5 break flow model are computed).

Details of the Marviken assessments are given in Section 3.5 of Reference 5 and are only summarized here. The calculated critical flow mass fluxes and the measured values are sampled at 1-second intervals. A total of 587 pairs of calculated and measured values from the 9 tests are collected. Figures 4.90 to 4.98 show the code-to-data comparisons of mass flow rates at the break. The calculations agree well with the data. The worst situation is in the subcooled-to-two-phase transition region where the differences are larger.

Figure 4.99 shows the comparison of the calculated mass flux versus the data. The figure clearly shows that the comparison points are uniformly scattered around the 45 degree line. The ratios of (calculated mass flux minus data)-to-data are used to compute the statistics. [

]

The ratios given in Figure 4.100 were evaluated first by separating the subcooled choking and two phase choking and then as an overall data set. [

]

4.3.1.9 Westinghouse/EPRI 1/3 Scale Tests

The W/EPRI 1/3-scale test assessments were performed to assess the ECC/steam mixing process during the reflood-accumulator and reflood-safety injection period in a typical PWR LBLOCA scenario.

The principal feature of the test apparatus was a simulated cold leg that was fabricated from a 10.42-in, inside diameter (I.D.) straight pipe. Two ECC injection points were provided so that the pipe lengths downstream of the injection point were either scaled to a typical PWR or were full length. Superheated steam from the boiler flowed through the inlet surge tank and an inlet flow chamber before entering the test section. The inlet flow chamber was designed to yield a uniform velocity profile entering the test section. Cold water from the storage tank entered the test section through either the scaled length ECC injection point or the full length injection point. The effluent fluid exited the test section into the outlet surge tank. The surge tanks upstream and downstream of the test section help maintain constant pressure boundary conditions for circumstances where large pressure oscillations occurred inside the test section. The test section was fitted at the top and bottom with thermocouples. This provided temperature data for both the vapor and liquid phase in the case of stratified flow inside the test section. Pressure drops along the test section also were measured.

One of the important phenomena identified in PWR LBLOCA is the mixing of the ECCS water and the steam in the cold leg during the LBLOCA refill and reflood phases. The controlling parameter is the interfacial condensation heat transfer coefficient. Its impact on the PCT calculation needs to be evaluated. To do this, the uncertainty range in the interfacial condensation heat transfer coefficient for the mixing process must be determined based on an assessment against relevant data. In this study, data from the W/Electric Power Research Institute (EPRI) one-third scale study was selected. This data has been determined to be appropriate and representative of conditions encountered in the reflood and post-reflood phases of a PWR LBLOCA.

Section 3.8 of Reference 5 documents the assessment results and a sensitivity study of the multiplier on the interfacial heat transfer coefficient. The results are used to support the overall application of the RLBLOCA methodology.

To confirm the appropriateness of the data, the results of a typical LBLOCA scenario for a W 3-loop PWR were examined. The range of conditions considered in the test matrix is similar to that found in the sample calculation. Hence, the test matrix selected is appropriate for the present assessment, and can be used to determine the uncertainty associated with the code's capability to predict the ECC/steam mixing process during the reflood period of a LBLOCA.

For the S-RELAP5 assessments, the difference between the liquid effluent temperature and the injection temperature was the primary data because it relates directly to the interfacial condensation heat transfer rate over the entire test section. The capability of S-RELAP5 in predicting the interfacial condensation heat transfer in the mixing of ECCS water and steam can therefore be assessed by calculating this temperature difference and comparing the calculated temperature difference results to measured data.

[

] To be consistent with the
FRA-ANP guidelines, a plant-consistent model is therefore developed for the assessments. The determination of the interfacial condensation multiplier is based on this plant-consistent model.

Nineteen runs were assessed; 9 correspond to the reflood phase after accumulator injection and the other 10 to the reflood accumulator injection phase. The primary result sought in this study is the effluent liquid temperature (i.e., the liquid phase temperature at the exit of the test section). For all the cases run, the thermal hydraulic variables were sufficiently steady at 100 seconds except for several reflood-accumulator tests. Hence the effluent temperatures at 100 seconds were used to compare with the measured data.

Table 4.6 compares the calculated and measured effluent temperature for all the cases, using the plant-consistent model. The information from Table 4.6 is plotted in Figure 4.101. The total amount of interfacial heat transfer is approximately proportional to the difference between the liquid effluent temperature and the inlet temperature (i.e., ECC liquid temperature). Denote this difference by ΔT . The ratio of the calculated ΔT and the measured ΔT approximates the ratio between the code-predicted condensation heat transfer and the actual value. Hence define R as

$$R = \frac{(T_{\text{effluent}} - T_{\text{in}})_{\text{measured}}}{(T_{\text{effluent}} - T_{\text{in}})_{\text{calculated}}}$$

Deviation from unity of R represents a code bias in predicting the interfacial condensation heat transfer during the ECC/steam mixing process. [

]

S-RELAP5 was assessed against selected tests from the W/EPRI 1/3 scale condensation experiment. A bias was defined that approximately represents the ratio of the experimental and code-calculated interfacial condensation heat transfer. This bias was used to assess the accuracy of the code in predicting the interfacial condensation heat transfer during the ECC/steam mixing process. [

]

4.3.1.10 FRA-ANP CCFL Tests

As described in Section 3.9 of Reference 5, a small-scale test facility was used to flow test the upper tie plates (UTPs) of interest and determine whether or not the S-RELAP5 calculation of CCFL was sufficient (i.e., accurate or conservative). UTPs from FRA-ANP designs for W 15 x 15 and 17 x 17 fuel assemblies and a CE 14 x 14 fuel assembly were obtained and flow tested in the mini-loop of the PDTF. The testing consisted of measuring the liquid penetration in an upflow air channel containing the UTP. Kutateladze parameters were calculated from the measured data and compared to the corresponding flooding curve predicted for the geometry by the S-RELAP5 CCFL model.

The mini-loop is a Lexan test loop designed to do part-array testing for air/water evaluations and/or flow visualization studies. It was configured to spray water into the top of the test chamber while air was injected into the lower portion of the test section. The test chamber was sized to contain a 5 x 5 bundle with four spacers and a UTP. Instrumentation is provided to monitor flows, pressures, temperatures, and water levels.

The generic test bundle consisted of a lower flow straightener, four spacers, and 24 rods in a 5 x 5 array. The bundle was situated in the test channel such that it was held a prototypic distance from the UTP test section. The UTP section was supported by the test channel and

not connected to the bundle. To ensure proper isolation of the UTP effect, the topmost spacer was situated approximately 12 in below the UTP. The same rod and spacer configuration was used throughout the evaluation. Care was taken to seal the edge of the UTP to prevent unintended bypass.

The mini-loop was operated at ambient temperature and atmospheric pressure for all test conditions. Water was inserted in a disperse spray above the top of the bundle. The facility was modified to provide a means to collect the water injected during the test by installing a collection tank.

Countercurrent flow limiting (CCFL) affects the liquid fallback from the upper plenum to the core during the refill and reflood portions of the LBLOCA transient. [

]

The experimental data was converted to Kutateladze parameters for comparison to Bankoff (Reference 9). The Bankoff correlation, as used in S-RELAP5, has provisions for Wallis or Kutateladze weighting, as well as slope and intercept as user input. [

] The intercept

is modified by Tien with:

$$c' = c \left\{ \tanh \left[0.9 \left(\frac{D_j}{L} \right)^{1/4} \right] \right\}^\beta$$

where the characteristic length L is given by

$$L = \sqrt{\frac{\sigma}{g(\rho_f - \rho_g)}},$$

and where

c	1.8 (user input)
β	1.0 (user input to choose Kutateladze weighting)
D_j	tie plate hydraulic diameter
g	gravity
σ	surface tension
ρ_f	liquid density
ρ_g	vapor density

For the geometries used in the experiments, the following hydraulic diameters and resulting c' were used to calculate the Bankoff flooding curves used for comparison purposes:

[]
[]
[]

Figures 4.103, 4.104, and 4.105 compare mini-loop data with Bankoff. In all cases, the measured data is conservative (acceptable agreement) with respect to the flooding curves using the RLBLOCA parameters (Reference 12).

4.3.1.11 UPTF Tests

Section 3.7 of Reference 5 documents assessments of S-RELAP5 using the Upper Plenum Test Facility (UPTF). The UPTF was operated by Kraftwerk Union AG (KWU) in support of the 2D/3D Refill and Reflood Program. It was designed to simulate a four-loop 3900 MWt PWR primary system, and was intended to provide a full-scale simulation of thermal-hydraulic behavior in the primary system during the end-of-blowdown, refill, and reflood phases of a PWR LBLOCA. Note that end-of-blowdown defined by UPTF experimenters differs from the blowdown period defined for the RLBLOCA PIRT and consists of the period when the accumulators are flowing but the system is still depressurizing. The specific tests assessed with S-RELAP5 include selected runs from the following test series, Tests 6, 7, 8, 10, 11, 12, and 29.

4.3.1.11.1 UPTF Tests 6 and 7

UPTF Tests 6 (Runs 131, 132, 133, 135, and 136) and 7 (Run 203) were designed specifically to examine downcomer countercurrent flow behavior during blowdown, ECC bypass, and lower plenum refill with cold-leg ECC injection. The ECC injection is activated in a PWR during the end-of-blowdown and refill phases of a cold-leg break LBLOCA transient. These interactions play a key role in determining the rate at which ECC water is able to refill the lower plenum. The tests were analyzed to demonstrate the ability of S-RELAP5 to self-limit countercurrent flow in the downcomer and predict reasonable refill behavior including ECC bypass compared to experimental data.

The S-RELAP5 assessment calculations included simulations of Test 6, Runs 131, 132, 133, 135, and 136 and Test 7, Run 203. For these runs, the UPTF system was configured to simulate the late blowdown and refill phases of a cold-leg break PWR LBLOCA. These tests all were initiated with no water inventory in the lower plenum. Steam injected in the core region traveled downward to the lower plenum, then exited the vessel via the downcomer and broken cold leg. An identical pattern of ECC injection was used for all the runs analyzed, with a constant injection rate into each of the three intact cold legs. A wide range of steam flow rates was used for the various runs and, depending on the downcomer steam flow rate, the ECC water entering the downcomer either bypassed to the broken cold leg or penetrated downward to fill the lower plenum.

The following general observations regarding UPTF Tests 6 and 7 were found to be true of both the experiments and their corresponding S-RELAP5 simulations.

- Very little water was delivered to the downcomer and lower plenum during the period that the intact cold legs were filling with ECC water. Only after the cold legs were filled did a significant amount of ECC penetration to the downcomer and lower plenum begin.
- When ECC penetration to the lower plenum did occur, the rate of that penetration tended to vary inversely with the rate of steam flow in the downcomer.
- During the period of ECC penetration, ECC water from cold legs 2 and 3 (opposite the broken cold leg) tended to penetrate directly downward to the lower plenum. ECC water from cold leg 1 (immediately adjacent to the broken cold leg) tended to be bypassed to the broken cold leg.
- Highly unstable flow conditions were observed in the downcomer during the entire period of ECC injection.

The specific LBLOCA refill phenomena addressed by the analyses of Tests 6 and 7 include the following:

- Downcomer multi-dimensional effects

Both calculated steam flow and calculated ECC water flow are shown to distribute themselves azimuthally in multi-dimensional patterns that were consistent with test results.

- Downcomer countercurrent and slug flow

The various runs were performed with a wide range of downcomer steam flow rates and with two phase flow conditions including countercurrent and slug flow. In all cases, the code was demonstrated to conservatively (adequate to reasonable agreement with data) predict downcomer penetration of ECC water with the RLBLOCA lower plenum plant nodalization.

- Downcomer condensation and non-equilibrium flow

The various runs were performed with a wide range of ECC subcoolings (and downcomer condensation rates) and in all cases, the code was demonstrated to conservatively predict downcomer penetration of ECC water with the RLBLOCA plant lower plenum nodalization.

- Downcomer entrainment and deentrainment

With the RLBLOCA plant lower plenum nodalization, the code conservatively predicted the entrainment of ECC water from the intact cold legs to the broken cold leg during the cold-leg filling period, and correctly predicted full or partial entrainment of ECC water to the broken cold leg during the lower plenum refill period.

- Lower plenum sweepout

The code was shown to overestimate the lower plenum sweepout rate when the standard RLBLOCA lower plenum nodalization is used (adequate agreement with data). A sensitivity study was performed that indicates that the use of a 2-D lower plenum model improves the code prediction of sweepout and liquid level.

Figures 4.106 through 4.111 show the lower plenum liquid level as calculated by S-RELAP5 with the RLBLOCA plant lower plenum nodalization and as measured for each test run. The

code is shown to consistently underpredict the lower plenum fill rate and overpredict the amount of lower plenum sweep out during the refill period. Underpredicting the lower plenum fill rate indicates that, in the full size UPTF facility, the S-RELAP5 code is overpredicting ECC bypass. Underpredicting the rate of lower plenum fill is conservative because it delays the beginning of core recovery, which will result in the prediction of higher PCTs.

4.3.1.11.2 UPTF Test 8

UPTF Test 8 was performed to investigate the thermal hydraulic behavior of ECC water injection during the end-of-blowdown, refill, and reflood phases of a postulated LOCA. Of particular interest in the test is the pressure and fluid oscillations occurring in the cold legs. These oscillations are induced by condensation of steam from the injection of the subcooled ECC water, the formation of a liquid plug in the cold leg (slug flow regime), and the transition to the stratified flow regime. The code assessment was performed for two Test 8 runs (Run 111 and Run 112) that differed by the value of the resistance to flow applied in the pump simulator of intact loop 2. The different resistance resulted in a different steam rate into the intact loop 2.

The primary results from the comparisons of S-RELAP5 to the UPTF data for Test 8 Run 111 and Run112 are as follows:

- A key test result was the measurement of a subcooled liquid plug filling the entire cross section of the cold leg (slug flow) at higher ECC injection rates. S-RELAP5 also predicted the plug formation at the start of the test for the higher ECC injection rates consistent with the test results.
- The experimental results and the S-RELAP5 prediction both indicate that condensation occurs at the face of the cold-leg plug.
- When the step change in the ECC flow from 400 to 250 (kg/s) occurs in the experiment, the S-RELAP5 calculation changes from slug flow to stratified flow. This corresponds directly to the start of a transition in the experiment from slug flow to fully developed stratified flow. This transition is marked by a high level of temperature oscillation that in the case of Run 112 clearly reaches the steam temperature.
- The S-RELAP5 cold-leg temperature solution is in good agreement with the measured UPTF data until the point where S-RELAP5 changes from slug flow to stratified flow. At that point, no single S-RELAP5 calculated temperature can be directly compared to the UPTF data.
- For these S-RELAP5 calculations, the predicted behavior was shown to be relatively insensitive for a maximum time step of less than 10 ms.

Figures 4.112 through 4.115 show the results from Test 8 Runs 111 and 112.

4.3.1.11.3 UPTF Tests 10 and 29

UPTF Tests 10, Run 081, and 29, Runs 211 and 212, were specifically designed to simulate upper core, upper plenum, and hot-leg fluid flow behavior during the reflood phase of a LBLOCA transient. These tests were analyzed to demonstrate the ability of S-RELAP5 to properly predict entrainment/deentrainment phenomena and to limit countercurrent flow at the UTP and upper plenum regions of a PWR during the LBLOCA reflood phase. The limiting of down flow into the core is important because water down flow into the core region provides a source of additional core cooling and reduces the likelihood of water carryout to the steam generators. The water carryout to the steam generators affects the predicted steam binding effects because of liquid vaporization in the steam generators

The S-RELAP5 assessment calculations included simulations of Test 10, Run 081, and Test 29 for a combination of Runs 211 and 212. For all of these runs, the UPTF system was configured to simulate the reflood phase of a cold-leg break PWR LBLOCA. UPTF Test 10, Run 081, and 29, Run 211/212, were separate effects tests that investigated core, upper plenum, hot leg and steam generator behavior during the reflood phase of a PWR LBLOCA with a cold-leg break. For these tests, the lower plenum and lower downcomer were filled with water to block steam flow directly from the core to the downcomer and cold legs. A mixture of steam and water was injected into the core simulator to simulate reflood steam generation and water entrainment. The injected steam and entrained water then flowed to the hot legs via the upper core support plate and upper plenum. From the hot legs, the steam/water mixture flowed into the steam generator simulators where water was separated from the mixture by cyclone separators. The separated water was stored and measured in holding tanks, while the steam (and any unseparated water) flowed onward through the pump simulators, intact cold legs, upper annulus and broken cold leg to the break junction.

Each test consisted of a sequence of phases using different steam and water injection rates. Run 081 was a 300-second transient consisting of four different flow phases. This test was flawed during the period from 50 through 150 seconds by the inadvertent leakage of steam from the lower plenum around the core barrel skirt into the downcomer and by accompanying lower plenum flow oscillations observed in the test data. This flawed test period involves the first

three phases of the test, and data from these phases is not compared with S-RELAP5 simulation results. The conditions for the four phases of this test are given in Table 4.7.

Runs 211 and 212 were 900-second transients consisting of six different flow phases. Each phase consisted of a period of constant steam flow rate and water flow rate, followed by a period of no flow. Test 211 was flawed by the inadvertent operation of drain valves in the steam generator simulator during the first two flow phases. Run 212 was a repeat of Run 211 with the drain valve problem fixed. Run 212 was flawed by oscillatory broken loop drain flow during phases 4 through 6. Consequently, the S-RELAP5 predictions will be compared to data from phases 1 and 2 (0 through 300 s) from Run 212, and data from phases 3 through 6 (300 through 900 s) from Run 211. The test parameters for the six phases in combined Run 212/211 are shown in Table 4.8.

The specific LBLOCA reflood phenomena addressed by the Test 10 and 29 analyses include the following:

- Steam generator steam binding
- Upper plenum two-phase convection
- Upper plenum countercurrent flow
- Upper plenum and hot-leg entrainment and deentrainment

The following general observations can be made regarding the S-RELAP5 simulations of UPTF Tests 10 and 29 using the CCFL inputs for the RLBLOCA methodology.

- Overall predictions of total water carryover to the steam generator simulators indicates that the code conservatively overpredicts (adequate agreement with data) the liquid carryover to the steam generators. This is conservative because it will result in an overprediction of the steam binding effect, which in turn reduces the reflood rate.
- Overall predictions of total fallback to the lower vessel region also was shown to be conservative in that the fallback to the core was underpredicted (adequate agreement with data). This is consistent with the overprediction of liquid carryover to the steam generators because more liquid will be present in the upper plenum to be carried over to the steam generators.

For UPTF Test 10 Run 081 the Kutateladze CCFL correlation is used in the S-RELAP5 code to limit down flow at the core UTP. Figure 4.116 presents a plot of Kutateladze parameters calculated from the S-RELAP5 results compared to the UPTF correlation. The comparison

shows that S-RELAP5 is correctly limiting liquid down flow, as noted by the linear upper limit of \sqrt{Kg} . [

] Figure 4.116 clearly shows the S-RELAP5 calculations are conservative relative to the UPTF correlation developed from the UPTF data.

For UPTF Test 29, Run 211/212, Figure 4.117 presents a plot of Kutateladze parameters calculated from the S-RELAP5 results compared to the UPTF correlation derived from the data. This comparison also shows that S-RELAP5 is correctly limiting liquid downflow noted by the linear upper limit of \sqrt{Kg} . Figure 4.117 shows that the S-RELAP5 calculation is conservative relative to the UPTF correlation derived from the data.

Figures 4.118 and 4.119 demonstrate the S-RELAP5 code overprediction of the liquid carryover to the steam generators. Figure 4.118 has been shifted in time to account for Test 10, Run 081, problems in the first part of the test to limit flow between the core and downcomer. Both plots clearly show that S-RELAP5 with the RLBLOCA plant nodalization conservatively overpredicts the carryover of liquid to the steam generators.

An additional set of S-RELAP5 simulations was performed using the CCFL input parameters recommended by KWU for the UPTF tests. These CCFL input parameters significantly reduced the conservatism in the S-RELAP5 predictions, indicating that the code is functioning appropriately with respect to CCFL inputs. The code prediction of carryover to the steam generators still is shown to be conservative relative to the UPTF test data. This indicates that the code entrainment/deentrainment model is conservative when applied with the RLBLOCA Kutateladze parameters in conjunction with the 2D upper plenum model.

4.3.1.11.4 UPTF Tests 10 and 12

UPTF Tests 10, Run 080, and 12, Run 014 were also specifically designed to simulate upper core, upper plenum, and hot-leg fluid flow behavior during the reflood phase of a LBLOCA transient. These tests differed from Test 10, Run 081, and Test 29 in that flow was allowed between the downcomer and core region and Test 12 included nitrogen injection. Analysis of these tests demonstrates the ability of S-RELAP5 to properly limit countercurrent flow at the UTP and upper plenum regions of a PWR during the LBLOCA reflood phase. This limiting of down flow into the core is important because water down flow into the core region provides a

source of additional core cooling and reduces the likelihood of water carryout to the steam generators with the associated steam binding effects.

UPTF Test 10, Run 080, was performed to examine countercurrent flow through the UTP and to examine co-current water down flow. The lower plenum was filled with water to a level of 1.2 m (3.94 ft), steam was injected into the core, and subcooled water was injected into the intact hot legs. The boundary conditions set up countercurrent flow of steam and water through the UTP as well as through regions of co-current water down flow.

UPTF Test 12, Run 014, was performed to examine countercurrent flow between the UTP and the upper plenum. The water level in the lower vessel at the start of the test was low enough (0.56 m, 1.84 ft) to allow steam to flow from the core to the downcomer and broken cold leg. Steam was injected into the core, and subcooled water was injected into the intact hot legs. These boundary conditions setup countercurrent flow of steam and water through the UTP.

The key parameters to be compared between S-RELAP5 simulations and test results are the down flow of water to the lower vessel region, Kutateladze countercurrent flow parameters calculated at the junctions between the upper plenum and core, and the upper plenum pressure. Reduced down flow of water to the lower vessel generally is considered to have a conservative effect because it leads to less core cooling. Figures 4.120 through 4.122 show results for UPTF Test 10, Run 080. Figures 4.123 through 4.125 give similar results for UPTF Test 12, Run 014.

For both tests, data and S-RELAP5 calculations were compared with two different sets of Kutateladze parameters. [

] For both sets of Kutateladze parameters, the S-RELAP5 code is demonstrated to conservatively limit the water downflow in the countercurrent flow mode. The degree of conservatism is significantly reduced when the UPTF experimental data parameters are used, but the code predictions remain conservative relative to the data in both tests (acceptable agreement).

The calculated UPTF water down flow also was compared with the S-RELAP5 calculated water down flow based on the two sets of Kutateladze CCFL input parameters. The results show that overall (co-current and countercurrent) S-RELAP5 conservatively underpredicts down flow. The small difference between the down flow results, despite the change in CCFL parameters,

indicates that the total down flow is primarily caused by co-current flow. This is consistent with the UPTF results which indicate break through of ECC liquid near the hot-leg upper plenum junction. The S-RELAP5 results are based on describing the core to upper plenum junction with the fuel bundle UTP area consistent with the current RLBLOCA methodology.

With respect to upper plenum pressure, the S-RELAP5 calculated upper plenum pressure and the measured data comparisons indicate that the S-RELAP5 code slightly underpredicts the pressure for all cases.

The final observation is that the presence of nitrogen in the system does not appear to have a significant impact on CCFL. One of the differences between Test 12, Run 14, compared to Test 10, Run 080, is that nitrogen was injected into the system. Comparisons of the Kutateladze parameters indicate that the presence of the nitrogen in the system does not affect either the S-RELAP5 calculation or the UPTF experimental results for CCFL.

4.3.1.11.5 UPTF Test 11

Assessment of UPTF Test 11 was made to validate the application of the S-RELAP5 CCFL model to the steam generator inlet plenum junction from the hot leg. UPTF Test 11 is a series of quasi-steady-state SETs conducted to investigate the countercurrent flow of steam and saturated water in the hot leg of a PWR. Countercurrent flow in the hot leg was simulated by venting steam from the primary system through the UPTF broken loop hot leg to the containment simulator downstream from the water separator. Simultaneously, a stream of saturated water was injected into the water separator inlet chamber. The test consisted of a series of flow conditions to map out the countercurrent flow curves at two different pressure conditions, 0.3 MPa (low pressure case) and 1.5 MPa (high pressure case).

The measured water level increase in the lower plenum of the test vessel was used to calculate the mean downflowing water rate by use of the volume versus elevation calibration curve. The upflowing water mass flow rate was separated by the cyclones and measured using the water level outside the cyclones in the water separator. At higher injected steam mass flow rates, a small part of the upflowing water was carried out by the steam to the containment simulator. To check the water mass balance, the water level in the water separator was measured and no water was drained from the water separator or from the lower plenum of the test vessel during the test.

Two S-RELAP5 input decks were created for each test series, one without the CCFL model and one with the CCFL option selected for the junction between the hot leg and inlet plenum. [

] The water and steam injection rates were input as boundary conditions into S-RELAP5 for both the low- and high-pressure test series. Figure 4.126 shows the simulation of the water and steam injection rates for the entire high-pressure (1.5 MPa) test series. At 12 seconds, water injection started and reached 9.8 kg/s within 0.5 second. Between 150 to 200 seconds, the water injection rate increased from 9.8 kg/s to 29.4 kg/s and then remained constant. After the initial ramp-up, the steam injection rate was held constant for 200 seconds and then increased to a higher value within a 50-second interval. This steam injection pattern was repeated for all the high-pressure test steam flow rates. For the low-pressure (0.3 MPa) test series, a similar simulation of the water and steam injection rates was used for the test calculation, as shown in Figure 4.127.

The calculated water downflow rates are listed in Table 4.9 for the low-pressure test series and Table 4.10 for the high-pressure test series. The calculated results, data, and data error bands are shown in Figure 4.128 with the steam injection rate plotted against the liquid mass downflow rate.

When the [

] good agreement between calculation and data is shown. For the high-pressure case (1.5 Mpa), complete carryover of water to the steam generator occurs at a steam flow rate of 40.2 kg/s, which is the same as the experimental value. For the low pressure case (0.3 Mpa), complete carryover occurs at a steam flow rate of 18.5 kg/s, which is lower than the experimental value of 20.5 kg/s (note, however, no experimental data points occur between 15.3 kg/s and 20.5 kg/s). For both test series, the calculated water downflow rates are slightly higher than the data in the region close to complete carryover and lower than the data in the lower steam flow region. [

]

Without the CCFL model, the steam flow rate for complete liquid carryover is calculated to be 55 kg/s and 24 kg/s, respectively, for the high-pressure and low-pressure cases. Complete water downflow is calculated to occur below the steam mass flow rate of 18.5 kg/s for the low-pressure case and below 40.2 kg/s for the high-pressure case. This is not supported by the

experimental data and is not conservative. [

]

The calculated results without the CCFL model show that the interphase friction package alone cannot properly calculate the countercurrent flow phenomena at the steam generator inlet plenum. [

]

4.3.1.12 CCTF Tests

The Cylindrical Core Test Facility (CCTF) Core-II Test Series was undertaken to provide a major and useful data base of LBLOCA reflood behavior in PWRs. Of particular interest were the simulations of reflood behavior after a LBLOCA in W 4-loop PWRs in which ECC is injected into the cold leg. CCTF is a full-height, 1/21 scale model of the primary coolant system of a 4-loop PWR plant. The facility was designed to reasonably simulate the flow conditions, including ECC flow behavior in the downcomer, and reactor core responses in the primary system of a PWR during the refill and reflood phases of a LOCA. Details of the CCTF assessments are reported in Section 3.12 of Reference 5.

The objective of these assessments is to ascertain S-RELAP5's capability to simulate reflood transients in conjunction with FRA-ANP RLBLOCA modeling guidelines. Therefore, the nodalization, time step, and other input parameters are set to those defined in the modeling guidelines (Reference 12) and all LBLOCA uncertainty multipliers are set to the nominal value of 1.0.

Four of the 29 tests (tests 54, 62, 67, and 68) were chosen as a diverse sample of behaviors to evaluate the performance of the model during vessel reflood. These CCTF tests were representative of a series of CCTF system gravity reflood tests with certain aspects of refill included. Calculations of these tests provide an understanding of key reflood phenomena and comparisons of predicted (calculated) and experimental (measured) results for assessment of various S-RELAP5 thermal-hydraulic models and their dynamic interactions. Table 4.11 summarizes the key test parameters of the four tests.

Table 4.12 shows that S-RELAP5 with an input model built on the current RLBLOCA modeling guidelines generates PCT that range from an overprediction by 157 K for the case with the worst agreement to an underprediction of the PCT by 17 K for the case with the best agreement.

4.3.1.12.1 Test Run 54

Test Run 54 simulated the reflood phase of a cold-leg ECC injection PWR LOCA with a nominal decay power (i.e., without augmenting American Nuclear Society (ANS) 1971 draft standard decay power by 20%), a system pressure of 0.2 MPa, and a low-pressure coolant injection (LPCI) flow rate of 0.011 m³/s.

The broken-loop hot-leg (BLHL) mass flow rate is in reasonable agreement with the data, but the calculated pump-side break mass flow rate, on average, is below the data by about 30%. The vessel-side break mass flow rate was not measured. Therefore, it is not possible to use vessel-side break mass flow rate comparisons to assess ECC bypass to the break. The good agreement between the calculated and the measured steam mass flow rates in the intact-loop hot legs (ILHL) indirectly indicates that the appropriate vapor generation rate is calculated in the core region. The calculated void fractions in the ILHLs and BLHLs are lower than the voiding shown by the data. The calculated void fraction in the intact-loop cold legs (ILCL) after the switch of ECC injection from accumulator core coolant (ACC) to LPCI also is lower than the measured data. This may be caused, in part, by observed inconsistencies among measured loop mass flow rates and poor calibrations of void fraction measurement (the void fraction was measured to be below 1.0 in the hot legs during the initial heatup period). Another possible cause could be a slight elevation change in the test facility that allowed the liquid to drain back into the downcomer resulting in a large data uncertainty for a small liquid fraction (below 5%) and stratified flow conditions. Therefore, no conclusion can be drawn about entrainment and deentrainment from the comparison of loop void fractions. In the cold-leg ACC injection period, the calculated void fraction in the ILCL agrees well with the data, indicating that the appropriate condensation rate is calculated in the cold leg under the accumulator ECC injection conditions.

Both the calculations and data show no asymmetrical or multidimensional effects of downcomer ECC penetration, mainly because no back steam flow occurs from the core to the downcomer. The lack of upward steam flow in the downcomer also precludes the issue of scaling on the downcomer ECC penetration behavior. The calculated downcomer differential pressure agrees

reasonably well with the data particularly during the accumulator injection period. Except for a short period of slightly lower calculated values after the switch from ACC injection to LPCI and slightly lower predictions later in the reflood period, the calculated core differential pressure is in good agreement with the data, indicating that the overall liquid inventory in the core is calculated properly. Another important parameter for the reflood process is the steam temperature in the core. Unfortunately, the steam temperature instrumentation did not correctly measure the superheated steam temperature in a steam-water mixture environment.

The heater-rod temperature histories are conservatively calculated, particularly for the high power rod bundles. At elevations above the mid-plane of the high-power rod bundles, the calculated temperature rise is somewhat higher and the calculated temperature rise period is longer, partly because of the over- and undercooling calculated for the accumulator ECC injection. The over- and undercooling sequence is partly attributable to the sudden and large system depressurization caused by the strong condensation associated with the ACC injection. The calculated PCT is 1147 K (1605 F) at 2.44 m elevation at approximately 257 seconds, compared to the measured PCT of 1113 K (1544 F) at 1.83 m at 130 seconds. The higher value of PCT at a higher elevation and later time is consistent with the general hydrodynamic behavior calculated by S-RELAP5. Figure 4.129 compares calculated versus measured maximum temperatures with core elevation for CCTF Test 54.

In summary, the assessment results have shown that the S-RELAP5 code calculates the important reflood phenomena occurring in the CCTF Reflood Test Run 54 well (reasonable or better agreement with data). The assessment demonstrates the successful application of S-RELAP5 to PWR LOCA analyses to support the conclusion that S-RELAP5 will produce acceptable licensing simulations of reflood behavior during the postulated LOCA of a cold-leg-injection PWR.

4.3.1.12.2 Test Run 62

Test Run 62 simulated the reflood phase of a cold-leg ECC injection PWR LOCA with a high decay power (i.e., augmenting ANS 1971 draft standard decay power by 20%), a system pressure of 0.2 MPa, and an LPCI flow rate of 0.011 m³/s.

The calculated pump-side break mass flow rate again is low by about 30% on average. The vessel-side break mass flow rate was not measured. Therefore, using vessel-side break mass

flow rate comparisons to assess ECC bypass to the break is not possible. The good agreement between the calculated and the measured steam mass flow rates in the ILHLs indirectly indicates that the appropriate vapor generation rate is calculated in the core region. The calculated void fractions in the ILHLs and BLHLs are lower than the data void fractions. The calculated void fraction in the ILCLs after the switch of ECC injection from ACC to LPCI also is lower than the measured data. This may be caused, in part, by observed inconsistencies among measured loop mass flow rates and poor calibrations of void fraction measurement (the void fraction was measured to be below 1.0 in the hot legs during the initial heatup period). Another possible cause could be a slight elevation change in the test facility that allows the liquid to drain back into the downcomer, resulting in large data uncertainty for small liquid fraction (less than 5%) and stratified flow conditions. Therefore no conclusion can be drawn about entrainment and deentrainment from the comparison of loop void fractions. In the cold-leg ACC injection period, the calculated void fraction in the ILCL agrees well with the data, indicating that an appropriate condensation rate is calculated in the cold leg under the accumulator ECC injection conditions.

Both the calculations and data show no asymmetrical or multidimensional effects of downcomer ECC penetration, mainly because no back steam flow occurs from the core to the downcomer. The lack of upward steam flow in the downcomer also precludes the issue of scaling on the downcomer ECC penetration behavior. The calculated downcomer differential pressure agrees reasonably well with the data particularly during the accumulator injection period. Except for a short period of slightly lower calculated values after the switch from ACC injection to LPCI, the calculated core differential pressure is in good agreement with the data, indicating that the overall liquid inventory in the core is properly calculated. Another important parameter for the reflood process is the steam temperature in the core. Unfortunately, the steam temperature instrumentation did not correctly measure the superheated steam temperature in a steam-water mixture environment.

The heater-rod temperature histories are well calculated, particularly for the high-power rod bundles. At elevations above the mid-plane of the high-power rod bundles, the calculated temperature rise is somewhat higher and the calculated temperature rise period is longer, partly because of the over- and undercooling calculated for the accumulator ECC injection. The over- and undercooling sequence is partly attributable to the sudden and large system depressurization caused by the strong condensation associated with the ACC injection. The

calculated PCT is 1241 K (1774 F) at 2.44 m elevation and 317 seconds, compared to the measured PCT of 1132 K (1578 F) at 2.38 m and 154 seconds. The higher value of PCT at a higher elevation and later time is consistent with the general hydrodynamic behavior calculated by S-RELAP5. Figure 4.130 shows the comparison of calculated versus measured maximum temperatures with core elevation for CCTF Test 62.

In summary, the assessment results have shown that the S-RELAP5 code calculates the important reflood phenomena occurring in the CCTF Reflood Test Run 62 with reasonable agreement to data. The assessment demonstrates the successful application of S-RELAP5 to PWR LOCA analyses to support the conclusion that S-RELAP5 will produce acceptably conservative licensing simulations of reflood behavior during the postulated LOCA of a cold-leg injection PWR.

4.3.1.12.3 Test Run 67 Description

Test Run 67 simulated the reflood phase of a cold-leg ECC injection PWR LOCA with a high decay power (i.e., augmenting ANS 1971 draft standard decay power by 20%), a lowered system pressure of 0.15 MPa, and an LPCI flow rate of 0.011 m³/s.

Again, the calculated pump-side break mass flow rate is low by about 30% compared with the data. The vessel-side break mass flow rate was not measured. Therefore, vessel-side break mass flow rate comparisons cannot be used to assess ECC bypass to the break. The good agreement between the calculated and the measured steam mass flow rates in the ILHLs indirectly indicates that the appropriate vapor generation rate is calculated in the core region. The calculated void fractions in the ILHLs and BLHLs are lower than the data void fractions. The calculated void fraction in the ILCLs after the switch of ECC injection from ACC to LPCI also is lower than the measured data. This may be caused, in part, by observed inconsistencies among measured loop mass flow rates and poor calibrations of void fraction measurement. The void fraction was measured to be below 1.0 in the hot legs during the initial heatup period. This resulted in a large data uncertainty for a small liquid fraction (below 5%) and stratified flow conditions. Therefore, no conclusion can be drawn about entrainment and deentrainment from the comparison of loop void fractions. In the cold-leg ACC injection period, the calculated void fraction in the ILCL agrees well with the data, indicating that the appropriate condensation rate is calculated in the cold leg under the accumulator ECC injection conditions.

Both the calculations and data show no asymmetrical or multidimensional effects of downcomer ECC penetration, mainly because no back steam flow occurs from the core to the downcomer. The lack of upward steam flow in the downcomer also precludes the issue of scaling on the downcomer ECC penetration behavior. The calculated downcomer differential pressure agrees reasonably well with the data during the accumulator injection period in particular. Except for a short period of slightly lower calculated values after the switch from ACC injection to LPCI, the calculated core differential pressure is in good agreement with the data, indicating that the overall liquid inventory in the core is properly calculated. Another important parameter for the reflood process is the steam temperature in the core. Unfortunately, the steam temperature instrumentation did not correctly measure the superheated steam temperature in a steam-water mixture environment.

The heater-rod temperature histories are conservatively calculated, particularly for the high-power rod bundles. At elevations above the mid-plane of the high-power rod bundles, the calculated temperature rise is much higher and the calculated temperature rise period is longer, partly because of the over- and undercooling calculated for the accumulator ECC injection. The over- and undercooling sequence is partly attributable to the sudden and large system depressurization caused by the strong condensation associated with the ACC injection. The calculated PCT is 1300 K (1880 F) at 2.44 m elevation and 304 seconds, compared to the measured PCT of 1143 K (1598 F) at 1.83 m and 164 seconds. The higher value of PCT at a higher elevation and later time is consistent with the general hydrodynamic behavior calculated by S-RELAP5. Figure 4.131 compares calculated versus measured maximum temperatures with core elevation for CCTF Test 67.

In summary, the assessment results have shown that the S-RELAP5 code calculates the important reflood phenomena occurring in the CCTF Reflood Test Run 67 acceptably well. The assessment demonstrates the successful application of S-RELAP5 to PWR LOCA analyses to support the conclusion that S-RELAP5 will produce acceptable licensing simulations of reflood behavior during the postulated LOCA of a cold-leg injection PWR.

4.1.3.12.4 Test Run 68

Test Run 68 simulated the reflood phase of a cold-leg ECC-injection PWR LOCA with a nominal decay power (without augmenting the ANS 1971 draft standard decay power by 20%), a system pressure of 0.2 MPa, and an increased LPCI flow rate of 0.025 m³/s.

Both the calculated pump-side break mass flow rate and the calculated BLHL mass flow rate are in good agreement with the data, however the measured results are suspect because they show relatively large negative flow rates during the initial heat-up (refill) phase. The vessel-side break mass flow rate was not measured. Therefore, vessel-side break mass flow rate comparisons cannot be used to assess ECC bypass to the break. The good agreement between the calculated and the measured steam mass flow rates in the ILHLs indirectly indicates that the appropriate vapor generation rate is calculated in the core region. The calculated void fractions in the ILHLs and BLHLs are lower than the data void fractions. The calculated void fraction in the ILCLs after the switch of ECC injection from ACC to LPCI also is lower than the measured data. This may be caused, in part, by observed inconsistencies among measured loop mass flow rates and poor calibrations of void fraction measurement. The void fraction was measured to be below 1.0 in the hot legs during the initial heatup period. This resulted in a large data uncertainty for a small liquid fraction (below 5%) and stratified flow conditions. Therefore, no conclusion can be drawn about entrainment and deentrainment from the comparison of loop void fractions. In the cold-leg ACC injection period, the calculated void fraction in the ILCL agrees well with the data, indicating that an appropriate condensation rate is calculated in the cold leg under the accumulator ECC injection conditions.

Both the calculations and data show no asymmetrical or multidimensional effects of downcomer ECC penetration, mainly because no back steam flow occurs from the core to the downcomer. The lack of upward steam flow in the downcomer also precludes the issue of scaling on the downcomer ECC penetration behavior. The calculated downcomer differential pressure agrees reasonably well, \cong 12% lower than the data shows. The calculated core differential pressure is in good agreement with the data providing an indication that overall liquid inventory in the core is properly calculated. Another important parameter for the reflood process is the steam temperature in the core. Unfortunately, the steam temperature instrumentation did not correctly measure the superheated steam temperature in a steam-water mixture environment.

The heater-rod temperature histories are in excellent agreement, particularly for the high-power rod bundles. At elevations above the mid-plane of the high-power rod bundles, the calculated temperature rise is somewhat lower and the calculated temperature rise period is generally longer, partly because of the over- and undercooling calculated for the accumulator ECC injection. The over- and undercooling sequence is partly attributable to the sudden and large system depressurization caused by the strong condensation associated with the ACC injection.

The calculated PCT is 1105 K (1529 F) at 2.44 m elevation and 210 seconds, compared to the measured PCT of 1122 K (1560 F) at 1.83 m and 164 seconds. The higher value of PCT at a higher elevation and later time is consistent with the general hydrodynamic behavior calculated by S-RELAP5. Figure 4.132 compares the calculated versus measured maximum temperatures with core elevation for CCTF Test 68.

In summary, the assessment results have shown that the S-RELAP5 code calculates the important reflood phenomena occurring in the CCTF Reflood Test Run 68 with reasonable agreement to data. The assessment demonstrates the successful application of S-RELAP5 to PWR LOCA analyses to support the conclusion that S-RELAP5 will produce acceptable licensing simulations of reflood behavior during the postulated LOCA of a cold leg injection PWR.

4.3.1.13 SCTF Tests

The Slab Core Test Facility (SCTF) Core-II Test Series was undertaken in part to obtain information that could be used to assess thermal hydraulic models in best estimate, evaluation models and other computer codes. The intent for these assessments was to use the SCTF-II test series to assess the accuracy of the S-RELAP5 computer code. Six tests from the series of 19 were chosen as a diverse sample of behaviors to evaluate the performance of the model during vessel reflood phenomena. The present study has two objectives: to assess the code's capability of simulating both forced and gravity reflood transients and to study the effect of radial nodalization on reflood behavior. Details of the SCTF assessment calculations are presented in Section 3.11 of Reference 5.

The SCTF test program is designed to investigate the two-dimensional (2D) thermal-hydraulic behaviors in the pressure vessel during the reflood phase of a PWR LBLOCA. To meet this objective, SCTF simulates a full-radius slab section of a PWR with eight bundles arranged in a row. The heating power for each bundle can be controlled independently.

In the SCTF test, the following two test modes were adopted: gravity feed with the ECC injection into the cold leg, and forced feed with ECC injection into the lower plenum by closing the bottom of the downcomer. Although the first mode is considered to be a better simulation of integral reactor behavior, the boundary conditions at the core inlet (mass flow rate and subcooling) are affected by parameter changes (change of system pressure and core heating, etc.). Therefore, to investigate the effect of the parameter changes on the 2D thermal-hydraulic

behaviors in the pressure vessel, the forced feed test mode was adopted to obtain more accurate boundary conditions at the core inlet.

The tests that were modeled in the calculation assessments were two "gravity reflood" tests (Tests S2-SH1 and S2-AC1) and four "forced reflood" tests (Tests S2-10, S2-11, S2-17, and S2-18). The S2-SH1 test is the SCTF-II gravity-reflood base-case test. During Test S2-SH1, the downcomer was not blocked from the lower plenum (i.e., hydraulic communication existed between the lower plenum and the downcomer). A combination of lower plenum injection and cold leg injection was used in Test S2-SH1. Test S2-AC1 differs from Test S2-SH1 in the ACC injection rate and duration.

The S2-10 test is the SCTF-II forced-reflood base case. In Test S2-10, ECC was injected into the lower plenum only, with no hydraulic communication between the lower plenum and the downcomer. The ECC injection rate was specified to match the core inlet flow rate achieved in the gravity feed test S2-SH1. Test S2-11 differs from S2-10 in that a high ACC flow rate was used to simulate test S2-AC1.

Test S2-17 and S2-18 are also forced reflood tests with the primary difference being in the radial power distribution. Test S2-17 has a flat power profile and Test S2-18 has a steep power profile with test conditions similar to a standard plant. The S2-18 test has a power profile that is consistent with the RLBLOCA methodology NPP nodalization (Reference 12). The assessment of these two tests with their widely different radial power distributions provide a good test for the S-RELAP5 code and NPP nodalization.

Table 4.13 shows the test conditions for each of the tests examined. The six SCTF Core-II reflood experiment tests were selected to assess forced reflood, gravity reflood, and the effect of radial nodalization. The assessment matrix is summarized as follows:

- Forced vs. Gravity Reflood (Phase I). In this assessment phase, two sets of counterpart tests were chosen to study the differences between forced and gravity reflood. The first set is consists of Tests S2-11 and S2-AC1 and the second set consists of Tests S2-10 and S2-SH1. A nominal nodalization of two bundles per core channel was modeled for this study.
- Effect of Radial Nodalization (Phase II). In this assessment phase, two tests were chosen to study the effect of radial nodalization on reflood behavior. These tests are S2-18 and S2-17. Three different nodalizations were used: the nominal nodalization, a fine-nodalization of one bundle per channel, and a plant-consistent nodalization (Reference 12).

Phase I Assessment Results: Forced vs. Gravity Reflood.

This phase studies the comparison between forced and gravity reflood for the same test conditions. The pair S2-11 and S2-AC1, the flooding rate is about 17.4 cm/s during ACC reflood and 1.6 cm/s during LPCI reflood and represent the highest combined injection rate in the SCTF-II test matrix. For Test S2-11, the calculated responses show reasonable agreement with the data except at the top elevations. At the two topmost elevations, the data show prolonged heat up when the calculation predicted quenching. The vessel pressure agreement is reasonable. The pressure in the vessel increases at the point of ECC injection because of steam generation. The extent of pressurization depends on the rate of steam venting through the hot leg. The vessel void fraction calculated results exhibit large oscillations, typical of reflood simulation. The average behavior follows the data trend.

For Test S2-AC1, the agreement between calculation and data is better than that observed in Test S2-11. In particular, the quench time along the heated length is better predicted at all elevations shown. The cladding temperature prediction at the two uppermost elevations also is better than for S2-11. However, the peak vessel pressure was overpredicted.

For S2-10 and S2-SH1, the flooding rate is about 3.7 cm/s during ACC reflood and 1.8 cm/s during LPCI reflood. These tests represent the lowest combined injection rate in the SCTF-II test matrix. The calculation is in reasonable agreement with the data for both tests.

The comparison of calculated and measured PCT and quench time for the Phase I assessments are presented in Table 4.14. The quench time was predicted to occur earlier than the data for both the high and low flooding rate tests. Thus, the quench front was predicted to advance faster than the data for these tests. For test S2-10, the PCT was overpredicted and for S2-SH1, the PCT was underpredicted. Conversely the time of PCT was overpredicted in S2-10 and underpredicted in S2-SH1.

In summary, the Phase I assessments show that S-REALP5 can simulate both forced and gravity reflood transients. The PCT for counterpart tests, S2-11 and S2-AC1 and Tests S2-10 and S2-SH1, have good agreement with data. For high and low flooding rates, the PCT was predicted within 55 F or less (good agreement with data).

Phase II Assessment Results: Effect of Radial Nodalization

This phase studies the effect of radial nodalization on the reflood behavior during a postulated LBLOCA incident. Tests S2-17 and S2-18 were selected for this study. The ACC flooding rate for Test S2-17 is about half of that for Test S2-18, while the LPCI flooding rates are about the same for both tests. The major difference between these two tests is in the core power distribution. Test S2-17 has uniform power across the core (all at 890 kW). Test S2-18 has a significant radial power distribution, with the peak bundle power (1210 kW) about twice as much as the peripheral bundle power (676 kW). The total power level for the two tests is almost the same (7120 kW for S2-17 versus 7118 kW for S2-18). The distribution of radial power renders these two tests ideal for studying core radial nodalization.

[

]

The input models for the individual nodalization and the plant-consistent nodalization were developed from the base model having the nominal nodalization. Three primary modifications are required:

- [

]

- [

]

• [

]

Figures 4.133 and 4.134 show typical measured temperature transients near the core midplane for SCTF tests 17 and 18, respectively. These figures also compare the calculated temperature transients for the individual assembly and plant consistent nodalizations. These and comparisons of temperature transients at other elevations for both tests show that the differences in radial nodalization have minimal impact on the cladding temperature results (Reference 5). In particular, the fluid conditions seen by the "hot" rod must be similar to produce the similar cladding temperature responses.

Table 4.15 summarizes the Phase II assessment results for the calculation with the highest PCT from the nodalization studies. For Test S2-17 the highest PCT is for the individual assembly nodalization and for Test S2-18 it is the RLBLOCA plant consistent nodalization. For both tests the PCT and bundle quench time is underpredicted relative to the data. However, the time of PCT is underpredicted for Test S2-17 and overpredicted for Test S2-18.

These results confirm that the use of the plant nodalization scheme is adequate to capture the PCT response. [

]

4.3.1.14 ACHILLES Tests

International Standard Problem Number 25 (ISP 25) is based on a test in the ACHILLES facility that simulated the latter phase of accumulator injection during a LOCA. ISP 25 tests the ability of system codes to be evaluated for the impact of the nitrogen cover gas in the accumulator on the LBLOCA. The accumulators in a PWR are pressurized with nitrogen. When the system pressure falls below the nitrogen pressure, the borated water from the accumulator flows into the primary system. When the accumulators empty of liquid, the nitrogen cover gas enters the primary coolant system where it flows to the upper part of the downcomer and causes the pressure to increase. The increased pressure depresses the liquid level in the downcomer, resulting in a surge of water into the core. The nitrogen gas bypasses the core and flows out through the break, and in a few seconds the upper downcomer pressure drops, the downcomer level recovers, and the nitrogen has no further effect on the transient.

The difference between a pressurization surge caused by steam and one caused by nitrogen is that the nitrogen does not condense. Thus, the nitrogen can act like a large piston pushing the fluid into the core. For the realistic LBLOCA methodology, it is important that the code does not overpredict the surge into the core and the transient cooling caused by this in-surge, thereby leading to an underprediction of PCT. The ability of S-RELAP5 to predict both system and fuel temperature responses was confirmed by comparing the calculated values to the measurements.

The ACHILLES test facility is designed to simulate the latter stages of accumulator injection in an LBLOCA. The simulated downcomer is connected to the bottom of the core and a valve is closed, before nitrogen injection begins, to hold the water in the downcomer until injection occurs. Another valve is open before injection begins and provides a flow path for the pumped water so that it does not enter the core. This valve closes on initiation of nitrogen injection. The simulated core has 69 simulated fuel rods with a geometry similar to that of a W 17 x 17 design. The simulation core has 8 spacer grids. The rods are housed in a piece of pipe. The exit region has a centrifugal separator to collect carryover water. The steam then joins the nitrogen bypass flow and exits.

The nitrogen tank is connected to the top of the simulated downcomer, and a valve, which is initially closed, opens to initiate the nitrogen flow. Nitrogen forces flow through the core by increasing the pressure on the downcomer. Nitrogen also flows through a bypass path to join the steam that has passed through the core, then it exits. A flowmeter measures the nitrogen flow from the tank and another flowmeter measures the bypass flow.

Each simulated fuel rod has multiple thermocouples on the surface of the rod. The PCT level (2.13 m) is the most heavily instrumented, with 66 thermocouples.

Achilles ISP 25 was analyzed using S-RELAP5 modeling consistent with the realistic LBLOCA methodology. S-RELAP5 was able to accurately predict the liquid surge into the core, liquid carryover to the upper plenum, and rod thermocouple readings. In particular, the surge into the core when the nitrogen flow is initiated is never overpredicted.

Predicted PCTs are good to excellent, which clearly is an acceptable outcome in light of the radial flow inhomogeneities observed in the Achilles test.

As the appropriate valves are operated to initiate the event, an immediate pressure transient occurs at the top of the downcomer. The initial pressurization of the downcomer causes a rapid surge of liquid into the simulated core. As the nitrogen leaves the system via the bypass, the pressure drops at the top of the downcomer, the levels in the core and downcomer recover, and the core reflooding now depends on the pumped water flow, which is entering both the downcomer and the core.

Figure 4.135 presents the range of variation in the thermocouples at the PCT elevation (2.13 m). The wide variation shown is not a consequence of power variation because the rods all are the same power. Three rods set the lower bound and all three of these rods are located next to the shroud in the test assembly. The early quench indicates that the flow field near the shroud is far different from that in the interior.

The remaining rods can be divided into a group that tracks the maximum fairly well and a group that falls well below the maximum, but not as dramatically as the three rods setting the lower limit. Thus, the test data shows that to get a reasonable prediction of core temperatures requires a multidimensional analysis.

The radial inhomogeneity is greater than would be experienced in a large-scale reactor core because the flow path on the periphery has hydraulic properties that are significantly different from the interior flow paths. While a reactor core is anisotropic and inhomogeneous, it does not have the range of variations this test assembly has. Thus, predicting the reflood behavior for this test assembly is significantly more challenging than for a PWR core.

For the S-RELAP5 assessments, the central 21 rods in the test assembly were modeled as one channel and the remaining 48 rods and the shroud were modeled as the other channel using the TWODEE component. The comparisons to data were made by comparing the predictions for the central channel with the measured values for the same 21 rods.

Calculated nitrogen flow rate was compared to measured results. The agreement is excellent until frost forms in the throat of the venturi at about 7 seconds (Reference 5). The time-to-empty agrees to within about 2 seconds. The calculated flow spikes a little early compared to the measured flow and then is slightly lower for the remainder of the blowdown.

The calculated liquid carryover at the core exit was compared to the measured carryover. The agreement with data is good, with the major discrepancy coming from the measured burst of flow at 20 to 50 seconds and the subsequent cessation of all liquid flow at the exit for nearly 50 seconds. Nothing in the thermocouple data distinguishes this time period.

The steaming rate at the core exit shows good agreement between the calculations and the measured data.

The downcomer level measurements generally are higher than the calculated results, indicating that the pressure drop through the core and the two sets of separators probably is higher than is modeled. No attempt was made to match this level because the core collapsed level, which is not very sensitive to pressure drop variations, matches quite well.

Calculated temperatures for the central region were compared to measured temperatures for the 21 rods in the middle of the assembly. The maximum, minimum, and average temperatures were compared with the calculated temperature for elevations from 1.08 m to 3.18 m. The calculated values are generally in good agreement with the measured values. The PCT elevation is 2.13 m and, at this elevation, the calculated PCT is about 30 K lower than the measured values. At all other elevations, the calculated peak temperature exceeds the measured values.

The impact of the nitrogen injection, which is the focus of this assessment, can be seen in the first 25 seconds of the transient. Figures 4.136 to 4.141 show the temperature comparisons on expanded time and temperature scales to emphasize the nitrogen effects. The rod thermocouples all show a transient temperature reduction at the beginning of the event. This initial cool-down is caused by the nitrogen in-surge that initiates the event. S-RELAP5 calculates a conservatively small cool-down compared to the data. In all cases, the calculated downward temperature transient accompanying the nitrogen injection is smaller than the measured temperature decrease, indicating that S-RELAP5 underpredicts the cool-down due to the nitrogen injection.

4.3.1.15 Multi-Dimensional Flow Testing

Flow blockage tests were performed using simulated pressurized water reactor (PWR) fuel assemblies (Reference 5). These tests provided data on single-phase flow redistribution for non-uniform inlet and outlet conditions. S-RELAP5 has a two-dimensional component used to

model multidimensional flows. These flow blockage tests have been used as a basis for evaluating the two-dimensional component in S-RELAP5. The comparisons to the measured data and to other codes that have been approved for flow distribution calculations show that the two-dimensional component in S-RELAP5 can be used to model multidimensional flow problems.

The S-RELAP5 assessment of these tests are presented in detail in Section 3.13 of Reference 5. No bias or uncertainty is derived from this assessment.

4.3.1.15.1 Summary

The radial flow split distributions of axial velocities calculated by S-RELAP5 show good agreement with data for all three tests considered. The comparison of S-RELAP5 with flow blockage data shows that the two-dimensional model in S-RELAP5 is sufficient to describe flow redistribution in multidimensional problems, and that it does as well as thermal-hydraulic design codes used for PWR core analysis in predicting the flows for these blockage tests (Reference 5).

4.3.1.15.2 Test Descriptions

The test assembly consists of two simulated PWR assemblies with a pin array representative of a 15 x 15 fuel assembly. The simulated assemblies are about 38 in long and are enclosed in a rectangular canister. For the bulk of the testing, the gap between the two simulated fuel assemblies was left open, but for some tests a perforated plate was inserted between the two simulated fuel assemblies. Because of the detail of the measurements and the nearly prototypic geometry (in the radial, or x-y, direction), these tests have become a standard benchmark test for flow redistribution codes.

The tests consisted of introducing asymmetric flow in the inlet region and measuring flow recovery in the bundle with a series of pitot tube arrays. The pitot tubes measure flow velocities at many points in each plane. The first array is 2.5 in above the inlet. The remainder are located at 5-in intervals, with the last one at 32.5 in level.

For the test series without a perforated plate between the two assemblies, two different test configurations were evaluated. The first configuration (Test 1) has a nominal 1100 gpm entering one fuel assembly and 550 gpm in the other. The second configuration (Test 2) has

one inlet blocked and a nominal 1500 gpm entering the other. In both cases, the exits are open. The case with the perforated plate inserted between the two assemblies (Test 3) has the inlet and outlet blocked on one assembly and has a nominal inlet flow of 1300 gpm.

4.3.1.15.3 Input Description

The test section was modeled in S-RELAP5 as a TWODEE component with 10 vertical (x) volumes and 14 horizontal (y) volumes. This, in effect, collapses the test assembly in the direction perpendicular to the asymmetric flows. Selection of 14 horizontal volumes resulted in volumes that corresponded to the pitot tube measurements. The vertical volumes had lengths that made the first volume match the bottom of the rodded region (4.5 in) and each of the others matches the elevation of a velocity measurement point (pitot tube location).

4.3.1.15.4 Results

A review of the data for Test 1 indicates that the real flows were probably 1138 gpm and 512 gpm for Bundles A and B, respectively. Figure 4.142 provides a comparison of the measured and calculated flow distributions at the last set of pitot tubes. The reported axial fluid velocities were calculated by S-RELAP5 with inlet flows of 1138 and 512 gpm. The measured velocities are almost all higher than the S-RELAP5 velocities at this level. Figure 4.143 compares the reported mass flow fraction in the high flow bundle, Bundle A, with that calculated by S-RELAP5.

A review of the data for Test 2 indicates the real inlet flow was probably 1281 gpm, rather than the nominal 1500 gpm for the test. This value was used in the S-RELAP5 model. Figure 4.144 compares the S-RELAP5 velocity distributions with the reported axial fluid velocities at the last set of pitot tubes. In general, the agreement is excellent. The largest discrepancy occurs on the side of the blocked bundle next to the wall. Here, S-RELAP5 calculates more of a tendency to back flow. The measurement velocities, which are based on pitot tube readings, show that the flow stops near the wall.

Figure 4.145 compares the fractional flow in the unblocked bundle, Bundle A. The agreement is good over most of the axial height of the bundle. Near the exit, the measured flow was nearly equal for the two bundles. The calculated flow distribution is still about 60/40 for S-RELAP5. The overall agreement is good.

Figure 4.146 compares the reported axial fluid velocities for Test 3 to those calculated by S-RELAP5. The agreement for these data is excellent for this and all levels. The most notable difference is the tendency of S-RELAP5 to predict reverse flow near the wall in the blocked assembly, very similar to the result in Test 2.

To assess the quality of the comparison to data, the XCOBRA-IIIC and THINC-IV flow predictions for Tests 1 and 2 were compared to the S-RELAP5 flow predictions. Figure 4.145 compares the S-RELAP5 calculations with the XCOBRA-IIIC calculations, the THINC-IV calculations, and the data for Test 1. The flow distribution calculated by S-RELAP5 is clearly in the best agreement with the data.

4.3.1.15.5 Conclusions

A series of flow blockage tests was analyzed using the two-dimensional component in S-RELAP5. S-RELAP5 was able to calculate the axial flow redistribution within the two test assemblies. Overall, S-RELAP5 does as well as, or better than, core flow distribution codes used for core flow and subchannel analysis of PWR cores. Calculated results were generally in reasonable agreement with the data.

4.3.2 Integral Effects Tests (IET)

The SETs presented in Section 4.3.1 assess the code capability and provide information to quantify the uncertainty to predict specific phenomena identified by the PIRT. In addition to the SETs, assessments are performed of integral effects tests (IET) to evaluate the overall code capabilities to predict the integrated LOCA scenario and the interacting phenomena in facilities of differing scale. Some of the facilities discussed with the SETs, such as SCTF, CCTF, and UPTF are large scale and include integral interacting-phenomena effects. However, these tests are still limited in that only a portion of the LOCA scenario is addressed. For this reason, FRA-ANP regarded these as separate effects tests.

Integral tests covering the entire LBLOCA scenario have been performed in the loss-of-fluid test (LOFT) facility, and the smaller scale Semiscale test facility. FRA-ANP has performed assessments of tests from both of these facilities. These assessments are reported in detail in Reference 5 and are summarized in the following sections.

4.3.2.1 LOFT Assessments

Assessments of the LOFT Tests L2-3, L2-5, LP-02-6, and LP-LB-1 were performed to justify the use of FRA-ANP's Realistic LBLOCA methodology and the S-RELAP5 code developed by FRA-ANP for realistic analysis of LBLOCA. This section of the methodology report documents the LOFT assessment calculations with the FRA-ANP RLBLOCA methodology. The assessment results demonstrates the accuracy of the RODEX3A and S-RELAP5 codes and the capability of simulating the LBLOCA phenomena observed during the LOFT tests, and provide assessments of the calculated results versus measured results to satisfy the rule change requirements.

4.3.2.1.1 LOFT Facility

The LOFT facility was designed to simulate a LOCA in a large W 4-loop PWR, and thus, to provide data with which to evaluate the adequacy and to improve analytical methods for analyzing LOCA transient response of a PWR. The LOFT results have been widely used to validate thermal-hydraulic codes that analyze PWR accident and transient phenomena. Key LOFT LBLOCA tests have been included in the CSAU assessment matrix (Reference 4) and RELAP5/MOD3 developmental assessment matrix. LOFT assessments have also been performed to verify RELAP5/MOD2 or MOD3 by various members of the NRC-sponsored International Code Assessment Program (ICAP).

LOFT was an NRC-sponsored nuclear test facility designed to simulate the nuclear and thermal-hydraulic phenomena that take place in a PWR LBLOCA. The LOFT facility was a 50 MWt experimental PWR designed to simulate the system response of a W 4-loop PWR during a hypothetical LBLOCA. The facility included five major subsystems, an intact loop, a broken loop, a reactor vessel, an emergency core cooling system, and a blowdown suppression system. The LOFT facility was instrumented so that system parameters could be measured during the tests.

The LOFT reactor had a single active intact loop that simulated the combined three intact loops of a W 4-loop PWR. The intact loops included an active steam generator, two primary coolant pumps (PCP) in parallel, a pressurizer, a loop seal, and the connecting piping.

The broken loop in the LOFT facility was an inactive flow loop during normal operation. The loop consisted of a hot leg, a steam generator simulator, a pump simulator, and a cold leg. It

became an active flow loop and simulated the broken loop of a 4-loop PWR during LOCA tests. The BLCL was divided into two parts: a pump side, that connected the pump simulator to the blowdown suppression system and the vessel side that connected the vessel downcomer to the blowdown suppression system. The steam generator and pump simulators provided flow resistances representative of a PWR during a LOCA. Both sides of the broken cold legs contained quick-opening blowdown valves (QOBV) that opened to initiate the transient.

The LOFT reactor vessel had an annular downcomer, a lower plenum, below core hardware, a nuclear core, above core hardware, and an upper plenum. The downcomer was connected to the intact and broken cold legs and the upper plenum was connected to the hot legs. The core contained 1300 fuel rods arranged in five square (15 x 15) and four triangular (corner) assemblies with an average linear heat generation rate (LHGR) of about 7.0 kW/ft at full power. The LOFT fuel rods and pitch were typical of a PWR 15 x 15 rod array, except that the active length was 1.68 m (5.5 ft) while that of a PWR is typically 3.66 m (12 ft). For Test LP-02-6, all the fuel rods in the central assembly except the outside row were pressurized with helium to 2.51 MPa (350 psig) and all fuel rods in the peripheral assemblies were unpressurized. In remaining tests, L2-3, L2-5, and LP-LB-1, all of the fuel rods were unpressurized.

The LOFT intact loop had two separate ECCSs connected to the cold leg. Each system contained an accumulator, an HPIS, and an LPIS. Only one ECCS was used during a LOCA test and the other was used as backup for plant protection in case of unplanned emergency situations that might occur during the test. The ECCS was not connected to the broken loop. For the LBLOCA tests, ECC was injected into the ILCL. The HPIS and LPIS were connected to the accumulator injection piping. The LOFT blowdown suppression system consisted of a header and a suppression tank that simulated the PWR containment pressure and temperature environment expected to occur during an LBLOCA.

LOFT was designed with a primary system volume-to-core power ratio similar to that of a PWR. The design objective for the LOFT facility was to produce, on a reduced scale, the significant thermal hydraulic phenomena with representative conditions and a representative sequence of events that could occur in a PWR during postulated LOCAs. Volumetric scaling generally was used for the design of LOFT components. Primary system components (e.g., lower plenum, core region, upper plenum, outlet piping, steam generator, and inlet piping) also were designed with relative volumes equivalent to those in a PWR. LOFT is a reduced-scale facility that is not

uniformly scaled by a consistent scaling criteria. Therefore, scaling distortions exist that must be considered when applying the results of the LOFT tests. Table 4.16 shows the PWR-LOFT scaling ratios to a PWR.

The accumulator gas volume is scaled so that the ratio of accumulator gas volume to accumulator liquid volume injected is made equal to that of a typical 4-loop PWR by adjusting the standpipe height. The LOFT accumulator liquid volume is scaled to represent three of the four accumulators of a typical 4-loop PWR, assuming that the liquid in the fourth accumulator is lost out of the break. The LOFT HPIS flow rate for the LB tests is volume-ratio scaled using the ratio of the LOFT to PWR total primary system fluid volume plus the single failure criterion and the assumption that flow from one of four lines of injection is lost out of the break. The LPIS flow rate is scaled based on the combined downcomer and core flow areas. The single failure criterion and the assumption that flow from one of four injection lines is lost out of the break are also used for LPIS scaling.

The major differences between the LOFT and a 4-loop PWR are summarized as follows:

- The LOFT has one active operating (intact) loop and a passive blowdown (broken) loop with only a steam generator and pump simulator, while a 4-loop PWR has four operating loops.
- The LOFT has two pumps connected in parallel in the operating loop, while a PWR has only a single pump in each loop.
- The LOFT core has a 1.68 m (5.5 ft) active fuel length, while PWR core lengths are at least 3.66 m (12 ft). The axial power distribution of the LOFT core is similar to a beginning-of-life, bottom-skewed power distribution in a PWR core.
- The LOFT has a short steam generator relative to a PWR.
- The LOFT cold leg ECC injection location is very close to the vessel inlet, while the PWR ECC injection lines are located near the pump outlet.
- Axial lengths and elevations of hydraulic components are not preserved relative to a PWR.

The LOFT scaling philosophy was to reduce the component coolant volume and flow areas by the core power ratio. The volume and power scaling was not achieved completely, and vertical scaling was not preserved. Despite these component differences and scaling distortions, the LOFT components were functionally similar to those of a PWR and provide sufficient similarity to permit the LOCA data to be used to validate the S-RELAP5 code for evaluating the PWR LOCA/ECCS performance.

4.3.2.1.2 LOFT Test Descriptions

Between 1976 and 1985, 50 LOFT tests were performed. The LOFT facility was designed primarily for performing LBLOCA tests; however, only five tests, L2-2, L2-3, L2-5, LP-02-6 (L2-6), and LP-LB-1 (LB-1), were LBLOCA tests with a heated nuclear core. The first three LBLOCA tests were sponsored by the NRC and the last two were conducted under the auspices of the OECD sponsored by an international consortium. LP-02-6 was conducted under OECD, but was totally funded and sponsored by the NRC. Test LP-LB-1 was the only LOFT LBLOCA test funded by the OECD consortium. The OECD Test LP-FP-01 also is a LBLOCA test simulating a German-type reactor accident scenario resulting in the fuel rod rupture and gap fission product release. It was therefore categorized as a fission product test rather than an LBLOCA test. Table 4.17 shows the characteristics and parameters of the LOFT nuclear LBLOCA tests.

FRA-ANP selected four LOFT LBLOCEs, L2-3, L2-5, LP-02-6, and LP-LB-1 for assessment with S-RELAP5. All of the selected LOFT tests simulate cold leg guillotine breaks. The major differences between these tests are: L2-3 and L2-5 were initiated from 75% power while LP-02-6 and LP-LB-1 were initiated from near 100% full power and the PCP flywheels were not attached during the coastdown of Tests L2-5 and LP-LB-1, but were attached when the pump speed was above 750 rpm (78.54 rad/s) in Test LP-02-6 and were left running for Test L2-3. These LOFT tests have been used to validate the S-RELAP5 code for the blowdown, refill, and reflood phases of an LBLOCA. The tests were selected for S-RELAP5 assessment for the following reasons.

- The test initial and boundary conditions most closely simulate the "design basis accident" LOCA conditions for typical W 4-loop PWRs.
- Test L2-3 provides scaling data when compared to Semiscale Test S-06-3.
- The LOCA phenomenology for Tests L2-5 and LP-LB-1 are similar to that expected for a W 3-Loop PWR, and the LOCA phenomenology for Test LP-02-6 is similar to that expected for a W 4-Loop PWR.
- Test L2-3 was designated as United States Standard Problem 10 for code assessment by the NRC.
- Test L2-5 was designated as ISP 13 for code assessment by the OECD.

- Other code assessment calculations of L2-5, LP-02-6, LP-LB-1 are available for comparison.

4.3.2.1.3 LOFT Assessment Summary

The LOFT assessment calculations were performed with an input model developed to be consistent with the nodalization used in other assessments and the nodalization to be applied for PWR plant calculations (Reference 12). The philosophy of developing the S-RELAP5 consistent input models is to use a similar nodalization scheme in terms of number and distribution of volumes, junctions, heat structures, and input specifications to represent corresponding components in the LOFT and plant models. Exceptions are made only where significant LOFT geometry differences justify a different, but consistent scheme.

Reference 5 contains detailed comparisons of the results of the LOFT L2-3, L2-5, LP-02-6, and LP-LB-1 tests with calculated results using the FRA-ANP LOCA realistic evaluation model. The LOFT test analytical results demonstrate the ability of S-RELAP5 to realistically simulate the key important system phenomena relevant to an LBLOCA that were observed during the unique LOFT LBLOCA test. These include: (1) system depressurization, (2) core flow reversal and core dry-out, or critical heat flux (CHF), (3) the fuel cladding temperature excursion and peak cladding temperature (PCT), (4) two-phase pump flow and critical flows at the breaks, (5) prevention of core bottom-up quench during the early blowdown period, (6) ECC downcomer penetration and bypass, and (7) core refill, reflood, and final quench.

As shown by the results presented in Reference 5, the FRA-ANP RLBLOCA evaluation model produced results in good agreement with the observations for LOFT Tests L2-3, L2-5, LP-02-6, LP-LB-1. The results are summarized as follows:

- The RODEX3A-calculated fuel initial centerline fuel temperatures were within 10% of the measured data.
- The S-RELAP5 code results provide good agreement with the hydraulic responses of the LOFT tests. That is, the calculated results either were within measured uncertainties, followed the major trends of the data if not within measured uncertainties, or were conservative with respect to the data if the phenomena were not simulated. The intact loop mass flow rates, break flow in the broken loop, and loop volume densities were all well-calculated. Coolant temperatures also were well calculated. Pressurizer draining was overpredicted, but because the pressurizer liquid tended to flow to the broken loop and was

removed from the system, that trend produced conservative results. Calculated pump speeds were accurately predicted up to the time where a two-phase mixture appeared. After that time, the pump speeds were lower than measured and, thus, acceptable.

- The code accurately calculated the thermal response (fuel centerline temperature and cladding temperature). The centerline temperatures closely match the data. The cladding temperature results generally were in reasonable agreement with the measured data. The hot rod PCT is very well calculated, considering test measurement uncertainty. The cladding quench times are significantly delayed with respect to the measured data. The early bottom-up core quenching found in Tests L2-3 and LP-02-6 were not simulated in the code calculations. The upper regions of the core showed delayed dry-out with respect to the test data. However, once the upper regions went through dry-out, the calculated rewet was much later than measured. In general, the code predicted higher than measured temperatures in the middle core region, lower than measured temperatures in the upper core region, and approximately measured temperatures in the lower region. In all cases, the calculated PCT was either within or greater than the measured PCT with analytical uncertainties included.
- The calculated ECC injection rates for the low pressure injection system (LPIS) and accumulator tended to underpredict the measured data and, hence, are acceptable.

4.3.2.1.4 LOFT L2-3 Assessment

Test L2-3 was the second LBLOCA test conducted in the LOFT facility in which the reactor core power provided the primary heat source. The test represented a hypothetical cold leg guillotine break that simulated a double-ended, offset, shear break in a commercial (1000 MWe) 4-loop PWR. The test was initiated at 75% thermal power (36 MWt) and a 12.22 kW/ft maximum linear heat generator rate (MLHGR).

The test was initiated by opening the QOBVs. Reactor scram commenced 0.1 seconds into the transient and was completed 1.6 seconds later, HPIS injection was initiated at 14 seconds, accumulator injection at 17 seconds at 4.18 MPa system pressure, and LPIS injection at 29 seconds. The core was reflooded at 55 seconds. During this test, the primary coolant pumps (PCP) operated continuously throughout the transient and were tripped off at 200 seconds.

The cladding temperature started rising as expected and, after 2 to 3 seconds into the transient, the ILCL mass flow exceeded the broken loop mass flow, causing flow diversion to the downcomer. That process eventually caused a bottom-up rewet of the core and the cladding was quenched momentarily. The conditions for core upflow quickly ceased and the core dry-out and heat-up resumed 10 seconds into the blowdown. The core heat-up continued until sufficient ECC injection caused quenching of the core at 55 seconds. The final rewet pattern was first the bottom, then the top, and finally the middle regions of the core.

The measured PCT was 914.0 K (1185.0 F) and occurred at 5 seconds. As indicated in Reference 5, a bias of $11.4 \text{ K} \pm 16.2 \text{ K}$ ($20.5 \text{ F} \pm 29.2 \text{ F}$) should be applied to the measured PCT to account for the 'fin cooling' effects on the surface mounted thermocouples. Thus the reportable PCT for LOFT L2-3 is 941.6 K (1235.2 F).

The S-RELAP5 LOFT input model for FRA-ANP assessments was developed at FRA-ANP. This model provides detailed thermal and hydraulic representations of all the major LOFT system components. It results from developing an LBLOCA analysis input model that is consistent with the nodalization scheme used in all assessment and PWR LBLOCA plant calculations (Reference 12).

The computer codes used to perform the LOFT assessment calculations were RODEX3A and S-RELAP5. RODEX3A is the FRA-ANP realistic fuel rod thermal-mechanical behavior analysis code. S-RELAP5 is an FRA-ANP-modified version of the INEEL RELAP5/MOD2 and MOD3 codes. The RODEX3A code provides input to calculate the fuel conditions and stored energy for all fuel types modeled by S-RELAP5 at the initiation of the realistic LBLOCA calculation. The RODEX3A models have been integrated with S-RELAP5 to provide a consistent realistic calculation of the thermal-mechanical responses of the fuel rods during the LOCA. The FRA-ANP input prescription (Reference 12) defines the acceptable nodalization, numbering system, and parameter inputs for an S-RELAP5 PWR plant or experimental facility input model.

The LOFT core components modeled by the RODEX3A code are the fuel rod coolant channel, the active fuel column, the gap, the cladding, upper fuel rod plenum free volume, and the fill and released fission gases (for pressurized rods only). The four fuel rod types represented by the S-RELAP5 heat structures differ by power level and initial fill gas pressure. The rod powers are modeled in accordance with the core axial and radial power distributions. The two hot rods and

the hot assembly rod are modeled as pressurized rods while the average core rod is unpressurized for Tests L2-5 and LP-02-6. For Test LP-LB-1, all fuel rods are unpressurized. RODEX3A calculations provide exposure-dependent input to the S-RELAP5 fuel model that calculates initial fuel rod conditions and stored energy. Therefore, pretest power and power histories were included in the initial stored energy calculation. For the analysis presented here, fuel information at 50 hours, as calculated by RODEX3A, was transferred to S-RELAP5.

A steady-state initialization calculation was made to obtain the desired initial conditions for the transient simulation. The calculated and measured initial conditions agree quite well and the calculated initial conditions generally are within the uncertainty band of the measured quantities (Reference 5). The calculated initial broken loop temperature of 560.8 K for the cold leg and 560.5 K for the hot leg come very close to measured values considering the large error bands quoted for the measured data, namely $554.3 \text{ K} \pm 1.8 \text{ K}$ for the cold leg and $565.5 \text{ K} \pm 1.8 \text{ K}$ for the hot leg.

The calculation for this analysis is a simulation of Test L2-3 from 10 seconds before the break initiation at 0 seconds up to 100 seconds. This time interval was chosen because the important phenomena and significant events of L2-3 occurred during this period.

For assessment purposes, the LOCA phenomena of primary interest are as follows:

- Fuel initial stored energy
- System blowdown and depressurization
- PCP performance
- DNB or CHF
- Bottom-up or top-down rewet
- Subcooled and two-phase critical flow through the break
- System refill and ECC bypass
- Core reflood and rod quench
- PCT.

Reference 5 discusses the assessed capability to calculate each of these LOCA phenomena; the details are not repeated here. Figure 4.148 compares the calculated and measured PCT versus core elevation. This figure refers to the PCT as a maximum cladding surface temperature, either calculated or measured at the various locations, during the LOCA transient history. The comparison shows that the calculated temperatures are quite close to the

measured temperatures below the 15-in elevation, much greater than the measurements from 15-in to 44-in elevation, and much lower than measurements above the 44-in elevation. The comparison can be considered acceptable because the calculated temperature trends followed the data trends, although the magnitudes did not compare well, and the calculated temperatures were overpredicted for the high power region. The highest PCT of 942 K (1236 F) was measured at the 15-in elevation while the calculated PCT was 1006 K (1351 F).

4.3.2.1.5 LOFT Test L2-5 Assessment

Test L2-5 was the third LBLOCA test conducted in the LOFT facility in which the reactor core power provided the primary heat source. The test represented a hypothetical cold leg guillotine break that simulated a double-ended, offset, shear break in a commercial (1000 MWe) 4-loop PWR. The test was initiated at 75% thermal power (36 MWt) and a 12.22 kW/ft maximum LHGR.

Operation of the LOFT PCPs differs from a typical PWR in that the LOFT pump rotors are electromagnetically coupled to their flywheel system. It is normal during LOFT tests to uncouple the pumps from their flywheels whenever the pump speed falls below 750 rpm (78.54 rad/s). During the L2-5 test, the two PCPs were tripped at 1 second and disconnected from their flywheels. This provided a rapid pump coast down. This operation of the pumps reduced the flow into the vessel to less than the flow to the break, thus preventing an early bottom-up fuel rod rewet. These simulated conditions are more typical of a 3-loop PWR than a 4-loop PWR. LOFT pumps normally coast down while connected to their flywheels that were designed to represent the normal pump coast down of commercial W 4-loop PWRs.

The Test L2-5 HPIS flow is 58% of Test L2-3 HPIS flow and is 75% of Test LP-02-6 HPIS flow because an improper small break HPIS flow condition was inadvertently specified for Test L2-5. The injections of high and low pressure ECCSs were delayed to 23.9 and 37.32 seconds, respectively, to simulate the expected delay in starting up the emergency power diesel generator to run the ECCS.

Before the transient started, the power level in the reactor core was steadily increased, then held at 36 MW \pm 1.2 MW for about 28 hours. This ensured that an appropriate decay heat power level would be obtained once the control rods were inserted into the reactor core. Test conditions before the beginning of the L2-5 test were as follows.

- The primary intact loop mass flow rate was set at $192.4 \text{ kg/s} \pm 7.8 \text{ kg/s}$.
- The hot leg pressure was $14.94 \text{ MPa} \pm 0.06 \text{ MPa}$.
- The primary coolant system hot and cold leg temperature were held at $589.7 \text{ K} \pm 1.6 \text{ K}$ and $556.0 \text{ K} \pm 4.0 \text{ K}$, respectively.

Test L2-5 was conducted to address conservatism in current licensing analyses. Many W plants are limited by Appendix K LOCA analysis results in which the calculated PCTs are predicted to occur during the reflood portion of the transient. Previous LOFT LB Tests L2-2 and L2-3 revealed that Appendix K requirements may be overly conservative because Appendix K criteria preclude the return to nucleate boiling (rewetting) before the end of blowdown. However, Tests L2-2 and L2-3 demonstrated that system hydraulic behavior can lead to an early rewet of the fuel cladding. This early rewet not only limits the PCT during blowdown [], but also removes a significant amount of stored energy from the fuel rod, thus reducing the reflood PCT. The cladding temperatures during reflood after blowdown rewet will be much lower than those occurring without rewet. Preventing the early rewet provides maximum core stored energy at the end of blowdown, and beginning of refill/reflood.

The test results showed that the early bottom-up core wide rewet that occurred in Tests L2-2 and L2-3 did not occur in Test L2-5 as planned. The PCT was 1078 K (1481 F), and because there was no early rewet and the hot rod temperature was fairly constant over a long period of time, there was no clear demarcation of blowdown and the reflood PCT was clearly the maximum. The cladding completely quenched at $65 \text{ seconds} \pm 2 \text{ seconds}$. The test was complete after LPIS was terminated at 107 seconds .

From Reference 5, a bias of $11.4 \text{ K} \pm 16.2 \text{ K}$ ($20.5 \text{ F} \pm 29.2 \text{ F}$) should be applied to the measured PCT to account for the 'fin cooling' effects on the surface mounted thermocouples. Thus, the reportable PCT for LOFT L2-5 is 1105.4 K (1530.1 F).

A steady-state initialization calculation was performed to reach the desired steady-state conditions for initiating the LOCA calculation. The calculated and measured initial conditions agree quite well and the calculated initial conditions generally are within the uncertainty band of the measured quantities. The calculated initial broken loop temperature of 556.0 K for the cold

leg and 558.0 K for the hot leg come very close to measured values considering the large error bands quoted for the measured data, namely $554.3 \text{ K} \pm 4.2 \text{ }^\circ\text{K}$ for the cold leg and $561.9 \text{ K} \pm 4.3 \text{ }^\circ\text{K}$ for the hot leg. The desired steady-state conditions were successfully achieved and the calculation accurately reached the L2-5 test initial conditions.

For the transient calculation, a short steady-state calculation before the break opening is carried out to ensure that the steady-state initial condition is properly maintained when switching from the steady-state input model to the transient simulation. The calculation for this analysis is a simulation of Test L2-5 from 10 seconds before the break initiation at 0 seconds up to 140 seconds. This time interval was chosen because the important phenomena and significant events of Test L2-5 occurred during this period.

The assessment of S-RELAP5 to predict each of the important LOCA phenomena is presented in detail in Reference 5. Figure 4.149 depicts the final comparison of the calculated and measured PCT versus core elevation. In this figure, the PCT is referred to as a maximum cladding surface temperature, either calculated or measured at the various locations, during the LOCA transient history. The comparison generally shows very good agreement and the differences between the calculated and measured PCT in the high power region between 15-in to 44-in elevations are quite small. Calculations and measurements both show a plateau region between the 15-in and 28-in elevations where maximum PCT occurs. The highest PCT of 1105.4 K (1530.1 F) was measured at the 24-in elevation and the calculated PCT was 1106 K (1531 F).

4.3.2.1.6 LOFT LP-02-6 Assessment

LOFT LP-02-6 was the fourth LOFT nuclear powered core LBLOCA test conducted with pressurized nuclear fuel rods and with a specification of minimum U.S. ECC injection rates. The maximum LHGR of 14.87 kW/ft was above the typical technical specifications currently used for licensing analyses of PWR fuel rods with the same approximate pellet diameter used in a 15 x 15 fuel pin array. Test LP-02-6 represented an NRC "design basis accident" test and was supposed to run at 100% power, 50 MWt, but because of questions concerning the integrity of the pressurized fuel rods in the central hot assembly, the power level was reduced to mitigate possible safety problems. LP-02-6 is an important LBLOCA test for code assessment because it addresses the issues relating to safety margins associated with the response of a PWR to the NRC "design basis accident" scenario, including delayed minimum ECC safeguards.

Test LP-02-6 simulated a cold leg guillotine break coincident with a loss-of-offsite power. It was conducted with a delayed and degraded high and low pressure ECC injection. During the test, the PCPs were tripped and coasted down with their flywheels attached. The result was an early partial core rewet from the bottom up. When PCP speed dropped below 750 rpm (78.54 rad/s), the flywheels were uncoupled from the pumps to increase the pump speed deceleration. The attached flywheels produced pump coastdown characteristics more typical of a commercial W 4-loop PWR.

Before the initiation of blowdown, the power level in the reactor core was steadily increased and then held at 46 MWt \pm 1.2 MWt to ensure that an appropriate decay heat power level would be obtained once the control rods were inserted into the reactor core. Test conditions at the beginning of the LP-02-6 test were as follows:

- The primary intact loop mass flow rate was 248.7 kg/s \pm 2.6 kg/s,
- The hot leg pressure was 15.09 MPa \pm 0.08 MPa, and
- The primary coolant system hot and cold leg temperatures were 589.0 K \pm 1.0 K and 559.0 K \pm 1.1 K, respectively.

The LOFT LP-02-6 results showed the early bottom-up rewet of the fuel rods because the PCPs were allowed to coast down normally and the pump flow exceeded vessel side-break flow during the early part of blowdown, causing the early rewet. The early quench of the fuel rods extended to two-thirds of the core. Following the blowdown, the core underwent a second heat-up caused by a second dry-out. Because of the large fuel rod stored energy removal during blowdown, the PCT of 1074.0 K (1474.0 F) occurred early in the blowdown. The cladding completely quenched at 56 seconds \pm 0.2 seconds. The test was complete after core reflood was completed at 59 seconds \pm 1.0 second.

From Reference 5, a bias of 11.4 °K \pm 16.2° K (20.5 °F \pm 29.2 °F) should be applied to the measured PCT to account for the 'fin cooling' effects on the surface mounted thermocouples. Thus, the reportable PCT for LOFT Test LP-02-6 is 1104.8 K (1529 °F).

A steady-state initialization calculation was performed to reach the desired steady-state conditions for initiating the LOCA calculation. The calculated and measured initial conditions

agree quite well and the calculated initial conditions are generally within the uncertainty band of the measured quantities. The calculated initial broken loop temperature of 557.6 K for the cold leg and 558.3 K for the hot leg come very close to measured values considering the large error bands quoted for the measured data, namely $553.0 \text{ K} \pm 6.0 \text{ }^\circ\text{K}$ for the cold leg and $560.0 \text{ K} \pm 6.0 \text{ }^\circ\text{K}$ for the hot leg. The desired steady-state conditions were achieved and the calculation accurately reached the LP-02-6 test initial conditions.

A short, steady-state calculation before the break opening is carried out to ensure that the steady-state initial condition is properly maintained when switching from the steady-state input model to the transient simulation. The calculation for this analysis is a simulation of Test LP-02-6 from 10 seconds before the break initiation at 0 second up to 140 seconds. This time interval was chosen because the important phenomena and significant events of Test LP-02-6 occurred during this period.

The assessment of S-RELAP5 to predict each of the important LOCA phenomena for LOFT LP-02-6 is presented in detail in Reference 5. Figure 4.150 compares the calculated and measured PCT versus core elevation. This figure refers to the PCT as a maximum cladding surface temperature, either calculated or measured at the various elevations, during the LOCA transient history. The comparison shows that the code overpredicted the measured temperatures except at the low power region near the core exit. The greatest differences between the calculated and measured PCT occur in the high power region between the 15 in and 44 in elevations. The highest PCT of 1104.8 K (1529 F) was measured at the 26-in elevation. The comparison shows that the calculated PCT of 1159.6 K (1627.6 F) is in good agreement with data and conservatively exceeds the measured PCT in the high power core region.

4.3.2.1.7 LOFT Test LP-LB-1 Assessment

The fifth LOFT LOCE, Test LP-LB-1, simulated a hypothetical double-ended cold leg guillotine break initiated from conditions representative of a PWR operating near its licensing limits. The initial core power was near the facility design limit of 50 MWt with maximum LHGR of 15.8 kW/ft. Included in the test's boundary conditions were loss-of-offsite power coincident with the LOCE, a rapid PCP coastdown, and a minimum safeguard ECCS injection assumption from a European PWR. To minimize possible fuel pin damage, all of the fuel rods in the core were initially unpressurized.

Similar to LOFT Test L2-5, the PCP flywheels were uncoupled from the pump rotors to affect a rapid pump coastdown and prevent an early bottom-up core rewet. In this test, the PCPs were tripped and uncoupled from their flywheels within 1 second after the start of the transient.

The ECC injection assumption for this test resulted in an accumulator liquid volume that was approximately 70%, and a pumped injection flow rate that was about 50% of that used in Test LP-02-6. The pumped injection was accomplished using the LPIS with a delay of nearly 32 seconds to simulate the delay in starting the emergency power diesel generator.

Before the start of the transient, the power level in the reactor core was steadily increased, then held at $49.3 \text{ MWt} \pm 1.2 \text{ MWt}$ to ensure that an appropriate decay heat power level would be obtained once the control rods were inserted into the reactor core. Test conditions at the beginning of the LP-LB-1 test are as follows.

- The primary intact loop mass flow rate was $305.8 \text{ kg/s} \pm 2.6 \text{ kg/s}$.
- The hot leg pressure was $14.77 \text{ MPa} \pm 0.06 \text{ MPa}$.
- The primary coolant system cold leg temperature was $556.6 \text{ K} \pm 1.0 \text{ K}$ with a fluid temperature increase of $29.5 \text{ K} \pm 1.4 \text{ K}$.

Similar to Test L2-5, Test LP-LB-1 was conducted to produce an LBLOCA that had a maximum of core stored energy at the end of blowdown by preventing an early bottom-up core rewet. Then using the high temperature conditions at the start of reflood, the test explored the reflood behavior of the system and provided information against which best estimate computer code simulations could be evaluated.

As desired, the early bottom-up core-wide rewet did not occur in Test LP-LB-1. By altering the PCP coastdown, an early bottom-up rewet was prevented. The test did have a partial top-down rewet that resulted in two peaks in the cladding temperature history. A blowdown PCT of 1261.0 K (1810.0 F) occurred at about 13 seconds and a refill/reflood peak of 1257.0 K (1803.0 F). The clad temperature at the peak power location remained at an elevated temperature for a long time. The cladding was completely quenched at $72 \text{ seconds} \pm 1 \text{ second}$. The test was terminated at 132 seconds.

From Reference 5, a bias of $11.4^{\circ}\text{K} \pm 16.2^{\circ}\text{K}$ ($20.5^{\circ}\text{F} \pm 29.2^{\circ}\text{F}$) should be applied to the measured PCT to account for the 'fin cooling' effects on the surface mounted thermocouples. Thus, the reportable PCT for LOFT LP-LB-1 is 1284.0 K (1851.5 F).

A steady-state initialization calculation was performed to reach the desired steady-state conditions for initiating the LOCA calculation. The calculated and measured initial conditions agree quite well and the calculated initial conditions are generally within the uncertainty band of the measured quantities. The calculated initial broken loop temperature of 560.0 K for the cold leg and 558.3 K for the hot leg come very close to measured values considering the large error bands quoted for the measured data, namely $552.0\text{ K} \pm 6.0\text{ K}$ for the cold leg and $561.0\text{ K} \pm 6.0\text{ K}$ for the hot leg. The desired steady-state conditions were achieved and the calculation accurately reached the LP-LB-1 test initial conditions.

A short steady-state calculation before the break opening is carried out to ensure that the steady-state initial condition is properly maintained when switching from the steady-state input model to the transient simulation. The calculation for this analysis is a simulation of Test LP-LB-1 from 10 seconds before the break initiation at 0 second up to 240 seconds. This time interval was chosen because, although most the important phenomena and significant events of Test LP-LB-1 occur before 100 seconds, the quenching of the core occurred much later in the calculation.

The assessment of S-RELAP5 to predict each of the important LOCA phenomena for LOFT test LP-LB-1 is presented in detail in Reference 5. Figure 4.151 compares the calculated and measured PCT versus core elevation. In this figure, the PCT is referred to as a maximum cladding surface temperature, either calculated or measured at the various elevations, during the LOCA transient history. The comparison shows that S-RELAP5 overpredicted temperatures in the high power region up to the 44-in elevation, and slightly underpredicted temperatures above 44 in. The measured PCT is 1284.0 K (1851.5 °F) at the 24-in elevation. That measurement includes a bias and uncertainty of $11.4\text{ }^{\circ}\text{K} \pm 16.2\text{ }^{\circ}\text{K}$ ($20.5\text{ }^{\circ}\text{F} \pm 29.2^{\circ}\text{F}$) caused by the fin cooling effects on the surface mounted thermocouple. The calculated maximum PCT of 1329 K (1932 F) also occurred at the 24-in core level and is in good agreement with the measured PCT. Based on Figure 4.151, the PCT at any elevation is within approximately 20% of the data, which is reasonable agreement.

4.3.2.2 Semiscale Tests

S-RELAP5 was assessed against the Semiscale LBLOCA tests S-06-3 and S-07-1. Test S-06-3 was performed in the Semiscale MOD-1 facility. The MOD-1 facility was scaled from the LOFT facility and Test S-06-3 was performed as a counterpart to LOFT Test L2-3. The results presented for this assessment are used to support the application of S-RELAP5 in PWR LBLOCA analysis and to verify the capability of the S-RELAP5 code to calculate integral LOCA phenomena in facilities of different scale.

Semiscale Test S-07-1 is a blowdown test performed in the Semiscale MOD-3 facility with cold-leg ECC injections. The results presented for this assessment are used to support the application of S-RELAP5 in PWR LBLOCA analysis and to verify the capability of the code to calculate blowdown film boiling heat transfer in the core.

4.3.2.2.1 Semiscale Facilities

MOD-1 Facility

The Semiscale MOD-1, 1½-loop facility was scaled to the LOFT facility, which in turn was scaled to a 4-loop PWR. It is designated a 1½-loop system because it is configured with one active loop and one passive blowdown loop. Subsequent Semiscale facilities have included components that have made the facility more typical of a PWR. All the other Semiscale facilities were designed with 1/1600 to 1/2000 volume scaling, with full height, in reference to a 4-loop, 3400 MWt PWR.

The MOD-1 system contains a reactor vessel with internals, including a 40-rod electrically heated core, an active intact loop scaled to represent three loops of a PWR and a broken loop scaled to a single loop of a PWR. The intact loop contains an active steam generator and an active PCP and is connected to the pressurizer. The broken loop contains hydraulic simulators for the steam generator and pump and break simulators or rupture assemblies connected to a blowdown suppression system. The blowdown suppression system simulates containment pressure.

The 40-rod electrically heated core has a PWR fuel pin pitch (0.563 in) and the heated length (5.5 ft) and outside diameter (0.42 in) are identical to the nuclear fuel rods of the LOFT core.

Semiscale Test Series 6 was performed to assist the LOFT program in planning the first nuclear test series. Test S-06-3 was performed as a counterpart to LOFT Test L2-3. For this test, the four central heater rods were operated at approximately 39.4 kW/m, 32 rods were operated at approximately 24.9 kW/m, and four rods were unpowered to simulate passive rod locations. This configuration yielded a peaked power profile that simulates that of the LOFT facility and provides a total core power of 1.004 MW.

The safety injection includes the HPIS, LPIS, and accumulators. For Test S-06-3, two HPIS pumps and two LPIS pumps delivered flow into the intact-loop cold leg along with the intact-loop accumulator. The primary coolant pump was powered for the entire transient.

MOD-3 Facility

The Semiscale MOD-3 facility is constructed with two fully active coolant loops. The intact loop, retained from the Semiscale MOD-1 system, was scaled to the LOFT facility, which in turn was scaled to a 4-loop PWR. The broken loop, on the other hand, was scaled directly to a 4-loop commercial PWR. The Semiscale MOD-3 facility was designed with 1/1600 to 1/2000 volume scaling and full height, in reference to a 4-loop, 3400 MWt PWR.

The vessel in the MOD-3 system consists of the upper plenum with internals required to represent guide and support tubes, upper head, 25-rod electrically heated core, and an external single pipe downcomer. The active intact loop is scaled to represent three loops of a PWR and the active broken loop is scaled to represent a single loop of a PWR. The intact loop contains a pump and the short Type I steam generator, and is connected to the pressurizer. The broken loop contains the taller Type II steam generator in addition to pump and break simulators or rupture assemblies connected to a blowdown suppression system. The blowdown suppression system simulates containment pressure.

The 25-rod electrically heated core is characterized by fuel pin pitch (0.563 in) and outside diameter (0.422 in) typical of a PWR. The heated length (12 ft) of the MOD-3 core is identical to a 4-loop PWR core.

Test S-07-1 was performed to establish the baseline performance of the MOD-3 system during a blowdown with cold-leg ECC injections. It was conducted to obtain core heat transfer and DNB characteristics of the heater rods. The MOD-3 system was initialized in the experiment to

a primary pressure of 15.95 MPa, total-loop flow of 9.4 kg/s and cold-leg temperatures of 559 K for the intact loop and 557 K for the broken loop at a core power level of 2.01 MW nominal. The system was subjected to a double-ended cold-leg break through a rupture assembly and two non-communicative nozzles. (Reference 5).

4.3.2.2.2 Semiscale Test Descriptions

Test S-06-3

In Test S-06-3, the MOD-1 system was initialized to a primary pressure of 15.769 MPa, cold leg temperature of 563 K, and inlet flow of 6.68 L/s (liters per second) at the initial core power level of 1.004 MWt. The system was subjected to a double-ended cold leg break through two rupture assemblies and two LOFT facility counterpart nozzles, each having a break area of 0.000243 m² (0.00262 ft²). The effluent from the primary system was ejected into the pressure suppression system.

After initiating blowdown, power to the heated core was reduced to simulate the predicted heat flux response of the nuclear fuel rods during a LOCA. Blowdown was accompanied by ECC injection into the cold leg piping of the intact loop. Coolant injection from the HPIS began at blowdown and continued until test termination (300 seconds). Coolant injection from the accumulator started at approximately 18.5 seconds after rupture and terminated at approximately 68.7 seconds. LPIS began at 25.5 seconds after rupture at a pressure of 1900 kPa and continued until test termination.

Test S-07-1

The specific test conditions simulated in the calculation are as follows:

- The 23 rods in the square matrix of the 25-rod electrically heated core were operated at approximately 36.9 kW/m with a flat radial power profile resulting in a total core power level of 2.01 MW nominal. One corner rod (Rod E-5) was unpowered and another corner rod (A-1) was replaced by a liquid level probe. The normalized axial power profile is a chopped cosine with peak axial power factor of 1.55 nominal (Reference 5).
- During the blowdown transient, power to the electrically heated core was automatically controlled to simulate the thermal response of nuclear heated fuel rods. The power history is modeled based on the measured core power decay.

- The accumulators for the intact (IL) and broken (BL) cold legs were pressurized with nitrogen to 4137 kPa (600 psia). IL accumulator injection began at 19 seconds and nitrogen discharge began at 72 seconds. BL accumulator injection began at 12.5 seconds and nitrogen discharge began at 35 seconds. The IL and BL accumulator injected flows are modeled based on the measured data. The accumulators are actuated in the calculation on time, not pressure, to match the injection timing of the experiment.

The simulation will extend from the time of pipe rupture until the time before nitrogen injection. Nitrogen was injected at 35 seconds, originating from the BL accumulator. Therefore, the simulation will extend for 35 seconds transient time after pipe rupture.

- The initial containment pressure is 246 kPa nominal. The transient containment pressure is modeled based on the measured data.
- The maximum break area corresponding to a double-ended break is 0.849 in² (5.48 cm²) and is modeled. This implies that each of the two blowdown nozzles had a break area of $0.849 \div 2$ or 0.424 in² (5.48 \div 2 or 2.74 cm²). This maximum break area was determined from the ratio of the maximum break area to the primary liquid volume of a PWR system applied to the primary liquid volume of the Semiscale MOD-3 system.
- The intact- and broken-loop primary coolant pumps coast down during the test. The IL and BL pump are modeled based on the measured data.
- HPIS flow into the intact and broken loops started at 3.5 seconds at a pressure of 12,410 kPa (1800 psia) and continued until test termination. The IL and BL HPIS injected flows are modeled based on the measured data. The HPIS pumps are actuated in the calculation on time, not pressure, to match the injection timing of the experiment.
- The LPIS started into the IL and BL at 27 seconds at a pressure of 2000 kPa (290 psia) and continued until test termination. The IL and BL LPIS injected flows are modeled based on the measured data. The LPIS pumps are actuated in the calculation on time not pressure to match the injection timing of the experiment.
- The measured fluid temperature in the IL and BL ECCS injection lines indicate that the ECCS (HPIS, LPIS and accumulator) water temperature is approximately 300 K (80.6 °F). Therefore, the IL and BL ECCS water are both modeled at a temperature of 300 K.

4.3.2.2.3 Test S-06-3 Assessment

Through a sensitivity study, the "best" discharge coefficients were determined to be 0.8 for the vessel side and 0.7 for the pump side break junctions for both the subcooled and two-phase flows. The nodalization of the input model was developed to be as consistent as possible with the LBLOCA input guidelines (Reference 12).

The S-RELAP5 initial condition results match reasonably well with the Semiscale Test S-06-3 data. The detailed comparisons of predicted versus measured results for the important transient phenomena are shown in Reference 5, and are not repeated here. The calculation results have been compared to test data for the three phases of the test (blowdown, refill, and reflood). While reasonable agreement is obtained between code results and data for the major thermal-hydraulic variables, the MOD-1 Test S-06-3 experienced apparent ECC bypass that could not be caught well by the LBLOCA methodology. This resulted in earlier refill being calculated and consequently earlier calculated reflood and quenching of the heater rods. The PCT of 1152 K in the test occurs at an elevation of 21 in above the bottom of the heated length at 20.7 seconds after pipe rupture. The calculated PCT of 1161 K occurs during blowdown at an elevation of 31.2 in above the bottom of the heated length at 26.5 seconds after pipe rupture. Figure 4.152 shows the calculated versus measured maximum temperatures as a function of elevation in the simulated core for Semiscale Test S-06-3.

4.3.2.2.4 Test S-07-1 Assessment

S-RELAP5 was assessed against Semiscale Test S-07-1. The calculation results have been compared to test data. Reasonable to good agreement is obtained between code results and data for the major thermal hydraulic variables including upper plenum pressure, break flow rates, coolant temperatures, and rod temperatures. The comparison demonstrates that S-RELAP5 is capable of simulating the blowdown film boiling heat transfer phenomena expected of a PWR LBLOCA transient. In particular, the code conservatively predicted the average of measured PCT at all elevations. For instance, the calculated maximum temperature at an elevation of 72.4 in is 1092 K compared to the average measured PCT of 1056 K at this elevation (based on eight thermocouple readings). In addition, the highest calculated PCT is 1108 K, compared to the highest measured (not average) PCT of 1101 K. Figure 4.153 shows the calculated versus measured maximum temperatures as a function of elevation in the simulated core for Semiscale Test S-07-1.

4.3.3 Methodology Treatment of PIRT Phenomena

Sections 4.3.1 and 4.3.2 reviewed the extensive assessment of the S-RELAP5 code with regard to capabilities to predict the important phenomena identified in the LBLOCA PIRT. In some cases statistical information was determined with regard to the mean values and uncertainties for predicting a specific phenomenon. Much of this information also is contained in Section 5 of the S-RELAP5 Code Verification and Validation, Report EMF-2102 (Reference 5). In other cases, the code, in its current configuration, was shown to calculate the phenomenon conservatively and no evaluation of the bias and uncertainty was performed. In these situations the conservatism associated with these phenomena was simply accepted as unquantified conservatism in the methodology. Table 4.18 summarizes the important PIRT phenomenon and how that phenomenon is being addressed in the methodology.

4.3.3.1 PIRT Phenomena Not Treated Statistically

From the comparison of the code predictions and data for both the SET and IET assessments, a number of important PIRT phenomena were found to be predicted conservatively by the code. The conservative prediction was either because of a conservative model in the code or the use of conservative input. These phenomena are indicated in Table 4.19 as being treated in the methodology as an "inherent conservatism" or an "input conservatism". By "inherent conservatism" is meant that a code model or combination of models has been demonstrated to conservatively predict these phenomena. By "input conservatism" is meant that the input being provided to the code has been demonstrated to be conservative and will be used in NPP analyses. These conservatisms are accepted in the methodology as an unquantified conservatism above that indicated by the statistical analysis. These phenomena will be discussed individually in the following sections.

4.3.3.1.1 Core 3-D Flow and Void Distributions

The core flow distribution and void distribution are determined by the initial power distributions and [

] In

effect this will result in a wide variation of calculated flow and void distributions in the core.

The ability of the code to calculate void distributions has been demonstrated in the SET assessments performed for the THTF level swell, GE level swell, and the FRIGG-2 tests. For all these assessments, the agreement between code prediction and measured void fractions was good to excellent (Section 4.3.1 and Reference 5). This indicates that the code is capable of calculating acceptable void distributions in the core.

The ability of the code to calculate flow distributions in the core was demonstrated in the SET assessments (Section 4.3.1 and Reference 5) performed for the multi-dimensional flow tests, CCTF, and SCTF. The multi-dimensional flow tests demonstrated that the code was capable of modeling and predicting the measured flows in these tests. In addition, the assessments performed for SCTF test S2-17 and S2-18 demonstrated that the combined code and core nodalization was capable of predicting the effects of changes in radial power distribution and associated flows during the reflood period of the LBLOCA. This was demonstrated by comparing the calculated with the measured PCTs for those tests.

The CCTF assessments further demonstrated that the combined code and core nodalization was able to predict the core flows and resulting PCTs in a cylindrical facility. The cylindrical facility is consistent with the input modeling used in the methodology NPP nodalization.

Based on the information in the previous paragraph, the combination of these assessments clearly demonstrates that the code is capable of realistically predicting the core flows and void distributions as the statistical parameters are being varied in the statistical analysis of the LBLOCA. In addition, the code prediction of flow and void distributions is an integral part of determining the code heat transfer biases and uncertainties. [

]

4.3.3.1.2 Liquid Entrainment in Core

The liquid entrainment in the core has been demonstrated to be conservatively calculated by the code and methodology nodalization. This is shown in the assessments performed for CCTF, UPTF, and FLECHT-SEASET and reported in Section 5.6 of Reference 5. In the CCTF tests examined, Tests 54, 62, 67, and 68, the conclusion was that the liquid entrained from the core into the upper plenum was overpredicted by the code during the early part of the test. This

overprediction occurred until about 400 to 500 s into the test, after that the code underpredicted the amount of liquid in the upper plenum. Only after quenching occurred in the test did the data indicate higher levels. Both the measured and calculated time of PCT occurred before the calculation began to underpredict the liquid in the upper plenum.

For the FLECHT-SEASET tests, as shown in Figures 4.61 through 4.69, the mass of water in the test section is underpredicted by the code and methodology nodalization. This is consistent with the results provided in Figures 4.70 through 4.75, which show that the code is overpredicting the water carryover from the test assembly.

For UPTF Test 10, Run 081, and Test 29, Run 212/211, the water level in the upper plenum was consistently overpredicted by the code and methodology nodalization. This overprediction by the code is shown clearly in Figures 4.154 and 4.155.

In conclusion, the code predicted liquid carryout from the core to the upper plenum was examined in three different test facilities. In all three test facilities, the amount of liquid carry out of the core into the upper plenum was overpredicted. Given these results from three different test facilities, it is concluded that the code and methodology prediction of core entrainment is conservative and no bias or uncertainty was developed to take credit for this conservatism.

4.3.3.1.3 Core Flow Reversal/Stagnation

The reversal and stagnation of flow in the core is the result of the size of the break and the rate of coolant loss versus the rate of coolant injection from the ECC systems. Generally, a combination of other phenomena occur to determine the limiting set of conditions that result in the worse situation where the flow in the core is essentially stagnant or has a low reflood rate for the longest period of time. This condition is addressed by the random variation of the other dominant phenomena. [

]

4.3.3.1.4 Upper Plenum Liquid Entrainment/de-entrainment

When liquid droplets are entrained in the core and carried up into the upper plenum they can remain there, fall back into the core (de-entrainment) or be carried out into the hot leg (entrainment). The major modeling concern for LBLOCA is that allowing too much liquid to fall back into the core would result in a top-down quench and a significant underprediction of the PCT. It would also reduce steam binding. To demonstrate conservatism, the calculated upper plenum collapsed liquid levels were compared to a series of tests and shown to be higher.

Tests at CCTF (54, 62, 67 and 68), FLECHT-SEASET (31805, 31203, 31302 and 31701) and UPTF (Test 10, Run 081 and Test 29, Run 211/212) were used to evaluate the balance of liquid droplet flows in the upper plenum. These tests simulated a PWR core using either steam and water (UPTF) or electrically heated, simulated fuel rods during the reflood period. The calculated liquid levels were compared to the measured liquid levels in the upper plenum region.

The liquid level in the upper plenum is generally overpredicted by S-RELAP5 for reflood conditions. This seems to be true for the prototypic upper plenum of the UPTF (Section 4.3.3.1.2 above), the scaled upper plenum in the CCTF (see Figures 4.156 through 4.159) and the atypical upper plenum of the FLECHT-SEASET tests (see Figures 4.160 through 4.163).

The conclusion is that, using the RLBLOCA methodology, S-RELAP5 tends to hold the liquid in the upper plenum to a slightly greater degree than testing would indicate when the liquid fractions are low. When substantial amounts of liquid are present, S-RELAP5 tends to carry over more than enough liquid and S-RELAP5 models liquid carry-over for the LBLOCA conservatively.

4.3.3.1.5 Counter Current Flow Limit (CCFL)

The CCFL phenomenon is addressed conservatively in the methodology by applying conservative input to the Kutateladze parameters. For the methodology, the following parameters will be used [] This has been shown to provide a conservative prediction of down flow at the UTP for the FRA-ANP specific UTP designs and in the UPTF assessment.

Figures 4.103 through 4.105 demonstrate the conservative comparison for the FRA-ANP current UTP designs for the W 15x15 and 17x17 fuel designs and for the CE 14x14 fuel design. Figures 4.116 and 4.117 and Figures 4.120 and 123 demonstrate the conservatism for the UPTF Test 10, Runs 080 and 081, Test 29, Run 212/211, and Test 12, Run 014. For all these tests, the selected Kutateladze parameters are demonstrated to be conservative.

This conservative set of Kutateladze weighting parameters were selected primarily to address the issue in the assessments (CCTF, SCTF, FLECHT-SEASET, THTF, Semiscale) where best estimate parameters are unavailable. To be able to use these assessments and still meet the CSAU requirement that the assessments use the same model as the NPP analysis, it was decided to use a conservative set of parameters.

4.3.3.1.6 Hot Leg Entrainment/de-entrainment

Liquid entrained into the upper plenum is carried through the hot leg to the steam generator, where it flashes to steam and increases the pressure drop. The more liquid reaching the steam generator, the more conservative the modeling. The liquid carry-over to the steam generator was calculated using modeling based on the RLBLOCA methodology and compared to measured carry-over values for a series of tests.

Tests at CCTF (54, 62, 67 and 68), FLECHT-SEASET (31805, 31203, 31302 and 31701) and UPTF (Test 10, Run 081 and Test 29, Run 211/212) were used to evaluate the carryover of liquid droplets in the hot leg and the steam generator. These tests simulated reflood conditions for a PWR by either introducing steam and water (UPTF) or by quenching electrically-heated, simulated fuel rods (CCTF and FLECHT-SEASET). CCTF used prototypic U-tubes in the steam generator and had a cyclone separator downstream of the steam generator exit. The UPTF was full scale and used cyclone separators in its steam generator simulators to trap water carried over by the hot leg. FLECHT-SEASET had a smaller (~4") horizontal pipe carrying the steam and water from the upper plenum to a separator and collector.

For the CCTF tests, the liquid is separated well downstream (~30') after the exit of the steam generator. Figures 4.164 through 4.167 compare the calculated level changes in the catch tank with the measured changes. The measurements are somewhat inaccurate (note the level decreases which affect the first three cases) and the piping from the steam generator exit to the catch tank introduces some uncertainties. The predicted trends are correct and for the tests

with higher flows (54 and 68) the predicted levels are either conservative or in reasonable agreement.

For the UPTF tests, the liquid is separated in the steam generator simulator. For the two tests, the calculated liquid accumulating in the catch tanks is quite conservative (See Figures 4.168 through 4.171).

For the FLECHT-SEASET tests, there is no steam generator. The hot-leg piping terminates in a separator, which has a tank with a pipe in the bottom leading to a drain tank. Figures 4.172 through 4.179 compare the calculated levels in the separator tank and the separator drain tank with the measured levels. Because of the tendency of the model to hold a larger quantity of liquid in the upper plenum initially than would be indicated by measurements (See Section 4.3.3.1.4), the calculated carry-over to the separator is delayed. The bottom line for these figures is that the calculation has the liquid carried over to these tanks arriving slightly later than the measurements would indicate, with the overall carry-over from the calculation being greater. This latter point shows that the liquid entrained and carried over by the hot-leg model is conservative.

4.3.3.1.7 Two Phase Pump Degradation

The pump two phase degradation is addressed in the methodology as a conservative input. Based on the sensitivity study described in Appendix B for a limiting break on both a 3-loop and a 4-loop plant, it is shown that this is not an important phenomenon for the limiting LBLOCA case. The use of the Semiscale two-phase degradation instead of the CE/EPRI two-phase degradation model produced essentially no impact on the 3-loop results and only an 18 F (10 K) for the 4-loop plant. However, it was shown that the use of the Semiscale pump degradation curves does provide a conservative bias to the model, so it was adopted as a minor conservatism.

4.3.3.1.8 Pump Differential Pressure Loss

The pump differential pressure loss is addressed in the methodology strictly as a best estimate. The S-RELAP5 code has the ability to input the pump specific homologous curves for the NPP being analyzed and this option is used. The homologous curves for the specific NPP pumps are obtained from the utility and, if plant data is available, a pump coast down is modeled to ensure that the curves are consistent with the plant data.

4.3.3.1.9 Non-Condensable Transport

The treatment of non-condensibles in the S-RELAP5 code was demonstrated to be conservative by the performance of an assessment of the ACHILLES ISP #25. The rod thermocouples in the test all clearly showed a reduction in temperature following the introduction of nitrogen into the system. The S-RELAP5 code conservatively underpredicted this cooldown, as shown in Figures 4.136 through 4.141. Thus, the impact of the nitrogen injection following the accumulator emptying of water will be conservatively predicted in the NPP analysis. However, as indicated in the sensitivity studies (Appendix A), the injection of nitrogen into the RCS system following the emptying of the accumulators was found to not significantly affect the final predicted LBLOCA event PCT.

4.3.3.1.10 Downcomer Entrainment

The S-RELAP5 prediction of the downcomer entrainment was demonstrated to be conservative through the assessment of UPTF Tests 6 and 7 (Section 4.3.1 and Reference 5). In these essentially full scale tests the lower plenum fill rate was measured as a function of time during the tests. Test 6 consisted of five different test assessments where the steam flow rate up the downcomer was varied with a constant ECC injection rate. One run from Test 7 was used in the assessments to extend the downcomer steam flow rate to a lower value.

The comparison of the lower plenum level for Test 6 is provided in Figures 4.106 through 4.110 and for Test 7 in Figure 4.111. These level comparisons show that S-RELAP5 underpredicts the lower plenum level for all the Test 6 and 7 assessments using the methodology NPP nodalization (Reference 12). This indicates that S-RELAP5 is overpredicting the entrainment of the ECC water and carrying it out the break. Thus, the results clearly indicate that the S-RELAP5 code overpredicts the bypass of ECC water in these full scale tests. Based on these results, it is concluded that the S-RELAP5 predictions will provide a conservative result with respect to ECC bypass, lower plenum fill, and core recovery. (For a discussion of the oscillations in the lower plenum level, see the discussion on lower plenum sweepout.)

4.3.3.1.11 Downcomer Liquid Level Oscillations

The downcomer liquid level oscillation is another phenomenon that is controlled primarily by other important phenomena. The ranging of these phenomena either will or will not produce the oscillations based on their specific ranging.

Manometer type downcomer liquid level oscillations have not been observed to any significant extent in the methodology NPP nodalization models. This appears to be the result of the boiling in the downcomer acting as a stabilizer for the phenomenon. Preliminary undocumented calculations in which the downcomer heat structures were uncoupled were able to produce manometer type downcomer level oscillations. The lack of these oscillations in the methodology NPP nodalization model is conservative because the effect of the oscillations is to drive water up into the core and provide an additional cooling mechanism. Thus, the fact that this phenomenon is not predicted by the methodology NPP model is acceptable.

4.3.3.1.12 Lower Plenum Sweepout

The conservatism of the S-RELAP5 lower plenum sweepout is also demonstrated in the essentially full scale UPTF Test 6 and 7 assessments with the methodology nodalization (Reference 12). Again these tests were performed with a constant ECC injection rate and with various steam flow rates up the downcomer. The measured versus code prediction of the lower plenum level is provided in Figures 4.106 through 4.110 for Test 6 and Figure 4.111 for Test 7.

In these figures the predicted lower plenum level shows a series of decreases. These decreases in the lower plenum level are a result of the prediction of liquid sweepout from the lower plenum. This sweepout is seen to be more pronounced in the higher steam flow rate assessments, Test 6, Runs 131, 132, 133, and 135, and less pronounced in the two lower steam flow rate assessments, Test 6, Run 136 and Test 7, Run 203. The measured data in these figures do not show these large sweepout events.

The large sweepout events predicted in the UPTF Test 6 and 7 assessments is a direct result of the methodology nodalization used in the lower plenum. Sensitivity studies were performed (Reference 5) that clearly showed that this sweepout prediction could be corrected with a more detailed model (i.e., a 2D lower plenum model). However, because many of the other assessments had already been run, it was decided to continue to use this lower plenum model and to simply accept the conservatism in the methodology.

4.3.3.2 PIRT Phenomena Treated Statistically

The parameters presented in this section are to be treated statistically in the FRA-ANP RLBLOCA methodology. The uncertainties developed from S-RELAP5 code assessments have been presented in Section 4.3.2 and Section 5 of Reference 5. For those parameters a

summary is provided giving the parameter bias and uncertainty and how it is to be applied in the methodology. In addition to these parameters, a few other parameters are being treated statistically based on analysis other than code assessment. The discussion on these parameters includes additional background and explanation of the objective of the statistical treatment. Table 4.19 presents a summary of the key statistical characteristics used in the FRA-ANP RLBLOCA methodology. The table provides a list of biases, standard deviations (for parameters treated with a normal probability distribution function), and range boundaries ($\pm 2\sigma$ for normal probability distribution functions).

4.3.3.2.1 Stored Energy

The analysis of stored energy uncertainty was performed by assessing RODEX3A predictions for centerline fuel temperature relative to data taken at the Halden Reactor Project. The results are presented in Section 5.8 of Reference 5. Using a normal probability distribution function, the mean error in centerline fuel temperature is 0.0 with a standard deviation of 130 °F. A bias in centerline temperature has been identified for burnup greater than 10 MWd/kgU. This is given by the expression:

$$Y\{\text{°F}\} = -4.2232 * X\{\text{MWd/kgU}\} + 39.183 \text{ °F}$$

The parameter is first sampled using a normal distribution with a mean of 0.0 and standard deviation of 130 °F. A test on "Time-of-Cycle" is performed to check if the bias is to be applied. If so, the bias is then added to the sampled centerline fuel temperature. In applying the sampled fuel centerline temperature, the S-RELAP5 multiplier, FUELK, is used in conjunction with a control system that tracks the centerline temperature of the peak power node. The FUELK multiplier is applied to the fuel pellet thermal conductivity. Using a control system applied during a steady-state S-RELAP5 calculation, this multiplier is driven to a value that results in shifting the fuel centerline temperature from a best-estimate value to the best-estimate value plus uncertainties as given by the equation above.

4.3.3.2.2 Oxidation

Energy released through the oxidation of cladding is calculated from the Cathcart-Pawel correlation (Reference 25) for oxide layer growth:

$$\frac{\delta_{\phi}^2}{2} = 0.01126 \exp(-35890 / RT)$$

R is the universal gas constant (1.987 cal/mole-K) and T is clad temperature. This appears in the S-RELAP5 Models and Correlations document (Reference 9) as

$$\frac{\partial \Delta r_{\phi}}{\partial t} = \frac{0.000002252}{2\Delta r_{\phi}} \exp(-18062 / T)$$

In Reference 25, uncertainties are provided for both the constant term and the exponential term. It is reported that the 90% confidence limits on the constant term is -23% to $+30\%$ and on the exponential term, it is $\pm 2.2\%$. A standard deviation is calculated from the upper 1-sided 95% probability point ($+30\%$, 2.2%). Assuming a normal distribution, this corresponds to 1.645 standard deviations; hence, the standard deviation is

$$\frac{30\%}{1.645} = 18.237\% \text{ on the constant term and } \frac{2.2\%}{1.645} = 1.337\% \text{ on the exponential term.}$$

4.3.3.2.3 Decay Heat

The FRA-ANP realistic LOCA evaluation model, S-RELAP5, calculates decay heat based on the 1979 ANSI/ANS standard (ANSI/ANS-5.1-1979, Reference 26). This standard is applicable to light water reactors containing Uranium 235 as the principal initial fissile material.

Fission contributions from Plutonium 239 and fast fission of Uranium 238 can be explicitly treated using the standard; other fissionable isotopes are treated as Uranium 235. Methods of accounting for the effect of decay energy from neutron capture in fission products are also described in the standard, and equations for decay of the capture product actinides Uranium 239 and Neptunium 239 are shown. The 1979 standard considers the reactor operating history and the average recoverable energy associated with fission of each of the above isotopes. Two types of reactor operation are presented, a fission pulse and a constant fission rate over an operating time period. Both methods yield decay power but do not account for the spatial distribution of the decay power deposition.

The decay heating described by the standard can be used for many types of calculations including LOCA analysis. However, considerations for LOCA are somewhat different from other

applications. LOCA is a hypothetical event which must be analyzed prior to reactor operation. Thus, the operating history and the concentration of fissionable isotopes will not be known prior to a LOCA. Fortunately, simplifying assumptions can be made which allow calculation of a realistic but slightly conservative decay heat curve as a function of time using the 1979 standard. The decay heat calculated with these assumptions bounds the more detailed decay heat curves that would result if the conditions at the initiation of LOCA were known. The assumptions are:

- infinite operating time at full power.
- All fissions assumed from U 235
- 200 MeV / fission (conservatively low)
- One standard deviation total decay heat of []

LBLOCAs are a short time event with PCT and quenching occurring on the order of 100 seconds and well within 1000 s. For this short decay time, decay energy tends to be dominated by short-lived fission products. A characteristic of short-lived fission products is that they approach equilibrium concentrations within a short operating time. The assumption of infinite operating time is equivalent to assuming equilibrium fission product inventory. While this assumption is bounding, it is also realistic with respect to the dominant short-lived fission product isotopes.

The ANS standard suggests a simplified method of calculating decay heat assuming Uranium 235 as the only fissionable isotope and applying a conservative multiplier. FRA-ANP makes the assumption that all fissions are from Uranium 235, and adjusts the uncertainty to account for the other isotopes.

The assumption of 200 MeV / fission converts power to fission rate. A low value is conservative. The components of this parameter and the uncertainties are described in more detail in following paragraphs.

Total decay heat using these assumptions was compared to more detailed calculations, and it was determined that use of a one standard deviation uncertainty of [] conservatively bounds total decay heat using these assumptions.

In addition to fission product decay heat, actinide capture product decay power is computed using the ANS standard equations, and added to the fission product decay heat.. In this calculation a conversion ratio appropriate for the time in cycle analyzed is obtained from core neutronics calculations. The ANS standard also provides equations to calculate the addition of decay heat from neutron capture in fission products. These equations are included in S-RELAP5 and the contribution to the total decay heat from this source is calculated and included.

4.3.3.2.4 Departure from Nucleate Boiling

Test results from the THTF Heat Transfer separate-effects test contributed to identifying a bias in the Biasi CHF correlation (Reference 5). [

] The CHF scaling is applied for RLBLOCA calculations, and the statistical information on heat transfer is used along with other test data (see next section) to derive the uncertainty parameters on film boiling heat transfer (FILMBL) and the dispersed flow heat transfer (FRHTC). (See following section).

4.3.3.2.5 Core Post-CHF Heat Transfer

The FLECHT-SEASET tests were used to assess S-RELAP5's capability to predict several phenomena associated with reflooding a heated bundle. This facility provided reflood data covering the LBLOCA range of pressures, subcoolings, and reflood rates using an electrically heated bundle with a center-peaked cosine power profile. The FLECHT skewed test data were added to provide additional data for an upskewed axial power profile.

The results (summarized in Section 4.3.1.6) showed that S-RELAP5 calculated maximum surface temperatures are generally higher than the measured data at all elevations. These trends were consistently observed for nearly all assessments of the S-RELAP5 heat transfer.

FLECHT and FLECHT SEASET data and data from THTF reflood tests were used to derive the multipliers to be used for film boiling heat transfer (FILMBL) and dispersed flow forced convection (FRHTC) as shown in Section 5.1 of EMF-2102 (Reference 5). [

]

The probability density functions are defined by the following two equations. The coefficients for the equations vary depending on whether they are to be applied to FILMBL (low void fraction) or FRHTC (high void fraction).

[]

[]

These are given in Table 4.20.

4.3.3.2.6 T_{min}

A set of seven FLECHT SEASET tests was used to evaluate the trends in T_{min} at low pressure. Quench temperatures improve at higher pressures; hence, a T_{min} uncertainty based on low pressure data was expected to bound high pressure data. This was validated with data from ROSA/TPTF, the ORNL/THTF and the Westinghouse G1/G2 tests. Examination of FLECHT SEASET data showed that based on observable conservatism, only the 3 in/s reflood rate test (Test #31302) was necessary to evaluate a bounding T_{min} uncertainty (Reference 5).

From the FLECHT SEASET data and from an evaluation of code uncertainty with regard to how the LBLOCA multiplier relates to T_{min}, [

] The uncertainty evaluation has been demonstrated to be a conservative bounding distribution relative to other datasets. As this value was based solely on data at 40 psia (2.76 bar), a penalty bias was included to cover the possibility of the system pressure falling below this value. The hydrodynamic film instability theory of Berenson was used to develop this pressure bias (Reference 5).

4.3.3.2.7 Break Flow

Break flow is a function of break area and critical flow uncertainty. [

]

The homogeneous-equilibrium critical flow model in S-RELAP5 was assessed by comparison to full-scale critical flow tests at the Marviken facility. This was presented in Section 4.3.1.8. From these assessments, [

]

4.3.3.2.8 Steam Binding

Steam generator liquid entrainment was examined in the code assessments for CCTF and UPTF.

For the purpose of measuring liquid entrainment in the steam generator, the facilities use a steam generator simulator. For the CCTF tests, liquid entrainment into the steam generator is determined by measurements of liquid levels in a collection tank from the separation of the two-phase mixture entering the simulator. The comparisons of measured and calculated liquid levels in the collection tank indicate that the amount of liquid carried over to the steam generator is in reasonably good agreement, given the uncertainties in the modeling. The uncertainty in the heat transferred from the steam generator simulator, the uncertainty in the extent to which the piping is adiabatic (as it is modeled in S-RELAP5), and the uncertainty in the dimensions of collection tank (dimensioned drawings were not available for the analysis) are significant. The assessment of the liquid carryover was based on conservatively low estimates of these uncertain values; even so, the results show reasonably good agreement.

[

]

[

]

Analyses of liquid entrainment from the upper plenum and hot legs (as discussed in Sections 4.3.3.1.2, 4.3.3.1.4, and 4.3.3.1.6) suggest that S-RELAP5 tends to carry over more than enough liquid and that liquid carryover for the LBLOCA is conservative. The large model uncertainty in the CCTF assessment requires the []

This bias is considered an additional conservatism in light of the UPTF results showing that carryover to the steam generator is conservative without the bias. The increased interfacial drag at the steam generator inlet will result in conservative carryover to the SG and will provide a bounding estimate of steam binding during a LBLOCA.

4.3.3.2.9 Cold Leg Condensation

S-RELAP5 was assessed against selected tests from the W/EPRI 1/3 scale condensation experiment. [

]

This bias was used to assess the accuracy of the code in predicting the interfacial condensation heat transfer during the ECC/steam mixing process. The results show that the mean bias, based on 19 data points, is [] using a nodalization consistent with plant nodalization. This indicates that S-RELAP5 slightly overpredicts the interfacial condensation rate on the average. For RLBLOCA analyses, a [] bounds the uncertainty range of the interfacial condensation heat transfer coefficient in the ECC/steam mixing process. It is to be applied in the system cold legs and in the downcomer. Condensation in the downcomer should not be that significant; however, sampling of a low condensation factor may prevent sufficient ECC mixing in the cold leg and this mixing would then be completed in the downcomer.

4.3.3.2.10 Accumulator Discharge

Accumulator discharge may be influenced by piping flow resistances and pressure. Most plants have can provide best-estimate data that maybe used to accurately model flow resistance;

hence, the largest uncertainty to accumulator discharge is accumulator pressure. To support a plant technical specification for accumulator pressure ranges, the accumulator pressure is sampled over a range, using a probability distribution developed specifically for the plant of interest. The information on uncertainty for this and other plant process parameters will be reported to the licensee with the safety analysis.

4.3.3.2.11 Reactor Vessel Hot Walls

The results from UPTF Tests 6 and 7 demonstrated that S-RELAP5 will overpredict ECC bypass; however, many parameters may contribute to this phenomena. The hot wall effect can be separated out since it is expected that there is a direct relationship with the degree of nucleate boiling in the downcomer and ECC bypass. To maximize the hot wall effect, heat transfer in the downcomer can be locked into nucleate boiling by raising the CHF point to a high value. In the FRA-ANP methodology, the hot wall effect [

]

4.3.3.2.12 Containment Pressure

Containment pressure is ranged [

] Sensitivity studies

have shown that lower containment pressure reduces PCT margins. [

]

4.3.4 Evaluation of Code Biases

This section assesses the effects of the defined code biases on the LBLOCA assessments. The biases were developed from uncertainty analyses performed on separate-effect tests. Although each bias developed has an uncertainty associated with it, the evaluation of the biases does not include the uncertainties.

Having defined the biases and uncertainties for use with S-RELAP5, an evaluation of the impact of these biases on the assessments was performed for the CCTF, LOFT, and Semiscale. The CCTF facility was selected from the various SET facilities because it is a large facility and has a cylindrical configuration consistent with the NPP core model. The two IET facilities were chosen because they provide a complete assessment for all phases of the LBLOCA scenario.

The following biases were included in all of the evaluation calculations and were taken from Table 4.19:

[]
[]
[]
[]
[]
[]
[]

4.3.4.1 Evaluation of Biases with CCTF

The biases were applied to each of the CCTF tests. The overall effects of the biases are shown by comparisons with unbiased results and measured temperatures. The comparisons are shown at the core elevation where the measured PCT occurred. In all the tests the measured PCT occurred at the 1.83 m elevation, while the calculated PCT in both the base case and the biased calculation occurred between the 2.3 and 2.5 m elevations. Therefore temperature comparison plots will be made at the 1.83 m elevation and at the 2.44 m elevation.

Also presented are rod temperature profile comparisons between measured, unbiased, and biased temperatures. In the profile plots, the temperatures presented are the maximums occurring at each elevation. The maximum temperature profile, referred to as a PCT plot, readily shows how the calculated temperatures compare with the measurements.

4.3.4.1.1 Summary and Conclusions

Inclusion of the biases resulted in improved but conservative PCT calculations in three of the four evaluation tests. In the fourth, which is a low PCT case, the inclusion of the biases improved the calculation of the general trends and produced a good comparison but slightly non-conservative PCT. [

]

4.3.4.1.2 Test 54

This test incorporates best estimate decay power (ANS x 1.0), a nominal cold leg ECC injection rate (0.011 m³/s), and nominal pressure (0.20 Mpa).

The comparison between measured, unbiased, and biased temperatures at the 1.8 m level where the measured PCT occurred is given in CCTF Figure 4.180. From the time reflood starts at 93 seconds up to the time that the rods quench, the heat transfer regime oscillates between dispersed flow film boiling and single phase steam heat transfer. [

] Similar trends are observed in Figure 4.181, where the comparison is made near the calculated PCT elevation. At this elevation, the calculation tracks the measured temperature almost exactly and the measured and calculated quench temperatures are nearly identical.

The PCT versus elevation plot is shown in Figure 4.182, where the biased and unbiased peak temperatures either exceed the measured temperatures or are within the range of the measured temperatures, except at the 1.425 m elevation, where the unbiased calculated temperature fall slightly below the lowest measured temperature. In the upper one third of the heated section, the code calculates higher temperatures than measured in both calculations. However all three figures show the code calculated the trends of the experimental data. Also, both the unbiased and biased calculations tend to overpredict the data near the calculated PCT location. The biased calculation, however, tends to fall between the data and the unbiased results.

4.3.4.1.3 Test 62

This test incorporates Appendix K required decay power (ANS x 1.2), a nominal cold leg ECC injection rate ($0.011 \text{ m}^3/\text{s}$), and nominal pressure (0.20 Mpa).

The comparison between measured, unbiased, and biased temperatures at the 1.8 m level where the measured PCT occurred and at the 2.44 m level where the calculated PCT occurred are given in CCTF Figures 4.183 and 4.184. The trends are similar to those shown for Test 54.

The PCT versus elevation plot is shown in Figure 4.185, where the biased and unbiased peak temperatures either exceed the measured temperatures or are within the range of the measured temperatures without exception. Also, both the unbiased and biased calculations tend to

overpredict the data near the calculated PCT location, but the biased calculation tends to be much closer to the data than do the unbiased results.

4.3.4.1.4 Test 67

This test incorporates Appendix K required decay power (ANS x 1.2), a nominal cold leg ECC injection rate (0.011 m³/s), and reduced pressure (0.15 Mpa). This test produced the greatest PCT in both the tests and in the calculation because of the combination of low pressure and higher decay power.

The comparison between measured, unbiased, and biased temperatures at the 1.8 m level where the measured PCT occurred and at the 2.44 m level where the calculated PCT occurred are given in CCTF Figures 4.186 and 4.187. Again, the trends are similar to those shown previously for Test 54 and 62, but because of the higher temperatures the effects of the biases are magnified.

The PCT versus elevation plot is shown in CCTF Figure 4.188, where, as in test 62, the biased and unbiased peak temperatures either exceed the measured temperatures or are within the range of the measured temperatures without exception. Also, both the unbiased and biased calculations tend to overpredict the data near the top half of the core, but the biased calculation tends to be much closer to the data than do the unbiased results.

4.3.4.1.5 Test 68

This test incorporates best estimate decay power (ANS x 1.0), an increased cold leg ECC injection rate (0.025m³/s), and nominal pressure (0.20 Mpa). This test produced the best agreement between the calculated PCT and that measured for the unbiased runs.

The comparison between measured, unbiased, and biased temperatures at the 1.8 m level where the measured PCT occurred and at the 2.44 m level where the calculated PCT occurred are given in Figures 4.189 and 4.190. As shown in both of these figures, the addition of the biases tends to produce PCTs at both locations that are slightly non-conservative. However, as shown in Figure 4.190, the underprediction is mainly the result of the initial temperature undershoot at the start of reflood. After the initial under shoot that ends at approximately 130 seconds the slope of the calculated temperature curve tracks that of the measured

temperature until 340 seconds, at which time the biased heat transfer rate becomes larger than that measured rate.

The PCT versus elevation plot for CCTF Test 68 is shown in Figure 4.191. The figure shows that both the biased and unbiased peak temperatures either exceed the measured temperatures or are within the range of the measured temperatures except at the measured PCT location where the biased temperature is under the lowest measured value. Also, both the unbiased and biased calculations tend to overpredict the data near the top third of the core. Because of the discontinuity in the measured temperatures near the core mid plane, visually deciding whether the biased or unbiased calculations produce the best overall comparison is difficult.

This test is the only one in which the biases produced a notable effect on any of the measured loop parameters (pressure drop, flow rate, void fraction, etc.). For this test the steam generator inlet interfacial drag bias of 1.75 produced a noticeable improvement in the agreement between the measured and calculated intact loop cold leg void fraction between the start of reflood and 350 seconds. After 350 seconds the biases produced little difference. The cold leg void fraction comparison is shown in Figure 4.192.

4.3.4.1.6 Conclusion Regarding Bias Evaluation in CCTF

Inclusion of the biases resulted in improved but conservative PCT calculations in three of the four evaluation tests. In the fourth, test which is a low PCT case, the inclusion of the biases improved the calculation of the general trends and produced a good comparison but slightly non-conservative PCT. [

]

4.3.4.2 Evaluation of Biases with LOFT

The integral tests used for the assessment were the LOFT Tests LP-LB-1, LP-02-6, L2-5, and L2-3. These tests were evaluated as part of the S-RELAP5 assessment, which provides a comparative basis.

The biases were applied to each of the LOFT tests. The overall effects of the biases are shown by comparisons with unbiased results and measured temperatures. The comparisons are shown at the core elevation where the measured PCT occurred. In Tests LP-LB-1 and L2-5, the calculated location of the PCT coincided with the measured location. From the Test LP-02-6 results, the elevation of the measured PCT was 26 in, while the calculated PCT occurred at the 24 in level. The difference in elevations is small enough to perform the analysis at the 26 in level. However, simulation of the L2-3 test resulted in a calculated PCT occurring at the 24 in elevation, while the measurements show the PCT occurring at the 15 in level. Thus two comparisons are evaluated, temperature comparisons at 15 in and 24 in.

Also presented are rod temperature profile comparisons between measured, unbiased, and biased temperatures. In the profile plots, the temperatures presented are the maximums occurring at each elevation. The maximum temperature profile, referred to as a PCT versus elevation plot, readily shows how the calculated temperatures compare with the measurements.

4.3.4.2.1 Summary and Conclusions

From the assessment calculations, S-RELAP5 was demonstrated to be conservative with respect to the measured PCT data from LOFT tests LP-LB-1, LP-02-6, L2-5, and L2-3. Those assessment cases were re-run with the code biases applied in the analysis. The S-RELAP5 calculated results from the biased calculations were in better agreement with the data and the PCT results were still conservative.

4.3.4.2.2 LOFT Test LP-LB-1

Figure 4.193 compares the measured, unbiased, and biased temperatures at the 24 in level where the measured PCT occurred. The initial temperature rise is calculated to occur slightly earlier than was measured, and the biased calculation shows an earlier rise than the base calculation. [

]

From 4 s to approximately 35 s, the code calculates the heat structure to be in the dispersed film-boiling regime. The code bias of 1.75 is applied. The biased results show peak temperatures closer to the measured data during this period. The bias calculation underpredicts the measured temperatures slightly between 25 and 35 s. Had the calculated peak temperature

been delayed to the measured value, the calculated temperatures would have been in excellent agreement with the measurement.

After 35 s the heat transfer regimes are predicted to enter the transition region between dispersed flow film boiling ($\alpha > 0.9$) and the Bromley film boiling region ($\alpha < 0.7$). At that point,

]

Both calculations follow the measured temperature excursion until 50 s. At that time, the measured temperature starts decreasing more rapidly and final quench occurs just before 70 s. The LP-LB-1 transient shows early quenching, primarily caused by top-down quenching in the upper core. The S-RELAP5 calculations do not effectively calculate that phenomenon.

The PCT versus elevation plot is shown in Figure 4.194. In that figure, the unbiased peak temperatures exceed the measured temperatures except at the 54 and 61 in elevations. The results from the biased calculation are shown with a dashed line. Those results are either within the measured uncertainties or exceed the measured temperature peaks except at the upper elevations. In the low power upper region of the core, the calculated dry-out is delayed relative to the data. After dry-out occurs, the code calculates quenching much later than measured. That calculated discrepancy is associated with the inability to adequately predict top-down quenching (see CCFL discussion in Section 4.3.3.1.5).

Except for top-down quenching, both figures show that the code calculated the trends of the experimental data. Also, both the unbiased and biased calculations tend to overpredict the data. The biased calculation, however, tends to fall between the data and the unbiased results, and tends to be within the measured uncertainty for ~20% of the data. [

]

4.3.4.2.3 LOFT Test LP-02-6

The LOFT LP-02-6 experiment is characterized by a short period of core quenching immediately after the blow-down peak temperatures occur because of a slow pump coast down. The

quenching occurred in the lower two-thirds of the core. The S-RELAP5 calculations do not show that brief core quenching.

The calculated temperatures from unbiased and biased cases are compared with measured temperatures at the 26 in core elevation, and are shown in Figure 4.195. The analysis of the effects of the biases on the calculated temperatures is similar to what was discussed for Test LP-LB-1 with alternative timings for the phenomenon occurrence. [

]

The Test LP-02-6 PCT versus elevation plot is shown in Figure 4.196. As was the case in the Test LP-LB-1 PCT plot, the calculated peak temperatures overpredict the measured peak temperatures, except in the upper core region. Unlike the Test LP-LB-1 PCT plot, the biased calculation shows little difference from the unbiased case, although the biased results fall between the measured and unbiased temperatures. The conclusion from the LP-02-6 assessment is that the code still is conservative, even with the application of the biases.

4.3.4.2.4 LOFT Test L2-5

The LOFT L2-5 experiment was designed to provide data for evaluation model assessment. The experiment is characterized by a rapid pump coast down and PCT occurring during the reflood portion of the experiment.

Figure 4.197 shows the calculated temperatures from the unbiased and biased cases compared with the measured temperatures at the 24 in core elevation. The results, and consequent bias analysis, are similar to those from the Test LP-LB-1 comparison except for the calculated overprediction of temperatures. The Test L2-5 experiment has a controversial power associated with it. The core was operated for 28 hours at 38 MW, then reduced to a reported 36 MW over a 2.5 hour period before the test. Additionally, the reported core power with uncertainty was 36 ± 1.2 MW, but the target power for the test had been 37.5 ± 1.0 MW. The calculation was performed using 36 MW. As shown in Figure 4.198, the unbiased calculated temperatures do not greatly exceed the measured temperatures as expected based on the other LOFT assessments.

Based on the current results, time shifting the calculated results so the PCT would occur at the same time as the data, the biased temperature decay would overlay the measured temperature

decay. Also, the unbiased temperature would greatly exceed the measured temperature. The implication is that the biased results are more accurate after PCT is reached.

Figure 4.198 shows the PCT versus elevation plot where the unbiased and biased peak temperatures are compared with the measured peak temperatures. In its present form, the biased calculation is within the measured uncertainties of the data above the 26 in elevation. However at the lower elevations, the figure shows both calculations underpredicting the data.

4.3.4.2.5 LOFT Test L2-3

The LOFT L2-3 test was one of the tests performed early in the LOFT experimental LBLOCA test series with a nuclear core. The prime characteristic of the L2-3 test is the total core quench immediately after the blowdown peak temperature occurred. The quenching was caused by the pumps running at 100% (i.e. no coast down) throughout the transient. The pump operation can cause an early core flow recovery as the pumps cause cold leg flow to exceed break flow. The LOFT facility was highly susceptible to this core quenching phenomenon.

The measured PCT occurred at the 15 in core elevation, as shown in Figure 4.199. That figure includes calculated temperatures from the unbiased and biased transients. The figure shows the blowdown peak well predicted from both calculations, while the reflood portion of the transient was overpredicted. Again, the code does not show the core quenching immediately after the blowdown peak. Missing the core quench immediately after blowdown contributes to the high temperatures calculated during reflood.

The code calculated a much higher PCT for the L2-3 test, which occurred at the 24 in core elevation. Those results are compared with data in Figure 4.200. The calculations show similar behavior as was seen in Figure 4.199. Although the biased results are closer to the data, both calculations overpredict the data and are conservative.

The PCT versus elevation plot is shown in Figure 4.201. From the calculated profile, the calculated results are skewed showing the peak temperatures centered at the 24 in core elevation. The measured results show a flat profile in that region because of the core wide quenching. The temperatures from the biased calculation are lower than the temperatures from the unbiased calculation. Both calculated results overpredict the measured temperatures.

4.3.4.2.6 Conclusions

The evaluation of the S-RELAP5 biases using LOFT shows the expected results from the application of the biases. That is, the biases bring the code predictions more into line with the measured data for all four LOFT tests evaluated. For three of the four tests the code continues to demonstrate conservatism relative to the measured data. For Test L2-5, where the code prediction with biases no longer overpredicts the data, there has always been a concern with respect to the actual power for this test. Most previous analyses of this test have indicated that the power level from which the test was initiated is likely higher than the reported value. Thus, it is concluded that the biases produce the expected improvement in the comparison of calculation and measurement and that the code continues to demonstrate conservatism relative to the measured data.

4.3.4.3 Evaluation of Biases with Semiscale

The code biases were used to make S-RELAP5 assessment calculations of the Semiscale Tests S-06-3 and S-07-1. Previous S-RELAP5 assessment results have shown that the calculated PCT from each Semiscale assessment occurred at a different elevation than was measured. From the S-06-3 assessment, the measured PCT occurred at the 21 in elevation, while the calculated PCT occurred at the 27 and 30 in elevations. From the S-07-1 assessment, the calculated PCT occurred at the 81.5 in elevation, while the measured PCT occurred at the 70.5 in elevation. Comparisons from both locations are presented for consistency.

4.3.4.3.1 Summary and Conclusions

The bias evaluation using the Semiscale tests showed the expected trends because the predicted PCT in the high powered central region of the hot rod was reduced when the biases were applied. However, in test S-06-3, the comparison with data was not improved while for test S-07-1 the comparison with data, particularly in the high power central region of the hot rod, was improved.

4.3.4.3.2 Semiscale Test S-06-3

Figure 4.202 shows the unbiased and biased calculated temperatures compared with data at the 21 in core location where the PCT was measured. At that location, the S-RELAP5 temperature from the assessment (unbiased) underpredicted the measured temperature. The calculated temperature from the bias case is lower than the temperature from the unbiased run,

the expected result. Figure 4.203 shows the calculated temperatures compared with data at the 29 in core elevation, the calculated PCT level. In that figure, both calculated temperatures initially overpredict the measured temperature during the first 50 s of the transient. Because of the [] the temperature from the biased calculation is lower than the temperature from the unbiased calculation.

Figure 4.204 shows the PCT versus elevation plot from the S-06-3 calculation. As shown in the figure, the calculated peak temperature profile is shifted higher in core elevation than was measured. As expected, the biased results are lower than the unbiased results in the vicinity where the calculated PCT occurred. However, the biased profile crossed over and exceeded the unbiased profile above the 2.7 ft core elevation, while the LOFT L2-3 results show the crossover occurring above the 3.6 ft core elevation (Figure 4.201). The biased results are acceptable because they are lower than the unbiased results at the calculated PCT location.

4.3.4.3.3 Semiscale Test S-07-1

Figures 4.205 through 4.207 show the Semiscale S-07-1 temperature comparisons between measured, unbiased, and biased temperatures. Figure 4.205 shows the comparison at the measured PCT node, Figure 4.206 shows the comparison at the calculated PCT location, and Figure 4.207 shows the PCT versus elevation plot. In all figures, the biased results are lower than the unbiased results and both calculations are conservative with respect to the data.

4.3.4.3.4 Conclusions

As expected, for both the Semiscale tests evaluated, application of the biases reduced the calculated PCT. For Test S-06-3, the overall comparison to the data was not improved. This is clearly shown in Figure 4.204 where the temperatures in the lower and upper parts of the rod are further from the data with the application of the biases. The results for Test S-07-1, with a 12 ft core, are more consistent with the expected trends. The PCTs from the biased calculation are lower than the unbiased calculation in the central high power portion of the rod and are in better agreement with the measured data. While the comparison with data at the top and bottom of the rod are essentially unchanged between the biased and unbiased calculations relative to the data, the magnitude of the PCT is in good agreement with the data.

4.3.4.4 Conclusions from Bias Evaluation

Overall the evaluation of the model biases showed the expected trends. The application of the biases resulted in a reduction in the maximum PCT predicted by the code, which is consistent with the observed tendency of the code to overpredict the data. In general, the reduction in PCT improved the comparisons between calculation and data, as should be expected if the developed biases are reasonable. This indicates that the biases developed from comparison of the code predictions and data for the SET assessments are affecting the code predictions consistent with the intent and expectations.

4.4 ***Determination of Effect of Scale (CSAU Step 10)***

The basis for the analysis of a LBLOCA is the entire methodology being used, not just the basecode, S-RELAP5. When S-RELAP5 is referenced in this section, it means the combination of the code and the associated methodology. As noted in Appendix C of Reference 4, there are two premises which the assessment process is based. The first premise is that the tests are scalable to a LBLOCA and the second is that the models in S-RELAP5 and the implementation result in scalability of the code predictions. For the first premise to be true, the selection of tests needs to be such that all of the important phenomena in a PWR LBLOCA are captured by one or more appropriately scaled tests. For the second premise to be true, the phenomenological models in S-RELAP5 should apply to both the PWR LBLOCA and the scaled test. The scaling of the tests and of the phenomenology will be discussed in the following paragraph.

Throughout the assessment program (Reference 5), S-RELAP5 was used to simulate a variety of tests. These tests are a significant portion of the basis for the RLBLOCA methodology, having been used to demonstrate the ability of S-RELAP5 to predict the test outcomes. Because of the cataclysmic nature of a design-basis LBLOCA, no tests exist that replicate it at full scale. All of the integral tests and some of the separate-effects tests are scaled. One exception is the UPTF, which is full-scale, but has no core and no steam generators. The ability of the scaled tests to capture the phenomena of the LBLOCA is then pivotal to the applicability of the assessments for S-RELAP5.

4.4.1 Test Scaling

Tests are scaled to preserve certain features of the full-scale phenomena. For this reason, tests with different scaling are used to address different phases or aspects of an LBLOCA. If a test is

considered appropriately scaled for the phenomena of interest, then assessment conclusions to that data is considered applicable to the full scale NPP.

It has been shown (Reference 28) that scaling a test facility based on preserving the ratio of the power to the volume (power-to-volume scaling) results in substantially the same system response throughout the simulation, except for the behavior in the downcomer. For the downcomer component, the heat transfer with the wall is an important phenomenon, and it does not scale the same way. The SEMISCALE results showed entirely different flow patterns in the downcomer compared to the analogous LOFT. The Ishii-Kataoka scaling laws (Reference 29) are more general and have specific scaling laws for different phenomena.

4.4.1.1 Blowdown

Power-to-volume scaling for the blowdown period was demonstrated in Reference 4. Five system tests with powers from $1/48^{\text{th}}$ of a typical PWR to $1/30,000^{\text{th}}$ were used as a basis for the comparison. Each of these facilities were scaled such that the ratio of power to volume was preserved. The peak temperature during blowdown was plotted as a function of linear power for each of these test facilities. The measured peak temperatures all fell within 350 F of a linear regression line (temperature versus LHGR). The data scatter for a single facility was as great as, or greater than, any differences between facilities. As a result, it is hard to conclude there are any scale effects occur in the blowdown peak. It is concluded that tests that preserve the power-to-volume ratio of a PWR will scale properly for the blowdown phase of the LBLOCA.

4.4.1.2 Refill

During refill and early reflood, scale dependent multi-dimensional flow behavior has been observed in the downcomer for facilities using power-to-volume scaling. The SEMISCALE and LOFT facilities were compared for analogous tests in Reference 28. Under ideal scaling, the two tests should have shown the same behavior. However, during the refill portion of the simulation, the downcomer flow was observed to be generally up for the SEMISCALE test before the pressure increase accompanying the emptying of the accumulator. For the analogous test in the LOFT facility, the flow was asymmetric; down for the regions near the intact loop and up for the region near the broken loop. This has been attributed differences in the downcomer gap and the distance between the cold leg penetrations. This allows multi-dimensional flow effects to dominate the flow in the LOFT facility, whereas they do not occur to the same extent in the SEMISCALE facility. The downcomer gap, volume and surface area-to-

fluid volume ratios do not scale between these two facilities in such a manner to preserve the transit time and the heat transfer to the fluid from the walls.

The UPTF facility (Reference 30) was designed to simulate a four-loop 3900 MWt PWR primary system and to provide a full-scale simulation of thermal-hydraulic behavior in the primary system during the end of blowdown and refill phases of a PWR LBLOCA. The reactor vessel, the core barrel, and the greater part of the vessel internals are full-sized representations of the reference PWR, as are the four hot and cold legs that simulate three intact loops and one broken loop. The dimensions of the test vessel are those of the reactor pressure vessel of the reference PWR, with the exception that the vessel wall is thinner. The downcomer annulus, which is formed by the vessel wall and the core barrel, has a gap width that varies from 0.25 m (0.82 ft) in the lower part down to 0.21 m (0.69 ft) in the upper part. The loop geometry and flow areas correspond to the 4-loop PWR.

With the exception of the wall thickness, the UPTF is full scale. The hot-wall effect should be slightly under estimated, because of the slight reduction in vessel mass and stored energy. However, there is an ample amount of metal in the vessel so that the UPTF tests should be applicable to the refill portion of an LBLOCA.

4.4.1.3 Reflood

Scaling issues associated with reflood were addressed in Reference 4, where the effects of refill scaling were removed from the data by comparing the temperature rise to reflood rates. The temperature rise considered is the change from the beginning of reflood to the PCT.

Temperature rise data were collected for 8 facilities with volumes scaled from 1/21st to 1/1700th, all of which were power-to-volume scaled. Figure 34 of Reference 4 compares the temperature rise for all 8 facilities to the reflood rate. The data were fit with a regression relation and the tolerance bands added. As with the blowdown data, the spread in the data for a single facility was as great as or greater than the difference between the facilities. Tests which scale by maintaining the power-to-volume are applicable to the reflood phase of a LBLOCA.

4.4.2 Code Scaling

The issue of code scaling is primarily determined by the ability of the correlations and closure relations used to describe complicated thermal-hydraulic phenomena that are not treated from a mechanistic, theoretical approach. Generally, phase transitions, heat transfer, phasic

interactions and CHF fall in this category. The models, correlations, and closure relations used in S-RELAP5 are described in Reference 9. To a lesser extent, the numerical implementation may be subject to scaling issues. Generally, issues of numerics are treated by addressing the converged nature of the nodalization and time step criteria. This way, demonstrates that the computer code can solve the mathematical model correctly over the applicable range for the tests and the LBLOCA. This leaves the issue of scaling of the correlations and the closure relations employed in LBLOCA analysis.

Code scaling evaluation will focus on those items identified by the sensitivity studies of PIRT phenomena as having the greatest impact on LBLOCA. Table 4.1 shows the results of sensitivity studies on the PIRT phenomena in a PWR LBLOCA. The models related to these and the scalability of each of these models are discussed in the following paragraphs.

Items related to fuel rod performance are not affected by scaling, because the basis for the fuel-stored energy and dynamic response are based on RODEX3A (Reference 7), which has been benchmarked to fuel rod data. Similarly, decay heat models require no scaling.

4.4.2.1 Post-CHF and Reflood Heat Transfer

When heat flux from the fuel rods and any other metal masses exceed the CHF, the heat transfer is calculated using correlations specific to the heat transfer regimes. The single-phase vapor, transition boiling and film boiling regimes constitute the post-CHF heat transfer regimes. For each of these regimes, the effects of radiation heat transfer also are considered. Single-phase vapor heat transfer is the maximum of the Sleicher-Rouse correlation (Reference 31) for forced flow regimes (turbulent and laminar) and the turbulent natural convection heat transfer recommended by Holman (Reference 32). In general, the Sleicher-Rouse correlation determines the heat transfer.

The natural convection heat transfer model is based on data from the flow between vertical plates. If the boundary layer is small compared to the diameter of the rod, then heat transfer through this layer would be very similar to that through the boundary layer on a plate. With the Prandtl number near unity and the rod diameter large compared to the boundary layer, the Holman formulation for natural convection heat transfer used in S-RELAP5 applies (Reference 33) as long as

$$\frac{D}{L} \geq 35 \cdot (Gr)^{-0.25}$$

where D is the rod diameter, L is the length used in calculating the Grashof number and Gr is the Grashof number. When these conditions are met, the flat plate solution does not differ by more than 5% from the solution for the cylinder. In the turbulent flow regime, this implies $0.02 \leq D/L \leq 0.2$. For a 17x17 fuel design, with a diameter of 0.376 in., the length can be as low as 1.9 in. and as large as 19 in. [

] These fall well within the range of applicability of the natural convection heat transfer correlation.

The Sleicher-Rouse correlation is valid for the following ranges:

$$0.6 < Pr < 0.9$$

$$10^4 < Re < 10^6$$

$$1 < \frac{T_w}{T_g} < 5$$

$$\frac{x}{D} > 40$$

The Prandtl number (Pr) for steam at pressures below 50 psia and temperatures above 1000 F are all less than 0.9 (Reference 34). For lower temperatures, the Prandtl number is around unity. The steam Reynolds number (Re) for a typical limiting LBLOCA is approximately 5,000 during the reflood phase. This falls slightly below the correlation limit for the Sleicher-Rouse correlation. Wall temperatures (T_{av}) easily meet the criterion, as does the length-to-diameter ratio (x/D).

For the Prandtl number and the Reynolds number, the Sleicher-Rouse correlation falls slightly short of covering the conditions present in the LBLOCA. For the Prandtl number, the difference is quite small and the extrapolation should have little effect on the scalability of the calculations. For the Reynolds number, the LBLOCA falls somewhat further outside the region of applicability of the Sleicher-Rouse correlation. Heat transfer correlations such as Seider-Tate (Reference 35), Dittus-Boelter (Reference 36) and Sleicher-Rouse all have nearly the same (linear) Reynolds number dependence. In Reference 31 the Sleicher-Rouse correlation was compared to 120 data points and the standard deviation of the error was 4.2%. The 95%

tolerance range on these data would be $\pm 8.3\%$ ($=t_{119,97.5} \times \sigma_{fit} = 1.98 \times 4.2\%$). Treating the dependence as linear (because it is very nearly so) the tolerances for the ratio of predicted Nusselt number to the measured Nusselt number for a Reynolds number of x_0 would be given by

$$\pm t_{n-2,1-\alpha/2} \cdot \sigma_{fit} \cdot \sqrt{1 + \frac{1}{n} + \frac{(x_0 - \bar{x})^2}{(n-1) \cdot \sigma_x^2}}$$

Where \bar{x} is the mean of the Reynolds number and σ_x is the standard deviation. Inserting values here for the mean value of Reynolds number and for the standard deviation, the uncertainty in the extrapolated value can be obtained. Figure 4.208 shows the data from Figure 1 of Reference 31 plotted with a linear x-axis. In this figure, the tolerance bands have been included. The uncertainty in the extrapolated value ($Re = 5000$) is not significantly increased as the turbulent regime is still applicable.

In conclusion, the model for single-phase vapor heat transfer used in S-RELAP5 can be applied to a full-scale PWR LBLOCA.

Transition boiling is not really a heat transfer regime in the sense that it can be characterized by a homogeneous, steady, heat transfer mechanism. It is a combination of dynamically varying heat transfer mechanisms, including nucleate boiling, film boiling and vapor heat transfer. The amount of time a region spends in one of these heat transfer modes determines the effective heat transfer rate. Very few measurements are available for transition boiling heat transfer and they do not cover a very wide range. In addition, the unsteady nature of the process makes modeling the process physically very challenging.

Despite the complexity of this regime, exact modeling of the heat transfer is not particularly important for the LBLOCA because most volumes in the core move through this heat transfer regime rather quickly and are not sensitive to the details of the modeling. The main requirement for simulating the LBLOCA is that the point at which the code predicts the beginning and end of the transition region be reliable. In addition, the heat transfer in the transition region should be significantly better than the vapor heat transfer and it should remain below the CHF.

The major assumption in modeling this regime is that it can be modeled by a combination of steady state boiling heat transfer to liquid and convective heat transfer to vapor. In this model,

the heat flux is bounded by the CHF at the lowest wall temperatures and it approaches the flux based on single-phase vapor heat transfer as the wall temperature rises. The heat transfer is based on a modified Chen correlation for transition heat transfer (Reference 18 and 37). This model makes a smooth transition from the CHF to the vapor, with the calculated fraction of liquid heat transfer based on the wall temperature. The Chen correlation has been tested against data and behaves adequately, which is sufficient for LBLOCA transition boiling.

Film boiling occurs when the wall temperature exceeds the minimum temperature for stable film boiling and the void fraction lies in the appropriate range. The coolant consists of vapor and water droplets in this mode. The heat transfer mechanisms consist of boiling heat transfer to liquid droplets, convective heat transfer to vapor, and radiative heat transfer to droplets.

[

]

[

]

4.4.2.2 Scaling from Tests

While analytical arguments (see prior section) can provide a basis for code scaling for selected cases, often the issue of scaling needs to be addressed by a comparison to test data. Code scaling and the tests making up the basis are discussed in the following paragraphs.

4.4.2.2.1 Film Boiling Heat Transfer

A series of tests was performed in the THTF at Oak Ridge National Laboratory to measure heat transfer at higher pressures and flows. These included 22 steady-state dry-out tests (Reference

44), 3 transient boil-off tests (Reference 45) and two sets of transient reflood tests (References 46 and 47). The reactor core was simulated by an 8x8 array of heated rods with dimensions corresponding to those of a W 17x17 fuel assembly. The axial power shape was uniform. The FLECHT-SEASET used 161 full-length simulated fuel rods and axially-dependent power shapes (Reference 48). Based on rod count, these two test facilities differ by a scaling factor of 2.5.

These tests were used to evaluate the film boiling heat transfer. Table 4.21 compares the ranges for LBLOCA calculations for parameters that affect heat transfer with the ranges covered by the THTF tests and FLECHT-SEASET. Given the near prototypic nature of the fuel rod simulators and the extent to which the tests span the applicable ranges for LBLOCA, it is concluded that the heat transfer models, including correlations and closure relations, in S-RELAP5 are sufficient to allow direct application to a PWR LBLOCA and that the uncertainties obtained from these tests are applicable.

4.4.2.2.2 Core Entrainment

Entrainment of water droplets by the steam flow in the core can affect the predicted core cooling flow. The primary determinant of entrainment is the drag exerted on the liquid droplets by the steam flowing up out of the core. This drag, in turn, depends on the vertical flow regime in the core model. The determinants of the model applicability to a PWR LBLOCA are primarily local and, in the core, principally related to the conditions within the flow channel between the fuel rods. The axial effects predominate in this phenomenon. Radial redistribution is a second-order effect, in that it makes fluid available in a channel or removes it. The RLBLOCA methodology makes use of the TWOODEE component in S-RELAP5 to model the radial behavior in the core.

The tests used in the assessments, CCTF (Reference 49), FLECHT-SEASET (Reference 48), and THTF (References 44, 45, 46, and 47), use bundles of full-length fuel rods. Achilles (Reference 50) also used full-length rods, but the gaps between the rods and the piping containing the rods caused some radial flow re-distributions which made it less suitable for confirming scaling of core entrainment. The LOFT and SEMISCALE Test S-06-03 cores were too short for entrainment scaling. Based on the comparisons to CCTF, FLECHT-SEASET and THTF, the core entrainment model in S-RELAP5 is conservative and will scale suitably to a full-scale PWR LBLOCA.

4.4.2.2.3 Critical Flow at Break

The choked flow model used for FRA-ANP RLBLOCA analyses is the homogeneous equilibrium model (HEM) and not the Ransom-Trapp model (Reference 51). Choking for break flow occurs when the flow velocity reaches the speed of sound in the break. The critical flow model is not scale dependent, however, the Marviken Full-Scale Critical Flow Test data were used to determine the S-RELAP5 critical flow multipliers and uncertainties (Reference 5) as discussed in Section 4.3.

The test facility consists of four major components: a full-scale BWR vessel, a discharge pipe attached to the bottom of the vessel, a test nozzle connecting to the downstream end of the discharge pipe and a rupture disk assembly attached to the downstream end of the nozzle. Nozzles of various length-to-diameter ratios are used in the tests. The Marviken test data have been widely used in assessing critical flow models of various system codes over a range of flows to confirm the scalability. The Marviken tests provide a suitable basis for code scaling verification and the determination of uncertainties.

4.4.2.2.4 Carry-over to Steam Generator

Steam binding in a LBLOCA is assumed to occur as a result of steam production in the steam generator. This steam production occurs when water carried over from the core enters the hot steam generator. The resulting vaporization expansion increases the pressure drop through the steam generator and produces steam binding that reduces the core reflood rate.

The results from three test facilities were used to benchmark and verify the RLBLOCA methodology and S-RELAP5: Tests 54, 62, 67 and 68 (Reference 49) at the CCTF, Tests 10 (Reference 52) and 29 (Reference 53) at the UPTF, and Tests 31203, 31302, 31701, and 31805 at FLECHT-SEASET (Reference 48). The FLECHT-SEASET tests have prototypic rods and spacers for PWR fuel, but the balance of the test facility bears little resemblance to a PWR. The UPTF is a full-scale simulation of a German PWR. The steam generators are replaced with steam separators and the pumps are simulated with mechanical resistance. The CCTF is scaled such that it is prototypic of a $\frac{1}{3}$ PWR in the dimension parallel to flow and scaled down (~ 0.2) in the orthogonal directions.

The UPTF has no core per se, and reflood is simulated with steam and water injection. The CCTF and FLECHT-SEASET have electrically heated rods in the core. The upper plenum

region was tested at full scale in the UPTF, as were the hot legs and the steam generator inlet plenum. The steam generator tubing geometry is prototypic in the CCTF (although the number of tubes is smaller). All these tests in the three facilities collected water carried over from the core under conditions representing the reflood phase of the LBLOCA and all three have additional collapsed liquid level measurements. As presented in Section 4.3, a study on carryover to the steam generator was performed using the CCTF. From that study, a bias on interfacial drag was determined to conservatively bound this phenomenon. The results of the CCTF (with bias), UPTF, and FLECHT-SEASET evaluations indicate that S-RELAP5 overpredicts the entrainment of liquid from the test bundle (Section 5.6 and Reference 5). While each test by itself has some deficiencies in terms of simulating a PWR and in terms of scale, the combination of the three tests provides a substantial basis for evaluating modeling of the drag between the two phases during reflood at full scale.

4.4.2.2.5 Pump Scaling

The S-RELAP5 code has normalized single phase homologous curves for a full scale W reactor coolant pump as code default. The use of full scale data for the pump makes code scaling moot for the pump. These homologous curves are set to applicable values by entering plant specific values for rated head, torque, moment of inertia, etc.. The coastdown of the pump is driven by the torque and moment of inertia of the rotating mass. The torque includes the effects of friction and back EMF (pump torque) and of the loop pressure losses (hydraulic torque). The single phase pump head and torque curves are adjusted for two-phase degradation based on experimental data. The EPRI two-phase degradation data (Reference 54) is based on pumps that are similar to PWR coolant pumps and represent best estimate parameters. However, as a result of the sensitivity studies performed, the Semiscale two-phase degradation data produced a slightly conservative PCT and is used in the RLBLOCA methodology.

4.4.2.2.6 Cold Leg Condensation

Cold leg condensation was evaluated at a scaled EPRI test facility (Reference 55) to determine the accuracy of the calculated interfacial heat transfer between the ECC water and the steam in the cold leg. The principal portion of the test apparatus was the simulated cold leg, which was fabricated from straight pipe with an ID of 10.42 in. Two injection points were provided so that the pipe lengths downstream of the injection point approximated either a typical PWR cold leg scaled down to about one-third or the full length of the cold leg. The cold leg pipe length

downstream of the injection point for a typical Westinghouse PWR is about 16 and the cold leg ID is about 2.7. In the EPRI 1/3 scale test, the full length is approximately 15.6 feet, and the scaled length is 6.

For vertical components and for horizontal components not in either the stratified or slug flow regimes, the condensation model is based on a model by Carpenter and Colburn (Reference 56) as formulated in Collier's book on heat transfer (Reference 57). For stratified and slug flow in horizontal components the heat transfer also is taken from Reference 57. These models are relatively insensitive to geometry and are expected to scale from the 1/3 scale tests to full scale. In addition, these condensation effects were considered in the UPTF (see Section 4.3.1.11.2), which is full scale.

4.4.2.2.7 Bypass of Downcomer by ECC Water and Lower Plenum Sweep-Out

The scalability of the code predictions for the bypass of downcomer water is of particular interest because tests with fixed power-to-volume scaling do not show the same phenomena (LOFT L2-3 versus SEMISCALE counterpart Test, S-06-3, Reference 5). The major difference between these two tests was the behavior of the flow in the downcomer during the accumulator injection phase. In the LOFT test, the flows were down in the region of the downcomer near the intact loop and up near the broken loop before the accumulator empties. In the SEMISCALE test, it was up in both segments until the accumulator emptied. The differences were attributed to the scaling, which preserved power-to-volume but did not preserve downcomer volumes, gaps, and surface area-to-fluid volume ratios between the two tests.

The UPTF test facility has full-scale downcomer, cold legs and hot leg. This makes code scaling a non-issue for this comparison to test data. Test 6 (References 58 and 59), Runs 131, 132, 133, 135, and 136, and Test 7 (References 60 and 61), Run 203, were specifically designed to examine downcomer counter current flow behavior during blowdown, ECC bypass, and lower plenum refill with cold leg ECC injection. These interactions play a key role in determining the rate at which ECC water is able to refill the lower plenum. The tests were analyzed to demonstrate the ability of S-RELAP5 to self-limit counter current flow in the downcomer and predict reasonable refill behavior including ECC bypass compared to experimental data. The code comparisons focused on steam-water flow phenomena in the intact cold legs, the downcomer, and the lower plenum during the end-of-blowdown/refill phases of a LBLOCA.

In these tests, steam was injected in the core region, where it traveled downward to the lower plenum, then into the bottom of the downcomer. It then rose through the downcomer and exited at the broken cold leg. ECC injection (with and without nitrogen) entered from the cold legs at the top of the downcomer. Depending on the upward flow rate of the steam in the downcomer, the ECC water from the cold legs either bypassed to the broken cold leg or flowed down into the lower plenum.

These tests were such that the code modeling for the several important phenomena could be compared to full-scale measurements, for the downcomer, multi-dimensional effects, condensation and non-equilibrium flow, countercurrent and slug flow and entrainment and de-entrainment. Since the steam was flowing out the bottom of the core, these tests also addressed lower plenum sweep out. The results of these assessments indicated that S-RELAP5, with the RLBLOCA nodalization (Reference 12), overpredicted the ECC bypass and lower plenum sweep out.

4.4.2.2.8 Loop Oscillations

Test 8 at the UPTF (References 62 and 63) investigated the behavior during the end-of-blowdown, refill, and reflood phases of a postulated LOCA with ECC injection. The focus of the test evaluations was the pressure and fluid oscillations in the cold legs. These oscillations arise when the steam is condensed by the ECC water and forms a liquid plug in the cold leg. The flow rate falls and the flow in the cold leg transitions to the stratified flow regime, allowing the steam flow to increase again. This sweeps the liquid out again.

Test 8, Runs 111 and 112 was performed by isolating one intact loop at the pump simulator, opening a second intact loop to stabilize the pressure drop between the upper plenum and the downcomer, opening the break valves on the broken loop, injecting steam into the test vessel, and varying ECC water injection into the third intact loop cold leg downstream from the pump simulator. Thus the principle portion of the system relevant to the UPTF Test 8 used in this analysis consists of the cold leg piping for the third loop from the steam generator simulator to the pump simulator (including loop seal), the pump simulator, and the cold leg piping from the pump simulator to the vessel downcomer; all of which are full scale.

The S-RELAP5 calculations for this test indicated that the code predicted the formation of a cold leg sub-cooled liquid plug and condensation at the face of that plug. This was consistent with

the data for the test, indicating that the code is capable of calculating the appropriate phenomena in a full-scale facility.

Table 4.1 Parameters Perturbed for PIRT Sensitivity Studies

Table 4.1 Parameters Perturbed for PIRT Sensitivity Studies (*Continued*)



Table 4.1 Parameters Perturbed for PIRT Sensitivity Studies (*Continued*)



Table 4.2 Assessment Matrix



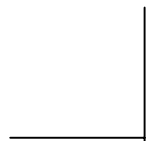
Table 4.3 Assessment Matrix Tests and Phenomena Addressed



Table 4.3 Assessment Matrix Tests and Phenomena Addressed (*Continued*)



Table 4.4 Large Break LOCA Nodalization



**Table 4.5 PDTF SMART Tests Chosen for S-RELAP5 Verification
and Validation**

Test Designator	Test Description
KH01B	Reported HTP spacer test with constant flooding rate of 4 in/s
KH02B	Reported HTP spacer test with constant flooding rate of 2 in/s
KH03B	Reported HTP spacer test with constant flooding rate of 1 in/s
KH05A	Reported HTP spacer test with variable flooding rate from 8 to 1 in/s

Table 4.6 Comparison of Effluent Temperature for the Plant-Consistent Model, Westinghouse/EPRI

Run Number	Liquid, Data	Liquid, Calculated	Vapor, Data	Vapor, Calculated
5-18	189.0	195.30	188.0	239.61
5-24	222.0	238.65	281.0	280.71
5-25	281.0	268.24	282.0	485.01
5-27	229.0	220.96	226.0	489.91
5-34	228.0	229.35	221.0	415.71
5-52	209.0	200.98	230.0	237.75
5-53	184.0	194.72	184.0	234.22
5-57	280.0	275.63	282.0	489.34
5-60	231.0	220.52	233.0	466.19
6-41	195.0	198.91	197.0	267.11
6-65	182.0	198.95	182.0	226.42
6-67	160.0	154.05 ^a	159.0	235.07
6-69	172.0	173.83	175.0	497.47
6-73	168.0	192.22	169.0	224.37
6-83	174.0	195.14	156.0	223.78
6-88	172.0	170.89	174.0	510.17
6-93	134.0	133.00 ^a	134.0	215.81
6-95	196.0	212.65	198.0	317.74
6-99	151.0	156.63 ^a	153.0	280.97

^a Oscillatory results. Values presented are time-averaged value from 70 to 100 seconds at 4-second intervals.

Table 4.7 Test Phase Parameters for Test 10 Run 081

Phase	Start Time (s)	End Time (s)	Steam Injection Rate (kg/s) (lb _m /s)	Water Injection Rate (kg/s) (lb _m /s)
1	35	75	125 276	60 132
2	75	135	125 276	16 35
3	135	196	110 243	16 35
4	195	255	87 192	16 35

Table 4.8 Test Phase Parameters for Test 29 Run 212/211

Phase	Start Time (s)	End Time (s)	Steam Injection Rate (kg/s) (lb _m /s)	Water Injection Rate (kg/s) (lb _m /s)
1	35	175	102 225	140 309
2	175	320	87 192	153 337
3	320	465	100 221	90 198
4	465	615	85 187	101 223
5	615	770	101 223	47 104
6	770	900	85 187	63 139

**Table 4.9 Calculated Water Downflow Rates for the 0.3 MPa
Test Series**

Steam Injection Rate (kg/s)	Water Injection Rate (kg/s)	Water Downflow Rate w/o CCFL (kg/s)	Water Downflow Rate w/ CCFL (kg/s)
4.6	30.5	30.5	30.5
10.5	30.5	30.5	28.2
11.0	30.5	30.5	25.1
12.4	30.5	30.5	17.9
12.9	30.5	30.5	15.3
15.3	30.5	30.5	5.8
18.5	30.5	30.5	0.0
20.5	30.5	27.0	
21.0	30.5	24.0	
22.0	30.5	20.0	
23.0	30.5	16.0	
24.0	30.5		

**Table 4.10 Calculated Water Downflow Rates for the 1.5 MPa
Test Series**

Steam Injection Rate (kg/s)	Water Injection Rate (kg/s)	Water Downflow Rate w/o CCFL (kg/s)	Water Downflow Rate w/ CCFL (kg/s)
8.3	29.4	29.4	29.4
9.3	29.4	29.4	29.4
18.1	29.4	29.4	29.4
24.0	29.4	29.4	19.1
28.0	29.4	29.4	10.0
31.0	29.4	29.4	5.3
32.6	29.4	29.4	3.5
33.5	29.4	29.4	2.6
36.0	29.4	29.4	1.3
40.2	29.4	29.4	0.0
42.0	29.4	29.0	
45.0	29.4	20.0	
48.0	29.4	15.1	
51.0	29.4	10.3	
53.0	29.4	7.3	
55.0	29.4	0.0	

Table 4.11 CCTF Test Conditions

Run	Core Power	LPCI Flow $\left(\frac{\text{m}^3}{\text{s}}\right)$	System Pressure (MPa)
54	ANSx1.0 + Actinide * 1.1	0.011	0.20
62	ANSx1.2 + Actinide * 1.1	0.011	0.20
67	ANSx1.2 + Actinide * 1.1	0.011	0.15
68	ANSx1.0 + Actinide * 1.1	0.025	0.20

Table 4.12 Summary Comparison of Measured and Calculated PCT, CCTF Tests 54, 62, 67, and 68

Run	Measured PCT (K)	Time of Measured PCT (s)	Calculated PCT (K)	Time of Calculated PCT (s)
54	1113	130	1147	257
62	1132	154	1241	317
67	1143	164	1300	357
68	1122	144	1105	210

Table 4.13 Test Data for SCTF-II Tests Modeled



Table 4.13 Test Data for SCTF-II Tests Modeled (*continued*)

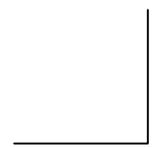


Table 4.14 Phase I Assessment Results, SCTF Tests

		S2-10	S2-11	S2-AC1	S2-SH1
PCT (K)	Data	1168.0	1085.0	1085.0	1166.0
	S-RELAP5	1193.0	1066.0	1073.0	1112.0
Time of PCT (s)	Data	193.5	125.5	127.0	251.5
	S-RELAP5	221.0	123.5	129.0	183.1
Quench Time (s)	Data	564.0	458.5	510.5	628.5
	S-RELAP5	471.0	235.0	309.0	403.0

Table 4.15 Phase II Assessment Results, SCTF Tests

		S2-17	S2-18
PCT (K)	Data	1080.0	1116.0
	S-RELAP5	1034.0	1069.0
Time of PCT (s)	Data	180.0	125.0
	S-RELAP5	168.3	135.7
Quench Time (s)	Data	540.0	500.0
	S-RELAP5	362.0	374.0

Table 4.16 PWR-LOFT Scaling Ratios

Parameters	PWR	LOFT	Ratio
Core Power (MWt)	3411	50	68/1
Total PCS Volume (ft ³)	12540	281	45/1
Upper Plenum/Head Volume (ft ³) (JAERI)*	1959 1450	31.8 31.8	62.1 41/1
Core Height (ft)	12	5.5	2/1
Core and Bypass Volume (ft ³)	920	11.1	83/1
Core Flow Area (ft ²) (JAERI)*	54.1 57.2	1.997 1.997	27/1 29/1
Lower Plenum Volume (ft ³)	1050	25.34	41/1
Downcomer & Inlet Annulus (ft ³)	721	24.25	30/1
Downcomer Flow Area (ft ²) (Including LOFT 0.25 in. Gap)	45.5 45.5	1.527 1.840	36/1 25/1
ILHL Volume (ft ³)	237	13.28	18/1
ILHL Flow Area (ft ²)	13.76	0.682	20/1
Steam Generator Volume (ft ³)	3231	49.4	65/1
Pump Suction Pipe Volume (ft ³)	378	12	32/1
Pump Suction Pipe Area (ft ²)	15.73	0.682	23/1
Pump Volume (ft ³)	168	7	24/1
ILCL Volume (ft ³)	255	15.61	19/1
BLHL Volume (ft ³)**	79	12.65**	6/1
BLHL Flow Area (ft ²)	4.586	0.682	7/1
BL Steam Generator/Simulator Volume (ft ³)	1077	19.4	55/1
Pump Suction Pipe Volume (ft ³)	126	unknown	-
Pump Suction Pipe Area (ft ²)	5.24	unknown	-
BLCL Pump Side Volume (ft ³)**	85	13.19**	6/1
BLCL Vessel Side Volume (ft ³)			
BLCL Vessel Side Flow Area (ft ²)	4.123	2.3	24/1
Break Flow Area (ft ²)	4.123	0.09231	45/1
Total Pressurizer Volume (ft ³)	1800	34	52/1

* JAERI data are given in the noted Reference 49

** LOFT BLHL Volume and BLCL-Pump Side Volume include portions of the RABV line volume.

Table 4.17 LOFT Nuclear Large Break Test Parameters

Test	Power (MWt)	MLHGR (KW/ft)	Pump Operation	Fuel Pressurized	ECC			PCT (K)
					HPIS	LPIS	Accum.	
L2-2 - Double end-cold leg break, with break area scaled to simulate PWR double-end cold leg break, US Appendix K ECC.	25	8	On	No	2/3	1/2	3/4	789
L2-3 - Similar to L2-2, with higher power and increased LHGR.	36	12	On	No	2/3	1/2	3/4	914
L2-5 - Similar to L2-3, with pumps turned off and decoupled from their external flywheels within 1 s, US Appendix K ECC with 58% L2-3 HPIS.	36	12.22	Off(A)	Yes	1/3	1/2	3/4	1078
LP-02-6 - Similar to L2-5, with pumps turned off but initial coast down with external flywheels, US Appendix K ECC, increased core power and MLHGR.	46	14.87	Off(N)	Yes	1/3	1/2	3/4	1077
LP-LB-1 - Similar to LP-02-6, with pump turned off and decoupled from their external flywheels within 1 s, UK minimum safeguards ECC, and slightly increased core power and MLHGR.	49.3	15.8	Off(A)	Yes	0/3	1/2	2/4	1261

A - atypical rapid pump coastdown,
N - normal pump coastdown.

Table 4.18 Important PIRT Phenomena and Methodology Treatment



Table 4.18 Important PIRT Phenomena and Methodology Treatment (*continued*)



Table 4.19 Summary of Evaluated Uncertainties of key PIRT Parameters

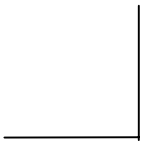


Table 4.20 Film Boiling HTC Distribution Fit Parameters



Table 4.21 Test Ranges for Film Boiling Heat Transfer Test Comparison

Parameter	Maximum		Minimum	
	Tests	LBLOCA	Tests	LBLOCA
Pressure (MPa)	8.2	10.8	0.13	0.22
Mass Flux Vapor (kg/s-m ²)	907	367	0	0
Mass Flux Liquid (kg/s-m ²)	4254	945	0	0
Void Fraction	1	1	0.13	0.13
Saturation Temperature °K	570	589	381	390
Vapor Temperature °K	1294	1160	384	391
Wall Temperature °K	1525	1400	390	396
Quality	1	1	-0.11	0

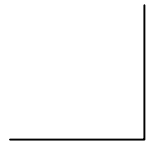


Figure 4.1 PCT Signature for 3- and 4-Loop NPP Base Case

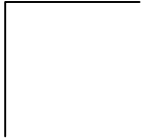


Figure 4.2 PIRT Sensitivity Histogram



Figure 4.3 Loop Nodalization for NPP



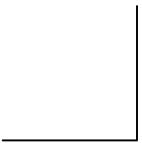
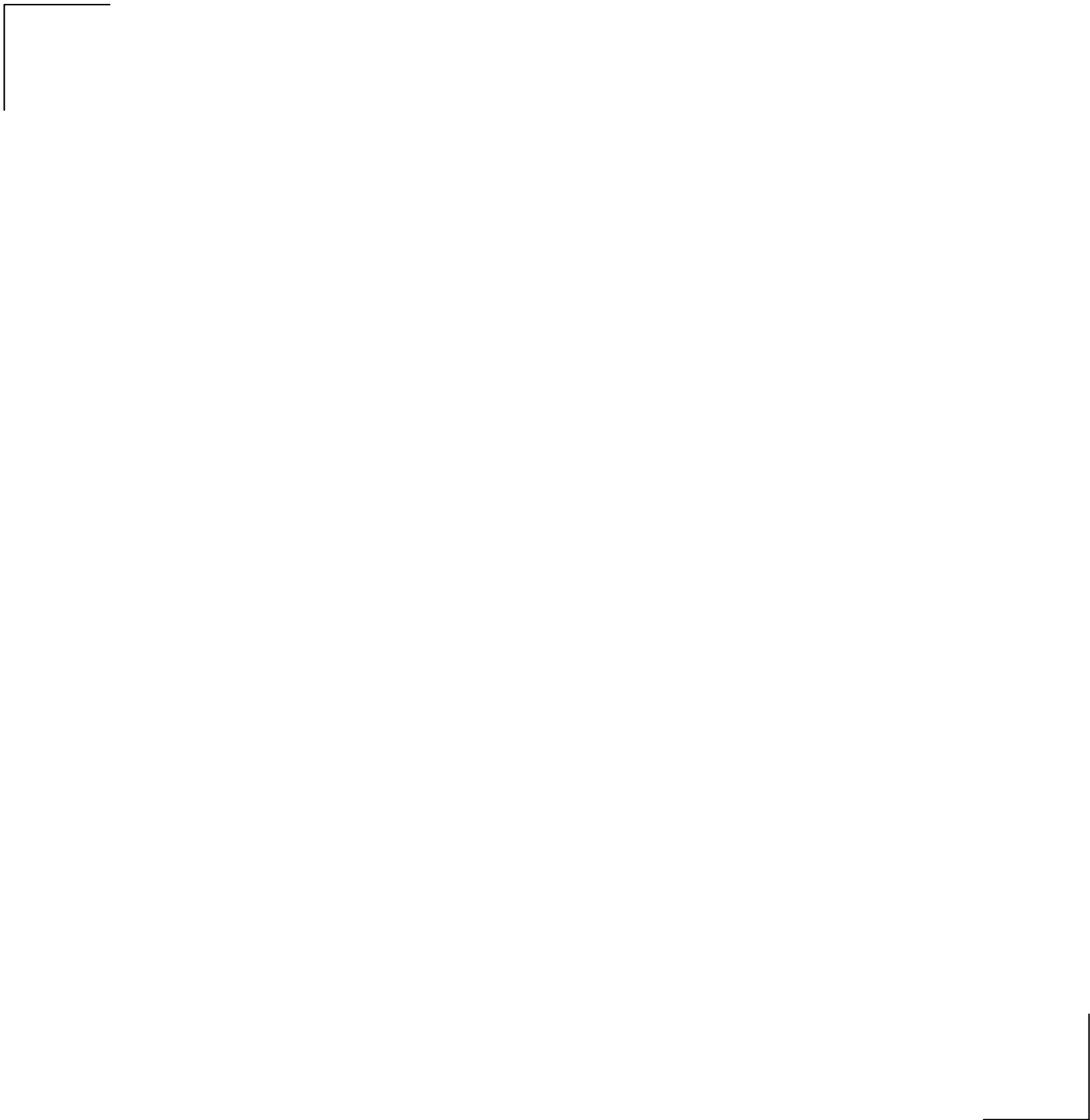


Figure 4.4 Reactor Vessel Nodalization for NPP



**Figure 4.5 CE 2x4 and Westinghouse 3- and 4-Loop Plant Vessel
Downcomer Configurations**



Figure 4.6 NPP Core Nodalization – Axial Plane



Figure 4.7 NPP Core Nodalization – Cross-Sectional Plane



Figure 4.8 NPP Upper Plenum Nodalization – Axial Plane

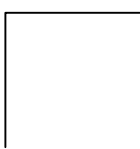


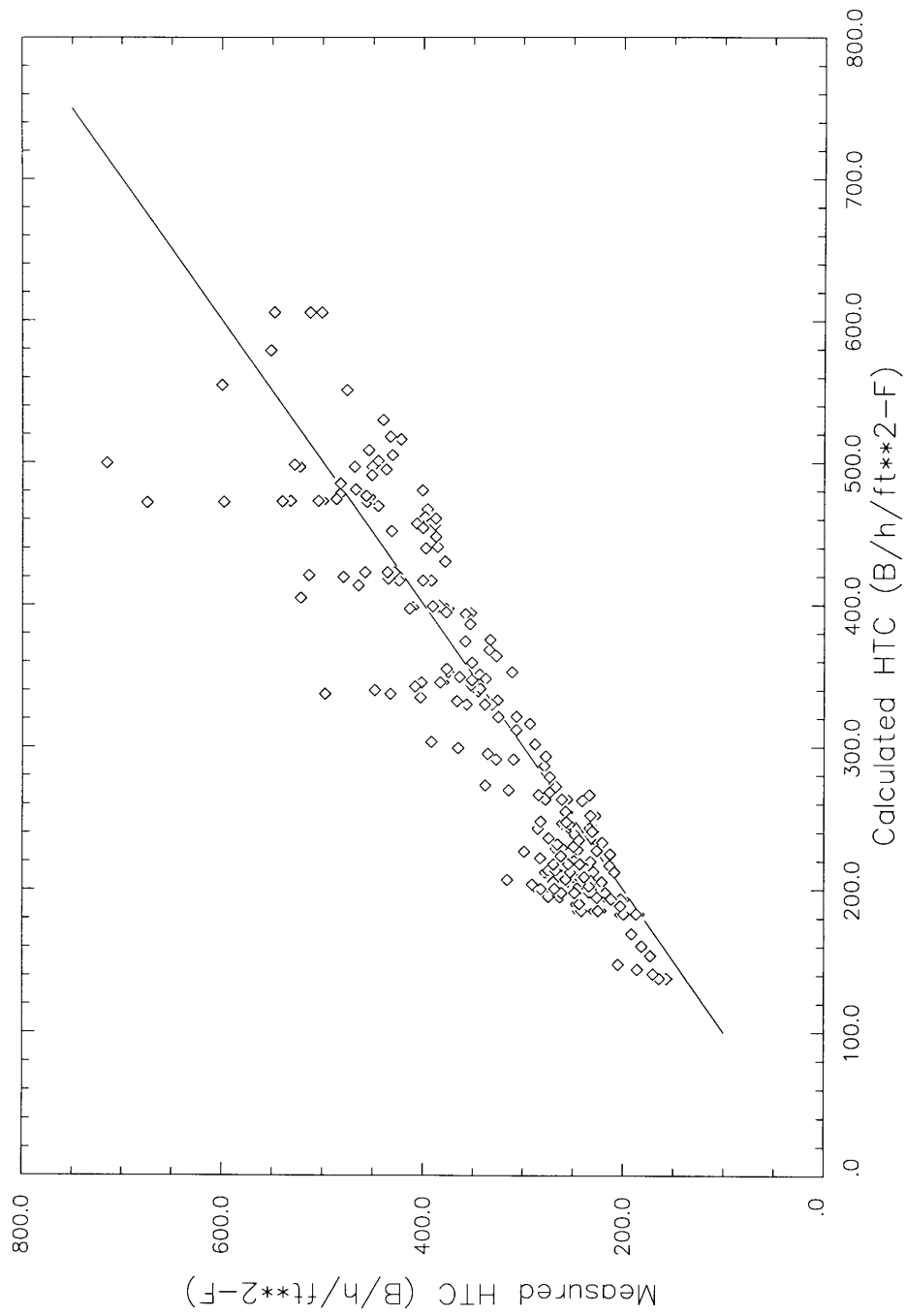
Figure 4.9 NPP Upper Plenum Nodalization – Cross-Sectional Plane



Figure 4.10 NPP Emergency Core Cooling System Nodalization

Figure 4.11 Double-Ended Guillotine Break Nodalization

Figure 4.12 Double-Ended Split Break Nodalization



**Figure 4.13 Comparison of Calculated HTC to Measured HTC, ORNL
THTF**

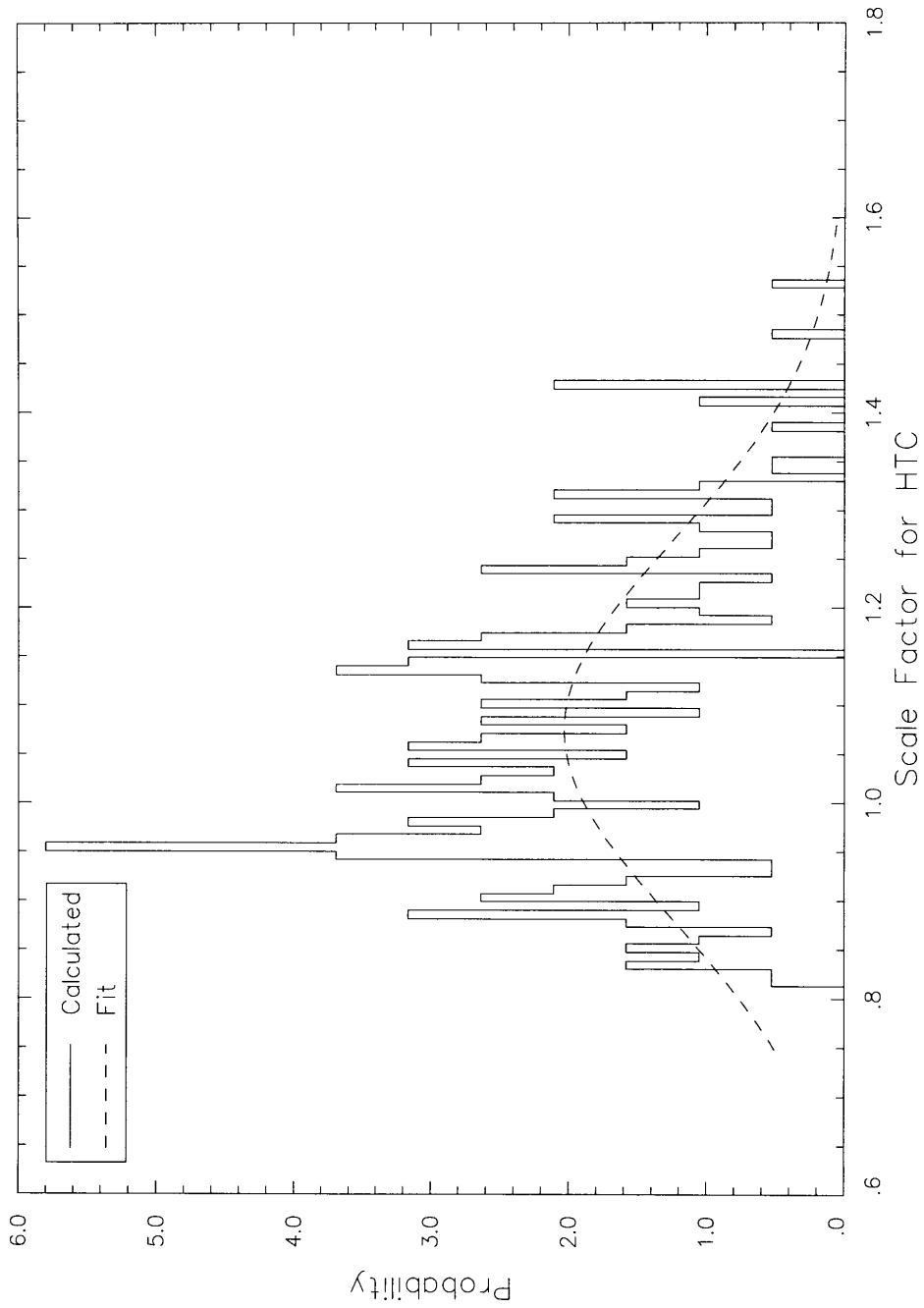


Figure 4.14 Frequency Distribution for Scale Factor for HTC, ORNL THTF

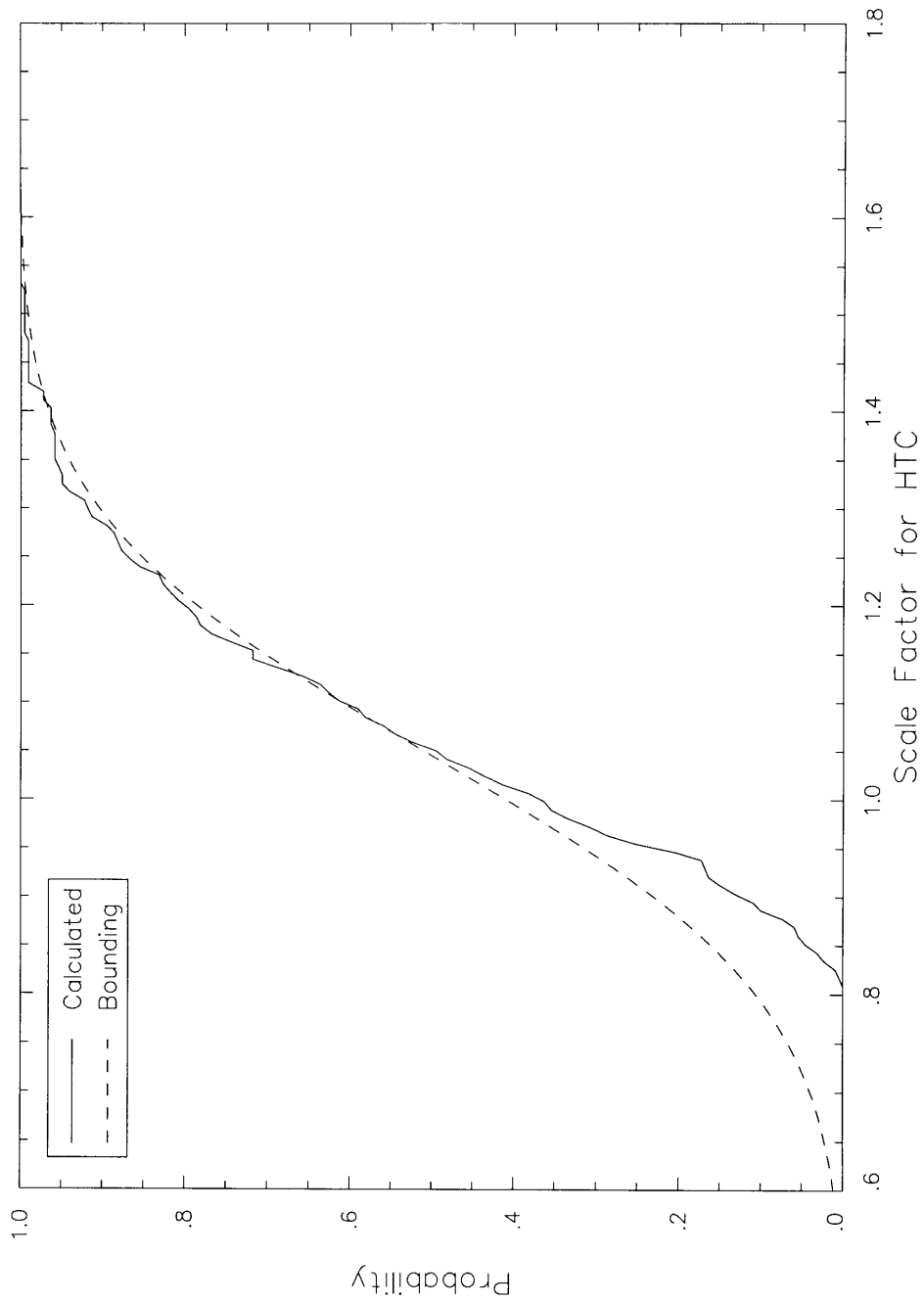


Figure 4.15 Bounding Distribution for HTC Scaling, ORNL THTF

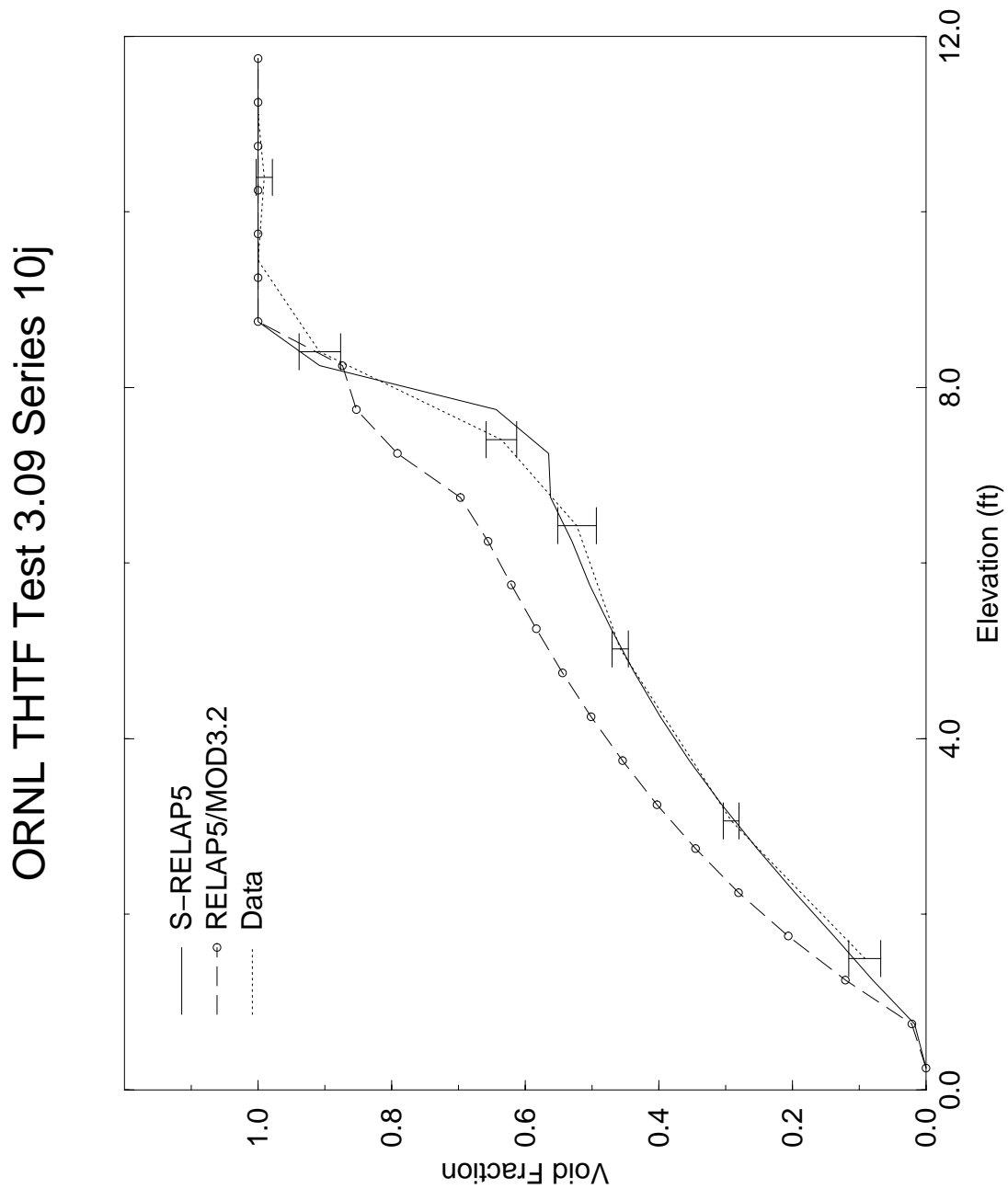


Figure 4.16 Comparisons of Void Profiles, ORNL THTF Test 3.09.10j

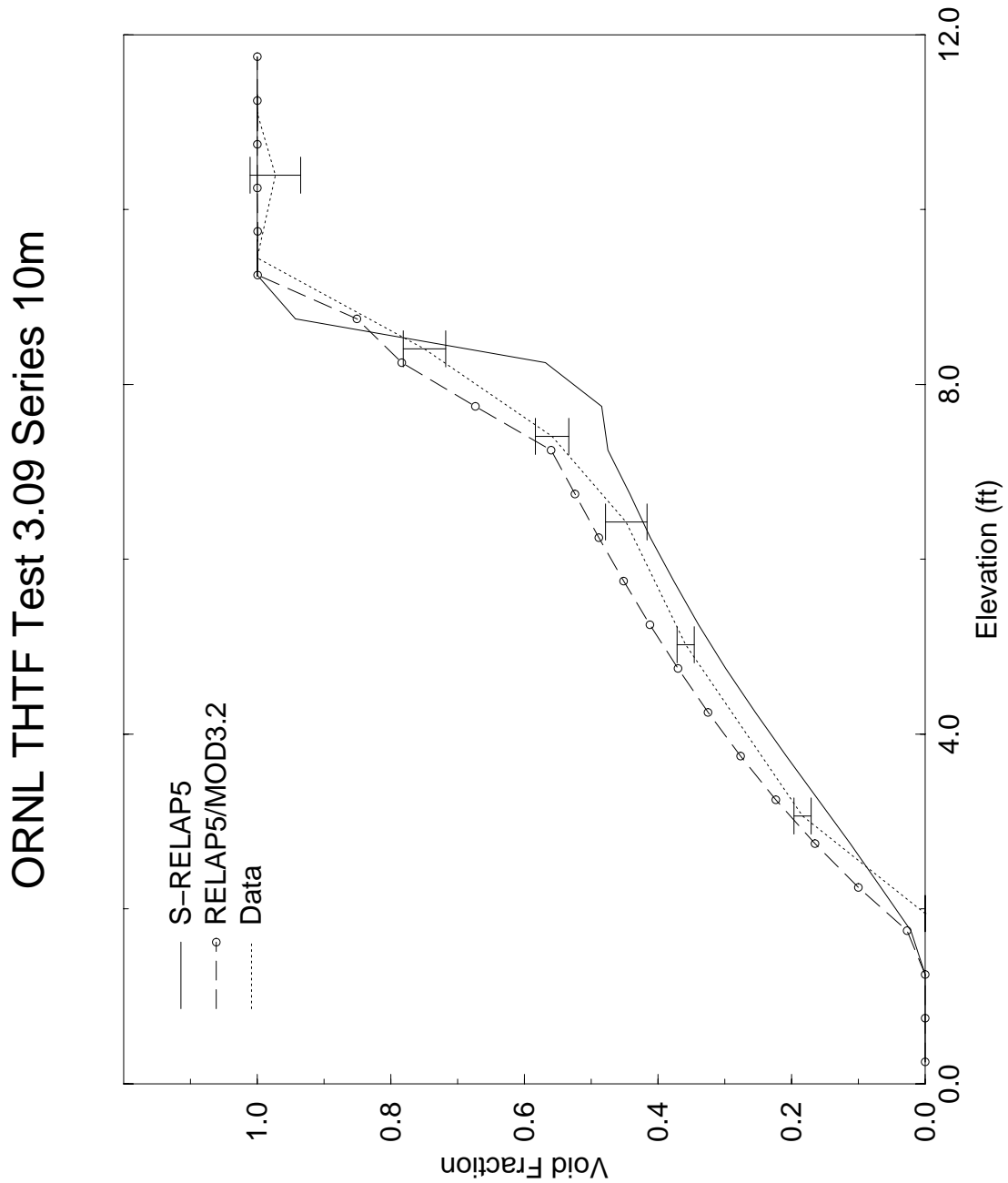


Figure 4.17 Comparison of Void Profiles, ORNL THTF Test 3.09.10 m

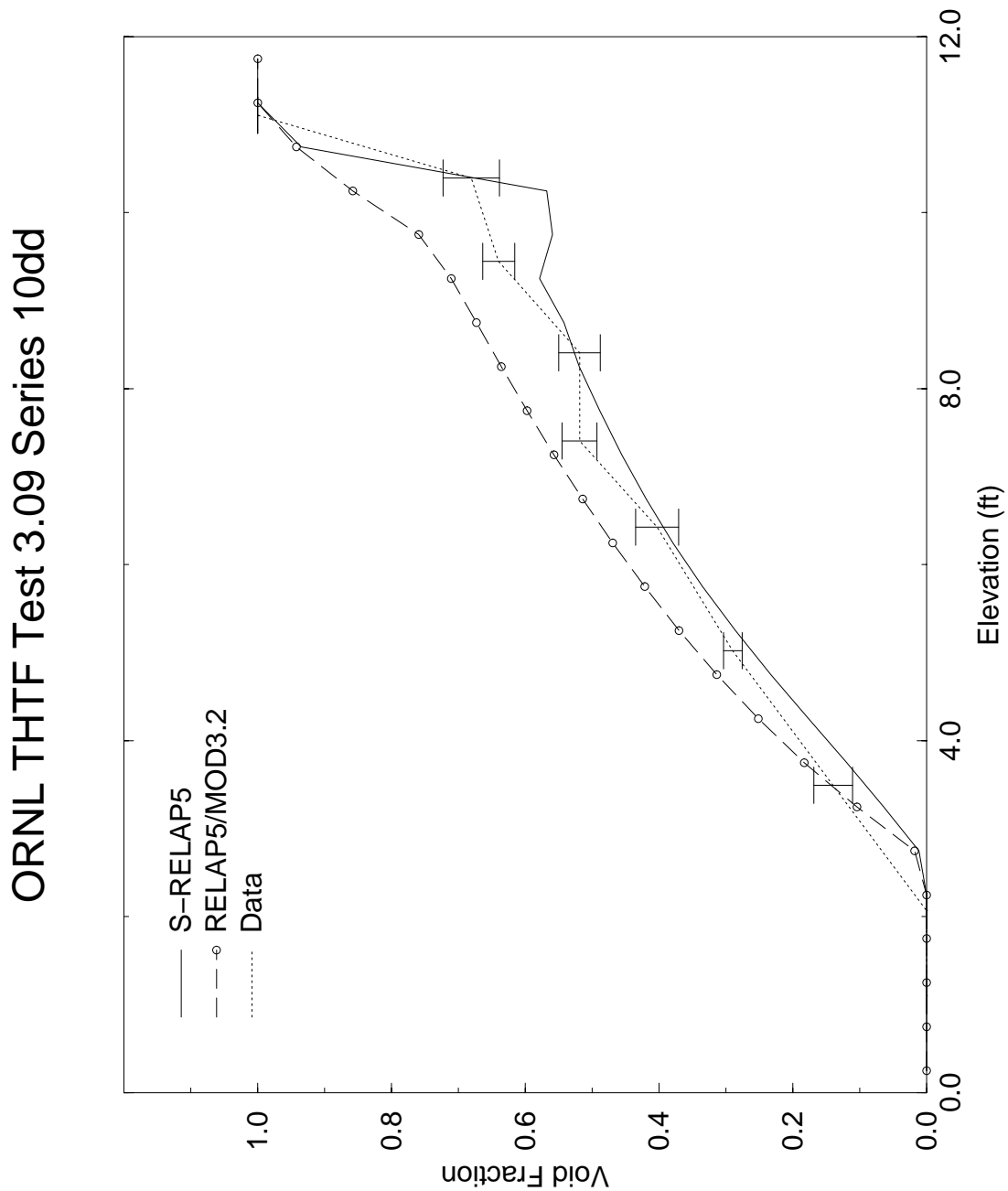


Figure 4.18 Comparison of Void Profiles, ORNL THTF Test 3.09.10dd

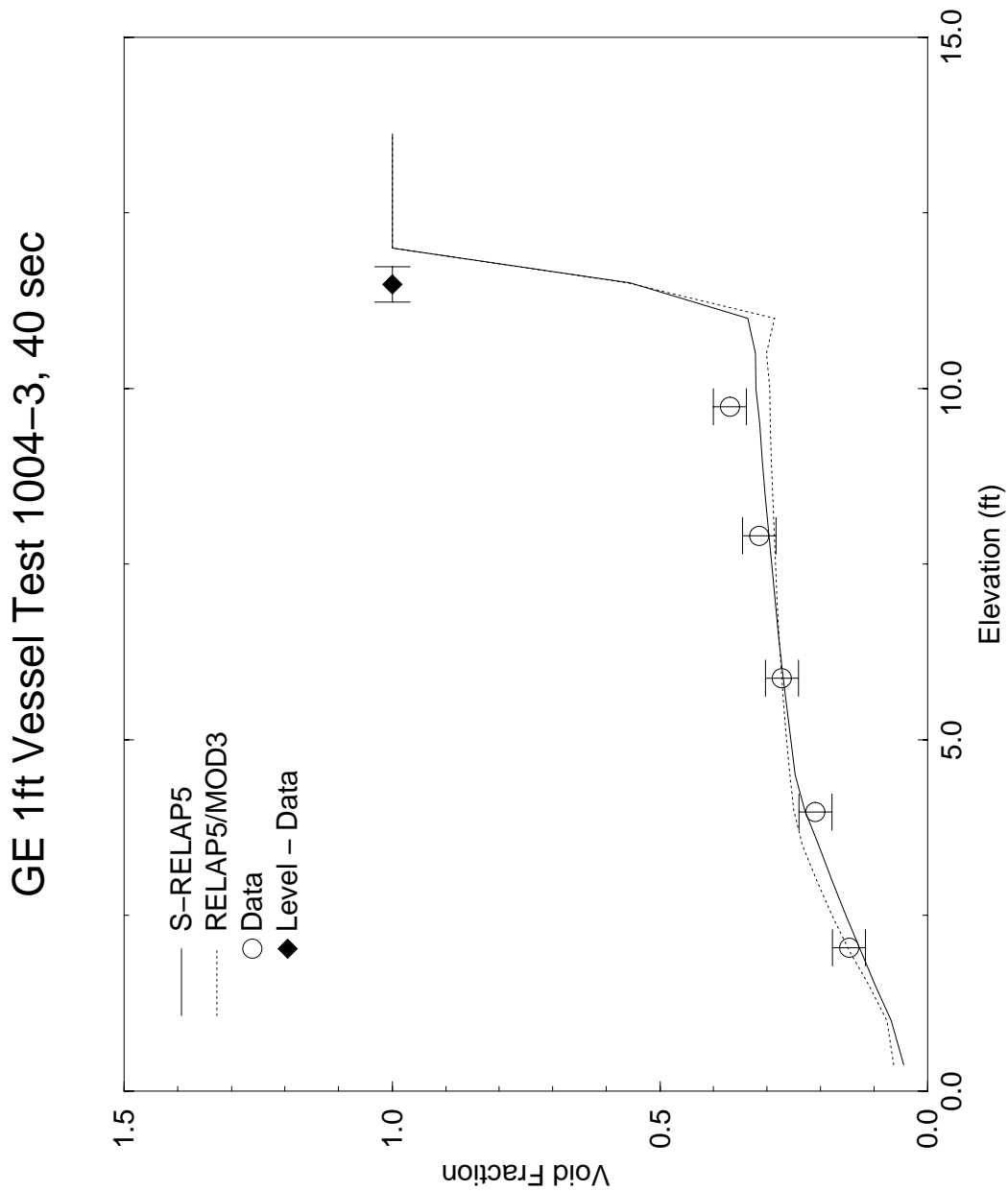


Figure 4.19 Void Profiles at 40 Seconds for the 1 ft GE Test 1004-3

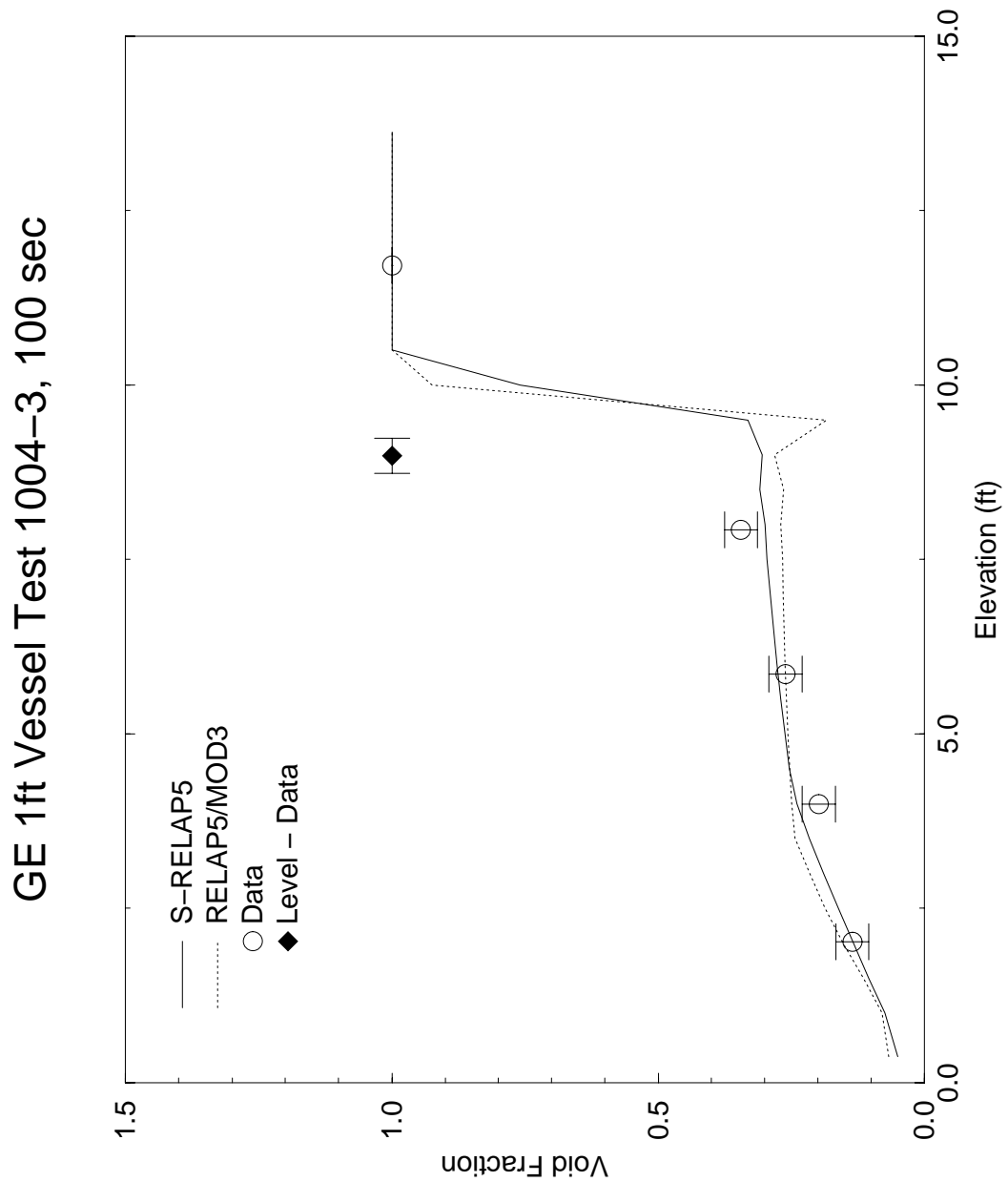


Figure 4.20 Void Profiles at 100 Seconds for the 1 ft GE Test 1004-3

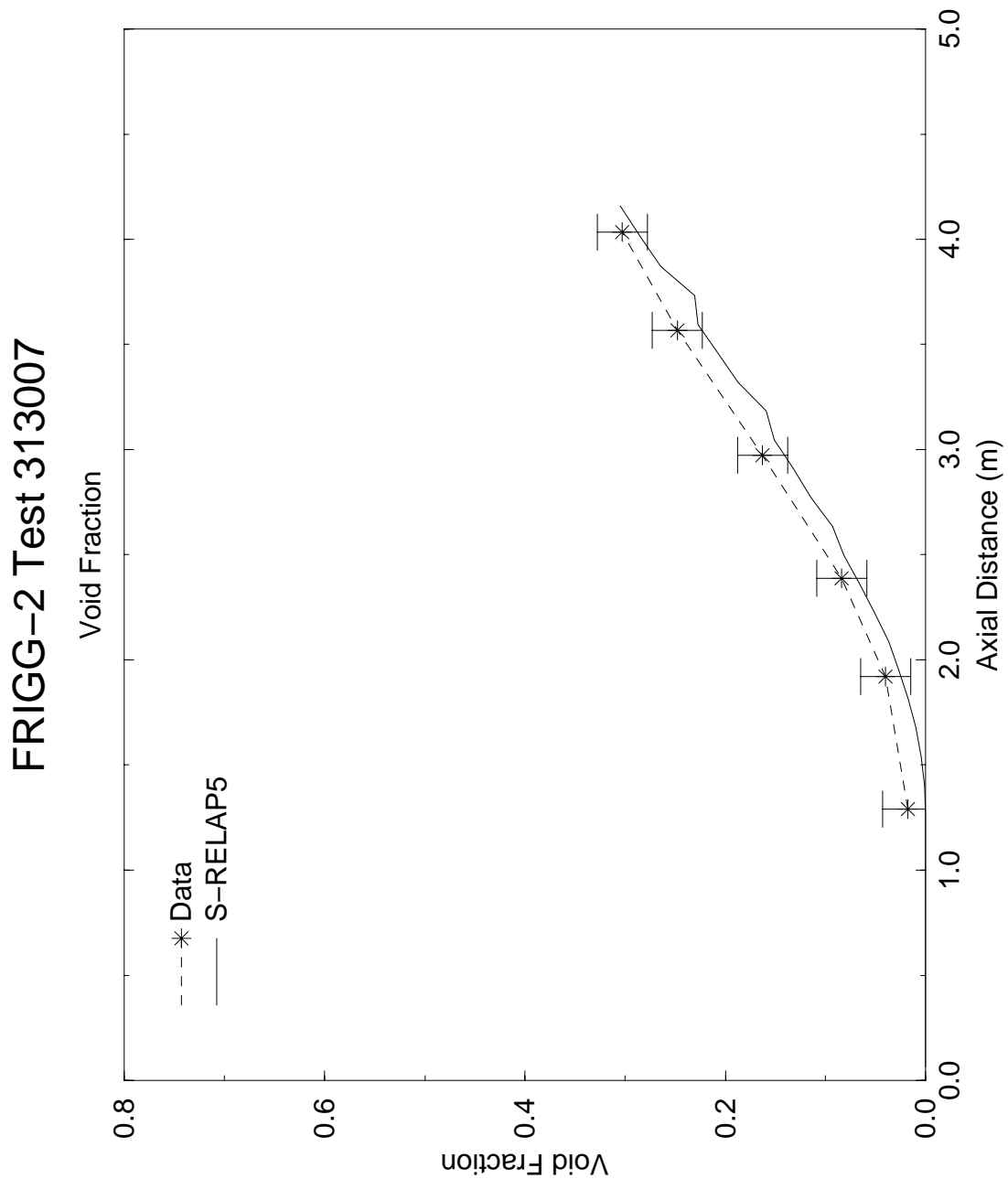
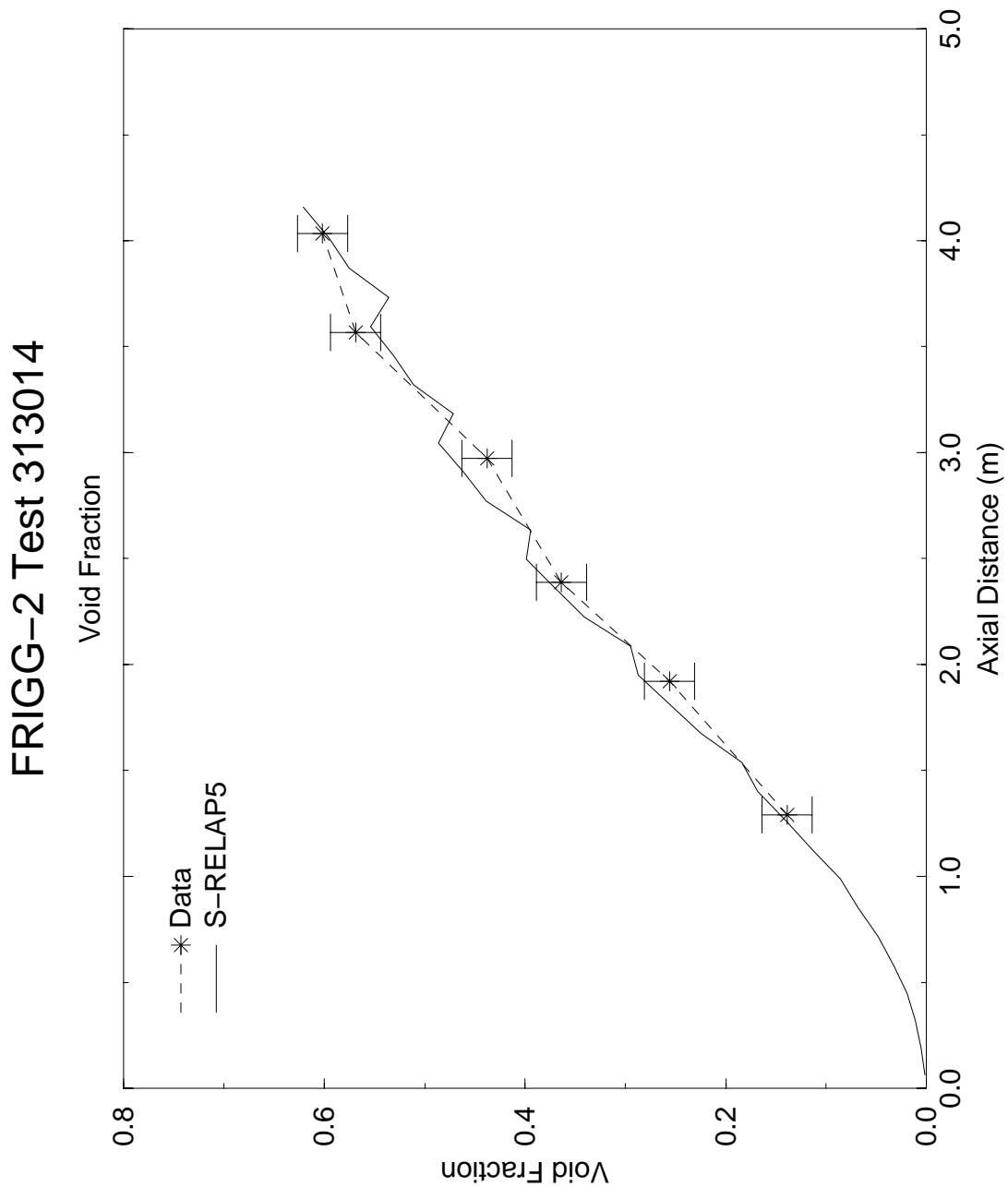


Figure 4.21 Comparison of Calculated and Measured Void Fraction, Frigg-2 Test 313007



**Figure 4.22 Comparison of Calculated and Measured Void Fraction,
Frigg-2 Test 313014**

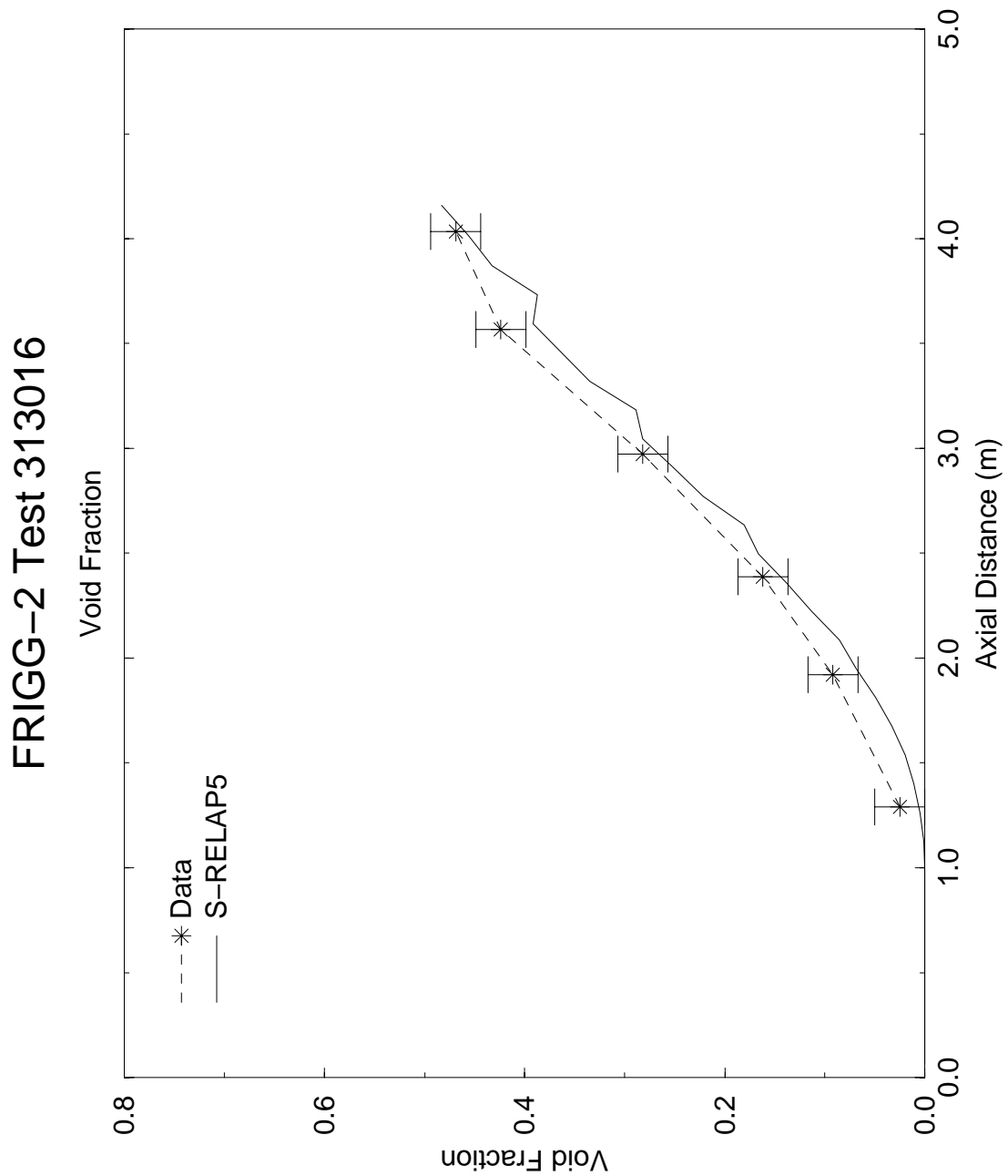


Figure 4.23 Comparison of Calculated and Measured Void Fraction, Frigg-2 Test 313016

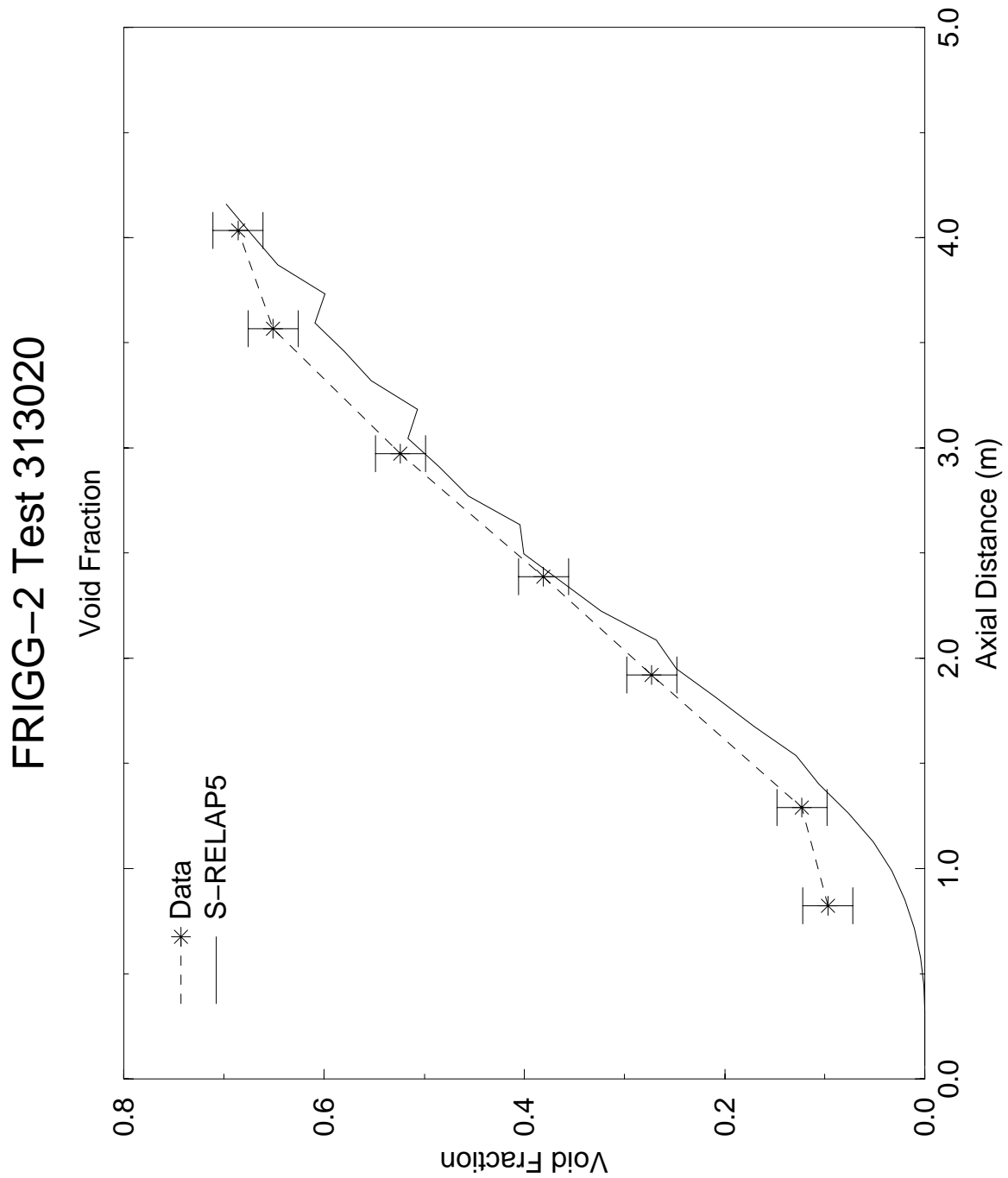


Figure 4.24 Comparison of Calculated and Measured Void Fraction, Frigg-2 Test 313020

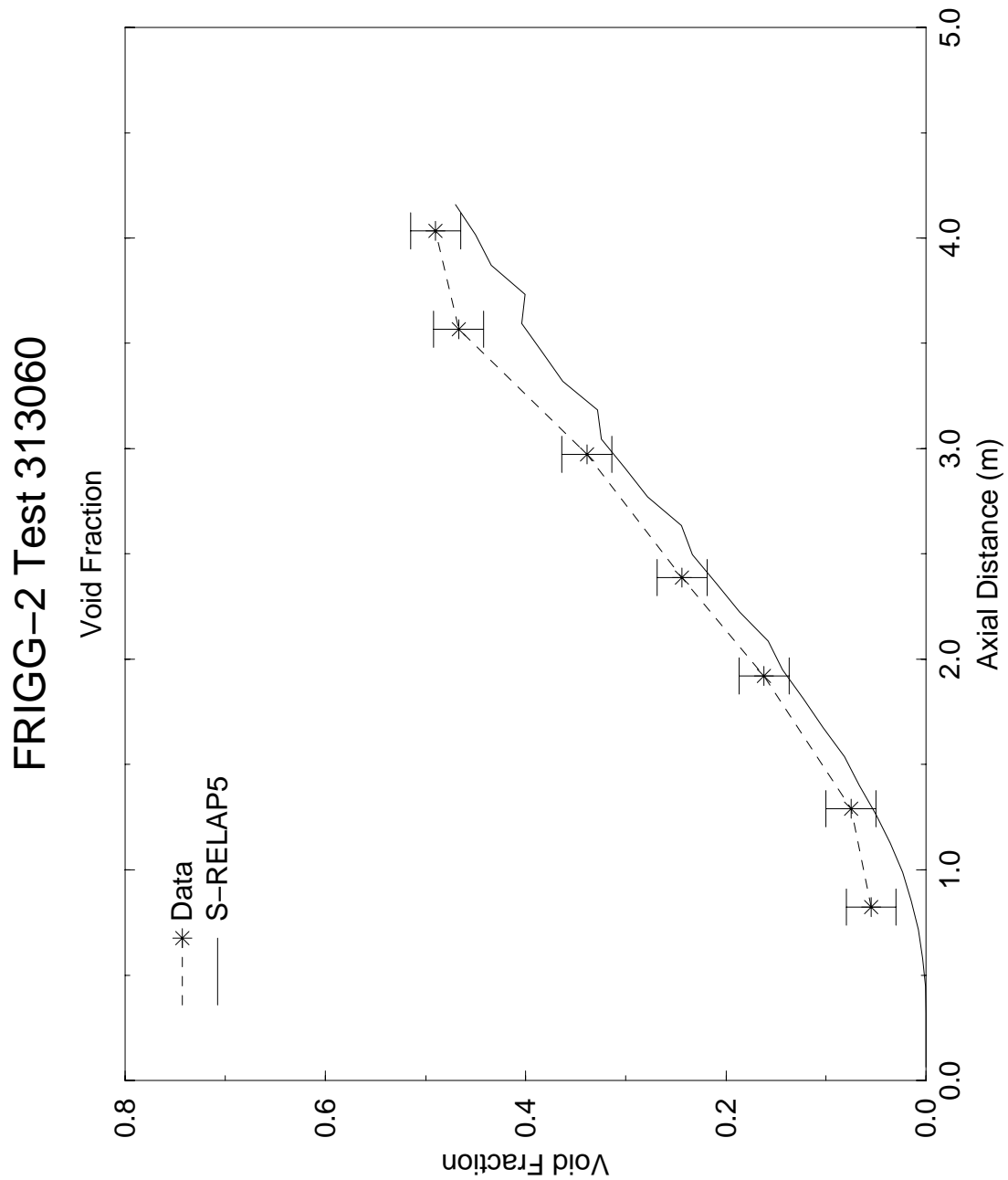
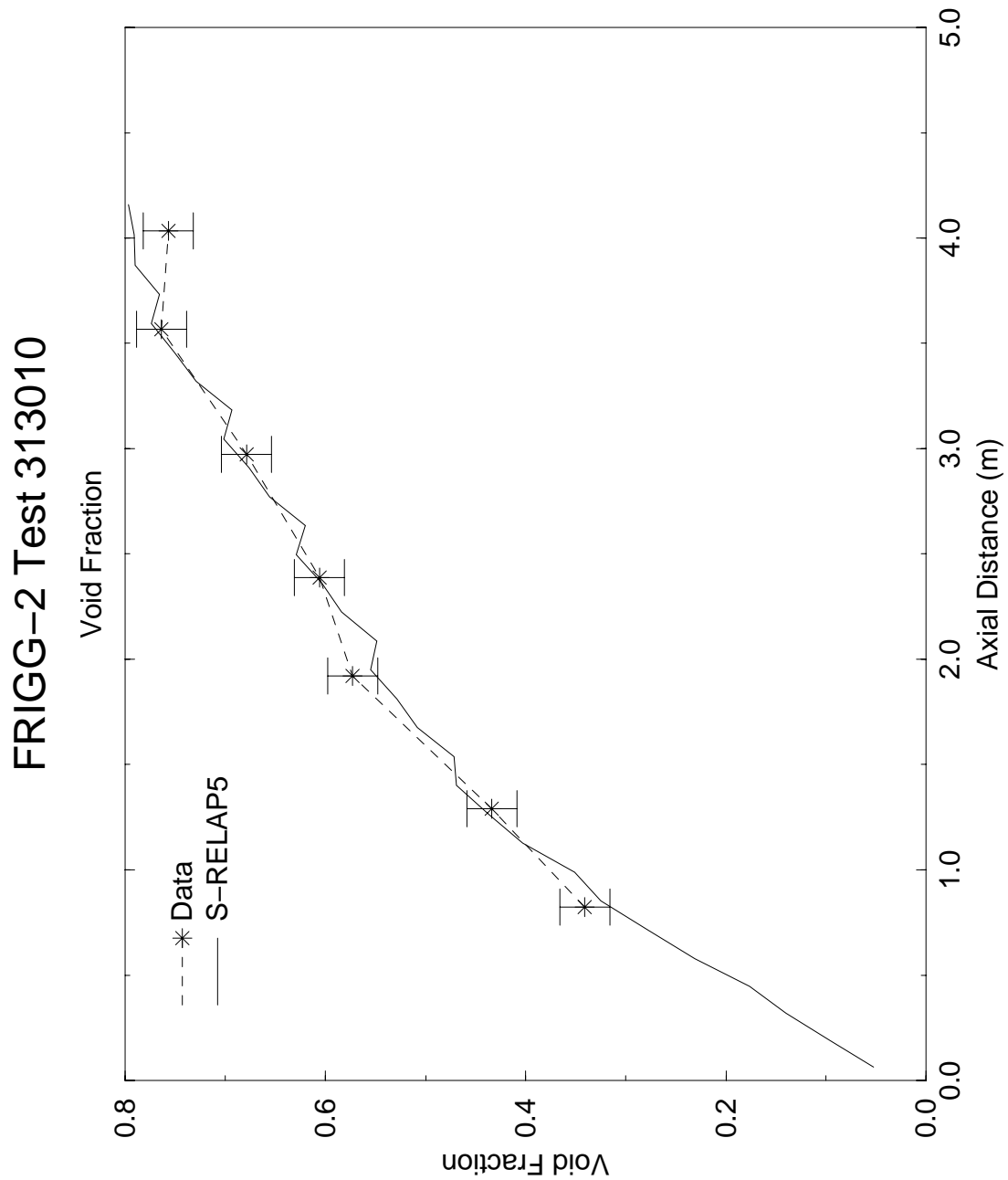


Figure 4.25 Comparison of Calculated and Measured Void Fraction, Frigg-2 Test 313060



**Figure 4.26 Comparison of Calculated and Measured Void Fraction,
Frigg-2 Test 313010**

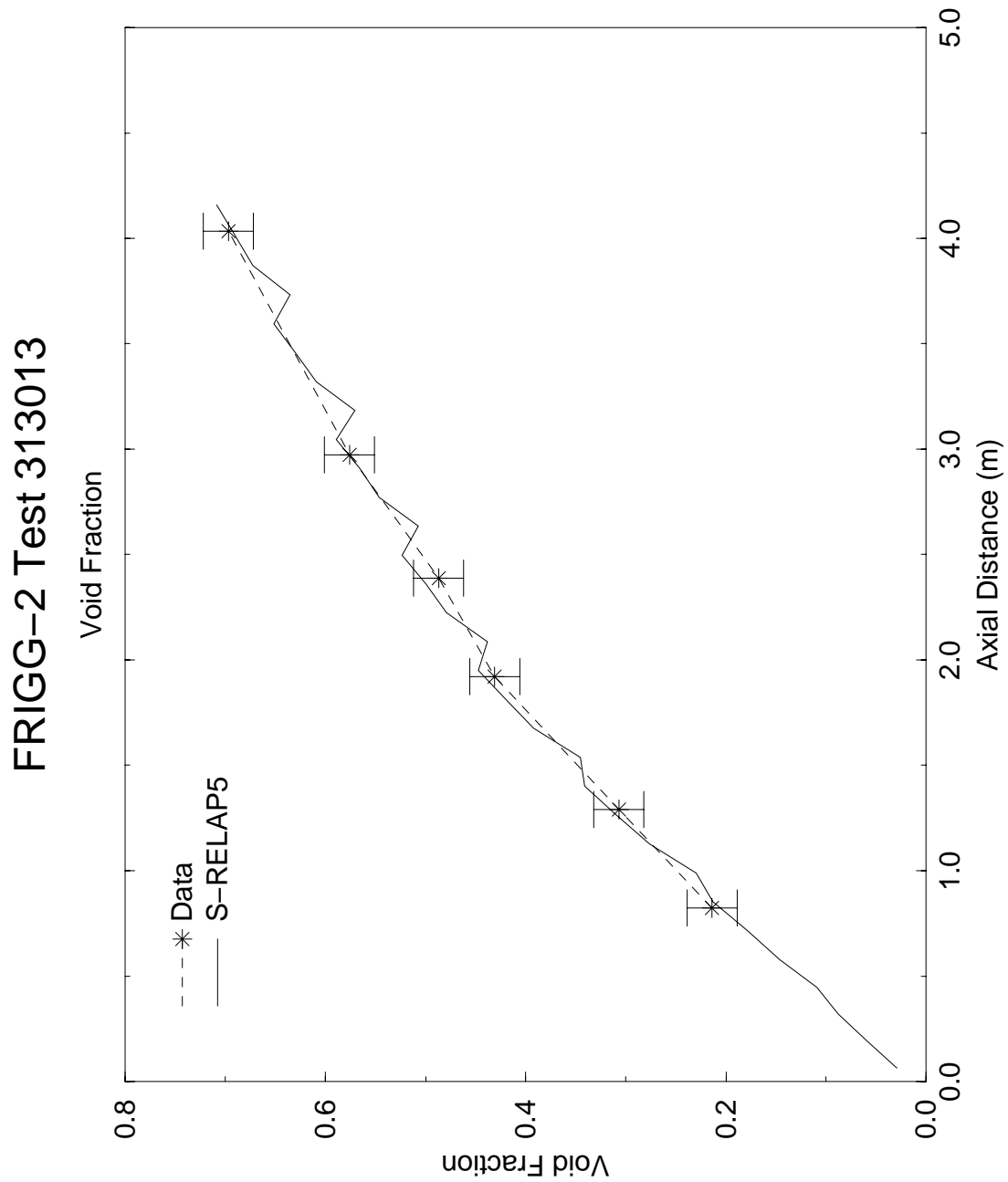


Figure 4.27 Comparison of Calculated and Measured Void Fraction, Frigg-2 Test 313013

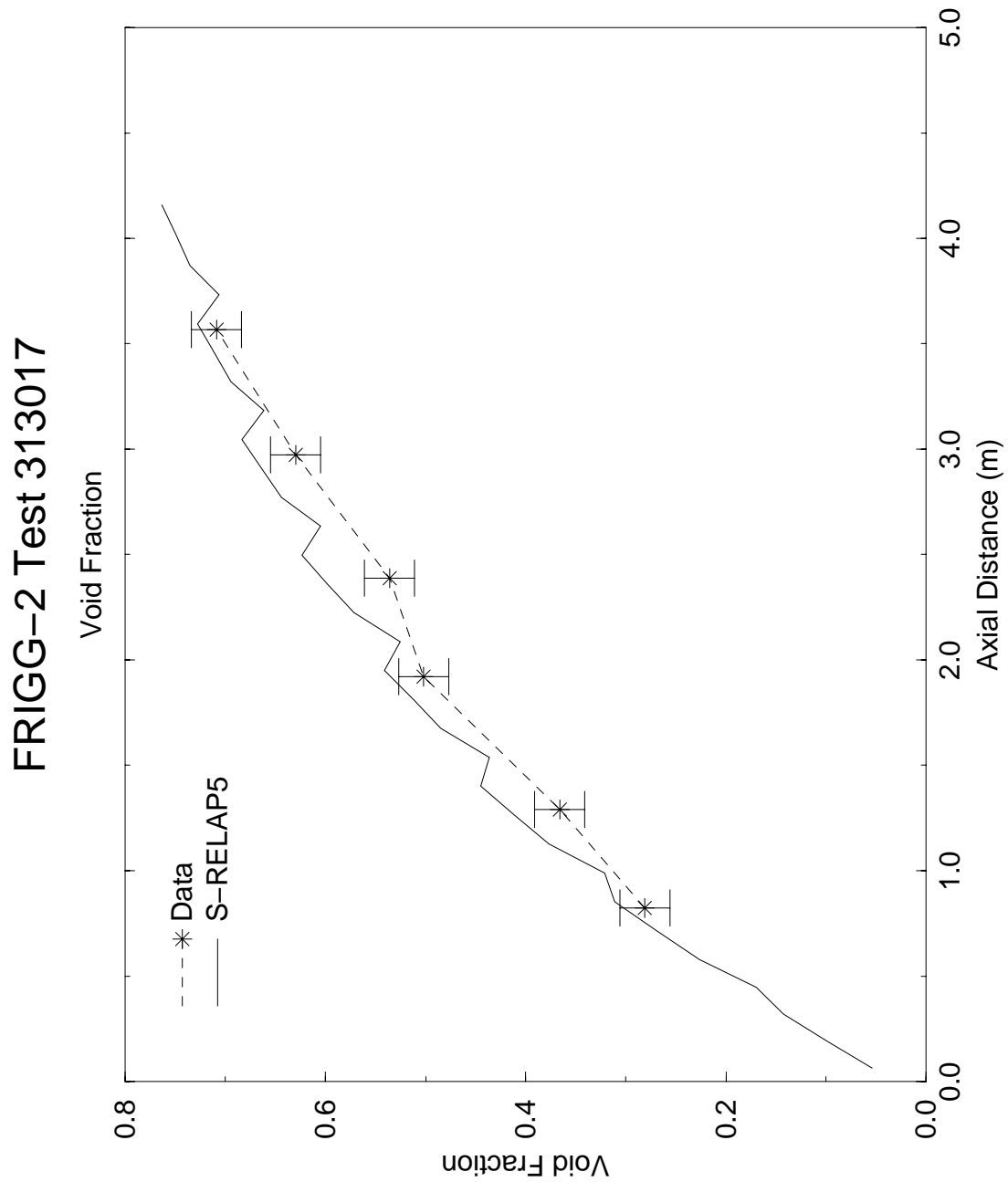


Figure 4.28 Comparison of Calculated and Measured Void Fraction, Frigg-2 Test 313017

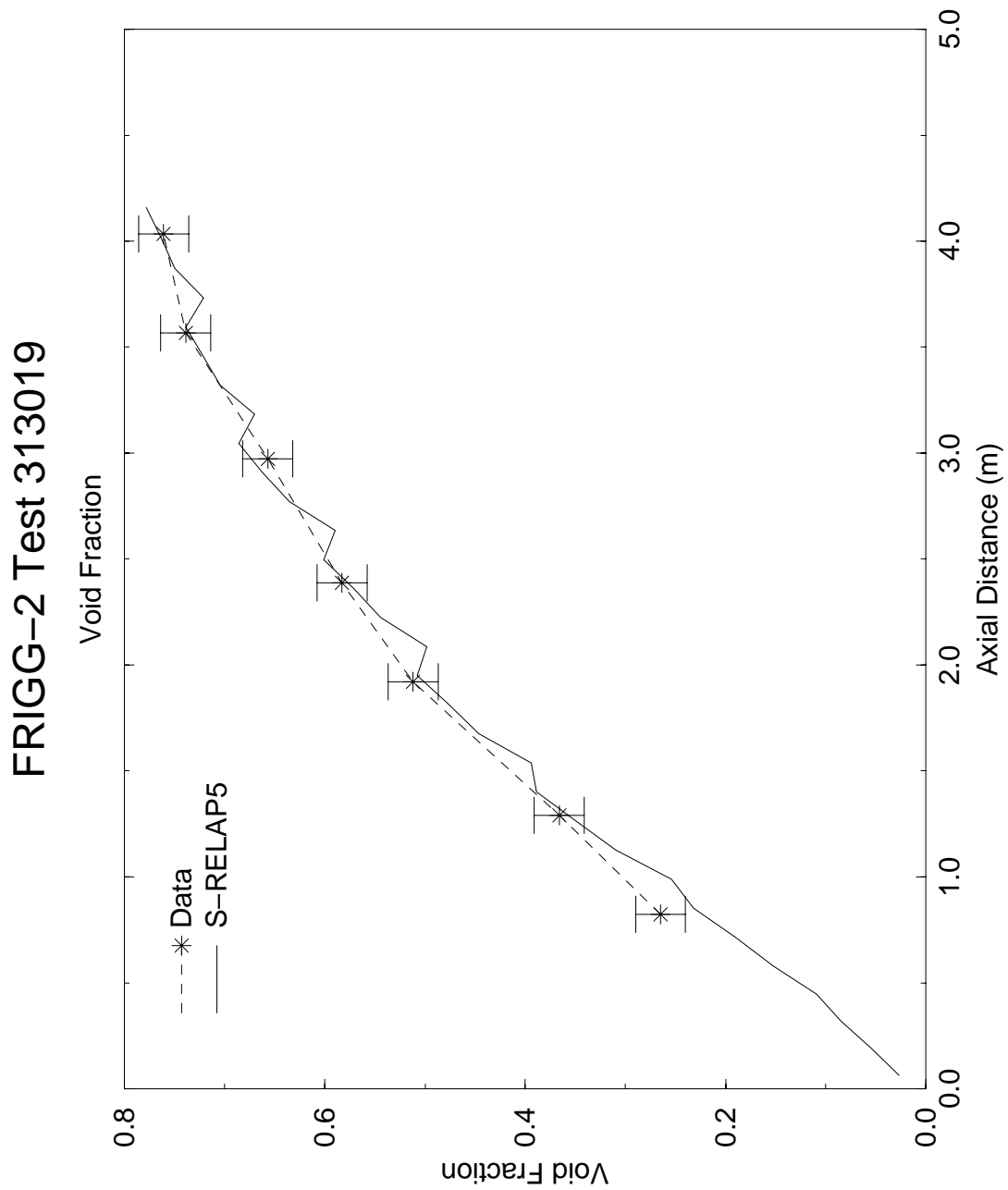


Figure 4.29 Comparison of Calculated and Measured Void Fraction, Frigg-2 Test 313019

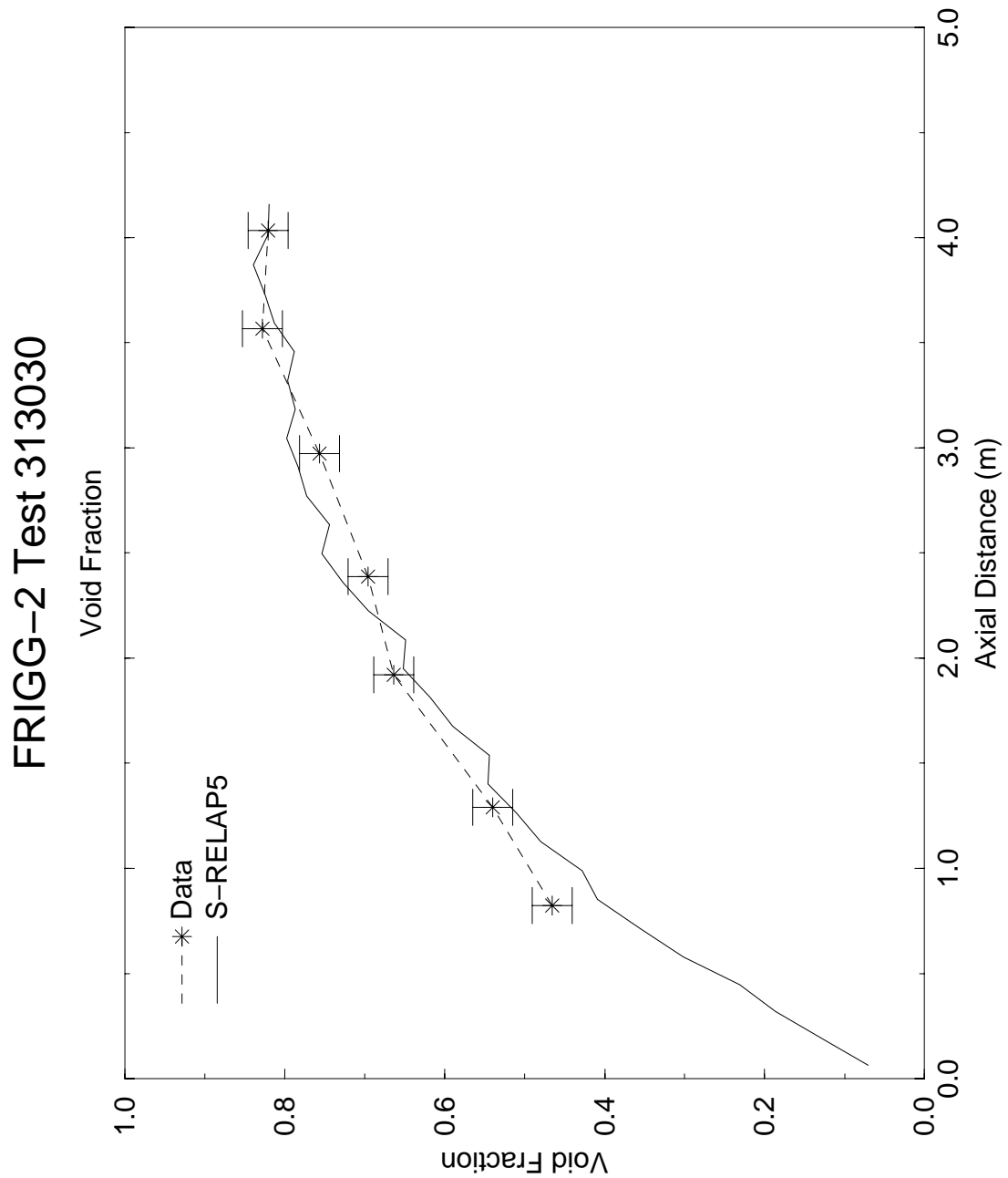


Figure 4.30 Comparison of Calculated and Measured Void Fraction, Frigg-2 Test 313030

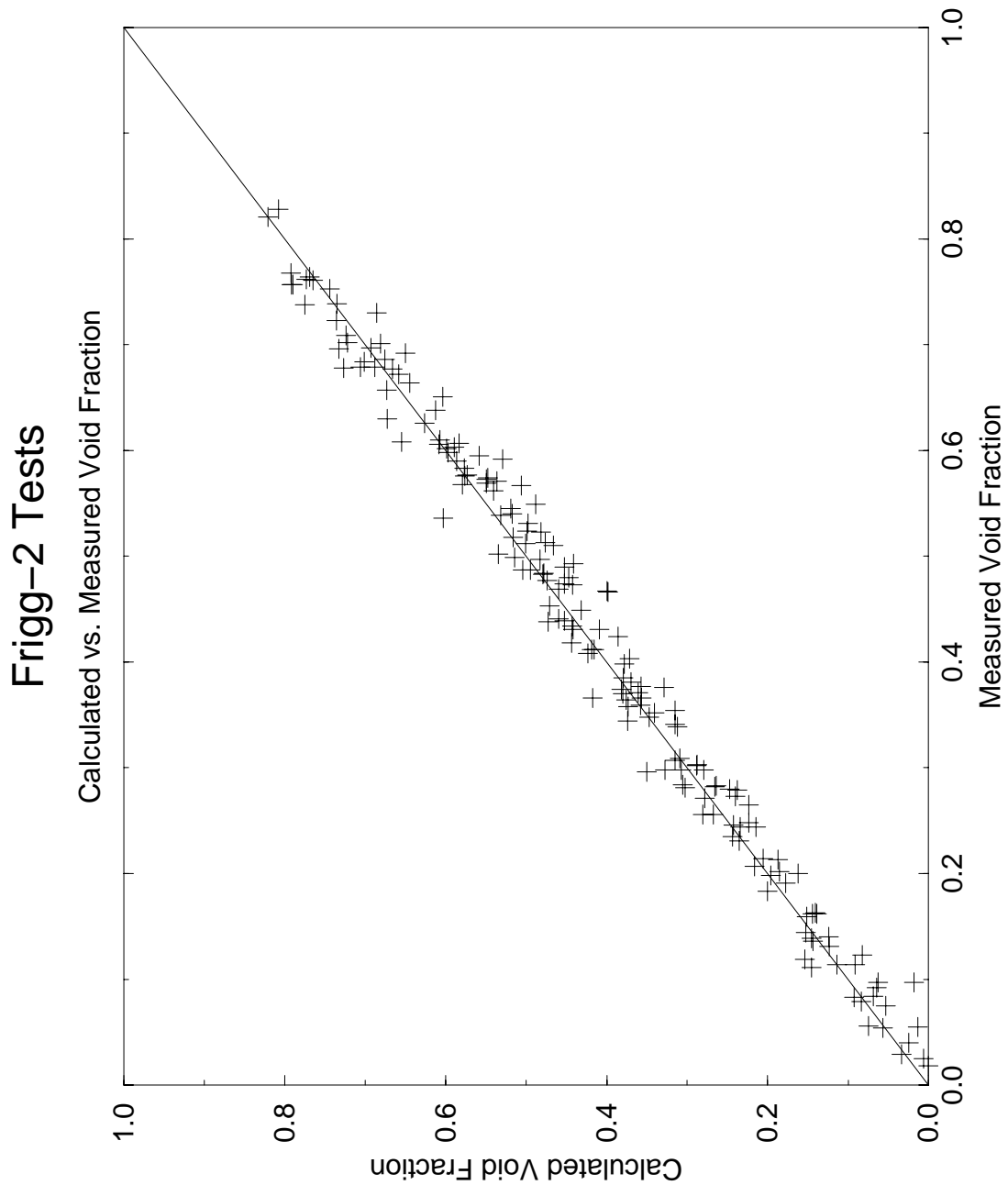


Figure 4.31 Comparison of Calculated and Measured Void Fraction at the Same Location for all 27 FRIGG Tests

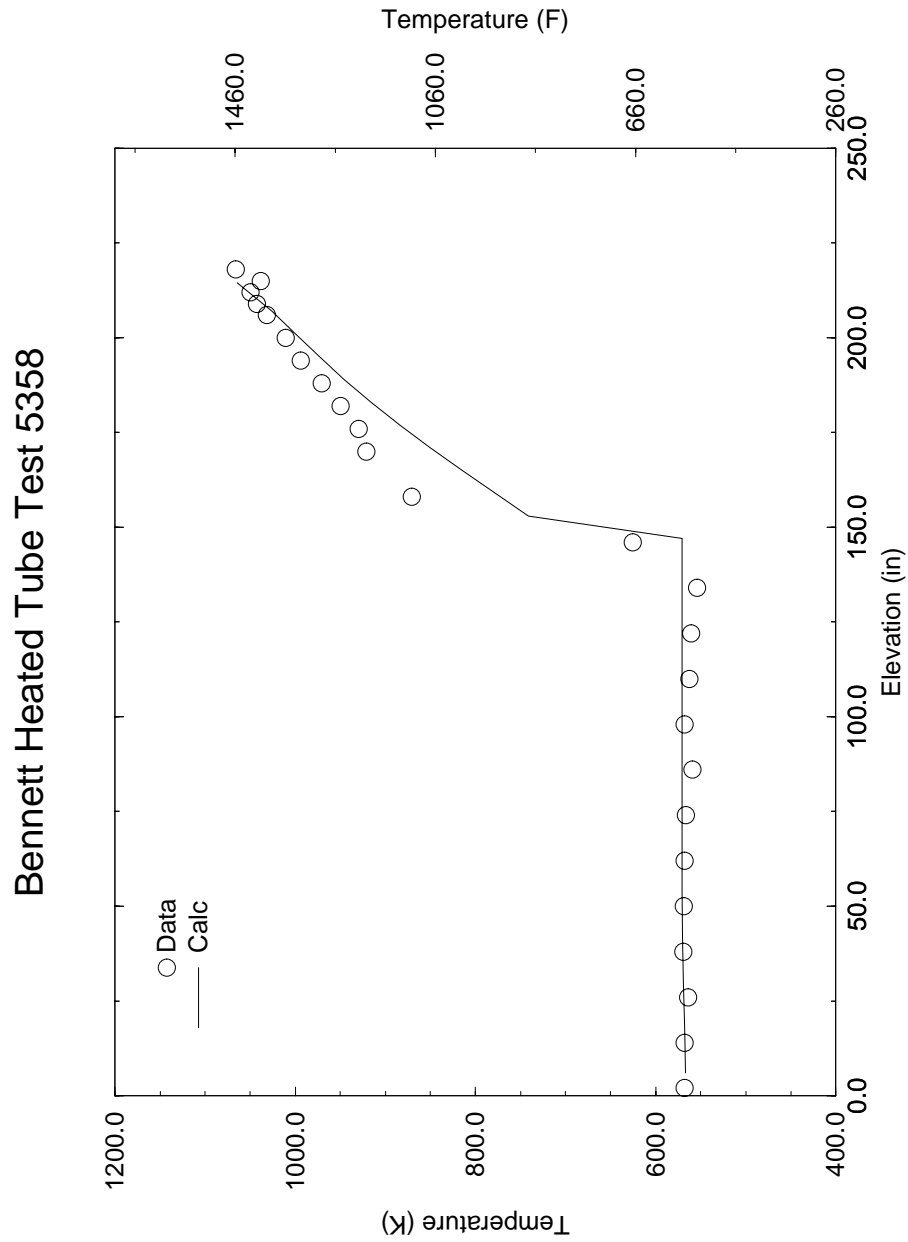


Figure 4.32 Wall Temperature Profiles, Bennett Heated Tube Test 5358

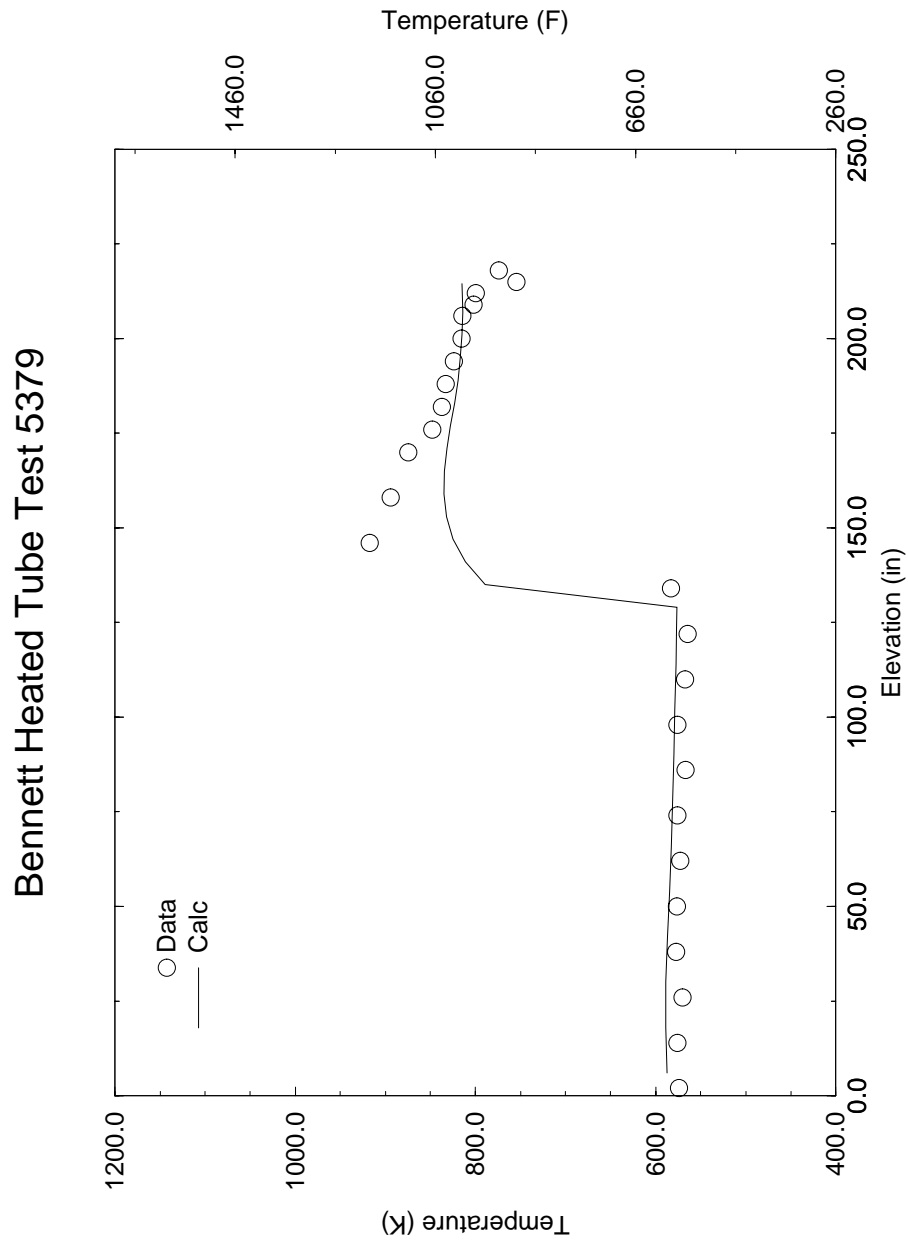
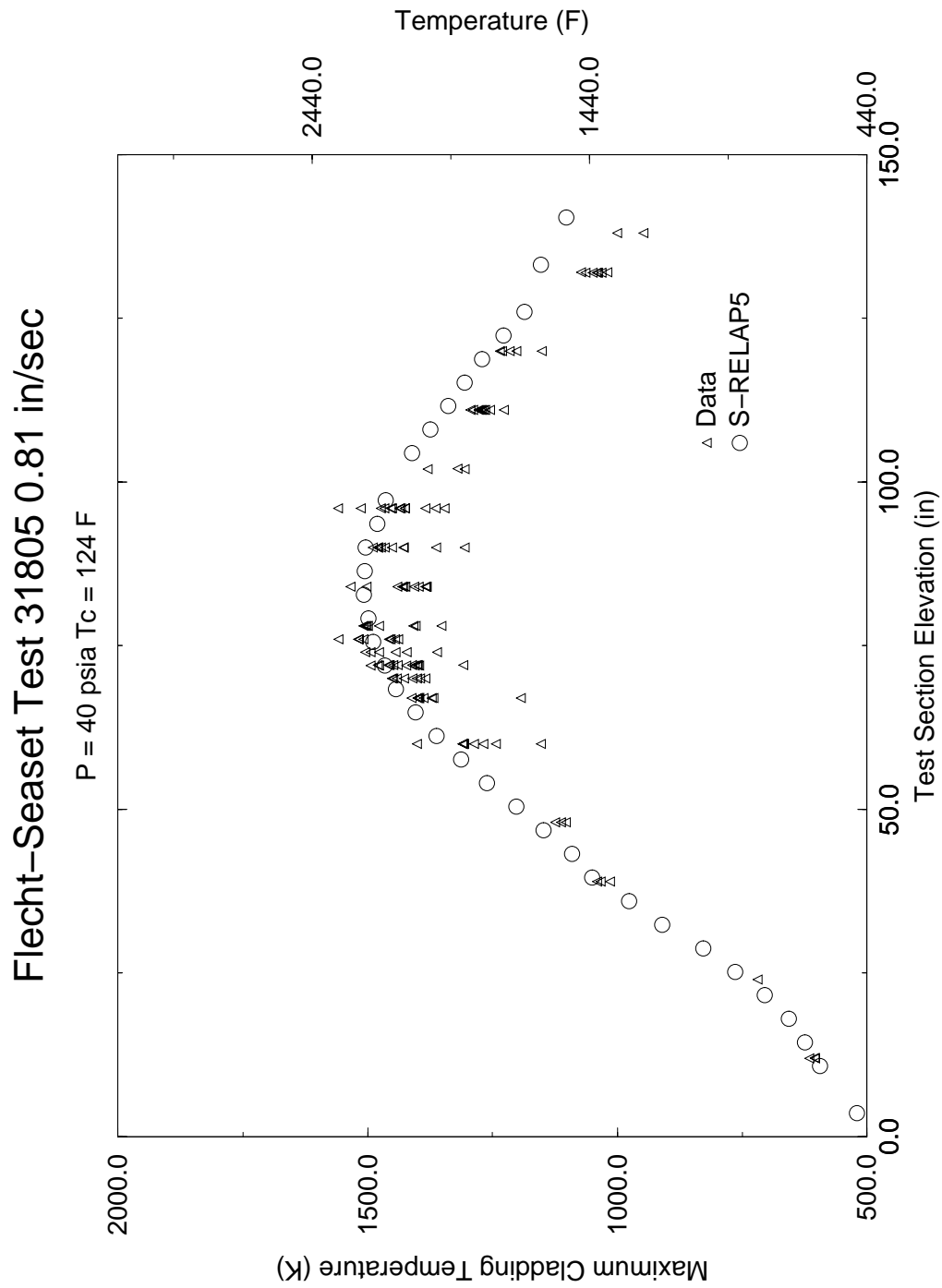


Figure 4.33 Wall Temperature Profiles, Bennett Heated Tube Test 5379



**Figure 4.34 Maximum Clad Temperature at All Measured Elevations,
FLECHT SEASET Test 31805**

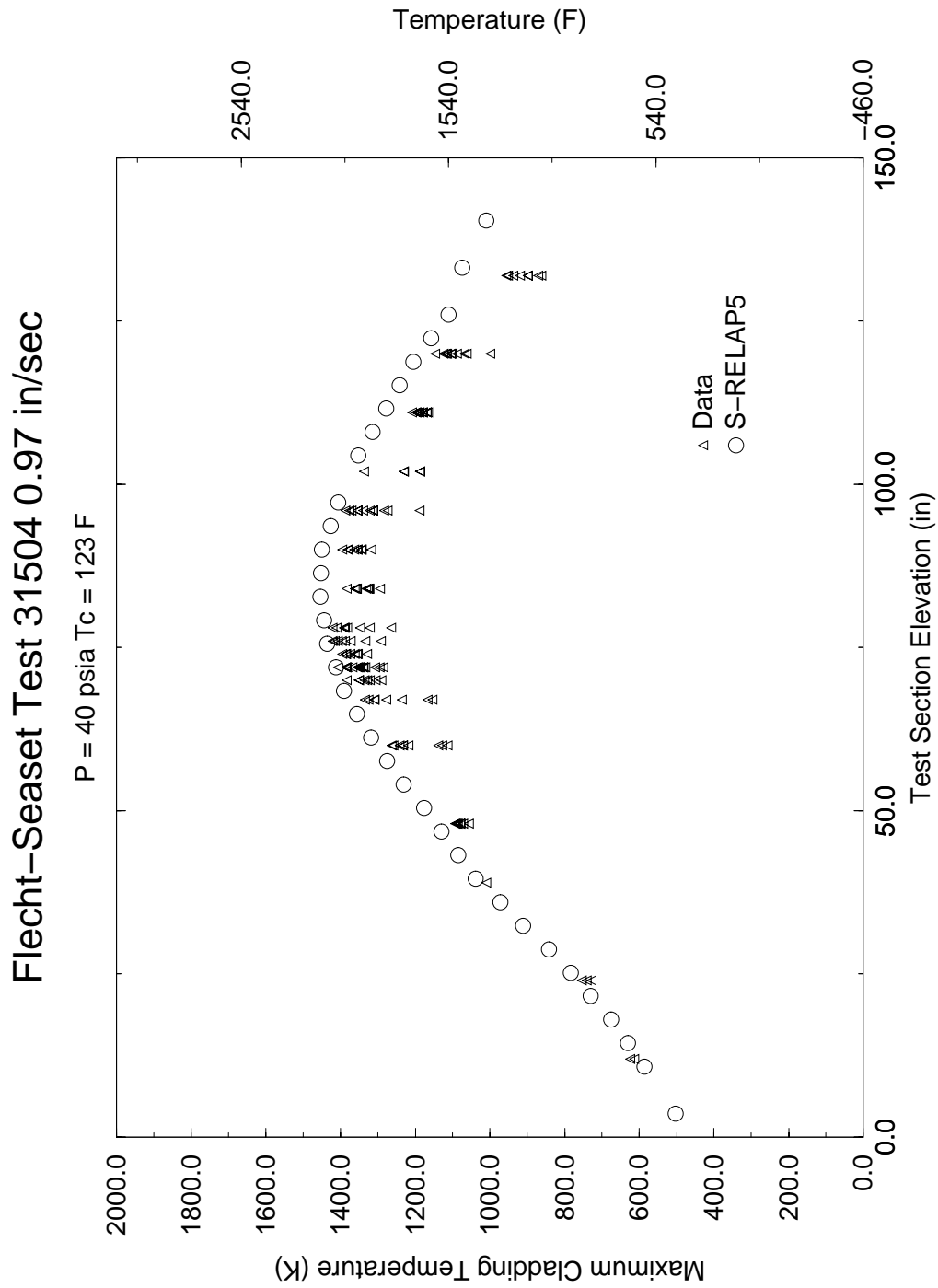


Figure 4.35 Maximum Clad Temperature at All Measured Elevations, FLECHT SEASET Test 31504

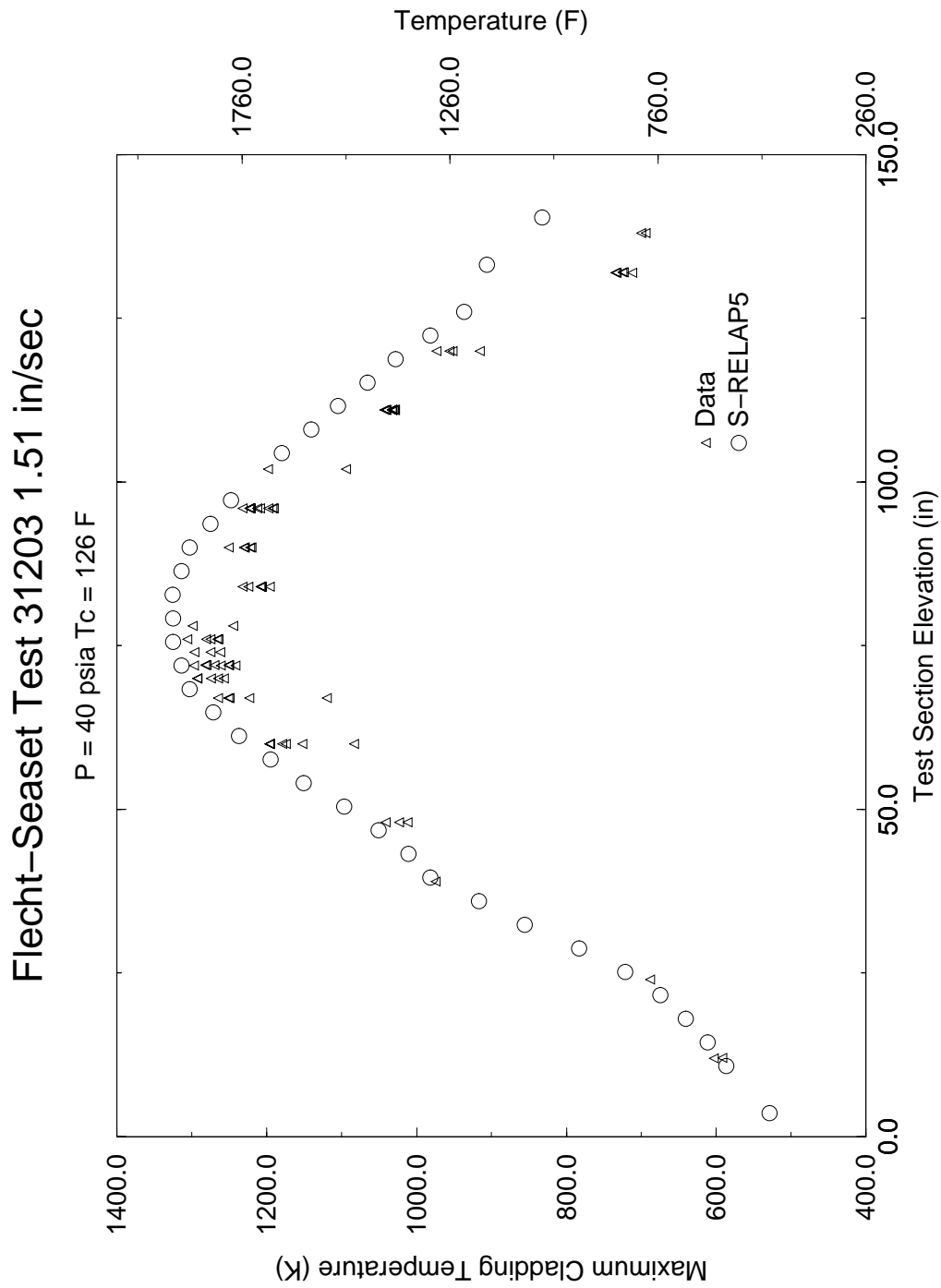


Figure 4.36 Maximum Clad Temperature at All Measured Elevations, FLECHT SEASET Test 31203

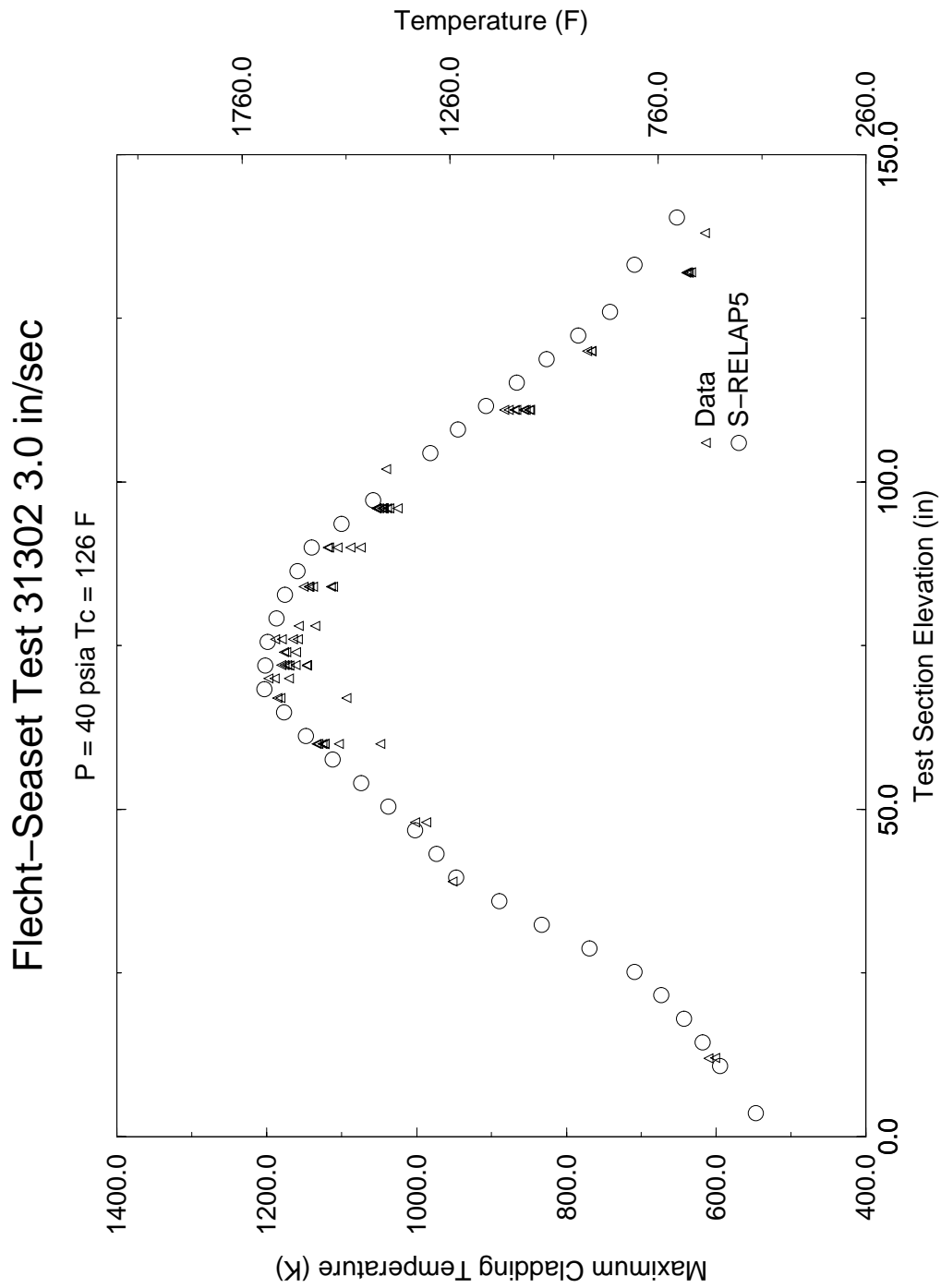


Figure 4.37 Maximum Clad Temperature at All Measured Elevations, FLECHT SEASET Test 31302

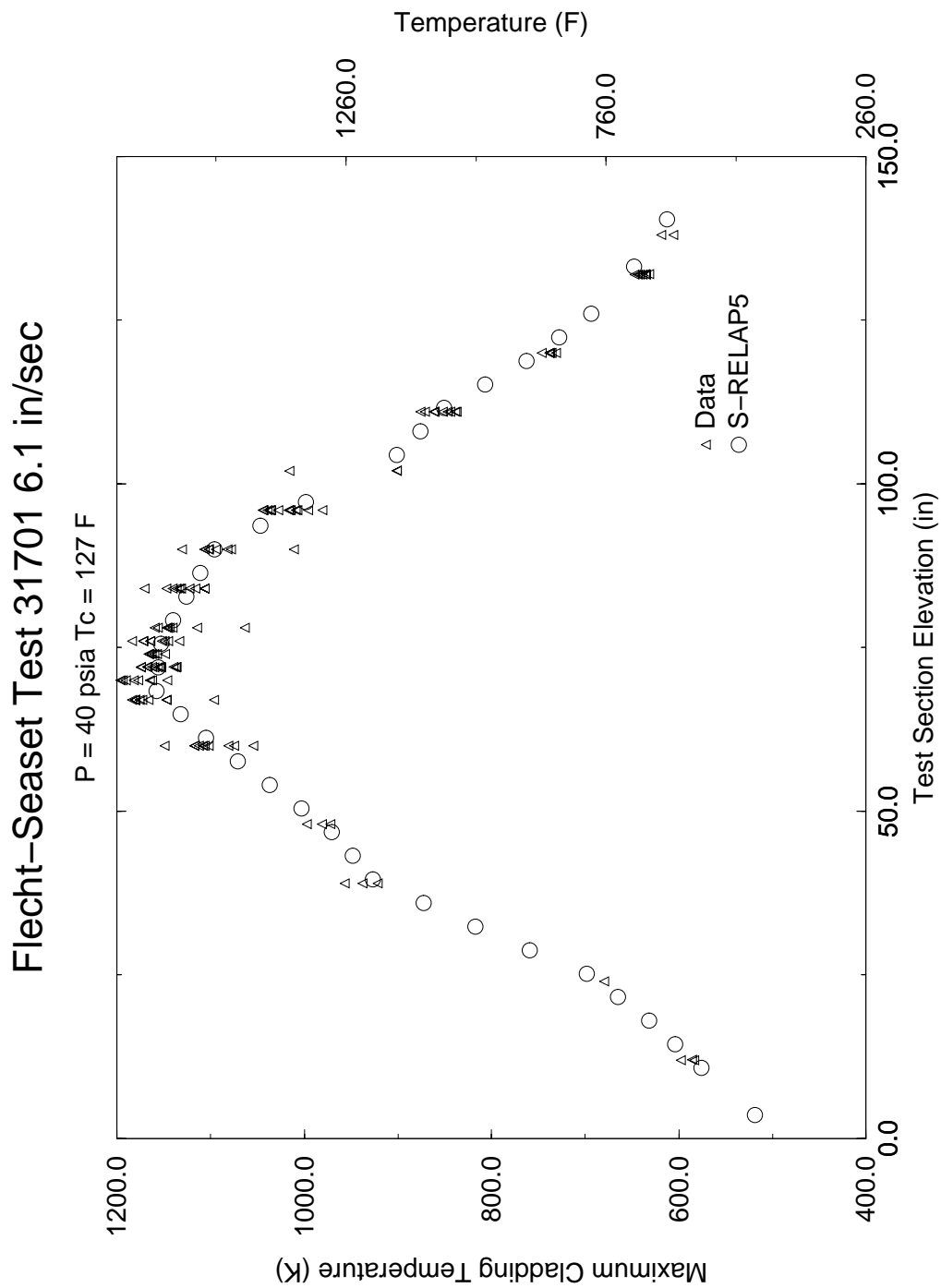


Figure 4.38 Maximum Clad Temperature at All Measured Elevations, FLECHT SEASET Test 31701

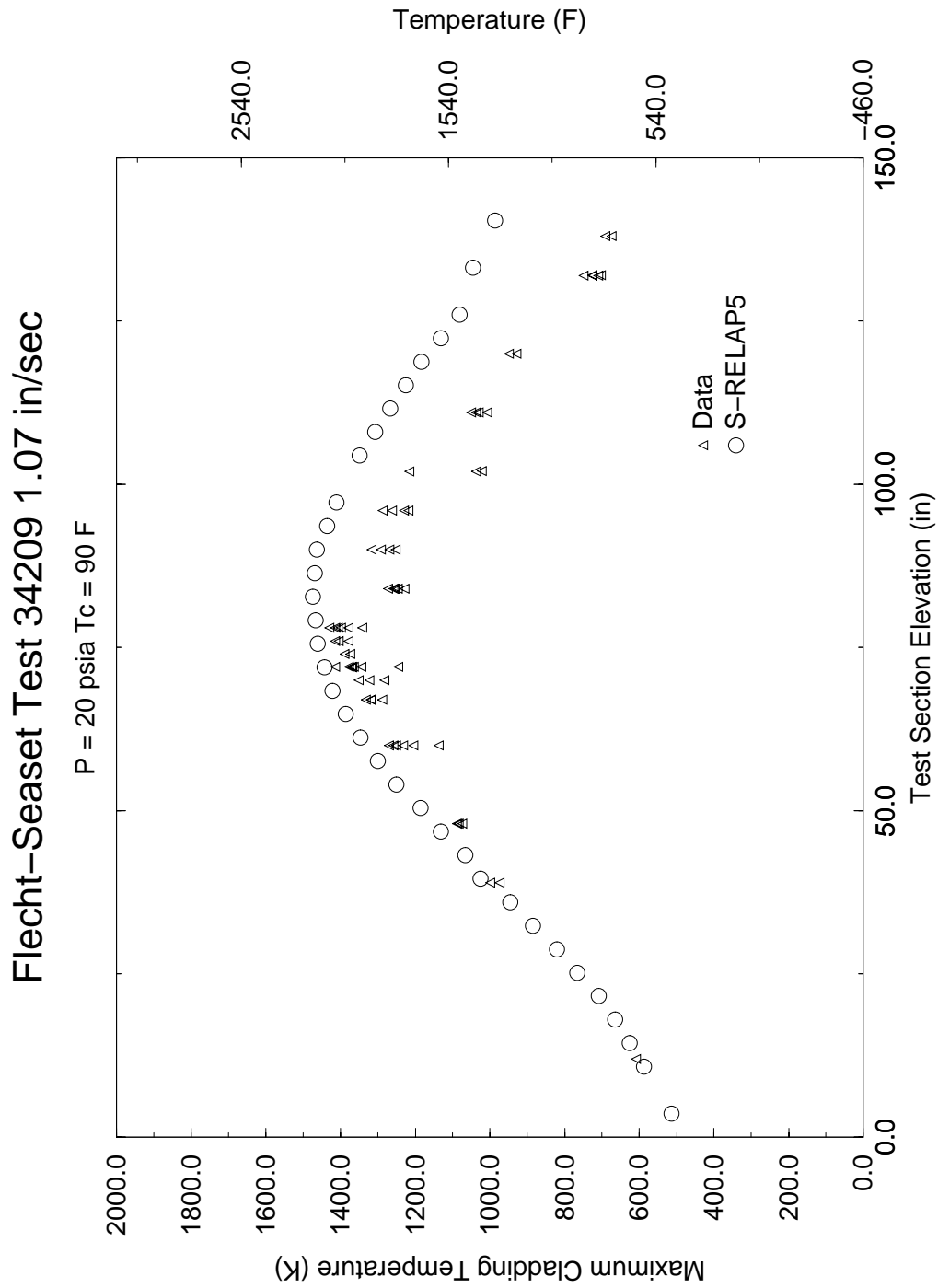


Figure 4.39 Maximum Clad Temperature at All Measured Elevations, FLECHT SEASET Test 34209

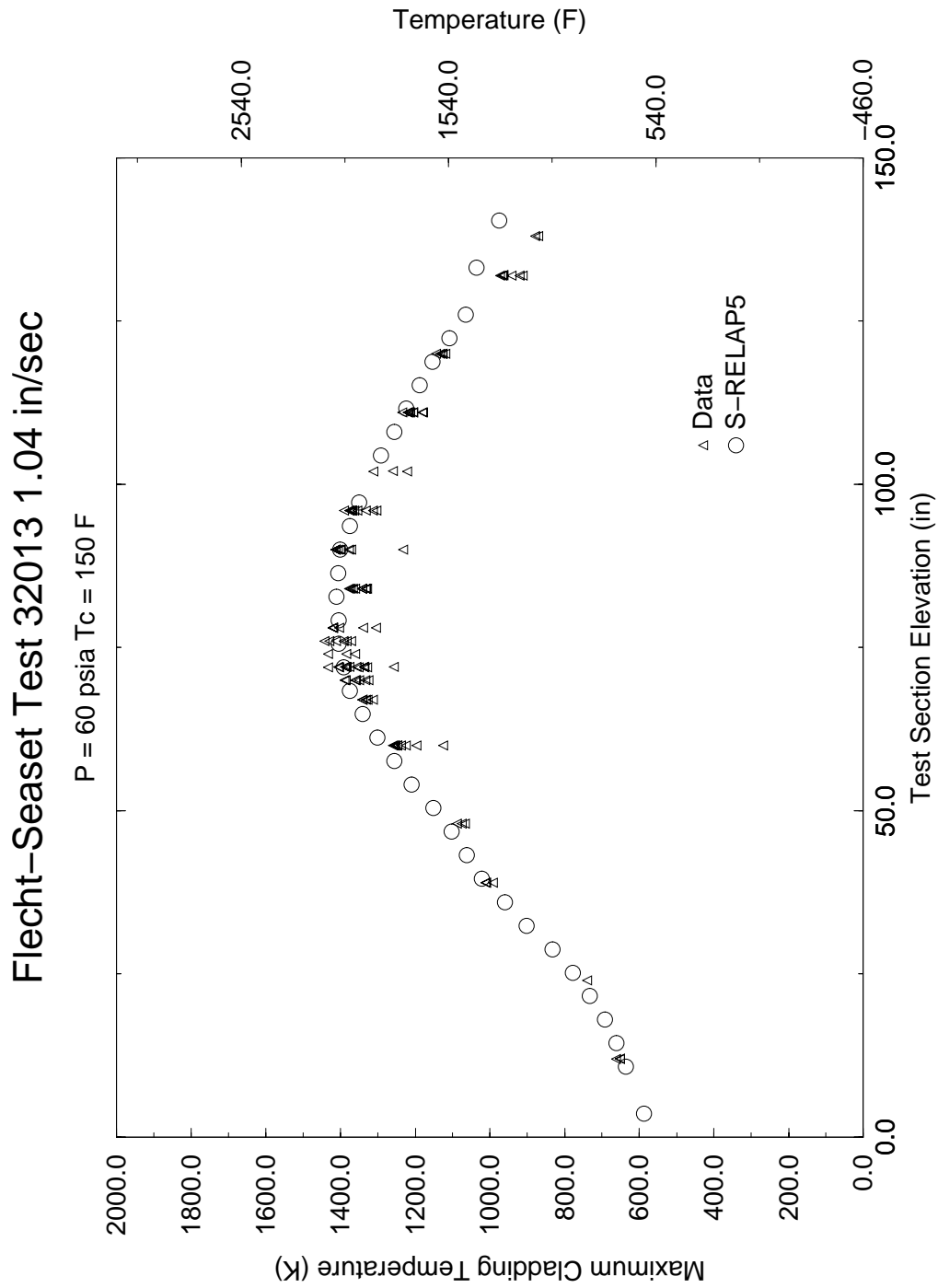


Figure 4.40 Maximum Clad Temperature at All Measured Elevations, FLECHT SEASET Test 32013

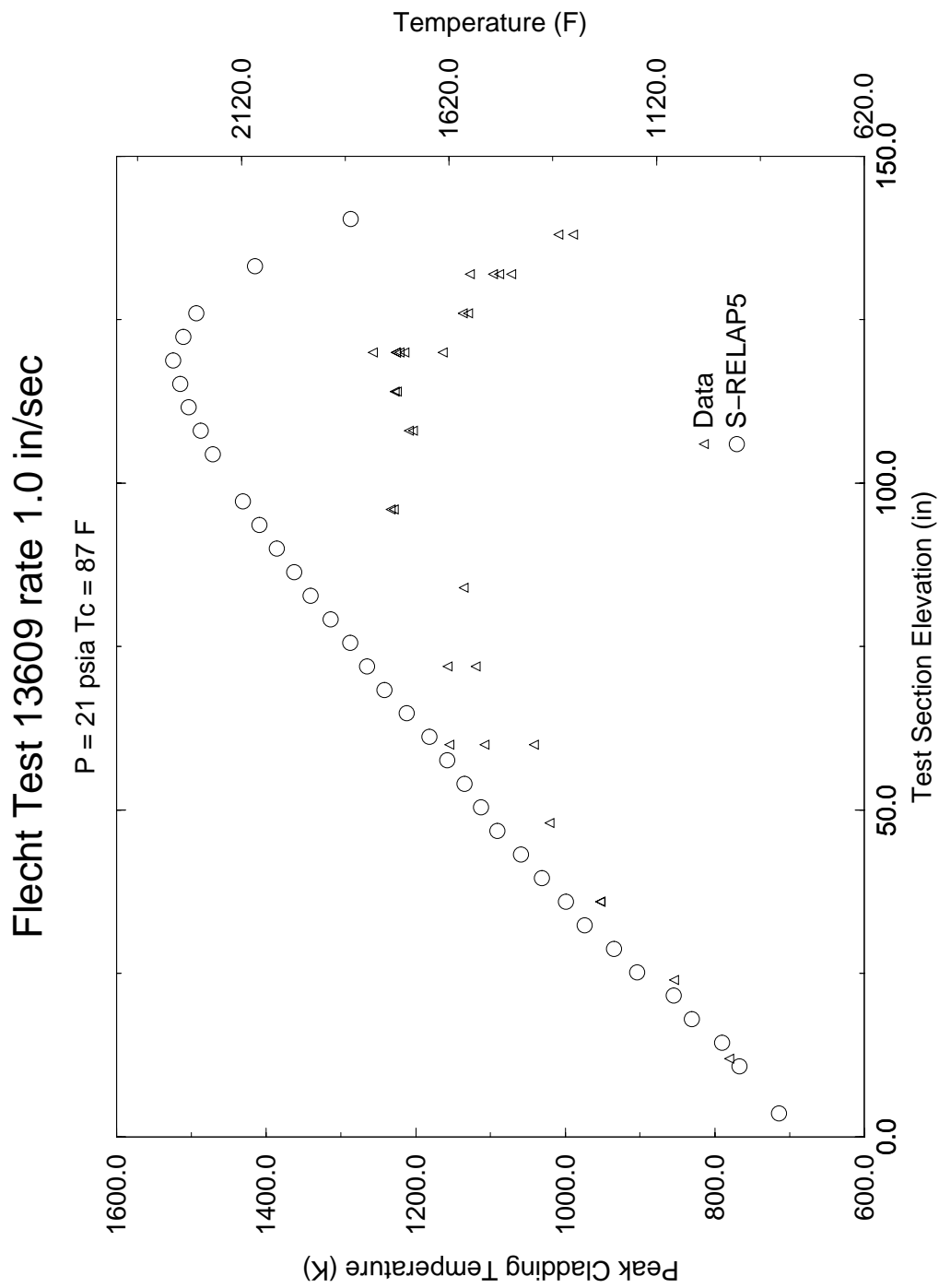


Figure 4.41 Maximum Clad Temperature at All Measured Elevations, FLECHT Skewed Test 13609

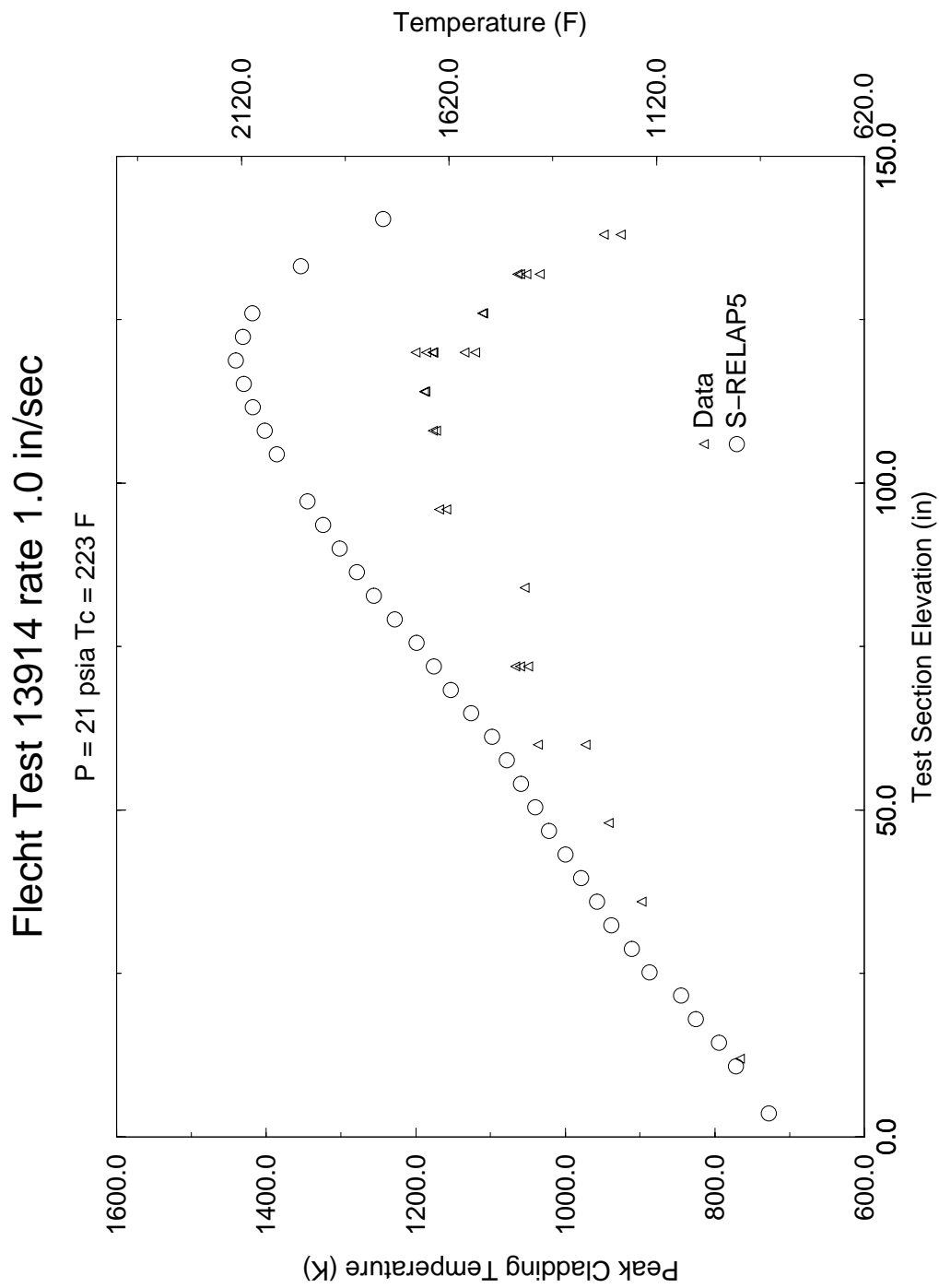


Figure 4.42 Maximum Clad Temperature at All Measured Elevations, FLECHT Skewed Test 13914

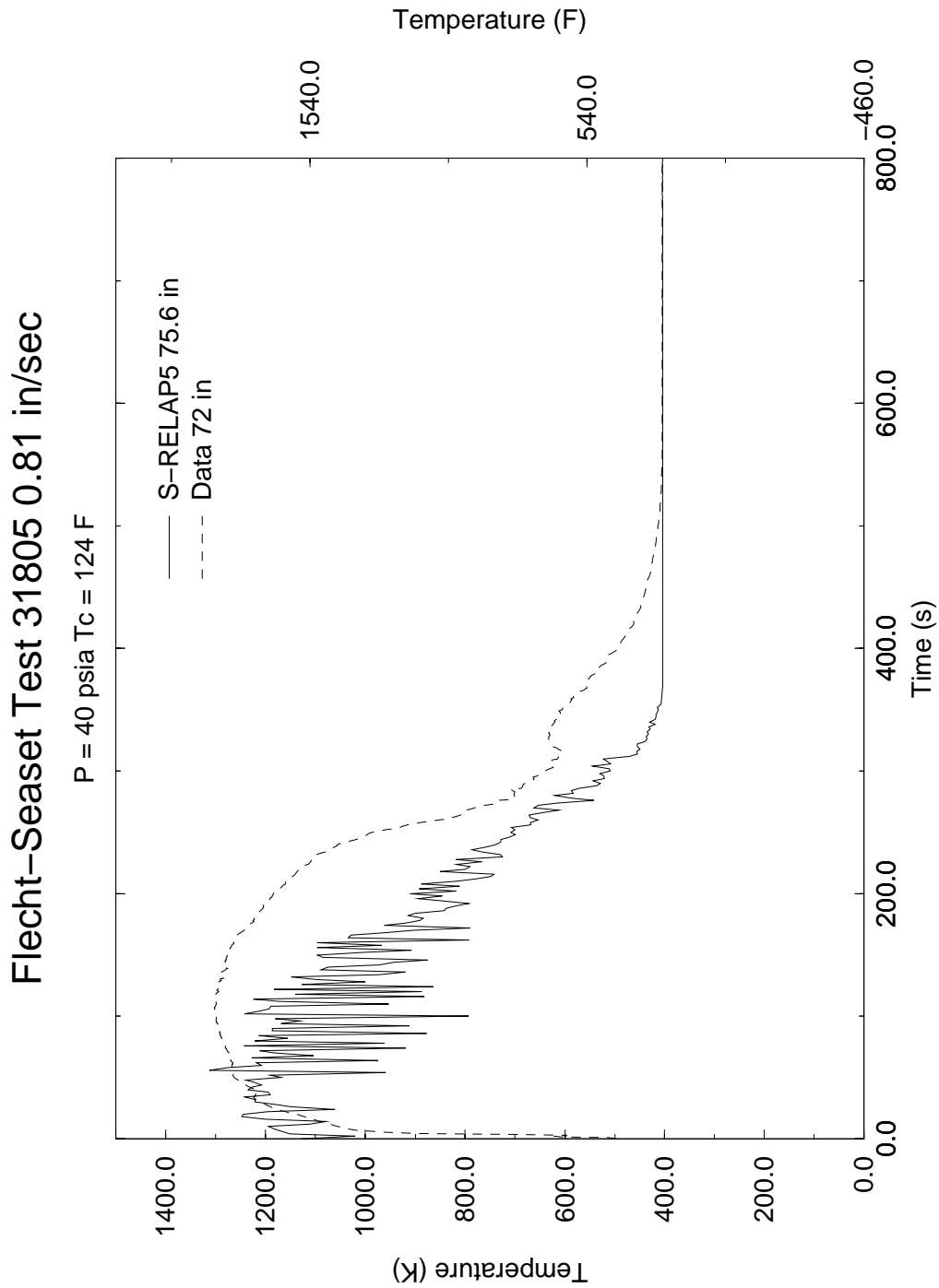


Figure 4.43 Steam Temperatures Calculated at 75.6 in and Measured at 72 in, FLECHT SEASET Test 31805

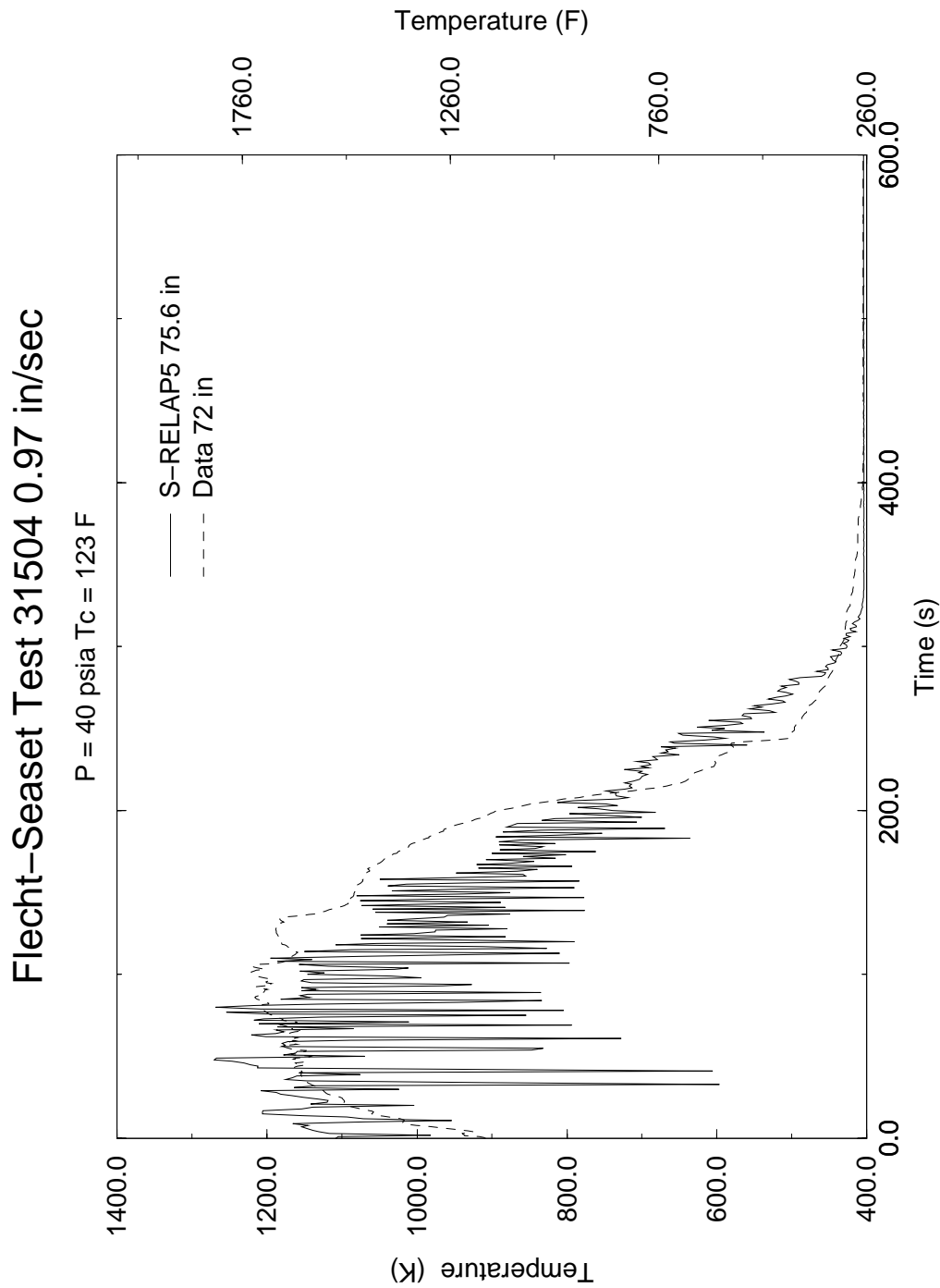


Figure 4.44 Steam Temperatures Calculated at 75.6 in and Measured at 72 in, FLECHT SEASET Test 31504

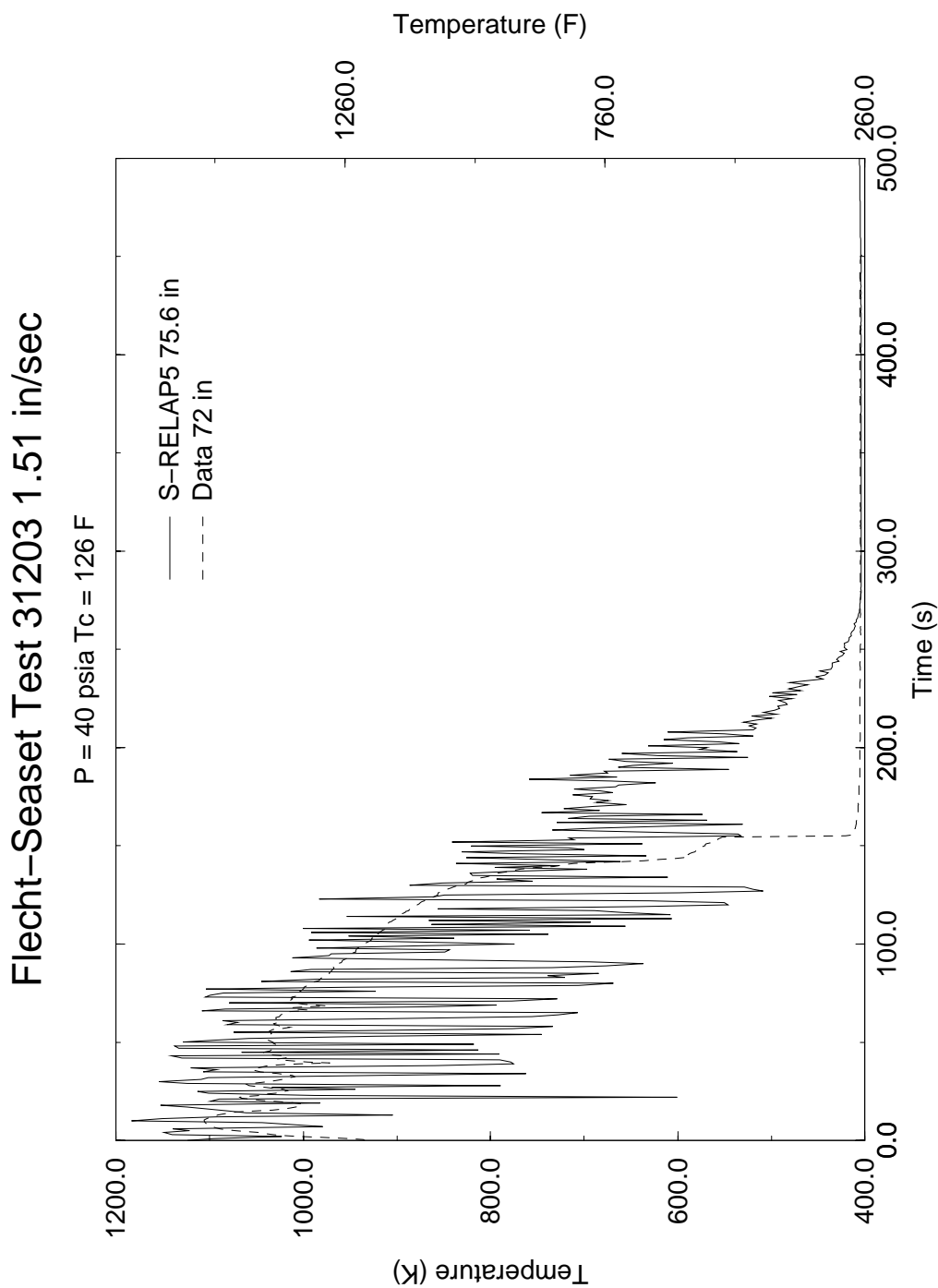


Figure 4.45 Steam Temperatures Calculated at 75.6 in and Measured at 72 in, FLECHT SEASET Test 31203

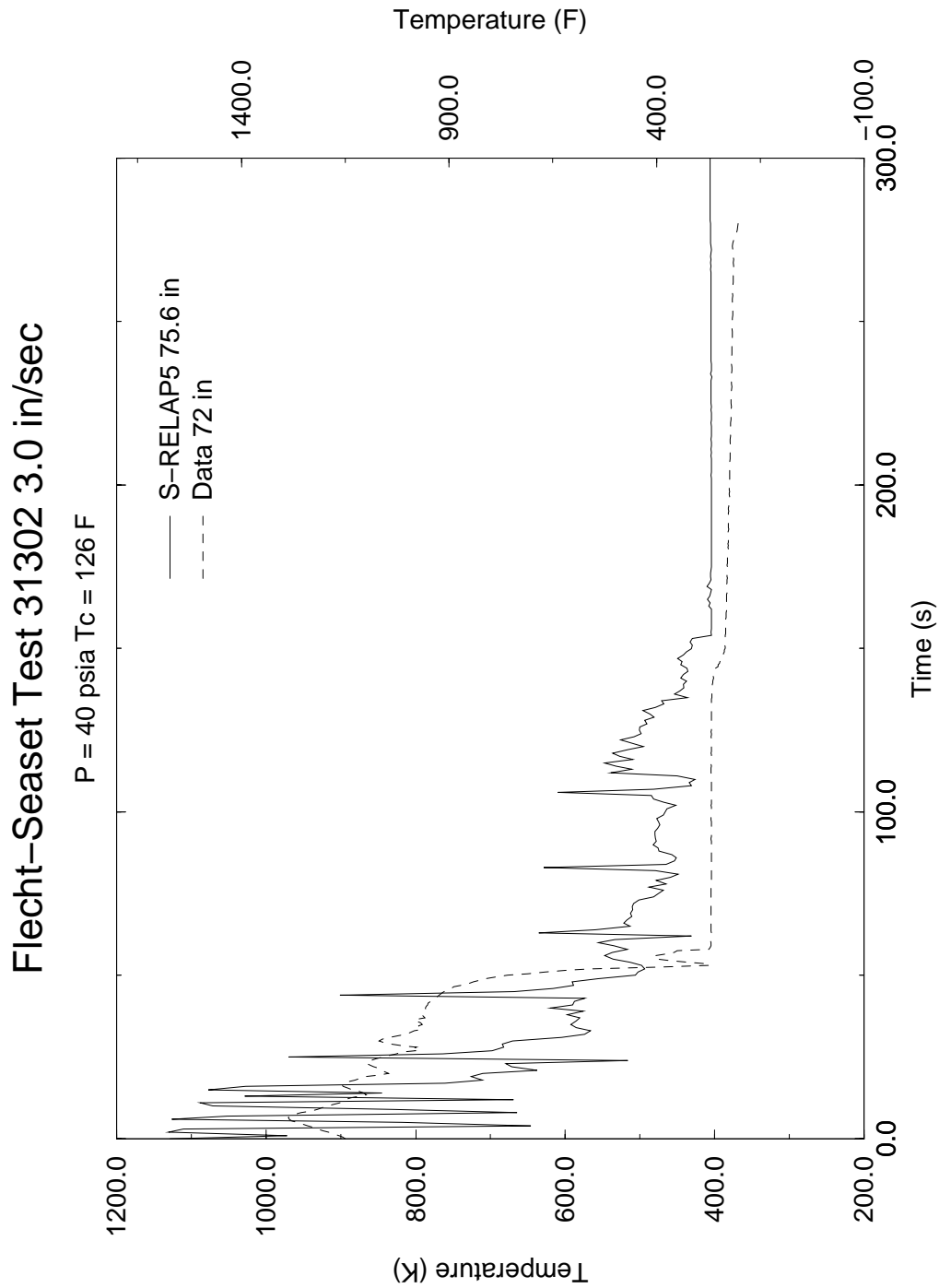


Figure 4.46 Steam Temperatures Calculated at 75.6 in and Measured at 72 in, FLECHT SEASET Test 31302

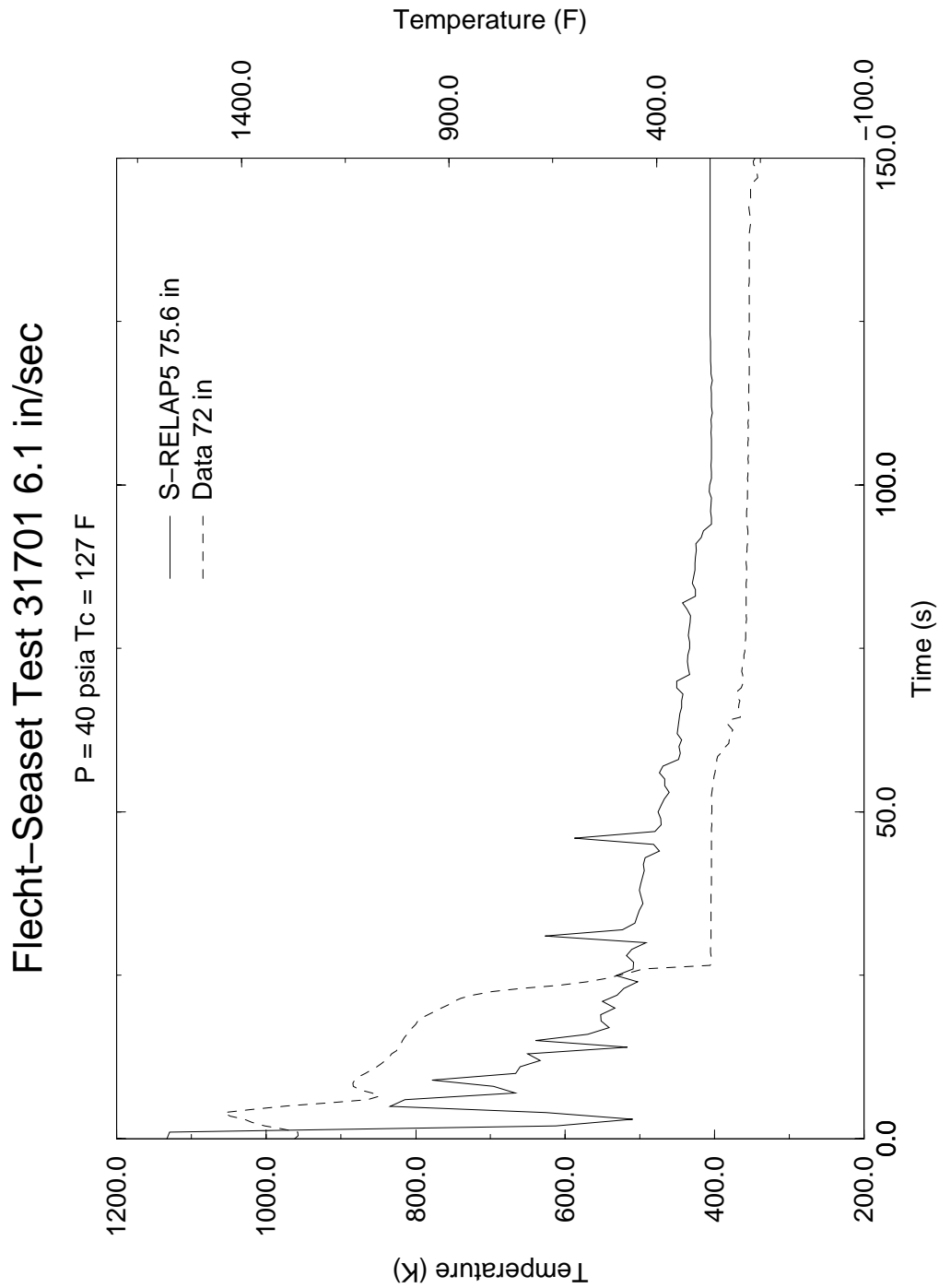


Figure 4.47 Steam Temperatures Calculated at 75.6 in and Measured at 72 in, FLECHT SEASET Test 31701

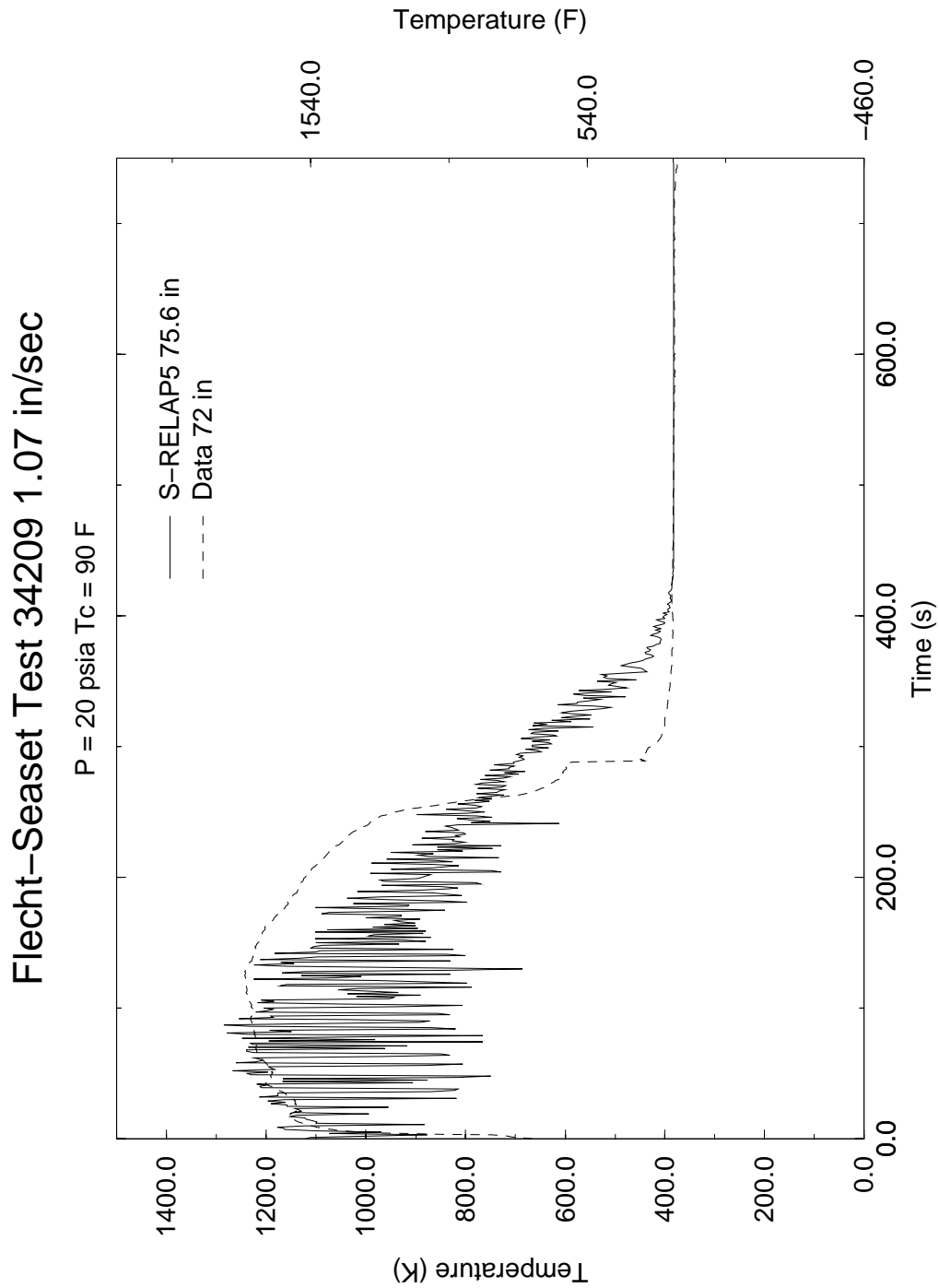


Figure 4.48 Steam Temperatures Calculated at 75.6 in and Measured at 72 in, FLECHT SEASET Test 34209

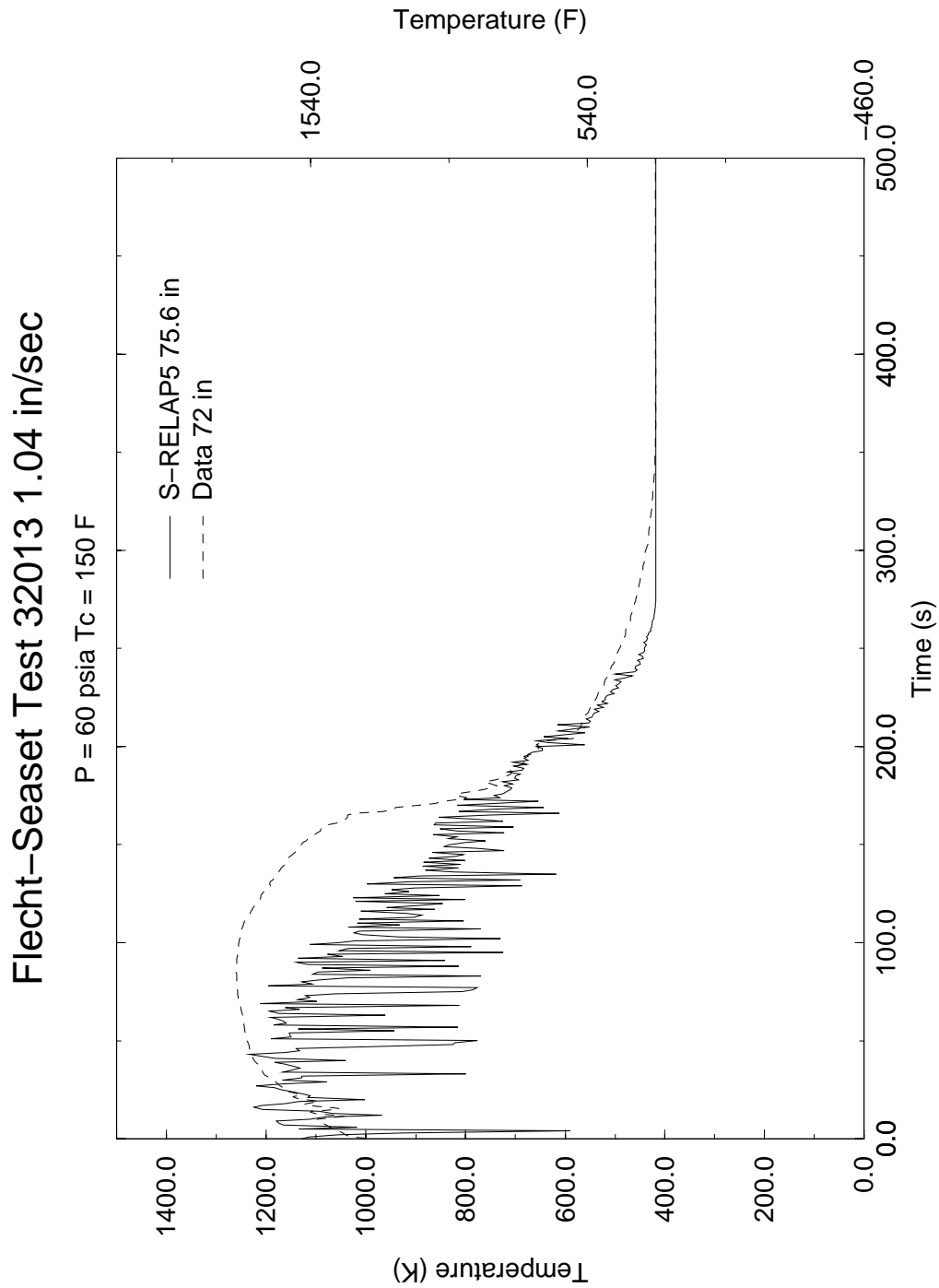


Figure 4.49 Steam Temperatures Calculated at 75.6 in and Measured at 72 in, FLECHT SEASET Test 32013

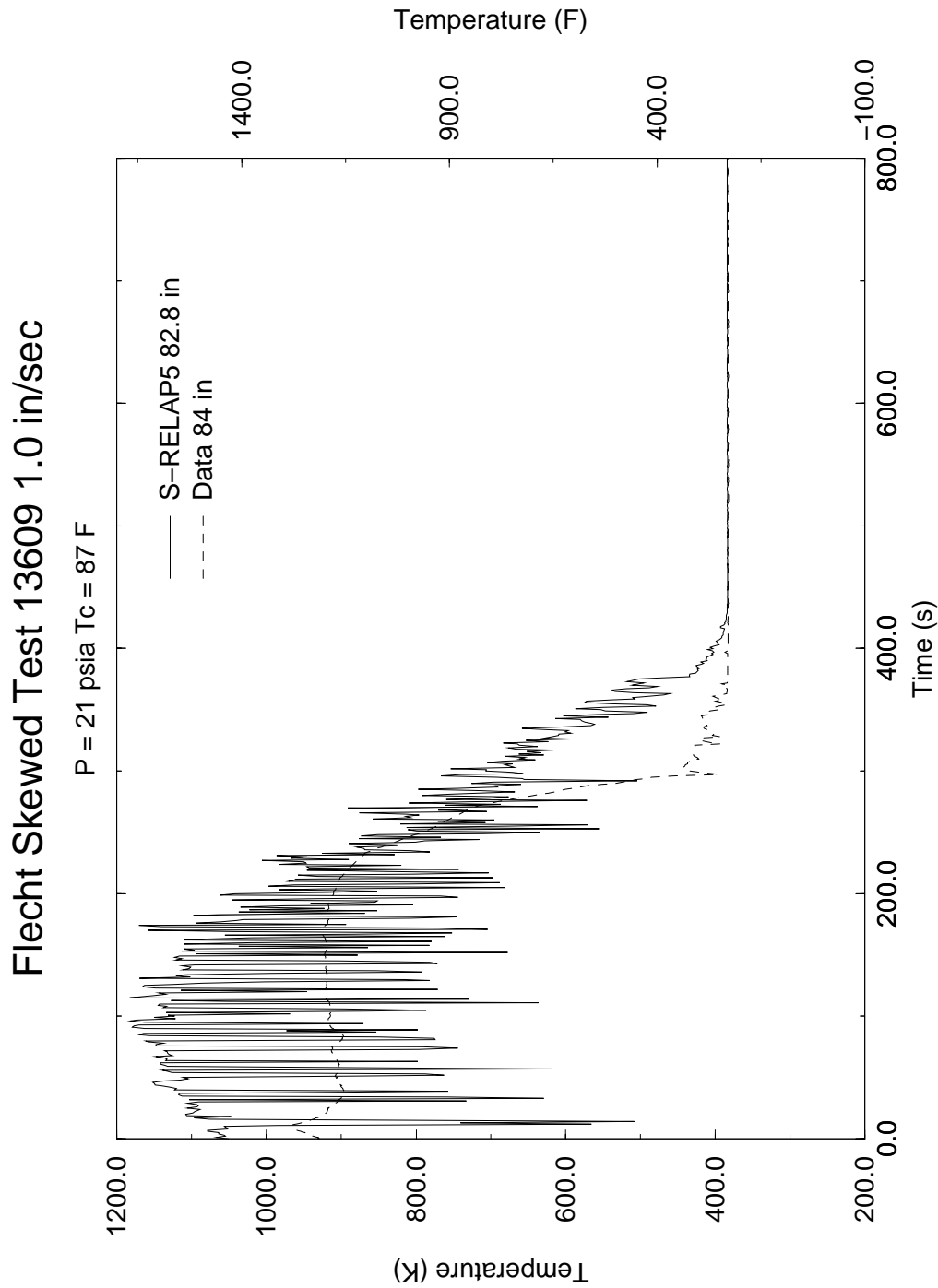


Figure 4.50 Steam Temperatures Calculated at 82.8 in and Measured at 84 in, FLECHT Skewed Test 13609

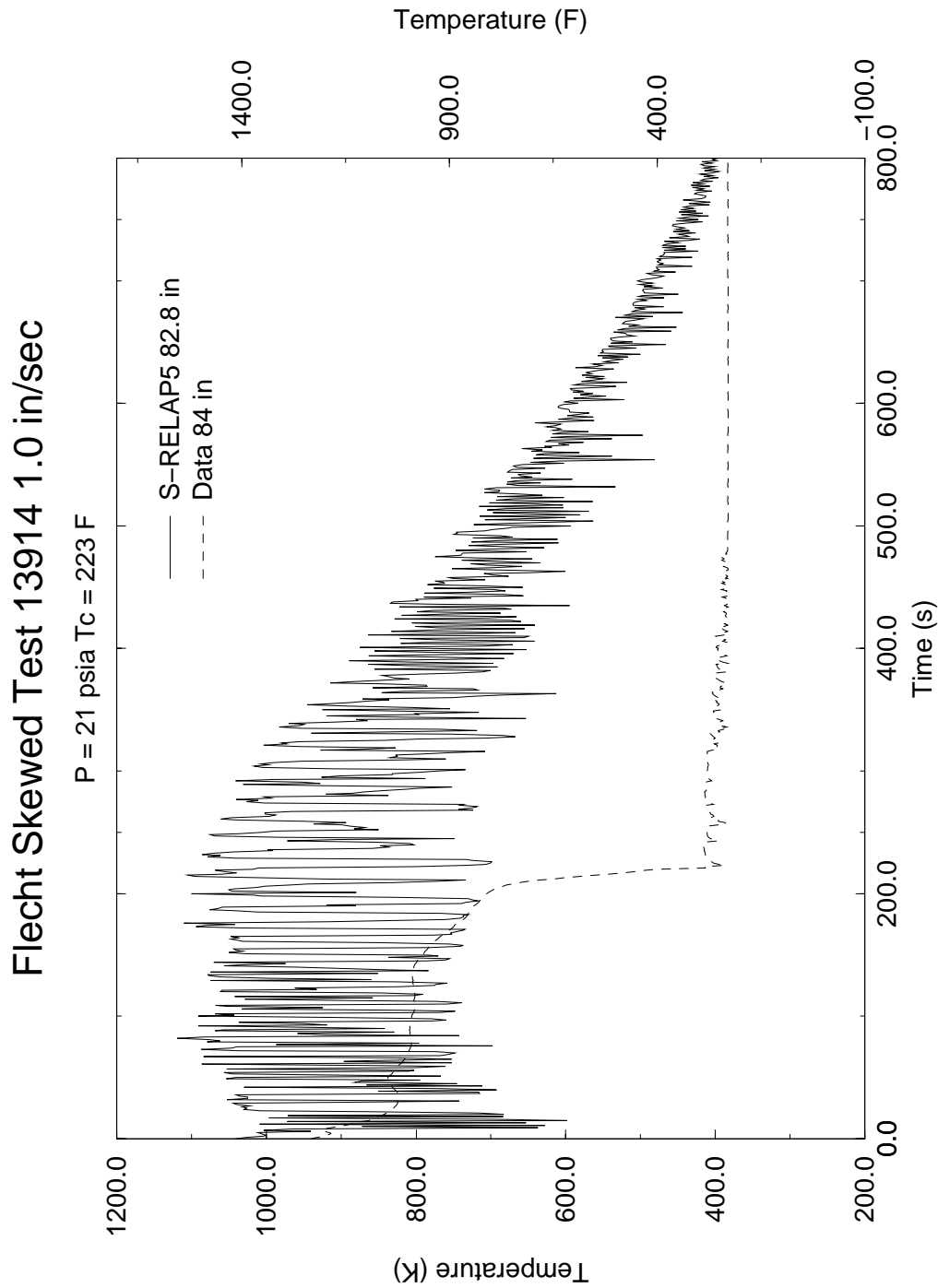


Figure 4.51 Steam Temperatures Calculated at 82.8 in and Measured at 84 in, FLECHT Skewed Test 13914

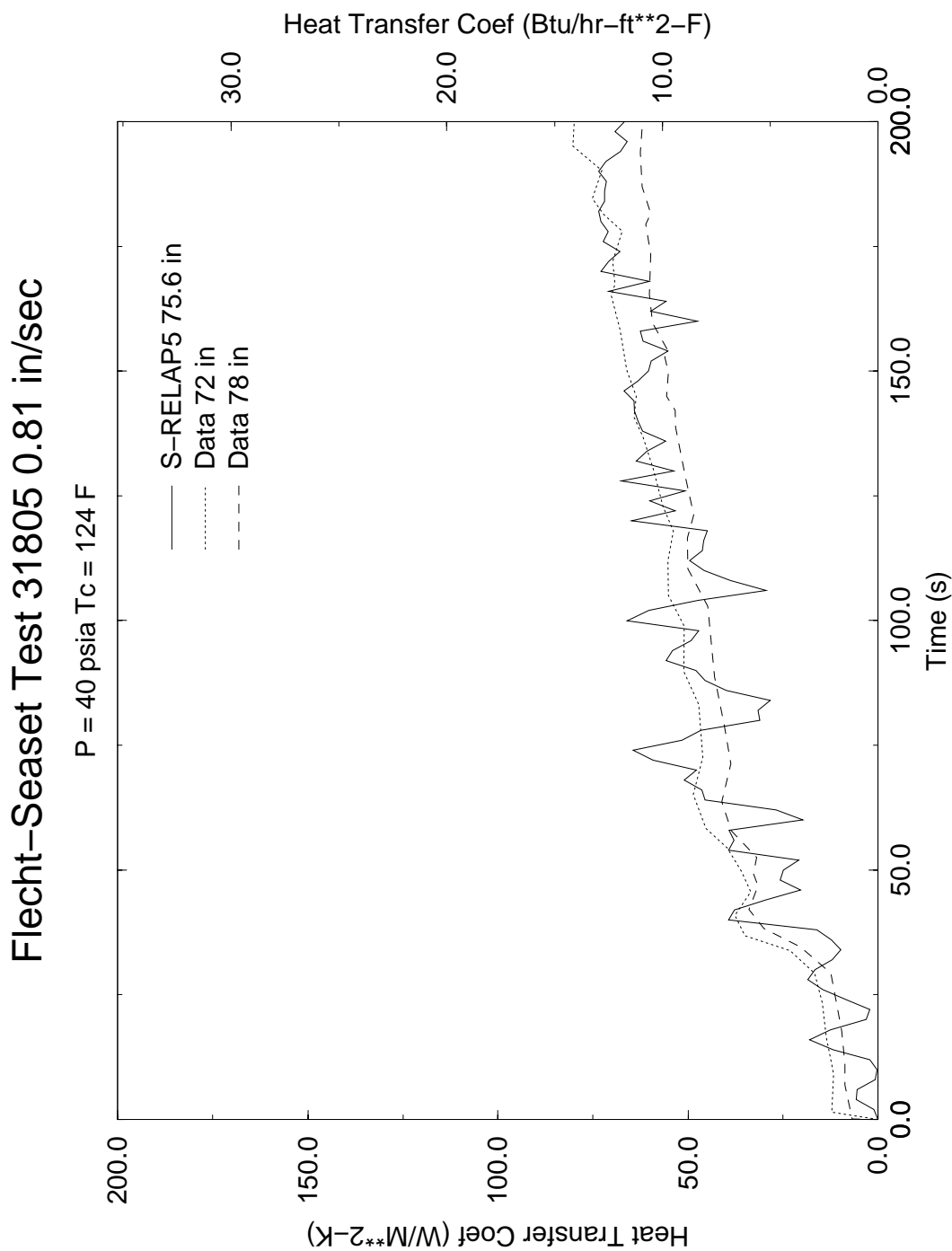


Figure 4.52 Comparison of Calculated and Measured Heat Transfer Coefficient, FLECHT SEASET Test 31805

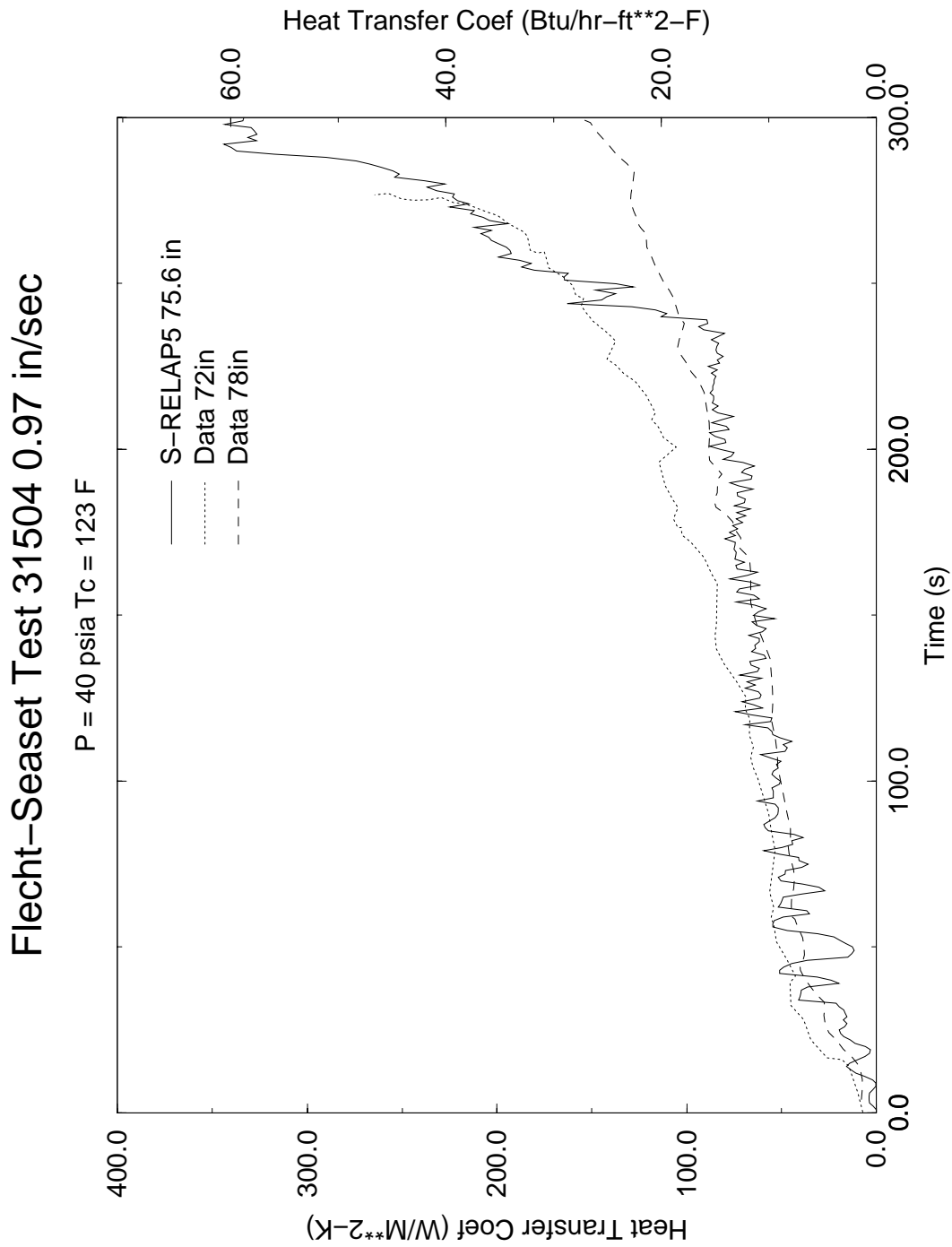


Figure 4.53 Comparison of Calculated and Measured Heat Transfer Coefficient, FLECHT SEASET Test 31504

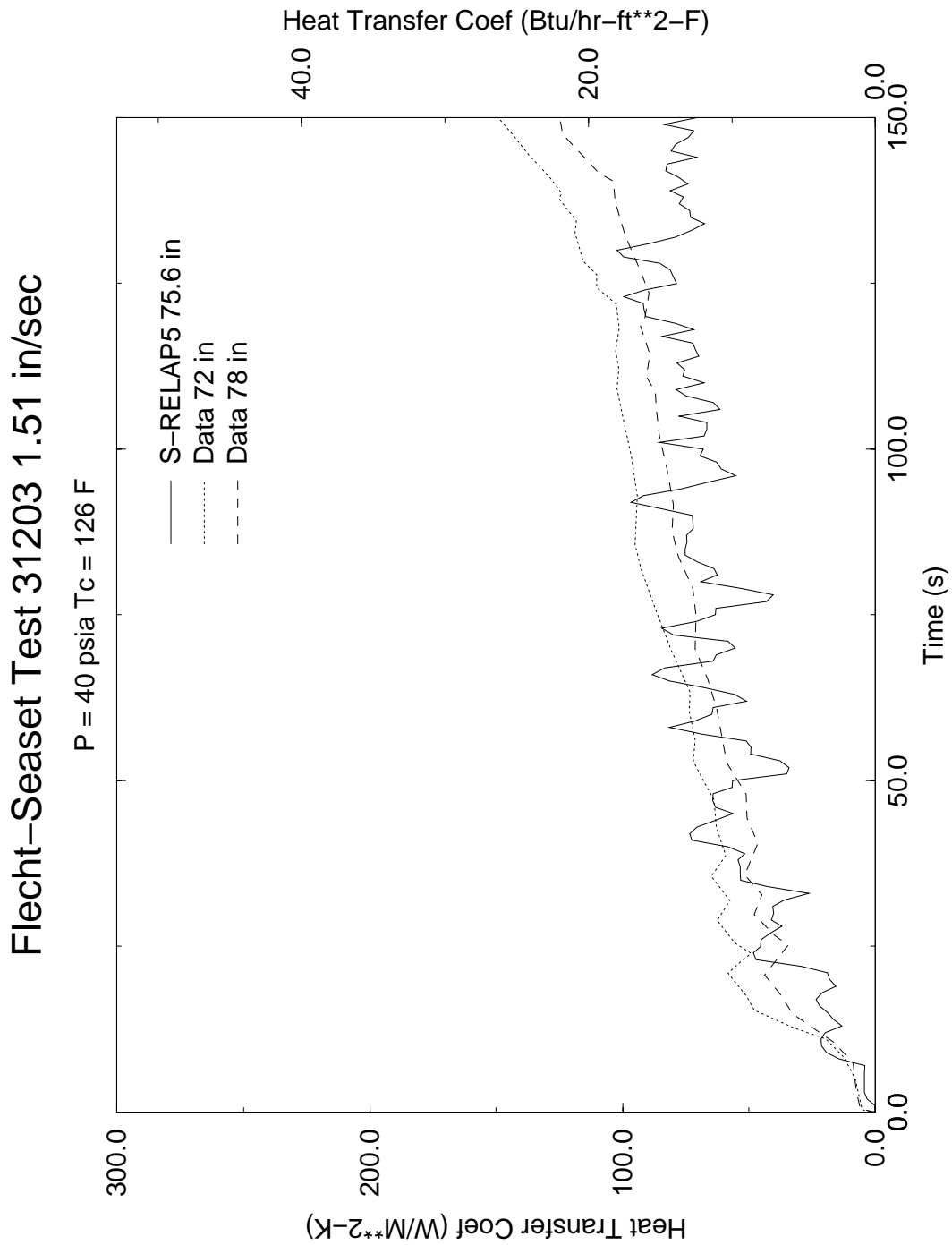


Figure 4.54 Comparison of Calculated and Measured Heat Transfer Coefficient, FLECHT SEASET Test 31203

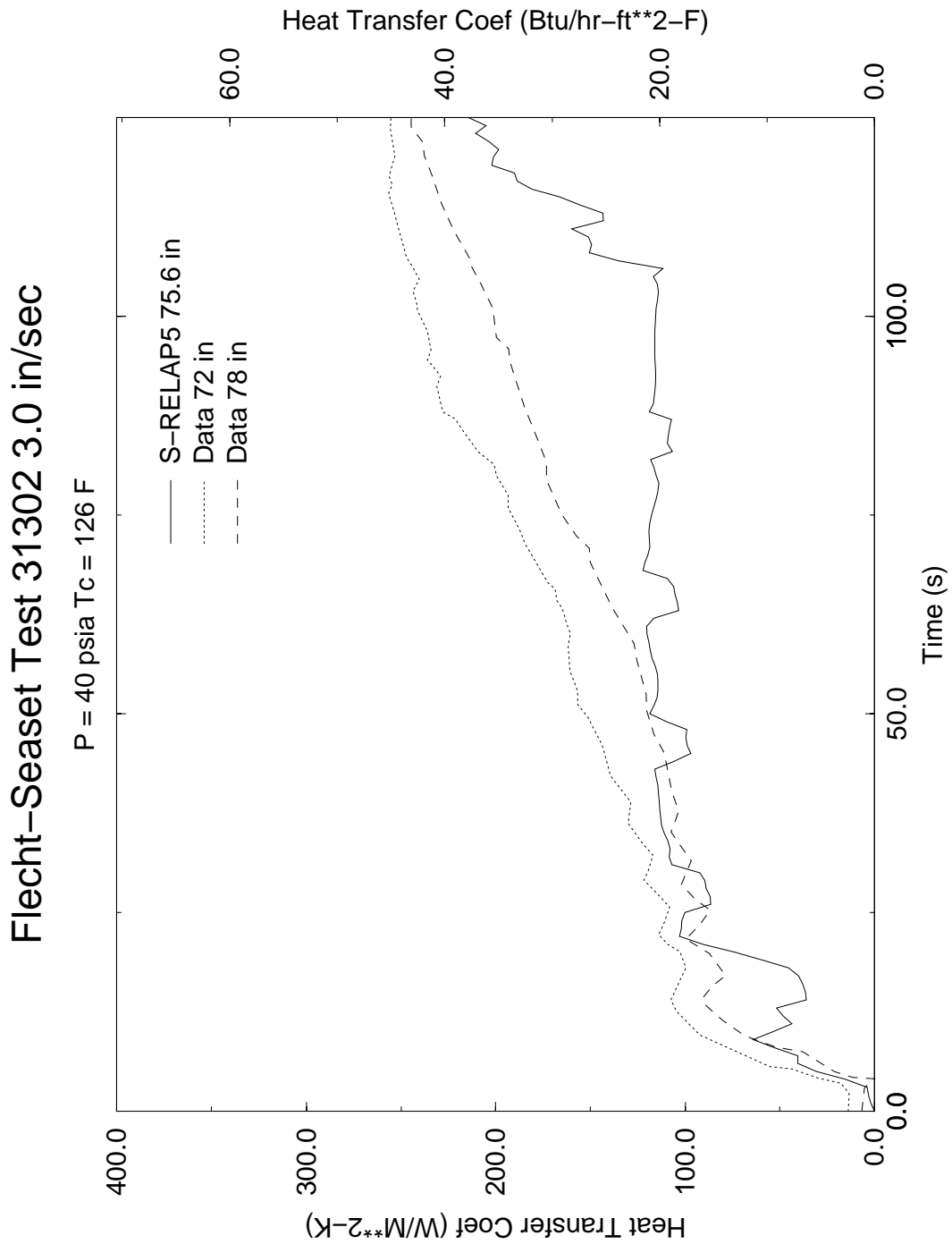


Figure 4.55 Comparison of Calculated and Measured Heat Transfer Coefficient, FLECHT SEASET Test 31302

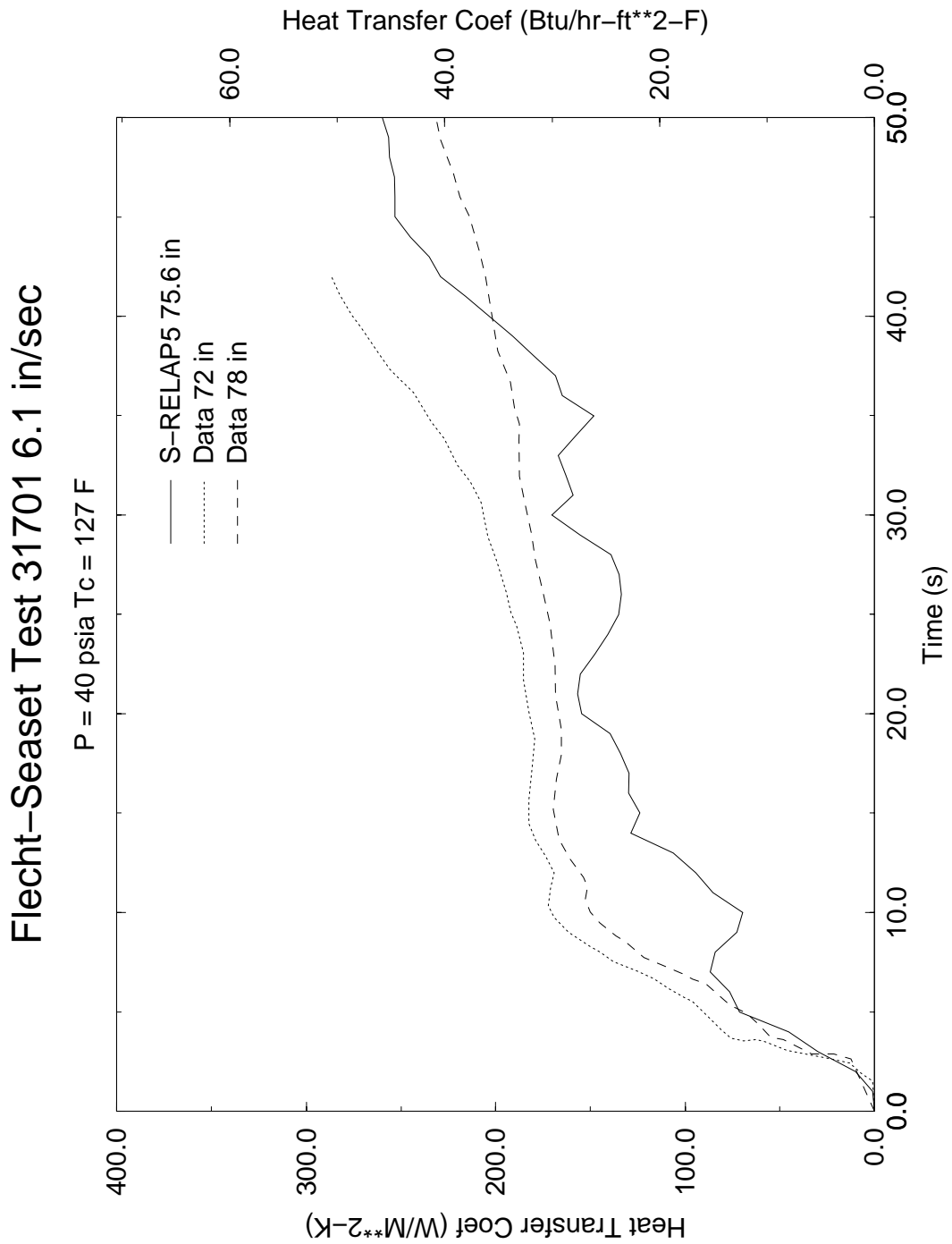


Figure 4.56 Comparison of Calculated and Measured Heat Transfer Coefficient, FLECHT SEASET Test 31701

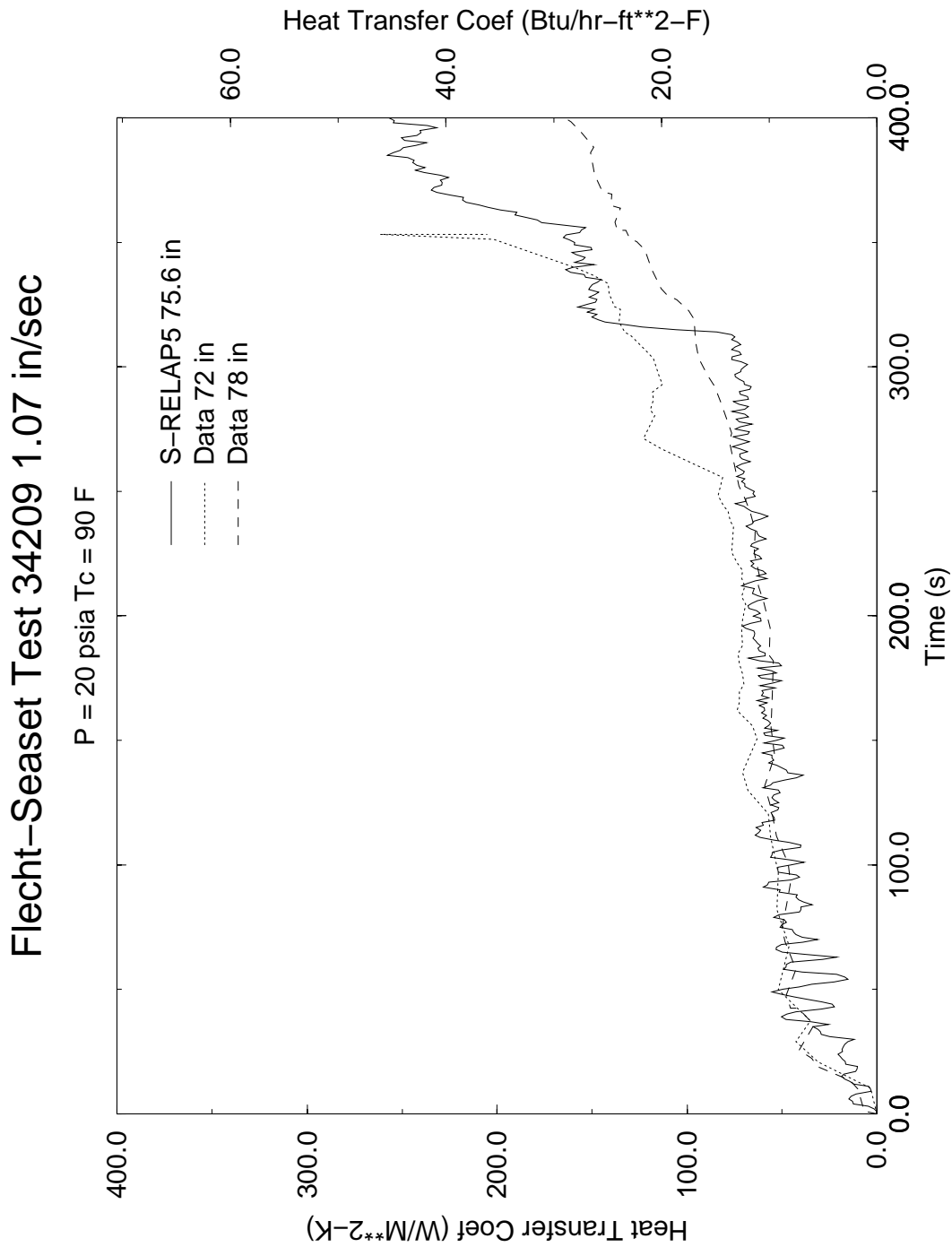


Figure 4.57 Comparison of Calculated and Measured Heat Transfer Coefficient, FLECHT SEASET Test 34209

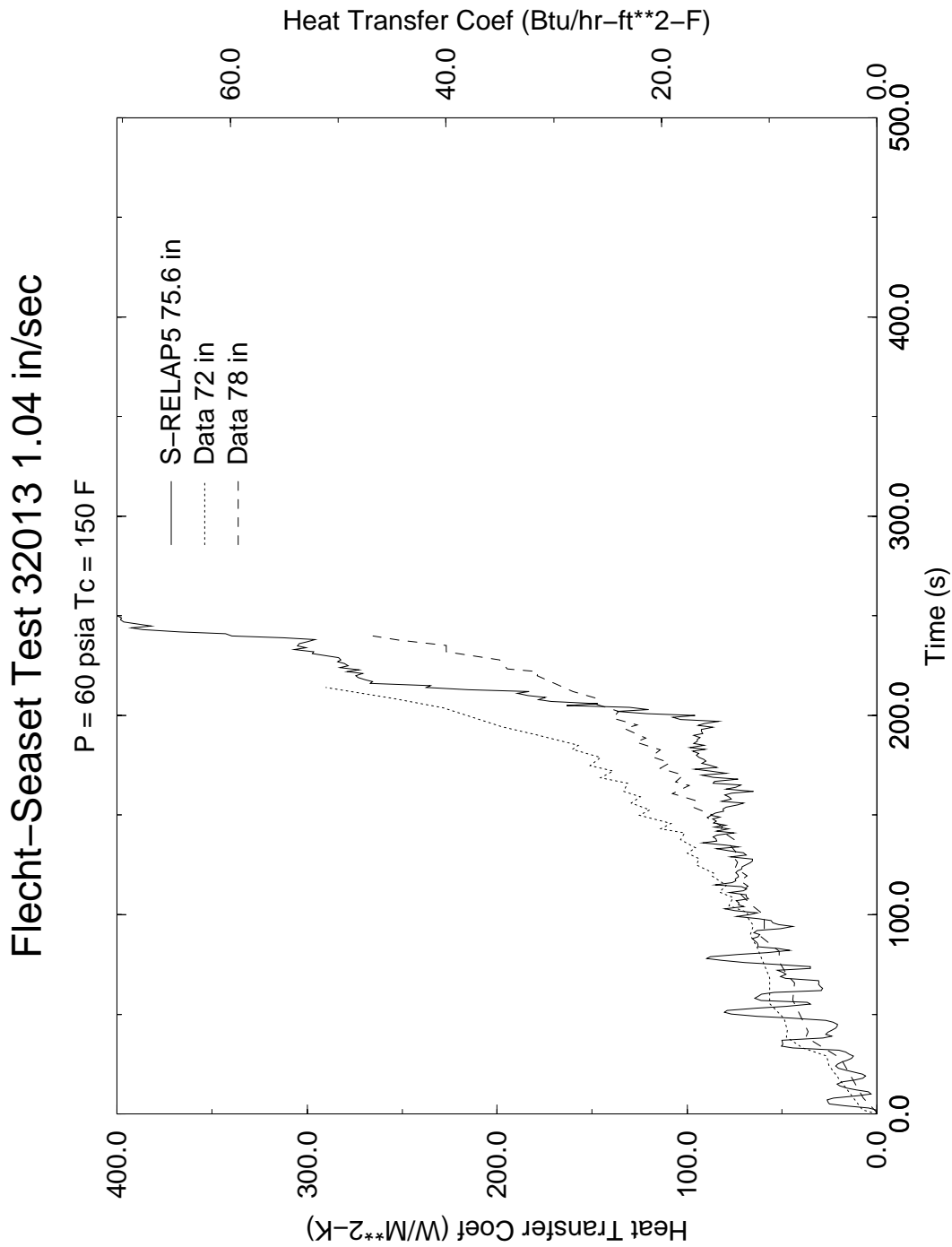


Figure 4.58 Comparison of Calculated and Measured Heat Transfer Coefficient, FLECHT SEASET Test 32013

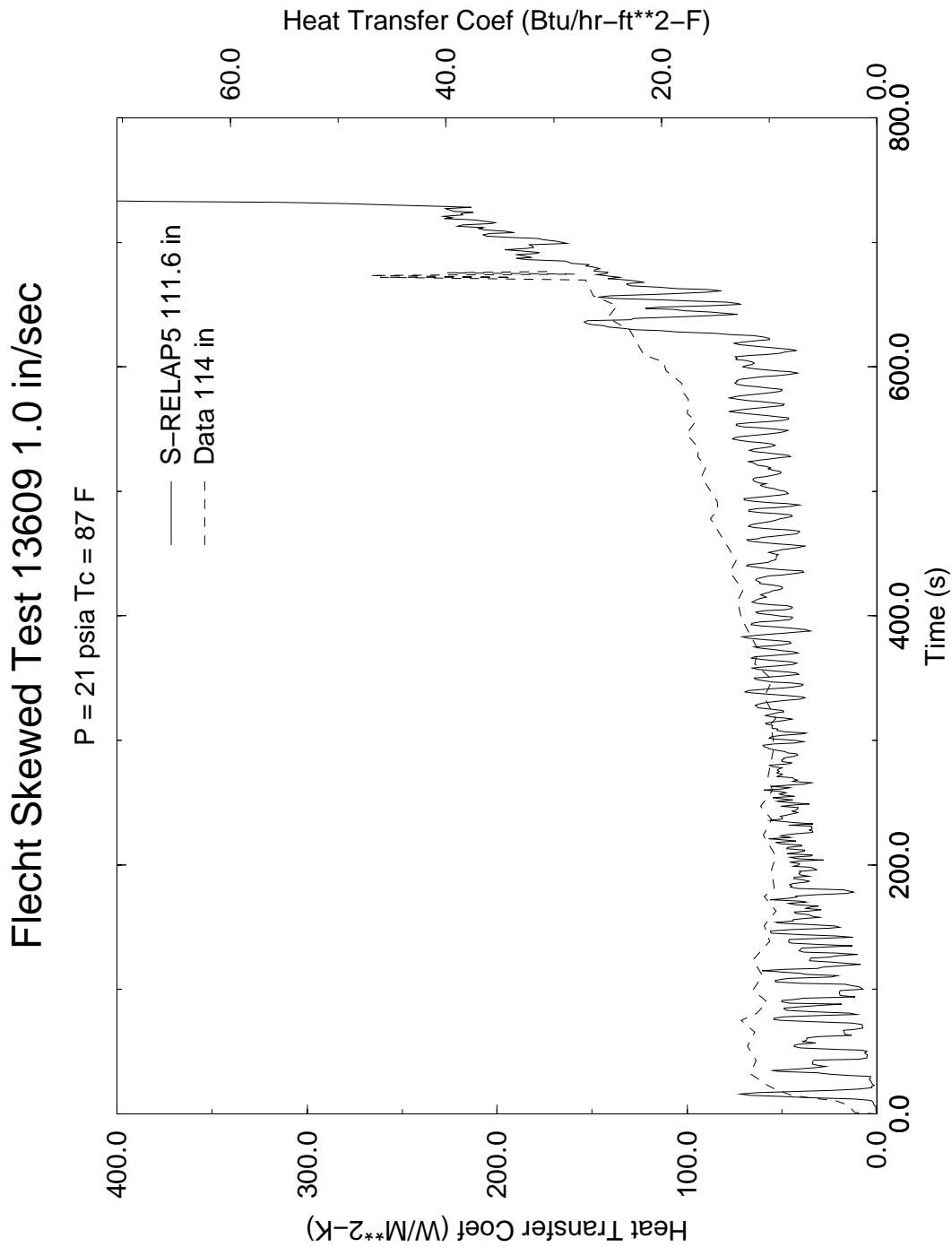


Figure 4.59 Comparison of Calculated and Measured Heat Transfer Coefficient, FLECHT Skewed Test 13609

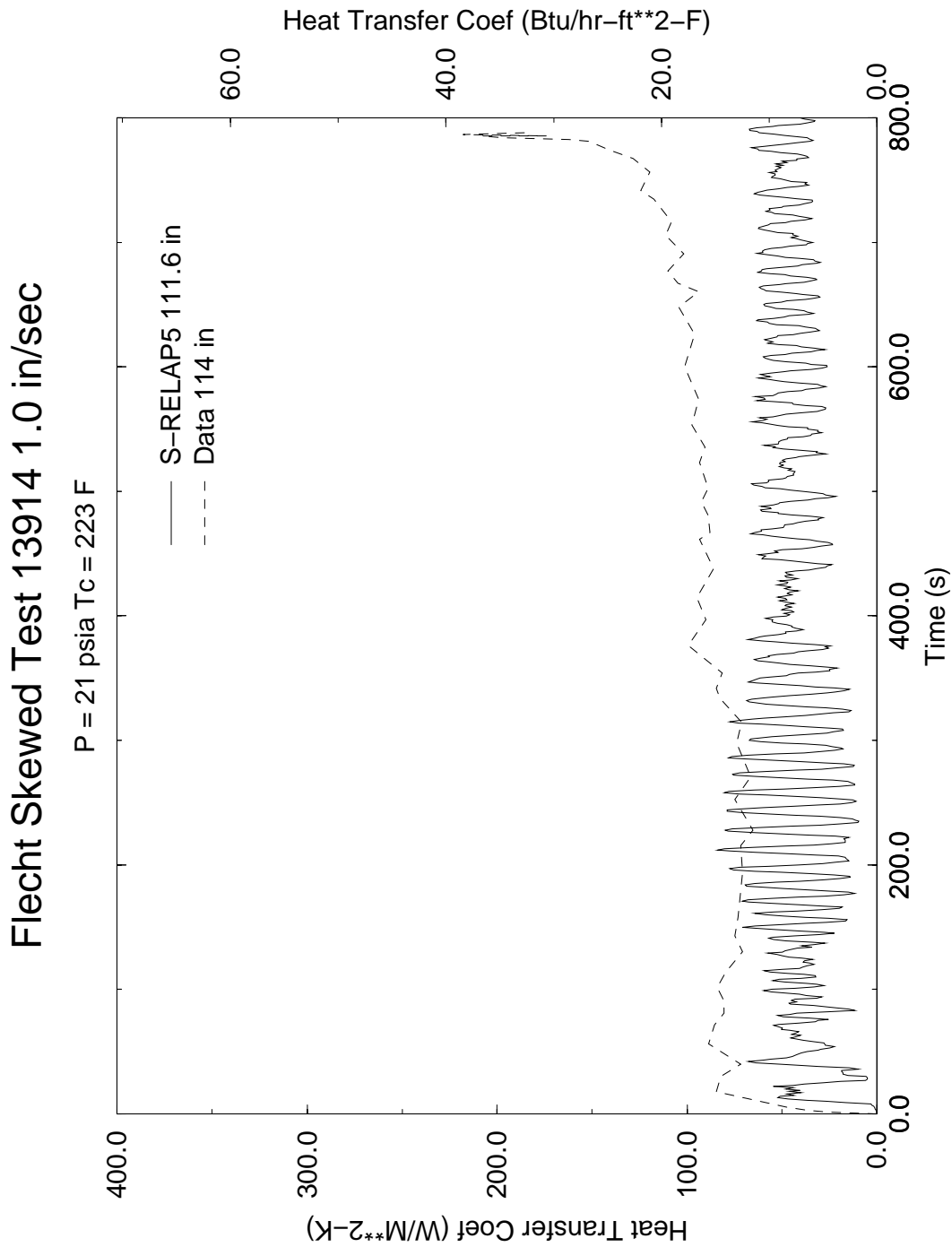


Figure 4.60 Comparison of Calculated and Measured Heat Transfer Coefficient, FLECHT Skewed Test 13914

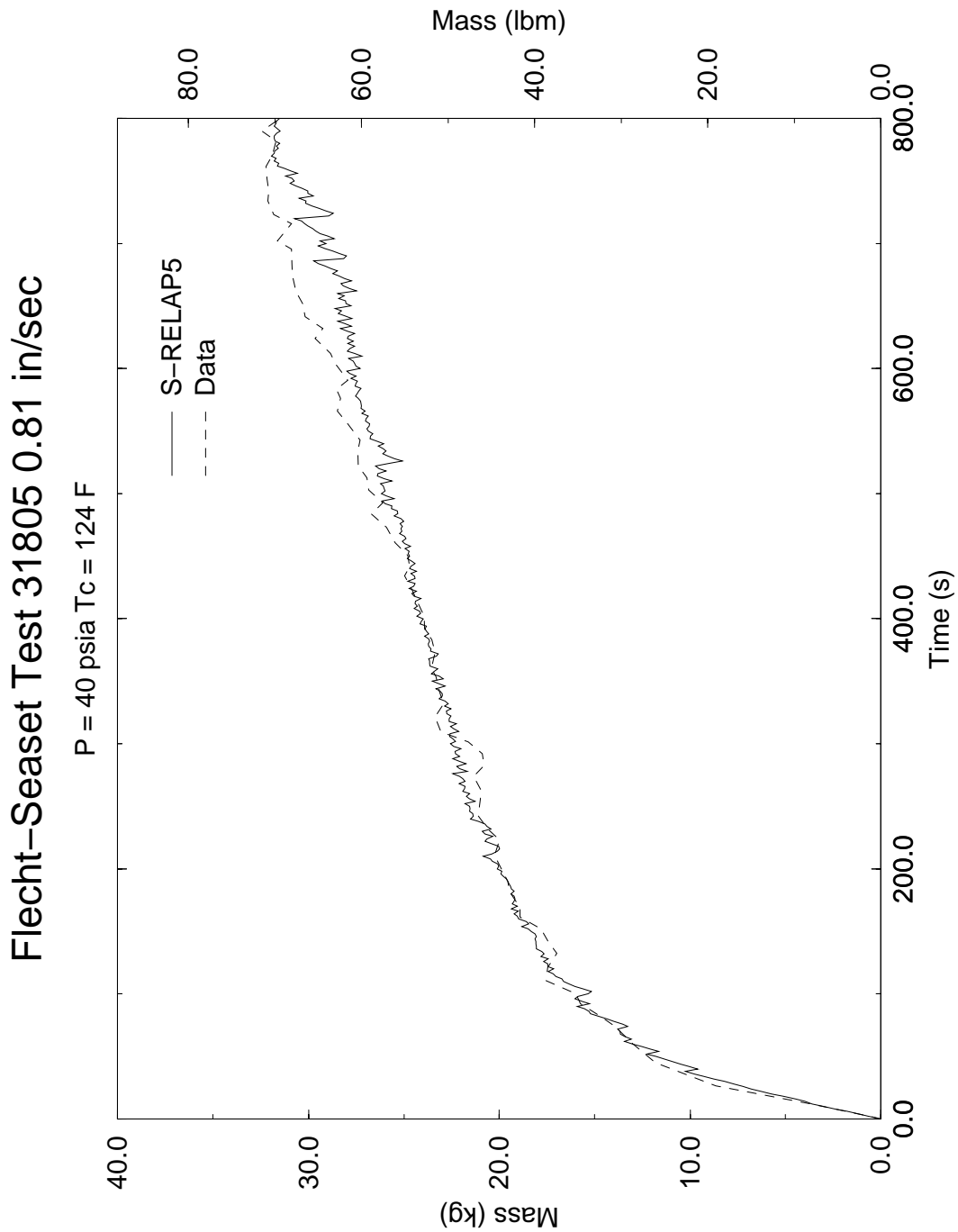


Figure 4.61 Accumulated Water Mass in the Test Section, FLECHT SEASET Test 31805

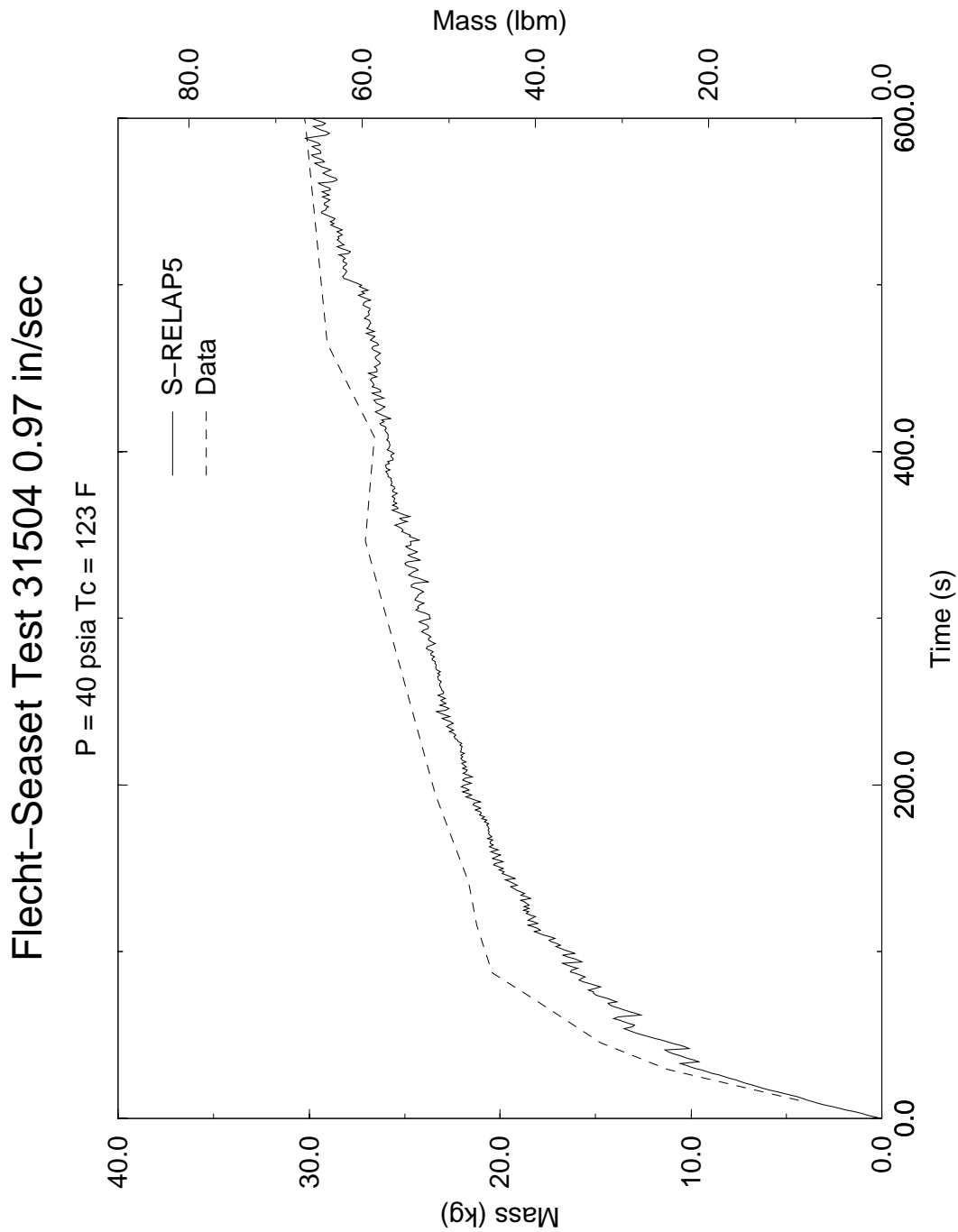


Figure 4.62 Accumulated Water Mass in the Test Section, FLECHT SEASET Test 31504

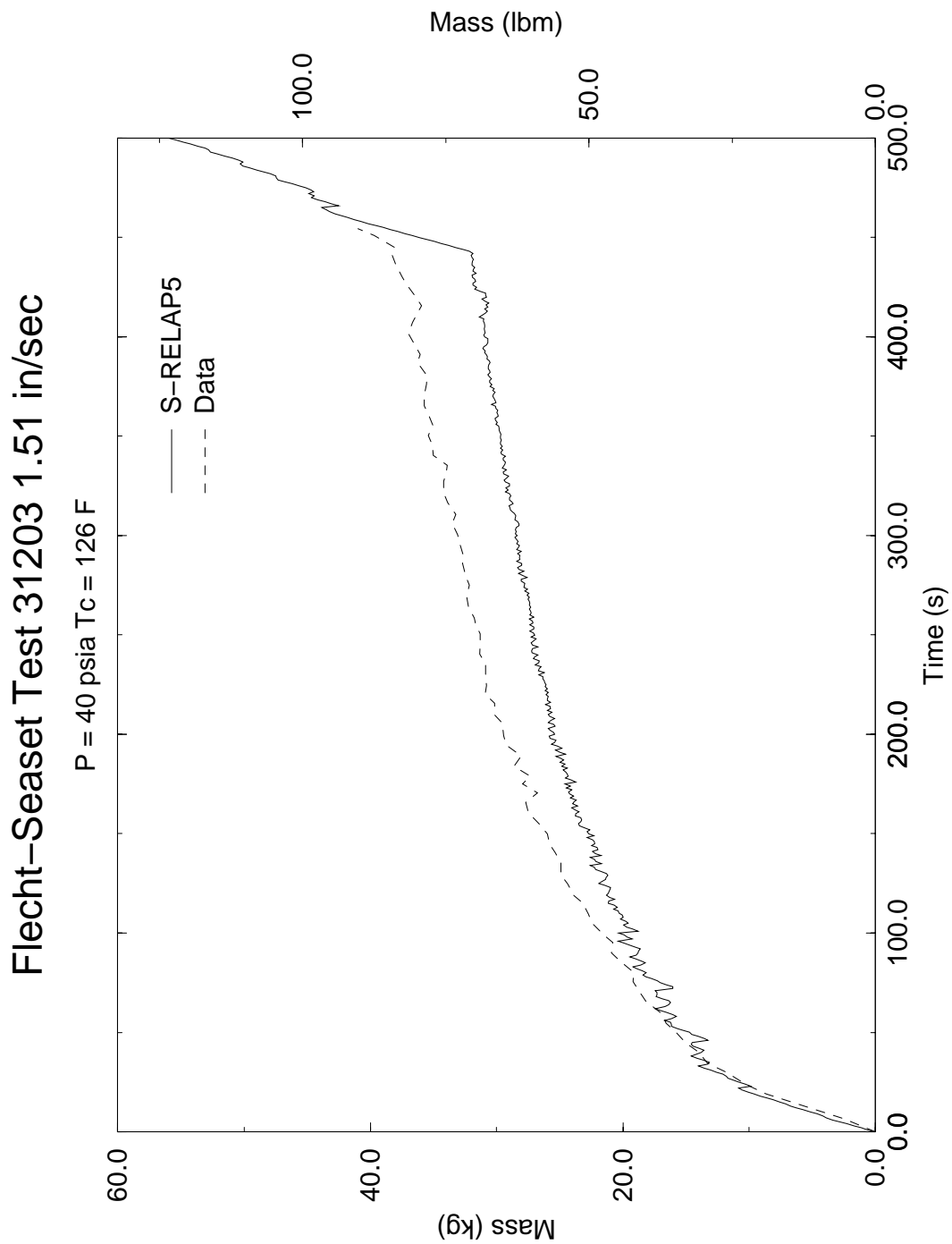


Figure 4.63 Accumulated Water Mass in the Test Section, FLECHT SEASET Test 31203

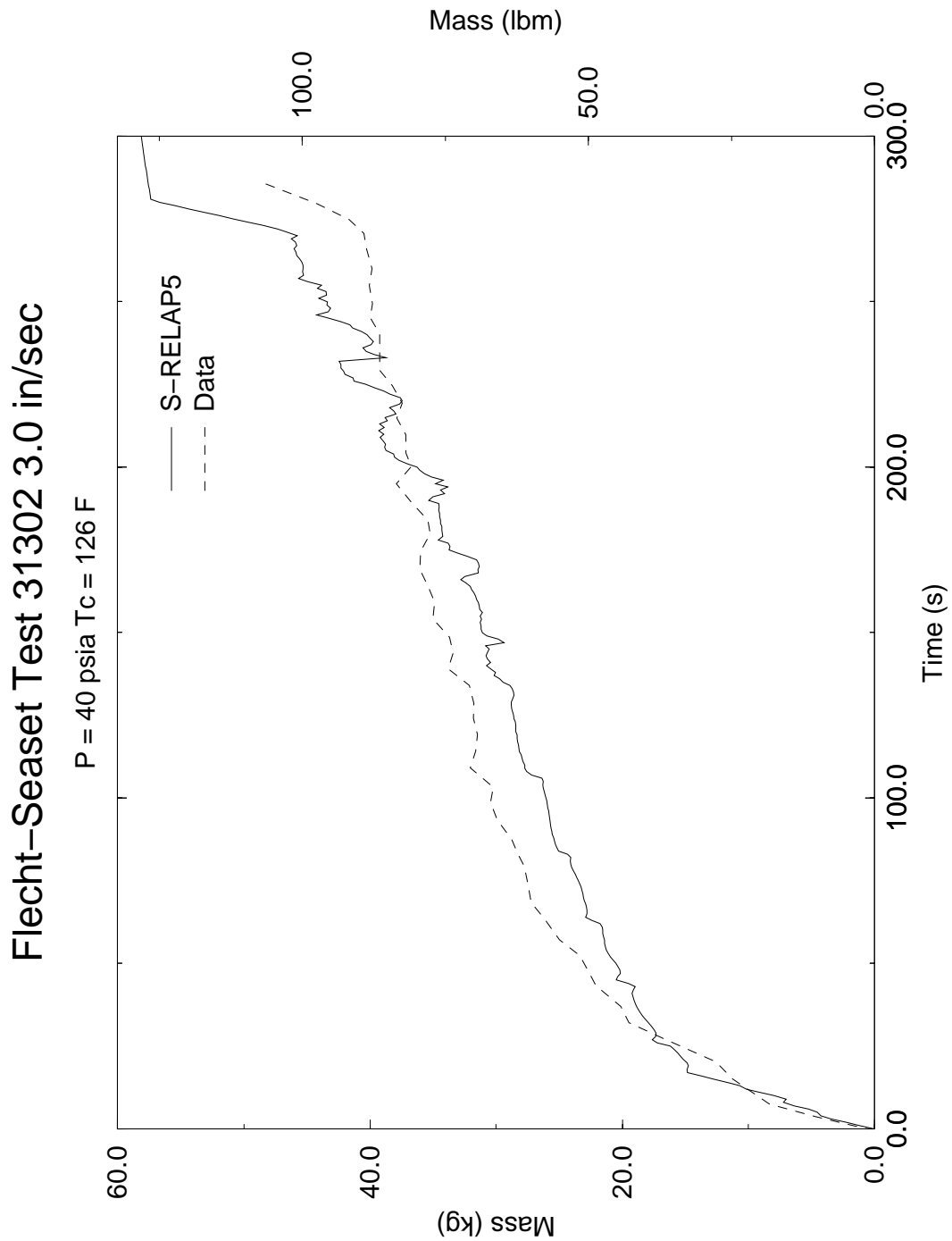


Figure 4.64 Accumulated Water Mass in the Test Section, FLECHT SEASET Test 31302

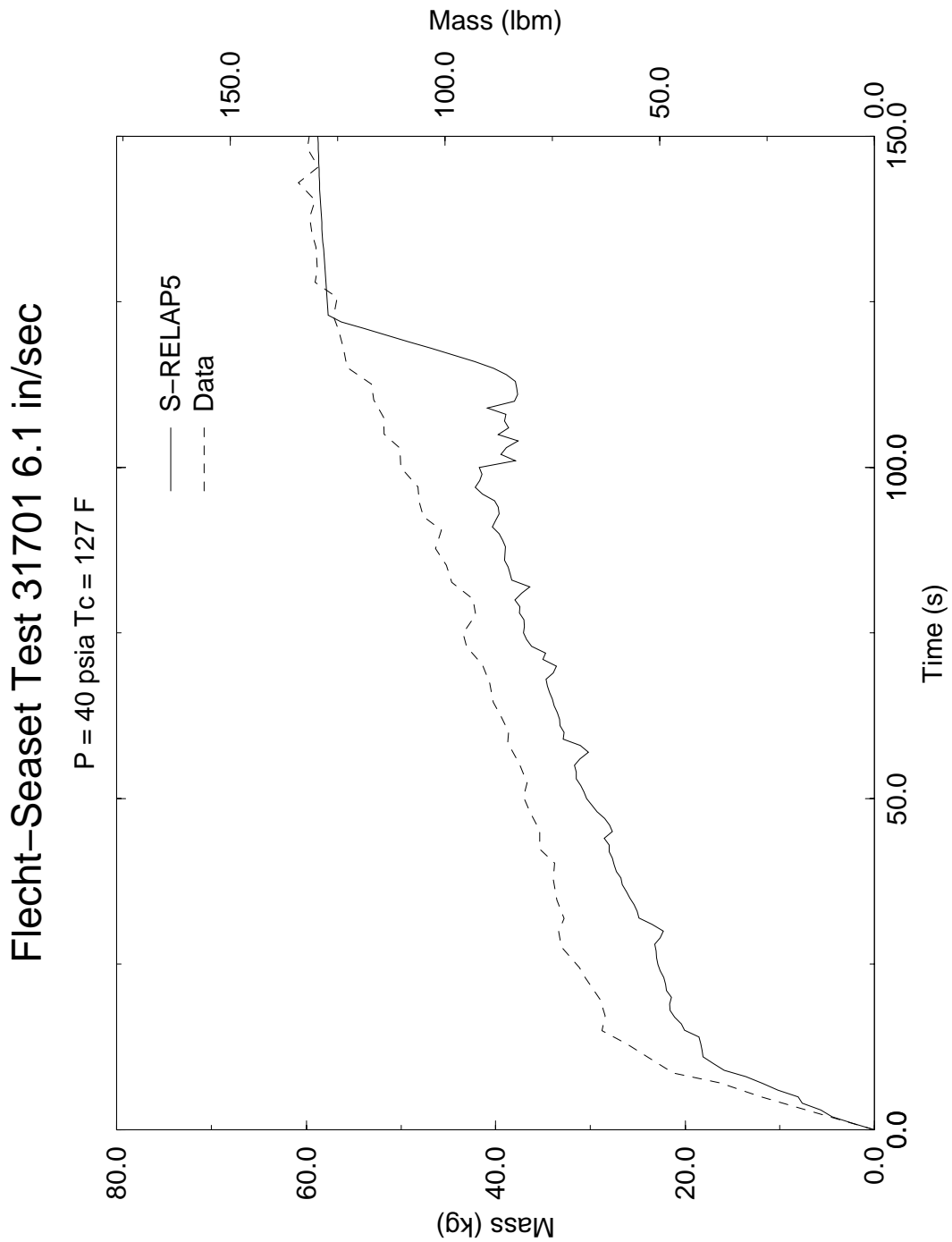


Figure 4.65 Accumulated Water Mass in the Test Section, FLECHT SEASET Test 31701

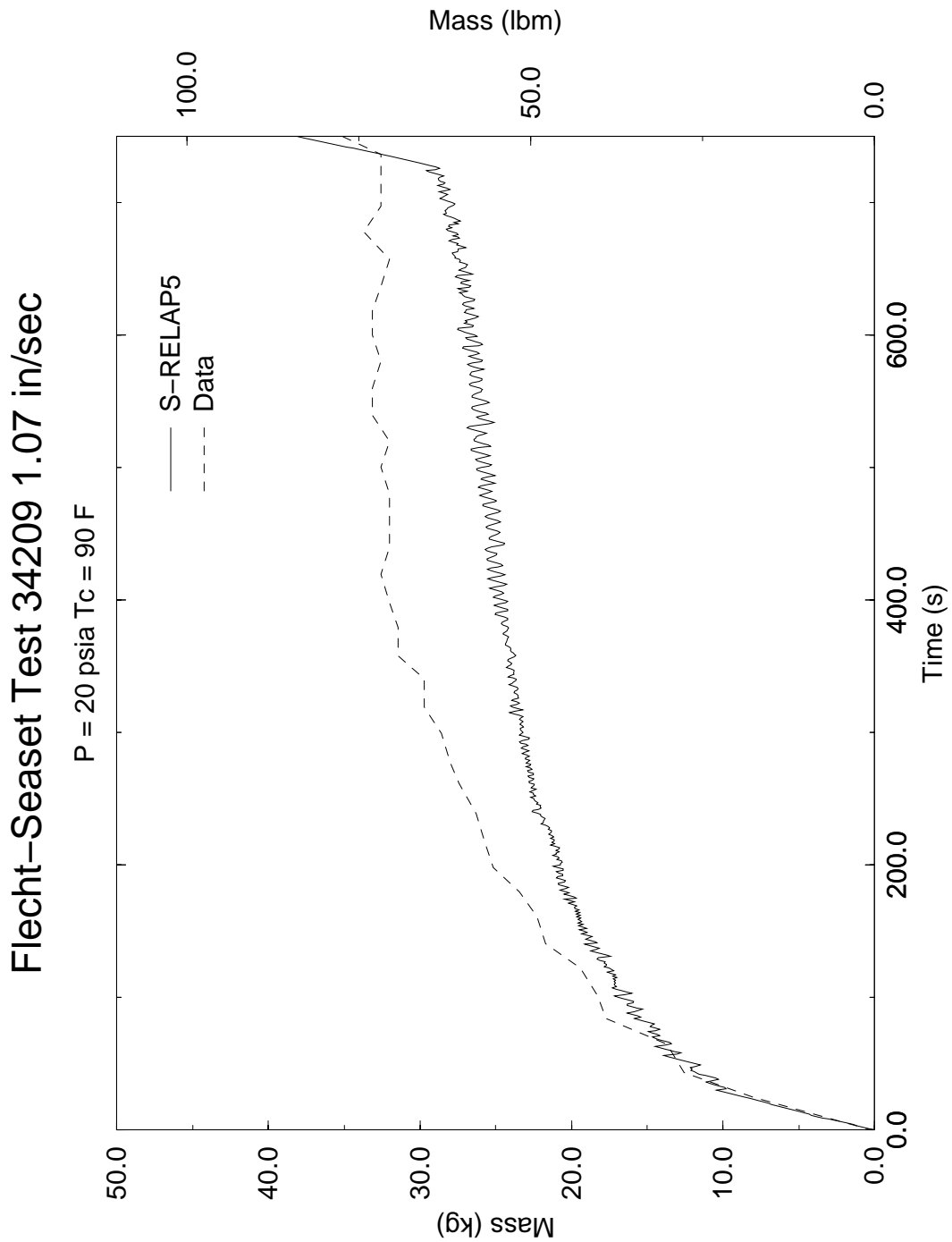


Figure 4.66 Accumulated Water Mass in the Test Section, FLECHT SEASET Test 34209

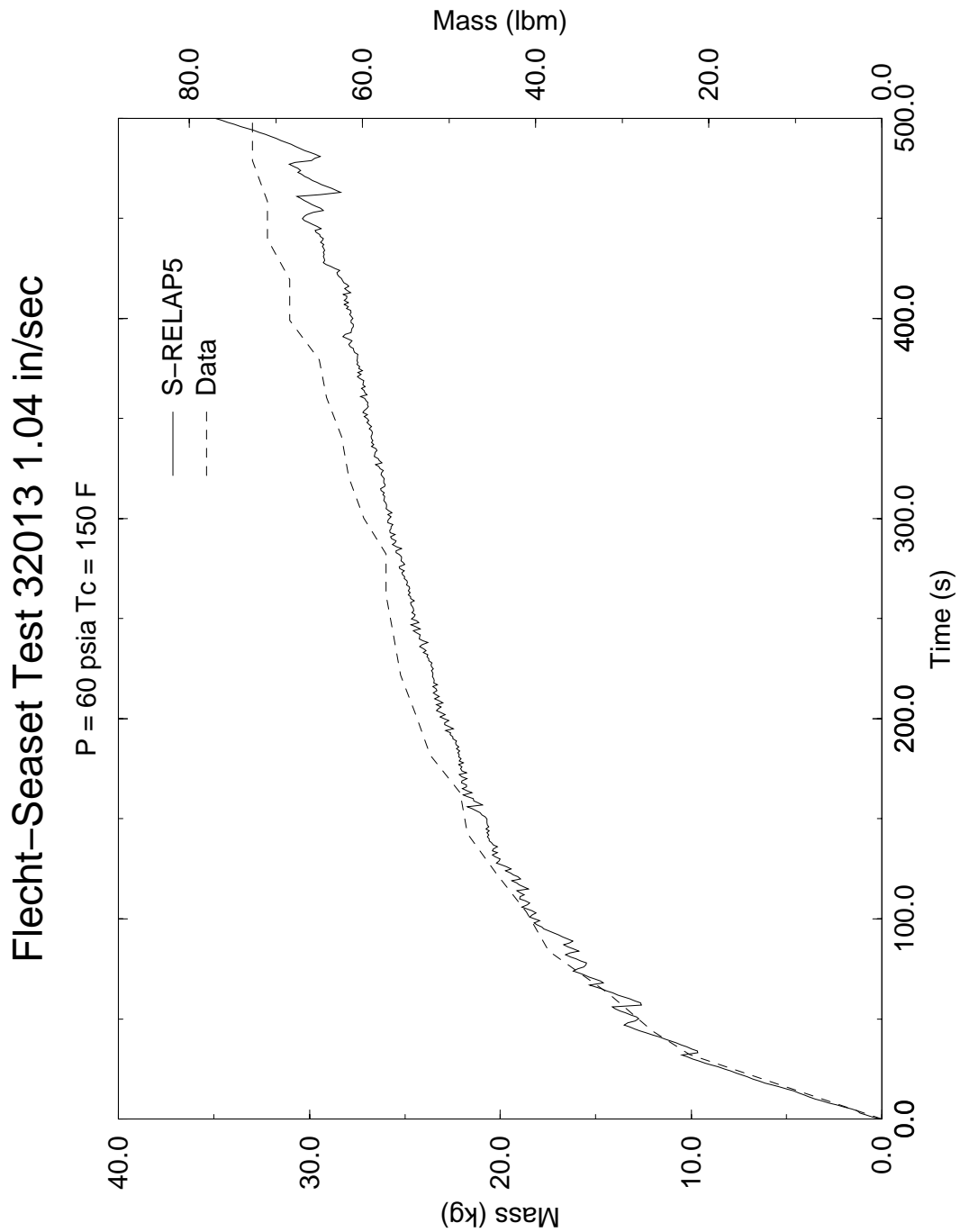


Figure 4.67 Accumulated Water Mass in the Test Section, FLECHT SEASET Test 32013

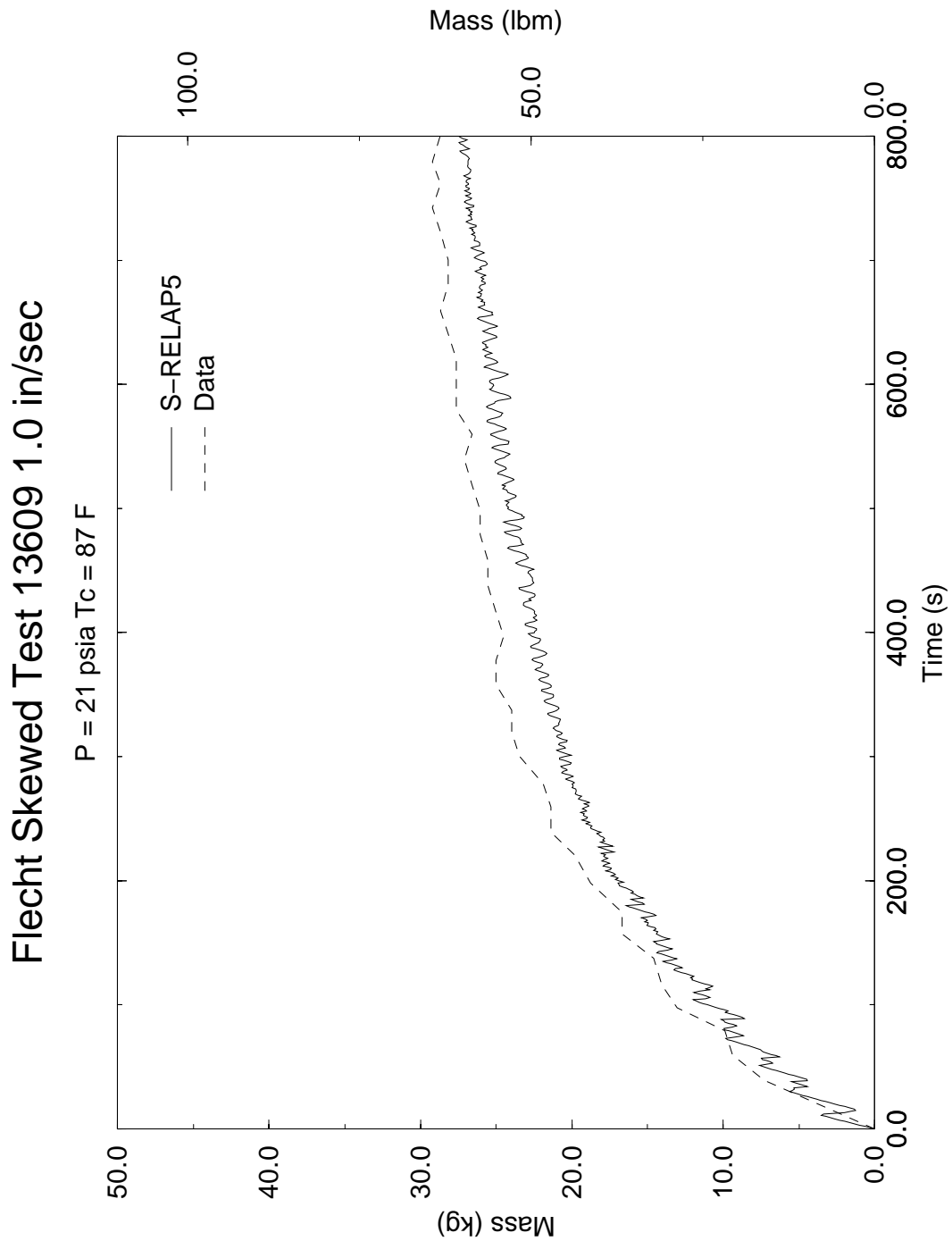


Figure 4.68 Accumulated Water Mass in the Test Section, FLECHT Skewed Test 13609

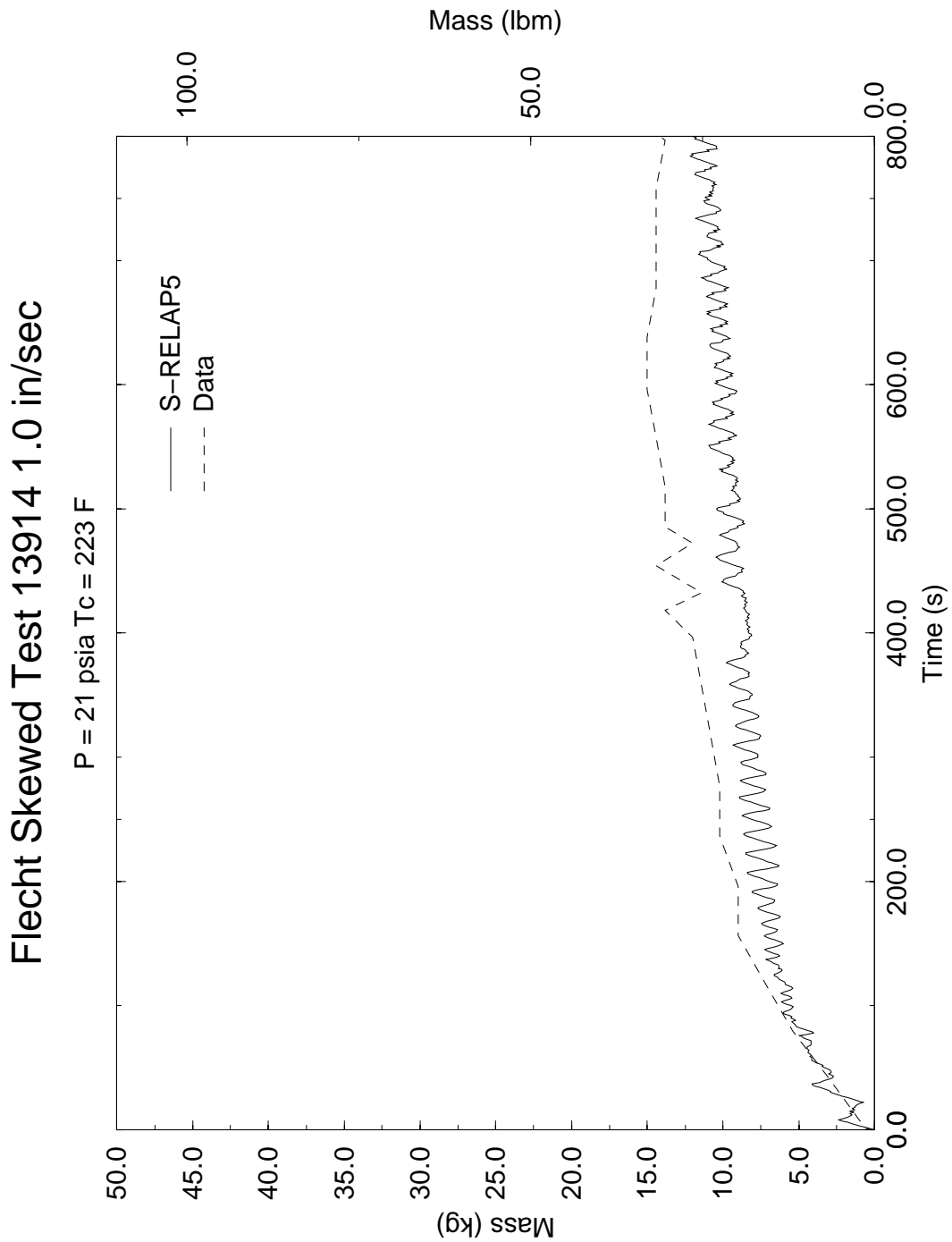


Figure 4.69 Accumulated Water Mass in the Test Section, FLECHT Skewed Test 13914

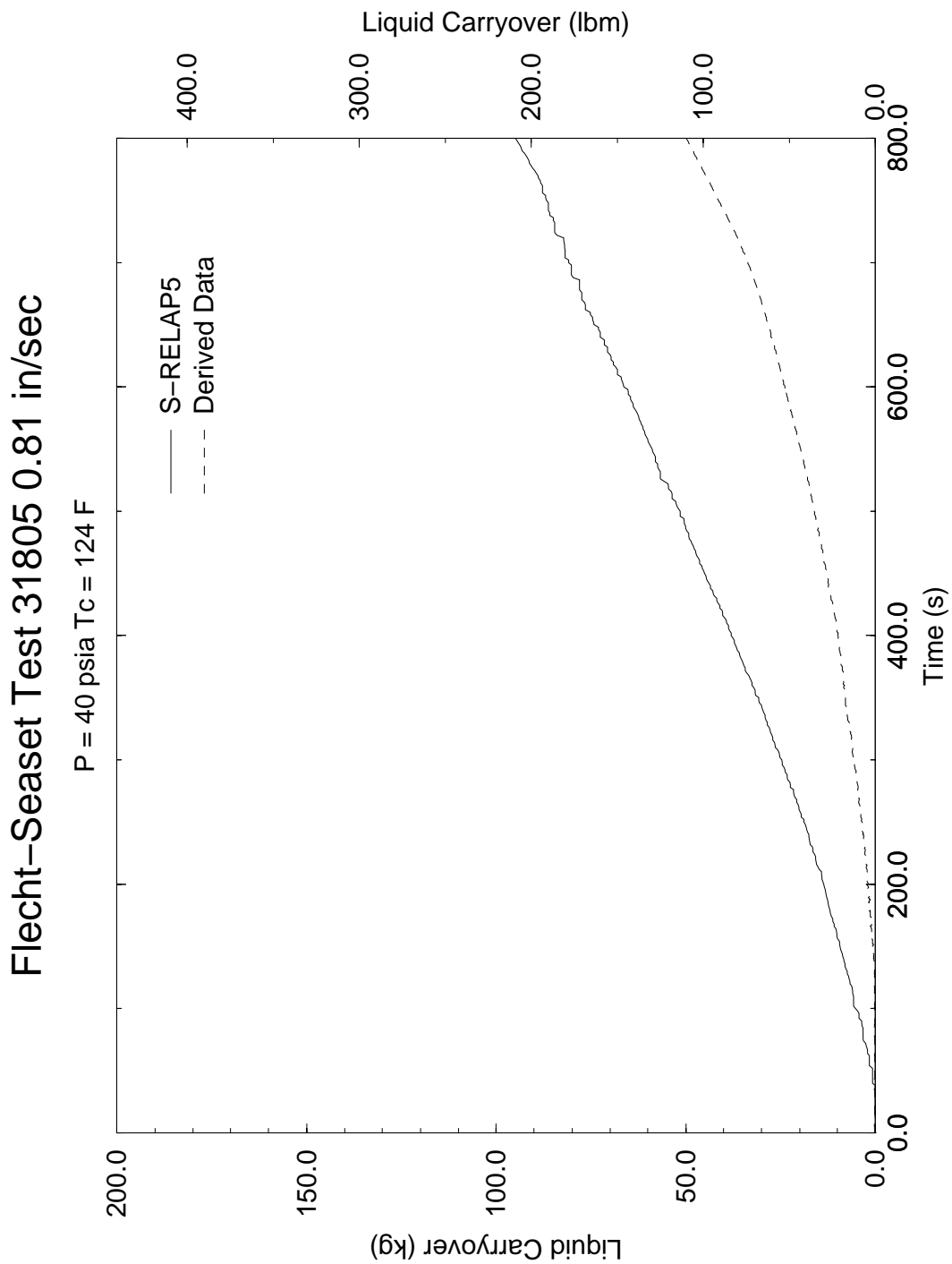


Figure 4.70 Total Liquid Carryover From Test Assembly, FLECHT SEASET Test 31805

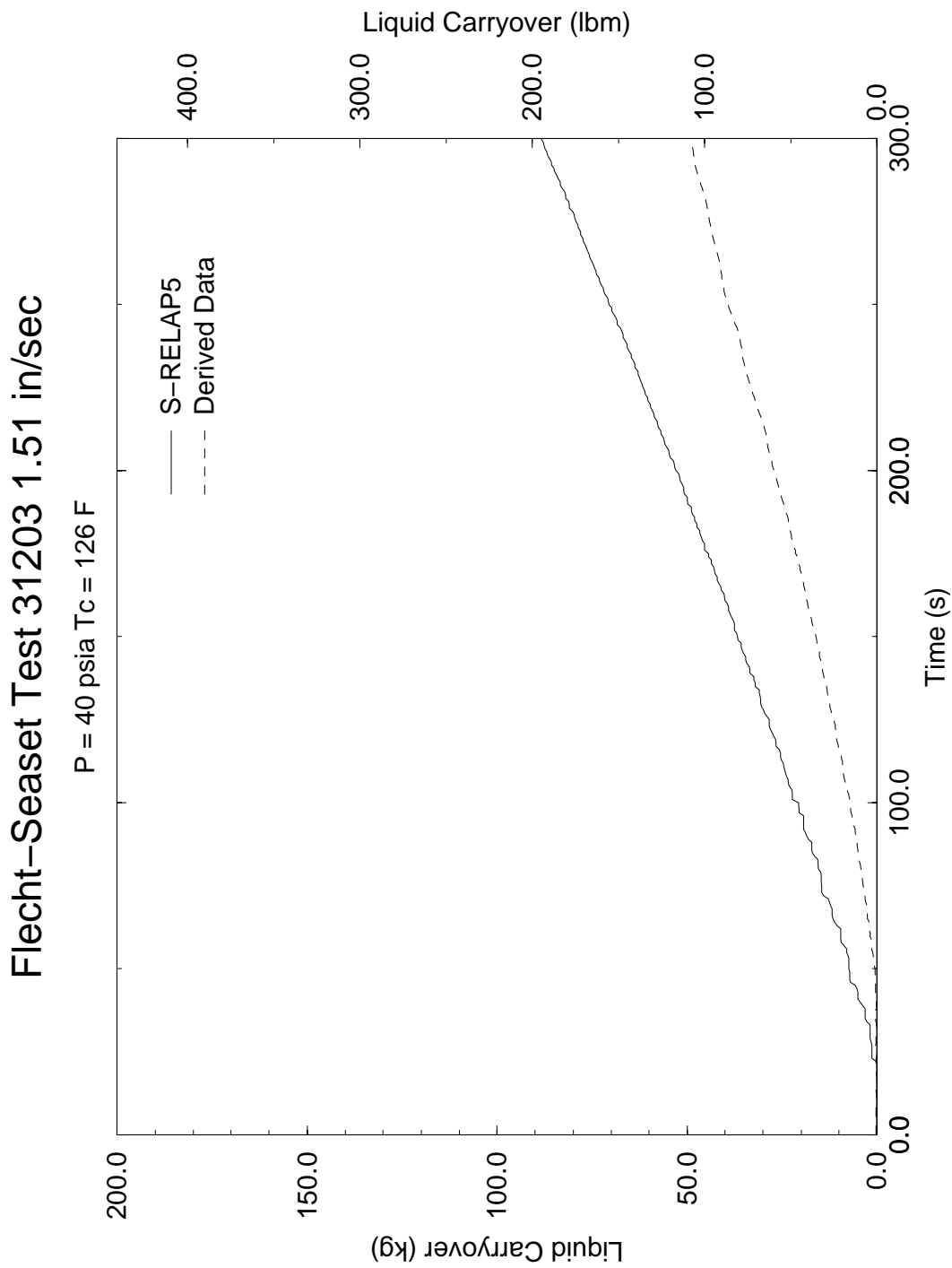


Figure 4.71 Total Liquid Carryover From Test Assembly, FLECHT SEASET Test 31203

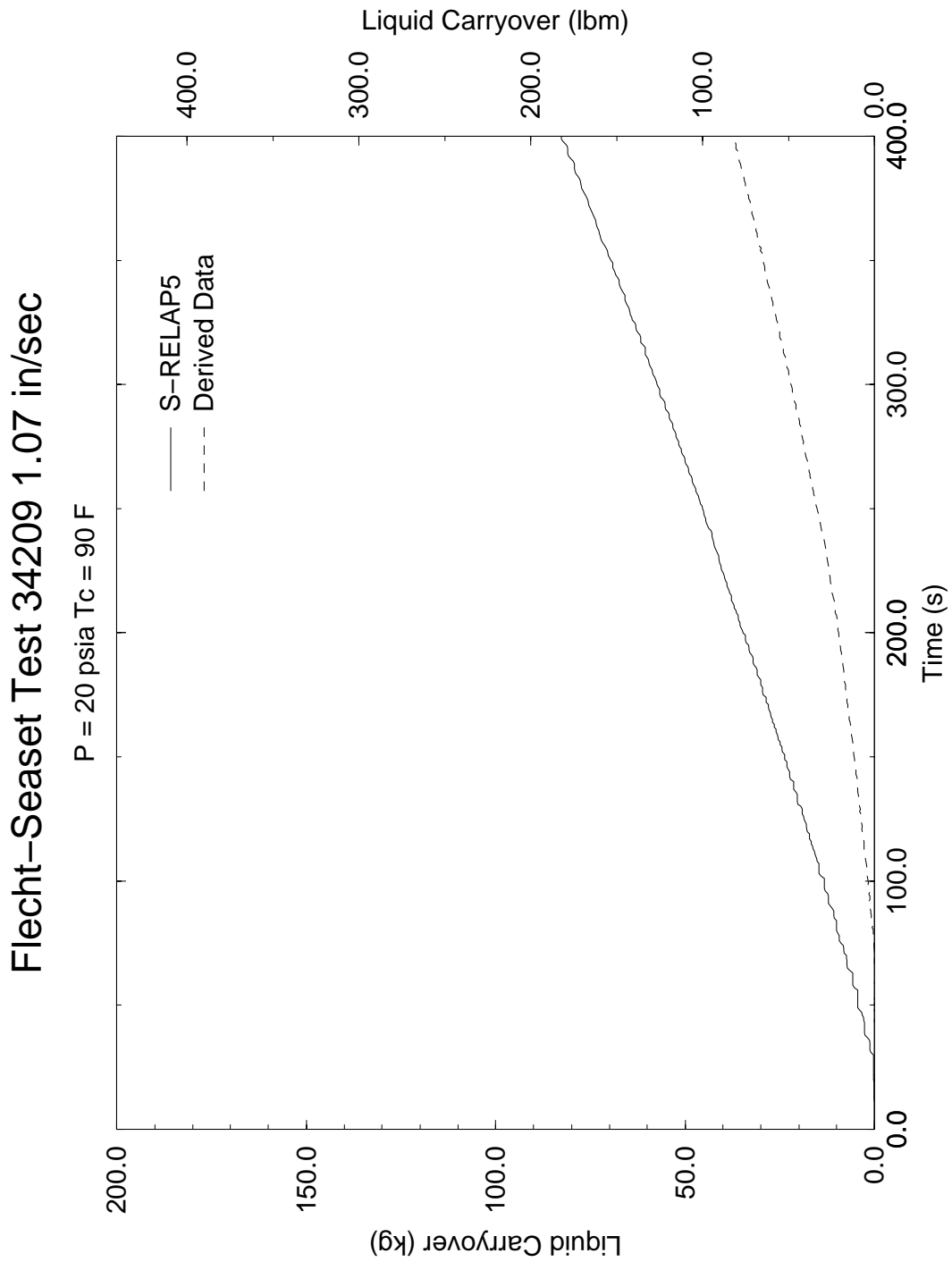


Figure 4.72 Total Liquid Carryover From Test Assembly, FLECHT SEASET Test 34209

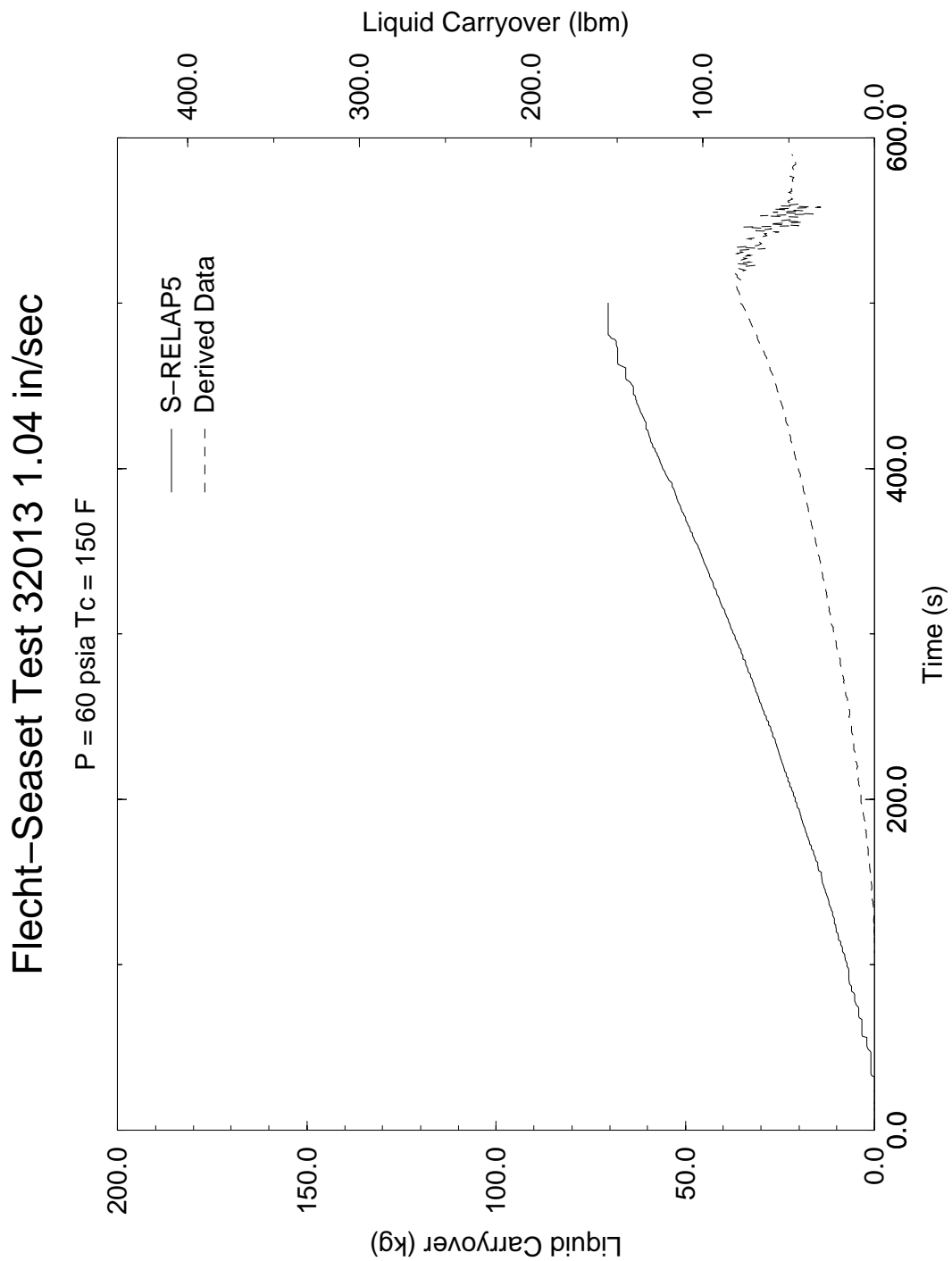


Figure 4.73 Total Liquid Carryover From Test Assembly, FLECHT SEASET Test 32013

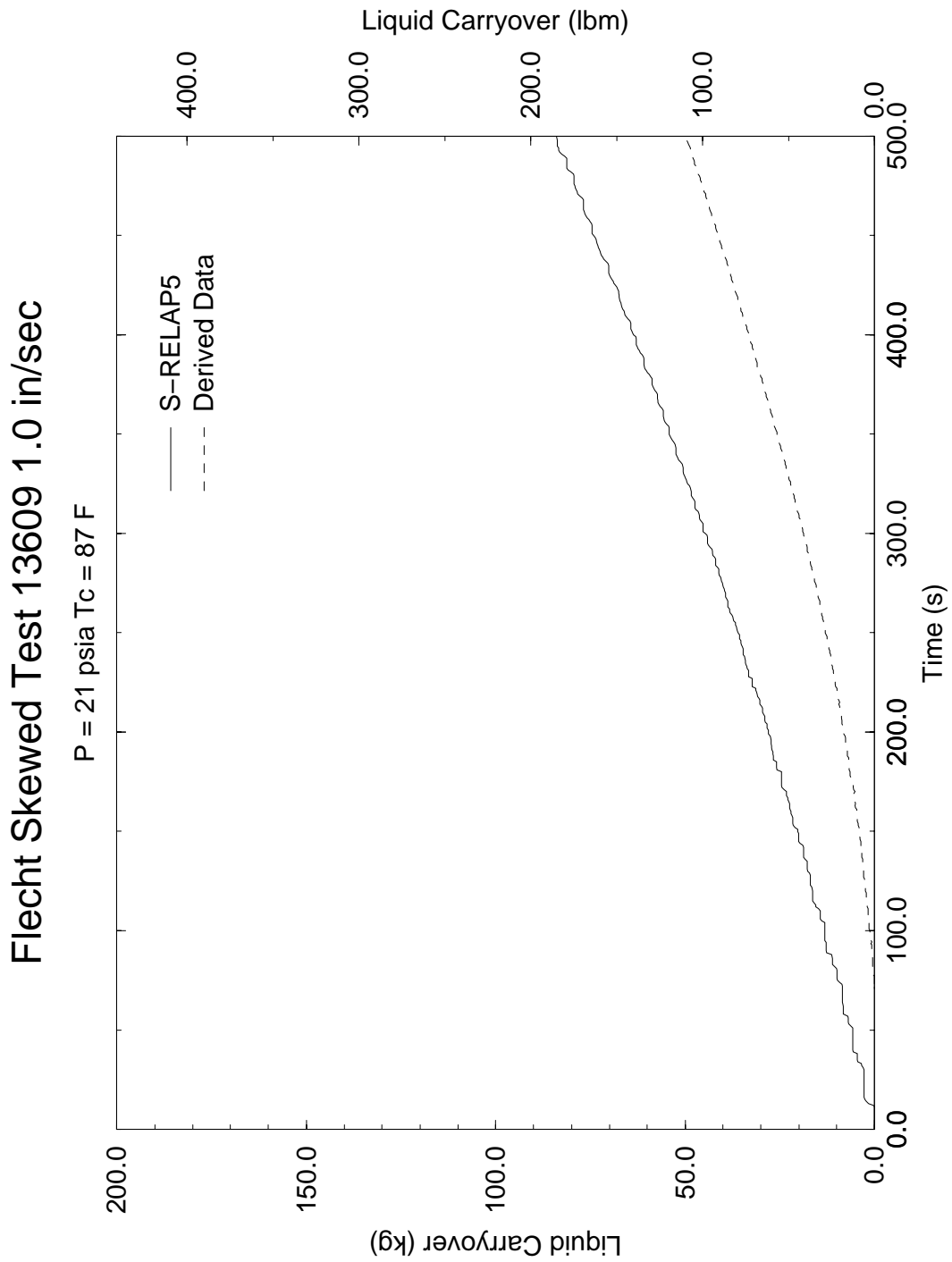


Figure 4.74 Total Liquid Carryover From Test Assembly, FLECHT Skewed Test 13609

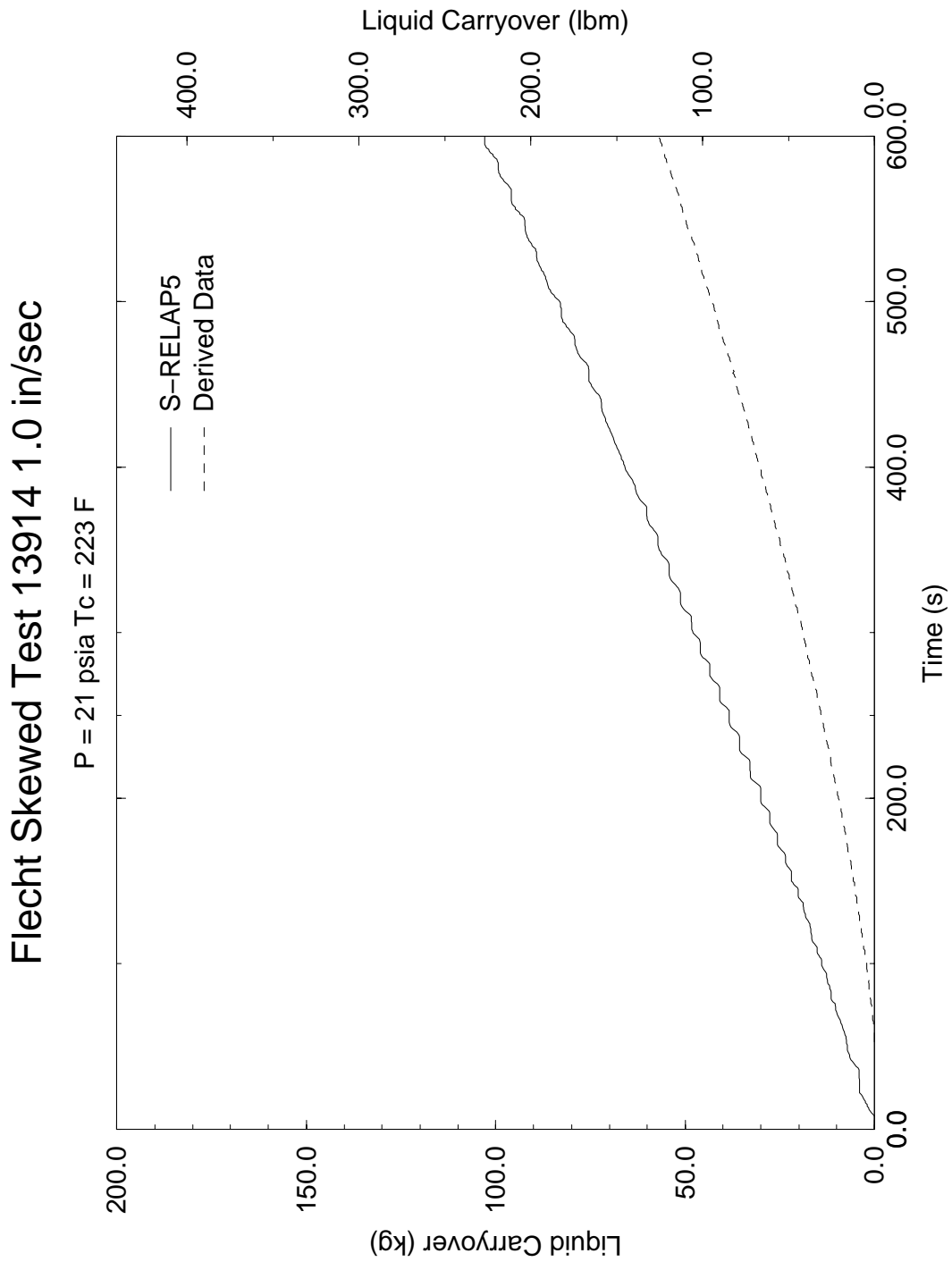


Figure 4.75 Total Liquid Carryover From Test Assembly, FLECHT Skewed Test 13914

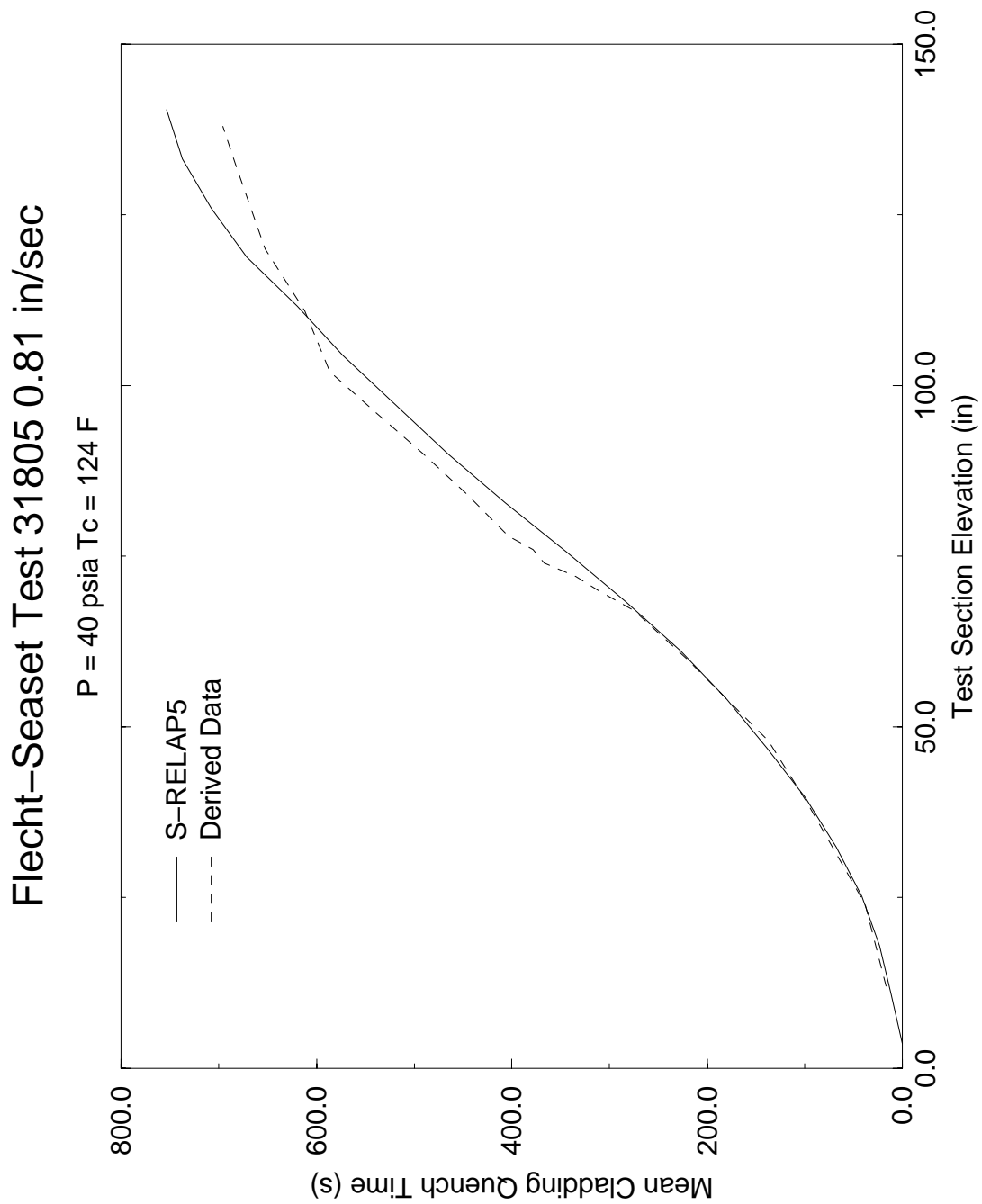


Figure 4.76 Average Rod Quench Time, FLECHT SEASET Test 31805

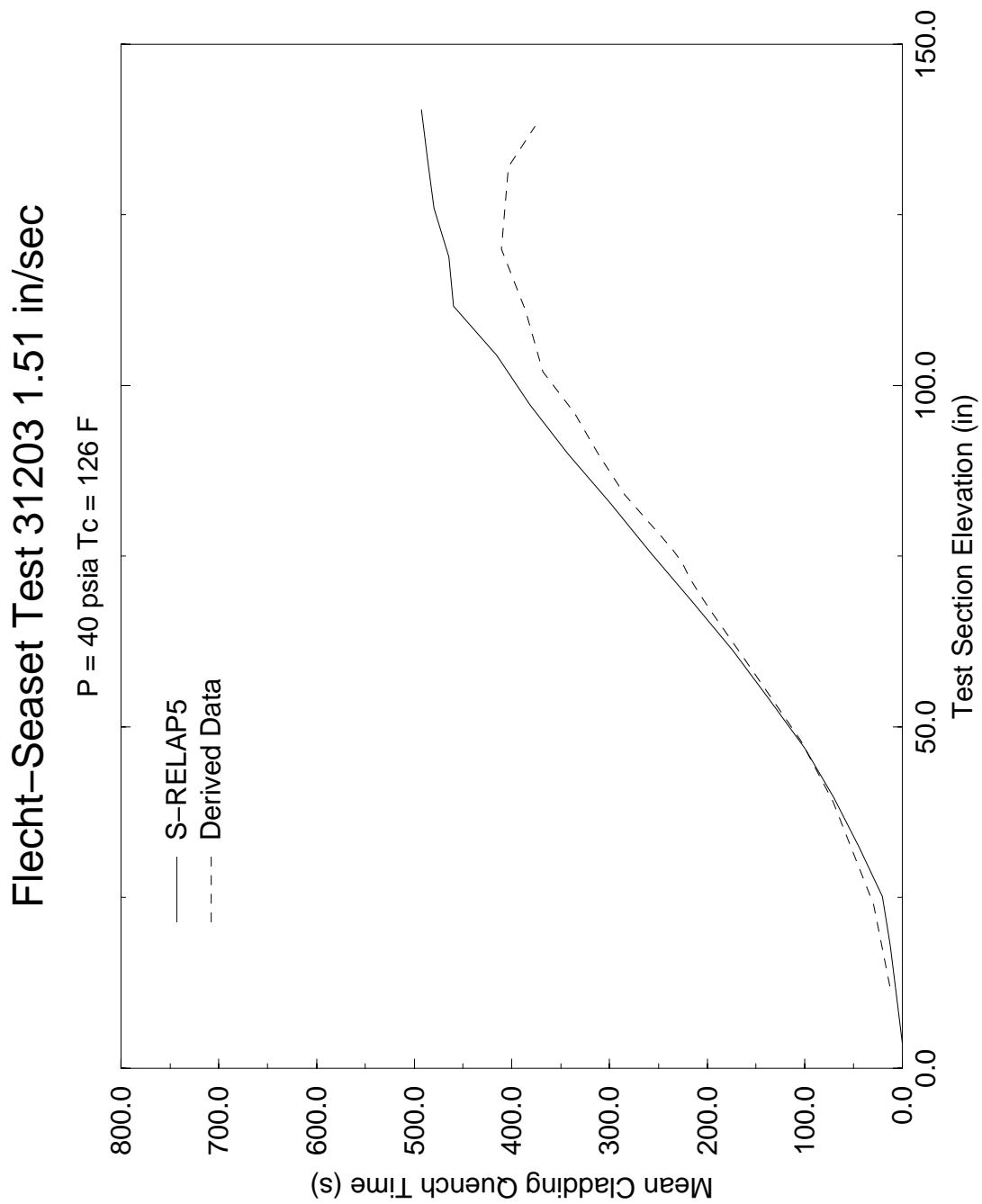


Figure 4.77 Average Rod Quench Time, FLECHT SEASET Test 31203

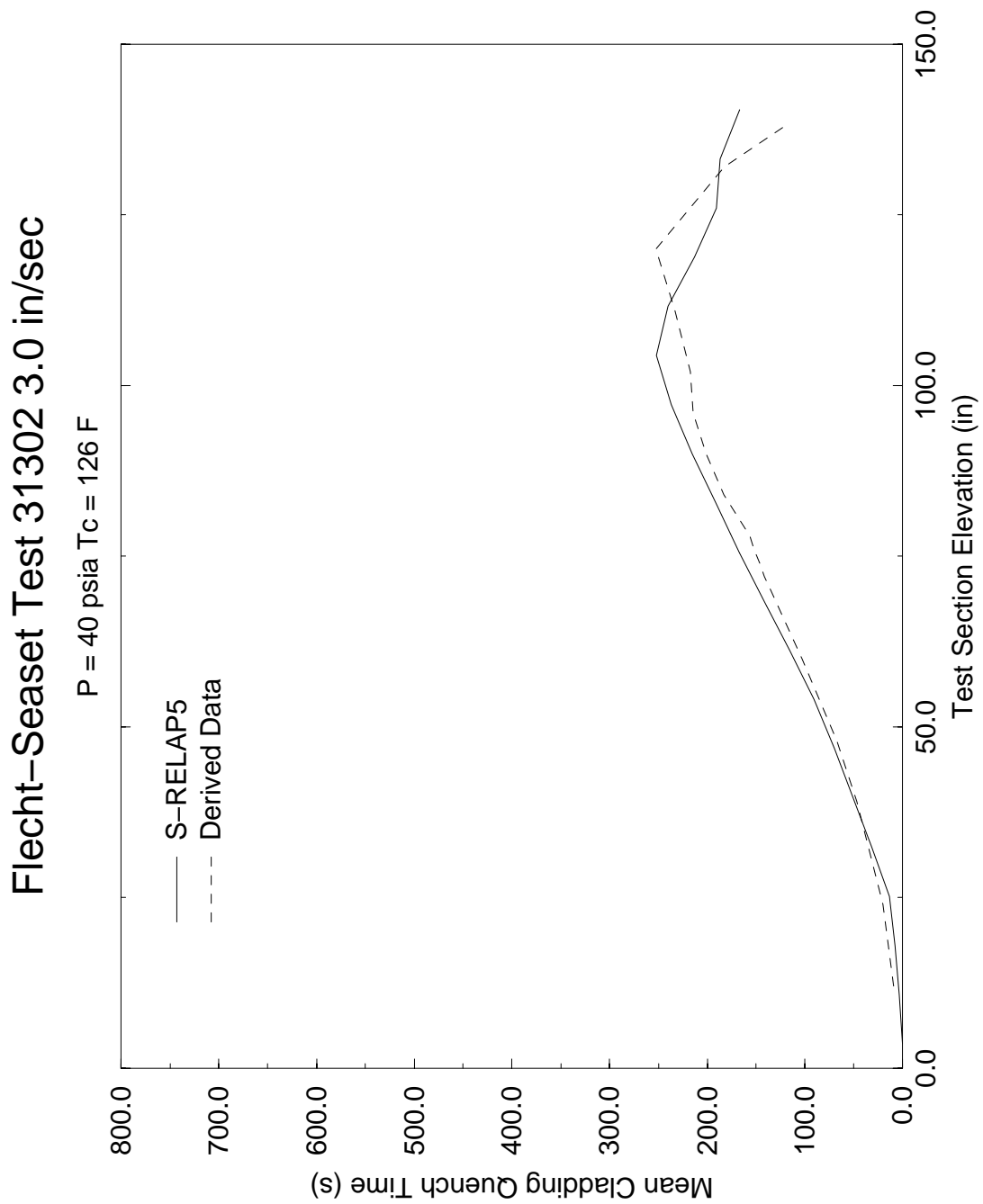


Figure 4.78 Average Rod Quench Time, FLECHT SEASET Test 31302

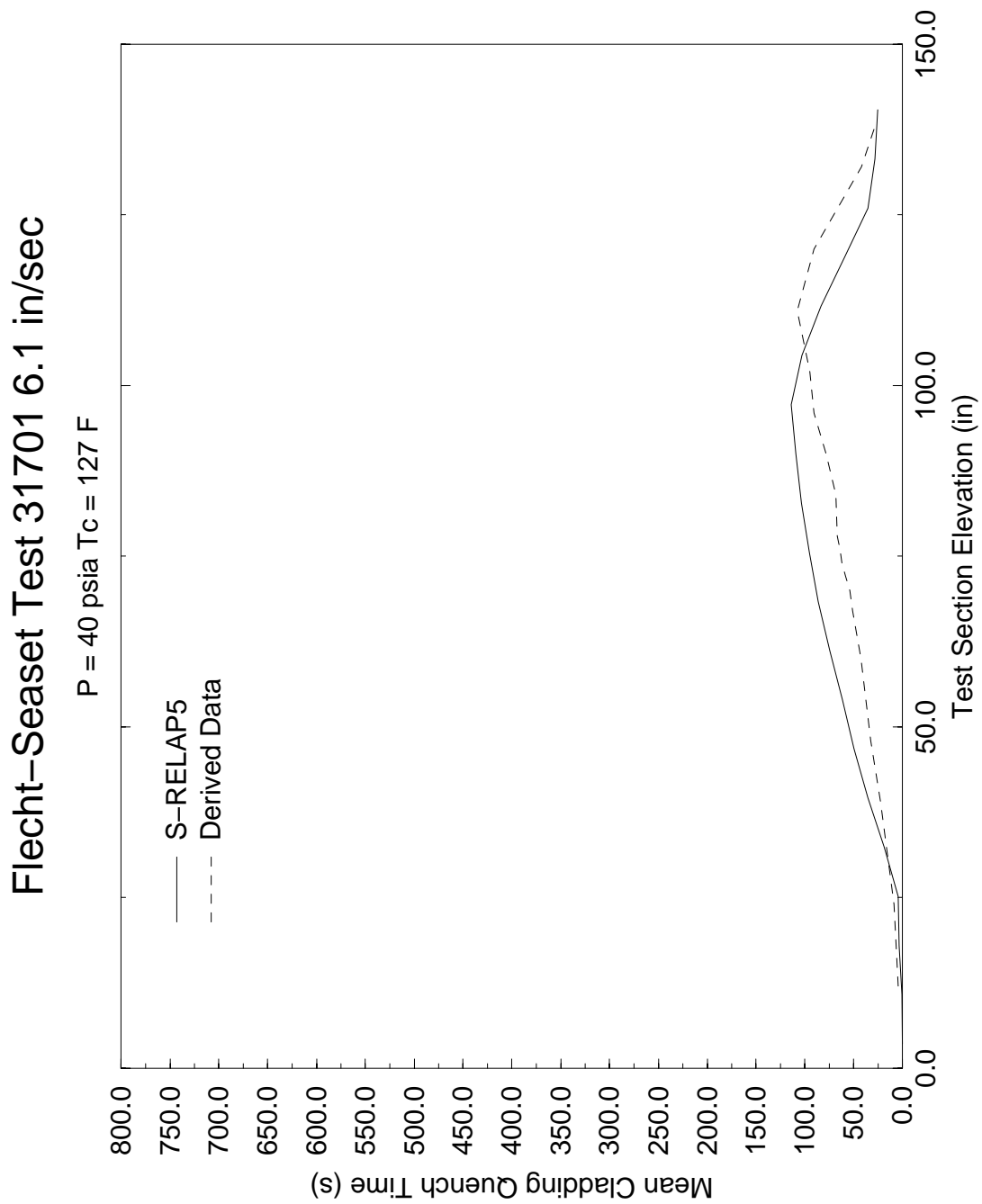


Figure 4.79 Average Rod Quench Time, FLECHT SEASET Test 31701

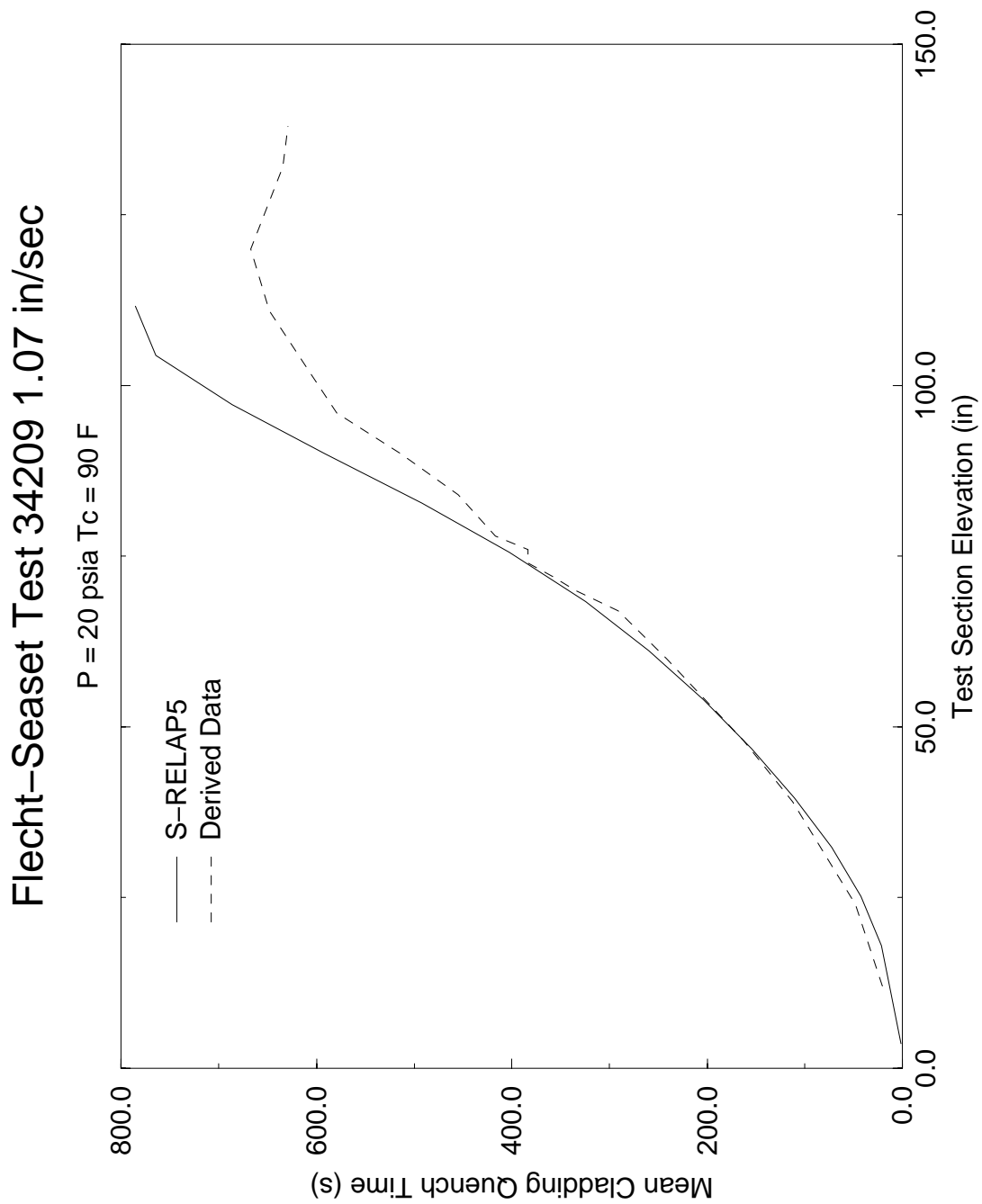


Figure 4.80 Average Rod Quench Time, FLECHT SEASET Test 34209

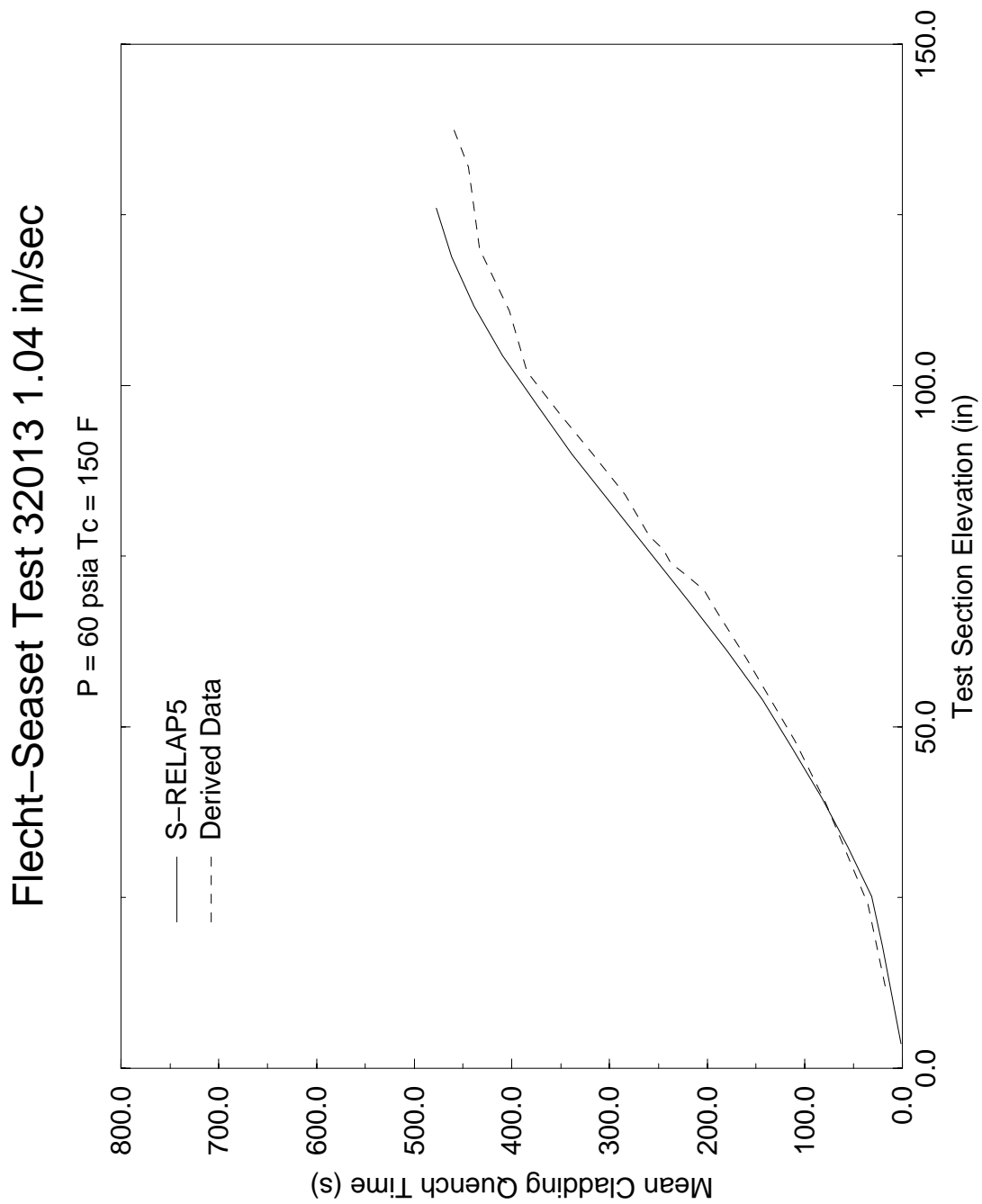


Figure 4.81 Average Rod Quench Time, FLECHT SEASET Test 32013

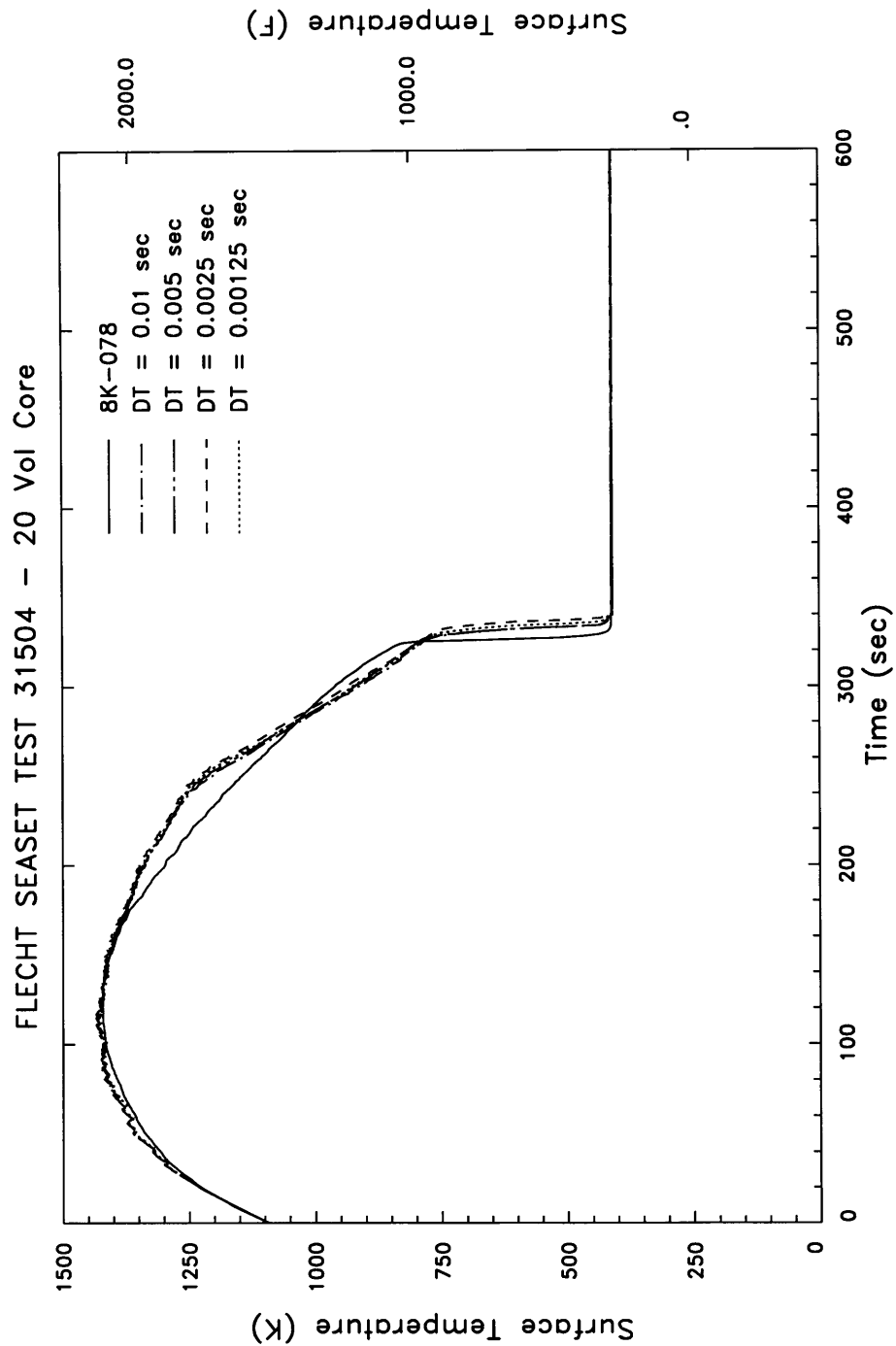


Figure 4.82 Calculated Rod Surface Temperatures at 79 in for the 20-Volume Test Section Cases With Various Time-Step Sizes, FLECHT SEASET Test 31504

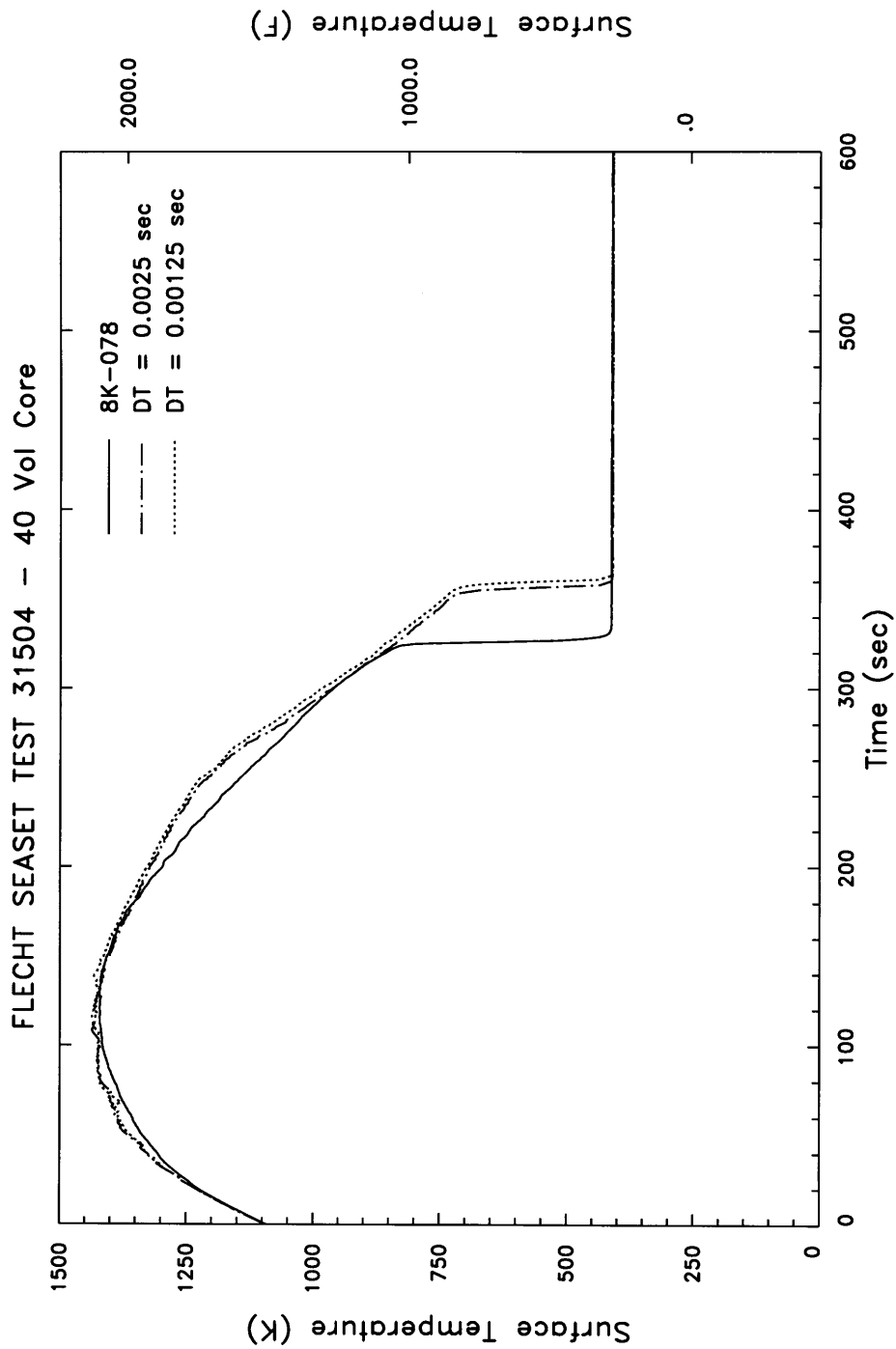


Figure 4.83 Calculated Rod Surface Temperatures at 79 in for the 40-Volume Test Section Cases With Various Time-Step Sizes, FLECHT SEASET Test 31504

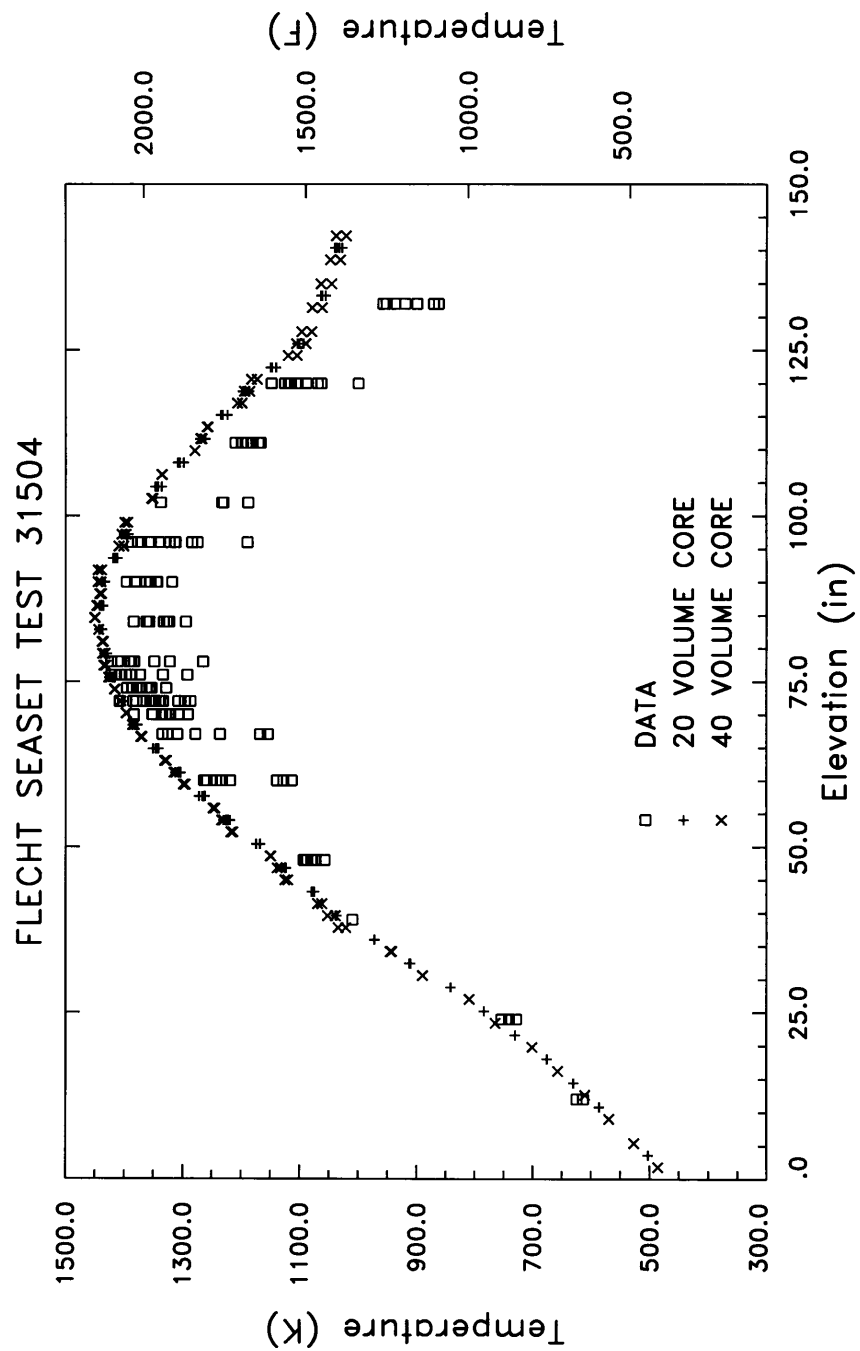


Figure 4.84 Maximum Cladding Temperatures vs. Axial Elevation, FLECHT SEASET Test 31504

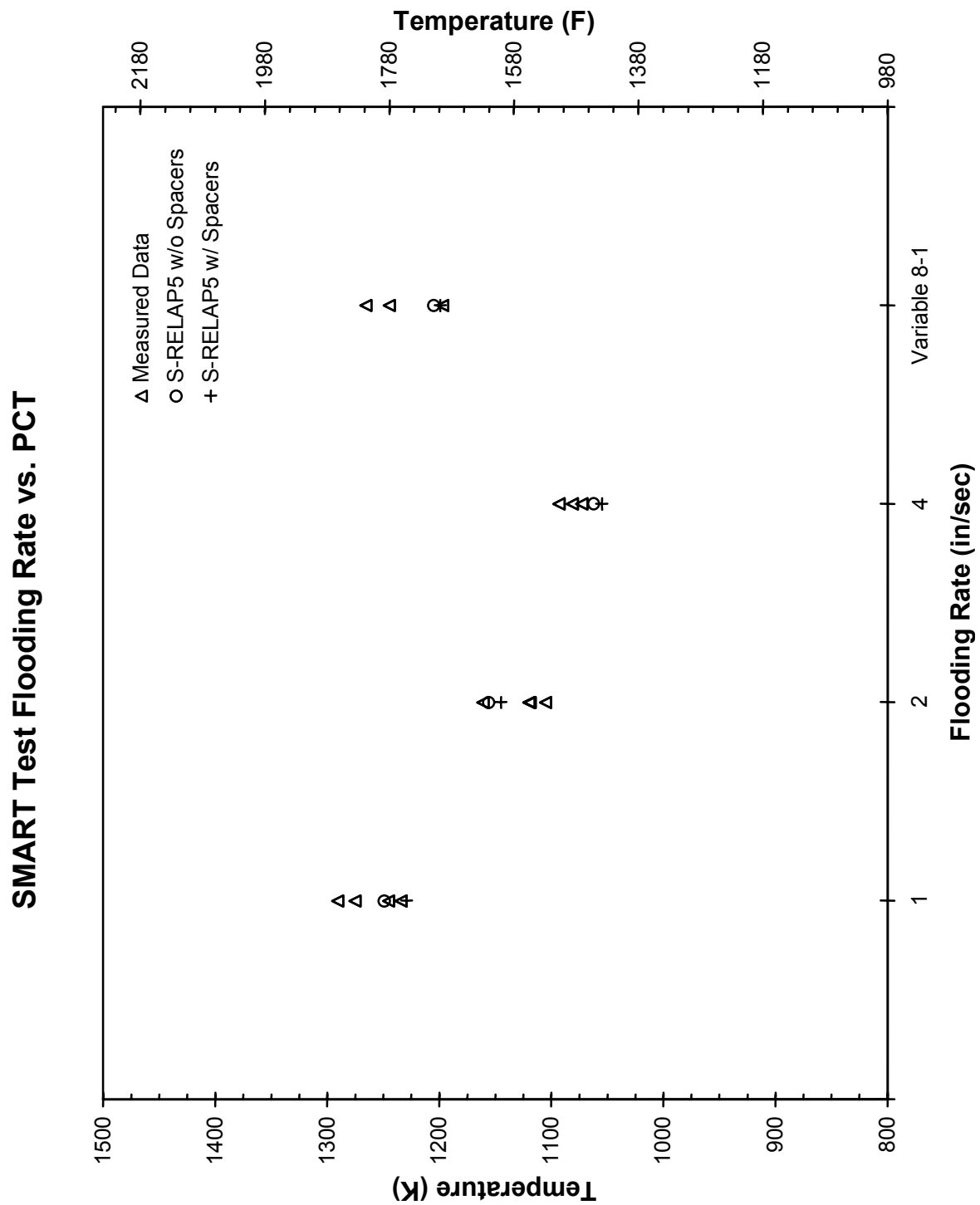
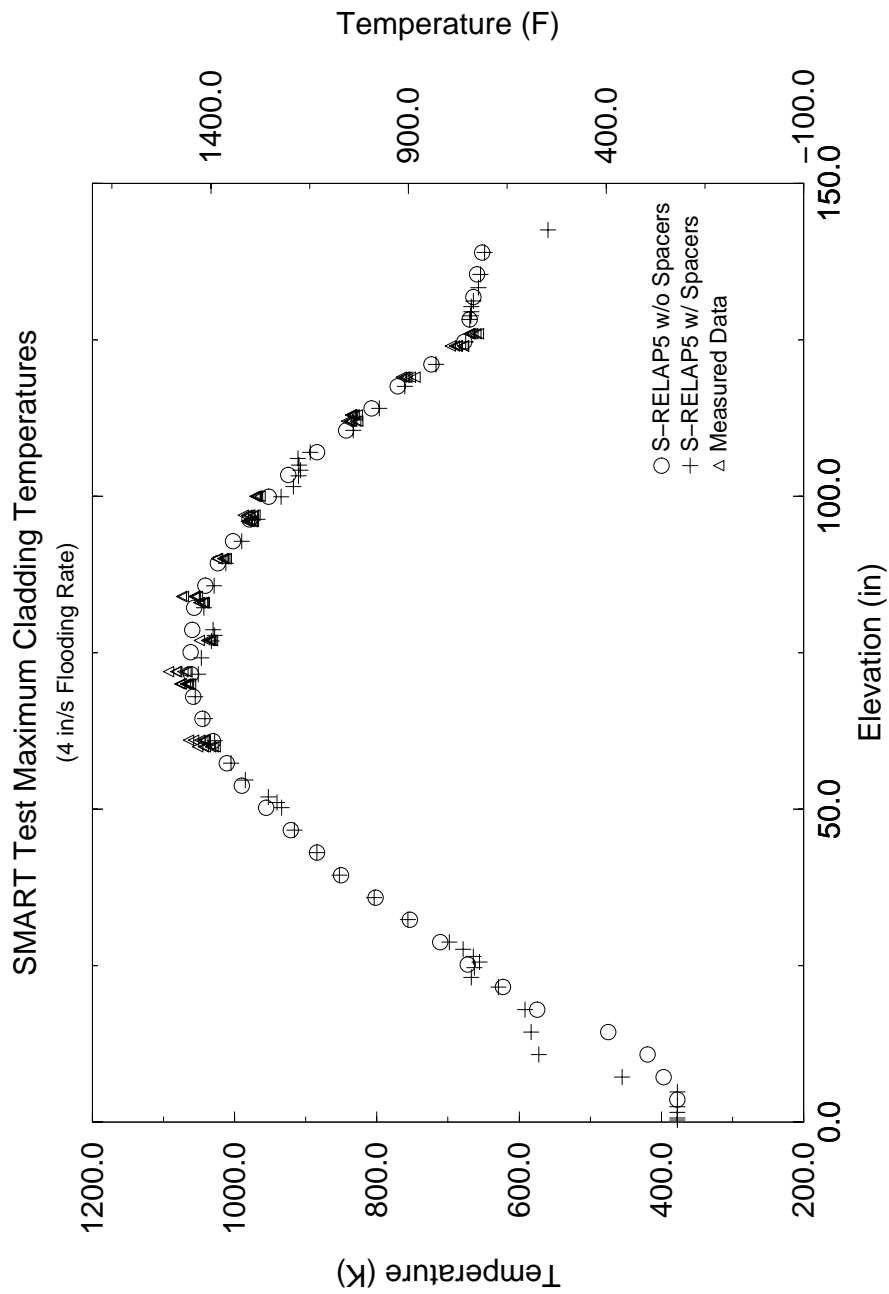


Figure 4.85 Comparison of Predicted PCT and Measured Data, PCTF SMART



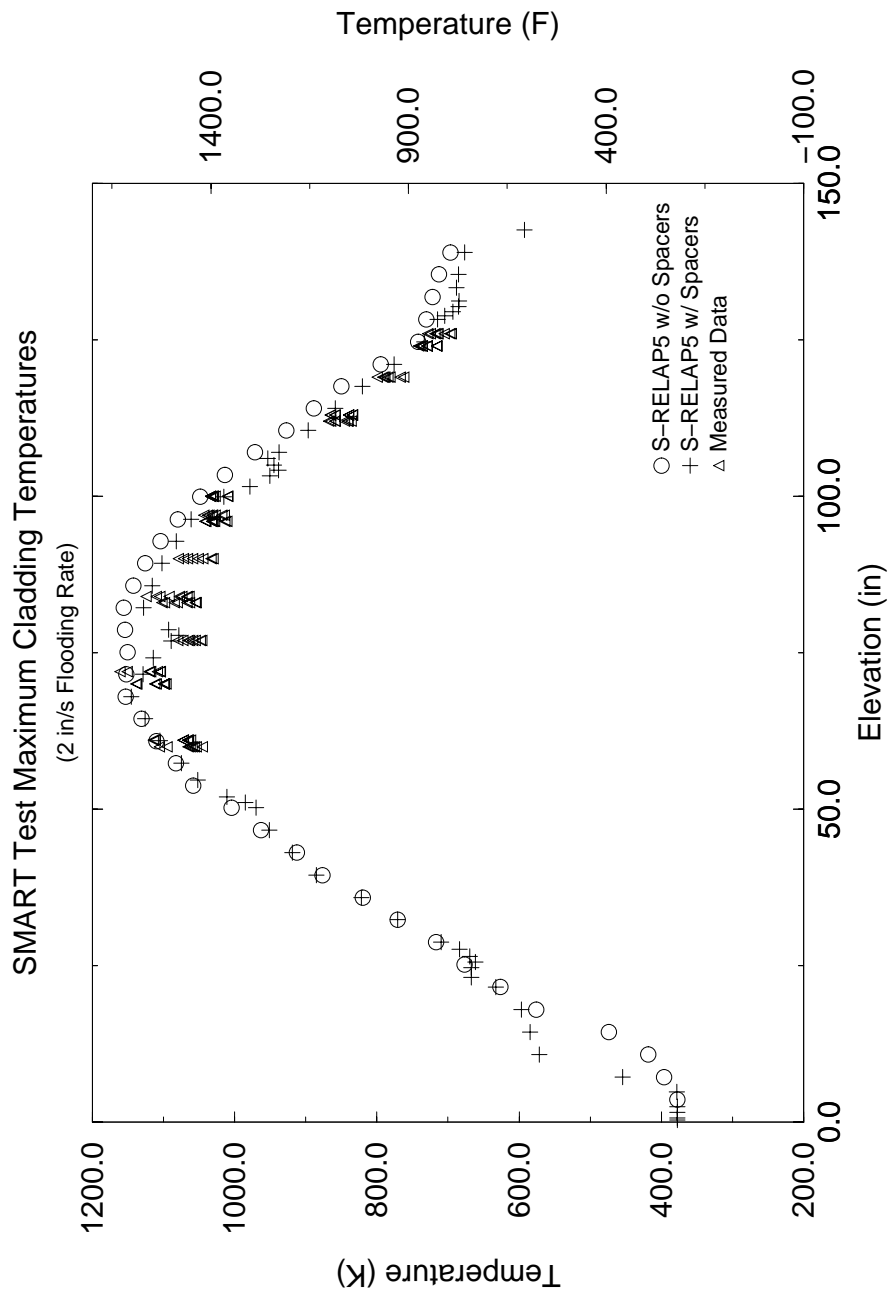


Figure 4.87 MCT vs. Elevation Comparison to Data for 2-in/s-Flooding-Rate Test, PDTF SMART

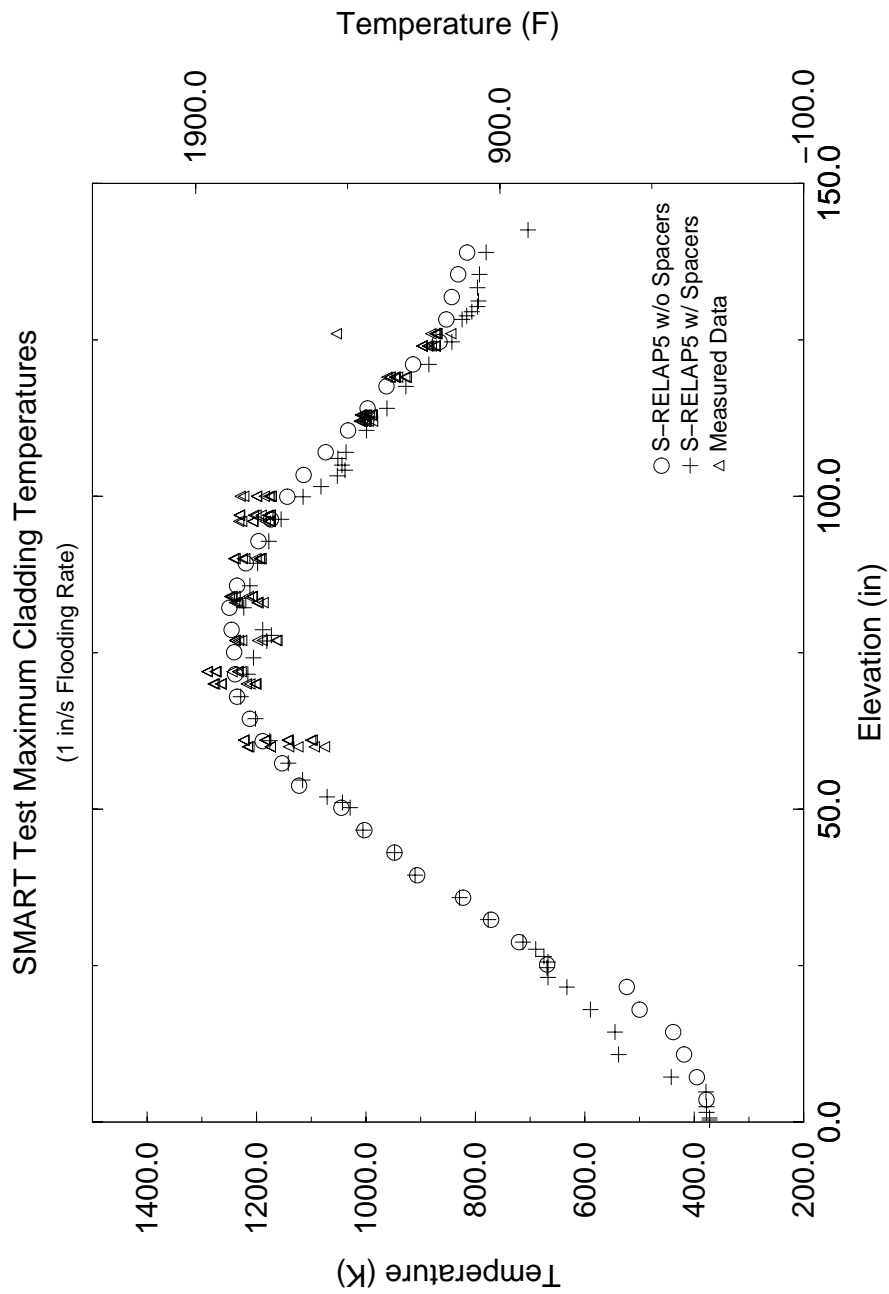


Figure 4.88 MCT vs. Elevation Comparison to Data for 1-in/s-Flooding-Rate Test, PDTF SMART

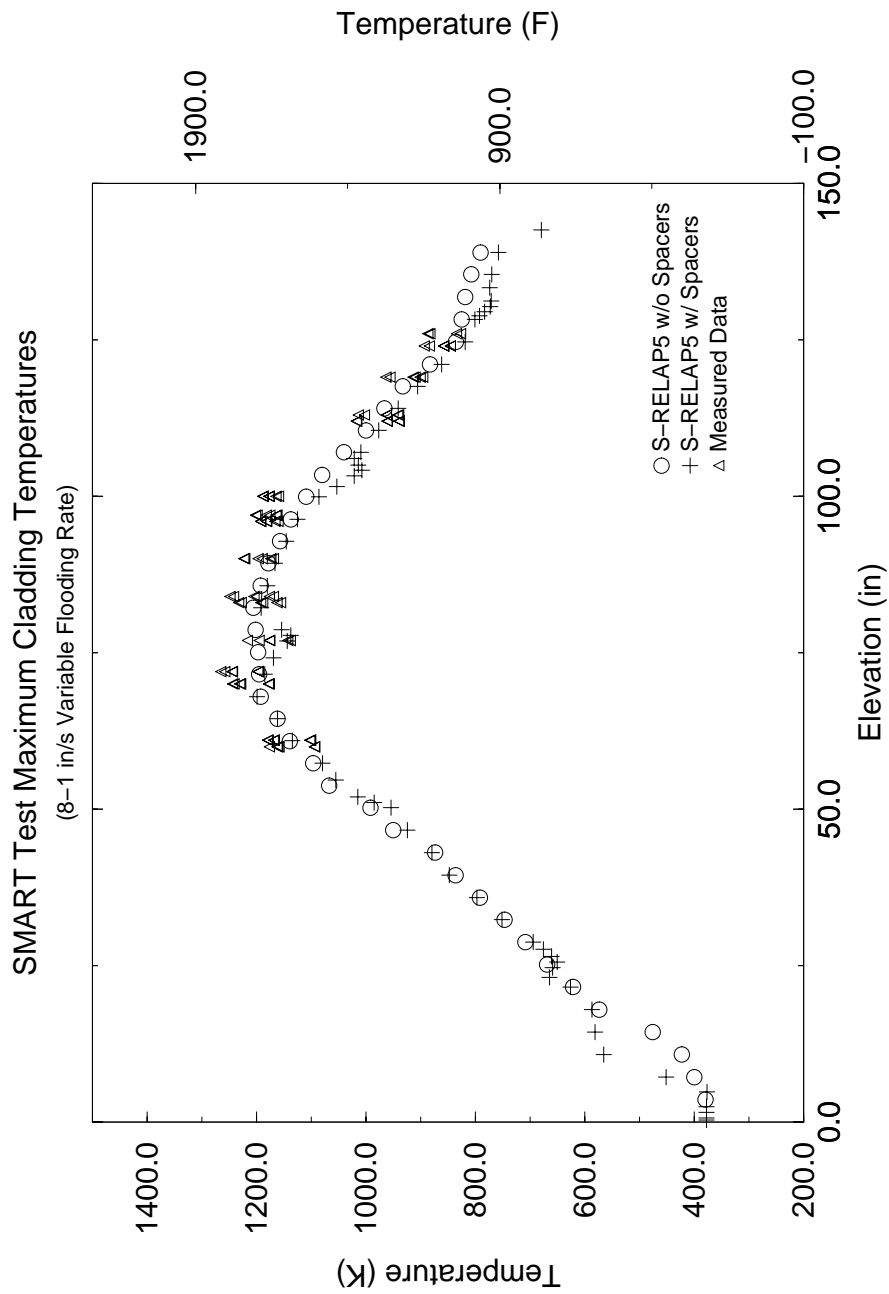


Figure 4.89 MCT vs. Elevation Comparison to Data for Variable-Flooding-Rate Test, PDTF SMART

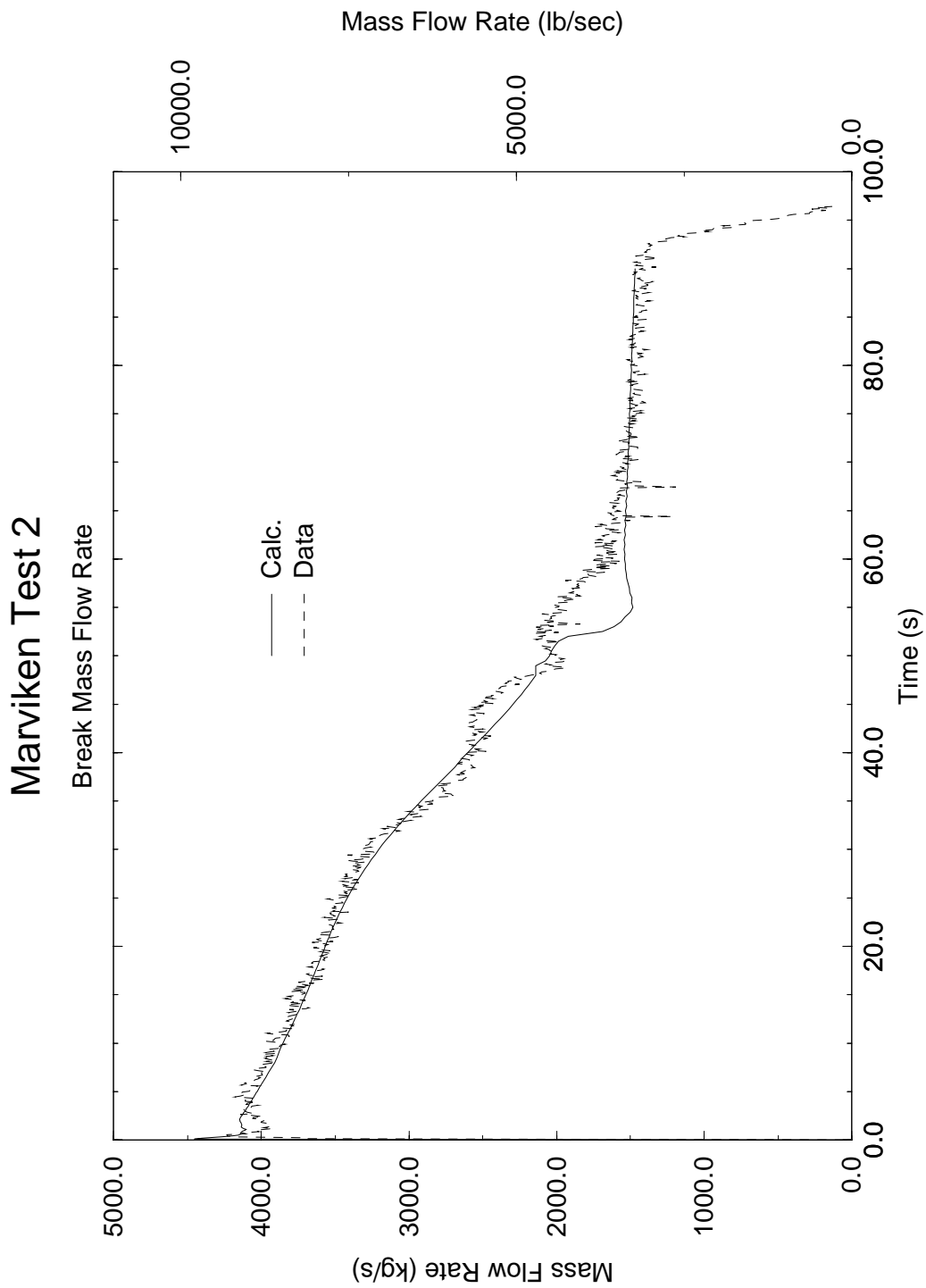


Figure 4.90 Comparison of Break Mass Flow Rates, Marviken Test 2

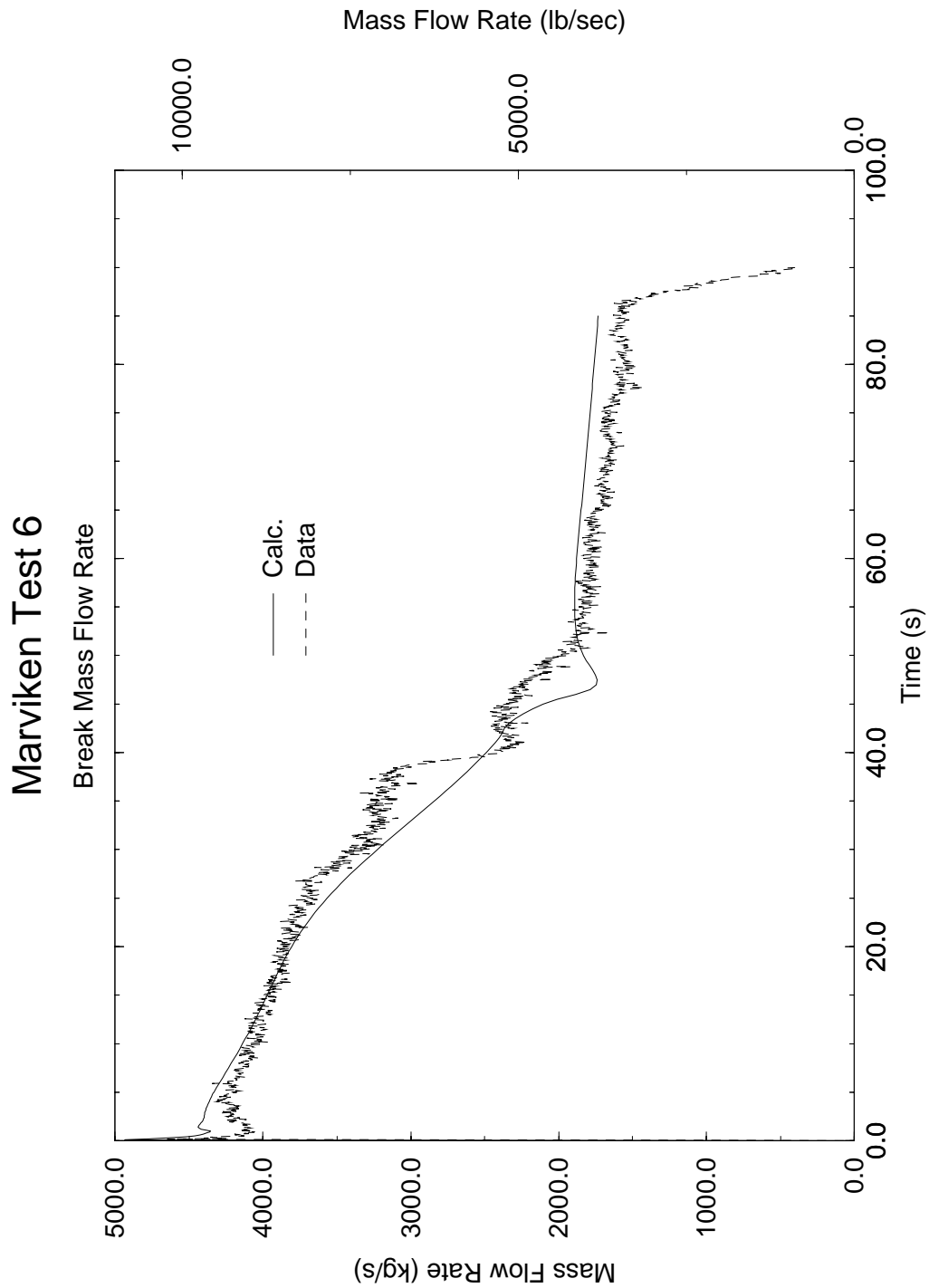


Figure 4.91 Comparison of Break Mass Flow Rates, Marviken Test 6

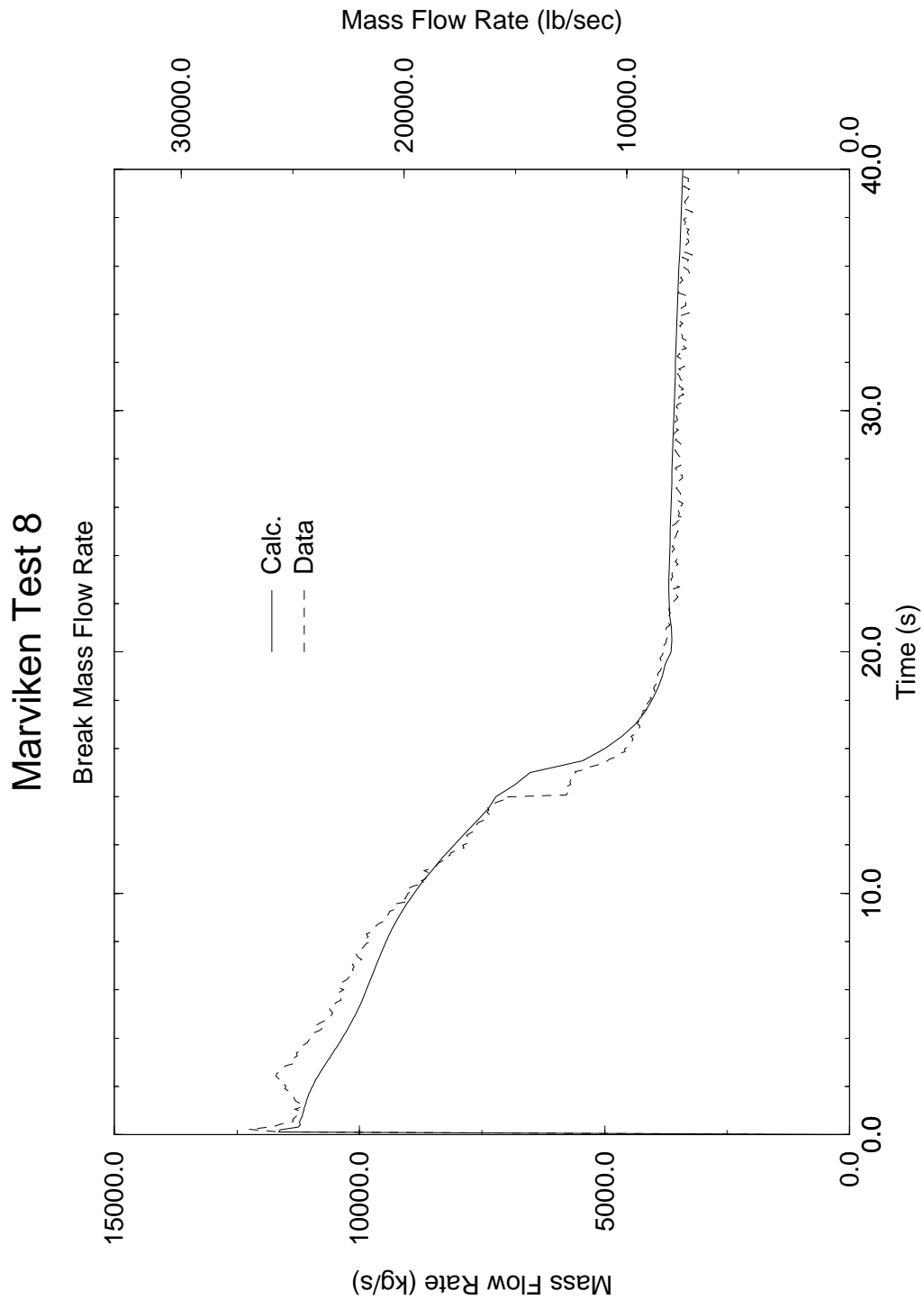


Figure 4.92 Comparison of Break Mass Flow Rates, Marviken Test 8

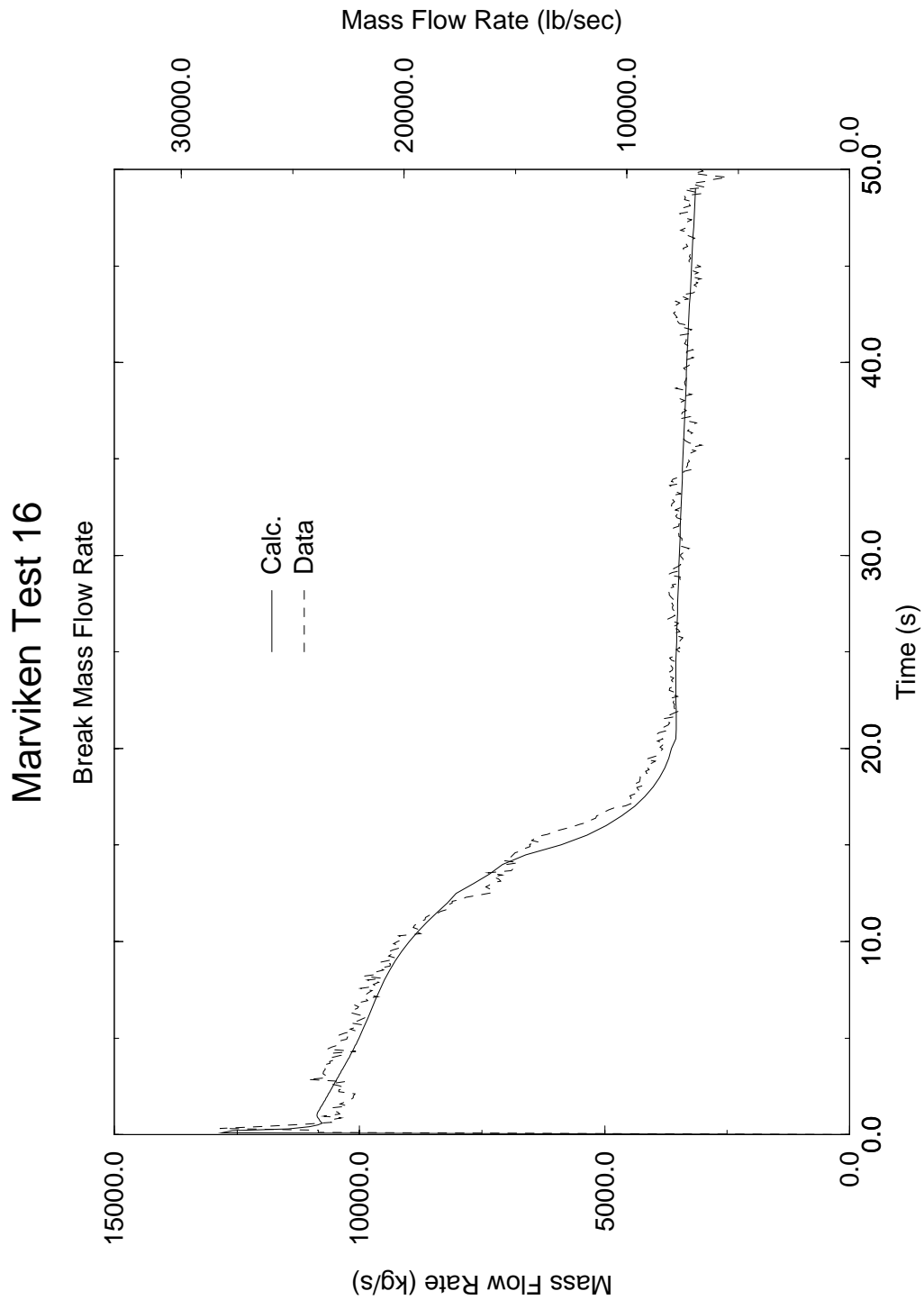


Figure 4.93 Comparison of Break Mass Flow Rates, Marviken Test 16

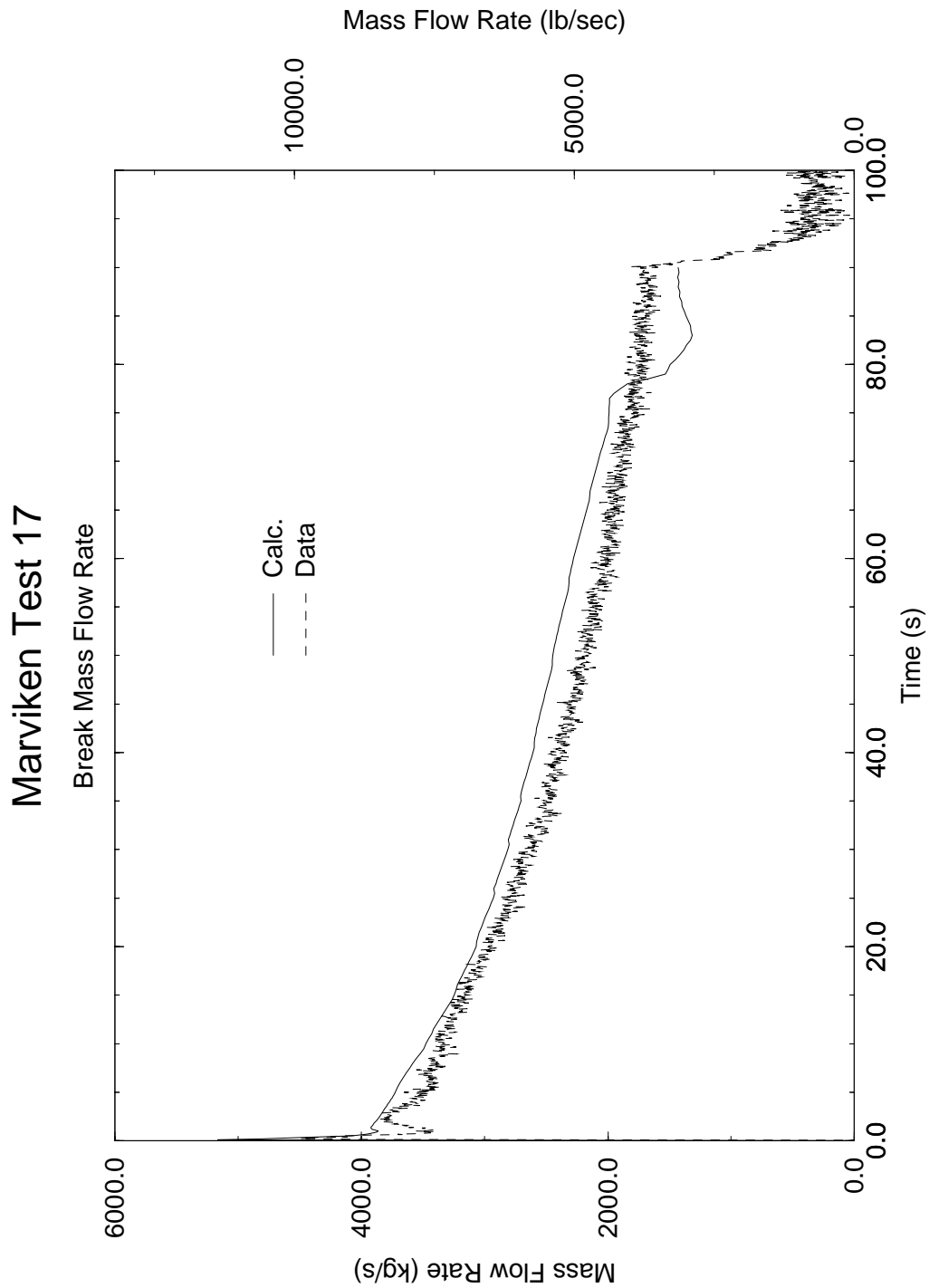


Figure 4.94 Comparison of Break Mass Flow Rates, Marviken Test 17

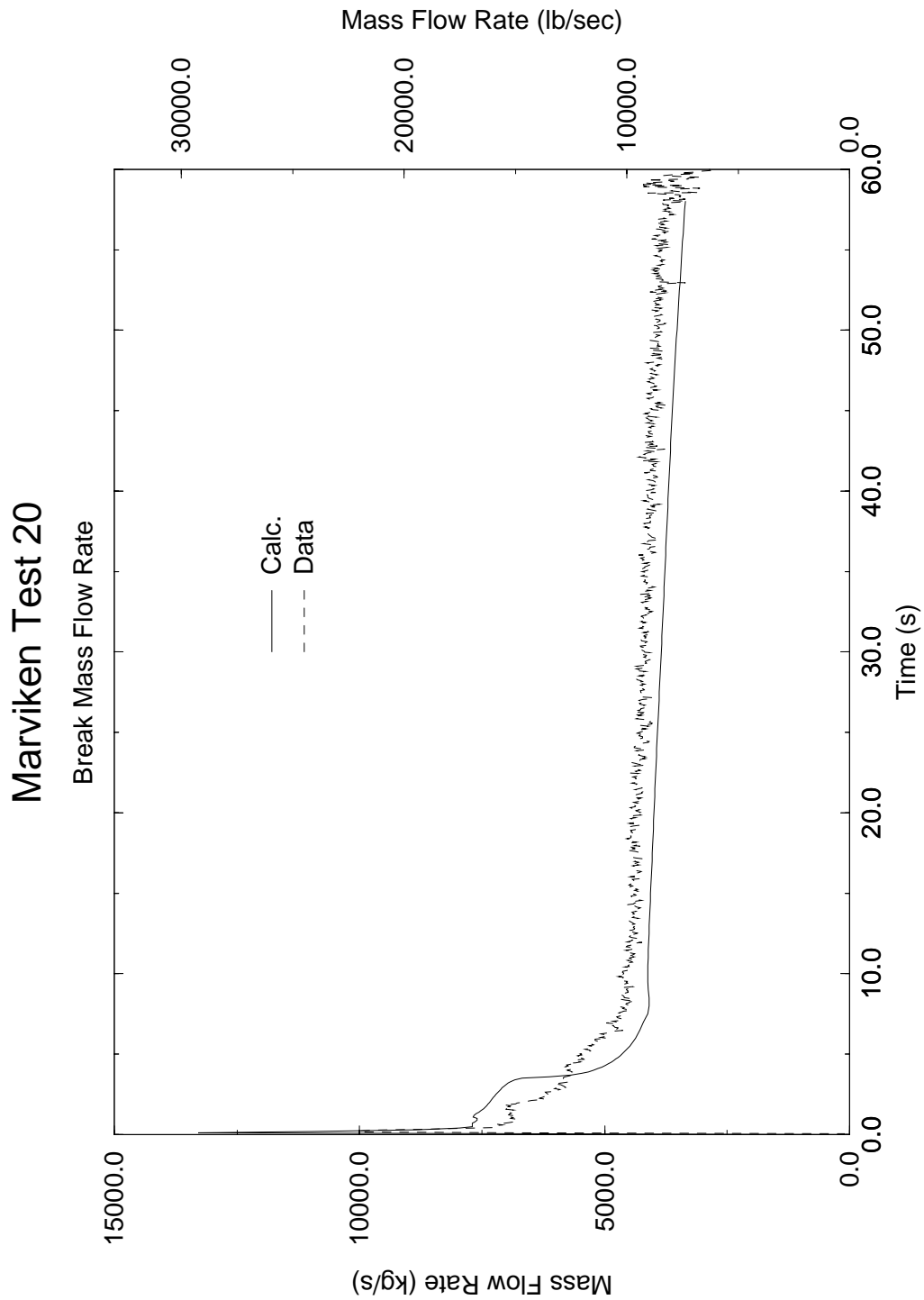


Figure 4.95 Comparison of Break Mass Flow Rates, Marviken Test 20

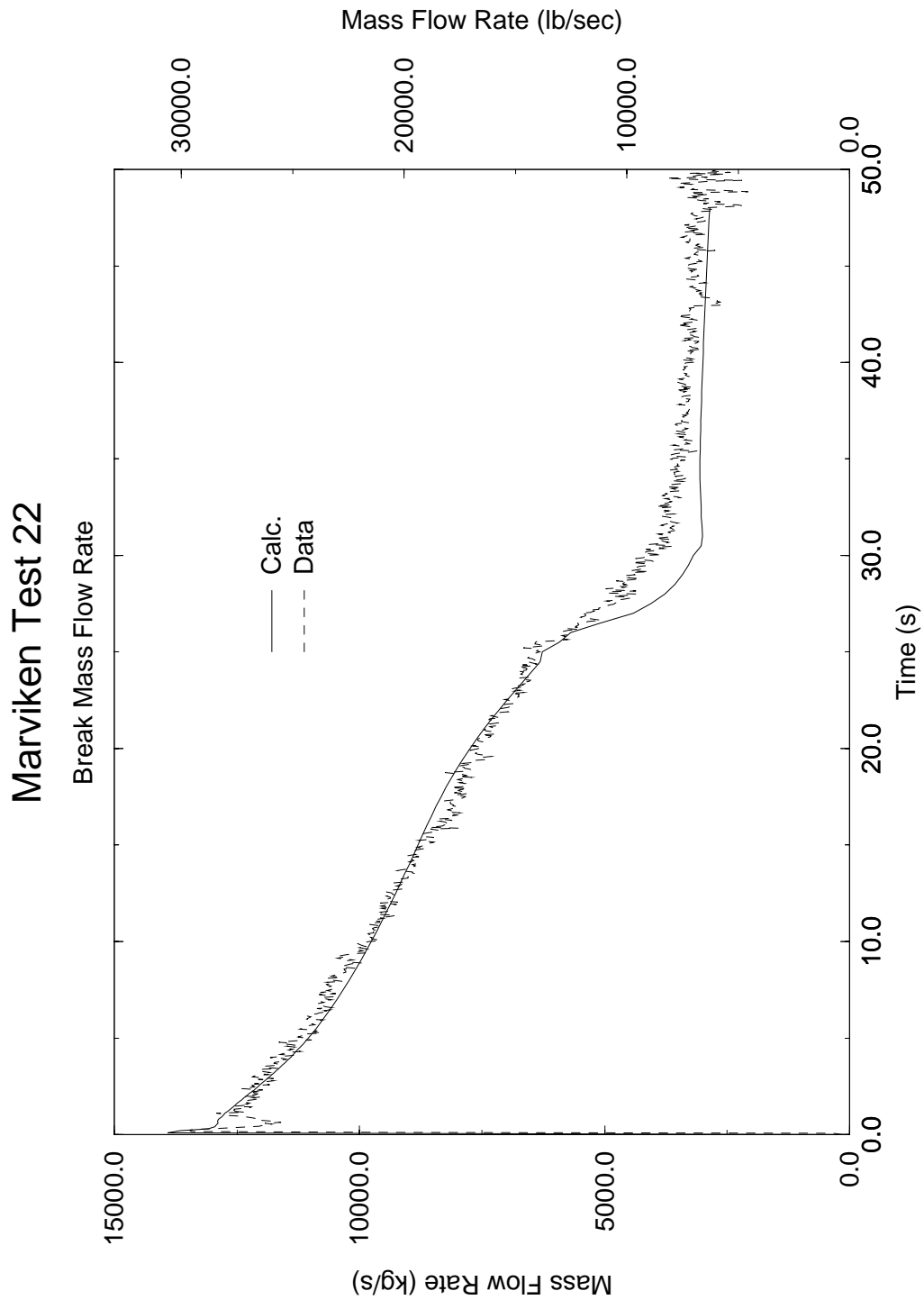


Figure 4.96 Comparison of Break Mass Flow Rates, Marviken Test 22

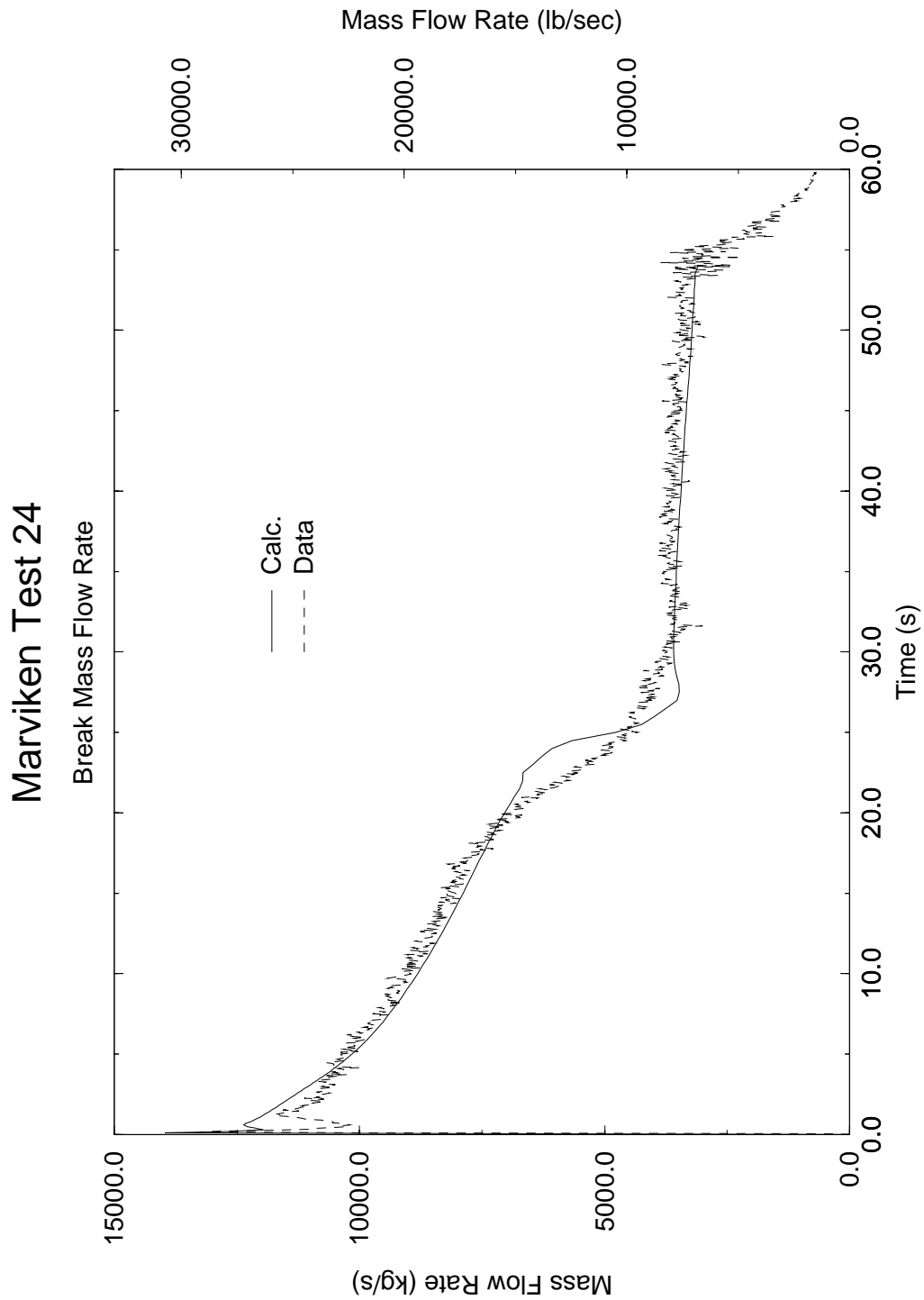


Figure 4.97 Comparison of Break Mass Flow Rates, Marviken Test 24

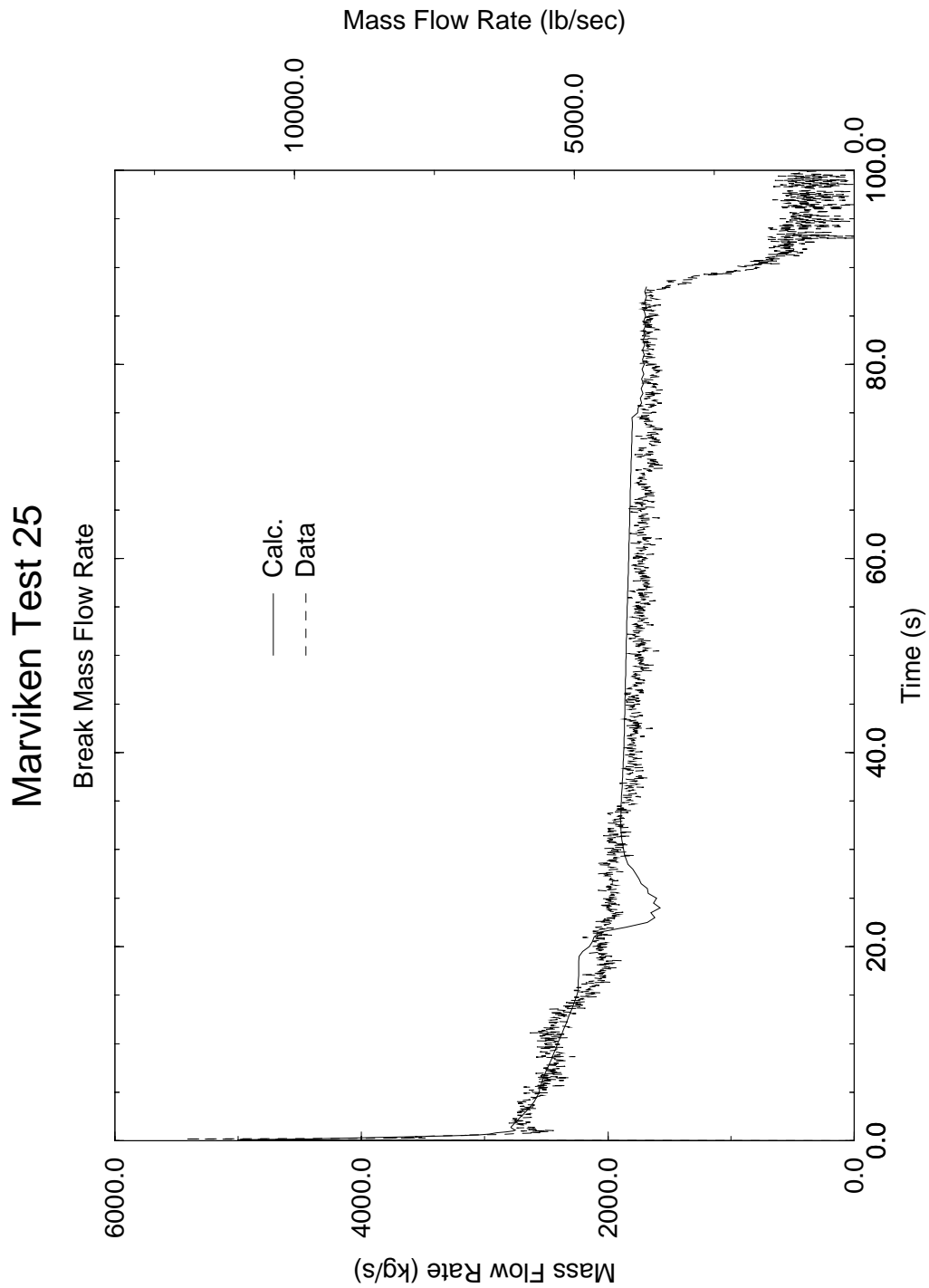
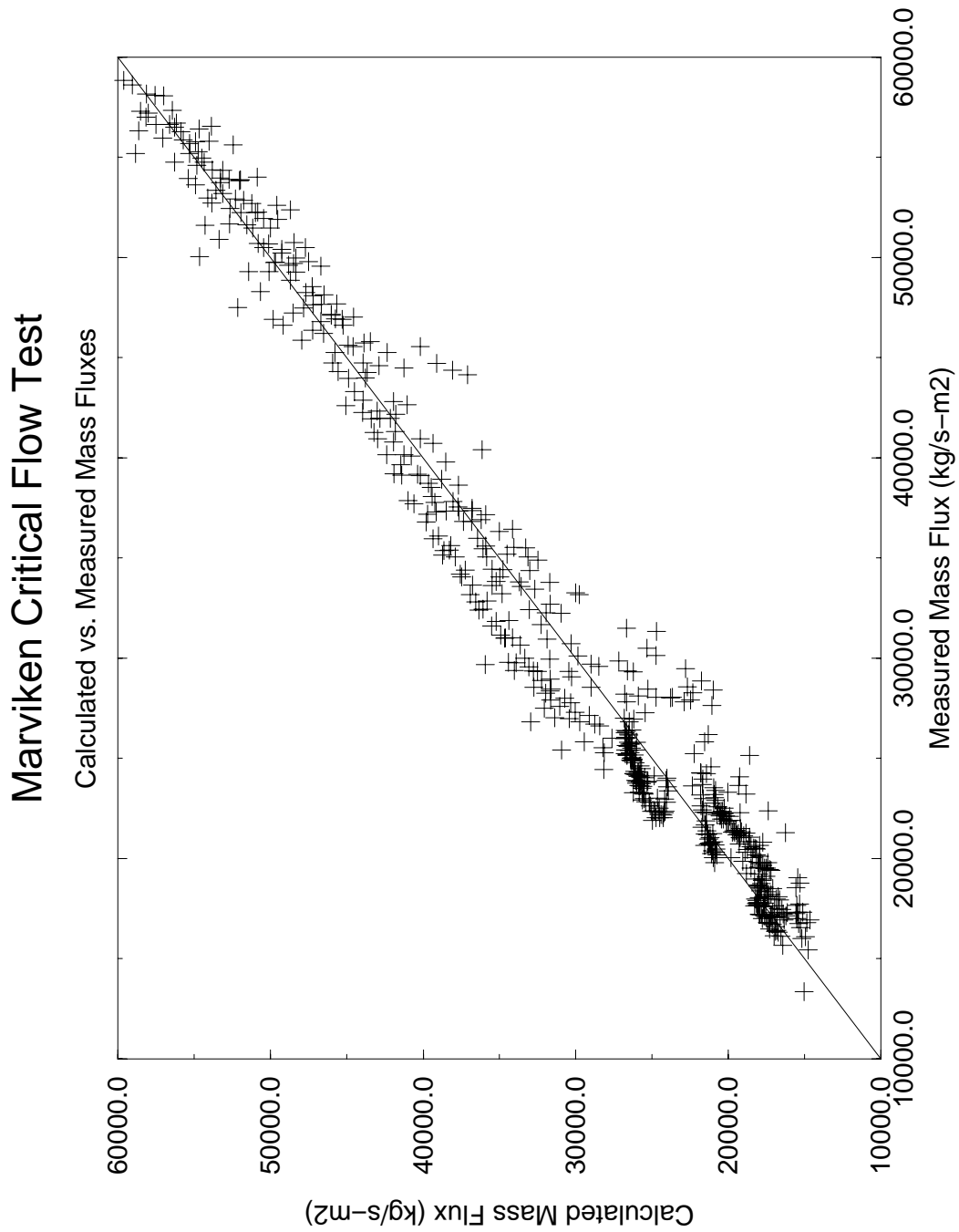


Figure 4.98 Comparison of Break Mass Flow Rates, Marviken Test 25



**Figure 4.99 Comparison of Calculated and Measured Mass Fluxes
(All Nine Marviken Tests)**

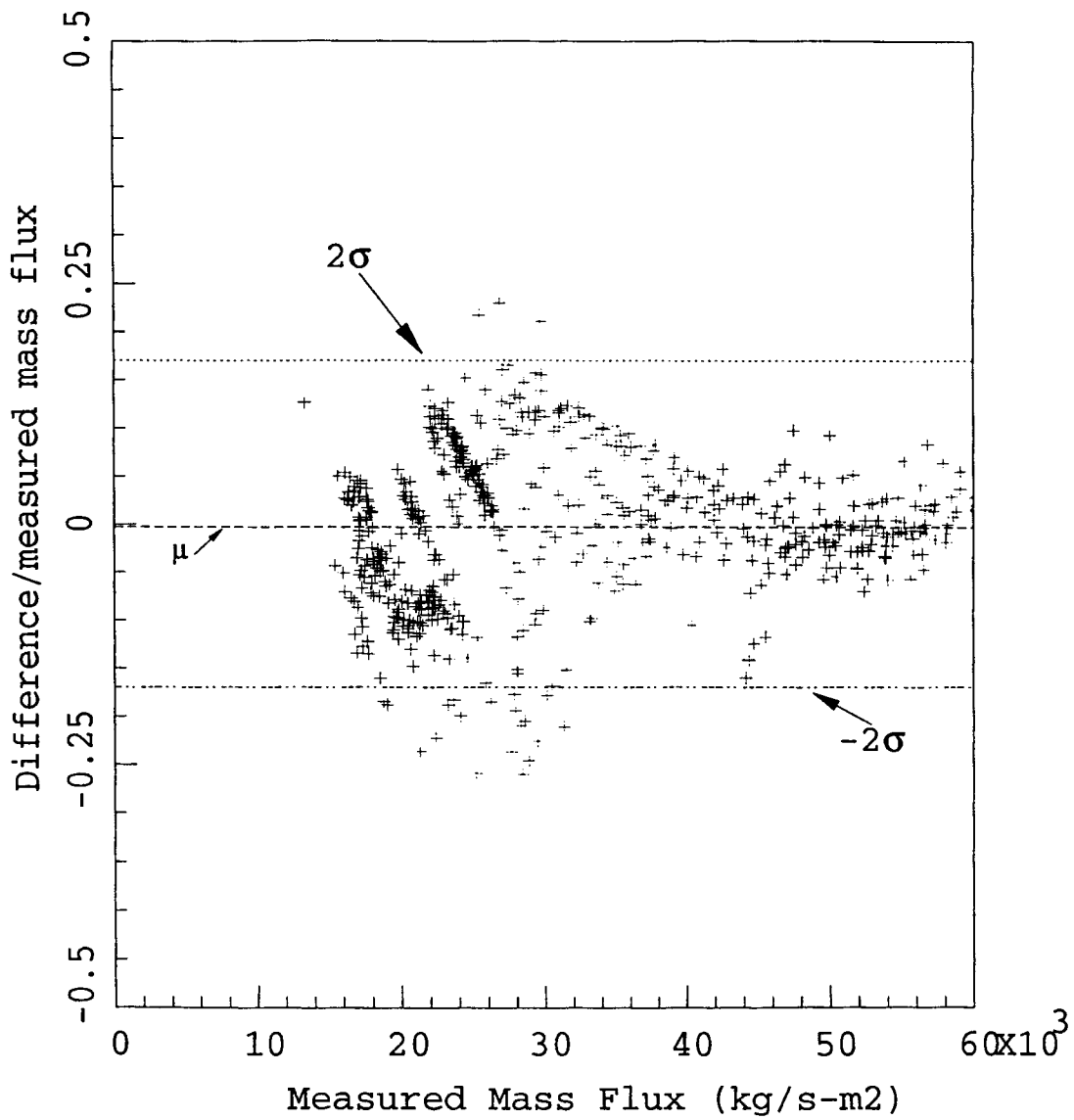


Figure 4.100 Break Flow Uncertainty, Marviken Tests

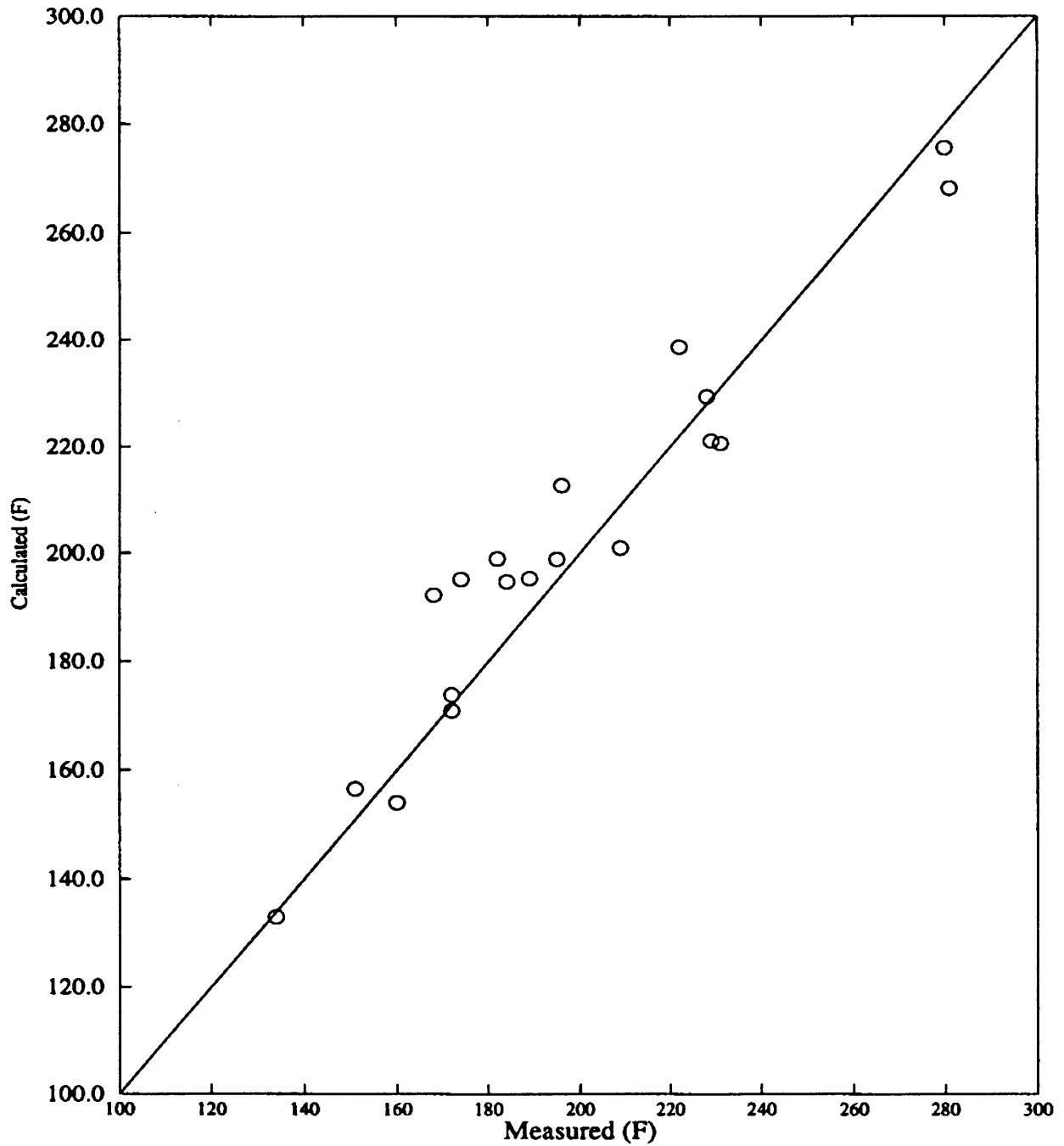
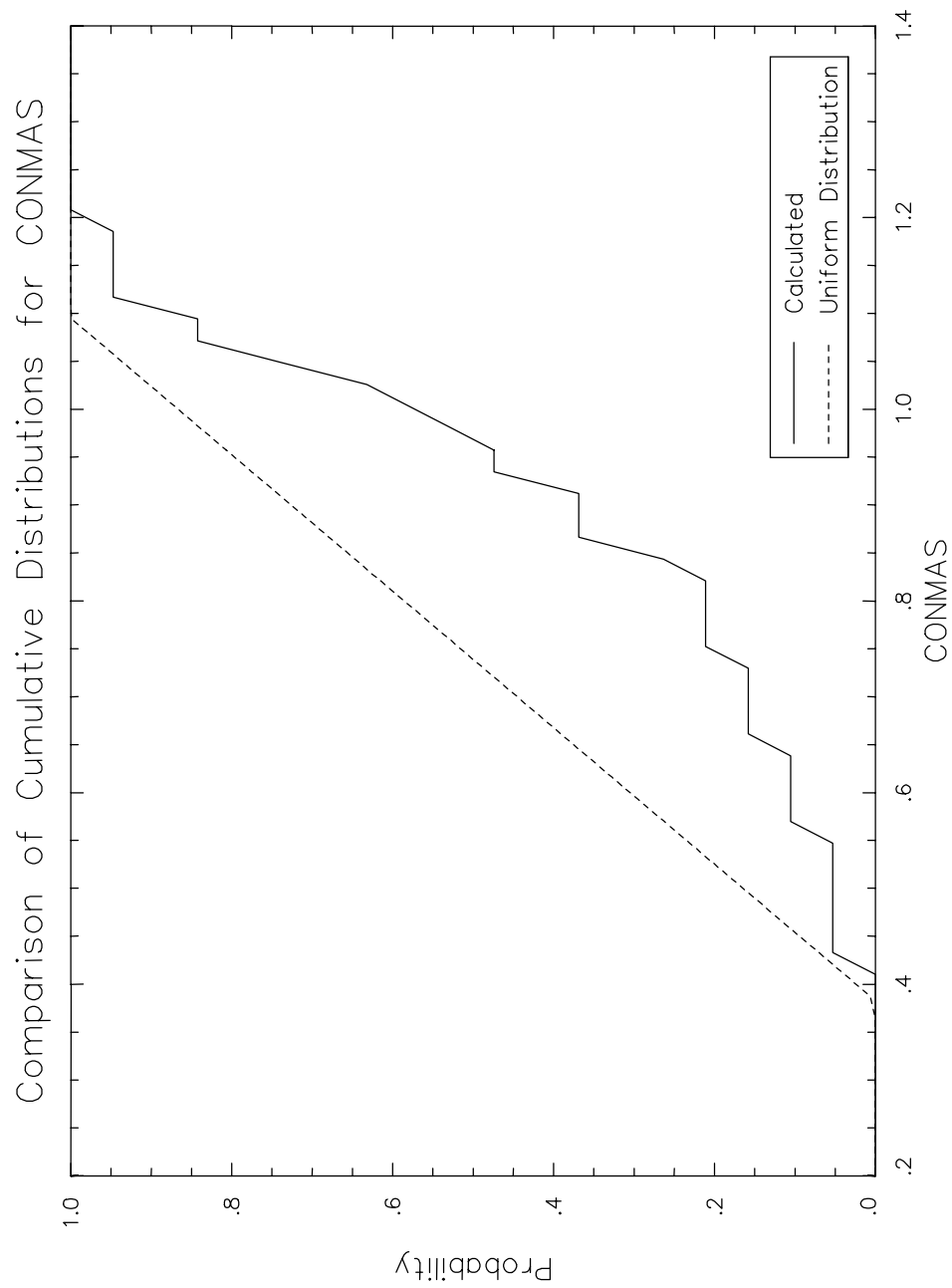


Figure 4.101 Comparison of Calculated and Measured Effluent Temperature for the Plant-Specific Model, Westinghouse/EPRI



**Figure 4.102 Cumulative Distribution Plots for CONMAS,
Westinghouse/EPRI**

PLOT FILE NAME: ow_17x17_ccfl.eps, JOB ID: plot_job.o2900, DATE: Mon May 21 09:21:00 PDT 2001

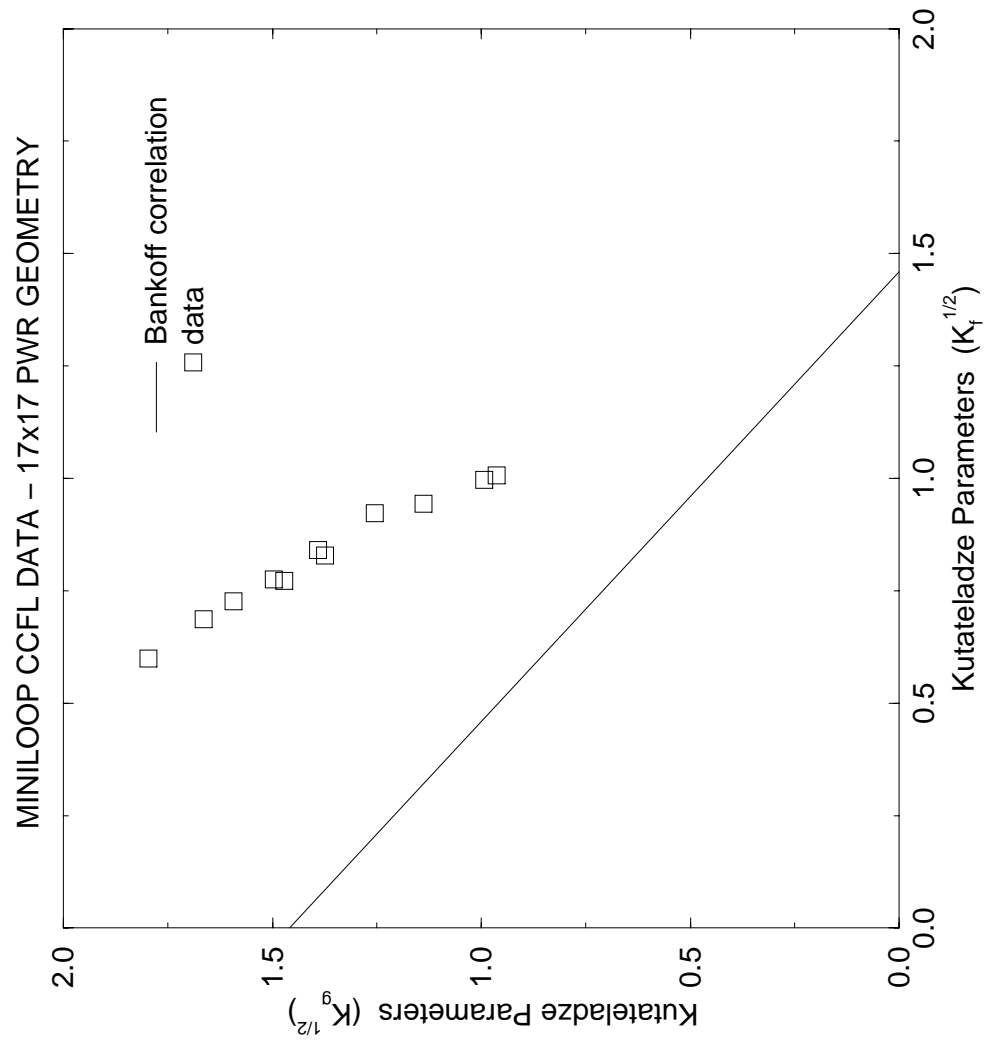


Figure 4.103 Comparison Between Mini-Loop CCFL Data of a Westinghouse 17 x 17 UTP and Bankoff

PLOT FILE NAME: 0w_15x15_ccfl.eps, JOB ID: plot_job.o2900, DATE: Mon May 21 09:21:00 PDT 2001

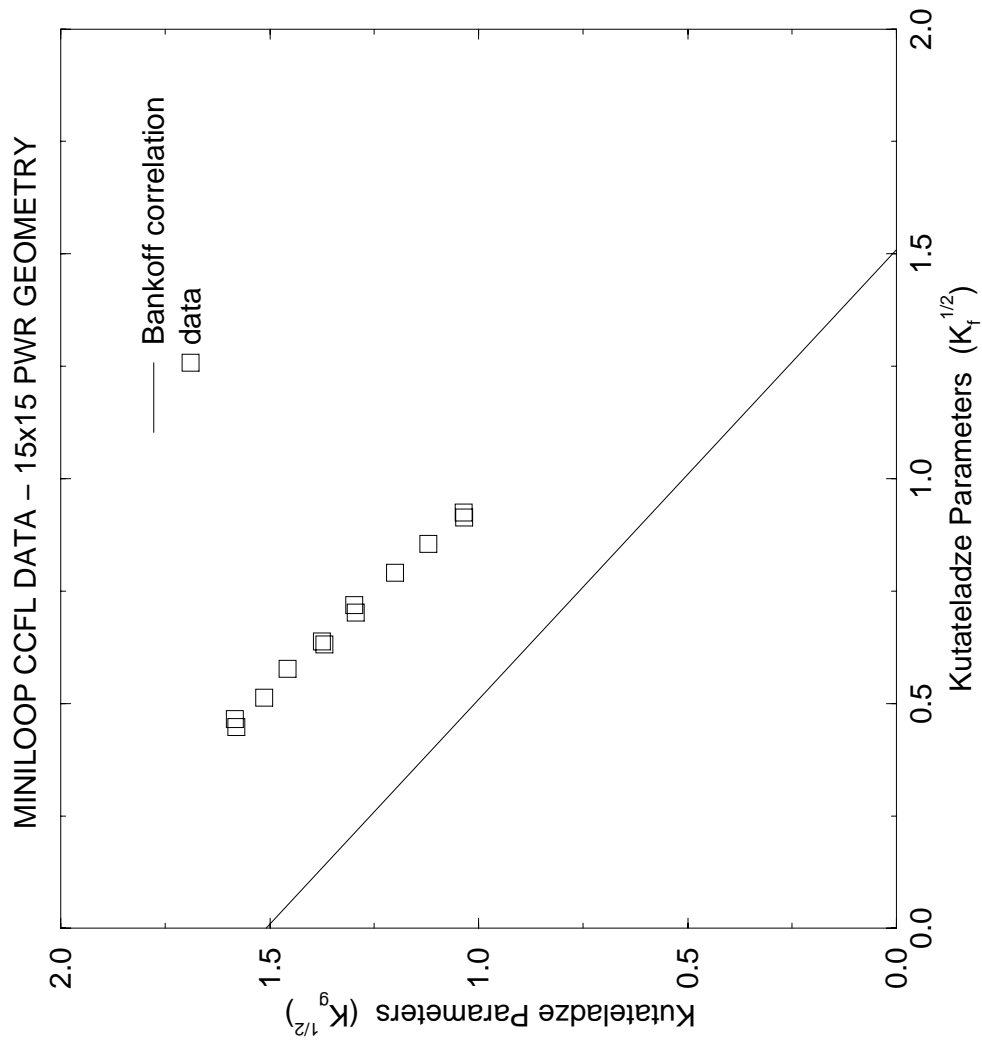


Figure 4.104 Comparison Between Mini-Loop CCFL Data of a Westinghouse 15 x 15 UTP and Bankoff

PLOT FILE NAME: oce_ccfl.eps, JOB ID: plot_job.o2900, DATE: Mon May 21 09:21:00 PDT 2001

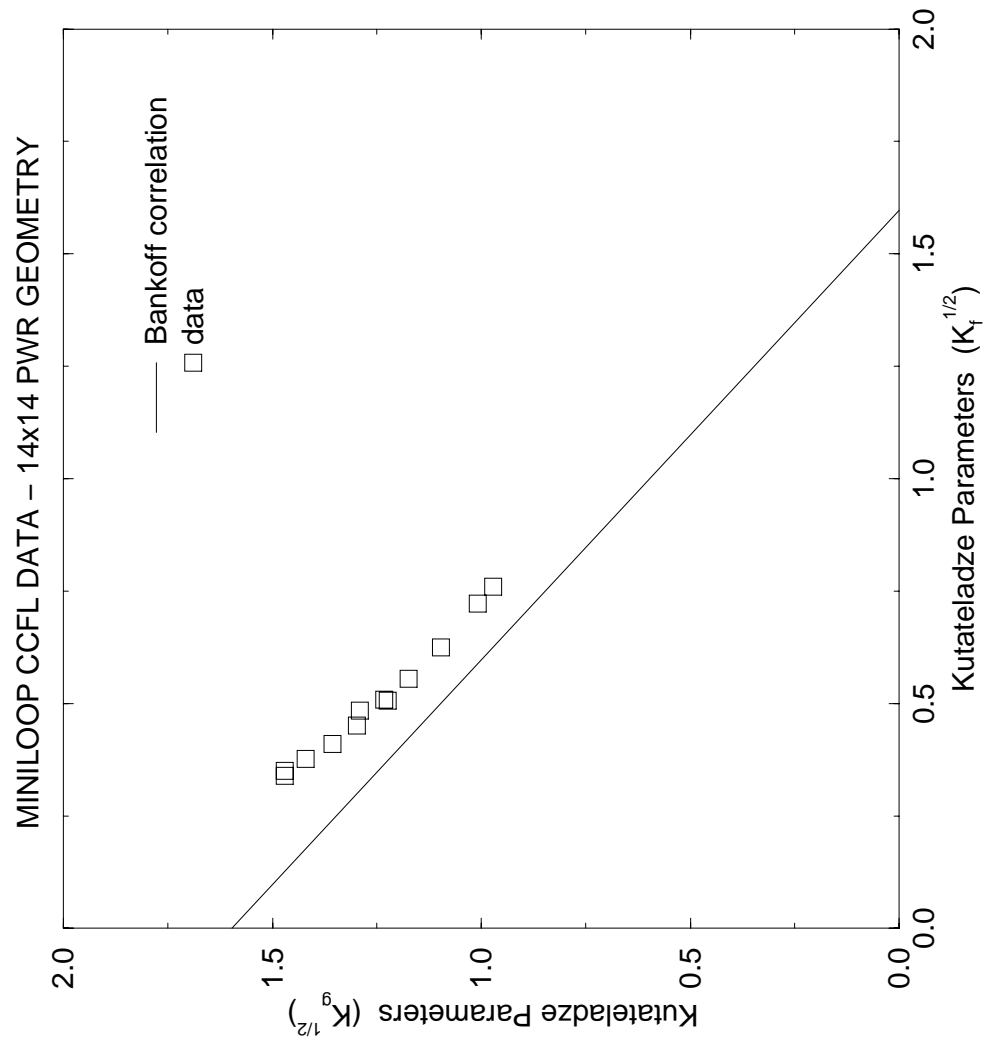
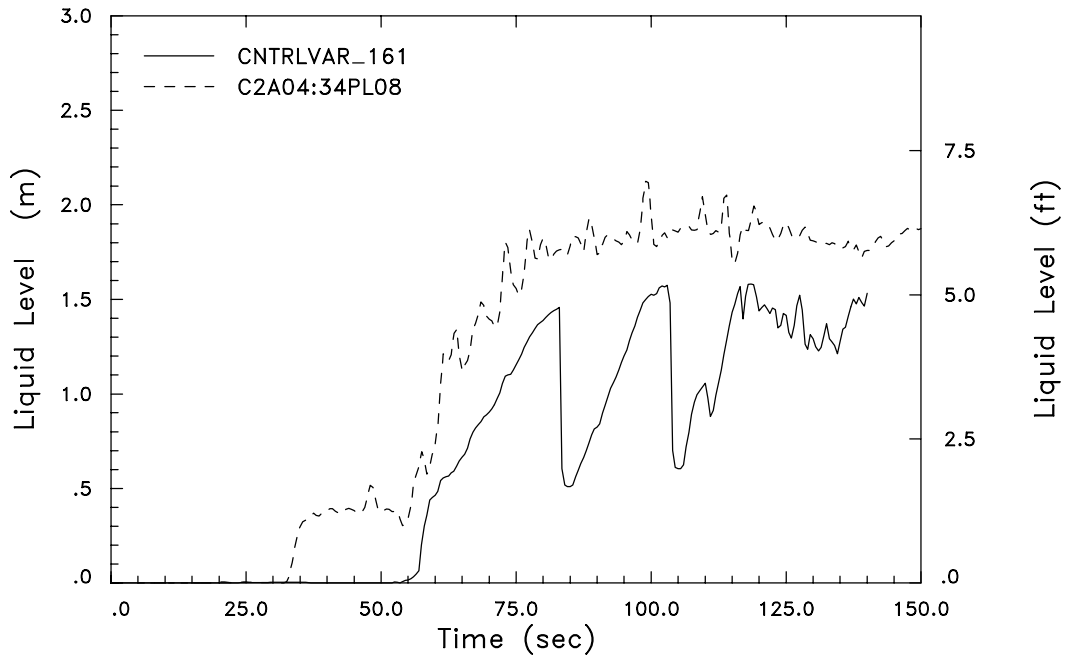
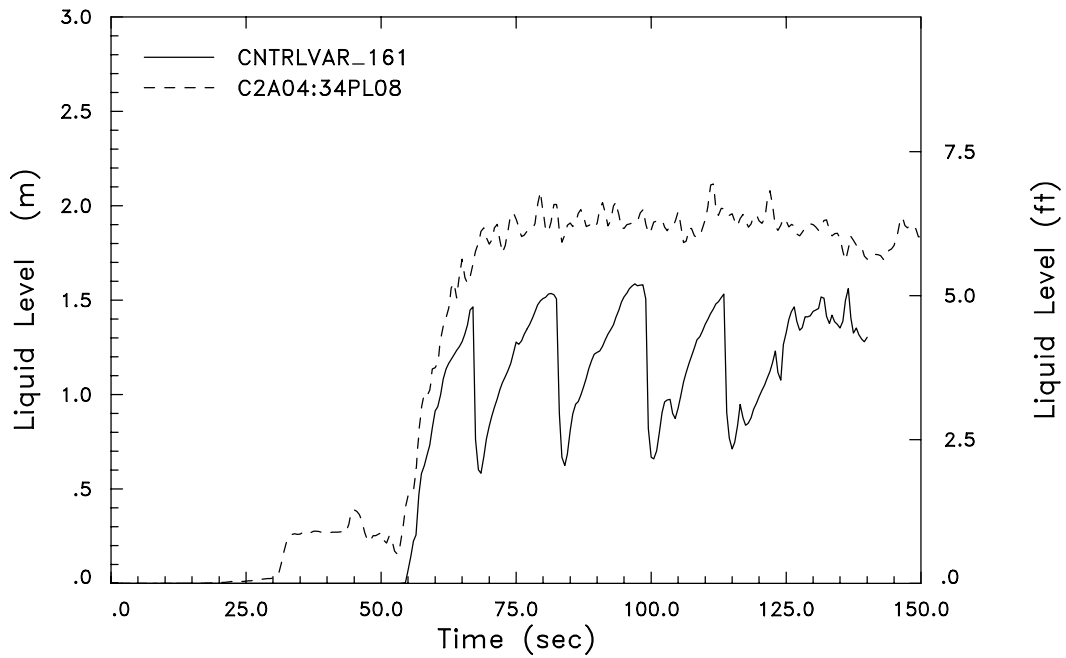


Figure 4.105 Comparison Between Mini-Loop CCFL Data of a Combustion Engineering 14 x 14 UTP and Bankoff



**Figure 4.106 Lower Plenum Liquid Level Comparison
UPTF Test 6 – Run 131**



**Figure 4.107 Lower Plenum Liquid Level Comparison
UPTF Test 6 – Run 132**

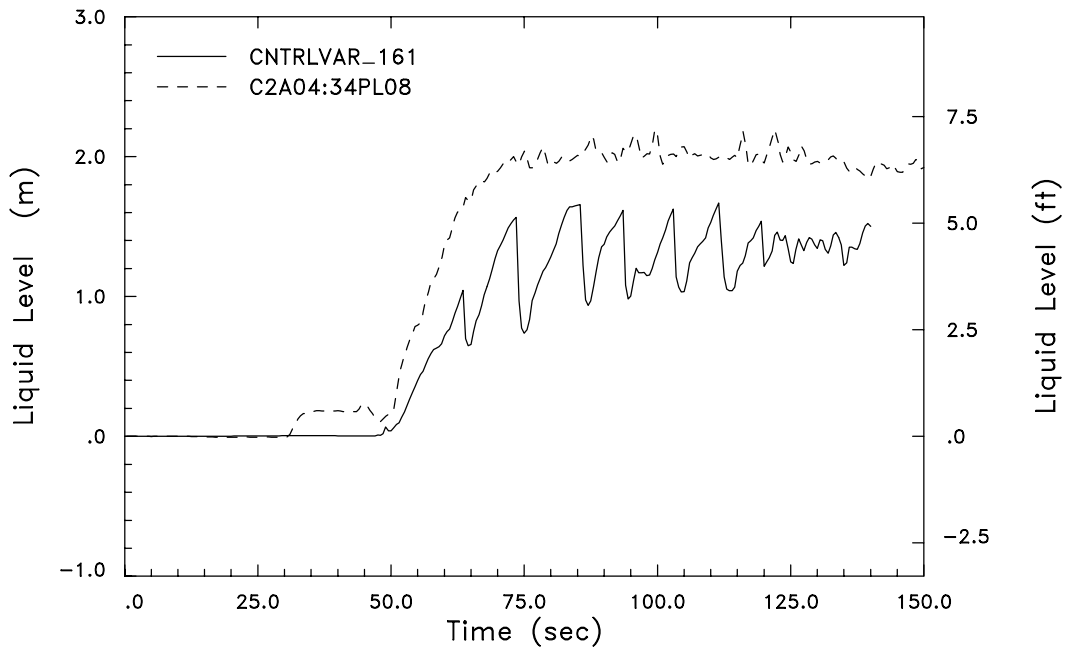


**Figure 4.108 Lower Plenum Liquid Level Comparison
UPTF Test 6 – Run 133**

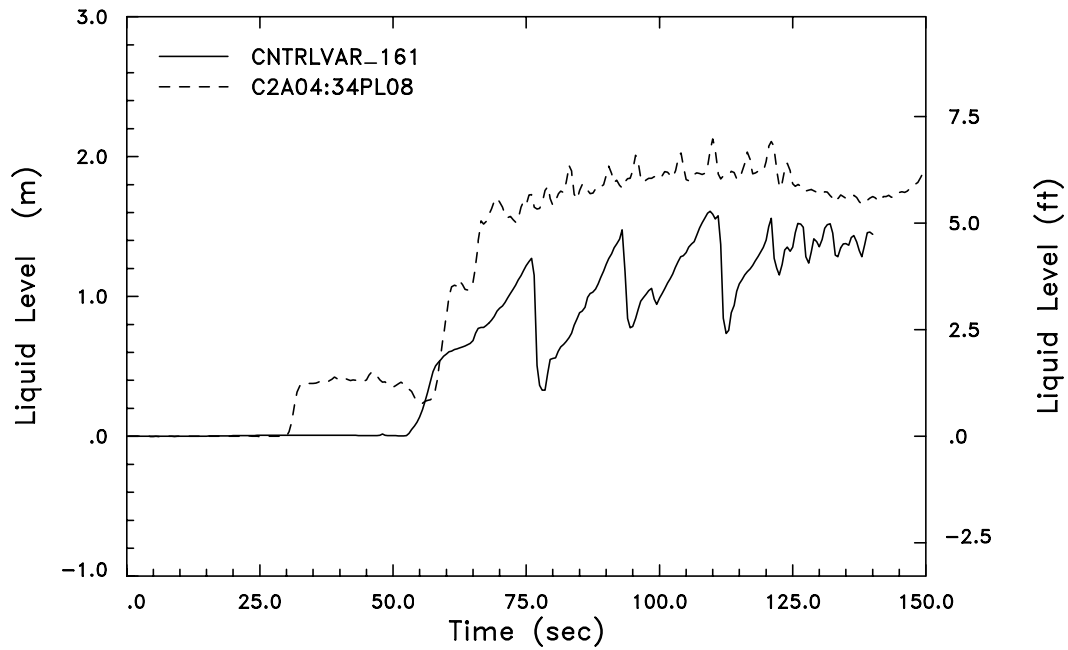


**Figure 4.109 Lower Plenum Liquid Level Comparison
UPTF Test 6 – Run 135**

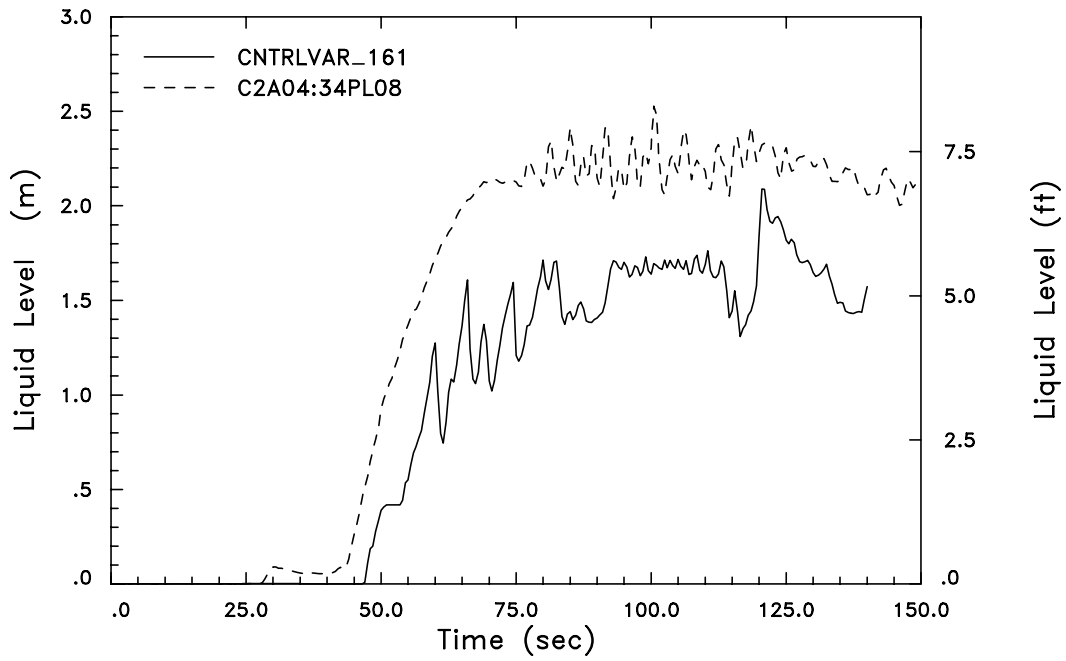


**Figure 4.110 Lower Plenum Liquid Level Comparison
UPTF Test 6 – Run 136**

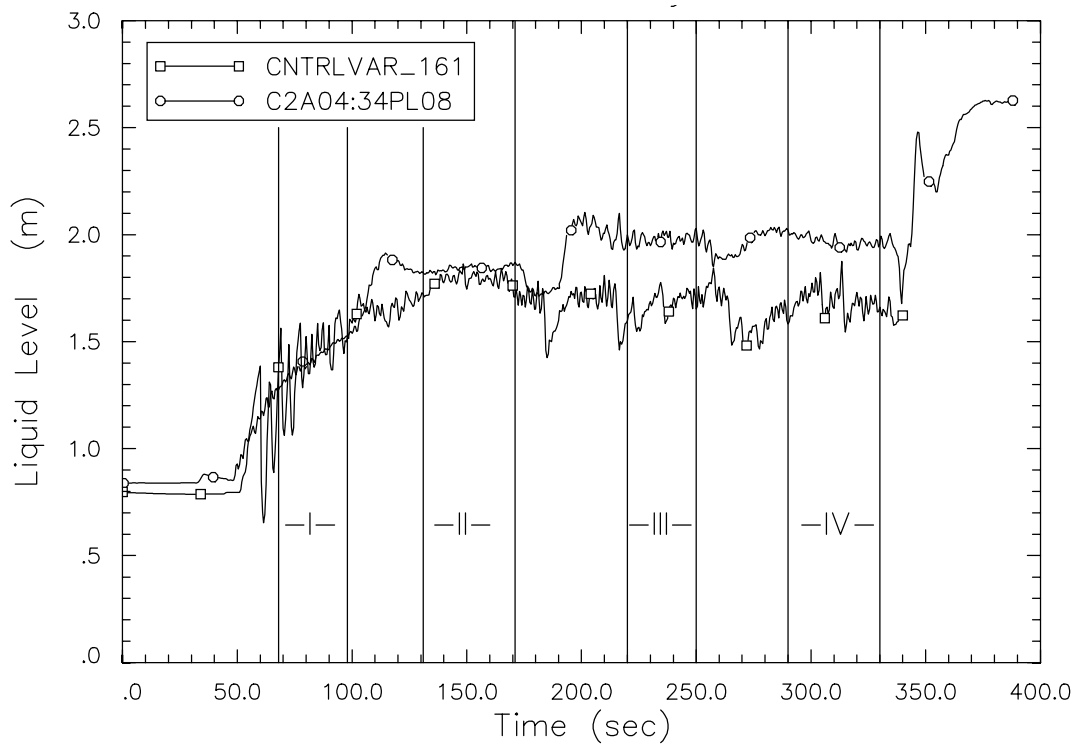


**Figure 4.111 Lower Plenum Liquid Level Comparison
UPTF Test 7 – Run 203**

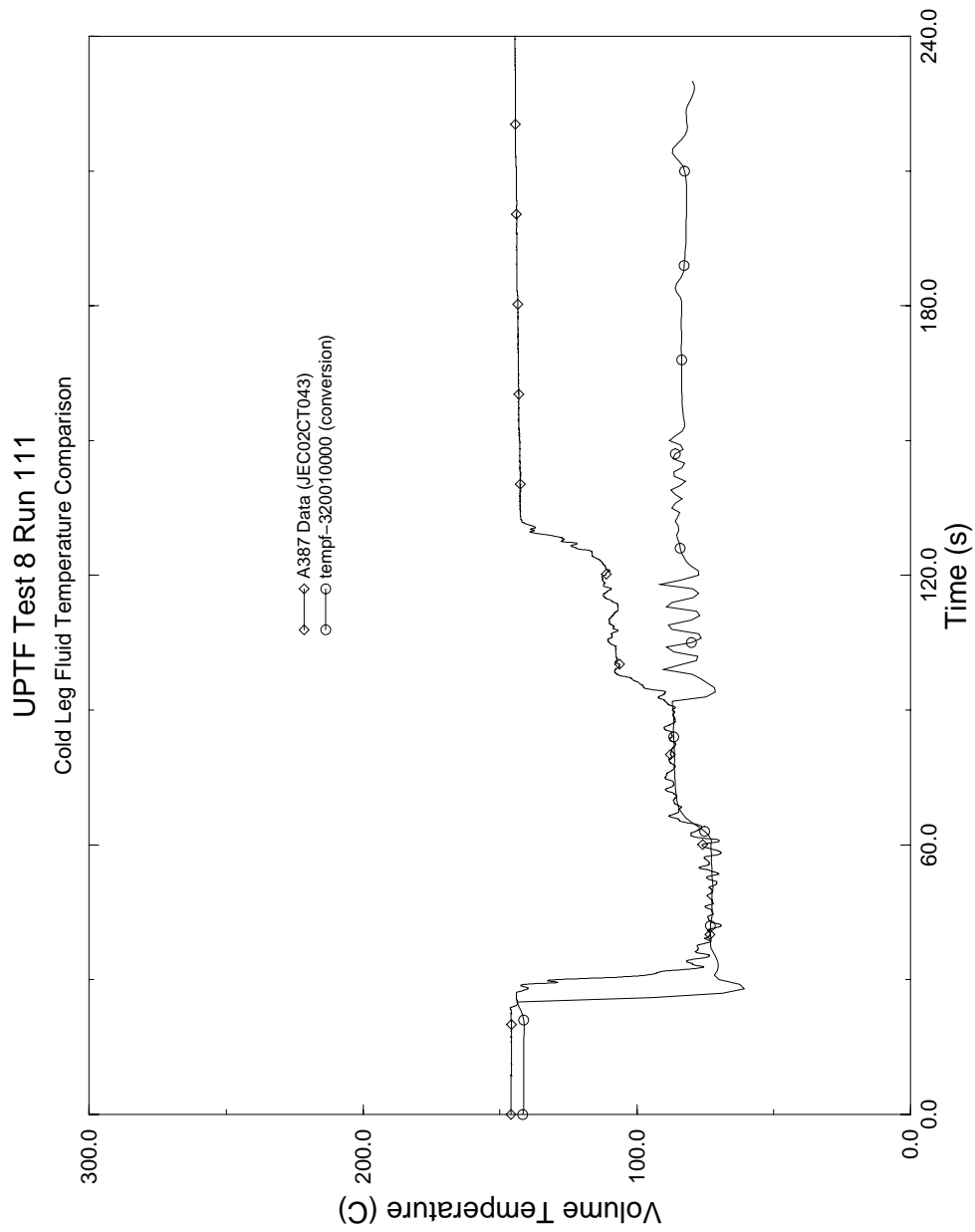


Figure 4.112 UPTF Data/S-RELAP5 Cold Leg Temperature Comparison, UPTF Test 8 Run 111

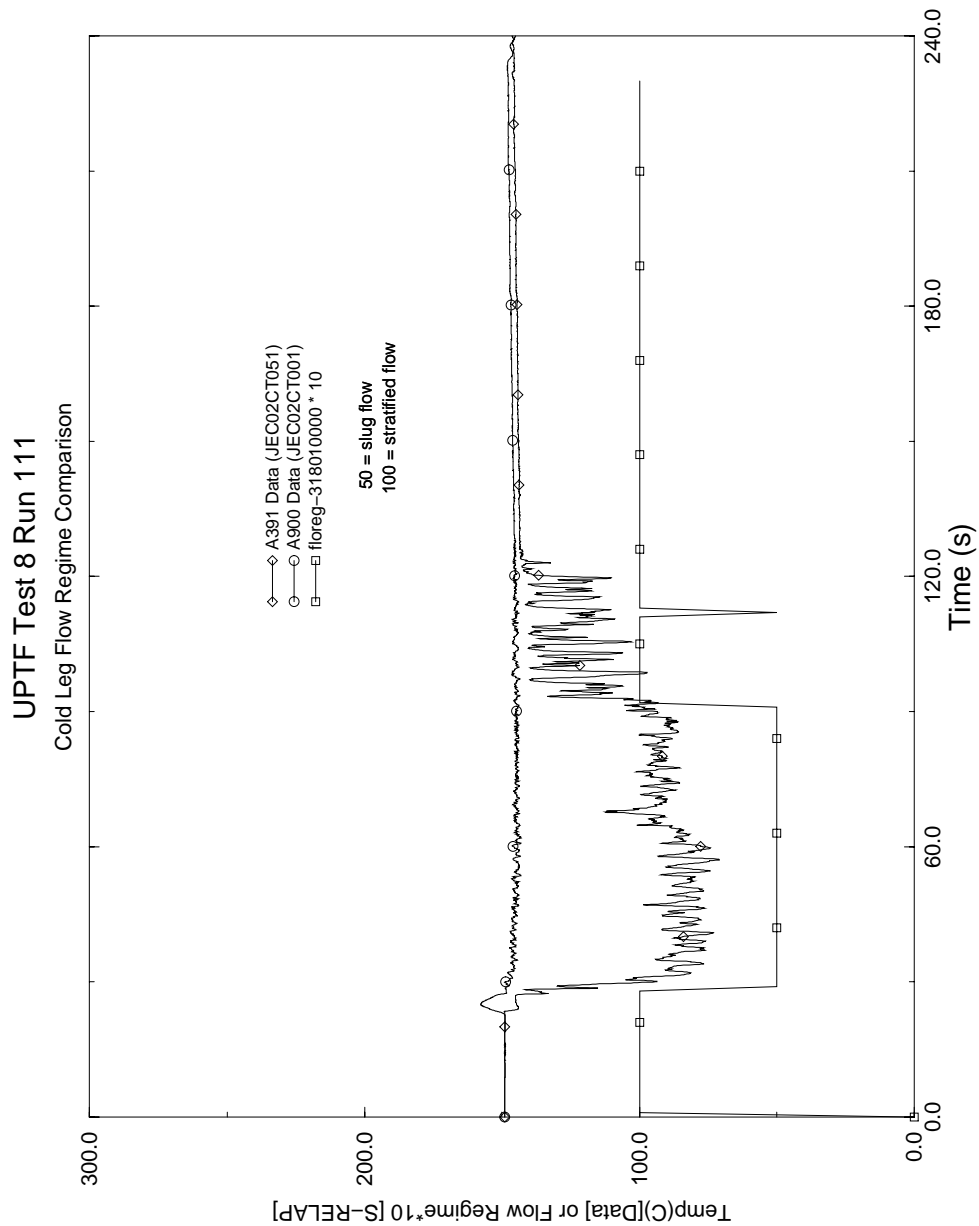


Figure 4.113 UPTF Data/S-RELAP5 Flow Regime Comparison, UPTF Test 8 Run 111

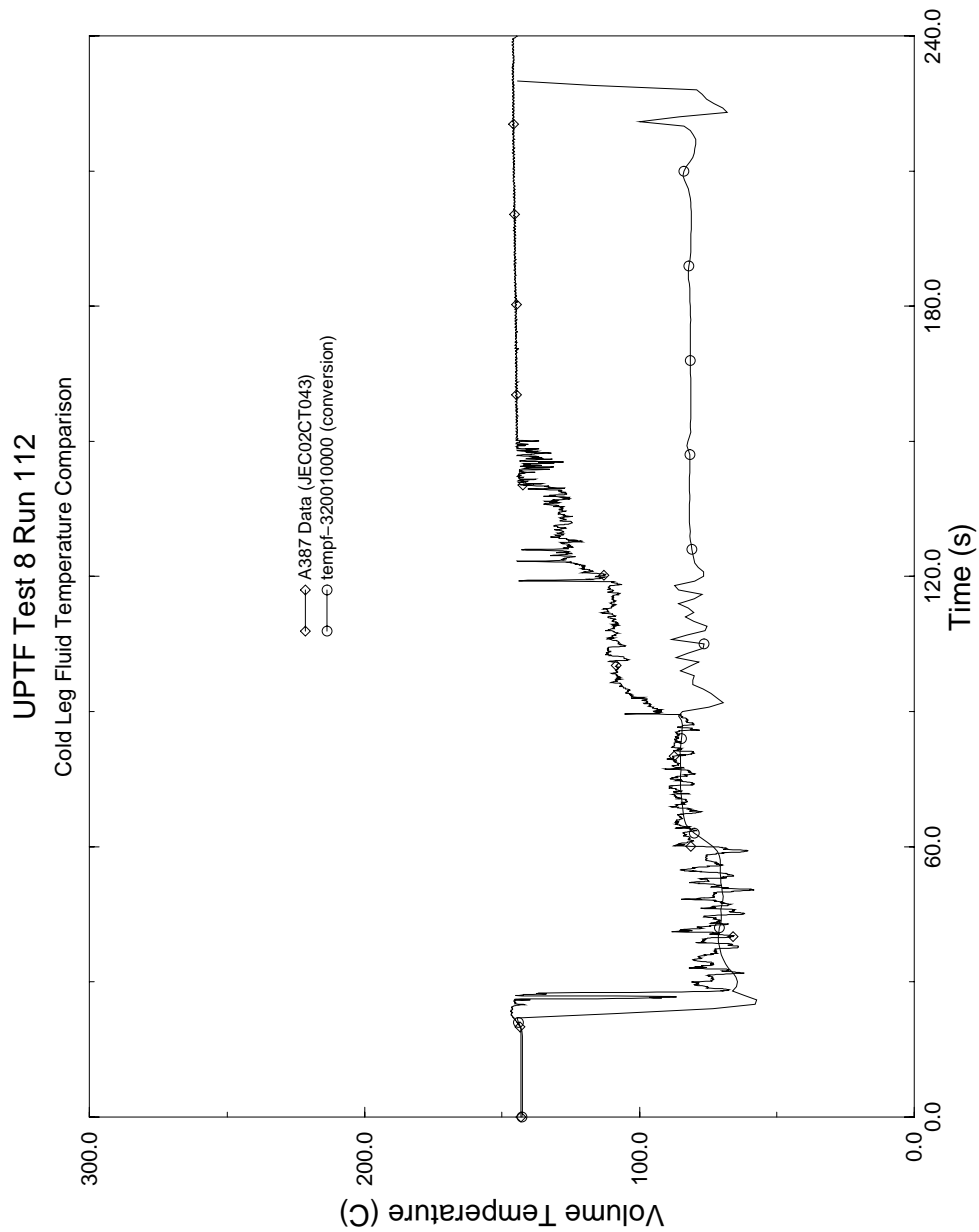


Figure 4.114 UPTF Data/S-RELAP5 Cold Leg Temperature Comparison, UPTF Test 8 Run 112

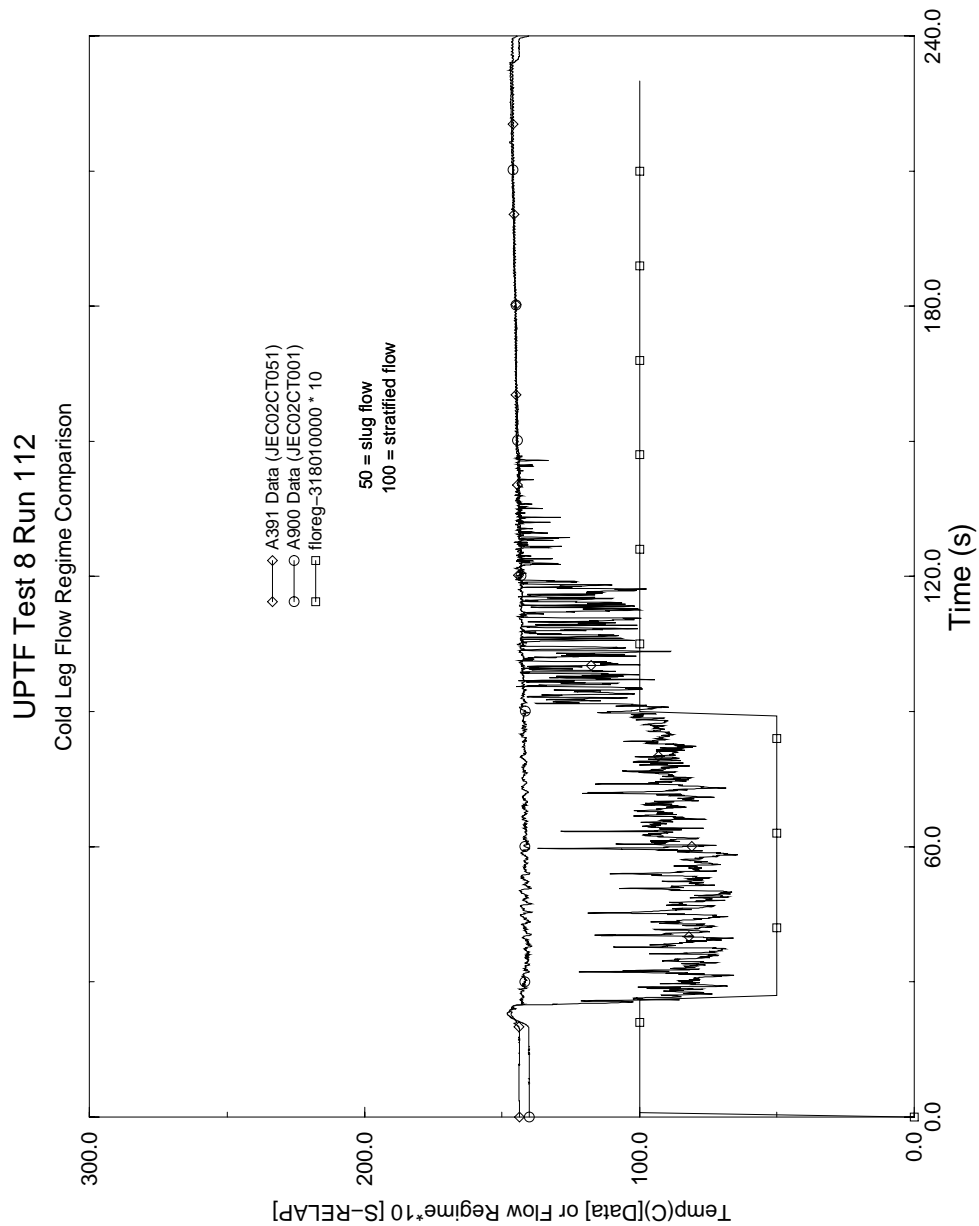


Figure 4.115 UPTF Data/S-RELAP5 Flow Regime Comparison, UPTF Test 8 Run 112

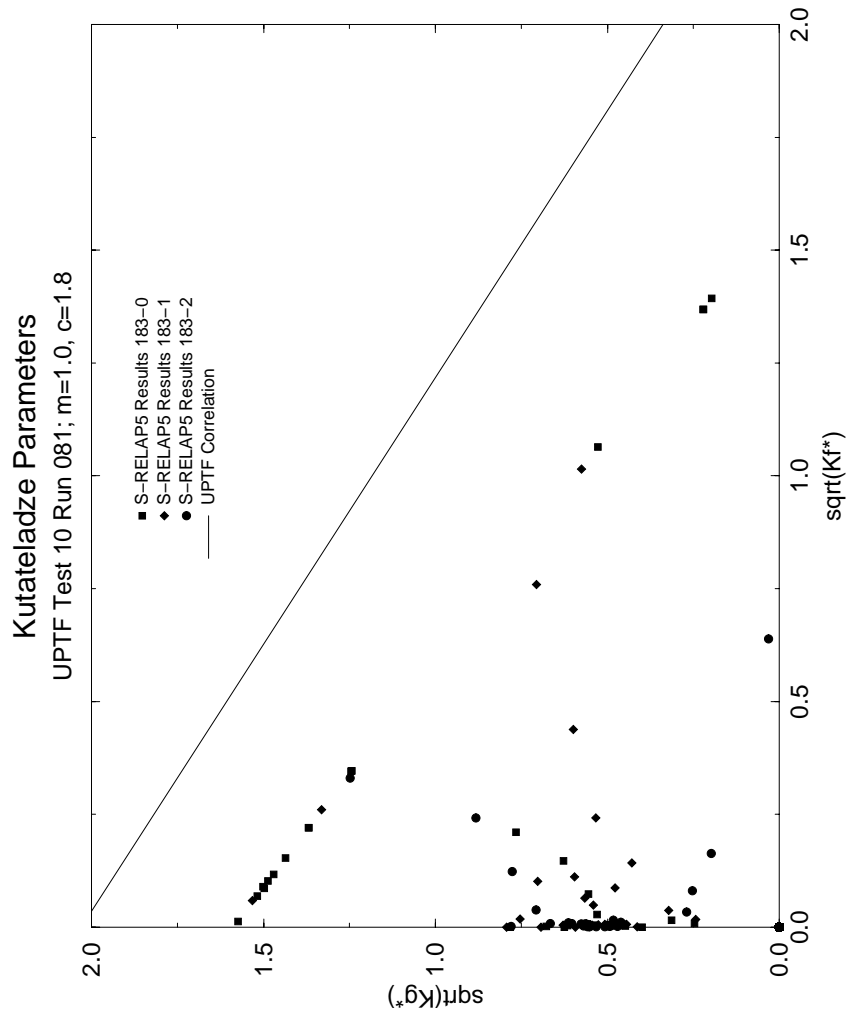


Figure 4.116 Countercurrent Flow of Steam and Water
UPTF Test 10 Run 081

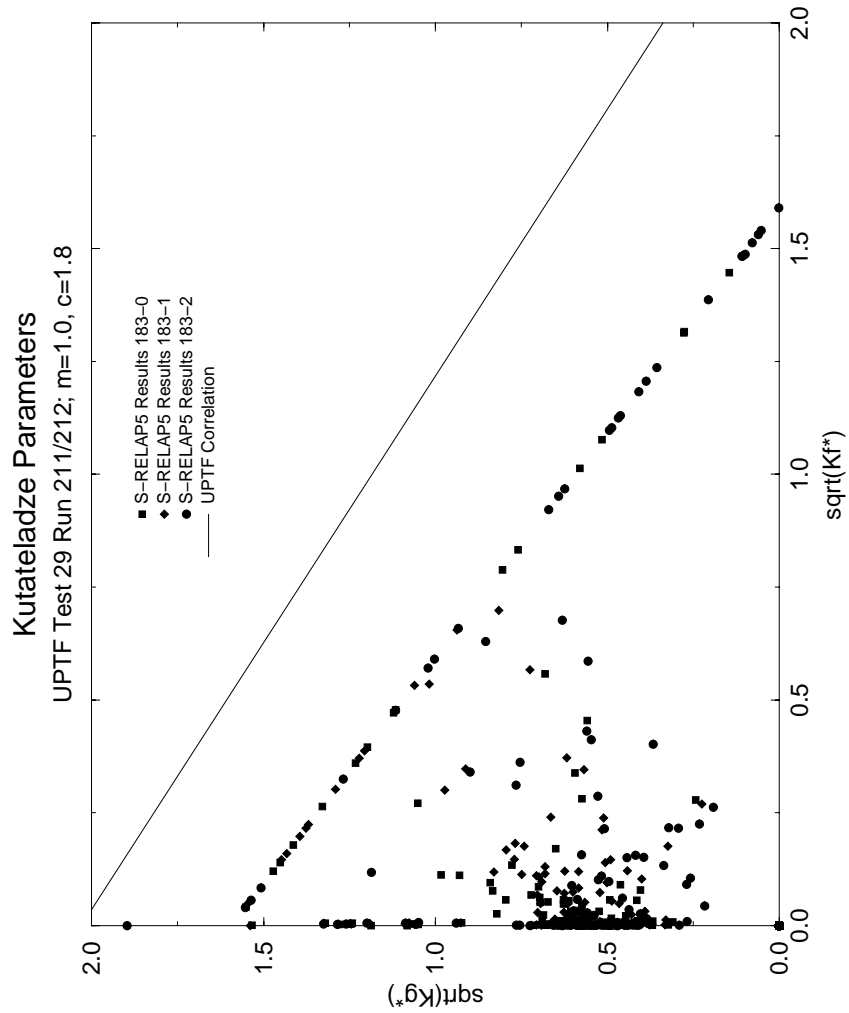
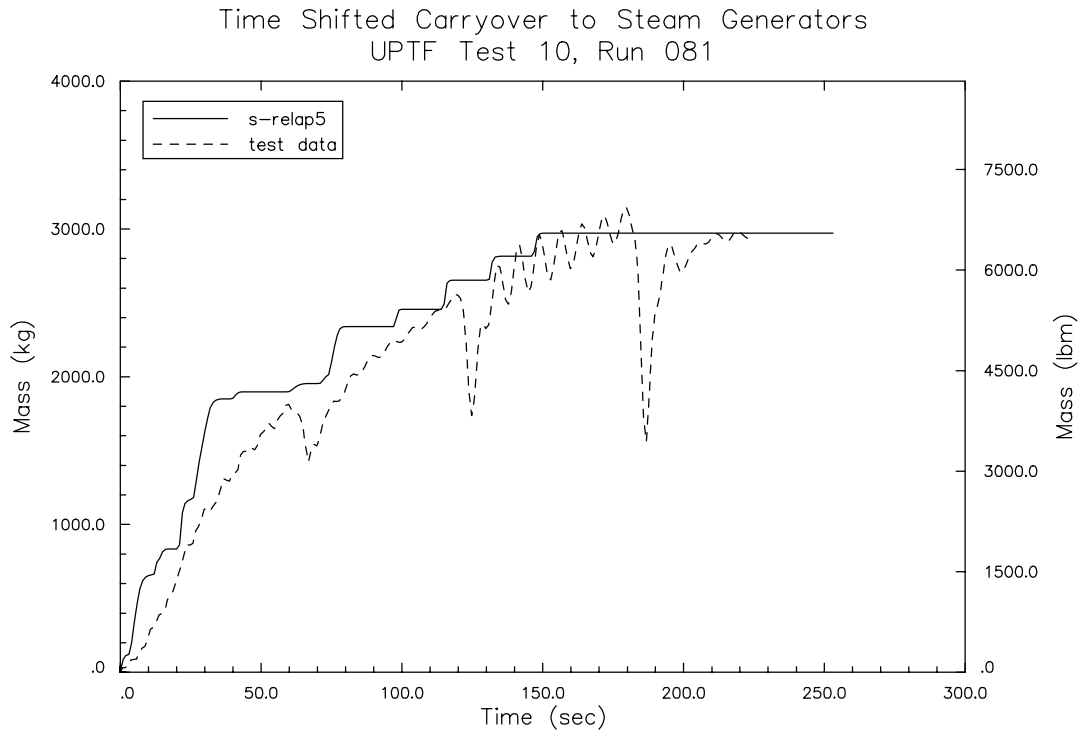
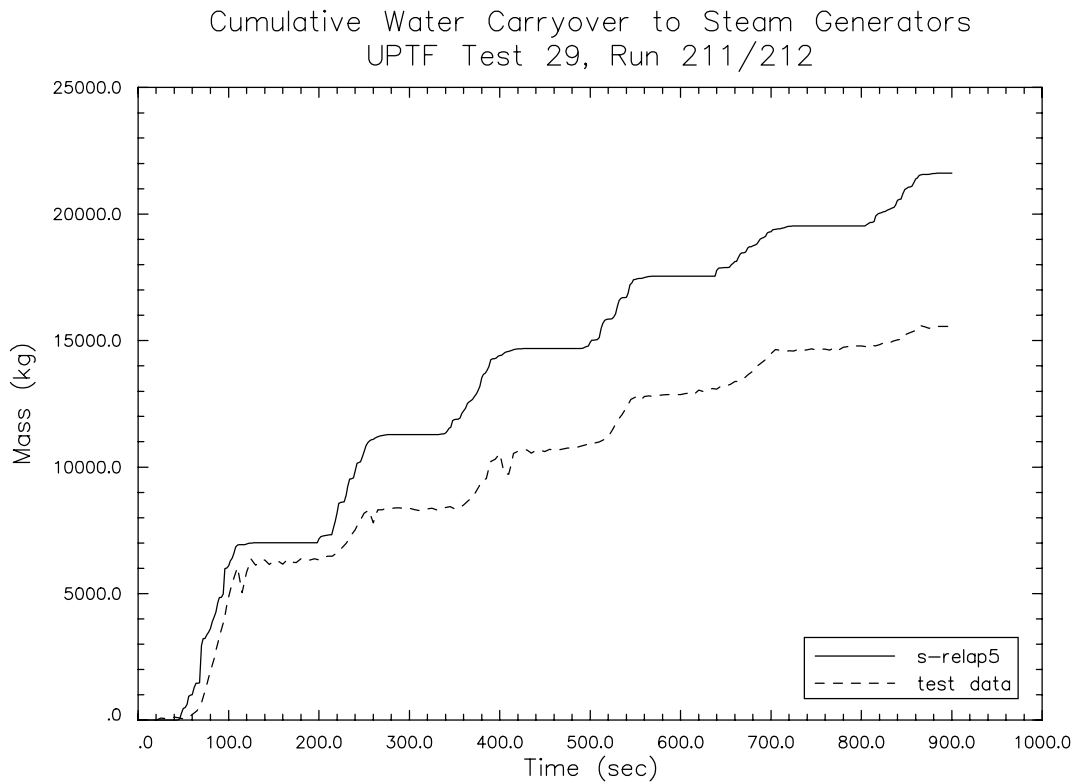


Figure 4.117 Countercurrent Flow of Steam and Water
UPTF Test 29 Run 212/211



**Figure 4.118 Carryover to Steam Generators Test 10 Run 081
Beyond 150 sec.**



**Figure 4.119 Cumulative Water Carryover to Steam Generators
Test 29 Run 212/211**

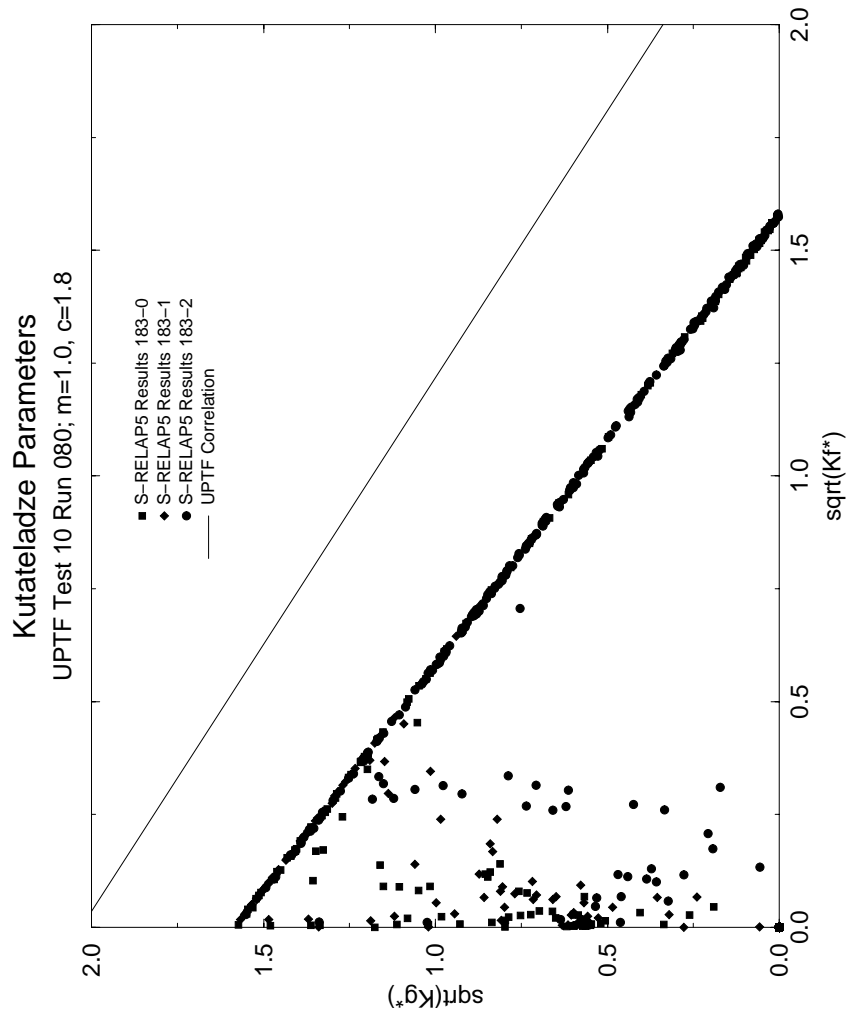


**Figure 4.120 Counter Current Flow of Steam and Water,
UPTF Test 10, Run 080**

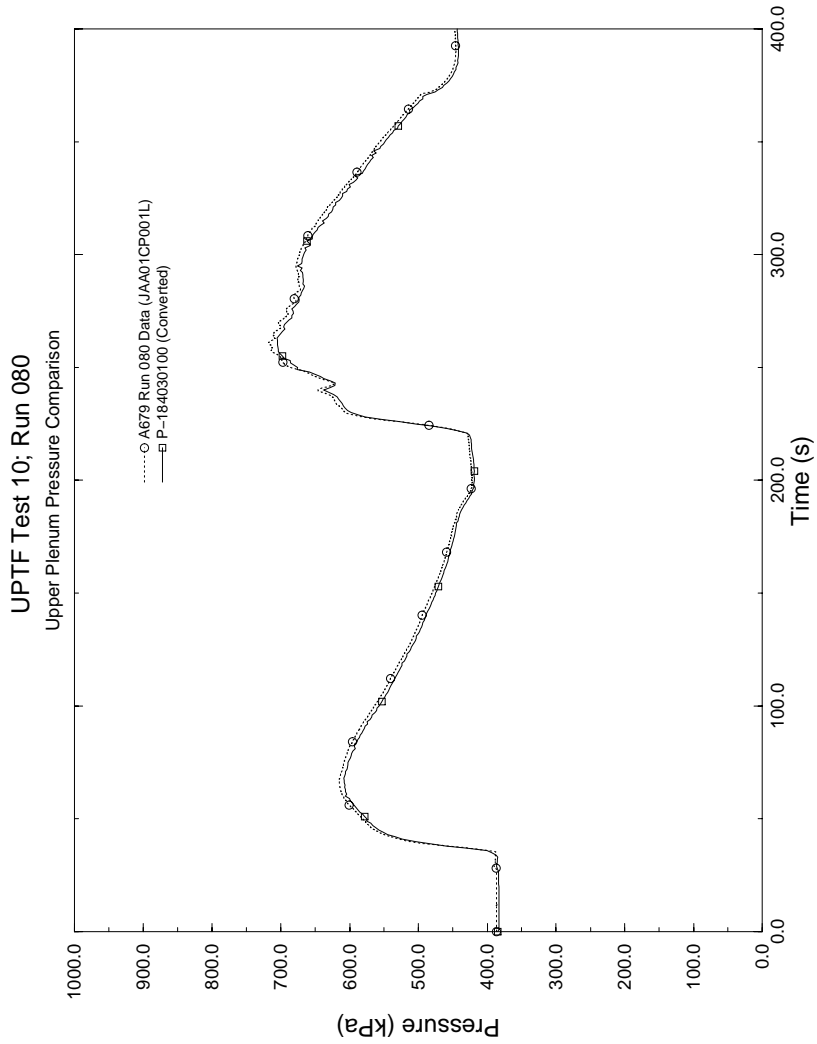


**Figure 4.121 Upper Plenum Pressure Comparison
Test 10, Run 080**

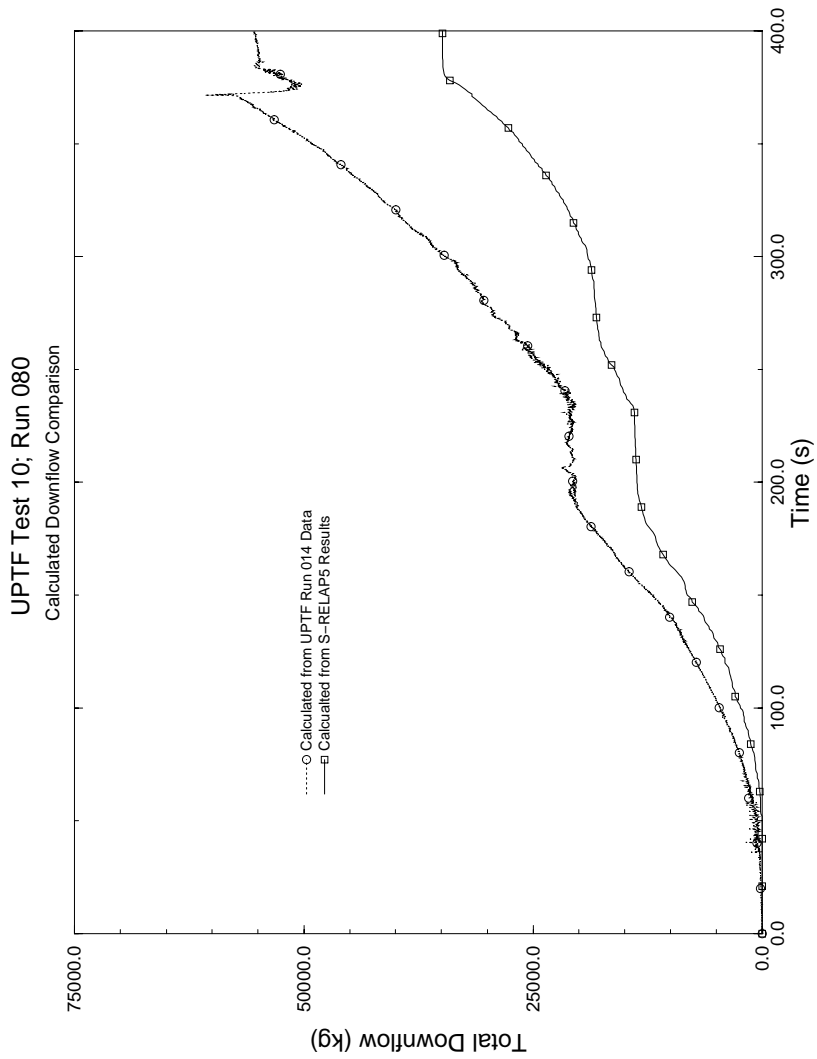


Figure 4.122 Calculated Downflow Comparison UPTF Test 10, Run 080 (m=1.0, c=1.8)

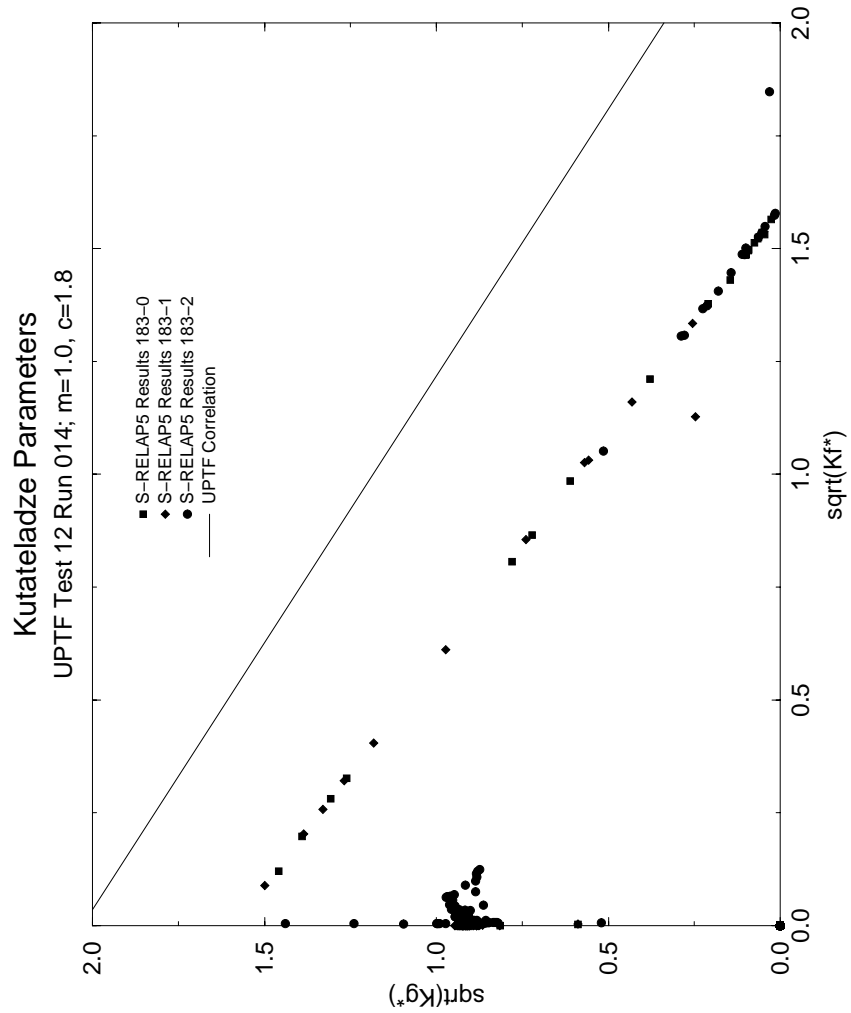
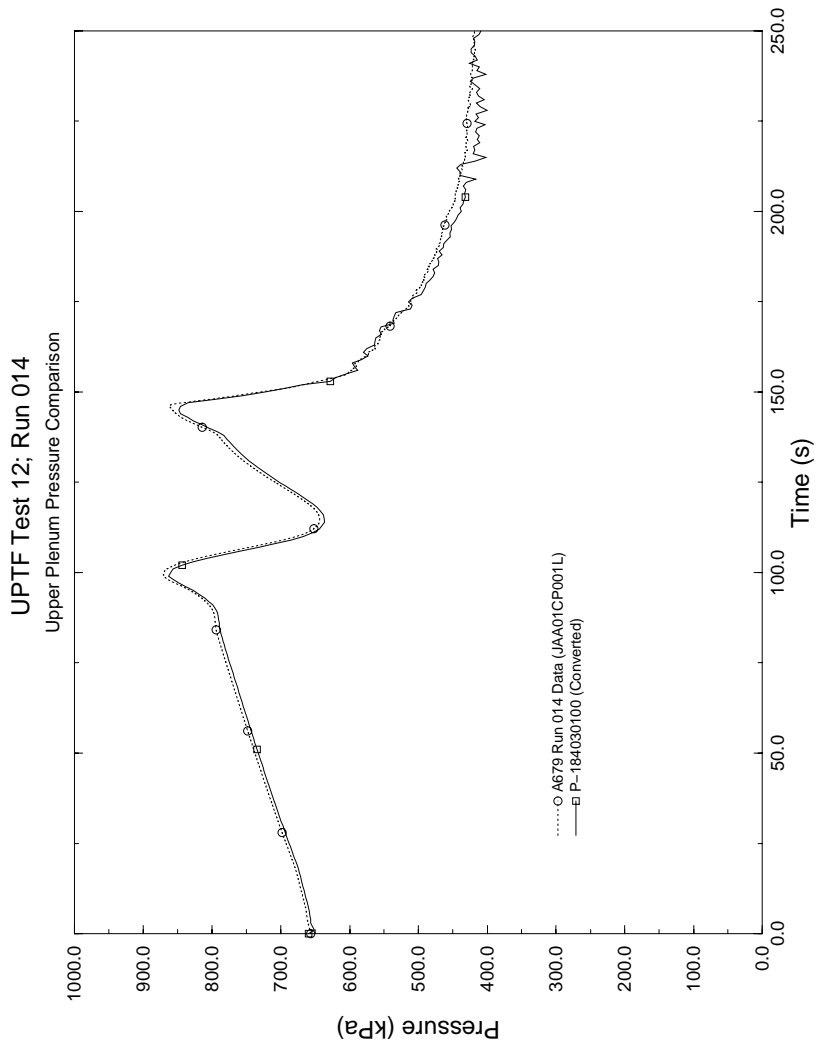


Figure 4.123 Counter Current Flow of Steam and Water, UPTF Test 12, Run 014



**Figure 4.124 Upper Plenum Pressure Comparison
UPTF Test 12, Run 014**

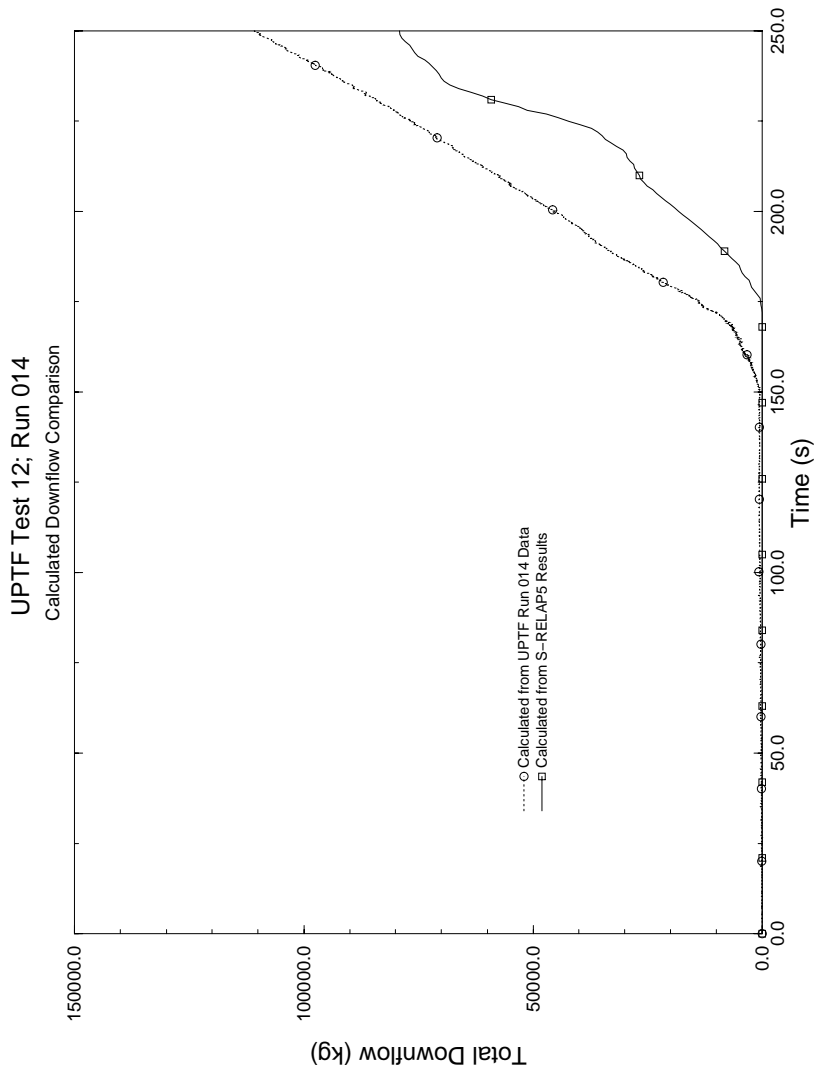
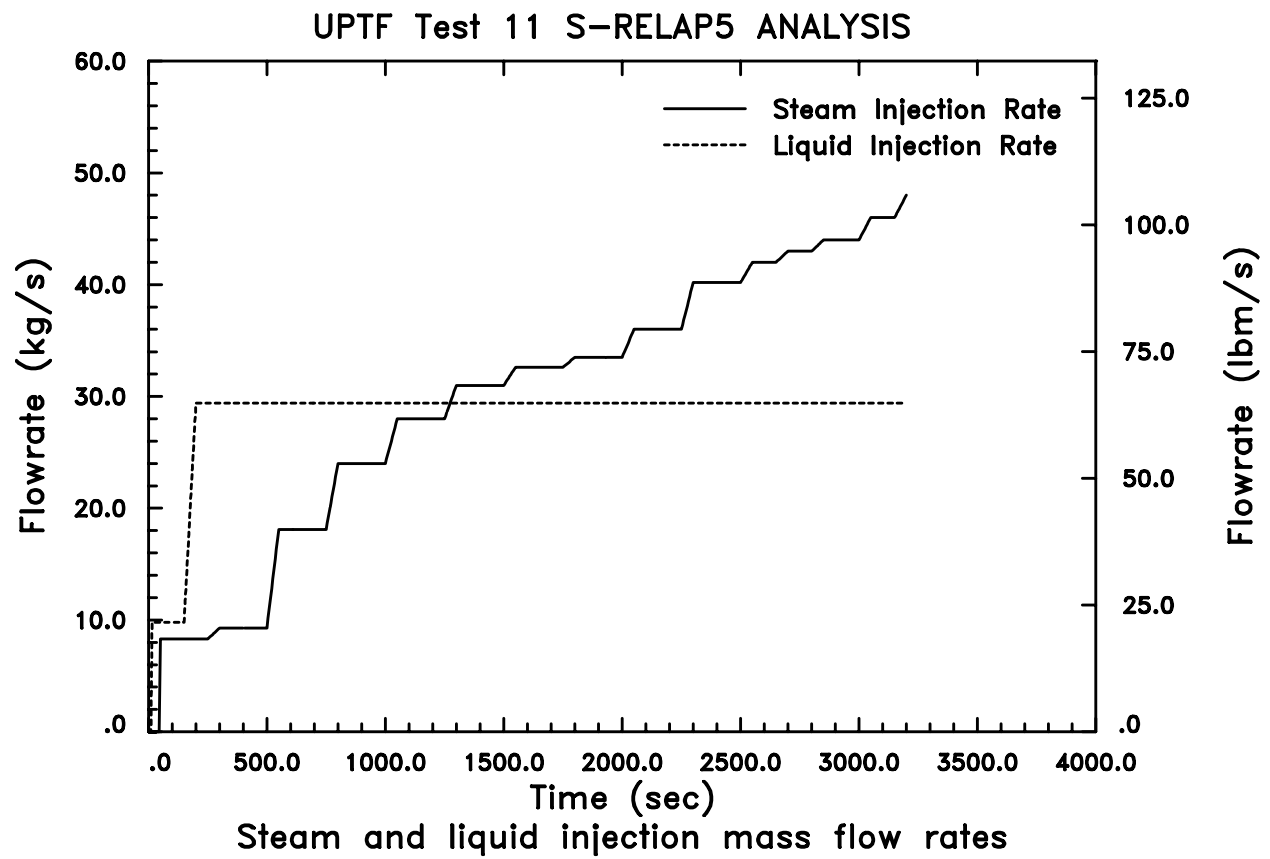


Figure 4.125 Calculated Downflow Comparison UPTF Test 12, Run 014 (m=1.0, c=1.8)



**Figure 4.126 Steam and Water Injection Rates for UPTF Test 11
1.5 MPa Series**

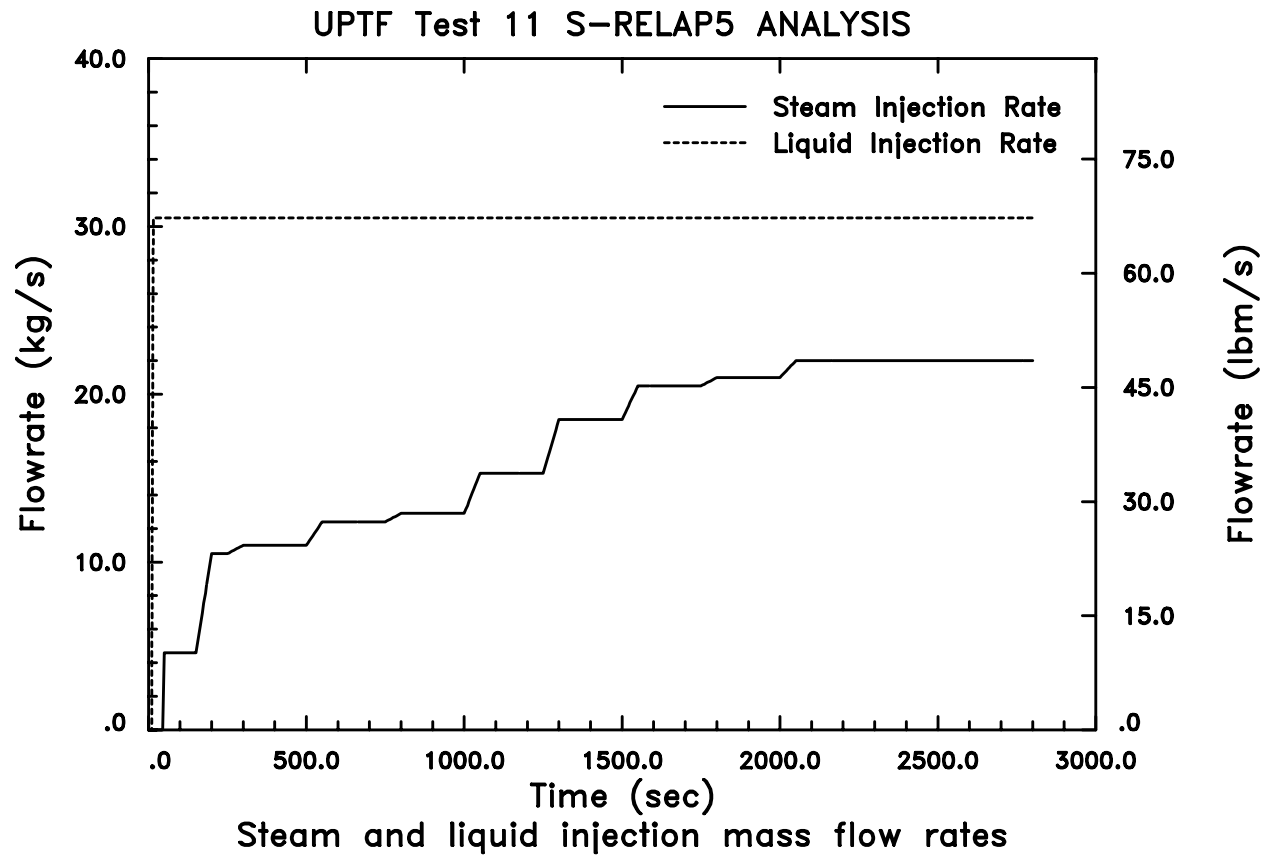


Figure 4.127 Steam and Water Injection Rates for UPTF Test 11
0.3 MPa Series

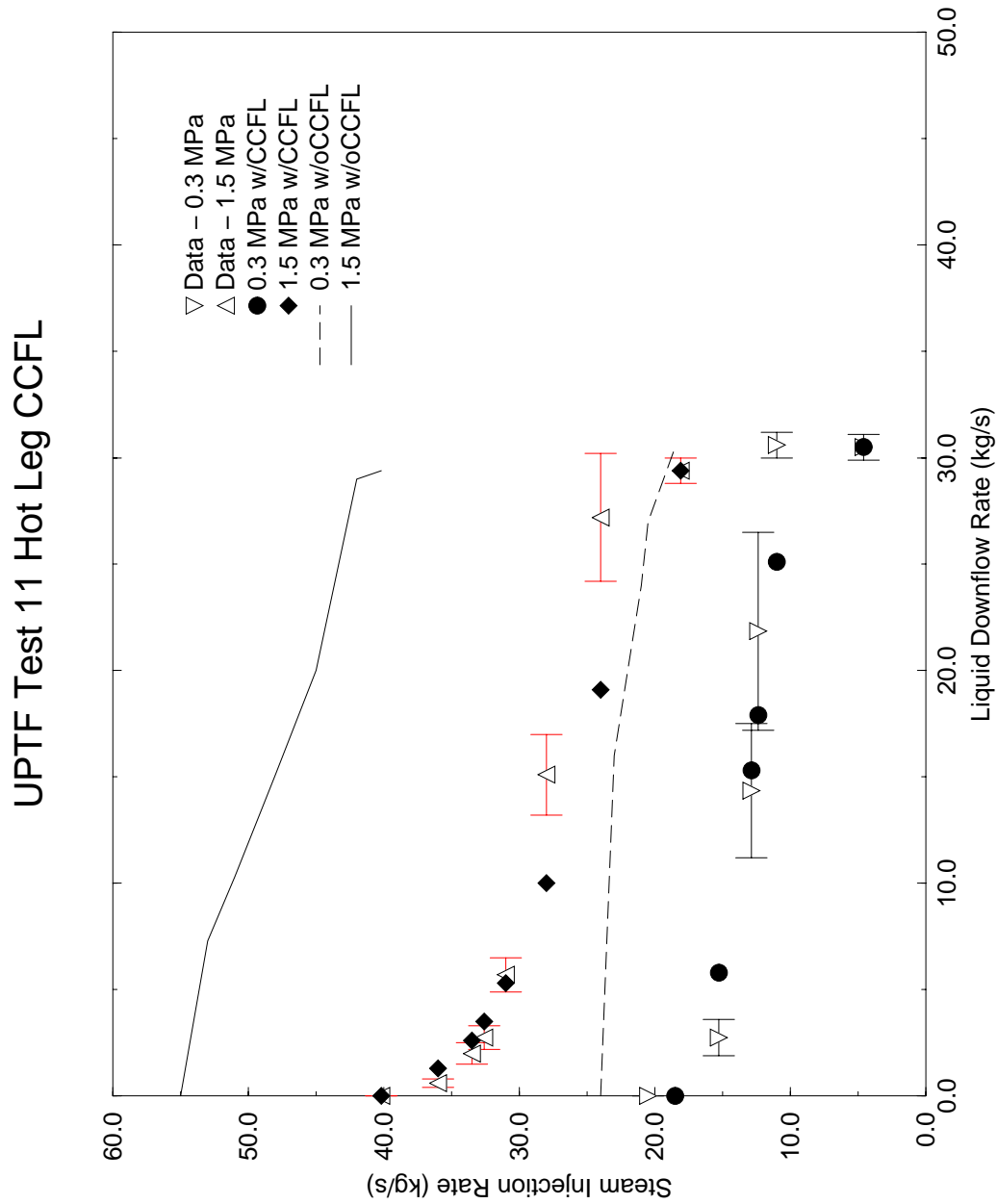


Figure 4.128 Comparison of UPTF Test 11 Data with S-RELAP5 Calculations

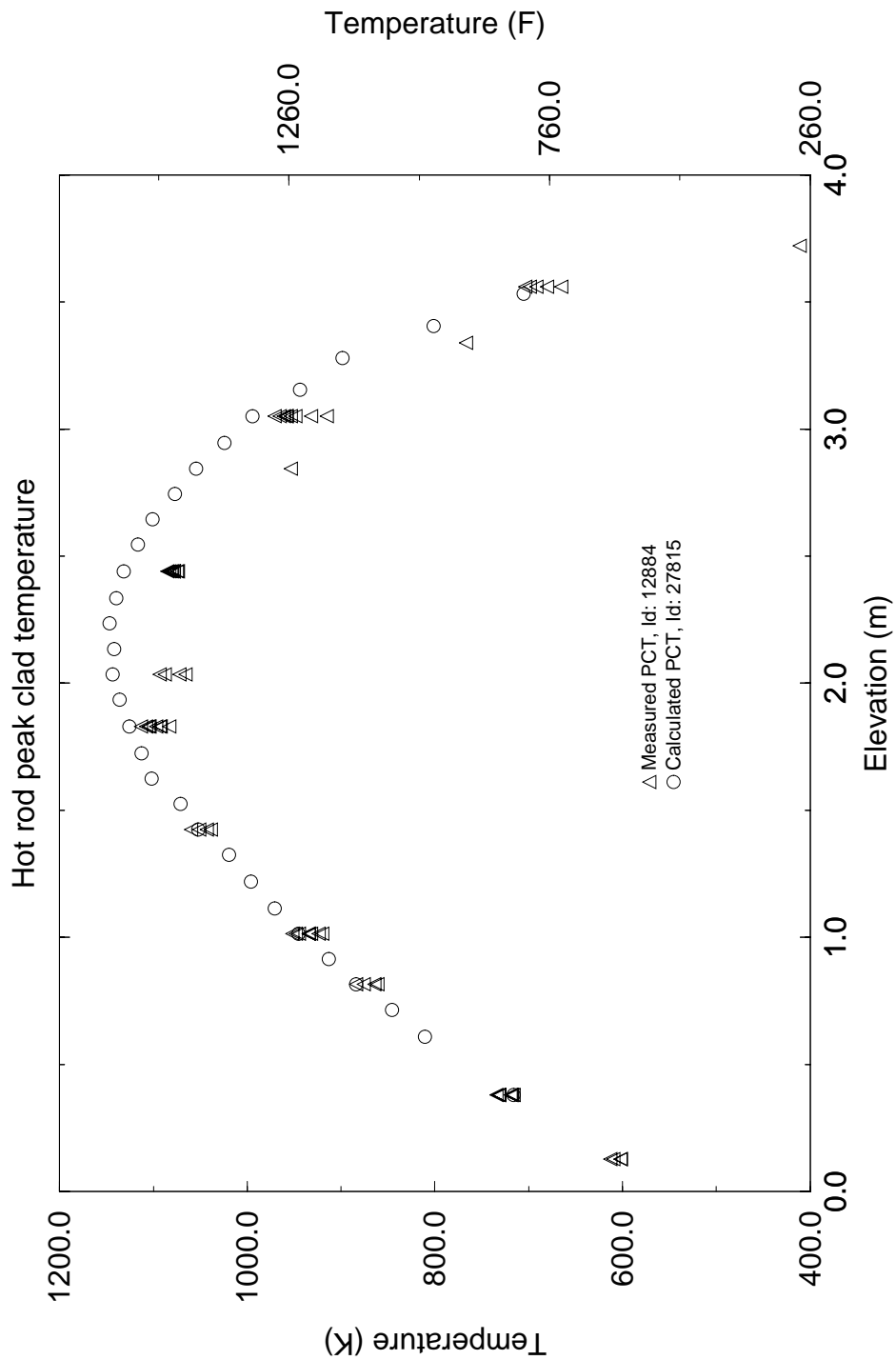


Figure 4.129 Comparison of Peak Surface Temperatures vs. Elevation for High Power Bundles, CCTF Test Run 54

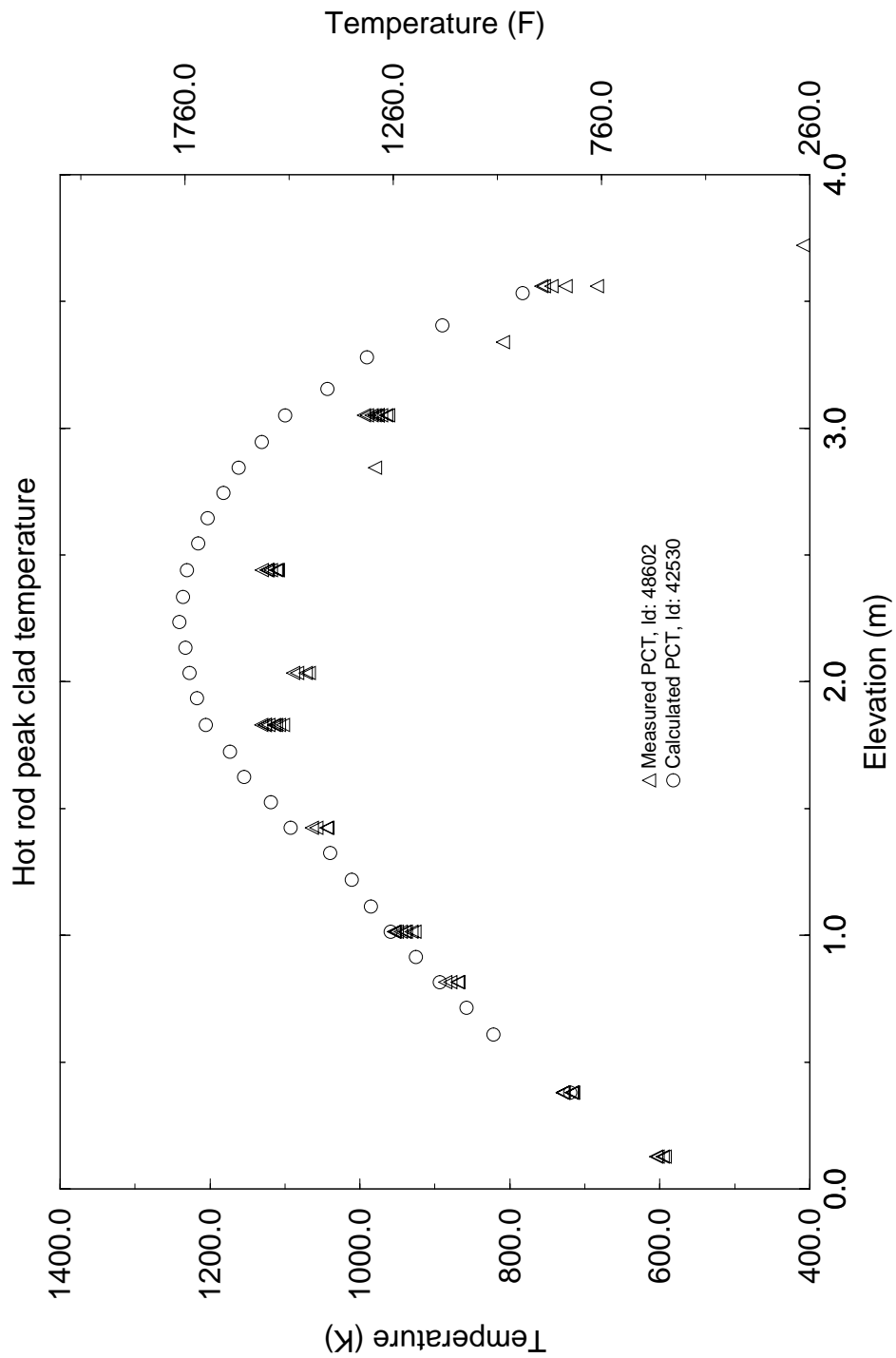


Figure 4.130 Comparison of Peak Surface Temperatures vs. Elevation for High Power Bundles, CCTF Test Run 62

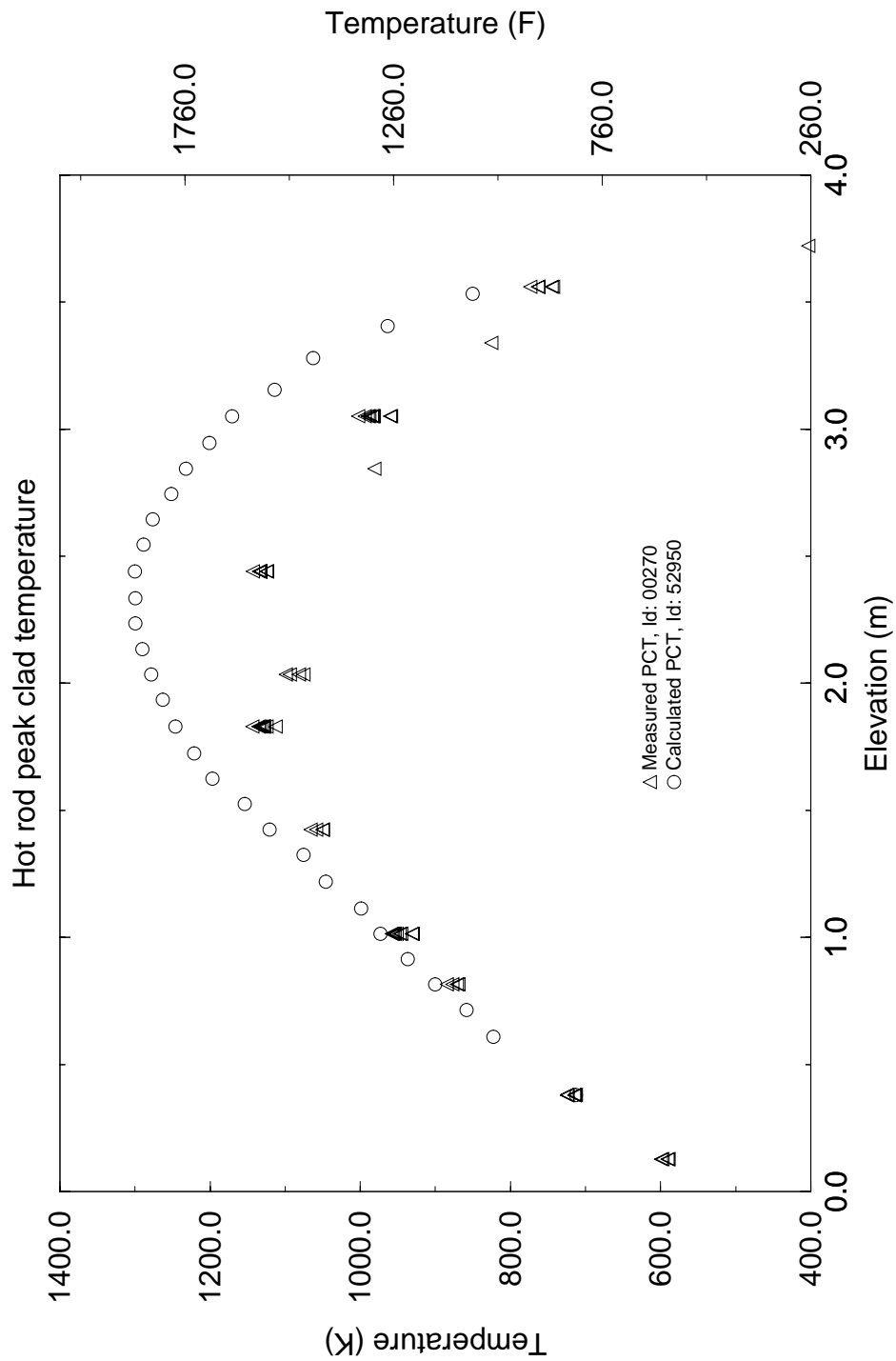


Figure 4.131 Comparison of Peak Surface Temperatures vs. Elevation for High Power Bundles for Test Run 67

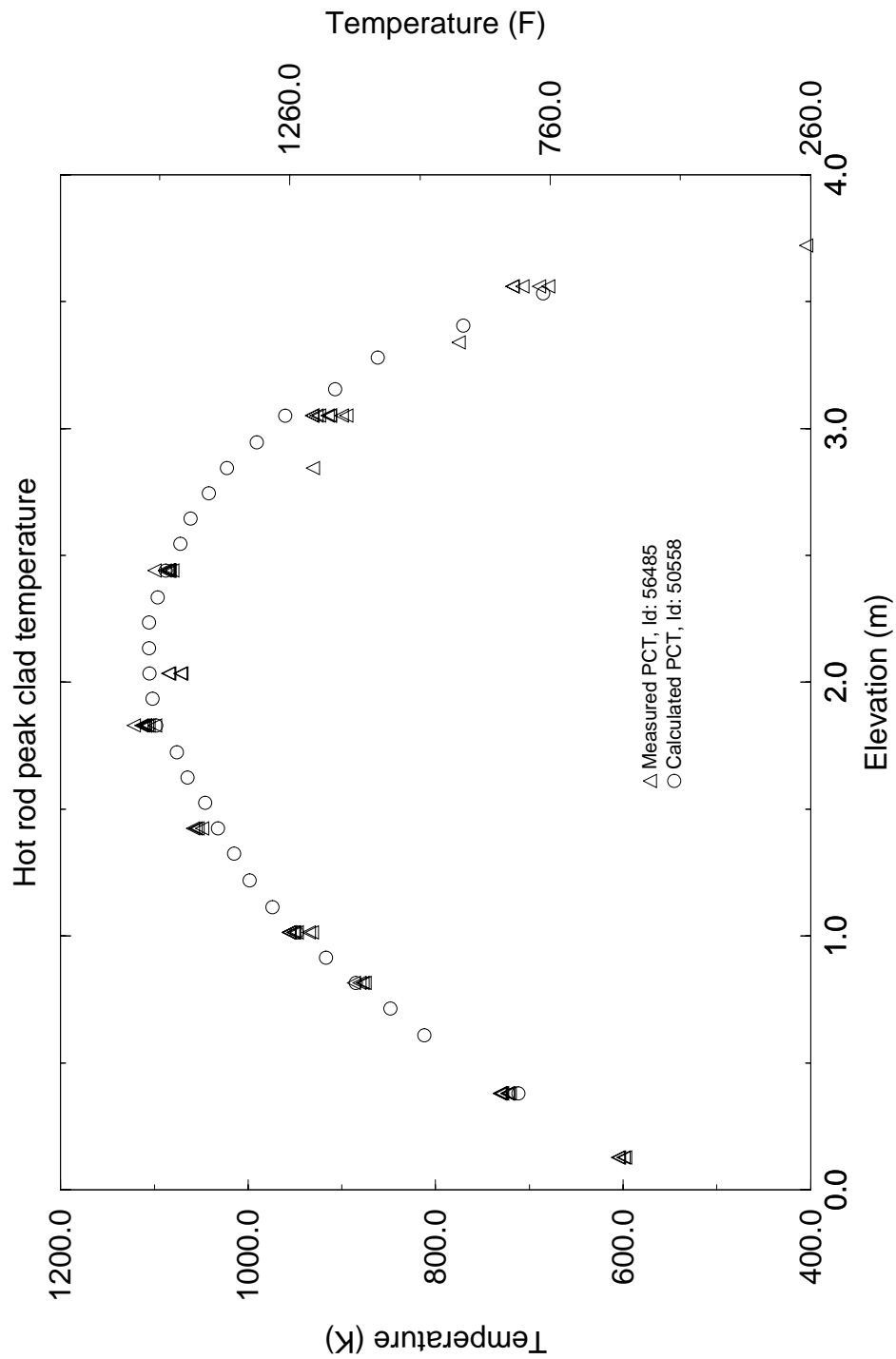


Figure 4.132 Comparison of Peak Surface Temperatures vs. Elevation for High Power Bundles, CCTF Test Run 68

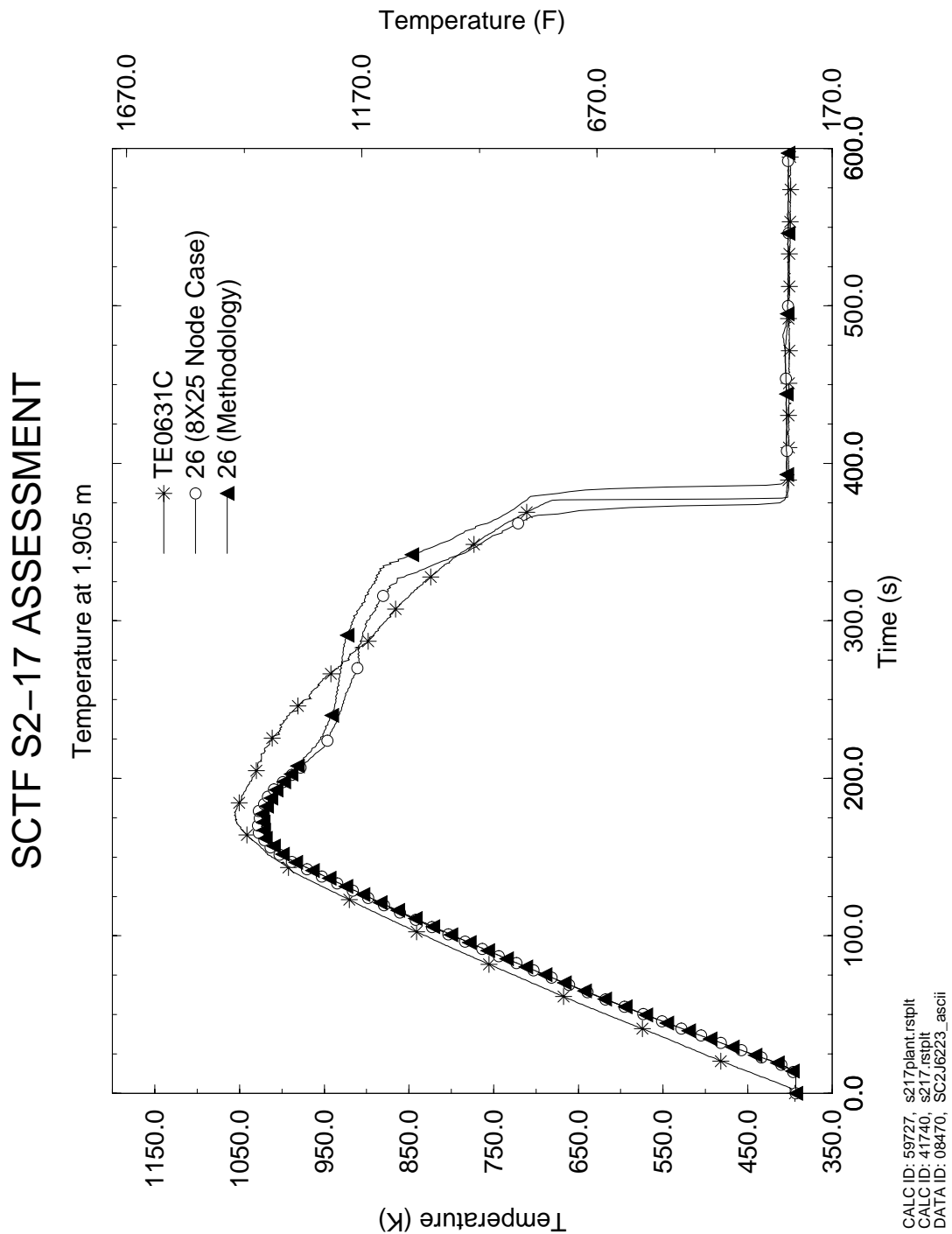


Figure 4.133 Temperature Comparison at 1.905 m, SCTF S2-17

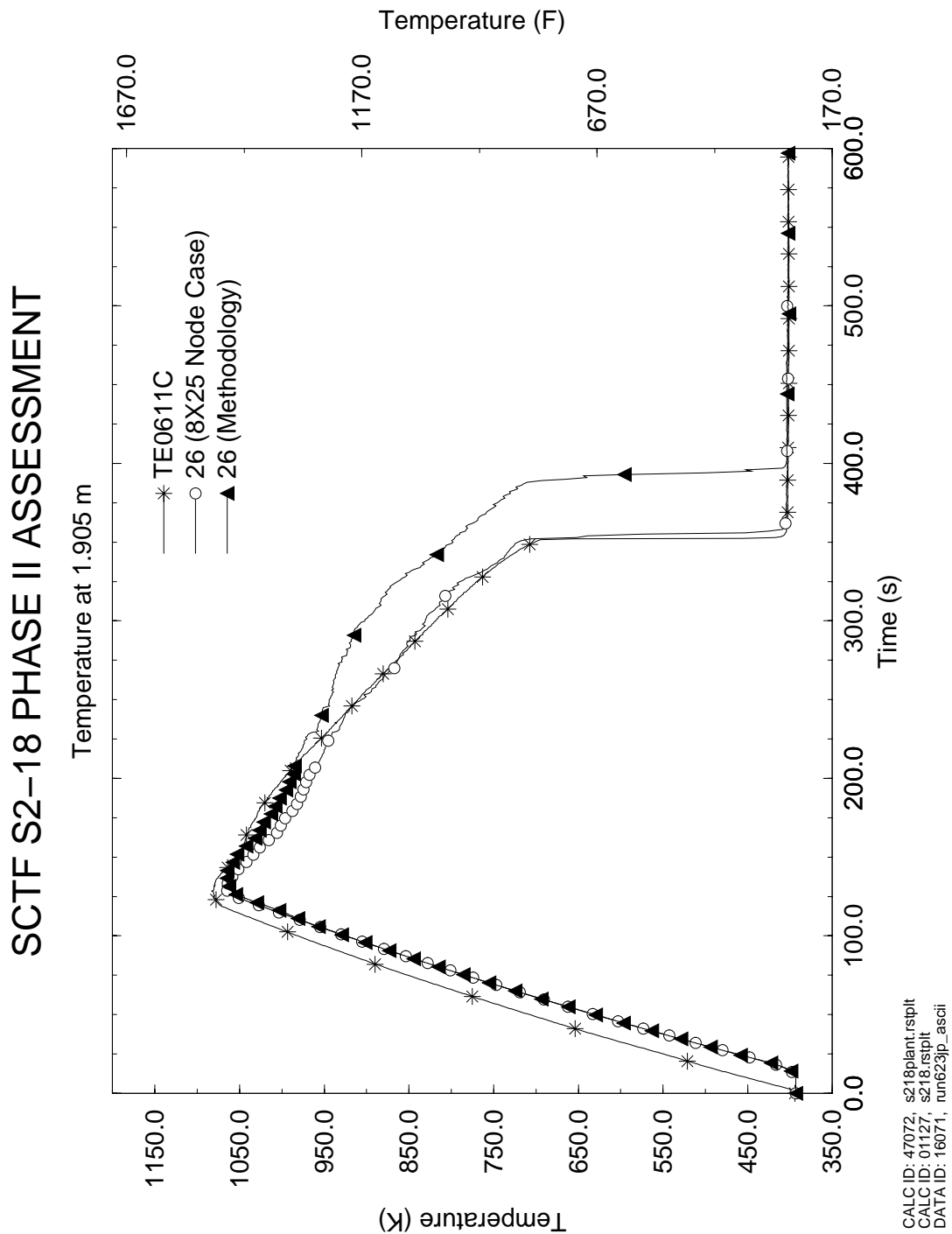


Figure 4.134 Temperature Comparison at 1.905 m, SCTF S2-18

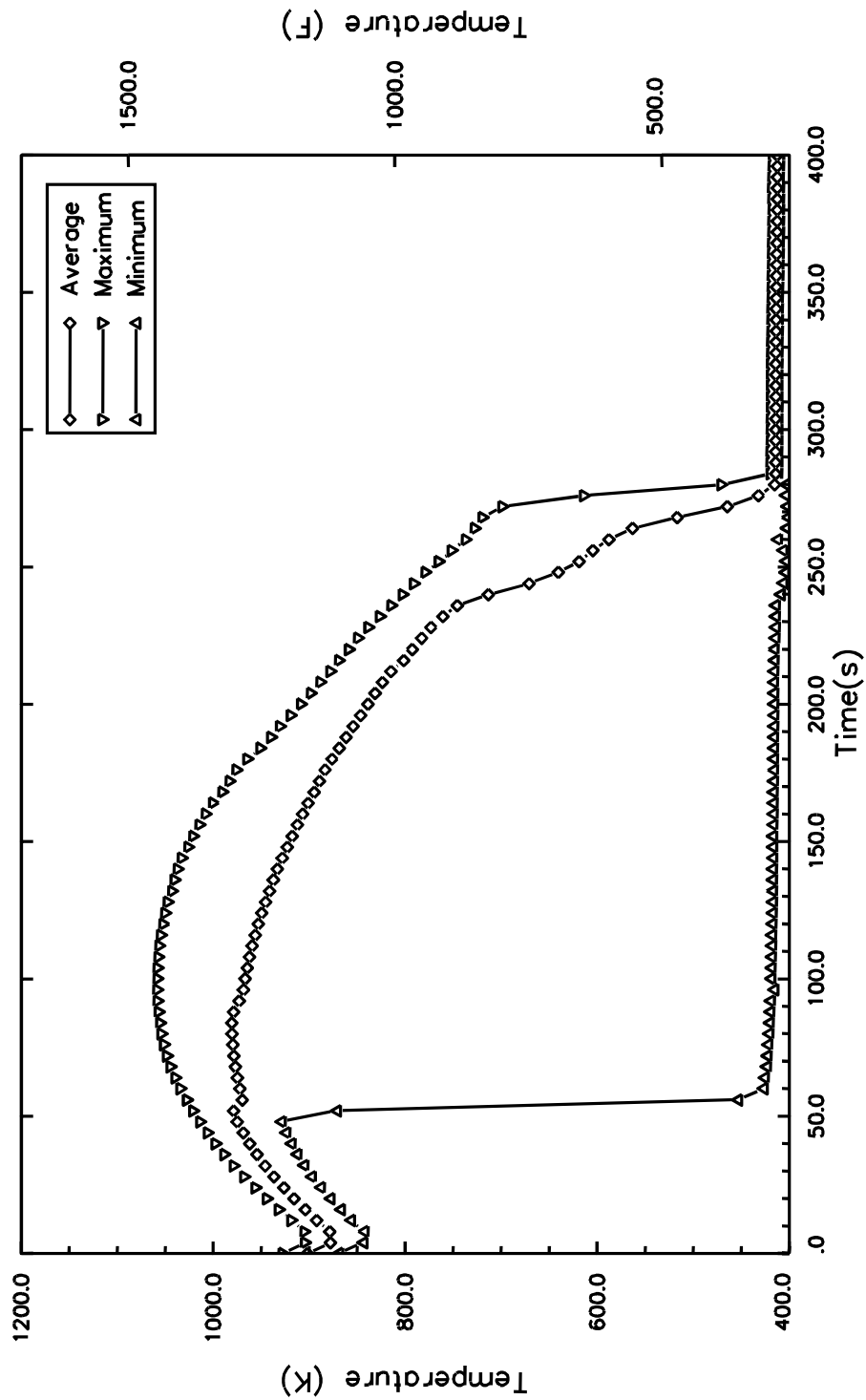


Figure 4.135 Thermocouple Variation Range at the PCT Elevation, ACHILLES ISP 25

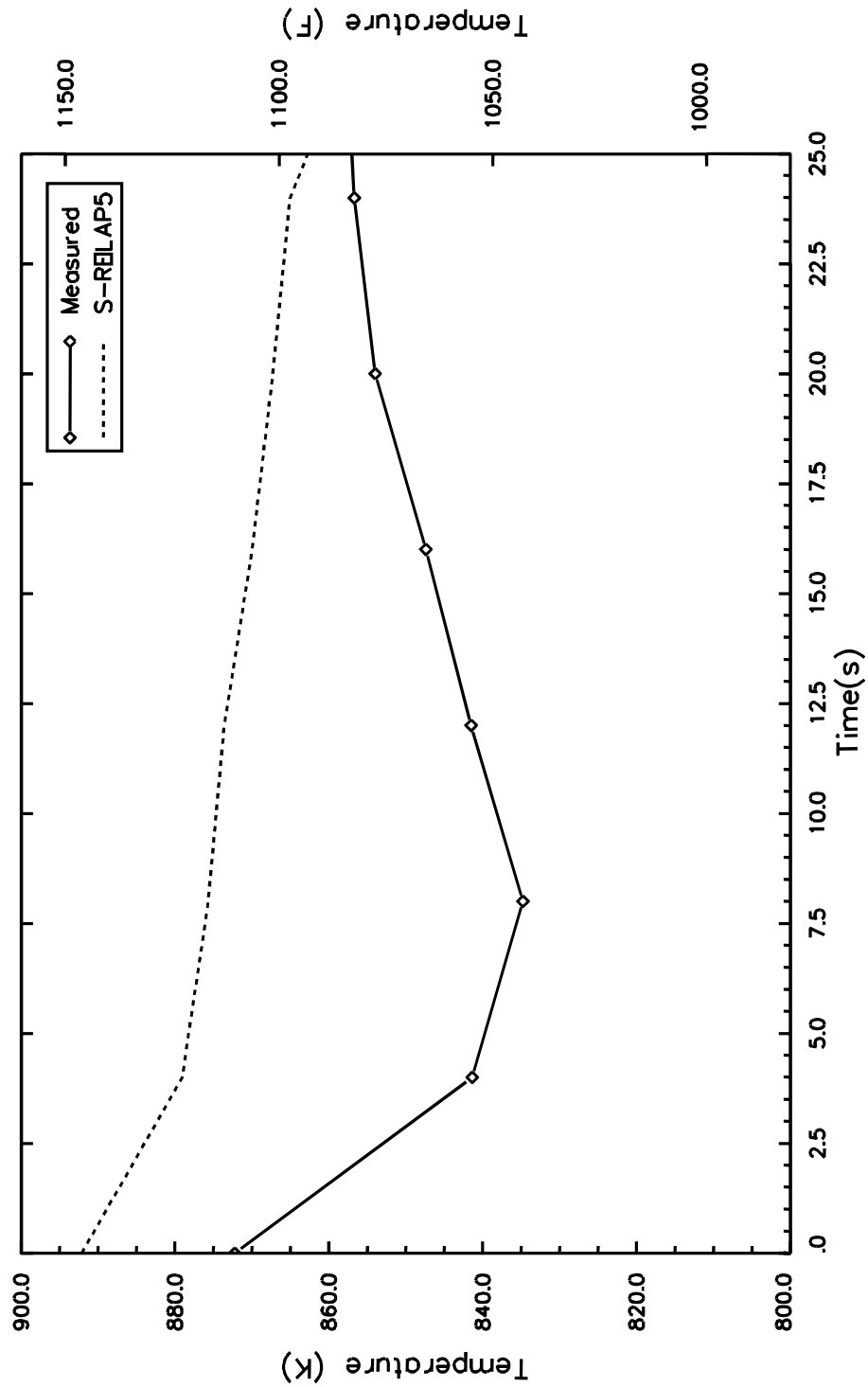


Figure 4.136 Nitrogen Insurge Impact at 1.08 m, ACHILLES ISP 25

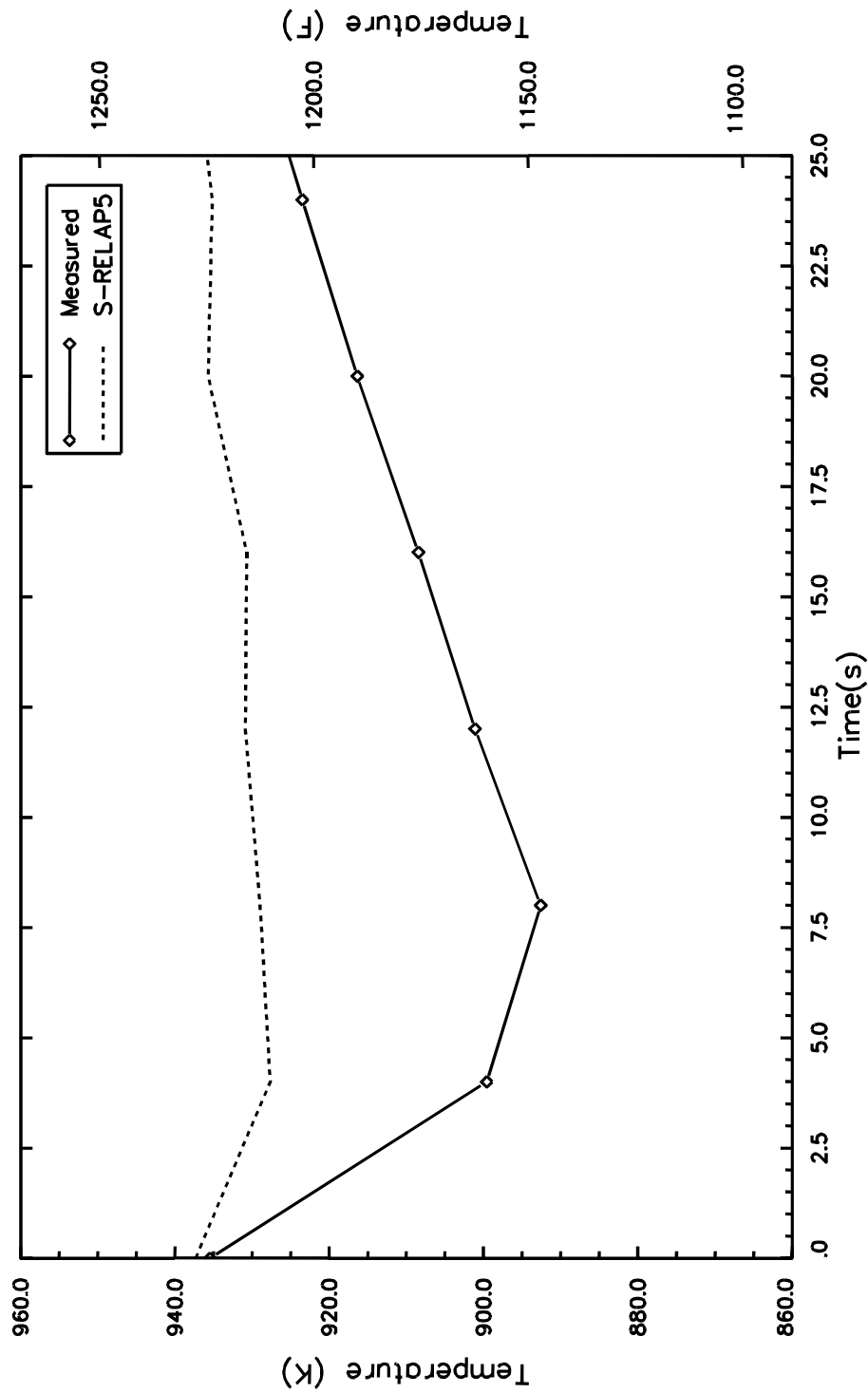


Figure 4.137 Nitrogen Insurge Impact at 1.81 m, ACHILLES ISP 25

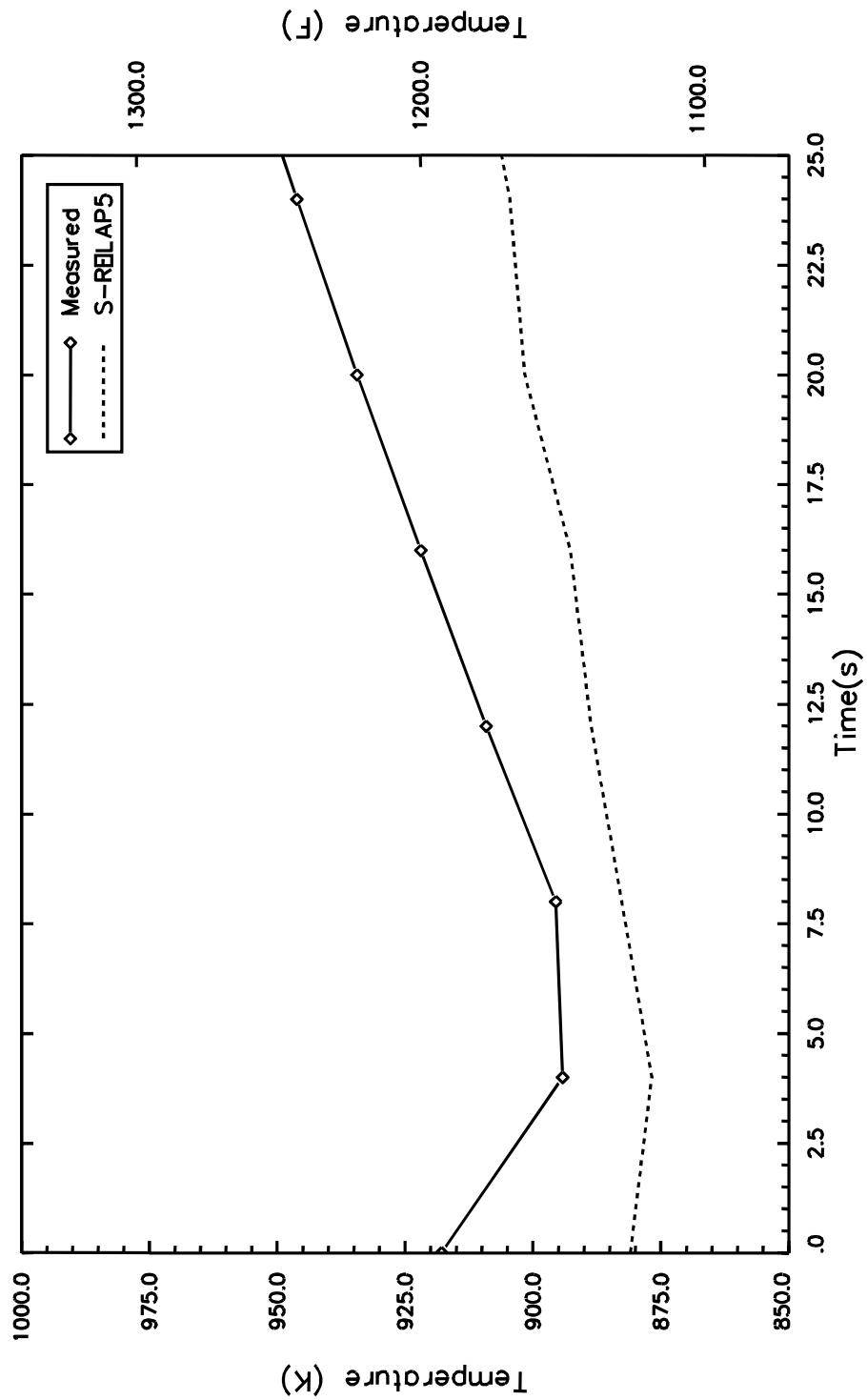


Figure 4.138 Nitrogen Insurge Impact at 2.13 m, ACHILLES ISP 25

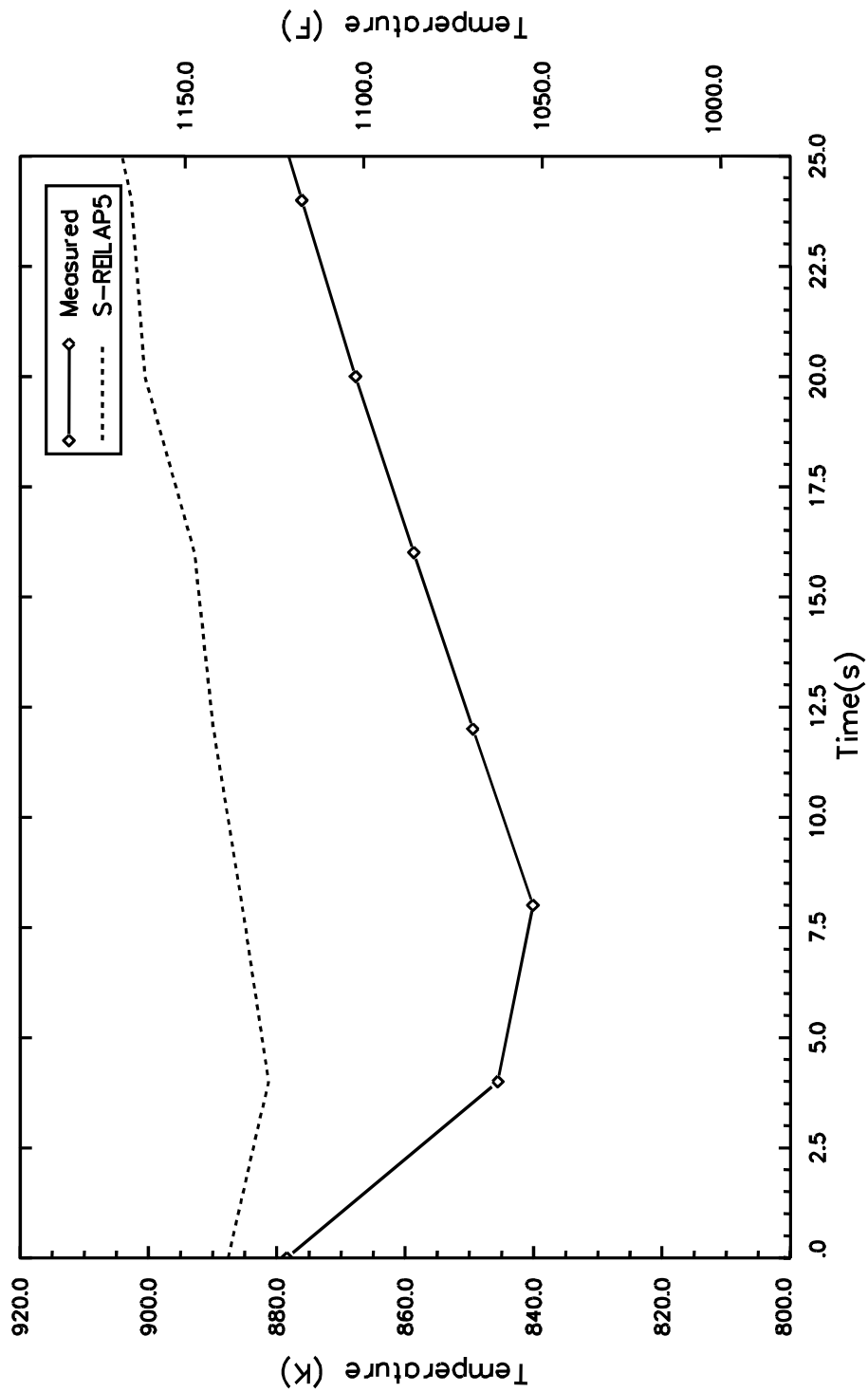


Figure 4.139 Nitrogen Insurge Impact at 2.33 m, ACHILLES ISP 25

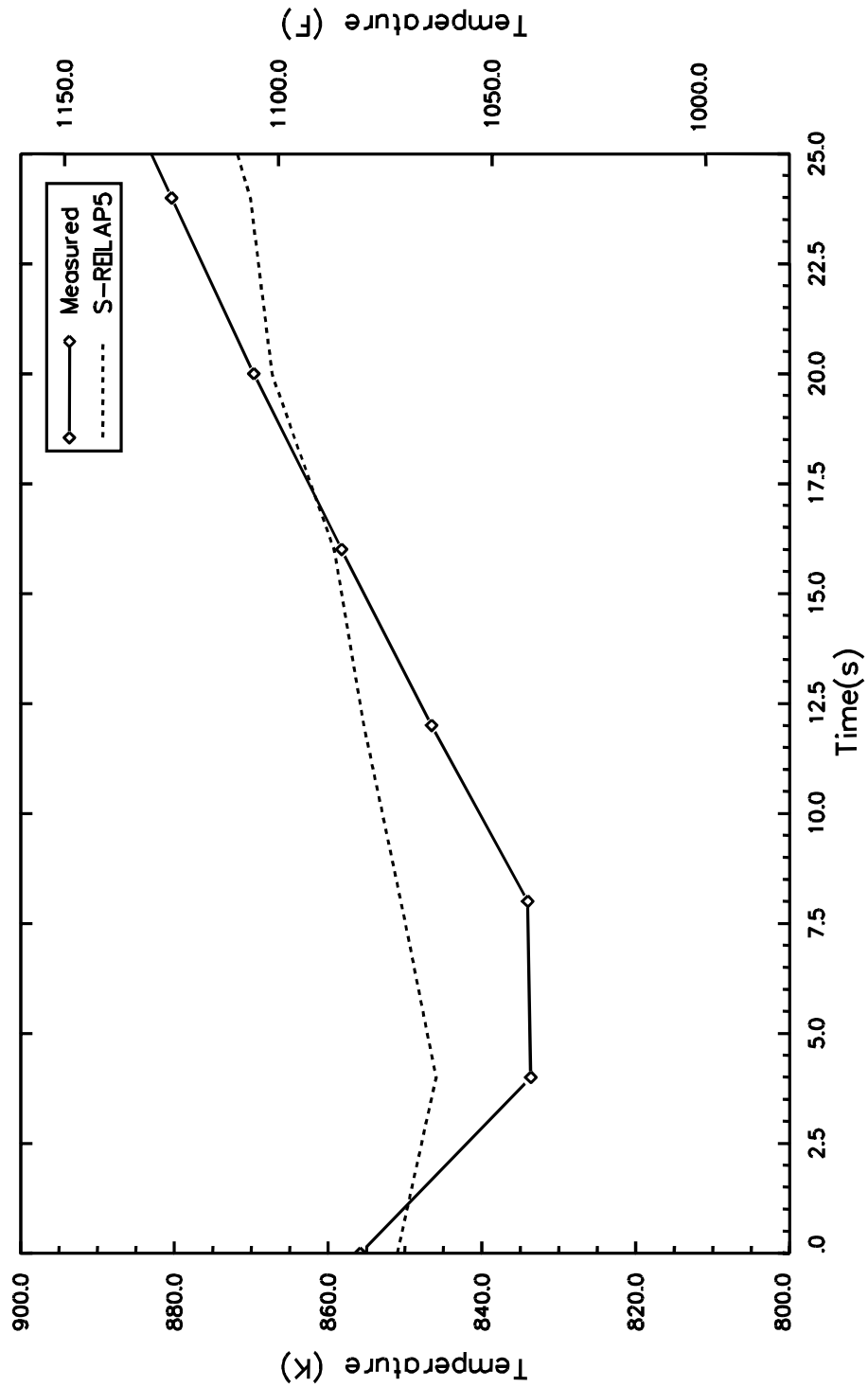


Figure 4.140 Nitrogen Insurge Impact at 2.65 m, ACHILLES ISP 25

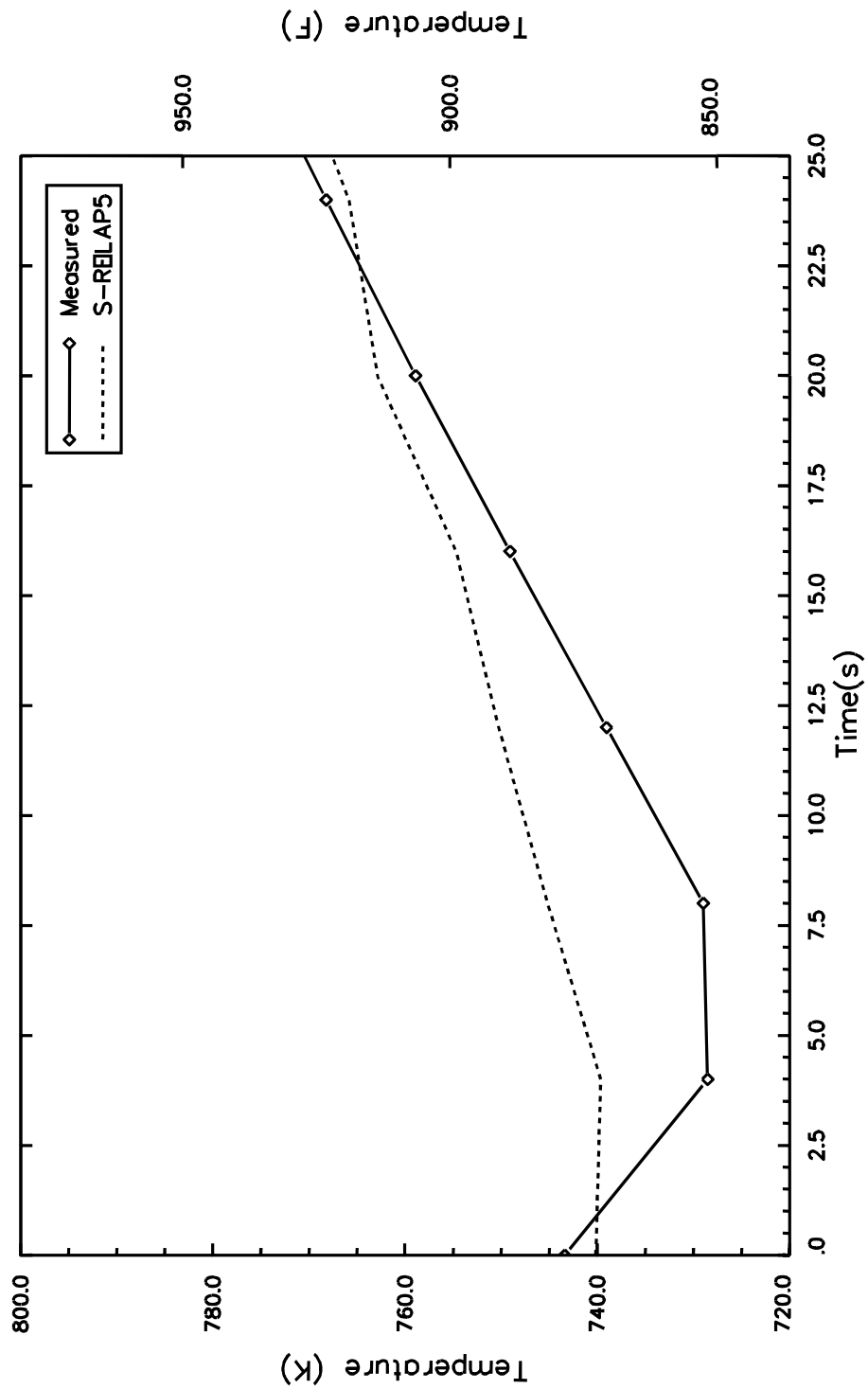


Figure 4.141 Nitrogen Insurge Impact at 3.18 m, ACHILLES ISP 25

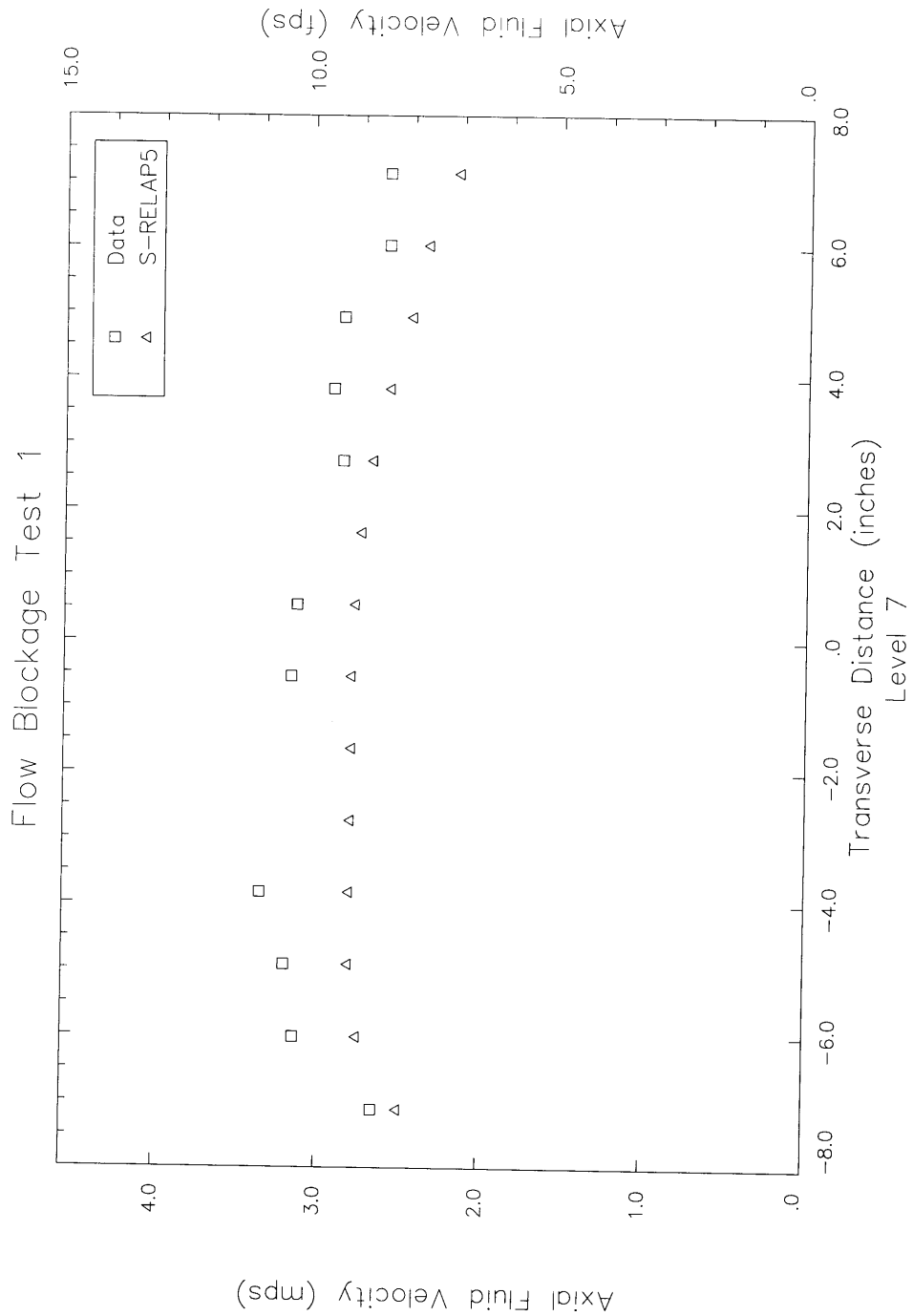


Figure 4.142 Axial Velocities at 32.5 Inches, Asymmetric Flow - Test 1

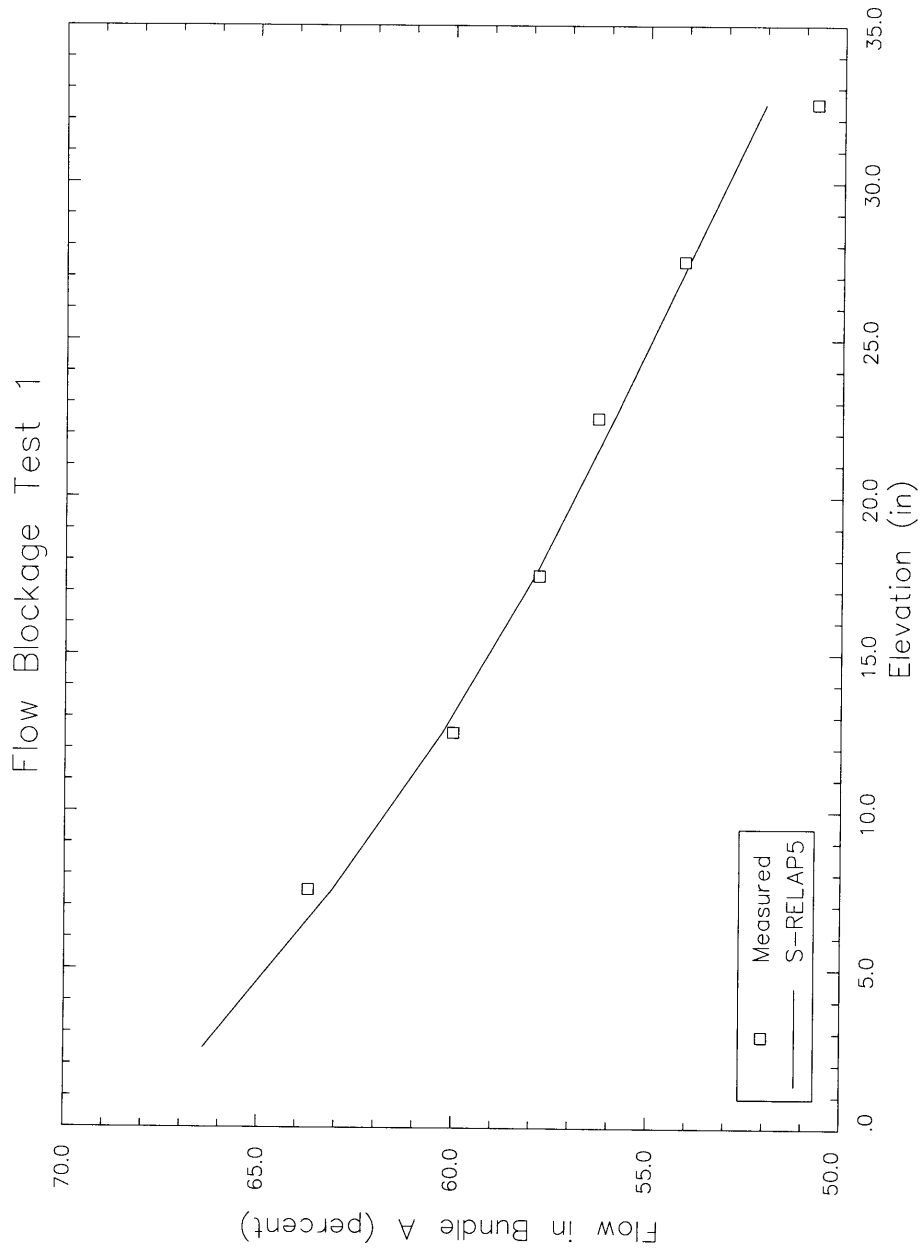


Figure 4.143 Axial Flow Fractions for Asymmetric Flow - Test 1

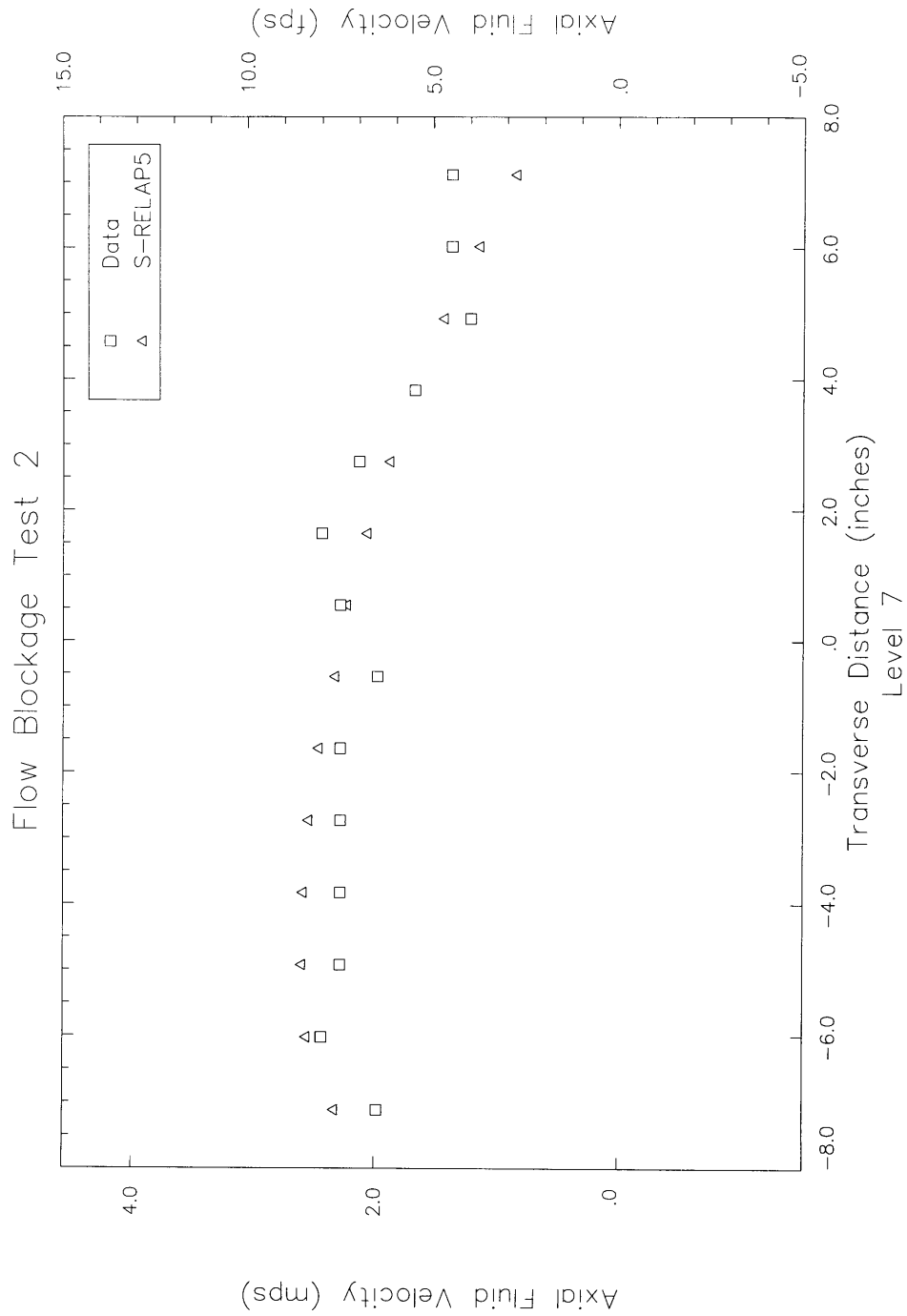


Figure 4.144 Axial Velocities at 32.5 Inches, for Asymmetric Flow - Test 2

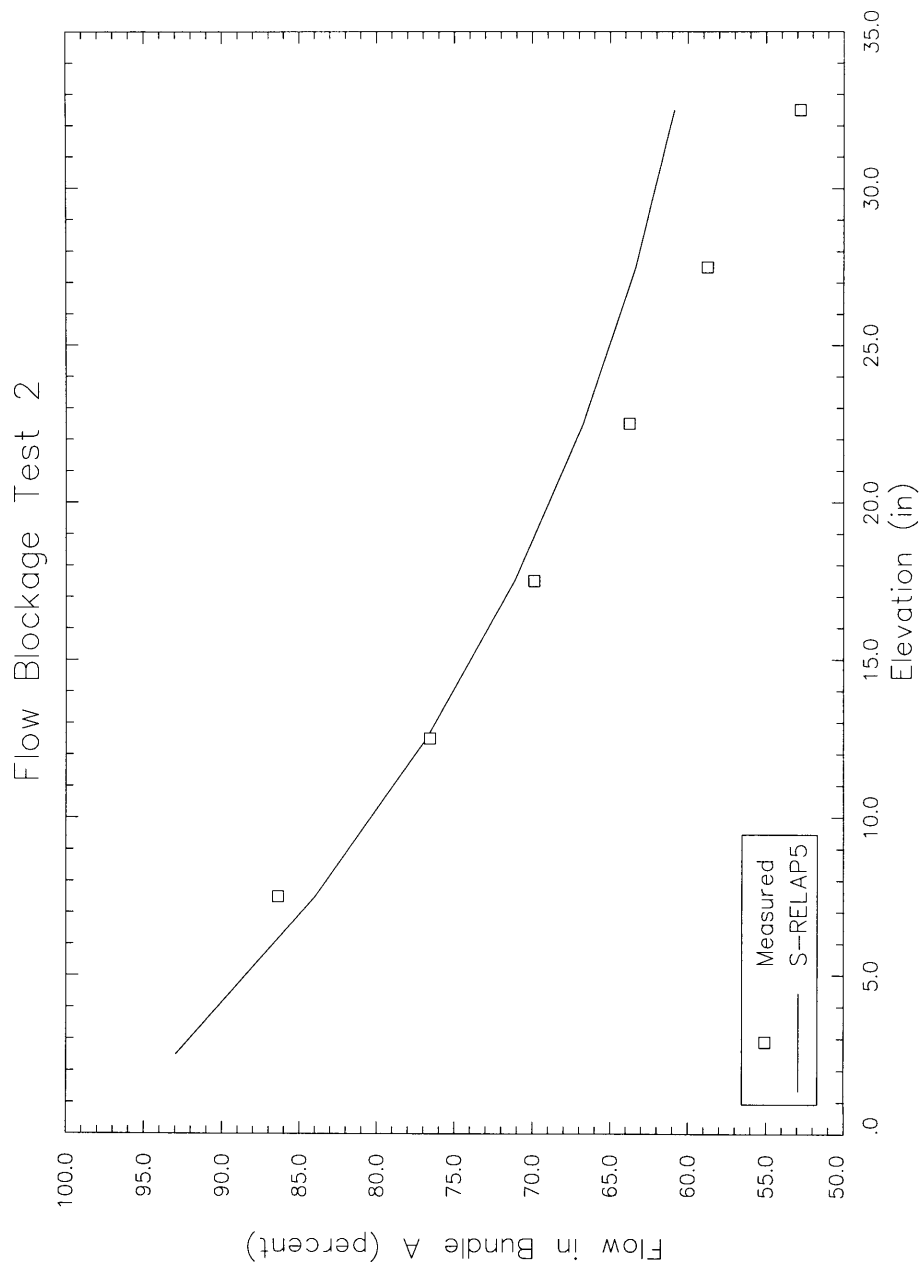


Figure 4.145 Axial Flow Fractions for Asymmetric Flow – Test 2

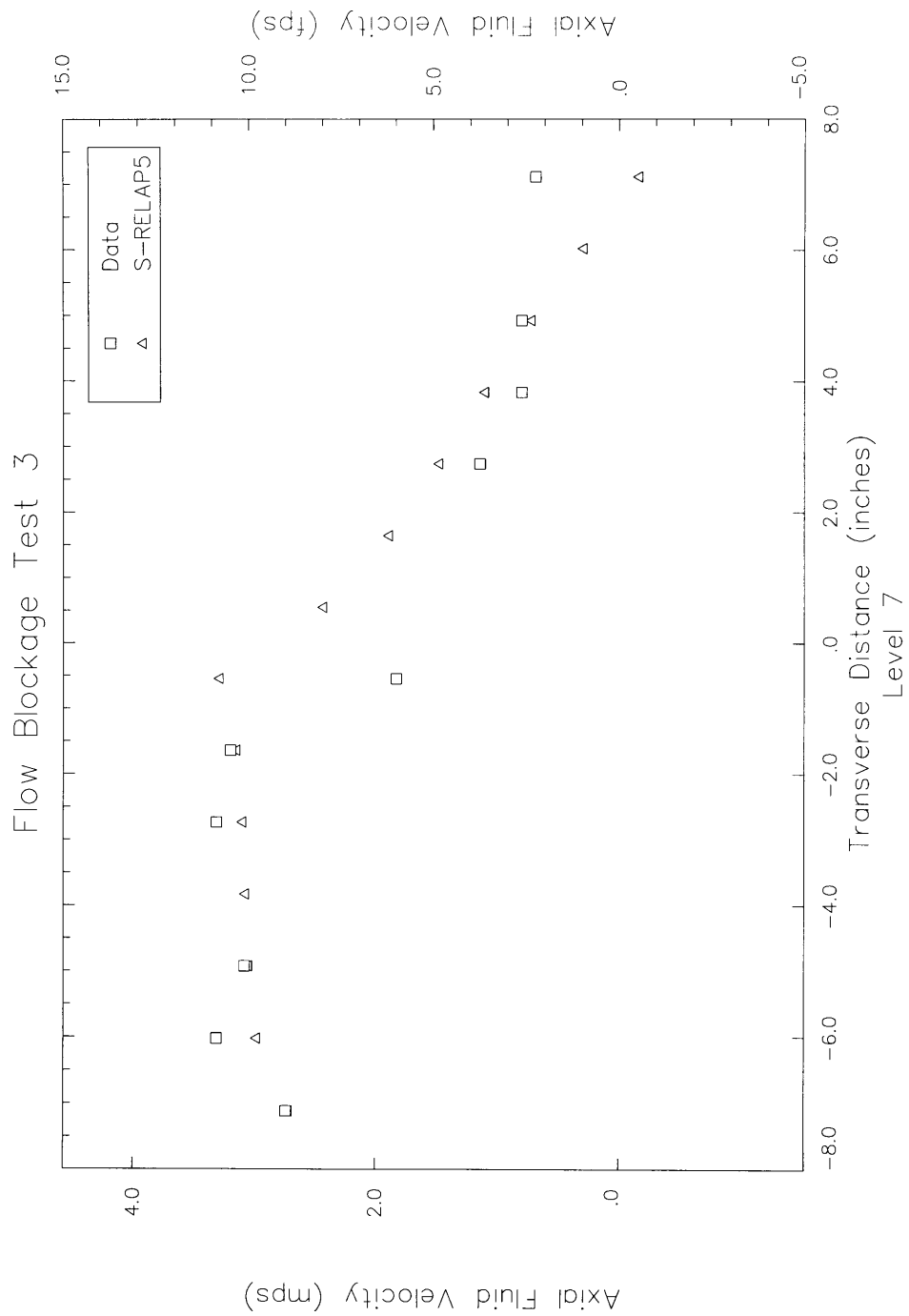


Figure 4.146 Axial Velocities at 32.5 Inches, for Asymmetric Flow - Test 3

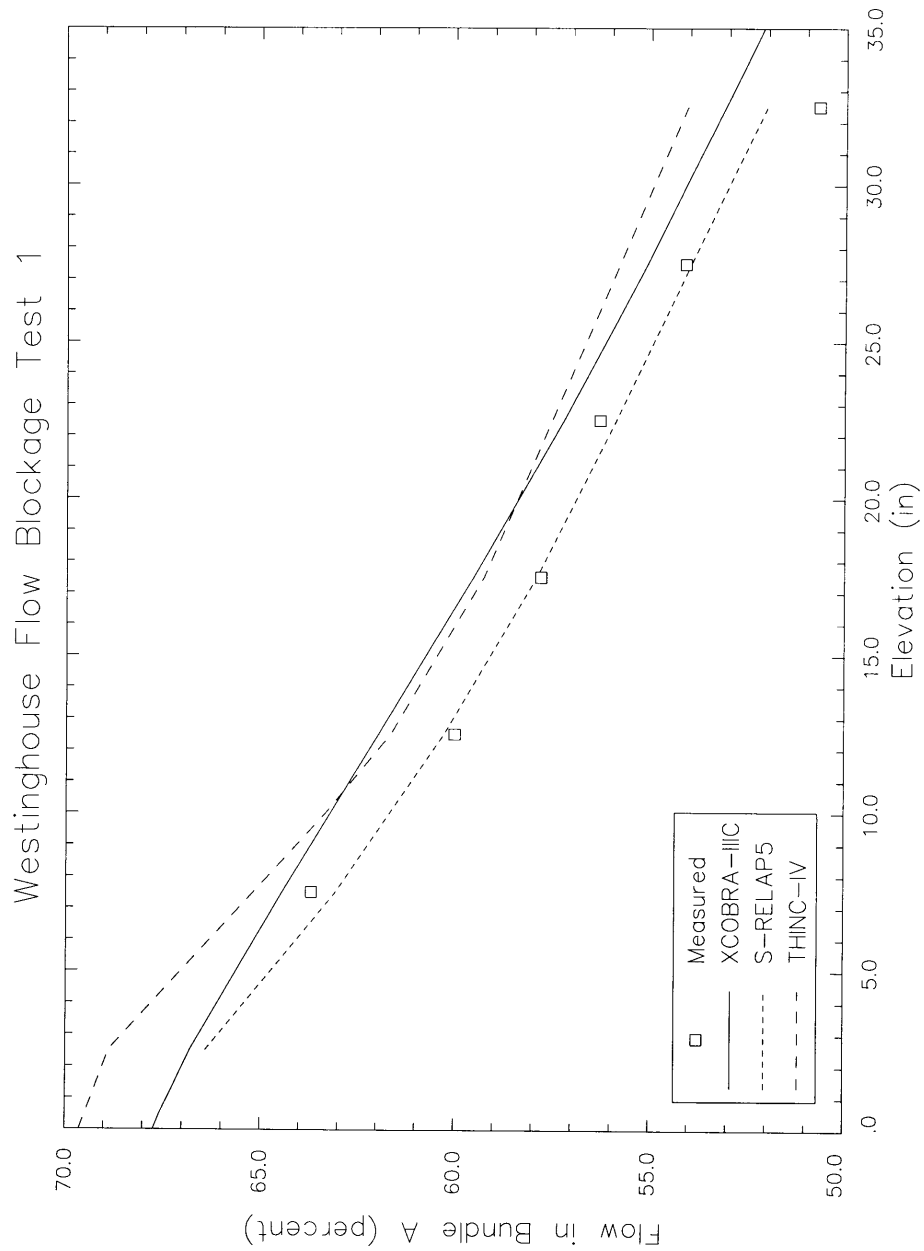


Figure 4.147 Comparison of S-RELAP5 with Design Codes for Asymmetric Flow - Test 1

LOFT L2-3 S-RELAP5 ANALYSIS PLOT FILE NAME: 012-3_pct_00.eps, JOB ID: make_pct_plot.o3184, DATE: Tue Jul 17 09:59:43 PDT 2001

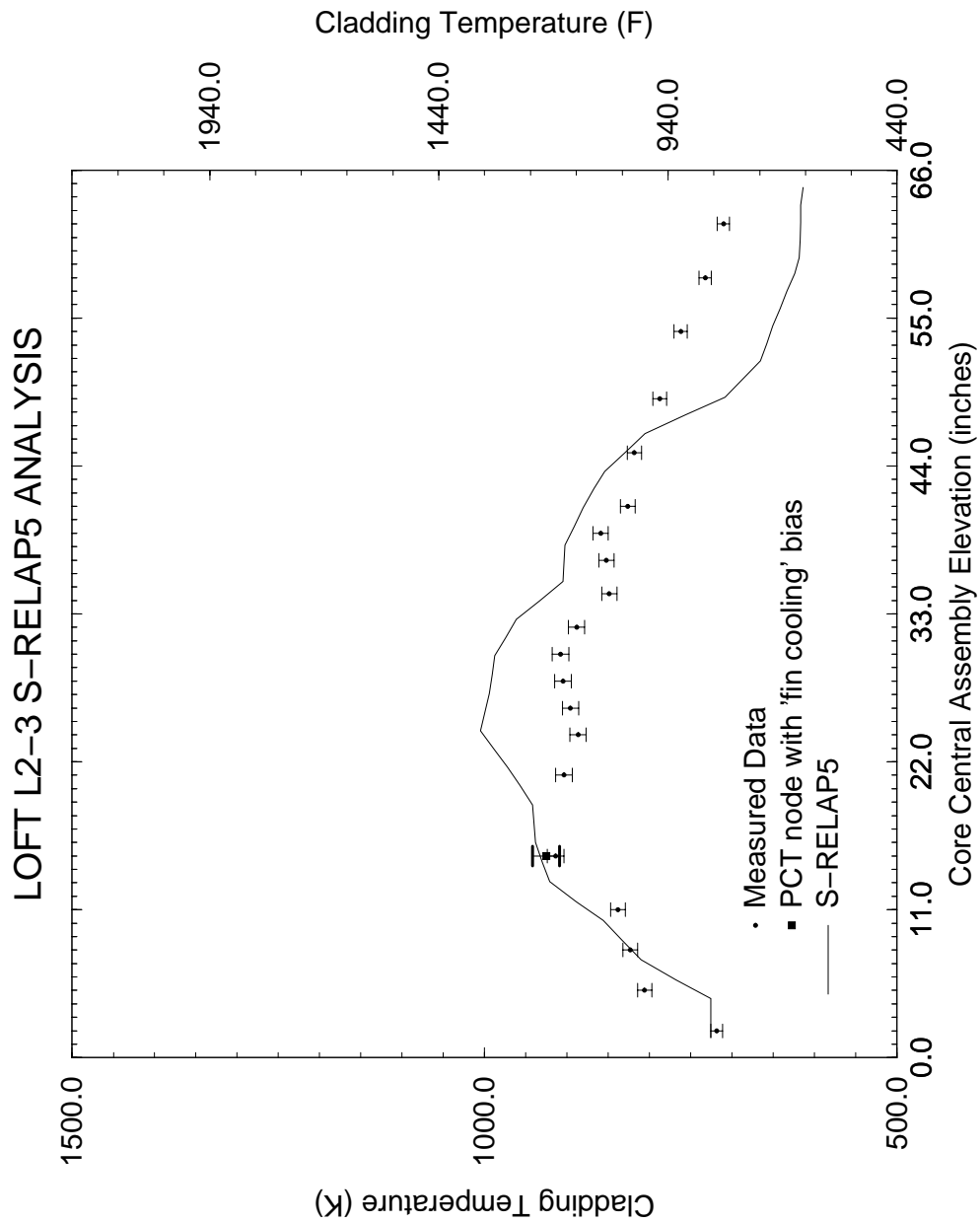


Figure 4.148 Comparison of PCTs Versus Core Elevations LOFT Test L2-3 with S-RELAP5

LOFT L2-5 S-RELAP5 ANALYSIS PLOT FILE NAME: 012-5_pct_00.eps, JOB ID: make_pct_plot.o3199, DATE: Thu Jul 19 14:43:03 PDT 2001

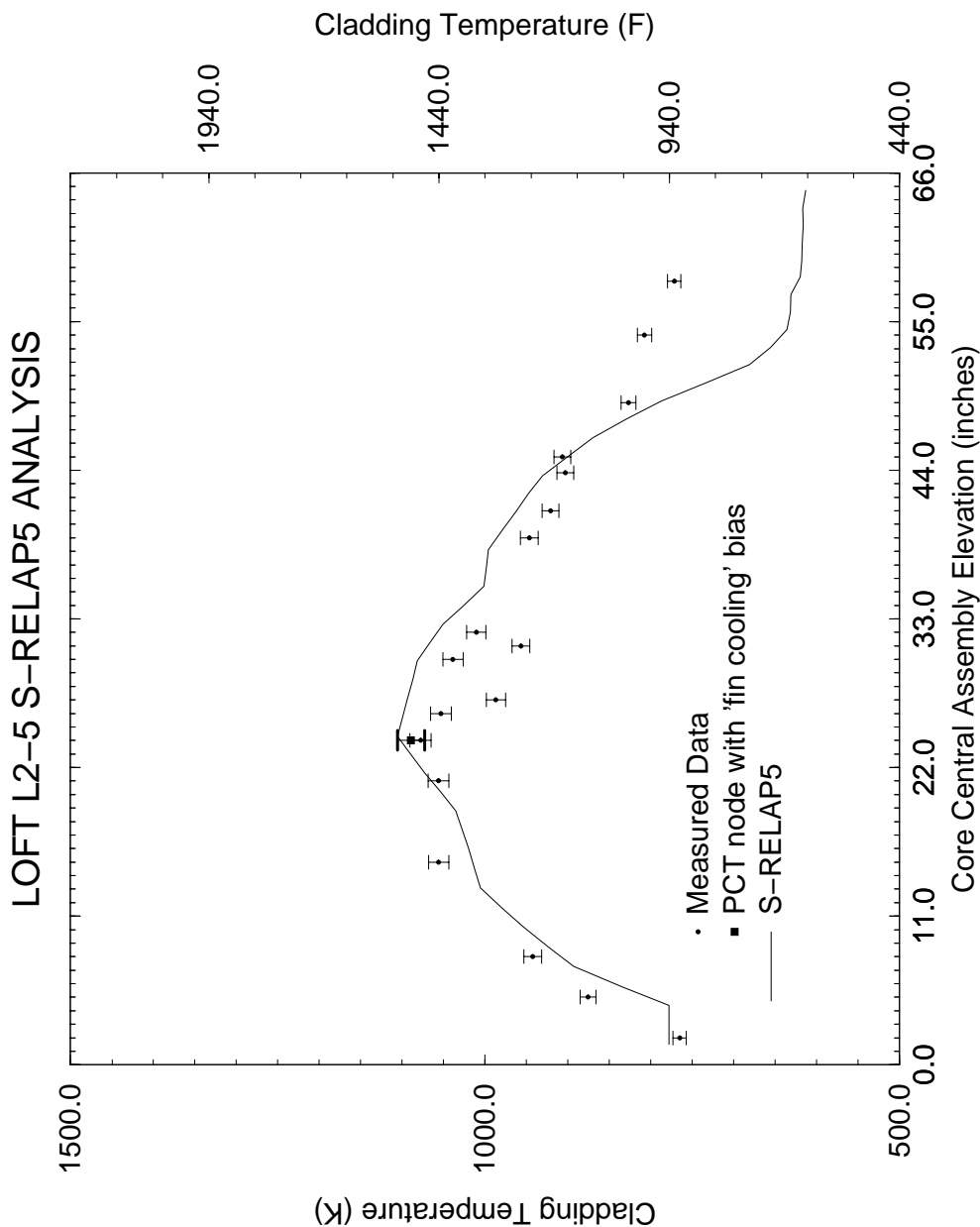


Figure 4.149 Comparison of PCTs Versus Core Elevations LOFT Test L2-5 with S-RELAP5

LOFT LP-02-6 S-RELAP5 ANALYSIS PLOT FILE NAME: 012-6_pct_00.eps, JOB ID: make_pct_plot.o3201, DATE: Thu Jul 19 15:14:29 PDT 2001

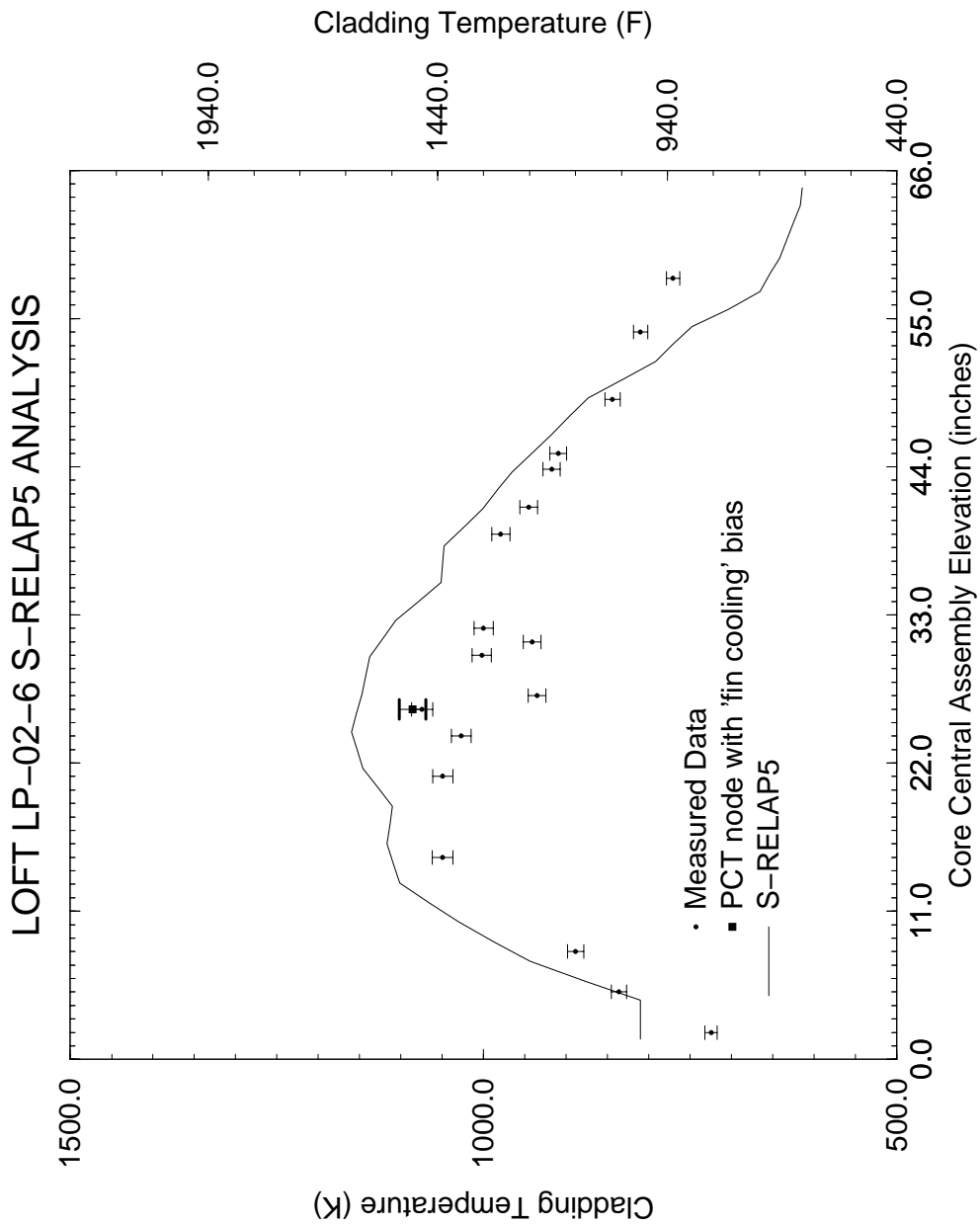


Figure 4.150 LOFT Test LP-02-6 Comparison of PCTs Versus Core Elevations

LOFT LP-LB-1 S-RELAP5 ANALYSIS PLOT FILE NAME: 0lb-1_pct_00.eps, JOB ID: make_pct_plot.c3185, DATE: Tue Jul 17 10:00:21 PDT 2001

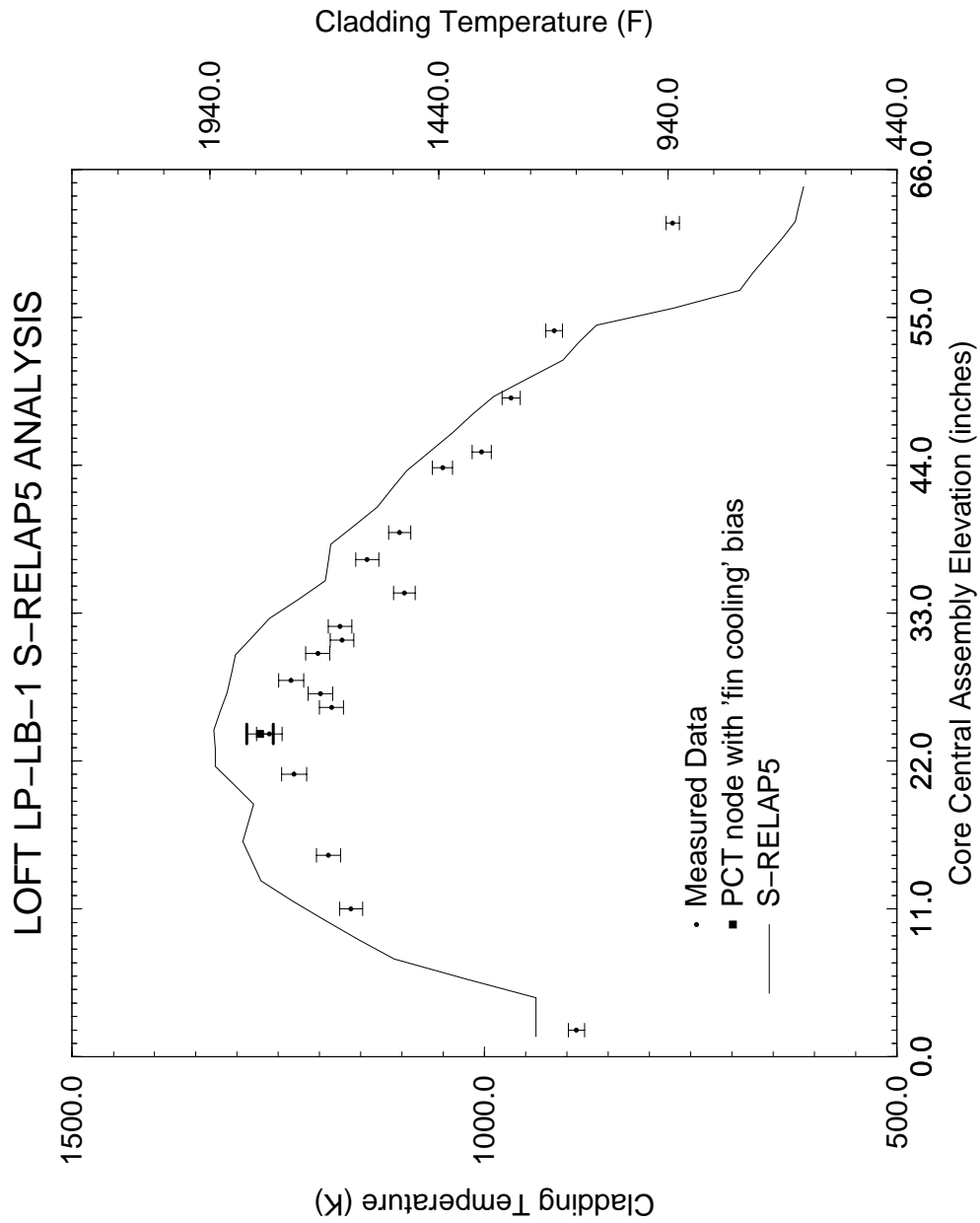


Figure 4.151 LOFT Test LP-LB-1 Comparison of PCTs Versus Core Elevations

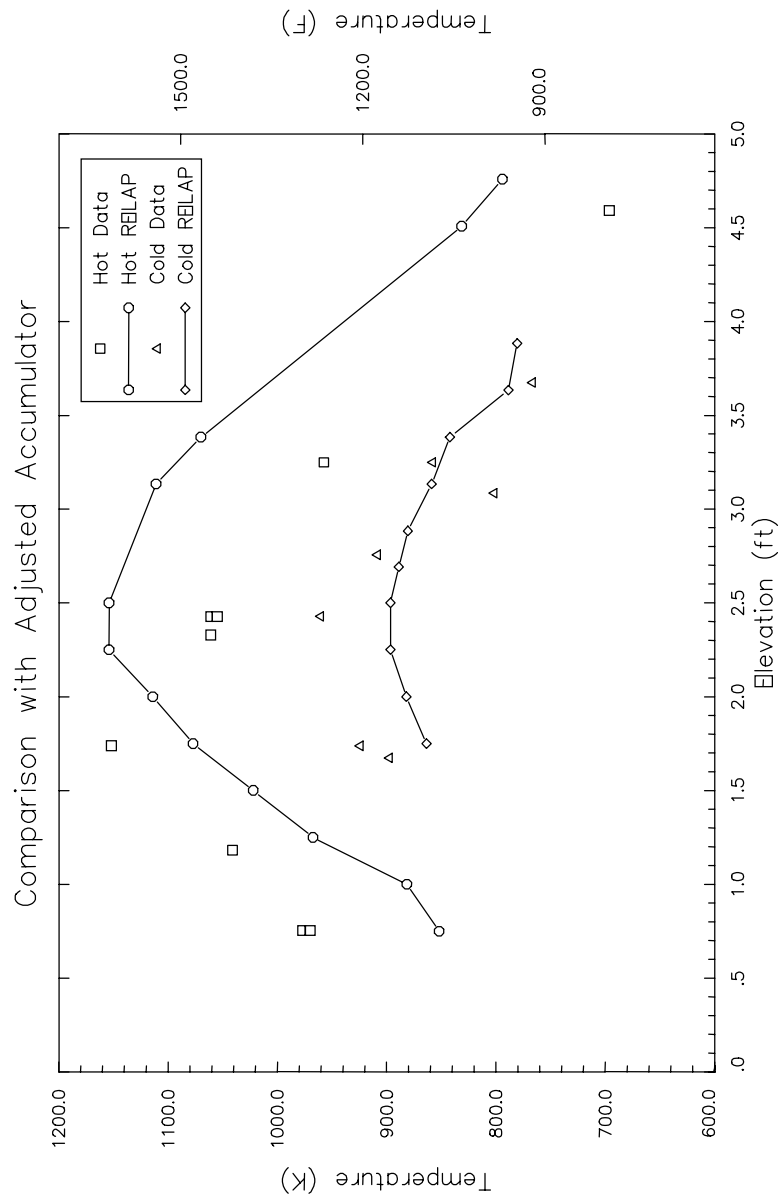


Figure 4.152 Assessment of Semiscale LBLOCA Test S-06-3, PCTs

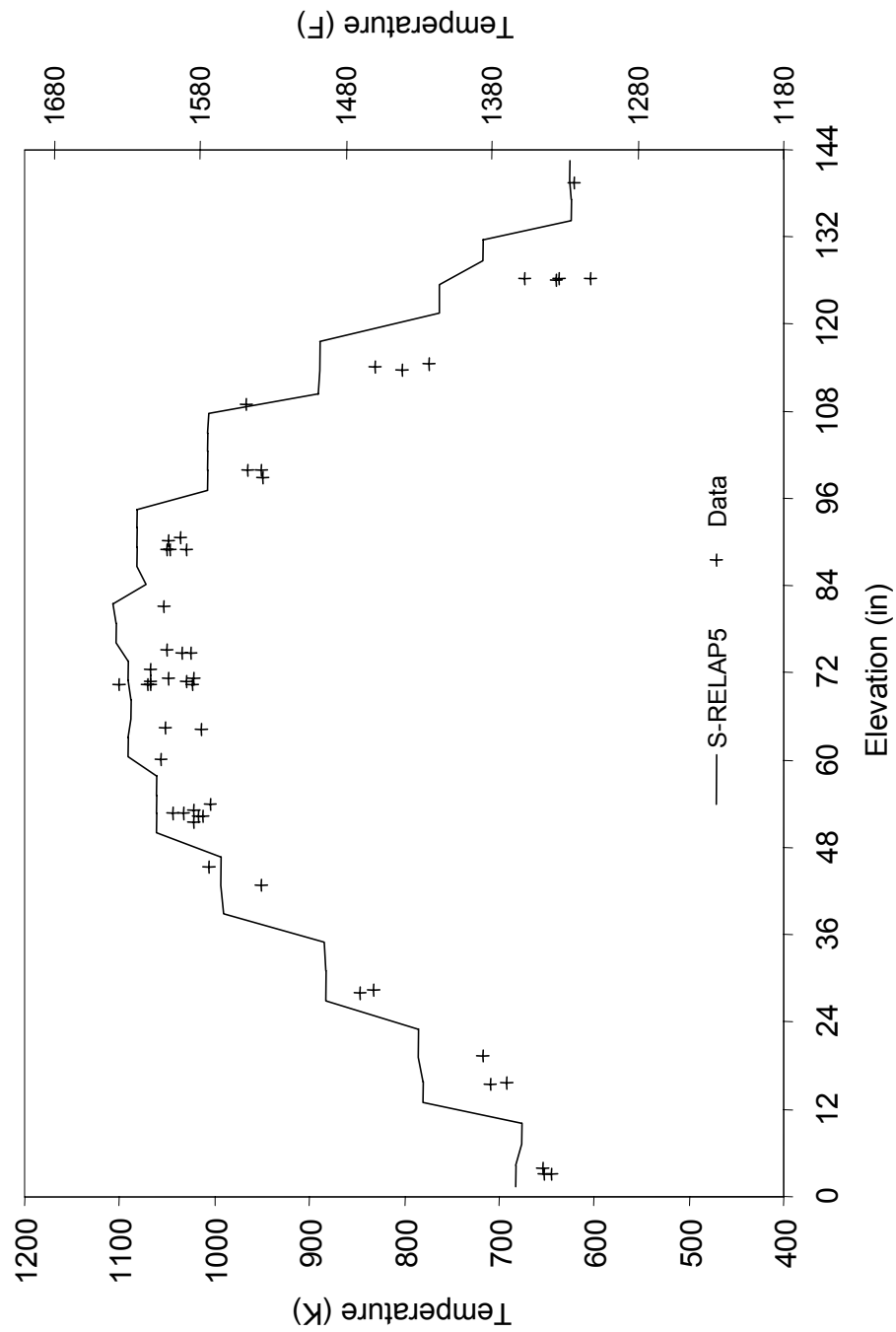


Figure 4.153 Assessment of Semiscale LBLOCA Test S-07-1, PCTs versus Elevation

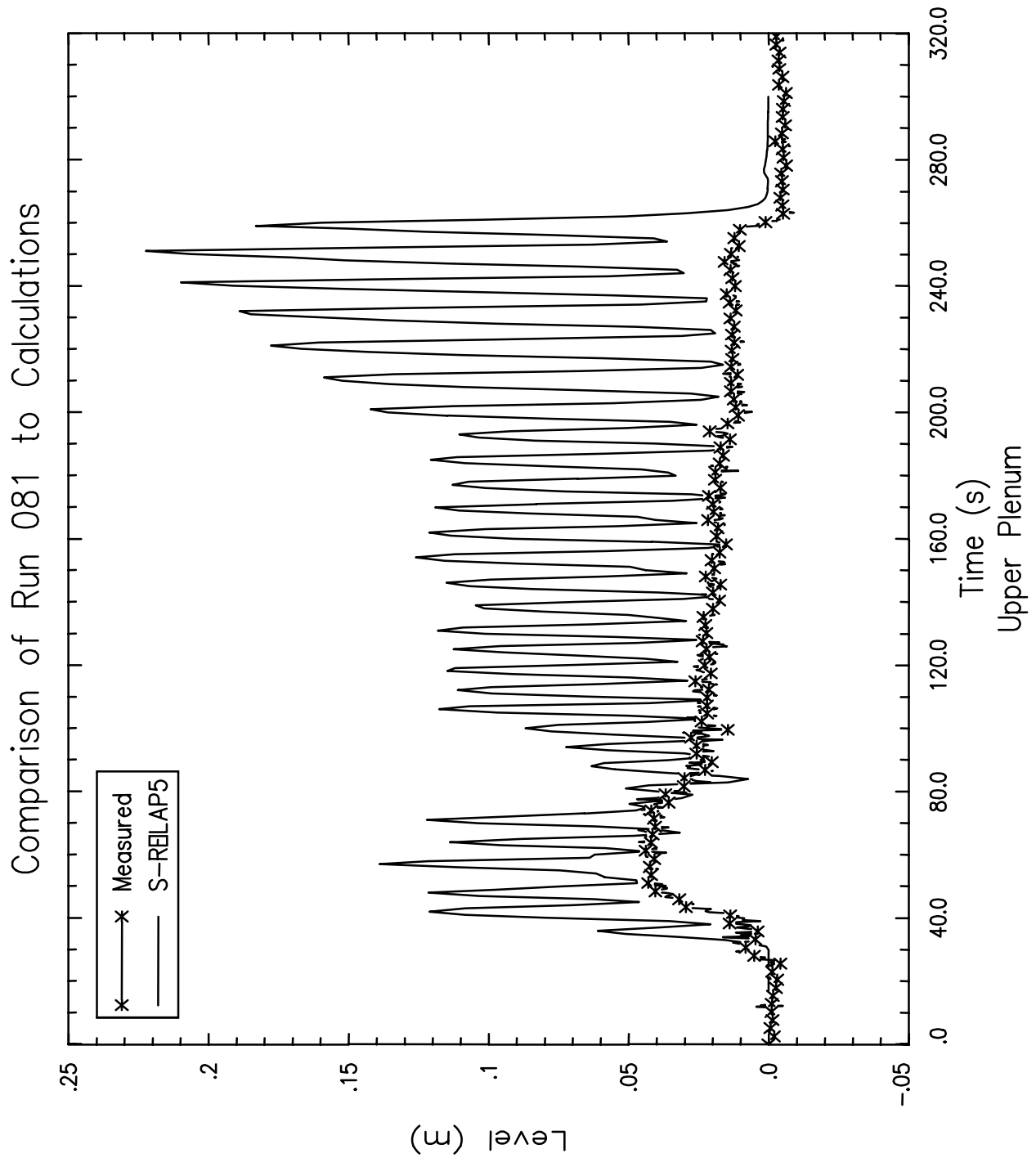


Figure 4.154 Upper Plenum Level, UPTF Test 10, Run 081

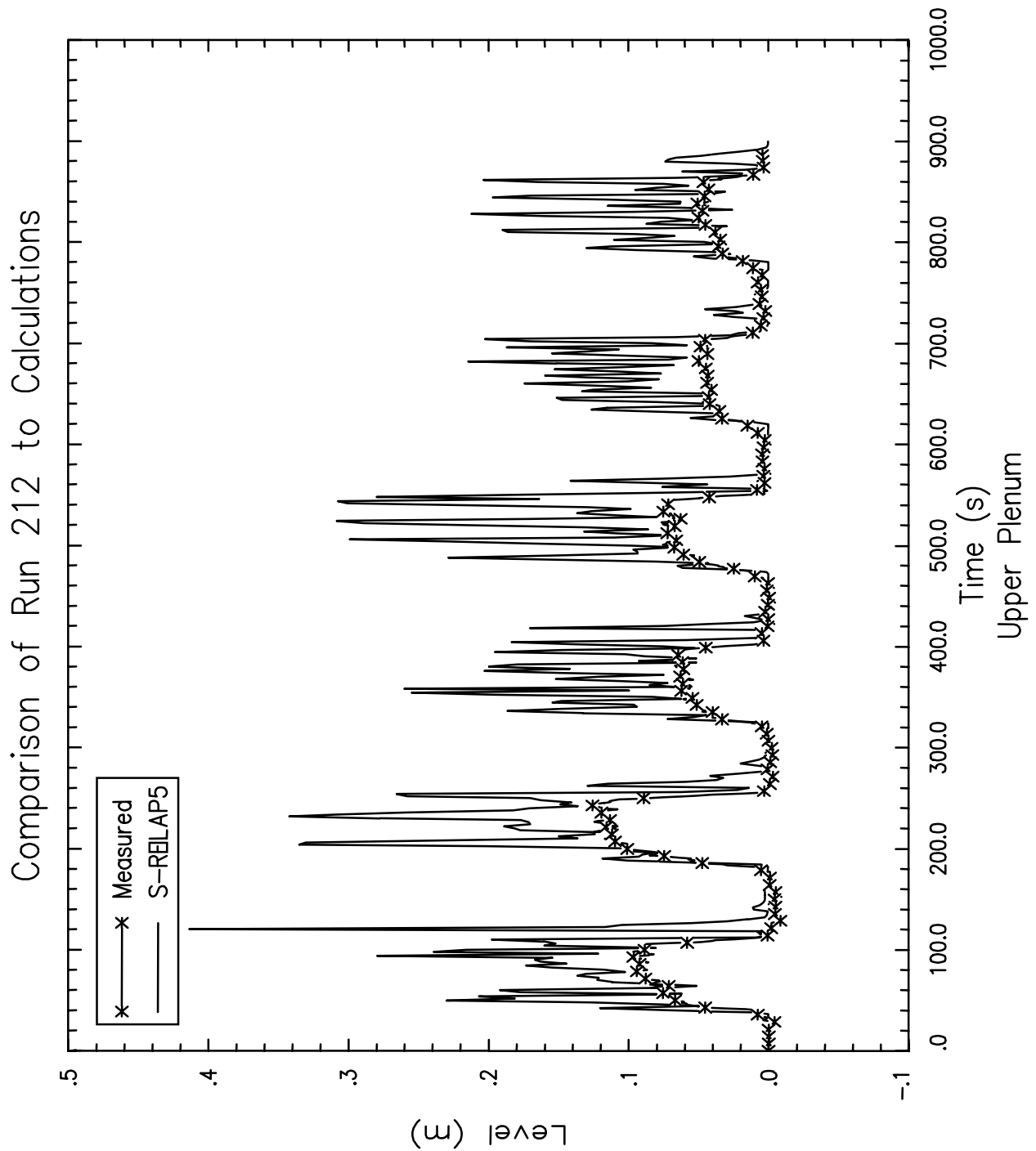


Figure 4.155 Upper Plenum Level, UPTF Test 29 Run 212/211

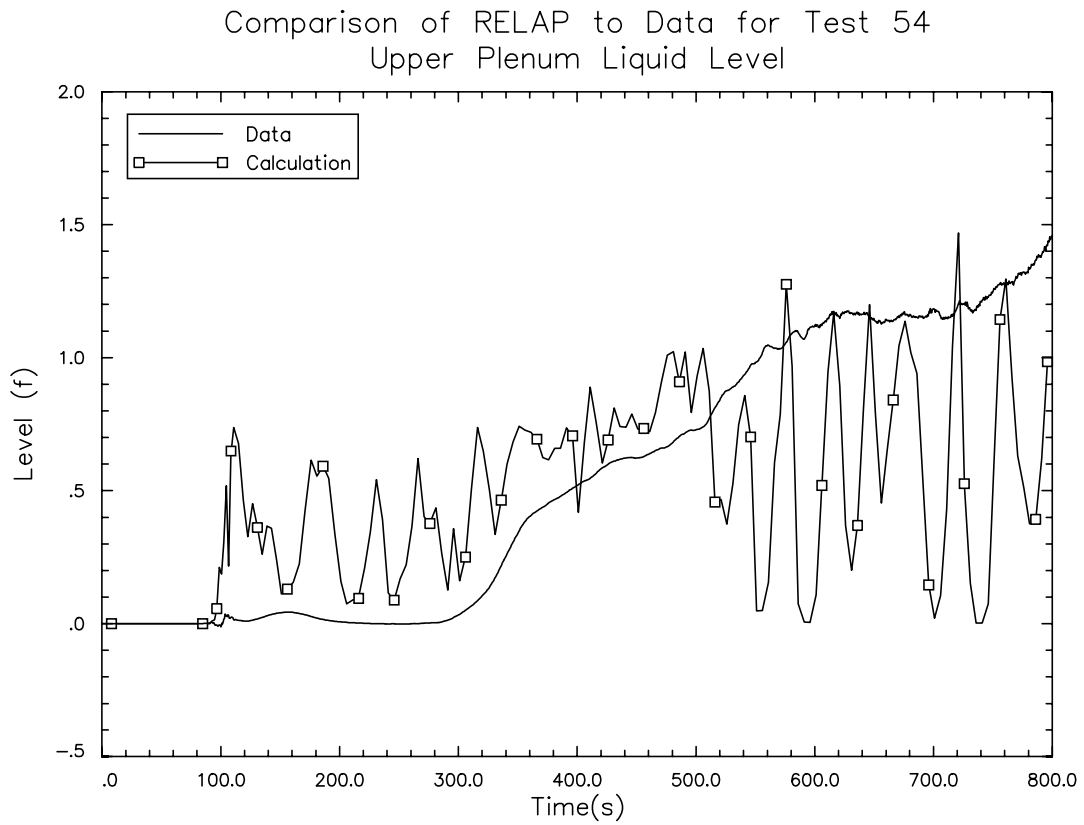


Figure 4.156 Liquid Level in Upper Plenum CCTF Test 54

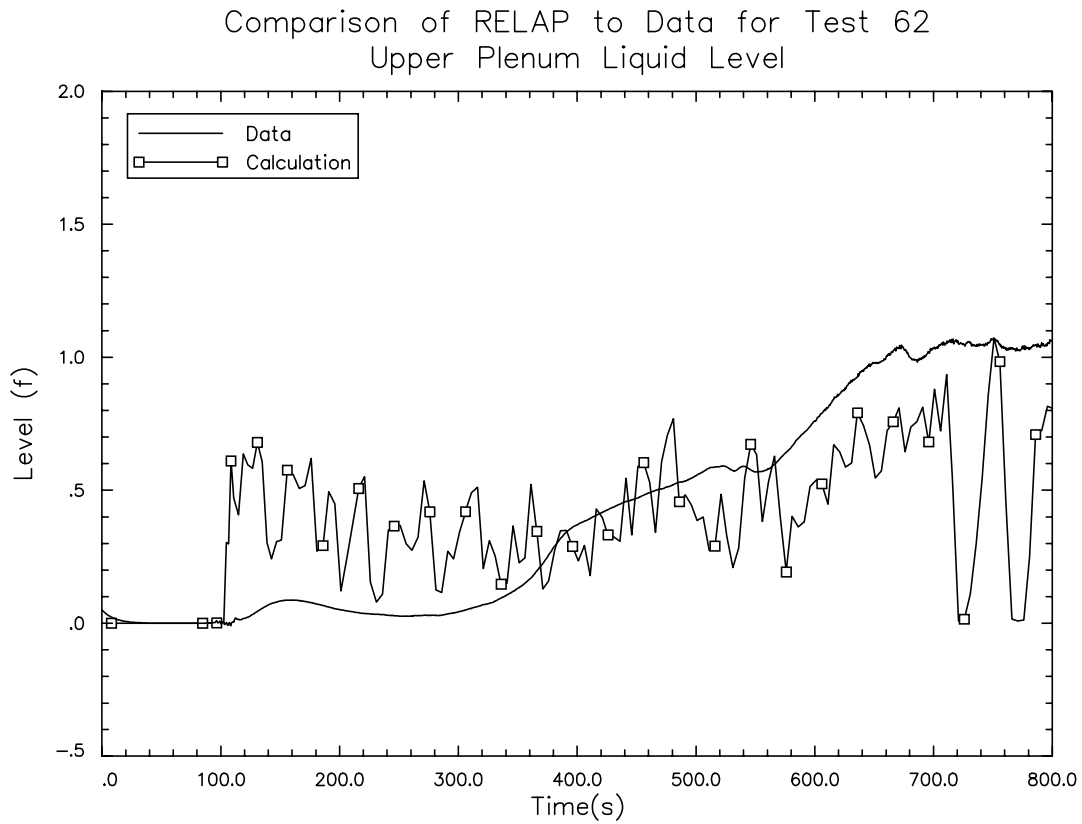


Figure 4.157 Liquid Level in Upper Plenum CCTF Test 62

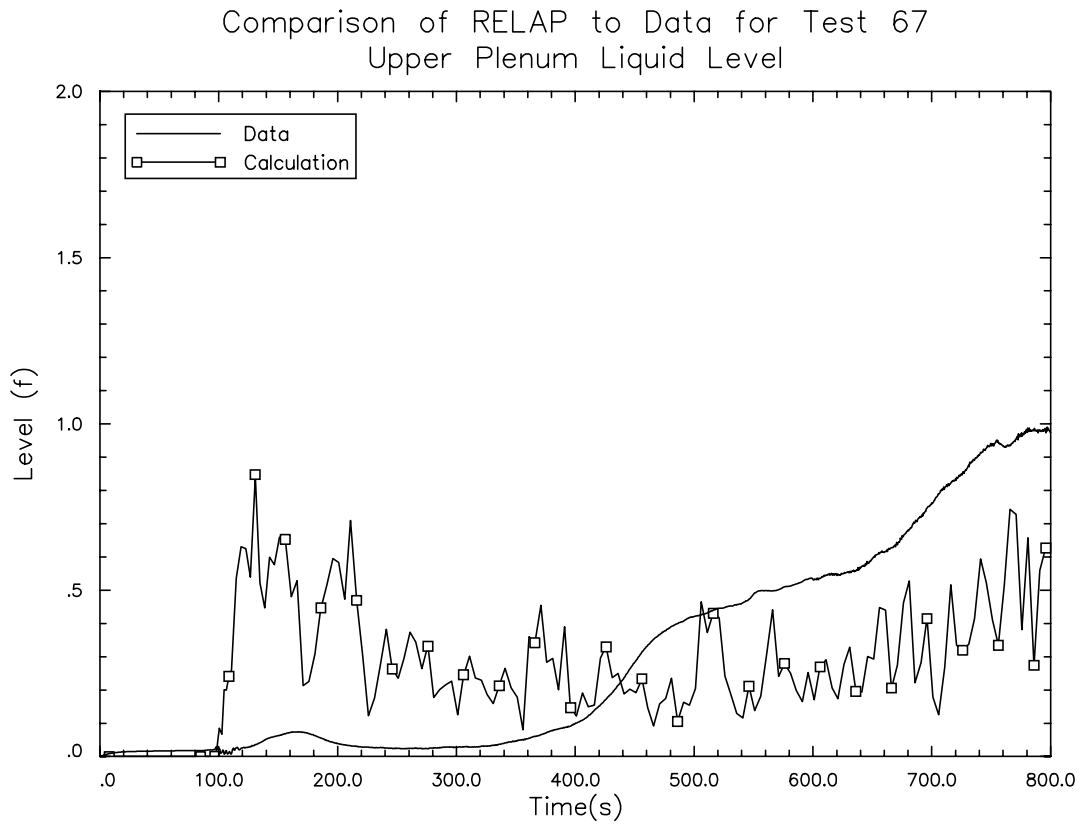


Figure 4.158 Liquid Level in Upper Plenum CCTF Test 67

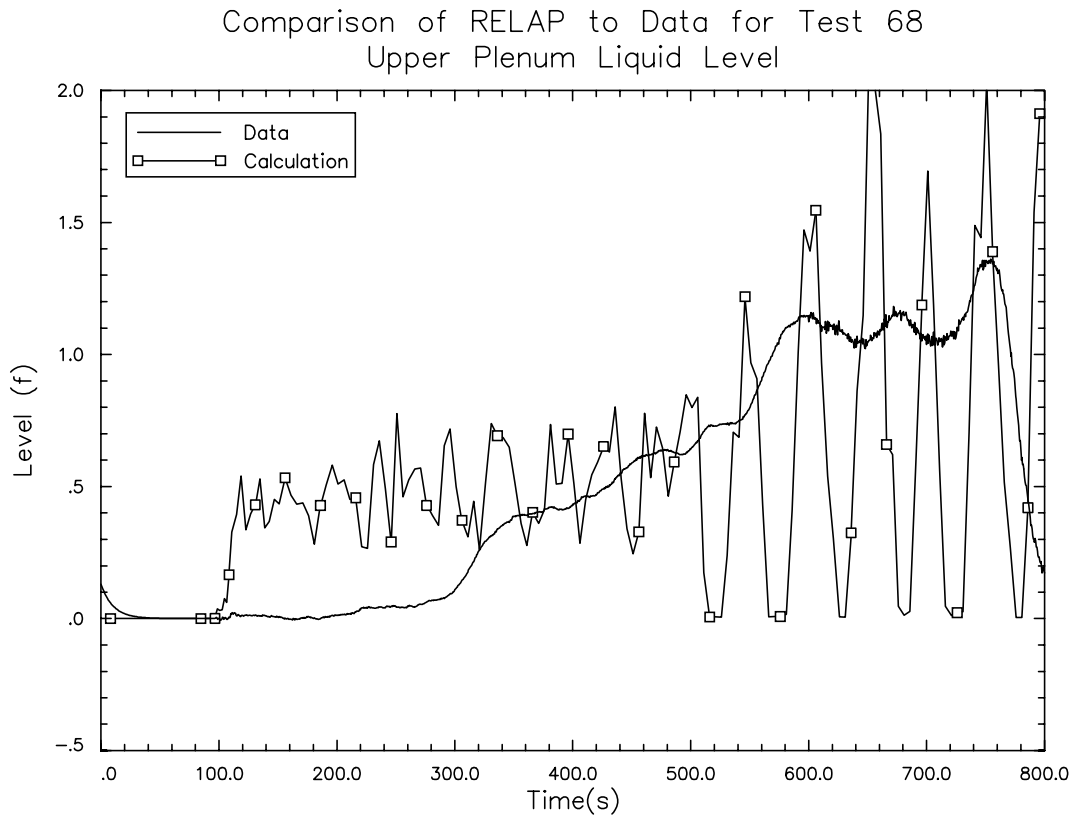


Figure 4.159 Liquid Level in Upper Plenum CCTF Test 68

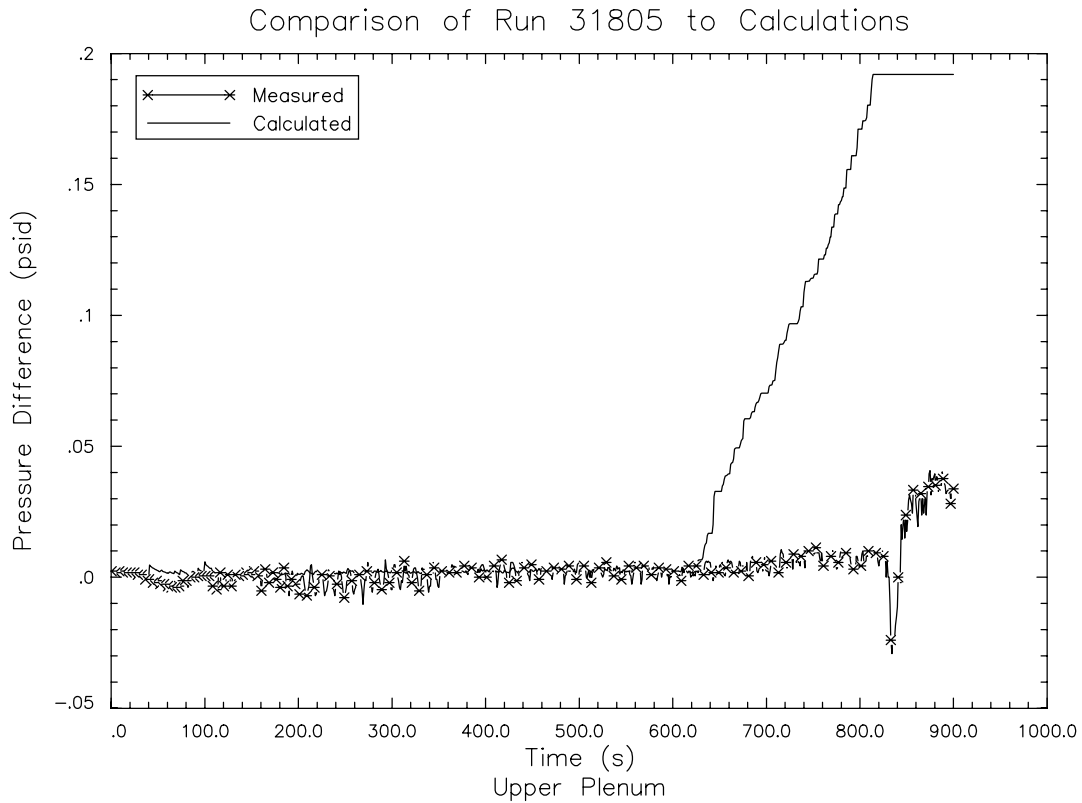


Figure 4.160 Upper Plenum Levels for FLECHT-SEASET Test 31805

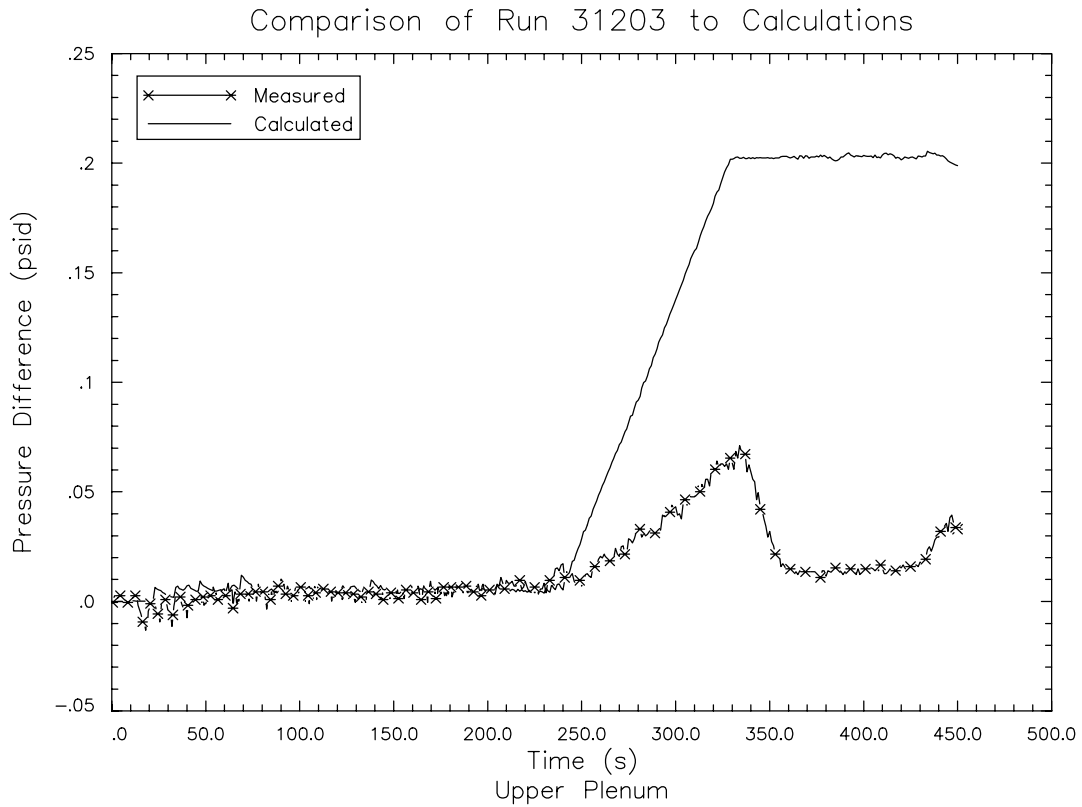


Figure 4.161 Upper Plenum Levels for FLECHT-SEASET Test 31203

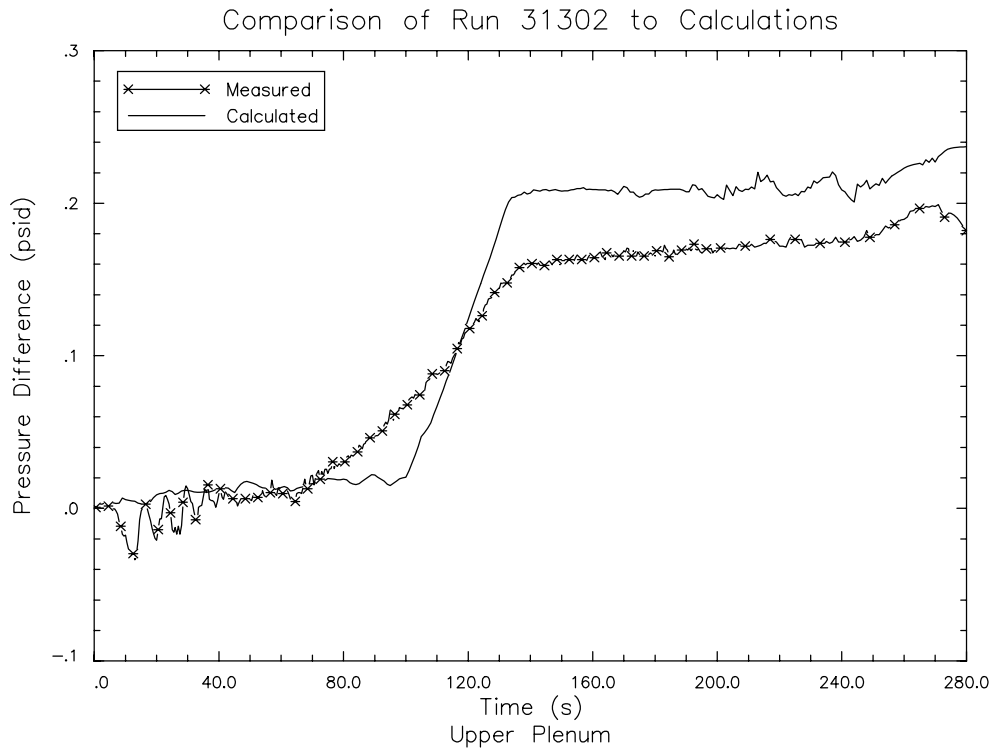


Figure 4.162 Upper Plenum Levels for FLECHT-SEASET Test 31302

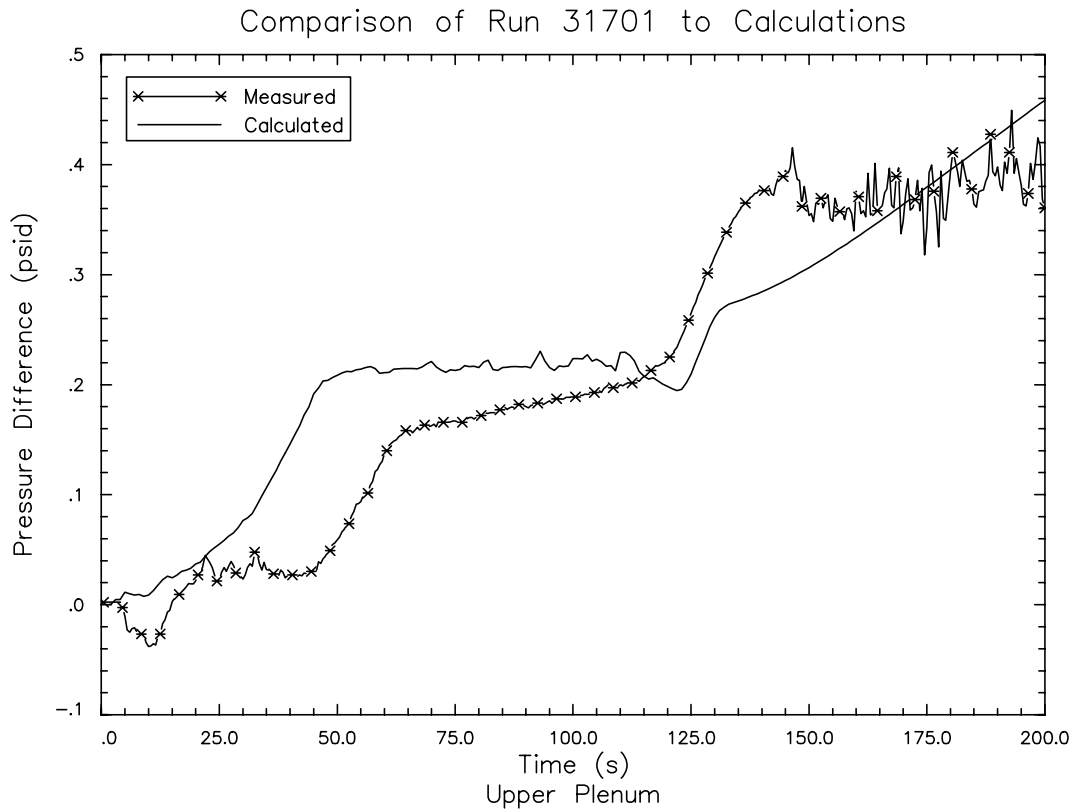


Figure 4.163 Upper Plenum Levels for FLECHT-SEASET Test 31701

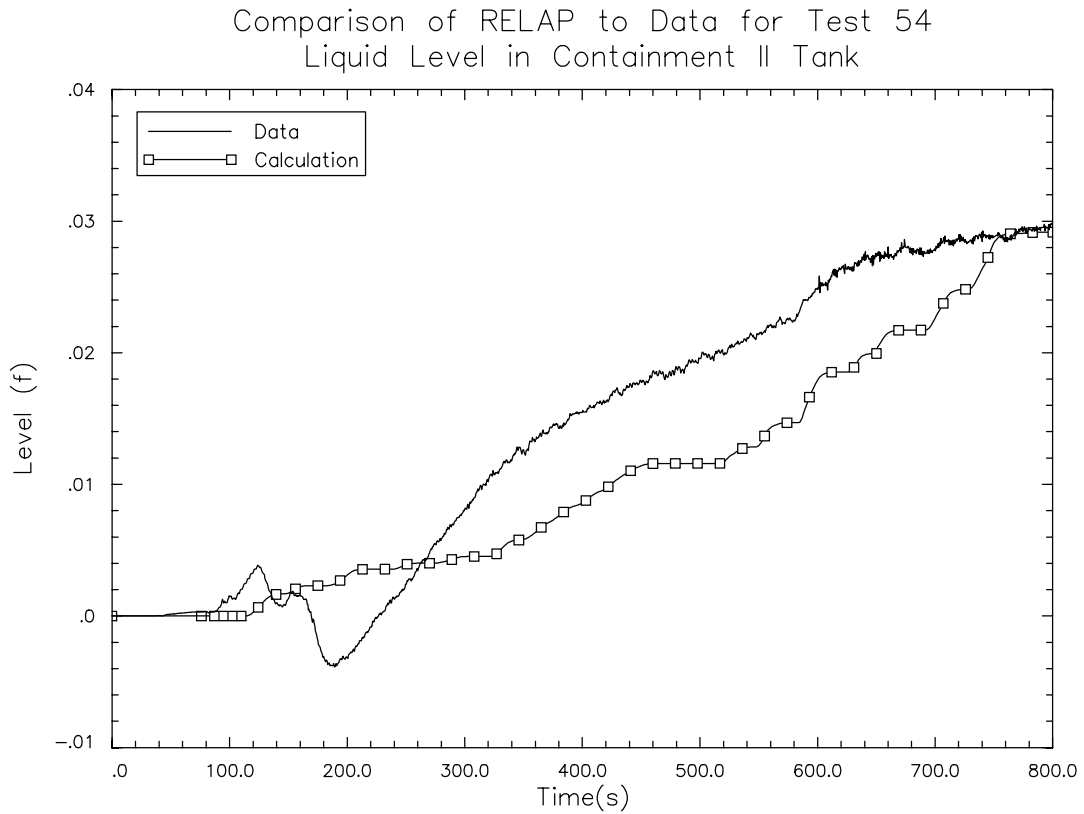


Figure 4.164 Comparison of Liquid Carryover for CCTF Test 54

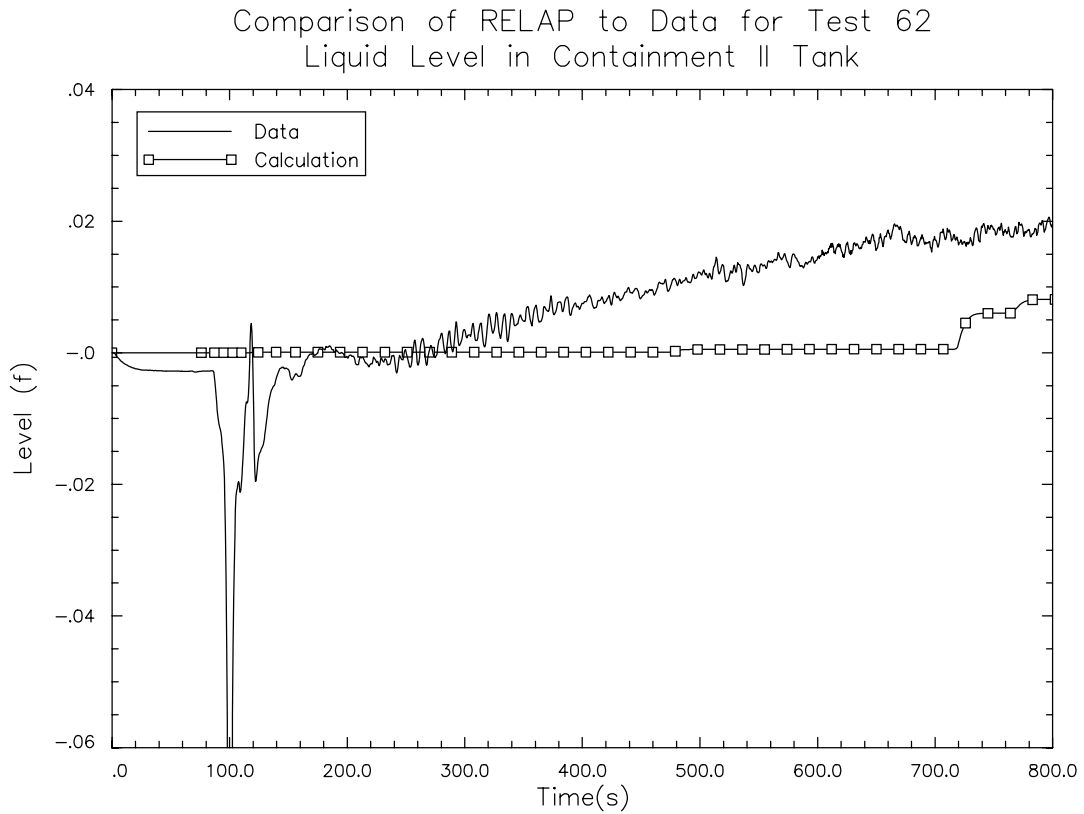


Figure 4.165 Comparison of Liquid Carryover for CCTF Test 62

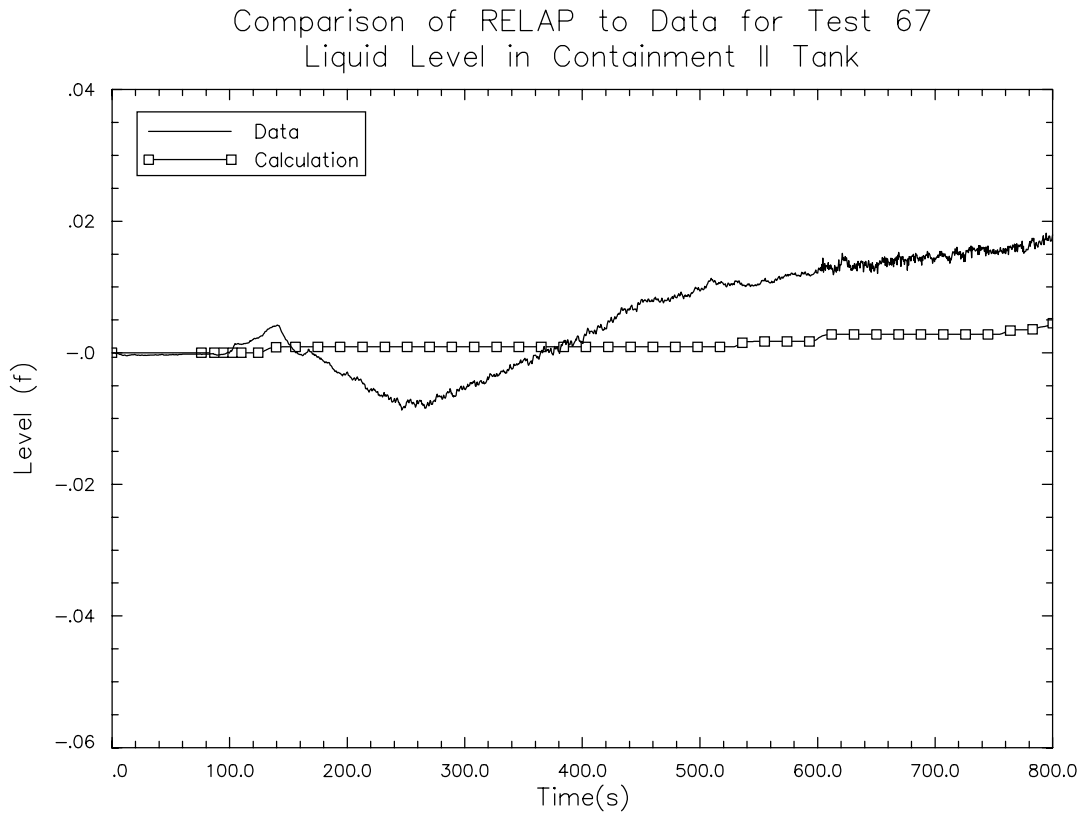


Figure 4.166 Comparison of Liquid Carryover for CCTF Test 67

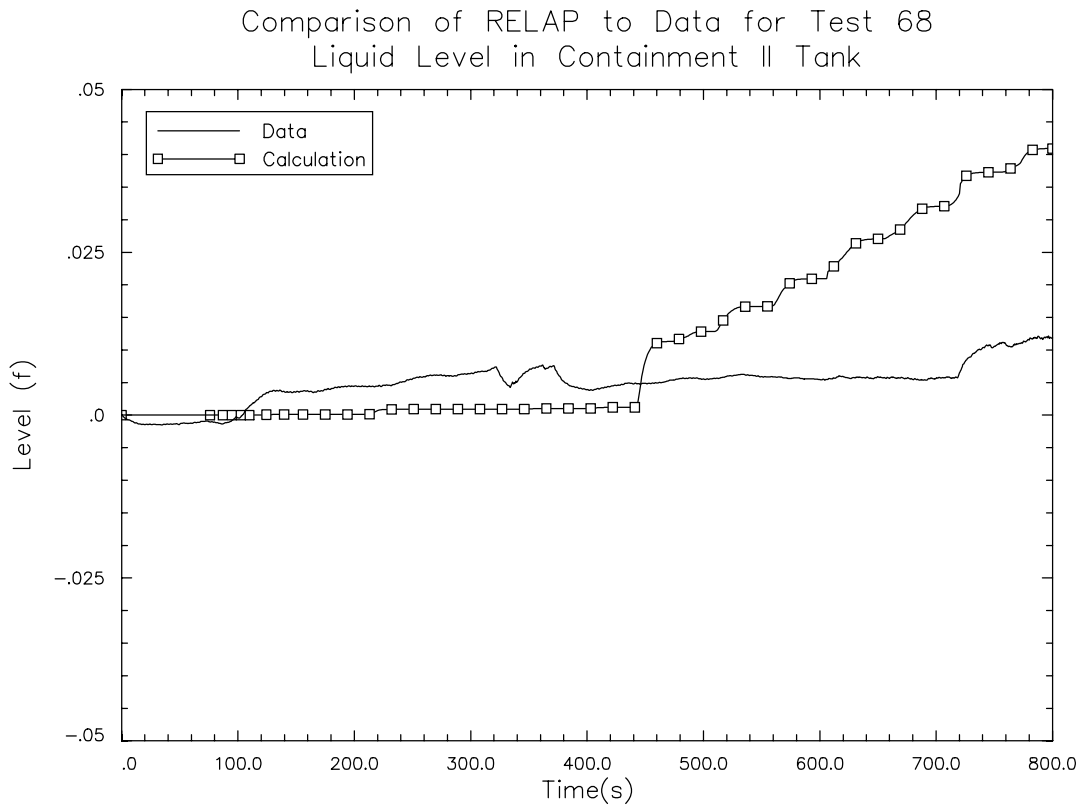


Figure 4.167 Comparison of Liquid Carryover for CCTF Test 68

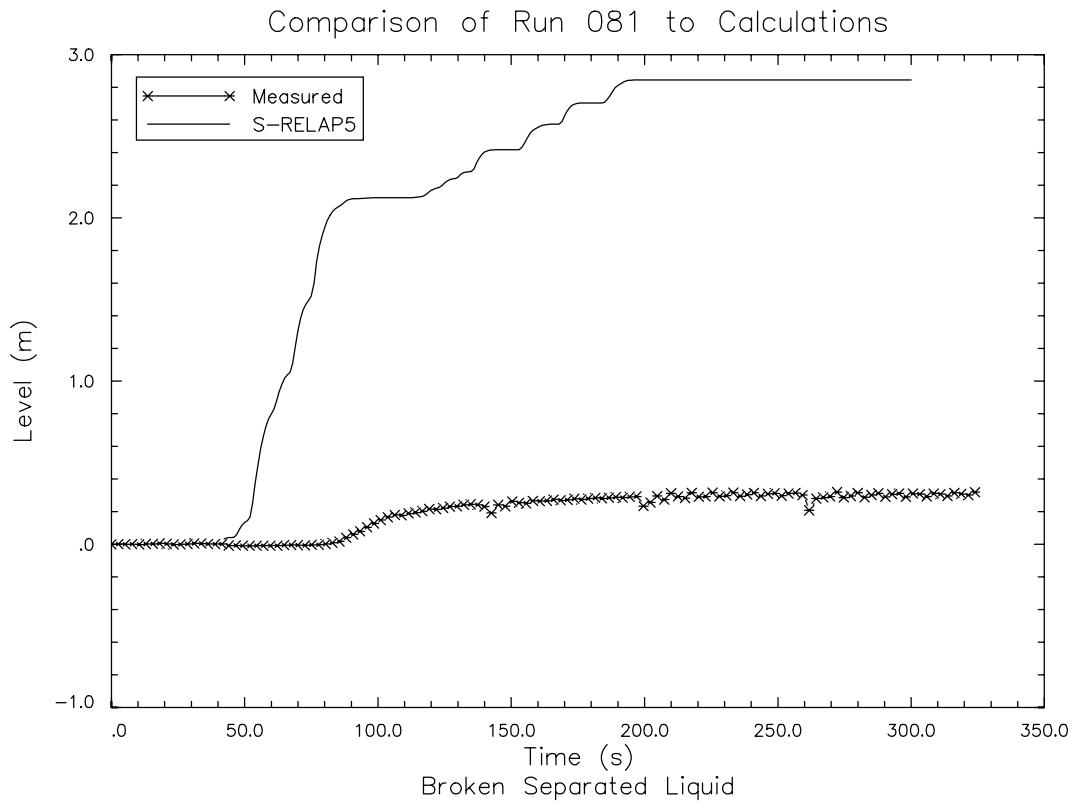


Figure 4.168 Level in Broken Loop Catch Tank - UPTF Test 081

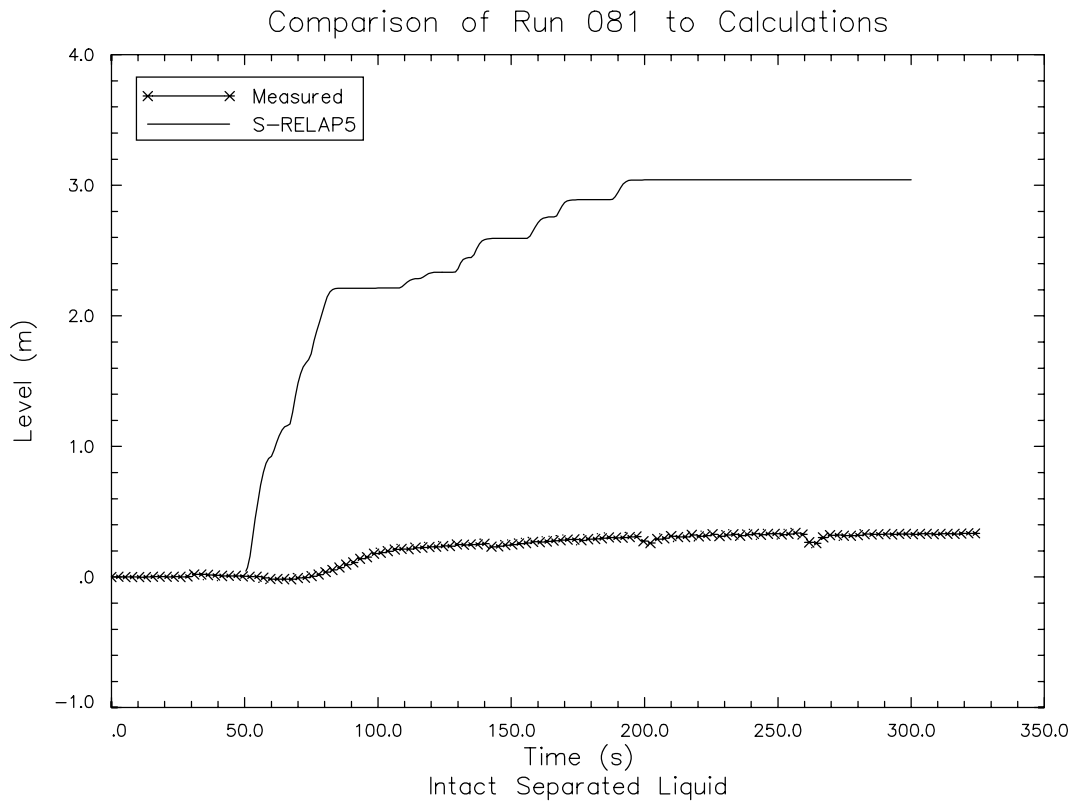


Figure 4.169 Level in Intact Loop Catch Tank - UPTF Test 081

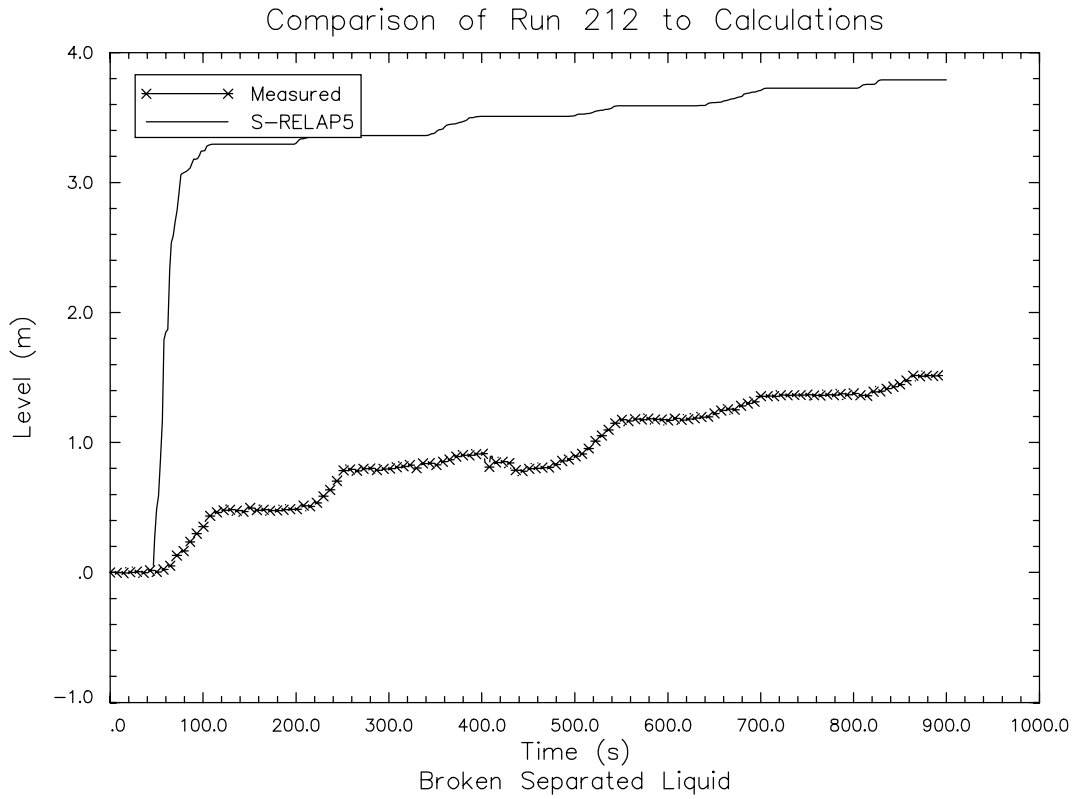


Figure 4.170 Level in Broken Loop Catch Tank - UPTF Test 212

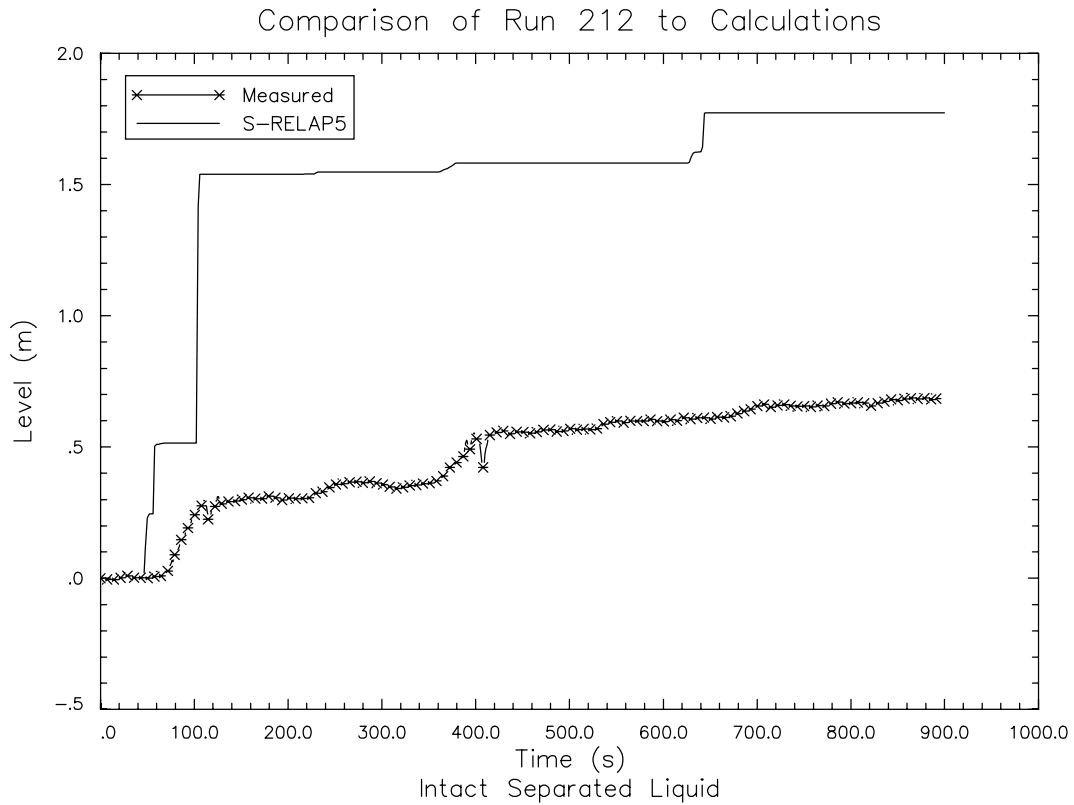
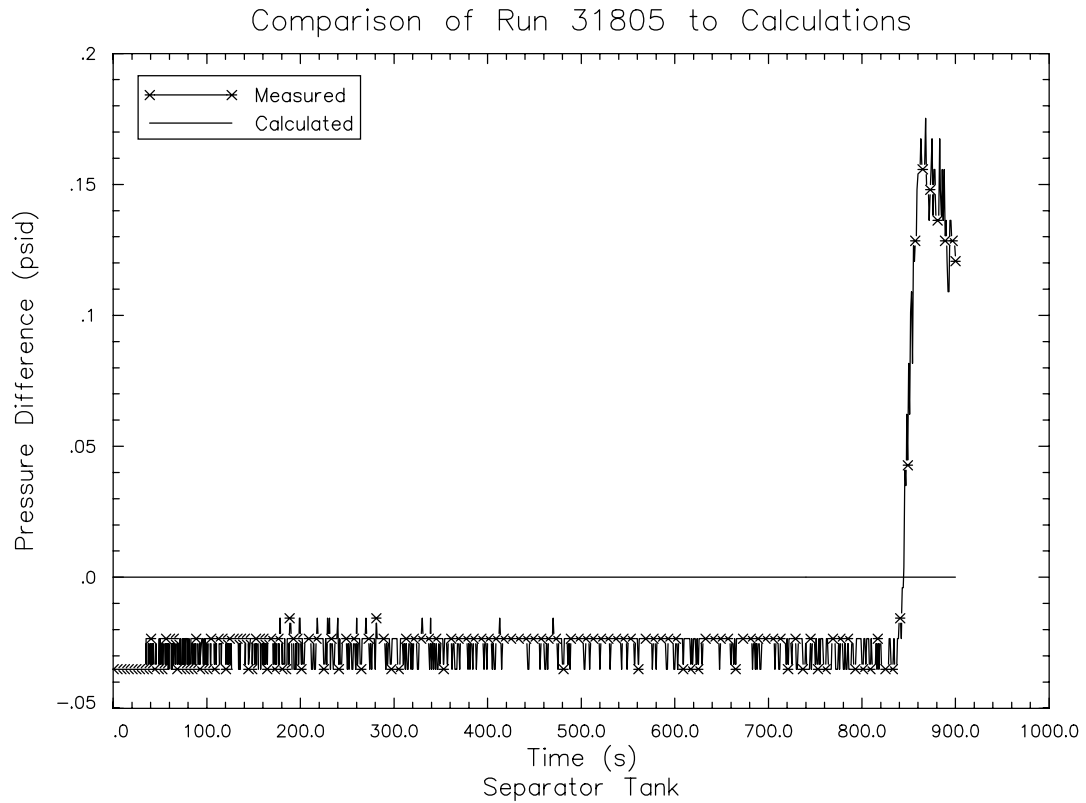
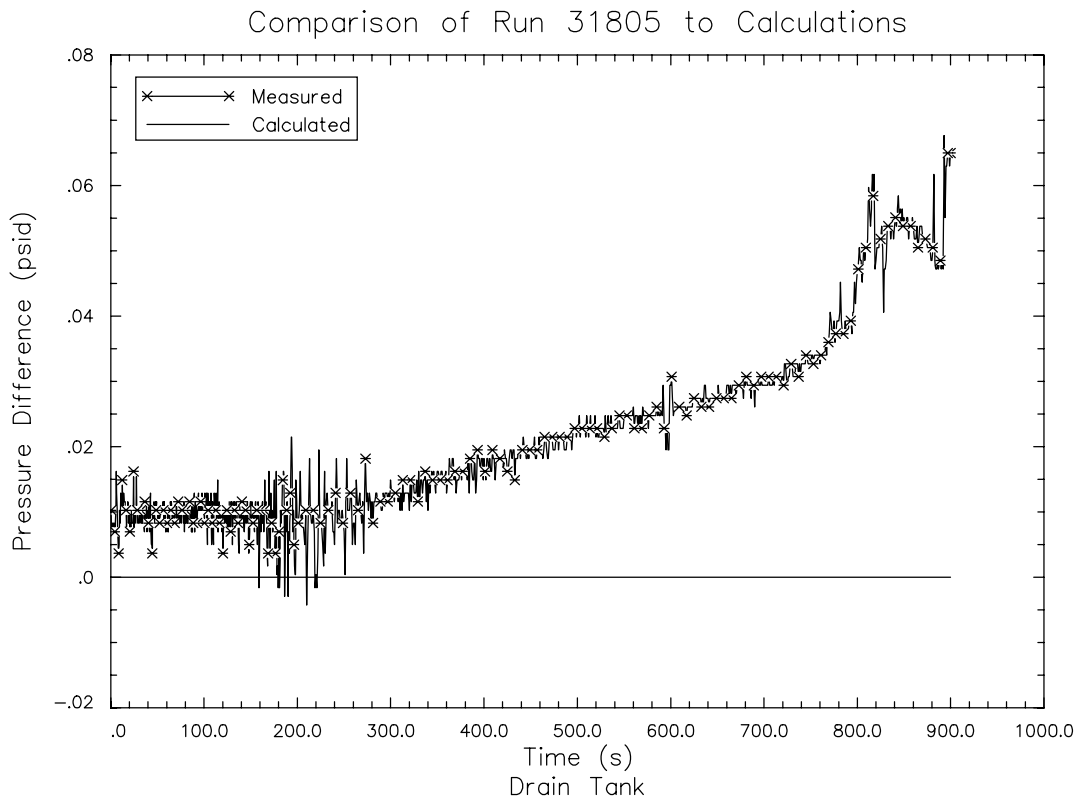


Figure 4.171 Level in Intact Loop Catch Tank - UPTF Test 212



**Figure 4.172 Level in Separator Tank for FLECHT-SEASET
Tests 31805**



**Figure 4.173 Level in Separator Drain Tank for FLECHT-SEASET
Tests 31805**

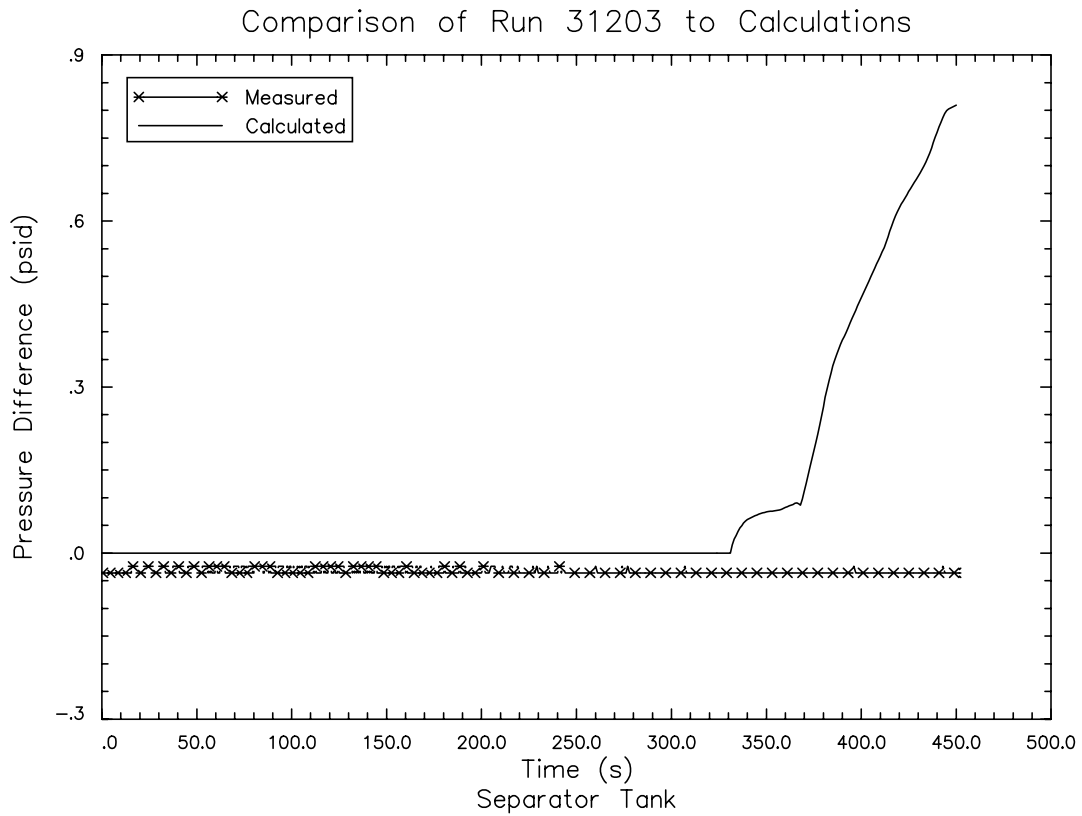


**Figure 4.174 Level in Separator Tank for FLECHT-SEASET
Tests 31203**

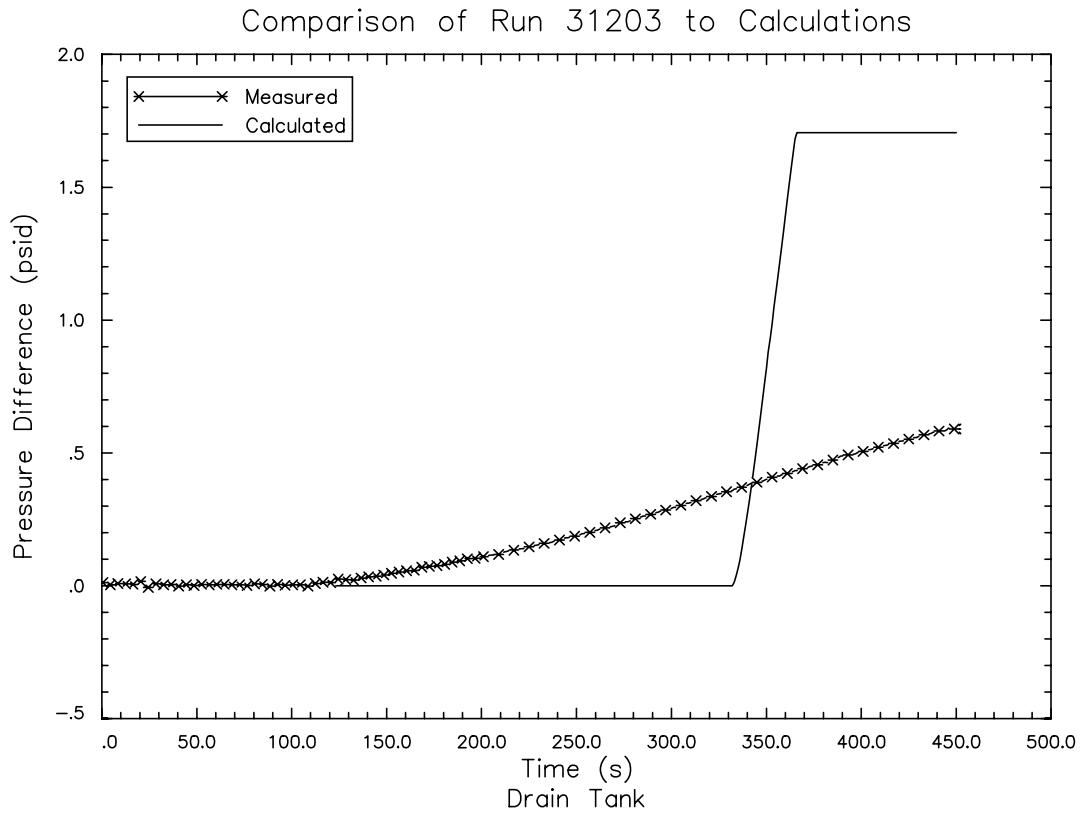


**Figure 4.175 Level in Separator Drain Tank for FLECHT-SEASET
Tests 31203**

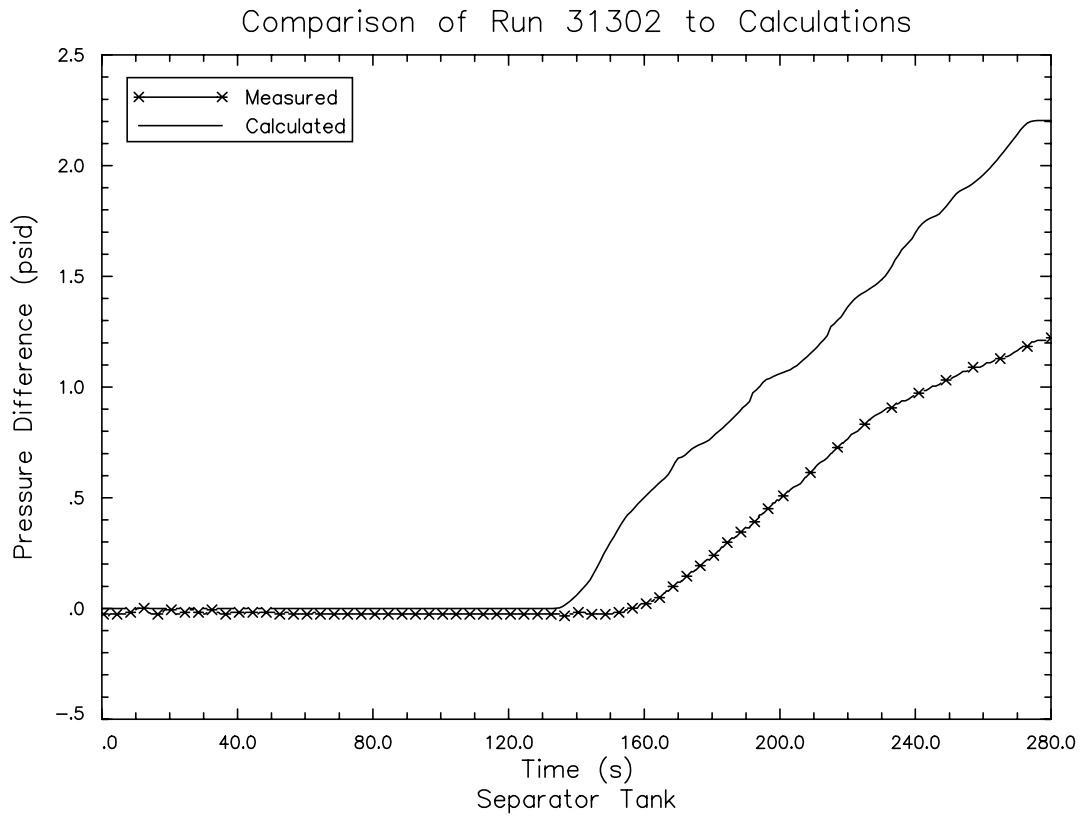


**Figure 4.176 Level in Separator Tank for FLECHT-SEASET
Tests 31302**

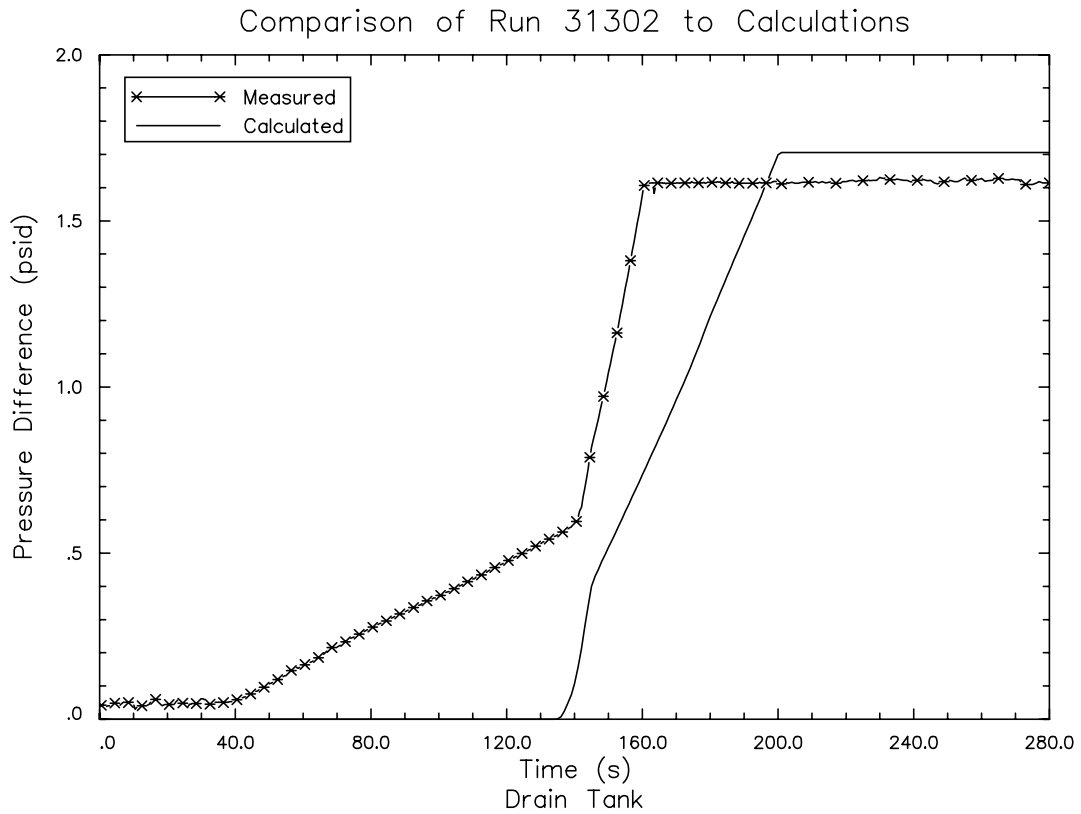


**Figure 4.177 Level in Separator Drain Tank for FLECHT-SEASET
Tests 31302**

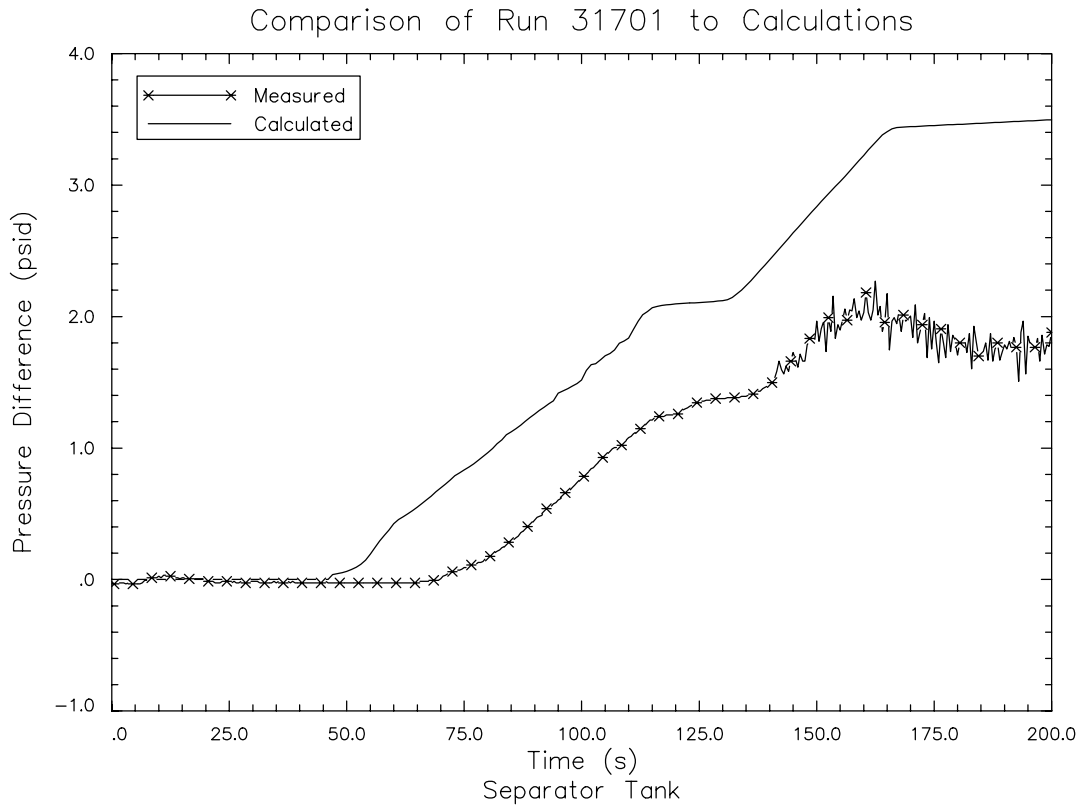


**Figure 4.178 Level in Separator Tank for FLECHT-SEASET
Tests 31701**

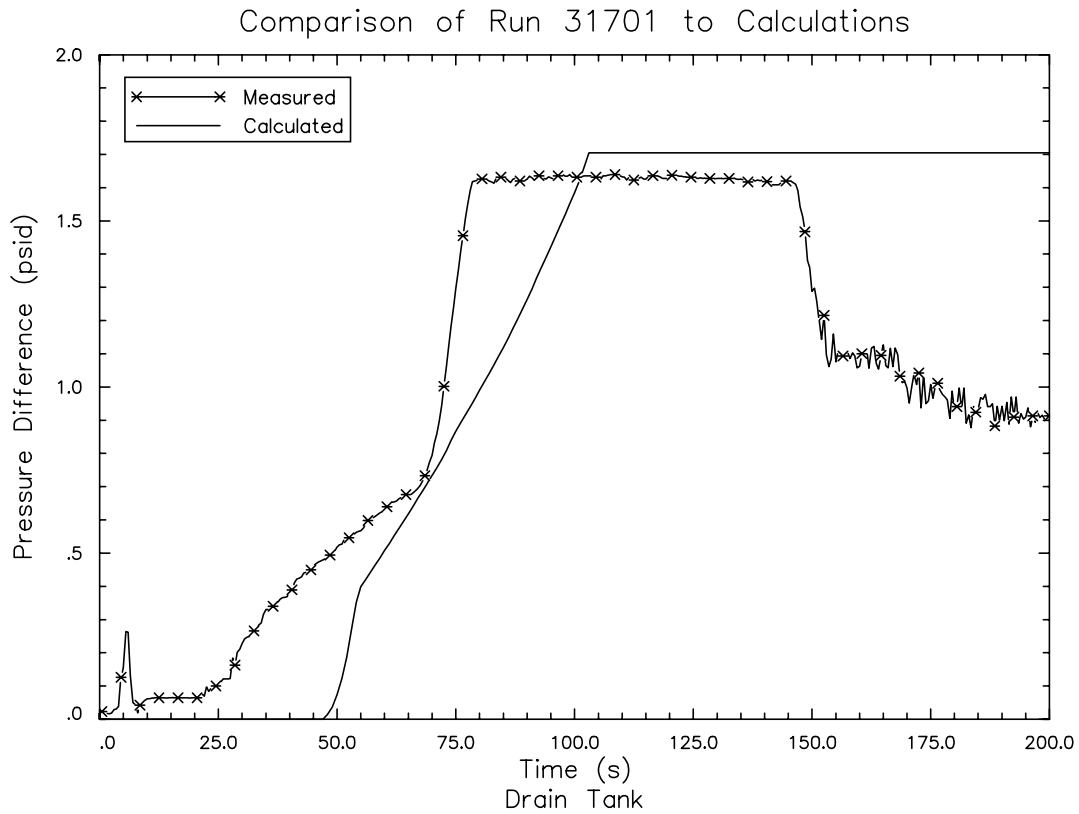


**Figure 4.179 Level in Separator Drain Tank for FLECHT-SEASET
Tests 31701**

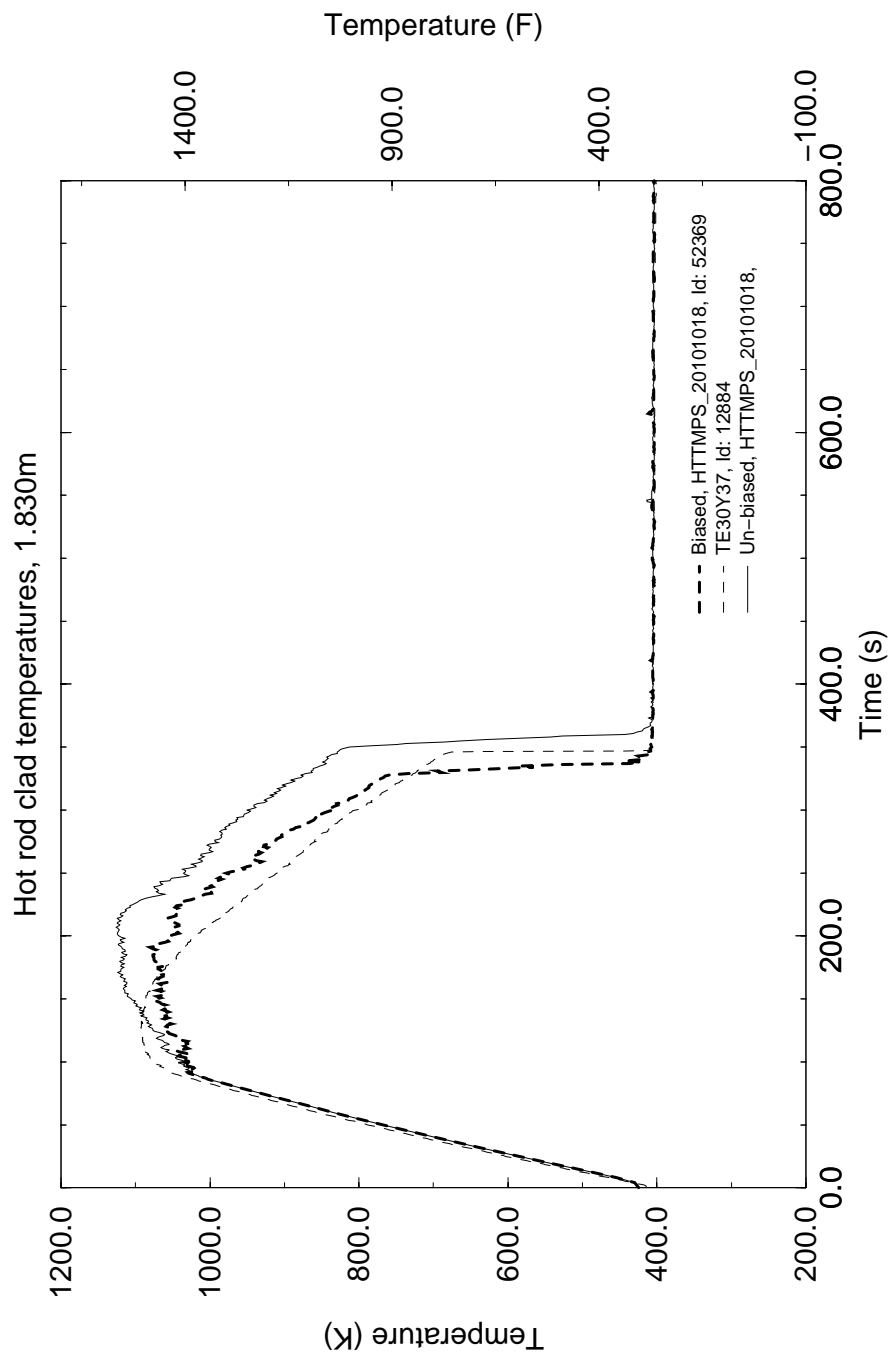


Figure 4.180 CCTF TEST 54 Temperatures at Measured PCT Node

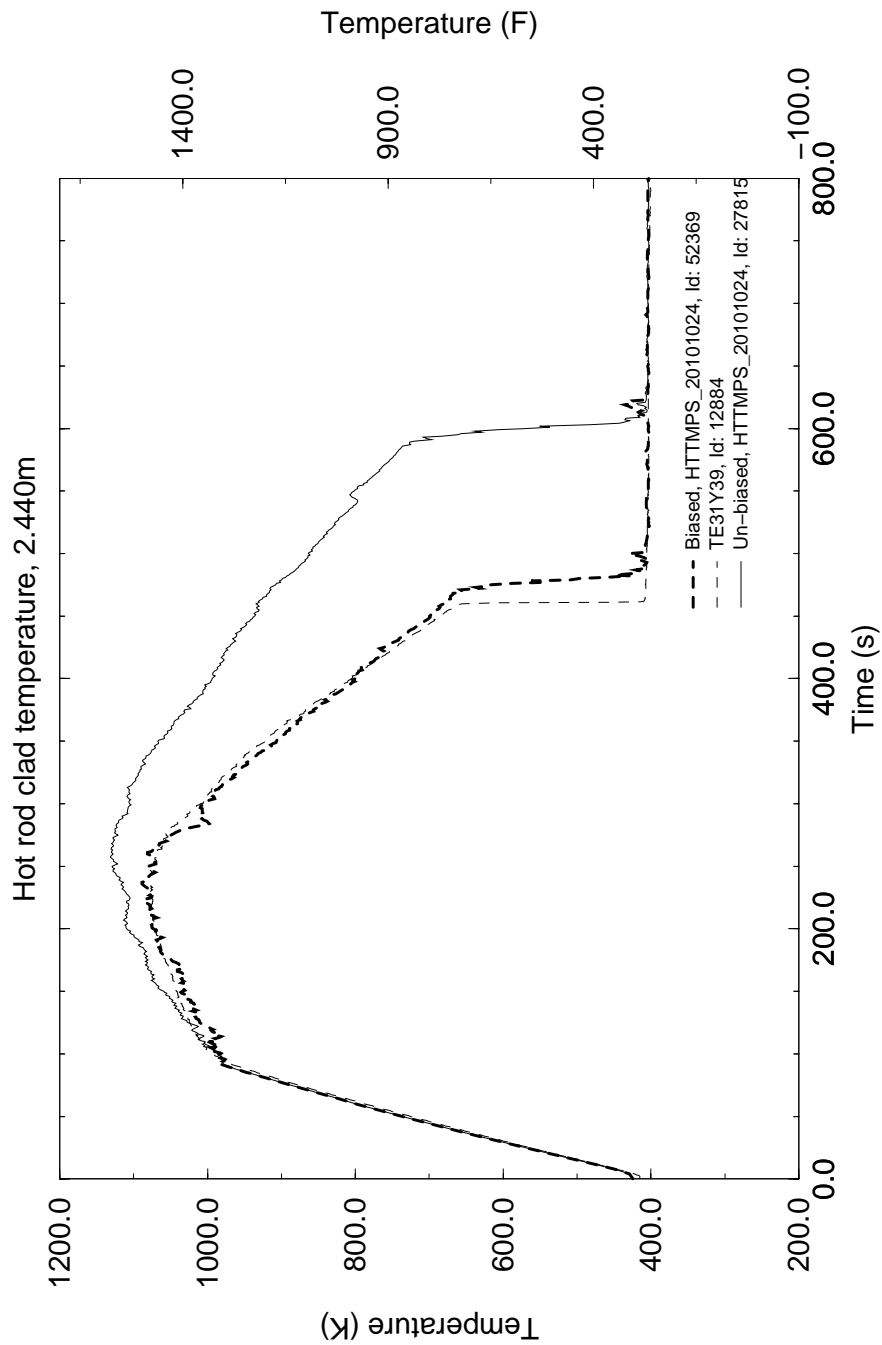


Figure 4.181 CCTF TEST 54 Temperatures Near Calculated PCT Node

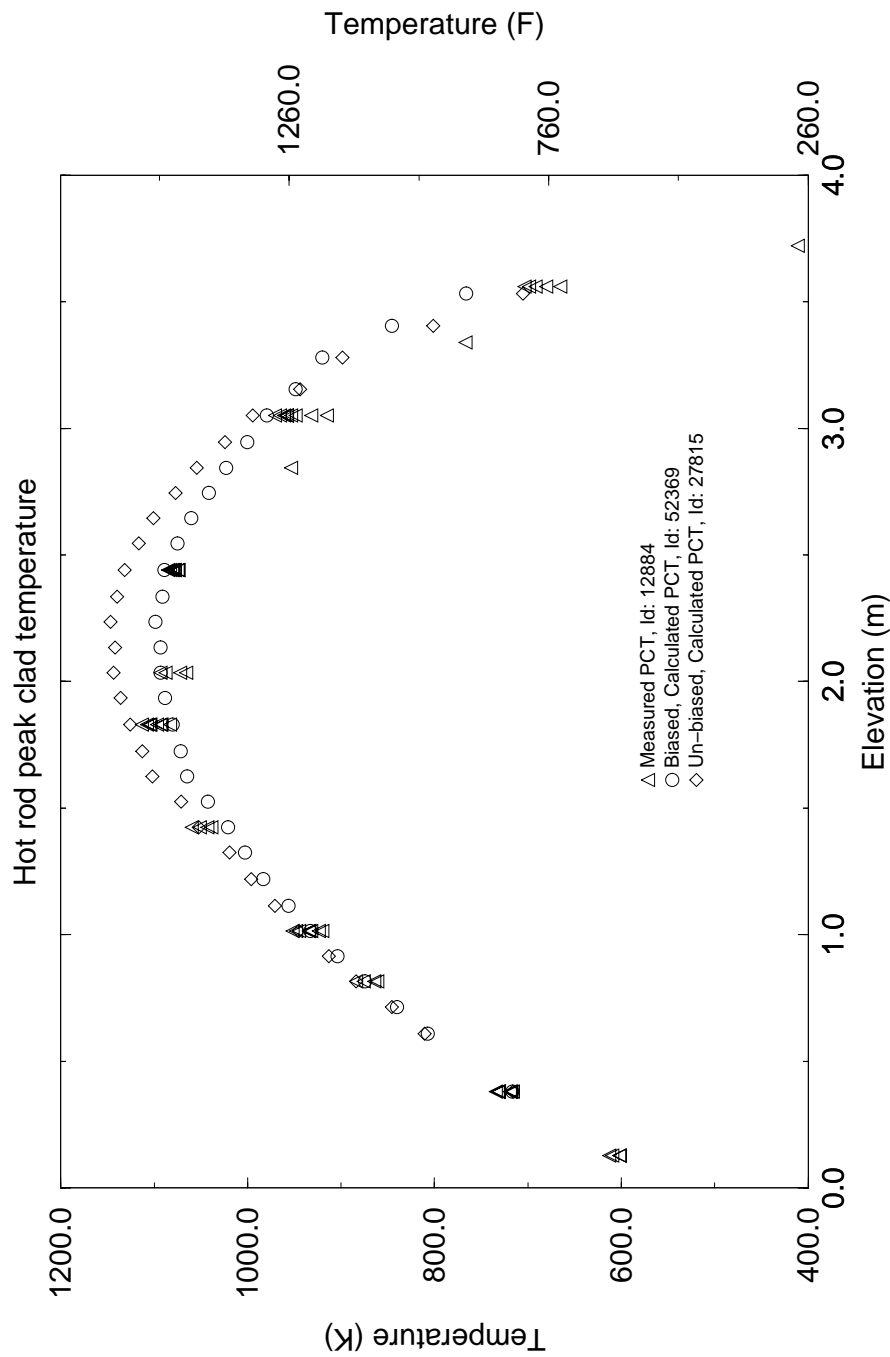


Figure 4.182 CCTF TEST 54 PCT Profile

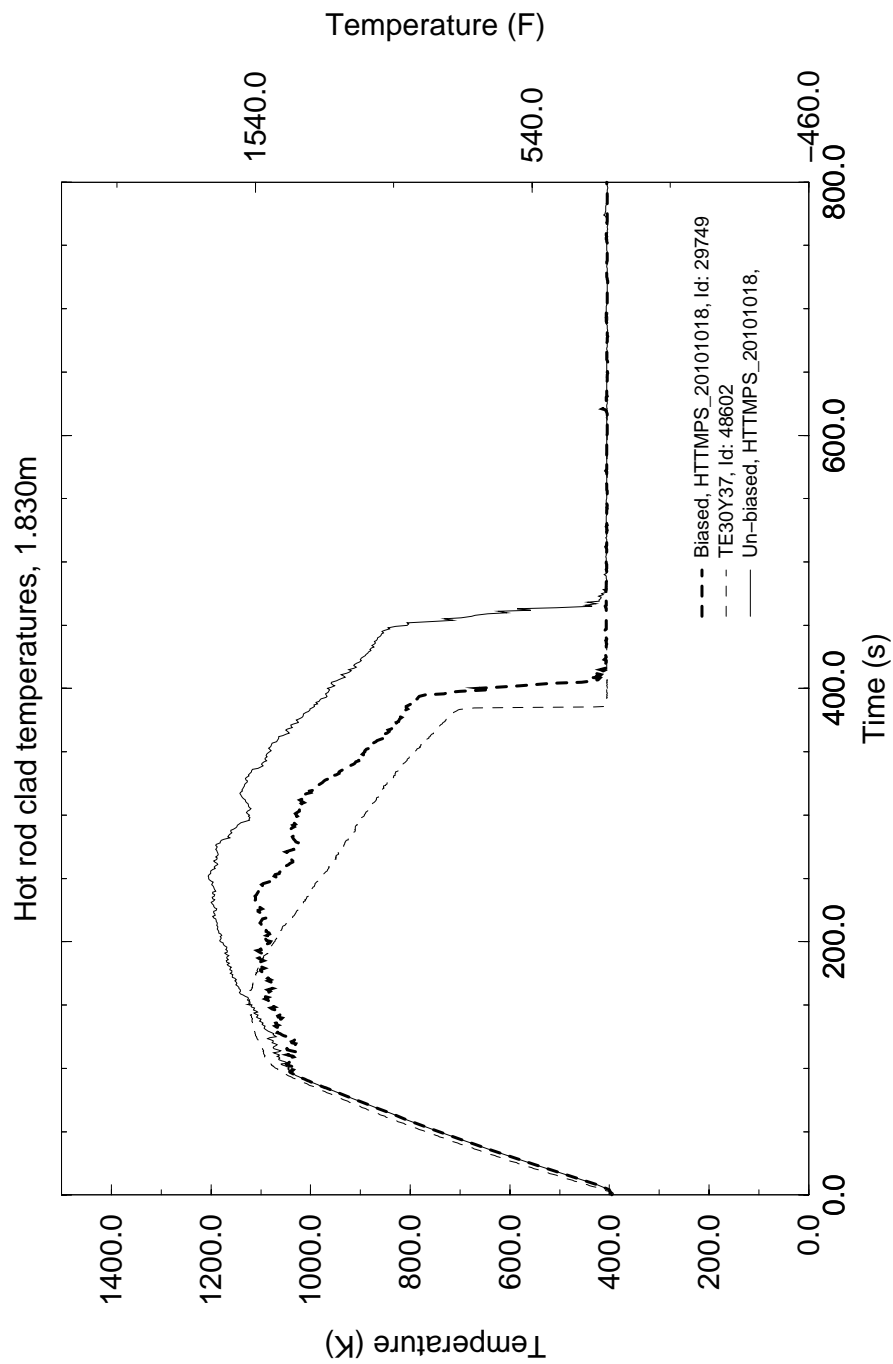


Figure 4.183 CCTF TEST 62 Temperatures at Measured PCT Node

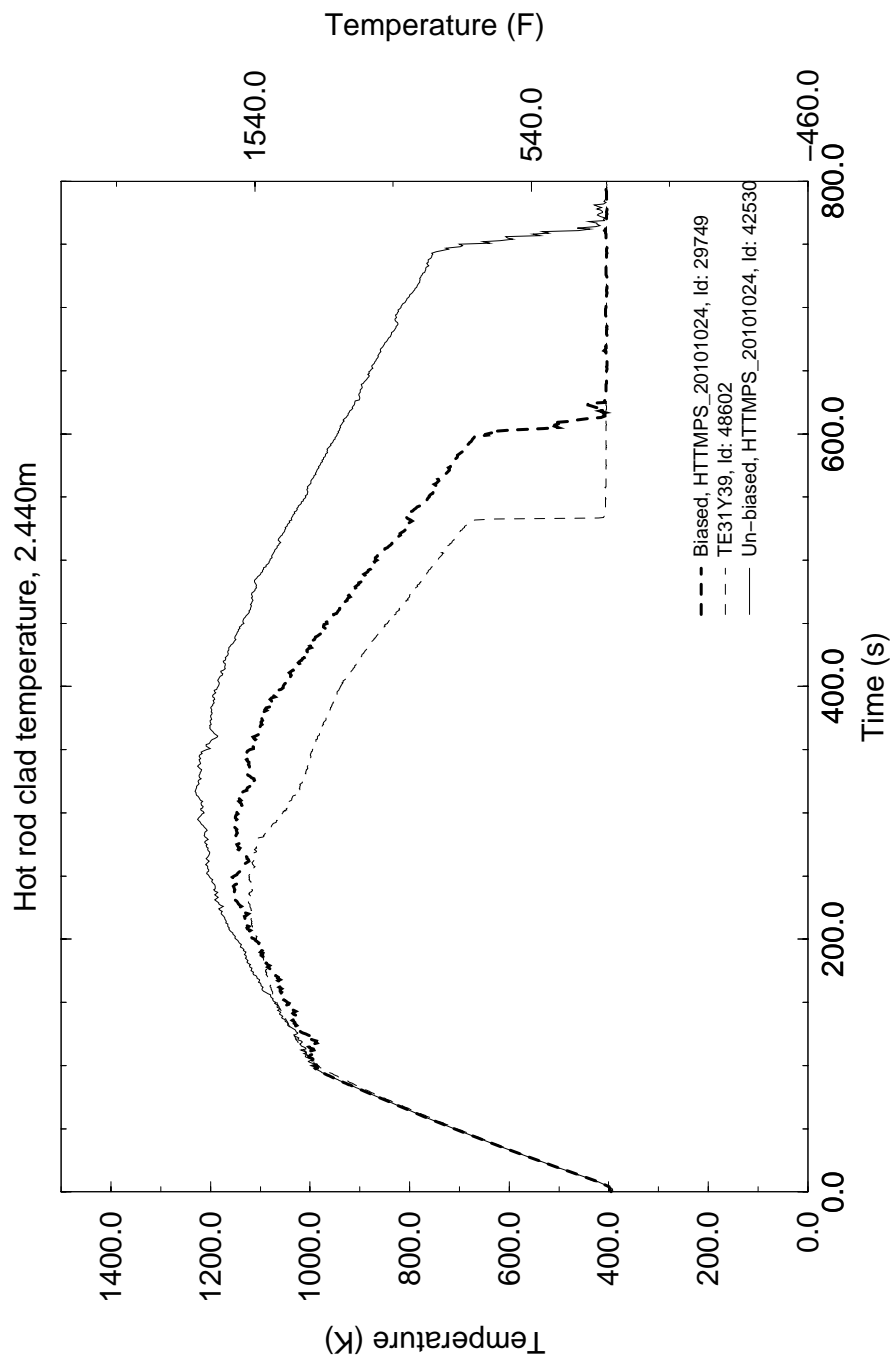


Figure 4.184 CCTF TEST 62 Temperatures Near Calculated PCT Node

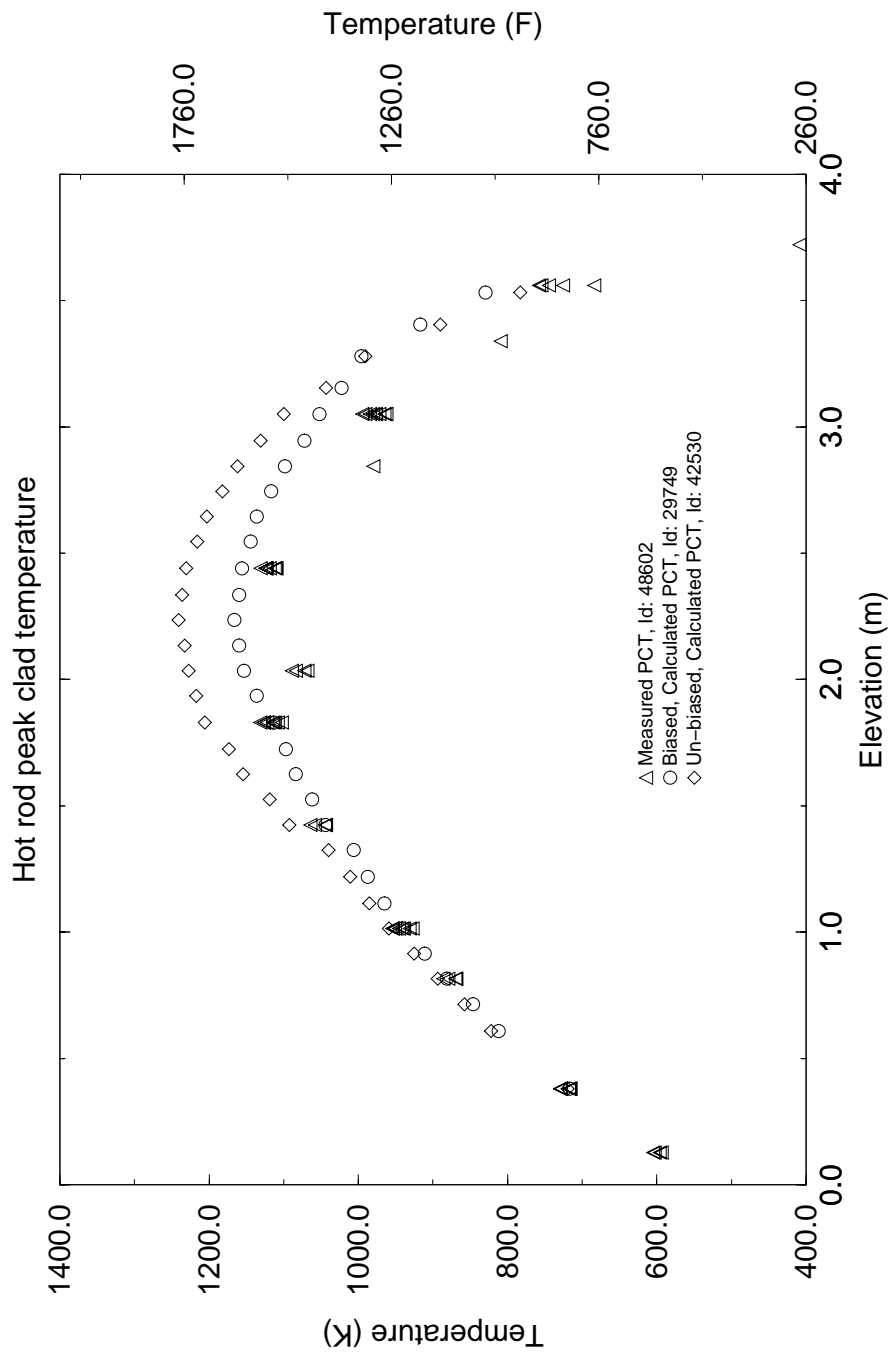


Figure 4.185 CCTF TEST 62 PCT Profile

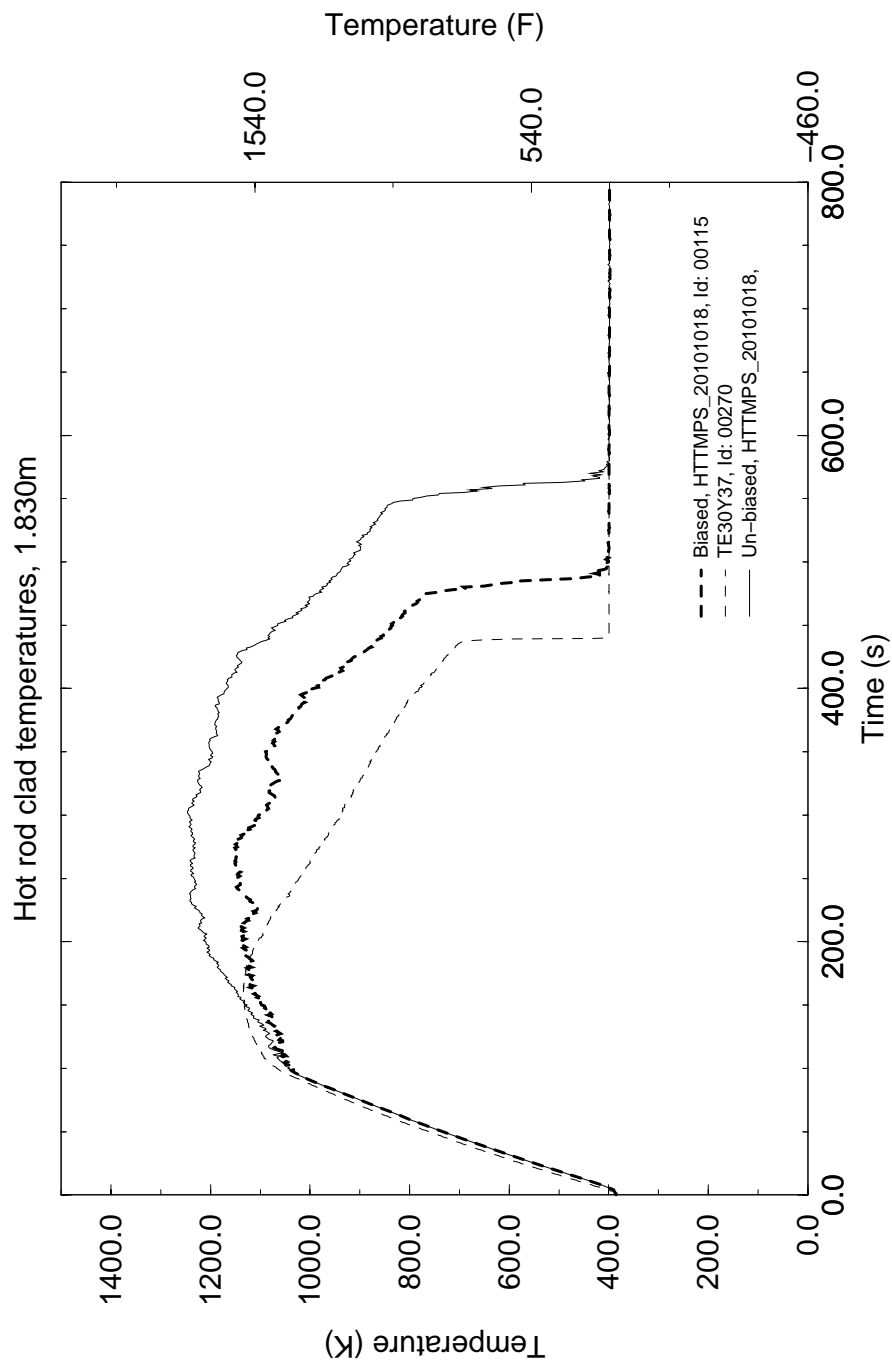


Figure 4.186 CCTF TEST 67 Temperatures at Measured PCT Node

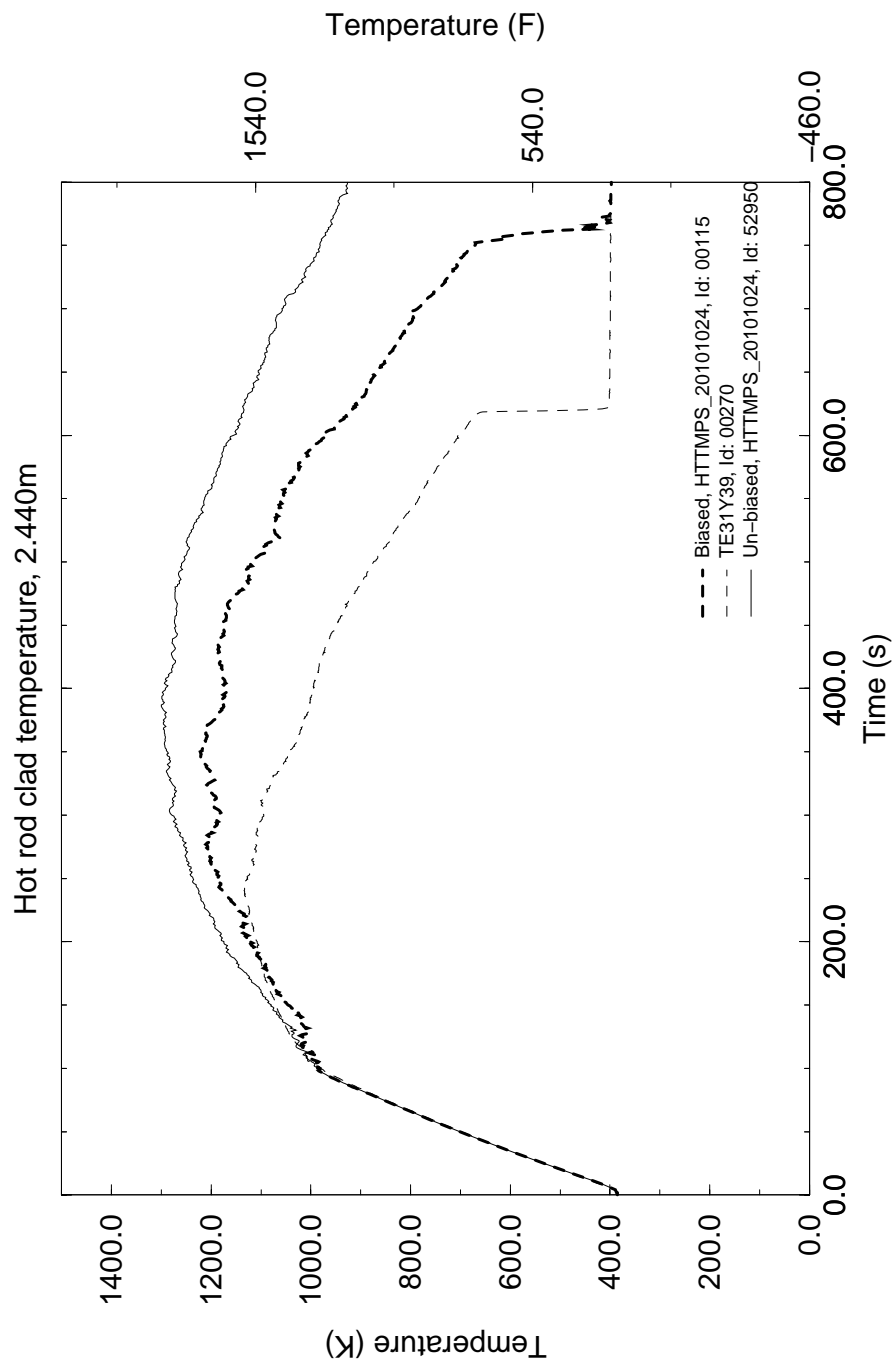


Figure 4.187 CCTF TEST 67 Temperatures Near Calculated PCT Node

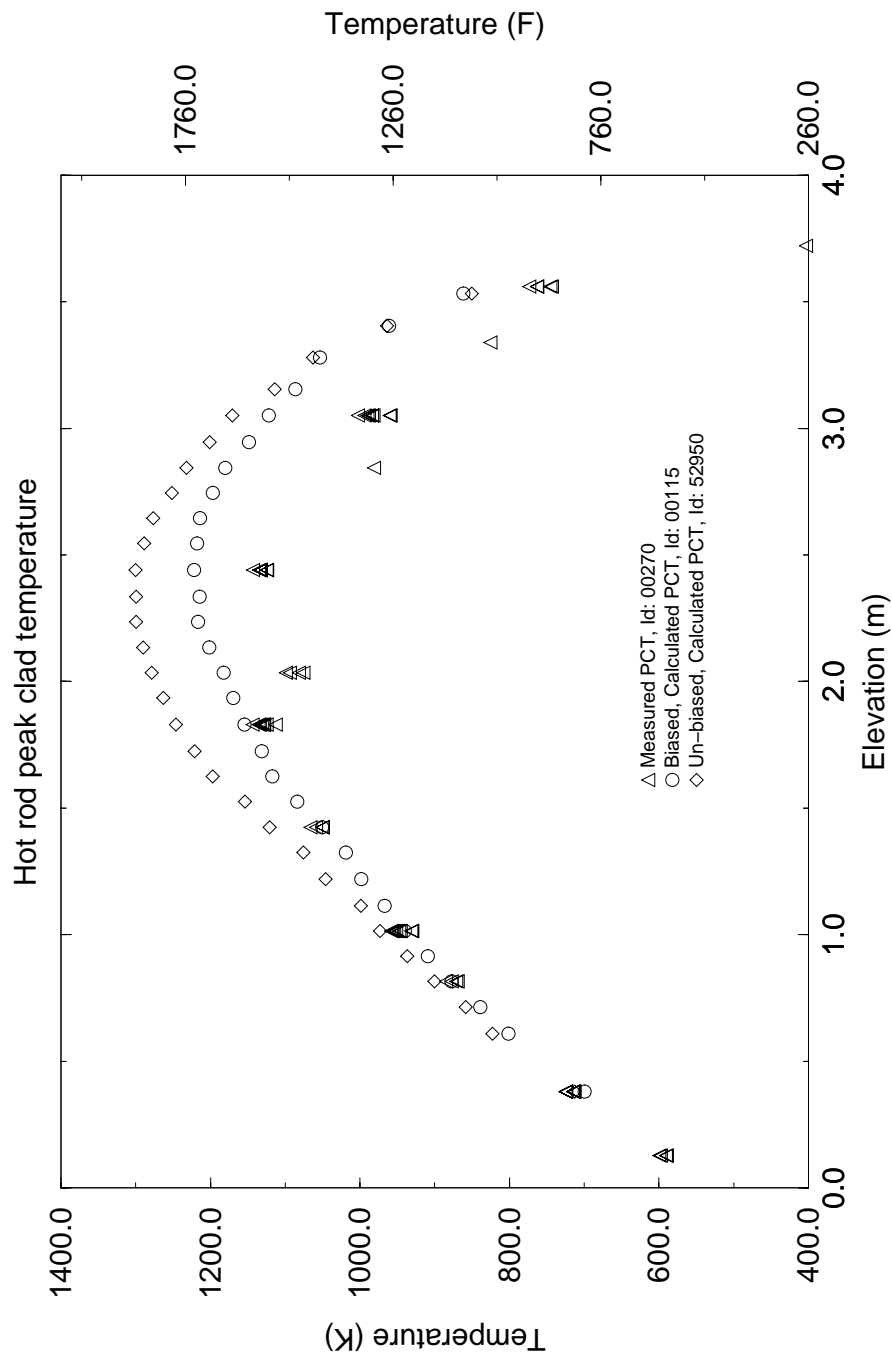


Figure 4.188 CCTF TEST 67 PCT Profile

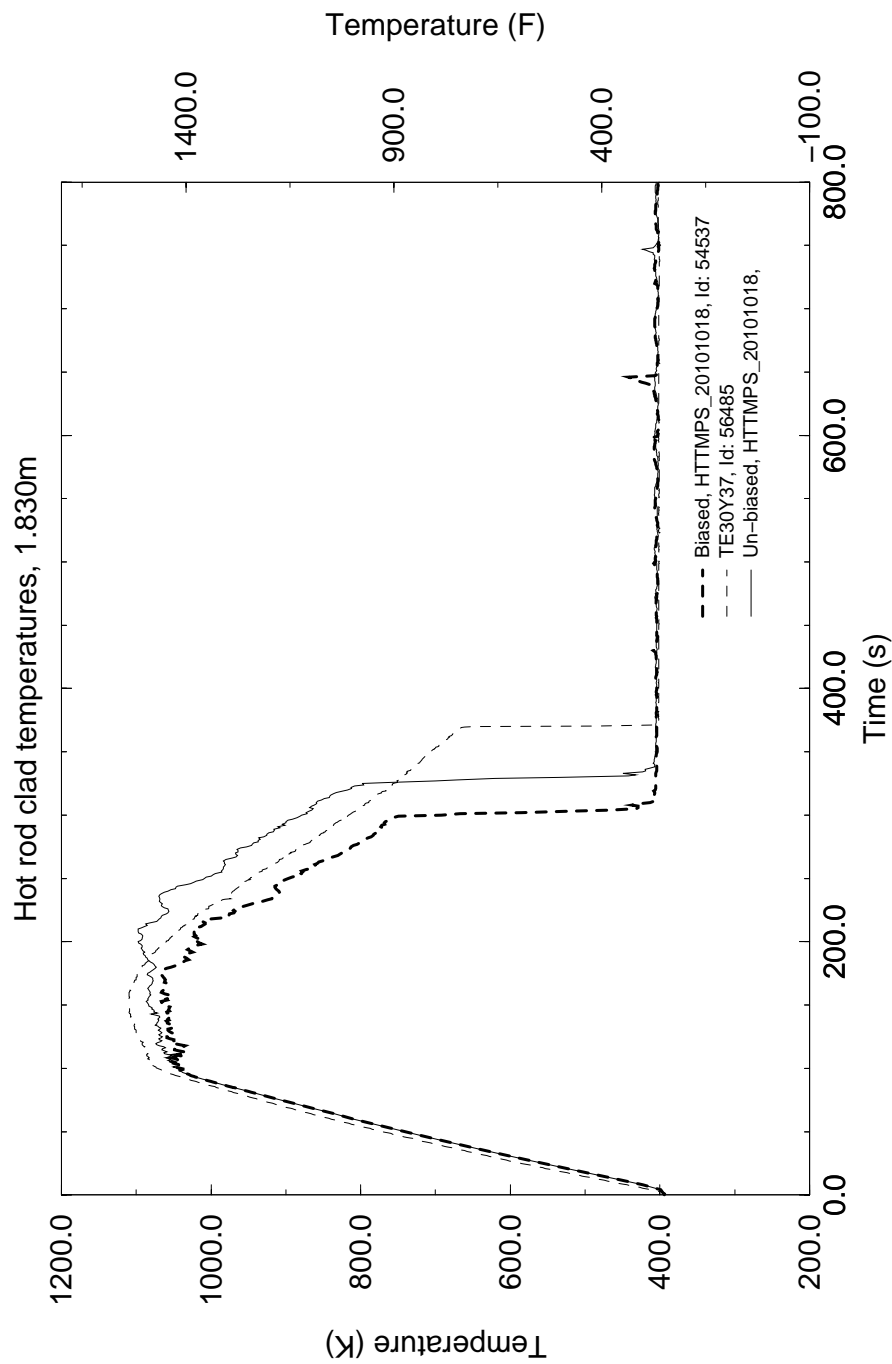


Figure 4.189 CCTF TEST 68 Temperatures at Measured PCT Node

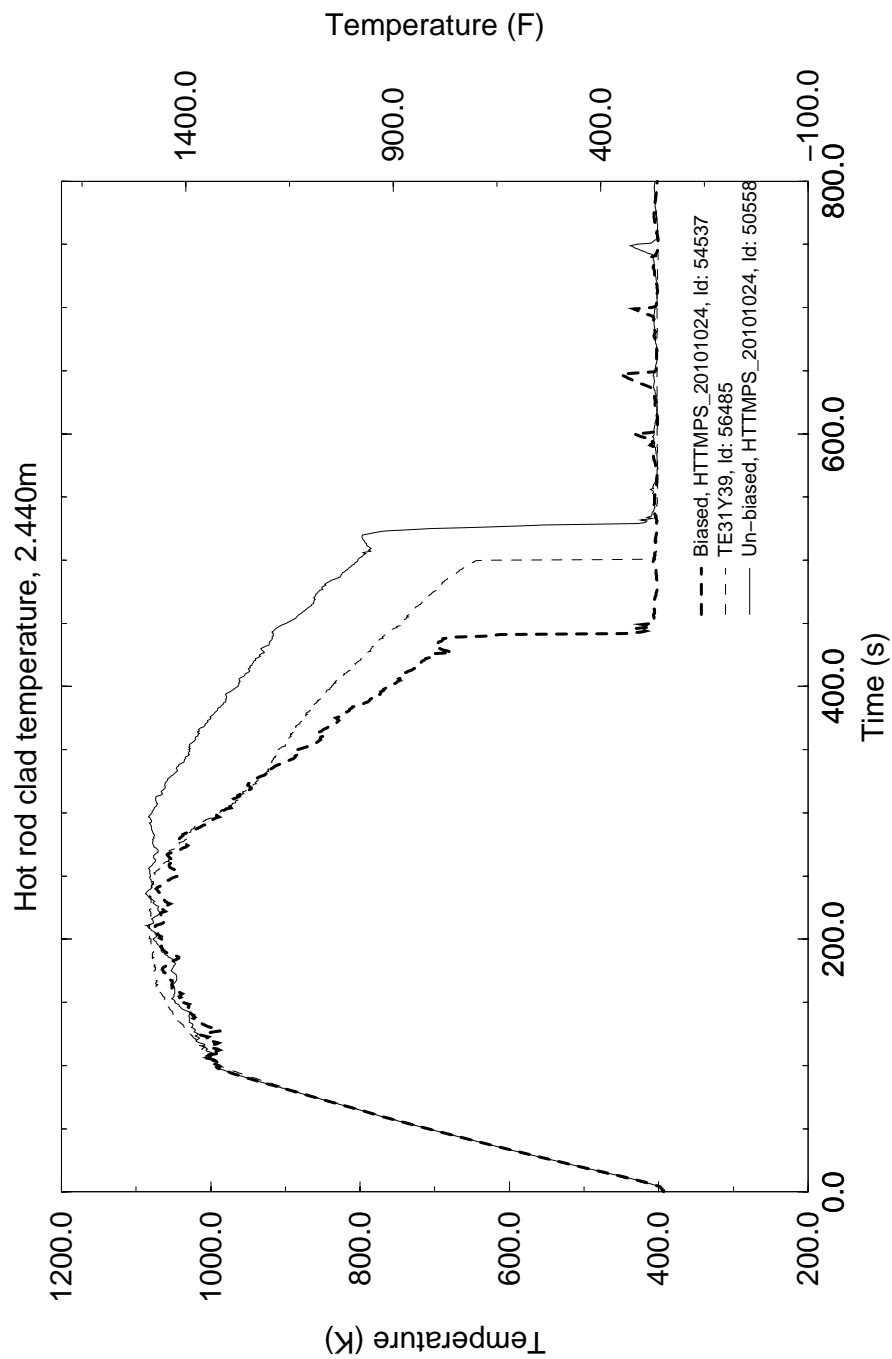


Figure 4.190 CCTF TEST 68 Temperatures Near Calculated PCT Node

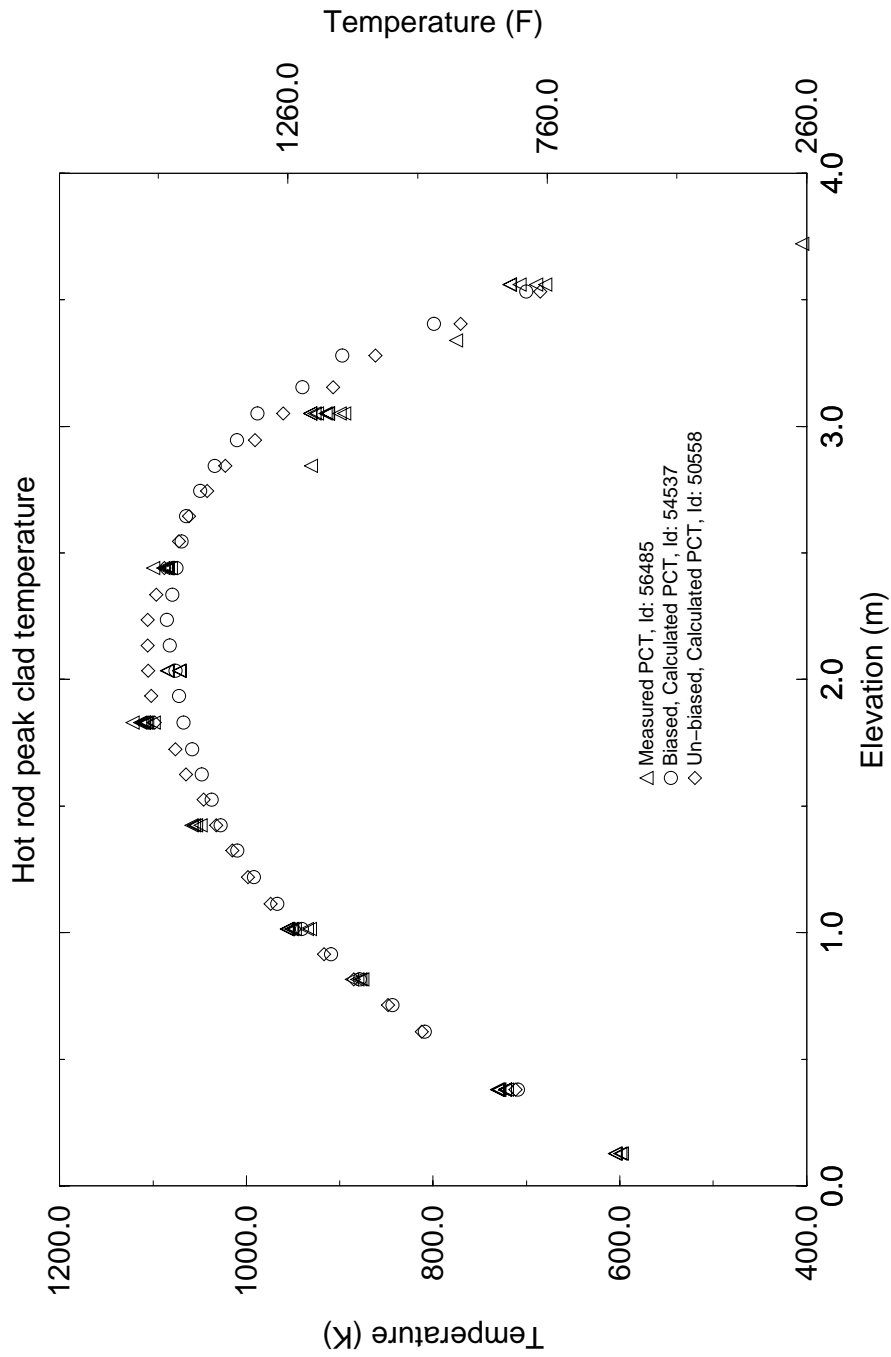


Figure 4.191 CCTF TEST 68 PCT Profile

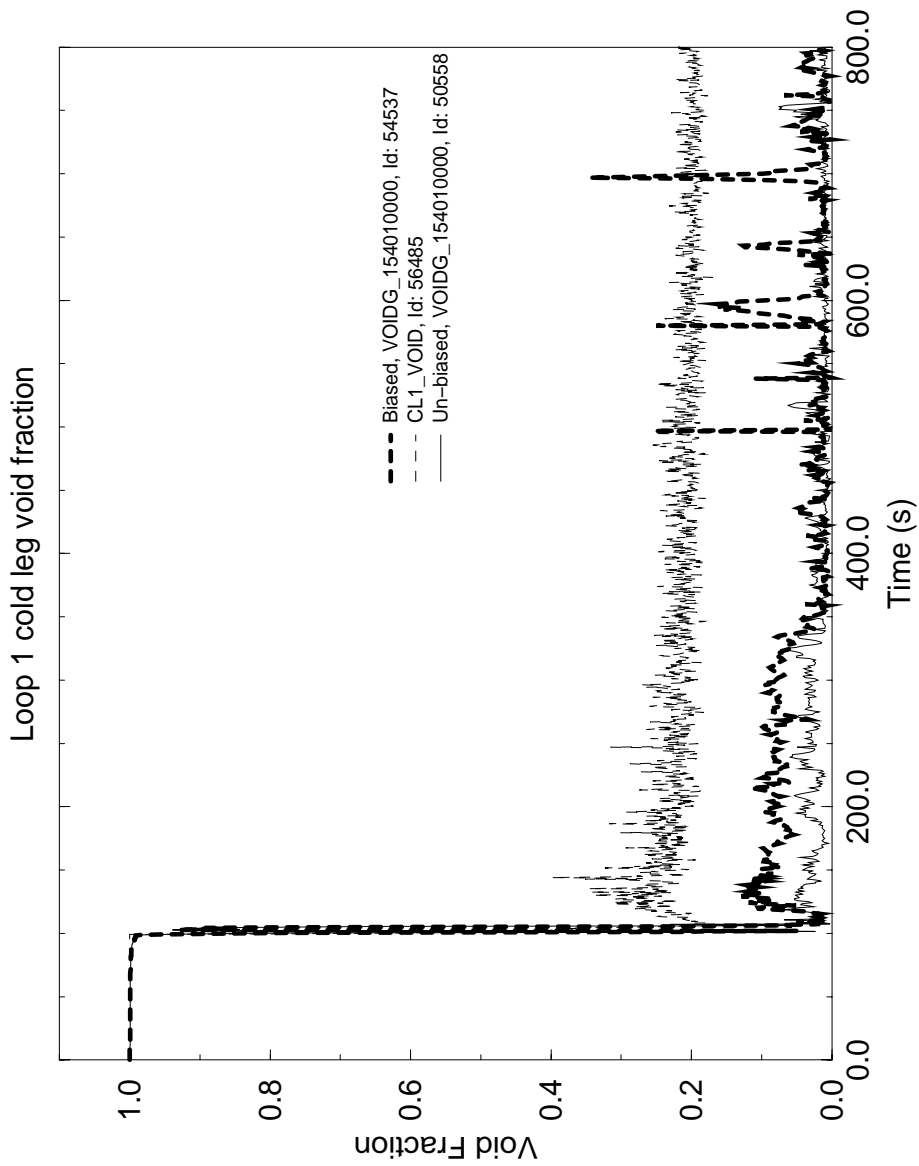


Figure 4.192 CCTF TEST 68 Intact Loop Cold Leg Void Fraction

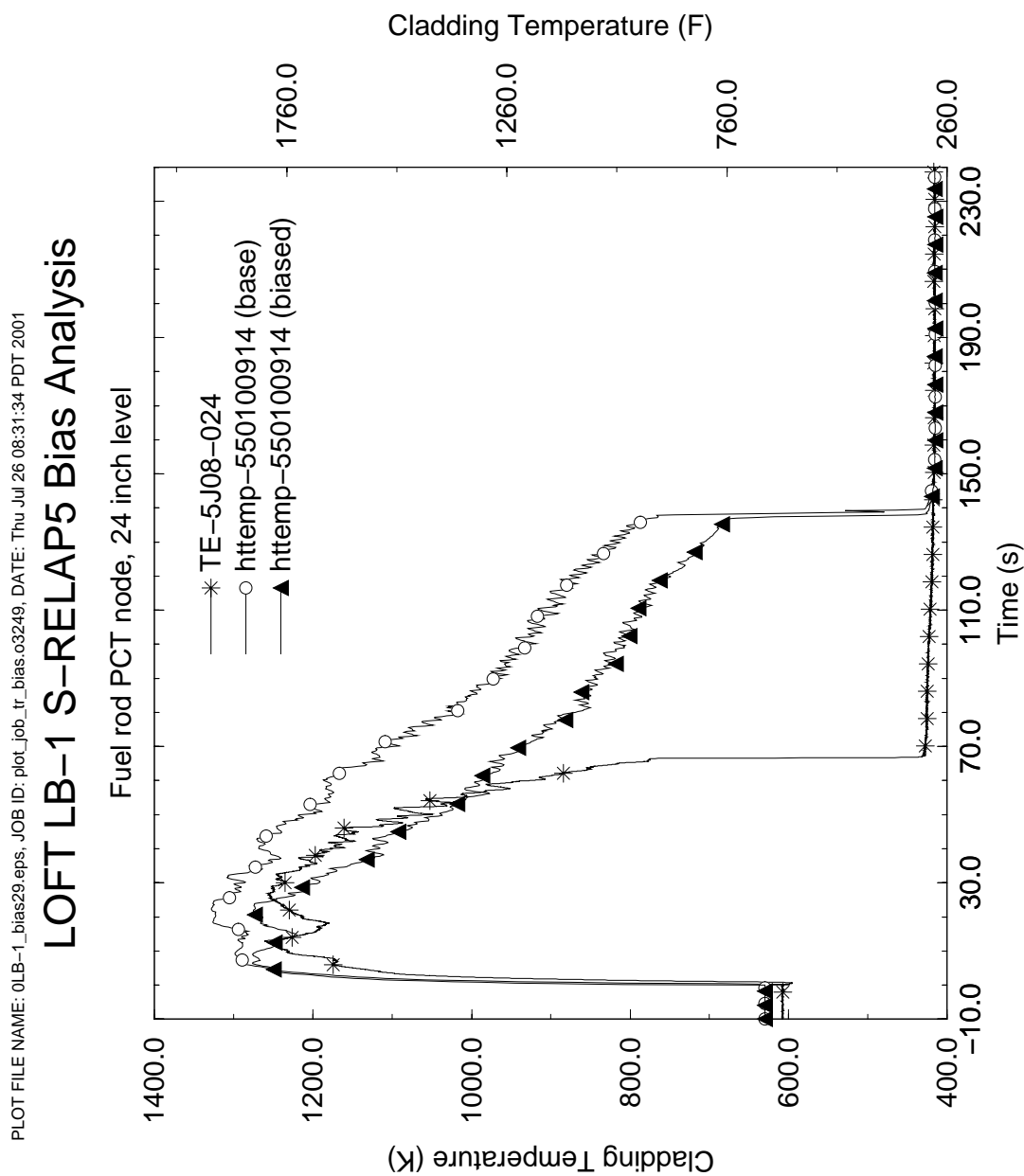


Figure 4.193 LOFT LP-LB-1 Temperatures at Measured PCT Node

LOFT LP-LB-1 S-RELAP5 ANALYSIS PLOT FILE NAME: 0lb-1_pct_00.eps, JOB ID: make_pct_plot_bias.o3250, DATE: Thu Jul 26 16:35:25 PDT 2001

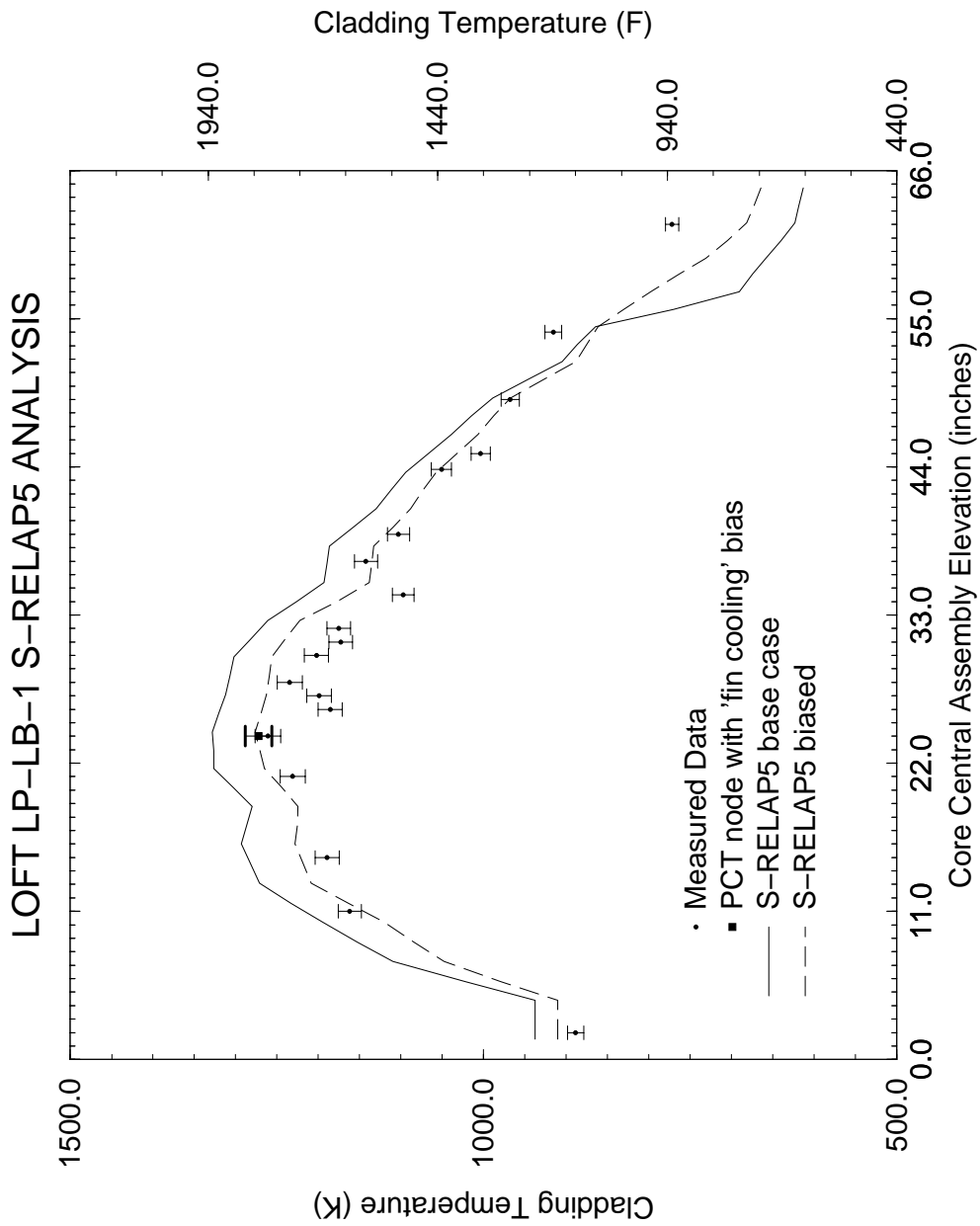


Figure 4.194 LOFT LP-LB-1 PCT Profile

PLOT FILE NAME: 0L2-6_bias29.eps, JOB ID: plot_job_tr_bias.o3248, DATE: Thu Jul 26 08:29:58 PDT 2001

LOFT L2-6 S-RELAP5 Bias Analysis

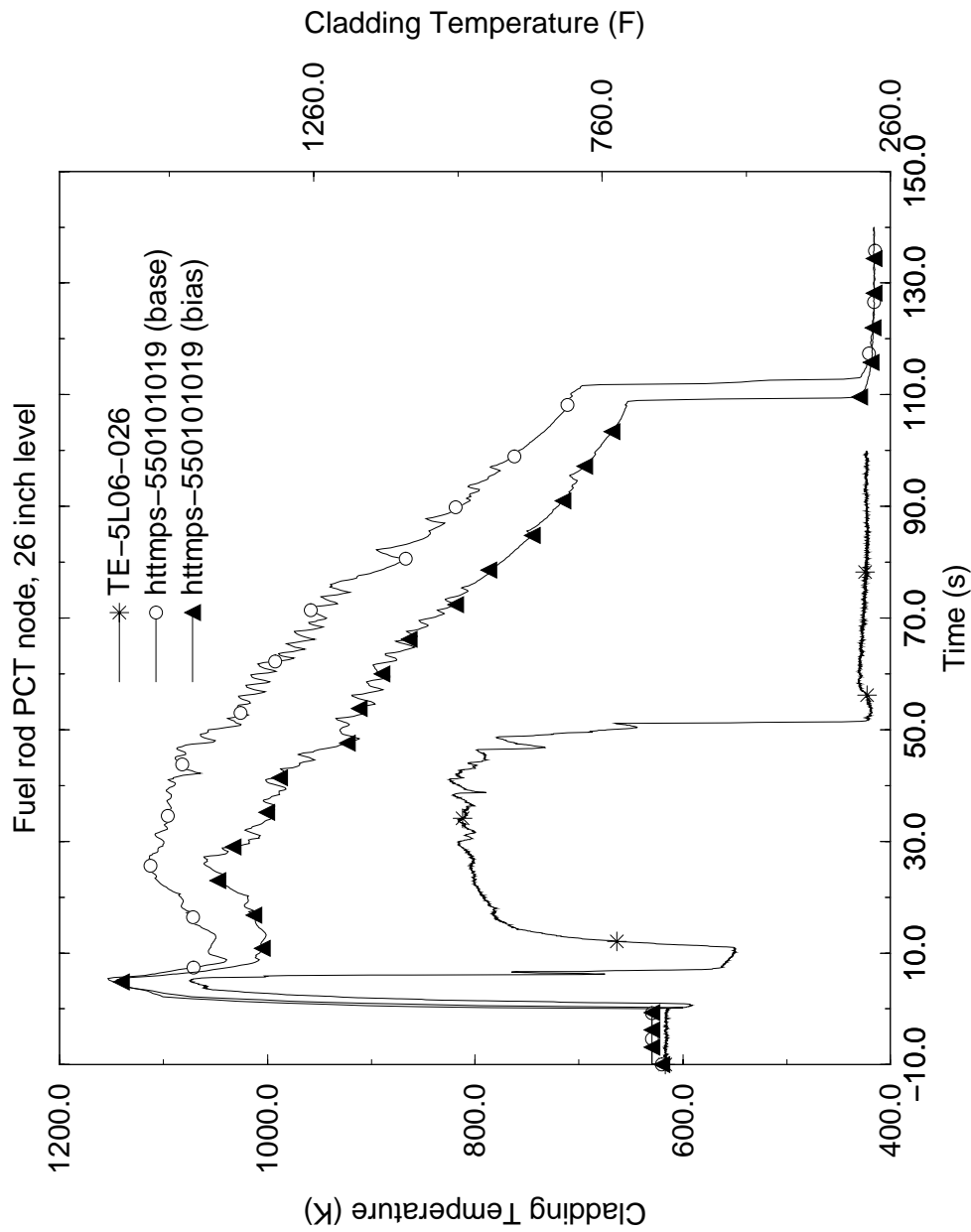


Figure 4.195 LOFT LP-02-6 Temperatures at Measured PCT Node

LOFT LP-02-6 S-RELAP5 ANALYSIS PLOT FILE NAME: 012-6_pct_00.eps, JOB ID: make_pct_plot_bias.o3251, DATE: Thu Jul 26 16:35:49 PDT 2001

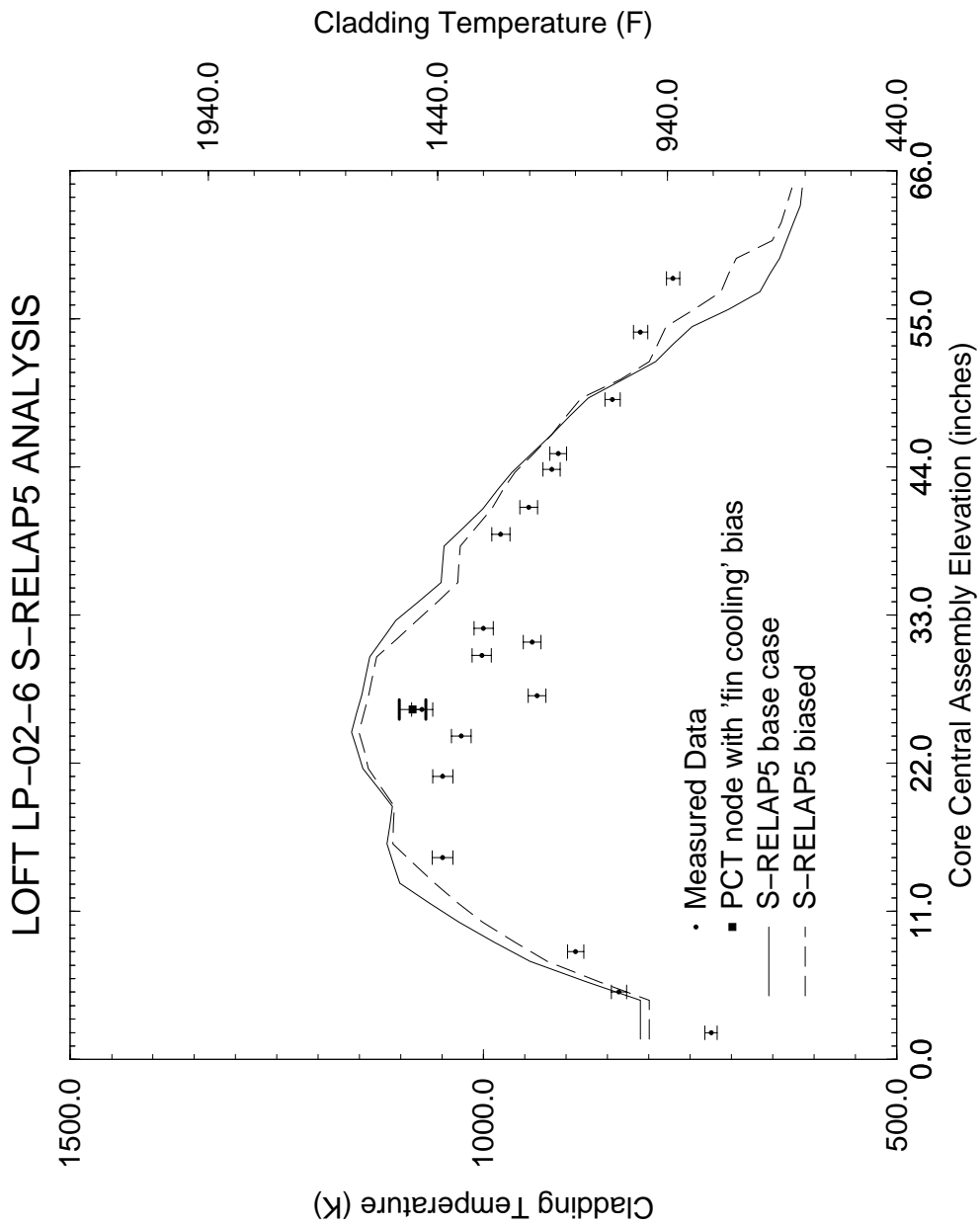


Figure 4.196 LOFT LP-02-6 PCT Profile

PLOT FILE NAME: 0L2-5_bias29.eps, JOB ID: plot_job_tr_bias.03247, DATE: Thu Jul 26 08:28:09 PDT 2001

LOFT L2-5 S-RELAP5 Bias Analysis

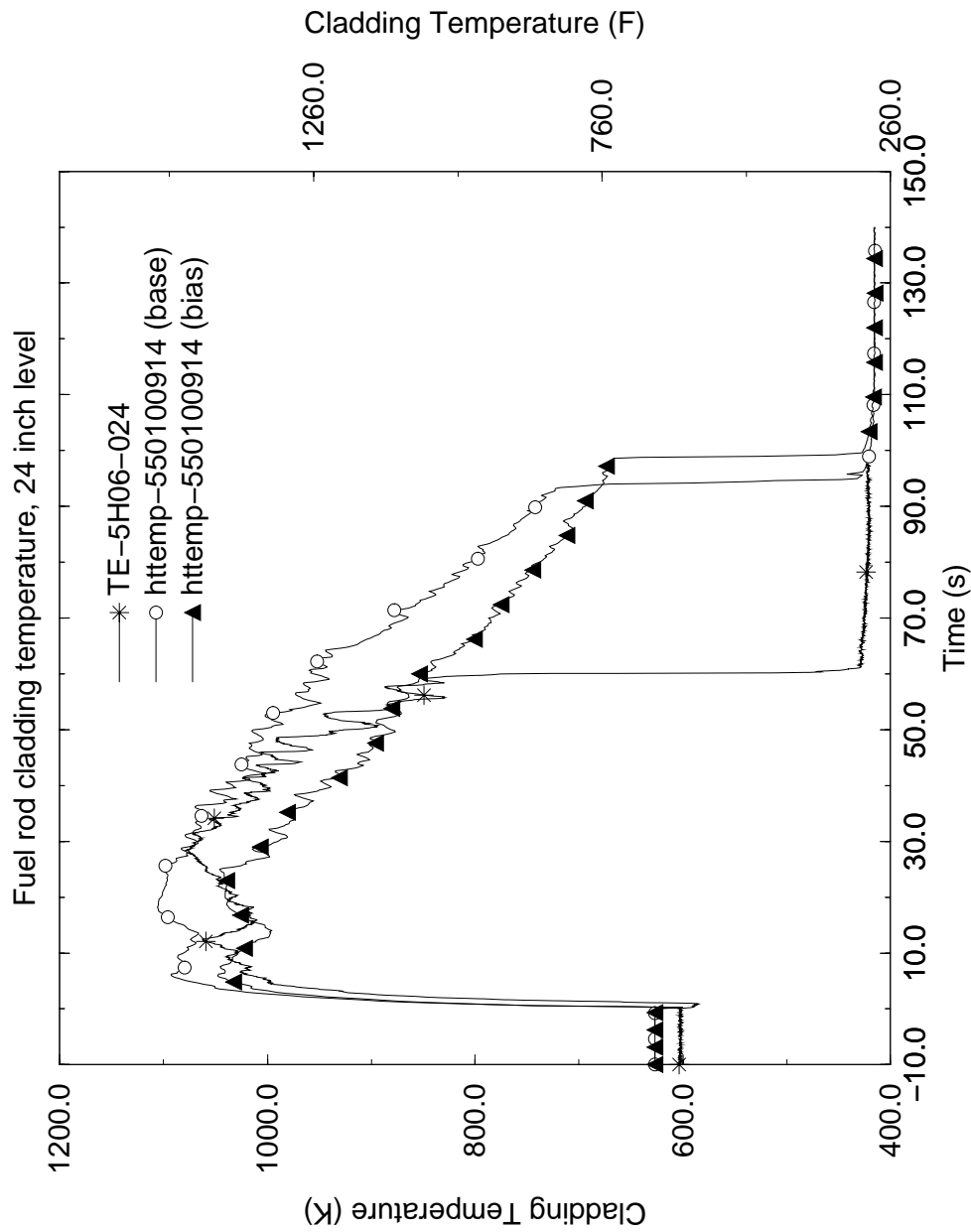


Figure 4.197 LOFT L2-5 Temperatures at Measured PCT Node

LOFT L2-5 S-RELAP5 ANALYSIS PLOT FILE NAME: 012-5_pct_00.eps, JOB ID: make_pct_plot_bias.o3252, DATE: Thu Jul 26 16:36:13 PDT 2001

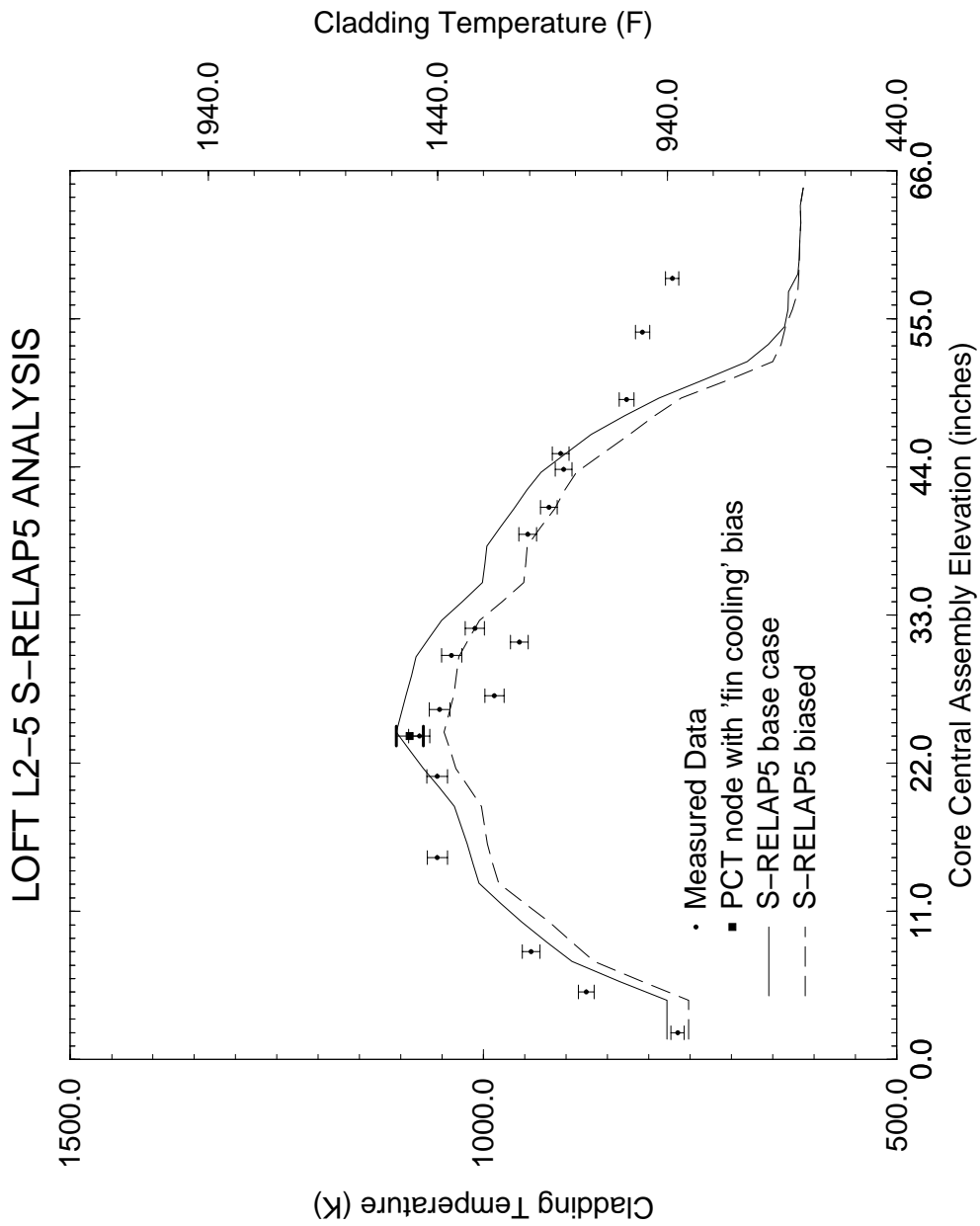


Figure 4.198 LOFT L2-5 PCT Profile

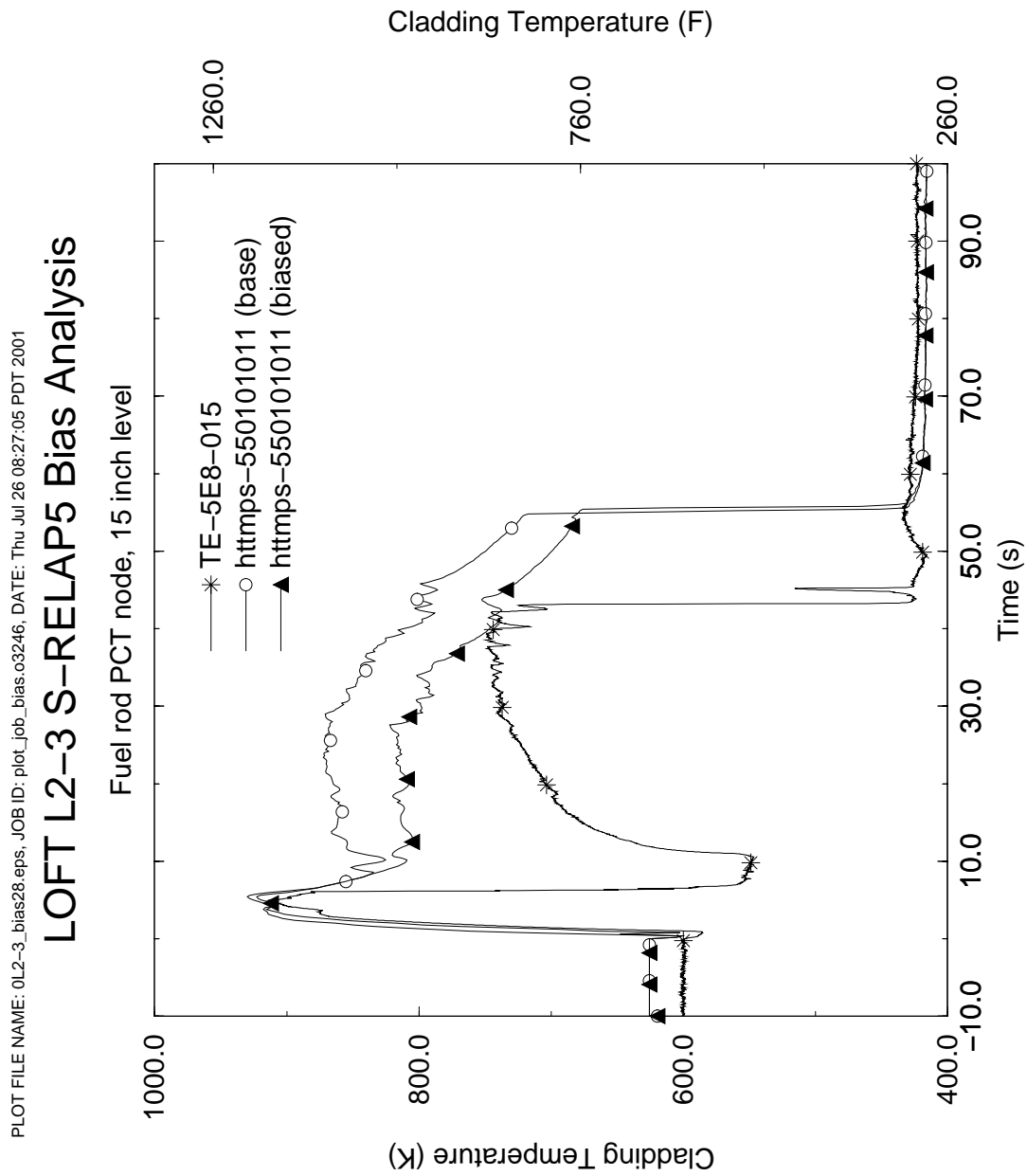


Figure 4.199 LOFT L2-3 Temperatures at Measured PCT Node

PLOT FILE NAME: 0L2-3_bias30.eps, JOB ID: plot_job_bias.o3246, DATE: Thu Jul 26 08:27:05 PDT 2001

LOFT L2-3 S-RELAP5 Bias Analysis

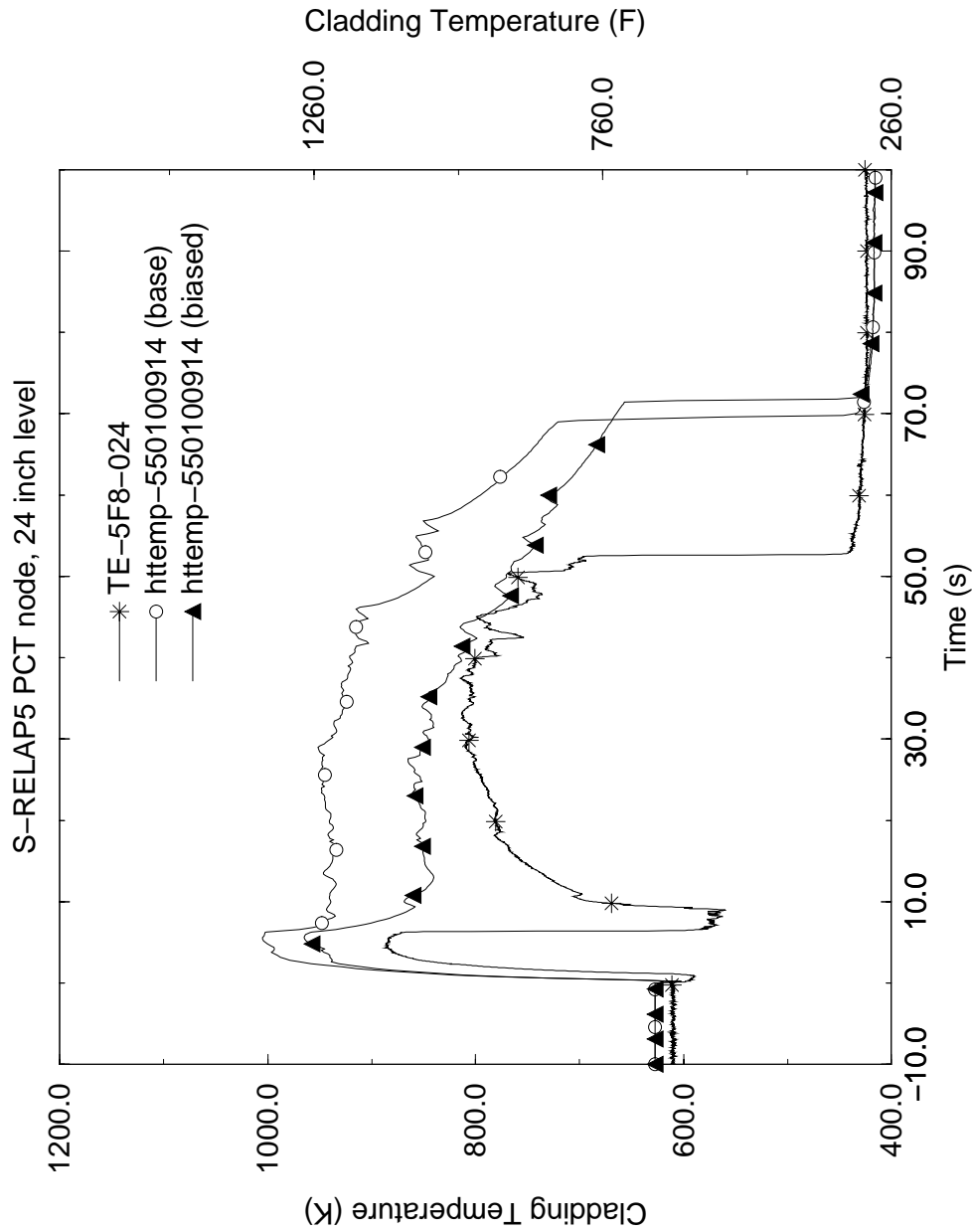


Figure 4.200 LOFT L2-3 Temperatures at Calculated PCT Node

LOFT L2-3 S-RELAP5 ANALYSIS PLOT FILE NAME: 012-3_pct_00.eps, JOB ID: make_pct_plot_bias.o3253, DATE: Thu Jul 26 16:40:49 PDT 2001

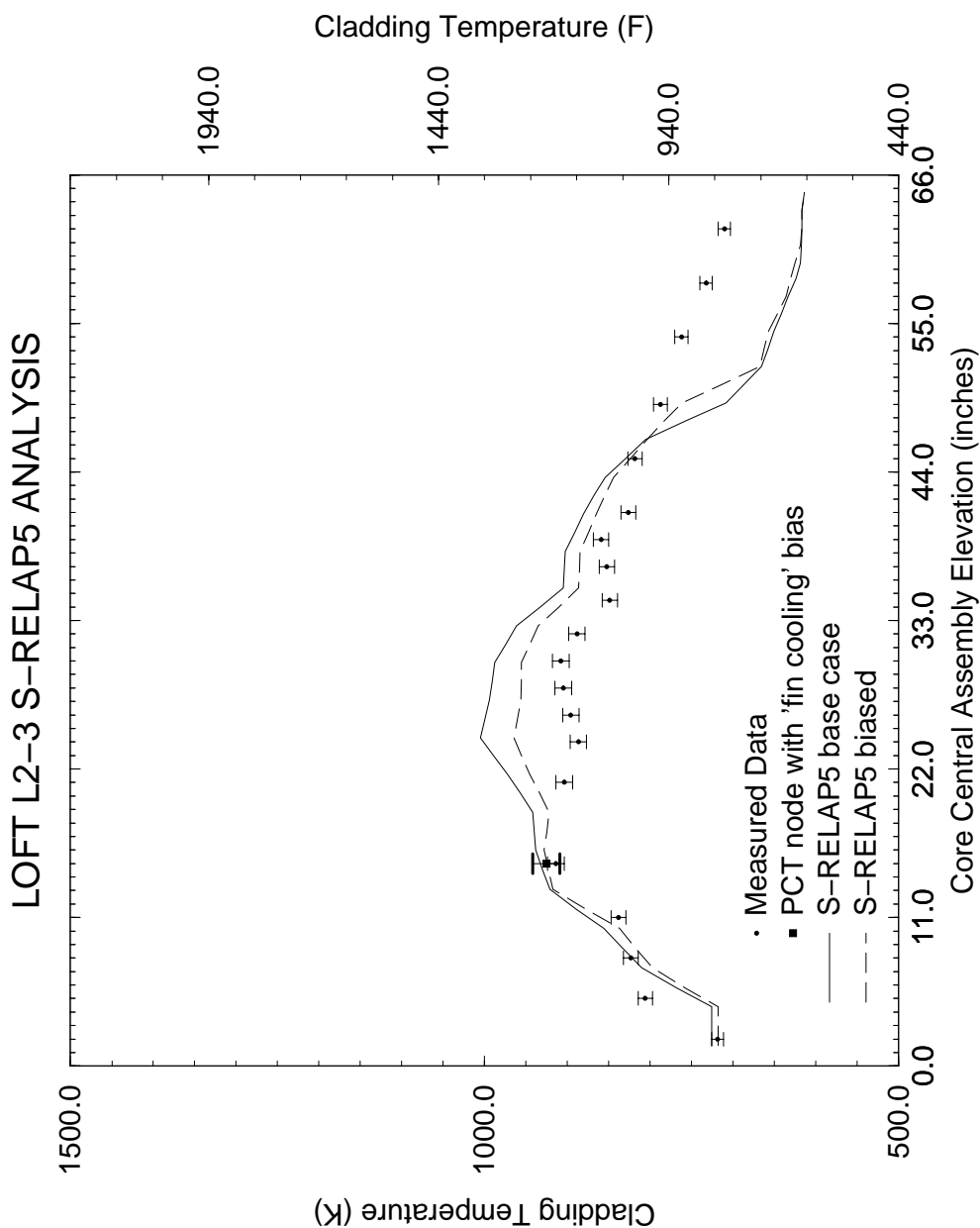


Figure 4.201 LOFT L2-3 PCT Profile

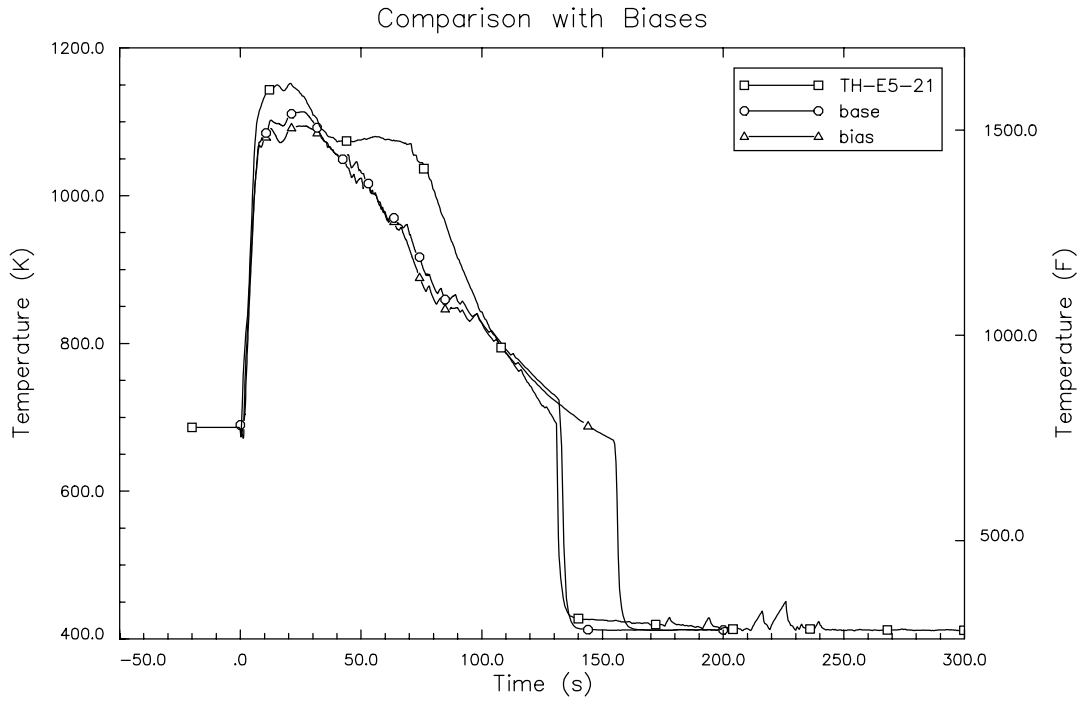


Figure 4.202 Semiscale S-06-3 Temperatures at Measured PCT Node

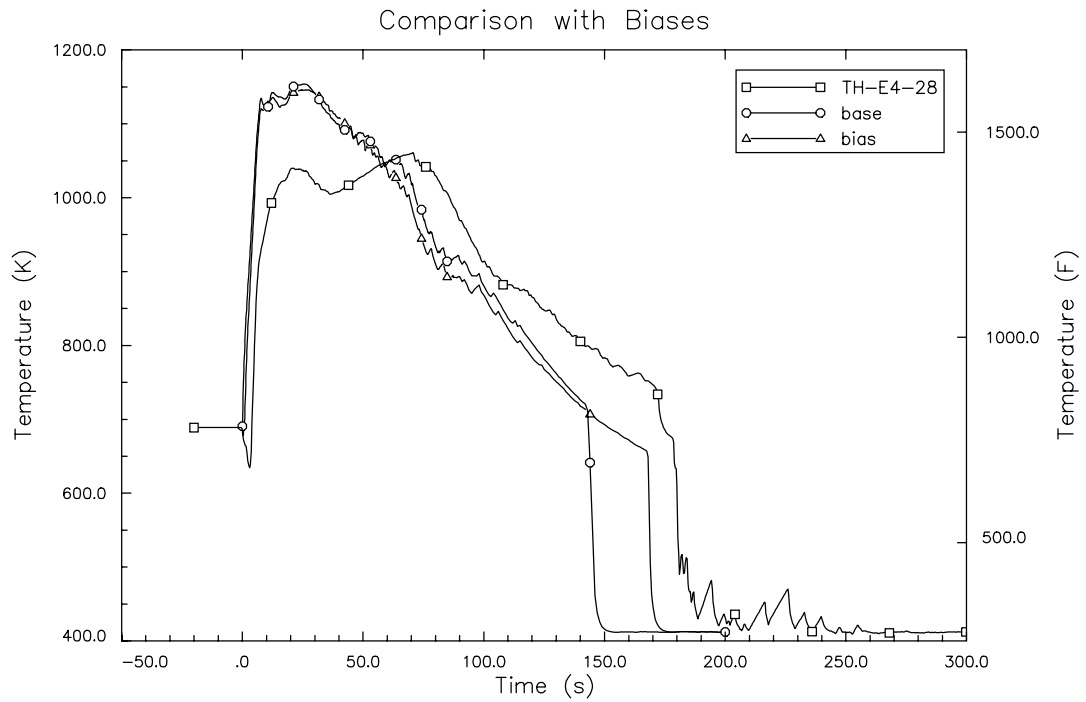


Figure 4.203 Semiscale S-06-3 Temperatures at Calculated PCT Node

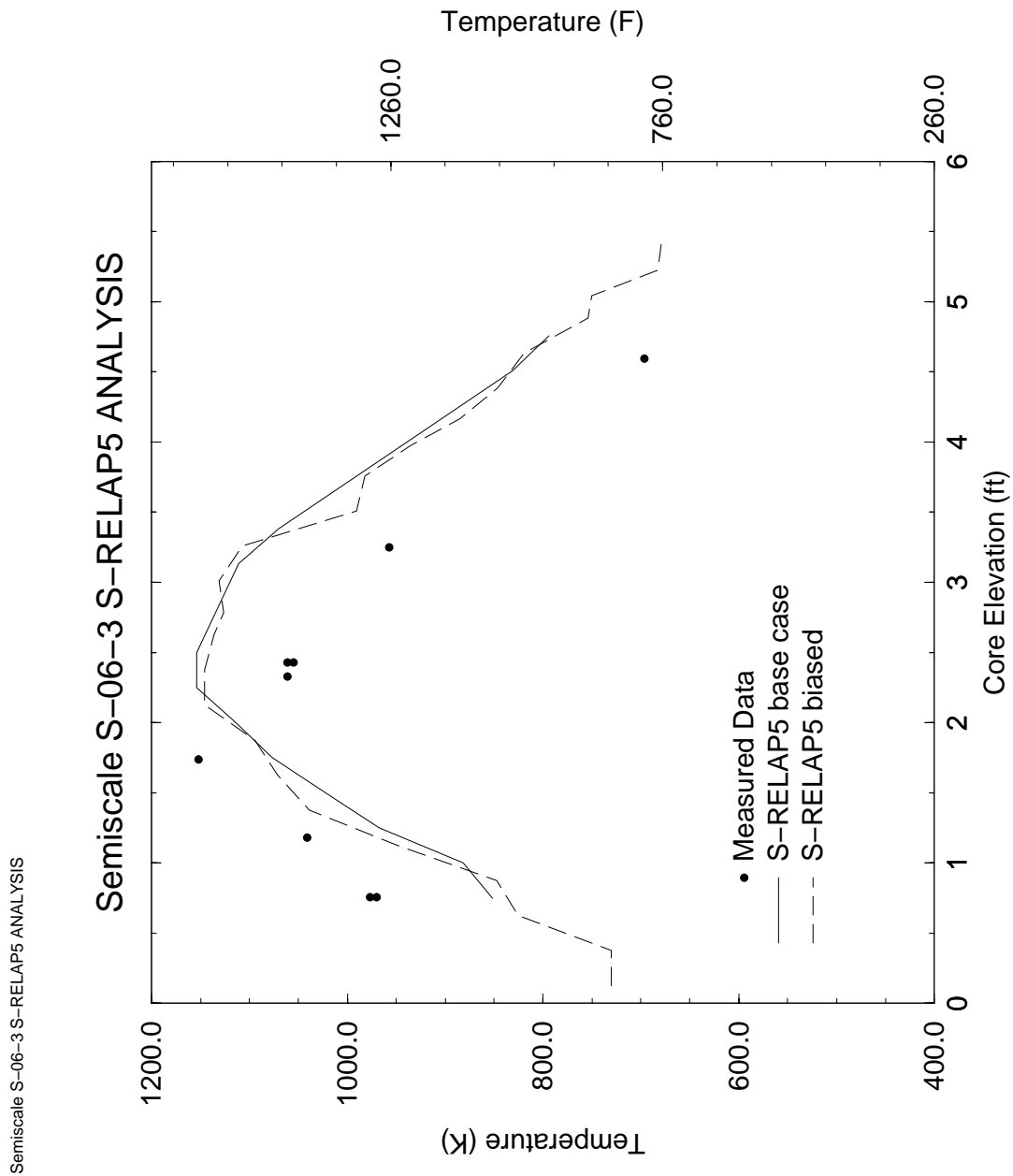


Figure 4.204 Semiscale S-06-3 PCT Profile

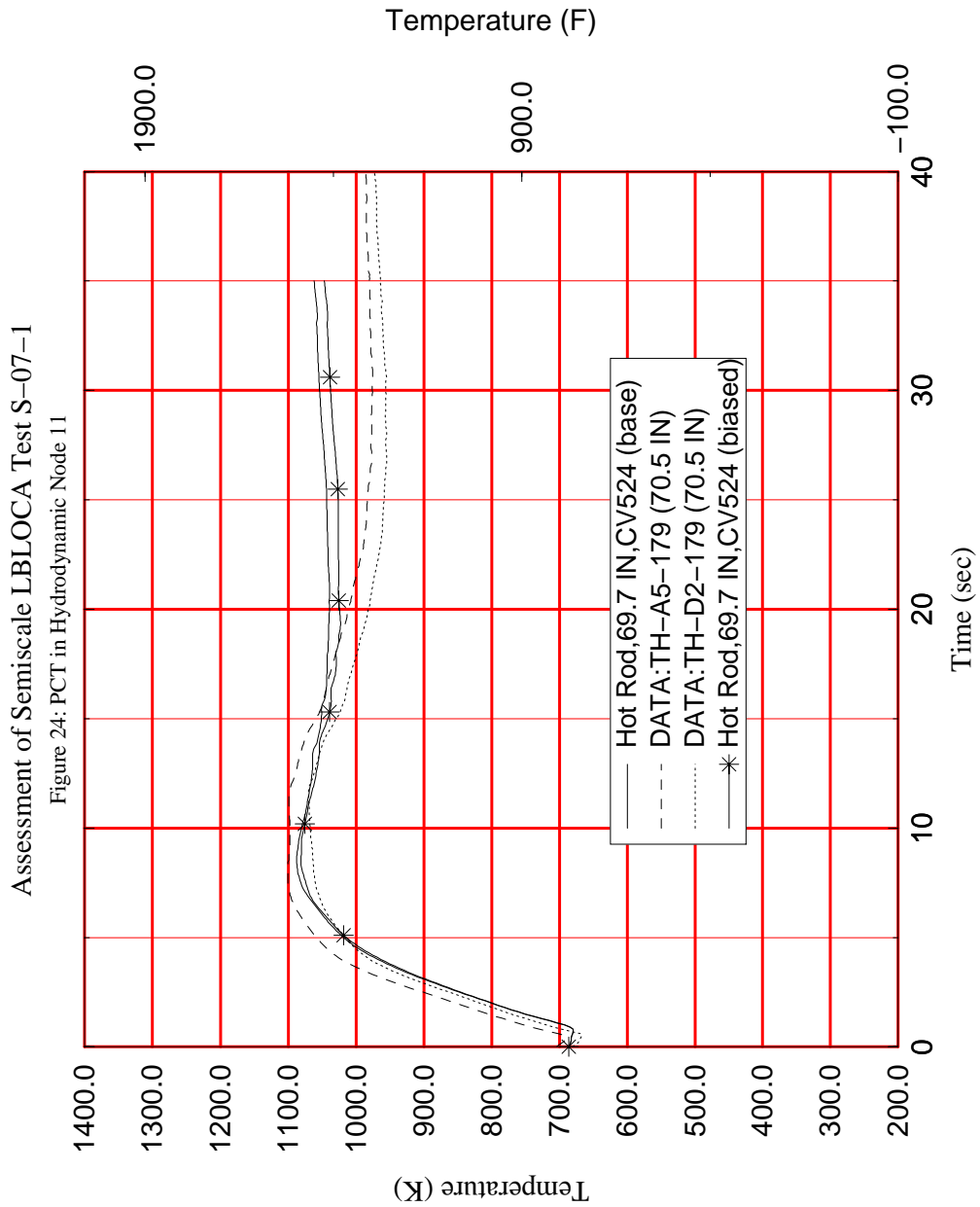


Figure 4.205 Semiscale S-07-1 Temperatures at Measured PCT Node

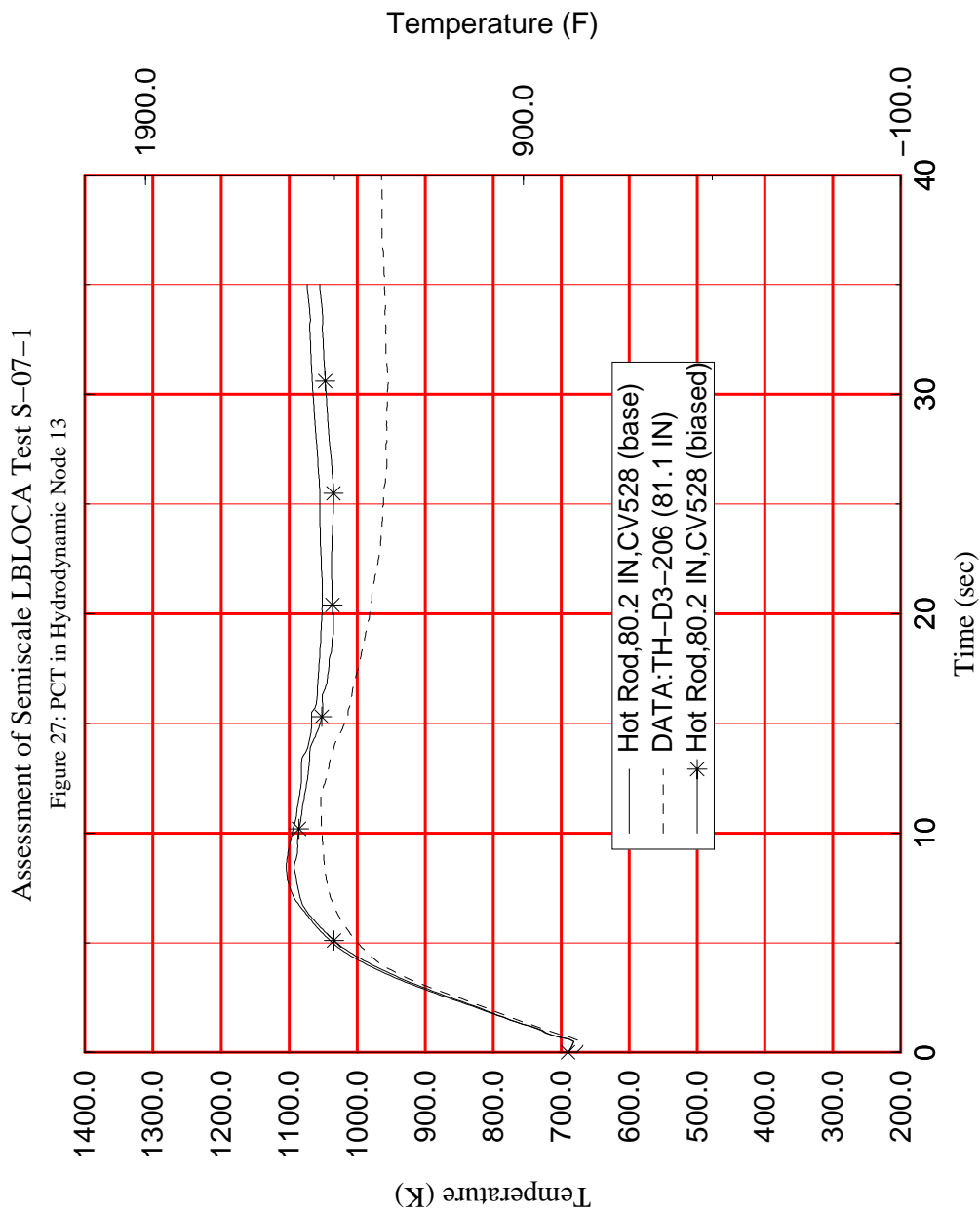


Figure 4.206 Semiscale S-07-1 Temperatures at Calculated PCT Node

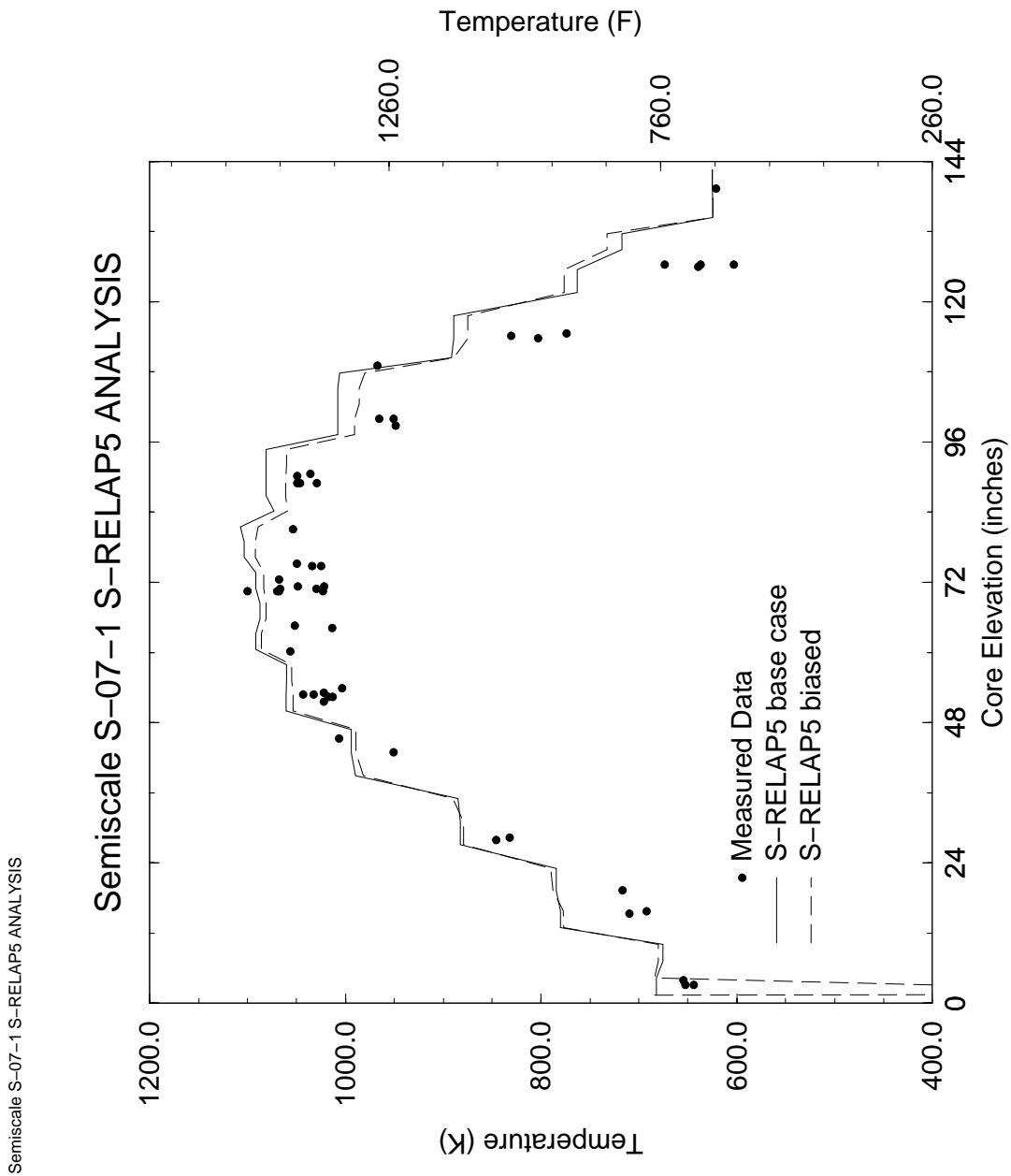


Figure 4.207 Semiscale S-07-1 PCT Profile

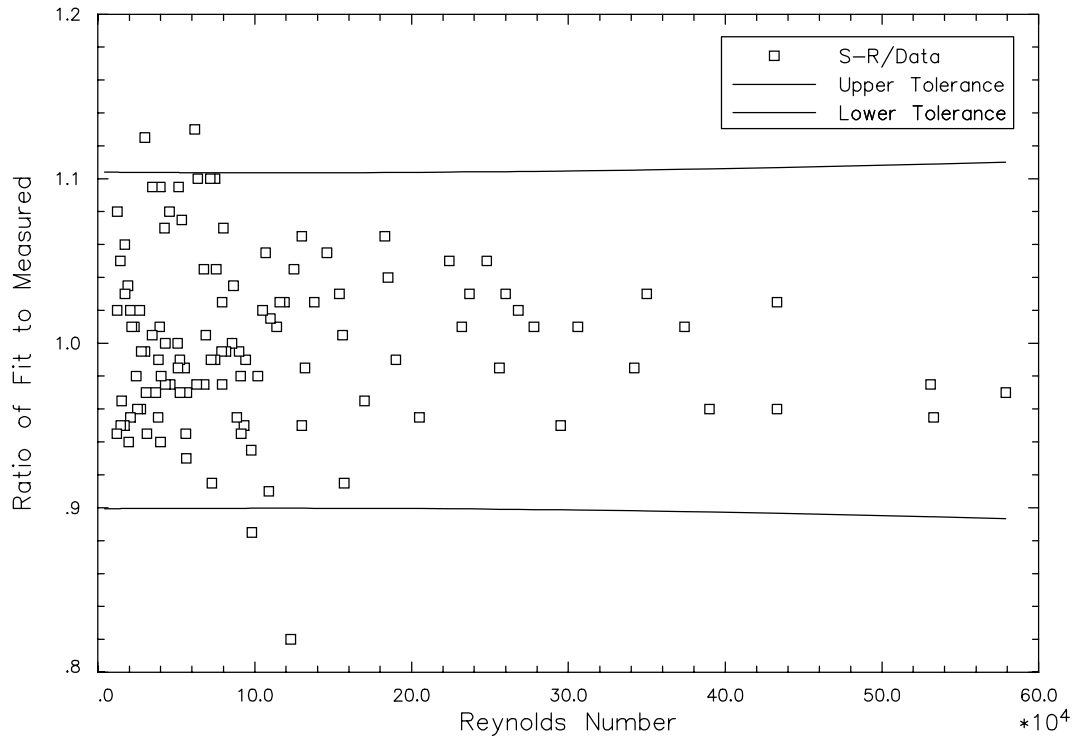


Figure 4.208 Sleicher-Rouse HTC for Steam Compared to Data

5.0 Sensitivity and Uncertainty Analysis

The objective of this section is to provide a statement of acceptability for each of the licensing criteria for the specified event. This is accomplished by evaluating the impact of the initial reactor state at the initiation of the specified event and determining a combined uncertainty statement. This combined uncertainty statement must address the biases and uncertainties in the important PIRT phenomena and the operating state of the NPP at the initiation of the event.

5.1 *Determination of Effect of Reactor Input Parameters and State (CSAU Step 11)*

The dynamics of a NPP may be characterized by design, phenomenological, and process (or operational) parameters. Design parameters are fixed values, such as a pipe diameter. Uncertainties associated with using design and phenomenological parameters are addressed by maintaining strict adherence to nodalization and identifying phenomenological uncertainties from code assessment studies applying well-defined nodalization guidelines. This is discussed in Sections 4.2 and 4.3, describing CSAU Steps 8 and 9. In contrast, process parameters characterize the state of operation and are, to various degrees, controllable by plant operators. Realistic variations can be expected in these parameters and uncertainty may be quantified with experimental and/or analytical studies.

5.1.1 Determining Important Process Parameters

From an operational standpoint, the NPP operating state is a function of the time in cycle (via burnup and power distribution) and the actual conditions present in the various NPP components. The deterministic approach to supporting the allowed variations in the NPP is to identify conservative bounds that are applied during safety analysis. Considering the complex nature of a NPP, such a declaration of conservatism can be given based only on the first order expectation of the effect of the given parameter on key LOCA parameters (e.g., PCT). Competing or compensating effects are possible; however, addressing these issues can be a challenging task in deterministic safety analysis. In contrast, treating these process parameters statistically accounts for higher order behavior by including all possible combinations in the sample space.

As part of the FRA-ANP RLBLOCA methodology development, a review was performed to identify the NPP parameters that are to be addressed in the performance of a LBLOCA

analysis. The identified parameters are provided in Table 5.1. The basis for inclusion in this list comes from three sources: PIRT, plant-specific technical specifications, and utility requests.

Determination of which process parameters to treat statistically begins with identifying the relationship a particular parameter has to any PIRT phenomenon. Table 5.2 lists process parameters determined to be important based on their potential influence to the moderate-to-high ranked phenomena given in Table 3.4. Process parameters that may only influence low ranked phenomena also should be included if an explicit limit is stated in a plant's technical specifications. Finally, utility requests may require the addition of still more process parameters. Such requests may be asked for support of plant procedures not explicitly mentioned in the technical specifications. To support the PIRT, the technical specifications, and any utility requests, these parameters will be explicitly treated by the RLBLOCA methodology. The preferred method for treating these parameters is statistically; however, conservative methods also can be used in the absence of adequate data to support a statistical approach.

5.1.2 Role of Sensitivity Studies

Quantifying the effect of individual process parameters is [

] Nonetheless, sensitivity studies on the parameters given in Table 5.1 have been performed and included in the histogram presented in Figure 4.2. The primary value of these calculations is to establish a perspective on the level of importance a safety analysis team might give in quantifying process parameter uncertainties. For example, having insufficient information to support adequately describing a highly sensitive parameter may reduce the margin for key LBLOCA parameters such as PCT; while a conservative or bounding value may be easily justified for a parameter producing little sensitivity in the PCT. Table 5.3 ranks the results from a set of sensitivities performed for process parameters on both 3- and 4-loop PWRs (highest to lowest). The list is abbreviated to include only those parameters having significant sensitivity on PCT (i.e., >50 F).

Sensitivity studies also may be used to justify not treating a parameter statistically. Parameters not treated statistically fall into two categories: those to be treated conservatively or those that are judged to be not significant. Parameters can be demonstrated to be insignificant by

sensitivity studies and/or by their relationship to low-ranked PIRT parameters. Conservatism should be demonstrated by sensitivity studies. The analysis team chooses which parameters to treat conservatively.

5.1.3 Quantifying Statistical Quantities

For the FRA-ANP RLBLOCA methodology there are a number of plant specific parameters which are treated statistically.

5.1.3.1 General

The identified process parameters shown in Table 5.1 are allowed to vary within a prescribed range throughout an operational cycle. The constraints on these ranges may be defined from a plant's technical specifications, some physical or operational limitation, or a utility request. For example, the accumulator pressure is allowed to vary within a prescribed operating range based on a plant's technical specification. Similarly, containment temperature is usually constrained by technical specification on high temperature; however, no limit may be expressed for the low-temperature range, which may come from plant data or by other means.

While process parameters are expected to vary with plant operation, design constraints, given in the form of plant technical specifications, will provide a one- or two-sided limit on the variation. It should be noted that not all process parameters such as fuel state are explicitly constrained by technical specifications. For those operational parameters such as fuel state, other parameters having a direct effect on the operational parameter of consideration are constrained by the plant Technical Specifications (e.g., power peaking for the fuel state).

Inherent in the FRA-ANP RLBLOCA methodology is [

] To treat a parameter statistically, the parameter uncertainty must be quantified in terms of biases and distributions. Quantifying this uncertainty with plant data is the best approach. At most plants, histories of core power, RCS flow rate, core inlet temperature, pressurizer and accumulator parameters, containment temperature, and diesel start times are available. In some instances, parameter uncertainties may need to consider two components of uncertainty: operational range and measurement. Operational uncertainty is defined as the true fluctuation of the parameter during normal

operation. Measurement uncertainty addresses the error associated with measuring the parameter.

From analysis of plant data, the statistical distribution and uncertainty can be quantified. While measurement uncertainty is most often characterized by a normal distribution, no particular uncertainty distribution is expected describing operational variations. The choice of distribution may have implications as to how a utility manages the process parameter of interest. For example, using a uniform distribution may be attractive to a utility in that it will support the most flexibility in how they control a given parameter. Conversely, uniform distributions may be more conservative in that equal likelihood is given for values that reduce operation margin.

Other distributions will be considered if supported by the data. Additionally, it is not likely that a parameter limited by a plant's technical specification will coincide with limits identified by plant data. Technical specifications often bound the nominal operational range. In this situation, the statistical distribution on measurement uncertainty may be adjusted to ensure that the Technical Specification limits are included in the parameter's sample space.

An assessment of plant data provided for key process parameters has been performed for an existing 3-loop NPP. Table 5.4 summarizes the results of this assessment in terms of statistical distributions. In applications to other plants, such distributions may be different.

5.1.3.2 Treatment of Time in Cycle

The time in cycle establishes the fuel rod properties and the lower bound for the global power peaking factor, F_q . [

] Power history calculations are performed using an NRC approved methodology (References 64 and 65). Typically, fuel rod data for 20 to 40 burnup steps are explicitly written from a cycle power history calculation. Fuel rod data is provided for the life of a fuel rod; however, sensitivity studies have been performed that show only fresh fuel assemblies are limiting (Appendix B).

In contrast to a traditional safety analysis, which assumes conservative fuel rod models consistent with Appendix K requirements, [

1.]
2. []
3. []
4. []
-]

The data produced by this method is used primarily to develop input for the RODEX3A code.

[]

5.1.3.3 Treatment of Axial and Radial Power Shapes

To support a plant's technical specification for the core peaking factor, F_q , the axial power shape must be adjusted from the nominal axial power shape extracted for the limiting fuel rod. During normal operation, F_q will most likely occur relatively near the nominal F_q represented in the power history files. []

[]

[

]

[

]

[

]

- []
- []
- []
- []
- []
- []
- []

5.1.4 Supporting Ranges Without Data

As shown in Table 5.1, some parameters lack explicit definition (technical specifications or data). For parameters for which no plant data is available, ranges may be established based on physical constraints or by analytical methods. Examples of physical limits include ranging the vessel upper head temperature to a maximum value of the hot leg temperature or ranging the diesel start delay on the LPSI pumps to a time corresponding to when RCS pressure drops below the back pressure delivered by the LPSI pumps. It may also be demonstrated that a particular parameter has a limited range of influence based on a set of sensitivity studies.

5.1.5 Reporting of Treatment of Process Parameters

Many decisions are required to establish plant specific treatment of process parameters. Such decisions must be reported or referenced when issuing a safety analysis report. Because the ranges and statistical description of the behavior of plant parameters may vary from plant to plant, the safety analysis report will require an explicit discussion of the treatment of key process parameters. If no changes are made in the treatment of process parameters for subsequent analyses, the earlier report may be referenced.

5.2 **Performance of NPP Sensitivity Calculations (CSAU Step 12)**

5.2.1 Statistical Approach

[

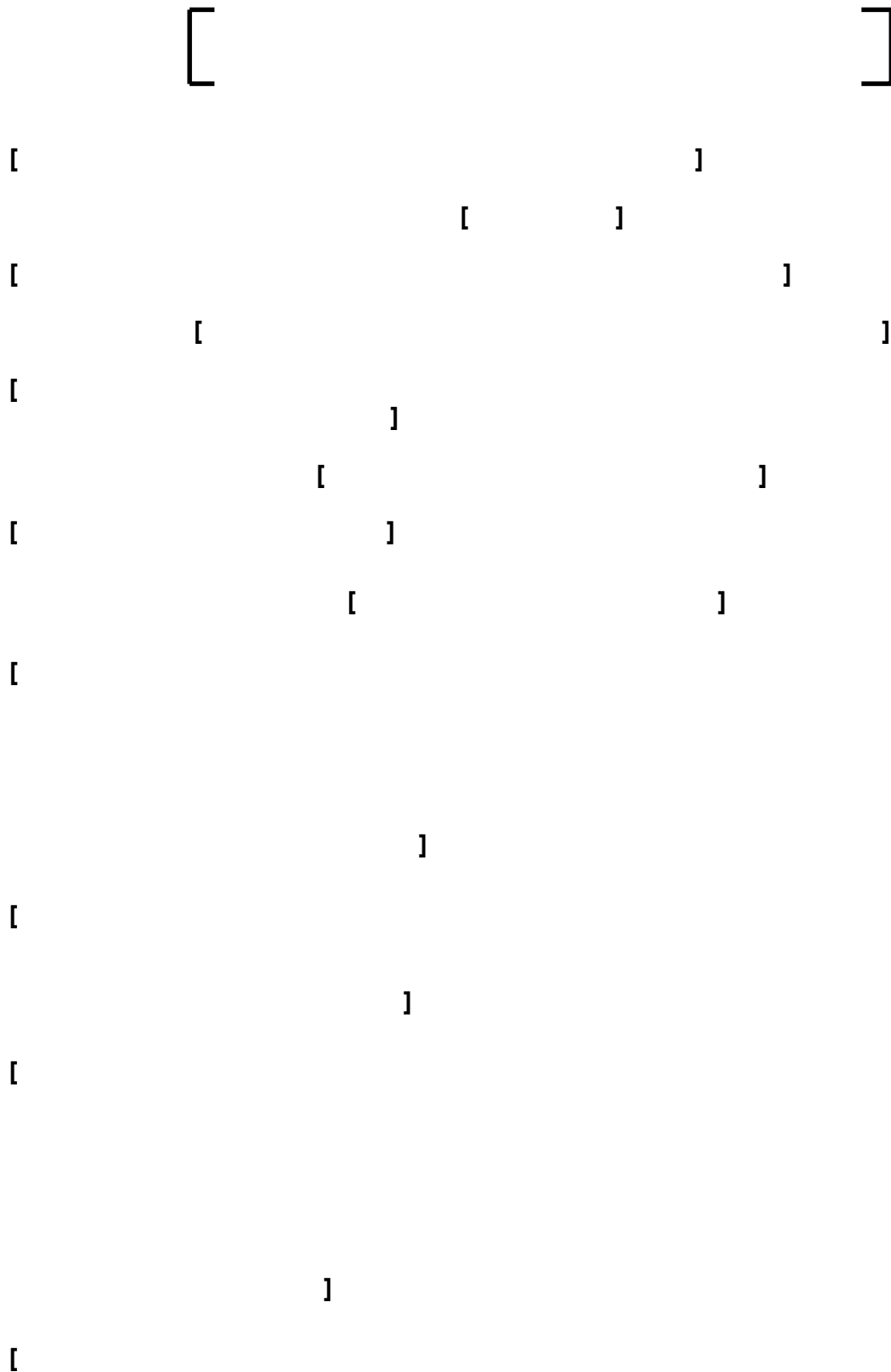
]

[

]

[

]



]

5.2.2 Application of Methodology

The FRA-ANP RLBLOCA methodology is a statistics-based methodology; therefore, the application does not involve the evaluation of different deterministic calculations. [

] The methodology results in a bounding value with 95% probability and 95% confidence in the PCT, total metal water reaction, and total core oxidation.

Application of this methodology relies on two computer codes: RODEX3A and S-RELAP5. All key LBLOCA parameters are calculated from S-RELAP5; RODEX3A is used to generate the initial fuel properties to be used by the fuel performance models in S-RELAP5. Performance of the RLBLOCA calculations relies on three analyst-created code input files describing the fuel, plant thermal-hydraulics, and containment thermal-hydraulics. The fuel model input is processed by the RODEX3A code, which will produce a binary file describing fuel properties. This file will be processed by S-RELAP5 during the steady-state initialization. During steady-state initialization, S-RELAP5 will process only the RODEX3A binary output file and the steady-state plant model input. The LBLOCA calculation is an S-RELAP5 "Restart" calculation. It relies only on the steady-state restart file, the S-RELAP5 LBLOCA transient input file, and the containment model input. The containment model input is similar to the original ICECON code (Reference 14), which evolved from the CONTEMPT code (Reference 20). Reportable LBLOCA parameters can be retrieved from the S-RELAP5 transient output file. Figure 5.1 depicts the calculational framework.

5.2.3 New RLBLOCA Analyses

[]

- []

- []

- []

- []

5.2.4 Ranging Uncertainty

[

] For this reason the RLBLOCA analyst must have available a validated random number generator. The most common type of random number generator available on most UNIX workstations produces a floating point value between zero and one. The random number generator provides sample values uniformly distributed.

Random number generators require that a random number seed be defined before processing the random number function. Most random number generators use a default random number seed when no seed is provided. The RLBLOCA methodology does not provide a random number seed and relies on the random number generator to pick the seed. The random number seed is recorded, in order allow reproduction of the of random numbers. This provides calculation traceability and a mechanism for reproducing a set of calculations.

Given that the random number generator provides uniformly distributed values between 0 and 1, other probability distributions must be mapped from these distributions. For this methodology, the common probability distributions applied to parameter uncertainty ranges are binary, uniform between two arbitrary numbers, and normal. A typical uniform random number generator produces values, r , ranging from 0 to 1.

A uniform probability distribution function ensures an equal probability of selecting any given value over the range of interest. Using the uniform random number generator, a sample, z , from a uniform probability distribution function ranging between two points, a and b , is defined as

$$z = a + (b - a) \cdot r$$

A normal probability distribution function is the natural limit to the combination of many random events. Using the uniform random number generator; two samples, z_1 and z_2 , for a normal probability distribution function can be created from two samples from a uniform distribution, r_1 and r_2 (Reference 70)

$$z_1 = \eta + \sigma \cdot \cos(2 \cdot \pi \cdot r_1) \cdot \sqrt{-2 \cdot \ln(r_2)}$$

and

$$z_2 = \eta + \sigma \cdot \sin(2 \cdot \pi \cdot r_1) \cdot \sqrt{-2 \cdot \ln(r_2)}$$

where η and σ are the mean and standard deviation of the normal distribution, respectively.

Similarly, other distributions can be related to a uniform random distribution, so that a variety of probability distributions can be treated in the LBLOCA calculation.

5.2.5 Parameter Initialization

The key parameters identified for ranging have been summarized previously in Tables 4.1 and 5.2. Table 5.6 presents these parameters as they relate to computer code input.

5.2.6 Calculation Order

[

] The key results are the PCT, maximum cladding nodal oxidation, and total core wide oxidation.

5.2.7 Subsequent RLBLOCA Analyses

[

]

[

]

5.3 ***Determination of combined Bias and Uncertainty (CSAU Step 13)***

This section presents the results of a sample RLBLOCA analysis for a W 4-loop plant. An actual licensing analysis is in progress for a W 3-loop plant and will be submitted by the utility following the utilities review and acceptance of the analysis (Reference 16).

This 4-loop sample problem was performed in accordance with the calculation framework shown in Figure 5.1 as described above and in more detail in Reference 13. The base input models for the fuel rod and NPP were developed as described above and in conformance with Reference 12. The input for the fuel rod code was developed based on an existing FRA-ANP 17x17 fuel assembly with 0.955 cm (0.376 in) fuel rods. The input for the NPP was developed based on information which was obtained for several different 3 and 4-loop plants and consequently can only be considered as representative of a 4-loop plant. However, the NPP input model is adequate to demonstrate the application of the FRA-ANP RLBLOCA methodology described in this report.

The parameters treated statistically are listed in Table 5.6 and the values for the specific parameters and ranges addressed are given in Table 5.7. The distributions assumed for this sample problem are those given in Table 5.4. [

] The results of these calculations are presented in Figures 5.2 through 5.28.

Figures 5.2 through 5.16 present scatter plots for the more important phenomena/parameters in the analysis. These scatter plots are provided to demonstrate that the methodology does select input which covers the phenomena/parameter ranges and associated distributions. In general, it is difficult to see the PCT dependence of an individual parameter from these scatter plots. This is primarily due to the fact that there are several major parameters and a conservative combination of these parameters is required to obtain the higher values of PCT. Based on this the following paragraphs will concentrate on a discussion of the LBLOCA criteria as addressed by the analysis.

[

]

[

]

[

]

[

]

[

]

[

]

[

]

[

]

[

]

[

]

[]

[]

[]

5.4 ***Determination of Total Uncertainty (CSAU Step 14)***

[] the biases and uncertainties determined during the code assessments are either directly addressed in the statistical analysis or demonstrated to be a code conservatism which adds an additional unquantified conservatism to the reported results. The final results for the 4-loop sample problem can be summarized as follows:

- The 95/95 calculated PCT was 1686 F which compares to the criterion for maximum PCT of 2200°F.
- The 95/95 calculated maximum nodal oxidation was 1.1% which compares to the criterion for maximum nodal oxidation of 17%.
- The 95/95 calculated maximum total oxidation was 0.02% which compares to the criterion for maximum total core oxidation of 1%.

Based on these results, it is concluded that the LBLOCA analysis for the sample W 4-loop plant meets the criteria for the LBLOCA event.

With respect to the identification of the degree of conservatism in the analysis, a comparison can be made to the 50/50 probability values for the PCT, maximum nodal oxidation, and the maximum total core oxidation. This comparison is provided in Table 5.12. As indicated in this table the 50/50 PCT at 1375°F is 311°F less than the 95/95 PCT. The 50/50 total core oxidation at 0.003% is nearly an order of magnitude less than the 95/95 value while the 50/50 maximum nodal oxidation at 0.34% is nearly one fourth that of the 95/95 value.

**Table 5.1 NPP Parameters for Consideration in the Performance of a
Realistic LBLOCA Analysis**



Table 5.2 Relationship of PIRT to Operational Parameters



Table 5.3 Ranked Importance of Process Parameters Relative to Plant Type

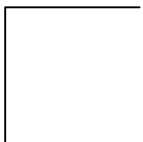
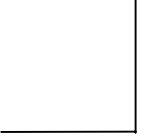
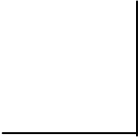


Table 5.4 Statistical Distributions Used for a Sample 3-Loop PWR



**Table 5.5 Number of Observations Required for a Desired
Tolerance: Non-Parametric Methods**

Table 5.6 Relationship of Uncertainty Parameters to Computer Code Input



**Table 5.7 Plant Operating Range and Fuel Design Supported by the
LOCA Analysis**

	<i>Event</i>	<i>Operating Range</i>
1.0	<i>Plant Physical Description</i>	
	<i>1.1 Fuel</i>	
	<i>a) Cladding outside diameter</i>	<i>0.376 in.</i>
	<i>b) Cladding inside diameter</i>	<i>0.328in.</i>
	<i>c) Cladding thickness</i>	<i>0.024 in.</i>
	<i>d) Pellet outside diameter</i>	<i>0.3215 in.</i>
	<i>e) Pellet density</i>	<i>95 % of theoretical</i>
	<i>f) Active fuel length</i>	<i>144 in.</i>
	<i>g) Maximum rod-average exposure</i>	<i>62,000 MWd/MTU</i>
	<i>1.2 RCS</i>	
	<i>a) Flow resistance</i>	<i>Analysis</i>
	<i>b) Pressurizer location</i>	<i>Analysis assumes location giving most limiting PCT</i>
	<i>c) Hot assembly location</i>	<i>Anywhere in core</i>
	<i>d) Hot assembly type</i>	<i>17x17</i>
	<i>e) SG tube plugging</i>	<i>≤ 10%</i>
2.0	<i>Plant Initial Operating Conditions</i>	
	<i>2.1 Reactor Power</i>	
	<i>a) Core average linear heat generation rate</i>	<i>Core power ≤ 102% of 3250 MWt</i>
	<i>b) Peak linear heat generation rate</i>	<i>≤ 2.62* (normalized)</i>
	<i>c) Hot rod average linear heat generation rate</i>	<i>≤ 1.8† (normalized)</i>
	<i>d) Hot assembly linear heat generation rate</i>	<i>< 1.731‡ (normalized)</i>
	<i>e) Hot assembly burnup</i>	<i>≤ 62000 MWD/MTU</i>
	<i>f) MTC</i>	<i>≤ 0 at HFP</i>
	<i>g) HFP boron</i>	<i>Normal letdown</i>
	<i>2.2 Fluid Conditions</i>	
	<i>a) Loop Flow</i>	<i>122.6 Mlb/hr ≤ M ≤ 142.1 Mlb/hr</i>
	<i>b) Core Inlet Temperature</i>	<i>550.0 ≤ T ≤ 556.6 °F</i>

* Includes 5% measurement uncertainty and 3% manufacturing uncertainty.

† Includes 4% measurement uncertainty.

‡ Value equivalent to hot rod peaking factor without 4% uncertainty.

Table 5.7 Plant Operating Range Supported by the LOCA Analysis (continued)

	<i>Event</i>	<i>Operating Range</i>
	<i>c) Upper Head Temperature</i>	<i>< Core Outlet Temperature</i>
	<i>d) Pressurizer Pressure</i>	<i>$P \geq 2175$ psig</i>
	<i>e) Pressurizer Level</i>	<i>$48.2\% \leq L \leq 58.2\%$</i>
	<i>f) Accumulator Pressure</i>	<i>$600 \leq P \leq 660$ psig</i>
	<i>g) Accumulator Volume</i>	<i>$929 \leq V \leq 945$ ft³</i>
	<i>h) Accumulator Temperature</i>	<i>$80 \leq T \leq 130$ °F (coupled to containment temperature)</i>
	<i>i) Accumulator fL/D</i>	<i>Current line configuration</i>
	<i>j) Minimum ECC boron</i>	<i>≥ 2925 ppm</i>
3.0	<i>Accident Boundary Conditions</i>	
	<i>a) Break location</i>	<i>Any RCS piping location</i>
	<i>b) Break type</i>	<i>Double-ended guillotine or split</i>
	<i>c) Break size (relative to cold leg pipe)</i>	<i>$0.05 \leq A \leq 0.5$ full pipe area (split) $0.5 \leq A \leq 1.0$ full pipe area (guillotine)</i>
	<i>d) Offsite power</i>	<i>On or Off</i>
	<i>e) Safety injection flow</i>	<i>Current per loop pump delivery (same as used in current Robinson Appendix K methodology)</i>
	<i>f) Safety injection temperature</i>	<i>≤ 100 °F</i>
	<i>g) Safety injection delay</i>	<i>≤ 20.5 seconds (with offsite power) ≤ 40 seconds (without offsite power)</i>
	<i>h) Containment pressure</i>	<i>Bounding current configuration</i>
	<i>i) Containment temperature</i>	<i>$80 \leq T \leq 130$ °F</i>
	<i>j) Containment sprays</i>	<i>≥ 8 seconds</i>
	<i>k) Single failure</i>	<i>1 LPSI, 1 HPSI</i>

**Table 5.8 Summary of Major Parameters
Describing Limiting PCT Case (Case 22)**

Time (hrs)	5850
Core Power (MW)	3297
Core Peaking (FQ)	2.44
Radial Peak (Fdh)	1.8000
Axial Offset	-0.163
Local Peaking (Fl)	1.098
Break Type	DEGB
Break Size (ft ²)	3.72 (~90%)
Offsite Power Availability	No
Diesel Start (s)	40.0
Decay Heat Multiplier	0.968

Table 5.9 Summary of Results for the Limiting PCT Case (22)

<i>PCT</i>	
<i>Temperature</i>	<i>1686 °F</i>
<i>Time</i>	<i>34 seconds</i>
<i>Elevation</i>	<i>9.4 ft</i>
<i>Metal-Water Reaction</i>	
<i>% Oxidation Maximum</i>	<i>0.8 %</i>
<i>% Total Oxidation</i>	<i>0.022 %</i>
<i>Total Hydrogen</i>	<i>0.5 lb</i>

**Table 5.10 Summary of Major Parameters Describing Limiting
Maximum Nodal Oxidation Case (3)**

Time (hrs)	4680
Core Power (MW)	3254
Core Peaking (FQ)	2.47
Radial Peak (Fdh)	1.8000
Axial Offset	-0.171
Local Peaking (FI)	1.12
Break Type	DESB
Break Size (ft ²)	1.808(~44%)
Offsite Power Availability	No
Diesel Start (s)	40
Decay Heat Multiplier	0.970

**Table 5.11 Summary of Results for the Limiting Maximum Nodal
Oxidation Case (3)**

<i>PCT</i>	
<i>Temperature</i>	<i>1665 °F</i>
<i>Time</i>	<i>45. 6 seconds</i>
<i>Elevation</i>	<i>8.86 ft</i>
<i>Metal-Water Reaction</i>	
<i>% Oxidation Maximum</i>	<i>1.1 %</i>
<i>% Total Oxidation</i>	<i>0.016 %</i>
<i>Total Hydrogen</i>	<i>0.35 lb</i>

Table 5.12 Comparison of 95/95 and 50/50 Statistical Results

	<i>95/95</i>	<i>50/50</i>
<i>PCT</i>	<i>1686 F</i>	<i>1375 F</i>
<i>Max O2 (Nodal value)</i>	<i>1.13 %</i>	<i>0.34 %</i>
<i>Total O2 (Core wide)</i>	<i>0.02 %</i>	<i>0.003 %</i>



Figure 5.1 Calculation Framework

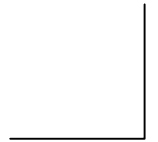
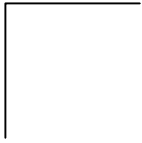


Figure 5.2 []



Figure 5.3 []



Figure 5.4 [

]





Figure 5.5 [**]**

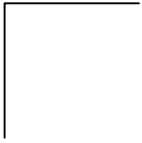


Figure 5.6 [

]





Figure 5.7 [

]





Figure 5.8 [

]





Figure 5.9 [

]



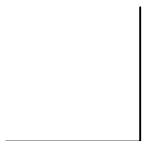


Figure 5.10 [

]



Figure 5.11 [**]**



Figure 5.12 [**]**

Figure 5.13 [

]



Figure 5.14 [**]**

Figure 5.15 [

]

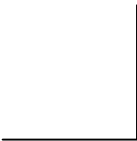


Figure 5.16 [**]**



Figure 5.17 []

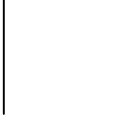


Figure 5.18 [

]



Figure 5.19 []

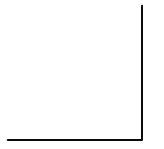


Figure 5.20 []



Figure 5.21 []



Figure 5.22 []



Figure 5.23 [

]

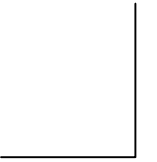


Figure 5.24 []

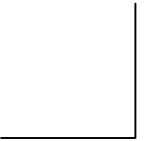


Figure 5.25 [
]



Figure 5.26 [

]



Figure 5.27 [

]

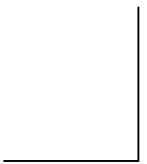


Figure 5.28 []

6.0 References

- 1) "Emergency Core Cooling Systems; Revisions to Acceptance Criteria," Federal Register, Vol. 53, No. 180, September 16, 1988, 10 CFR Part 50.
- 2) "Compendium of ECCS Research for Realistic LOCA Analysis," NUREG/1230, USNRC, December 1988.
- 3) "Best-Estimate Calculations of Emergency Core Cooling System Performance," Regulatory Guide 1.157, May 1989.
- 4) "Quantifying Reactor Safety Margins, Application of Code Scaling, Applicability, and Uncertainty Evaluation Methodology to a Large Break, Loss-of-Coolant Accident," NUREG/CR-5249, December 1989.
- 5) EMF-2102(P), Revision 0, S-RELAP5 Code Verification and Validation document
- 6) ANF-90-145(P)(A), *RODEX3 Fuel Rod Thermal-Mechanical Response Evaluation Model*, Volume 1, "Theoretical Manual," and Volume 2, "Thermal and Gas Release Assessments," April 1996.
- 7) EMF-1557(P) Revision 4, *RODEX3A: Theory and User's Manual*, November 2000.
- 8) EMF-2417(P) Revision 0, *RODEX3A Code Verification and Programmers Guide for Version USEP98*, July 2000.
- 9) EMF-2100(P) Revision 4, *S-RELAP5 Models and Correlations Code Manual*, January 2001.
- 10) EMF-2101(P) Revision 2, *S-RELAP5 Programmers Guide*, January 2001.
- 11) EMF-CC-097(P) Revision 7, *S-RELAP5 Input Data Requirements*, August 2000.
- 12) EMF-2054(P) Revision 2, *Code Input Development Guidelines for Realistic Large Break LOCA Analysis of a Pressurized Water Reactor*, July 2001.
- 13) EMF-2058, Revision 1, *S-RELAP5 Realistic Large Break LOCA Analysis Guideline*, July 2001
- 14) EMF-CC-039(P) Revision 2, *ICECON Code User's Manual: A Computer Program Used to Calculate Containment Back Pressure for LOCA Analysis (Including Ice Condenser Plants)*, March 1999.
- 15) EMF-CC-039(P) Revision 2 Supplement 1, *ICECON Code User's Manual: A Computer Program Used to Calculate Containment Back Pressure for LOCA Analysis (Including Ice Condenser Plants)*, December 1999.
- 16) EMF-2057, Revision 0, H. B. Robinson Unit 2 Nuclear Plant Realistic Large Break LOCA/ECCS Analysis, August 2001

- 17) NUREG-0800, U.S. Nuclear Regulatory Commission Standard Review Plan
- 18) NUREG/CR-4312, EGG-2396, Revision 1, RELAP5/MOD2 code Manual, Volume 1: Code Structure, Systems Models, and Solution Methods, March 1987
- 19) NUREG/CR-5535, INEL-95/0174, RELAP5/MOD3 Code Manual, August 1995
- 20) TID-4500, ANCR-1219, CONTEMPT-LT – A computer Program for Predicting Containment Pressure-Temperature Response to a Loss-Of-Coolant Accident, June 1975
- 21) EMF-2328 (P)(A), *PWR Small Break LOCA Evaluation Model, S-RELAP5 Based*, January 2000.
- 22) D. Fletcher and R. R. Schultz, RELAP5/MOD3 Code Manual, User's Guidelines, Volume 5, NUREG/CR-5535, January 1992.
- 23) R. R. Schultz, RELAP5-3D Code Manual, User's Guidelines, INEEL-EXT-98-00834, February 2001.
- 24) S. Shieh, V. H. Ransom, R. Krishnamurthy, RELAP5/MOD3 Code Manual, Validation of Numerical Techniques in RELAP5/MOD3, Volume 6, NUREG/CR-5535, August 1994.
- 25) J. V. Cathcart and R.E. Pawel, Zirconium Metal-Water Oxidation Kinetics: IV. Reaction Rate Studies, ORNL/NUREG-17, August 1977.
- 26) ANSI/ANS-5.1-1979, "American National Standard for Decay Heat Power in Light Water Reactors," approved August 29, 1979.
- 27) J. P. Unik and J.E. Gindler, "A Critical Review of the Energy Released in Nuclear Fission," ANL-7748, Argonne National Laboratory, Chemistry Division, March 1971.
- 28) "Comparisons of Thermal-Hydraulic Phenomena During Isothermal Loss-Of-Coolant Experiments and Effect of Scale in LOFT and SEMISCALE MOD-1," NURGE/CR-0410, December 1978.
- 29) "Similarity Analysis and Scaling Criteria for LWRs Under Single-Phase and Two-Phase Natural Circulation," NUREG/CR-3267, March 1983.
- 30) "UPTF: Program and System Description," U9 414/88/023, Siemens AG, KWU Group (Erlangen), November 1988.
- 31) Sleicher, C.A. and M.W. Rouse, "A Convenient Correlation for Heat Transfer to Constant and Variable Property Fluids in Turbulent Pipe Flow," International Journal of Heat and Mass Transfer, Volume 18, pp. 677-683, 1975.
- 32) Holman, J.P., *Heat Transfer*, 5th Edition, McGraw-Hill, New York, 1981.
- 33) Gebhart, B., *Heat Transfer*, 2nd Edition, McGraw-Hill, New York, 1971.

- 34) "ASME Steam Tables," Sixth Edition, ASME, New York, 1997.
- 35) Bird, R.B., W.E. Stewart and E.N. Lightfoot, *Transport Phenomena*, John Wiley and Sons, Inc., New York, 1960.
- 36) Dittus, F.W. and L.M.K. Boelter, "Heat Transfer in Automobile Radiators of the Tubular Type," *Publications in Engineering*, Volume 2, pp. 443-461. University of California, Berkeley, 1930.
- 37) Chen, J.C., R.K. Sundaram, F.T. Ozkaynak, "A Phenomenological Correlation for Post-CHF Heat Transfer," NUREG-0237, June 1977.
- 38) Forslund, R.P. and W.M. Rohsenow, "Dispersed Flow Film Boiling," *Journal of Heat Transfer*, Volume 90 (6), pp. 399-407, 1968.
- 39) Bromley, L.A., "Heat Transfer in Stable Film Boiling," *Chemical Engineering Progress*, Volume 46, pp. 221-227, 1950.
- 40) Berenson, P.J., "Film Boiling Heat Transfer from a Horizontal Surface," *Journal of Heat Transfer*, pp. 351-358, 1961.
- 41) Sun, K.H., J.M. Gonzales-Santalo and C.L. Tien, "Calculations of Combined Radiation and Convection Heat Transfer in Rod Bundles Under Emergency Cooling Conditions," *Journal of Heat Transfer*, pp. 414-420, 1976.
- 42) "FLECHT-SEASET Program, PWR FLECHT SEASET Unblocked Bundle, Forced and Gravity Reflood Task Data Evaluation and Analysis Report," NUREG/CR-2256, EPRI NP-2013, WCAP-8891, November 1981.
- 43) Taylor, D.D. et al, "TRAC-BD1/MOD1: An Advanced Best Estimate Computer Program for Boiling Water Reactor Transient Analysis, Volume 1: Model Description," NUREG/CR-3633, EGG-2294, April 1984.
- 44) "Dispersed Flow Film Boiling in Rod Bundle Geometry – Steady State Heat Transfer Data and Correlation Comparisons," NUREG/CR-2435, ORNL-5822, Oak Ridge National Laboratory, March 1982.
- 45) "An Analysis of Transient Film Boiling of High-Pressure Water in a Rod Bundle," NUREG/CR-2469, ORNL/NUREG-85, Oak Ridge National Laboratory, March 1982.
- 46) "Experimental Investigations of Bundle Boiloff and Reflood Under High-Pressure Low Heat Flux Conditions," NUREG/CR-2455, ORNL-5846, Oak Ridge National Laboratory, April 1982.
- 47) "ORNL Small-Break LOCA Heat Transfer Test Series I: High-Pressure Reflood Analysis," NUREG/CR-2114, ORNL/NUREG/TM-446, Oak Ridge National Laboratory, August 1981.
- 48) Loftus, M.J. et al, "PWR FLECHT-SEASET Unblocked Bundle, Forced and Gravity Reflood Task Data Report," NUREG/CR-1532, Volumes 1 and 2, June 1980.

- 49) "Data Report on Large Scale Reflood Test-43 – CCTF CORE-II Shakedown Test C2-SH2 (Run 054)," JAERI-memo 58-155, Japan Atomic Energy Research Institute, May 1983
- 50) Holmes, B.J, "I25 Comparison Report," NEA/CSNI/R(91)1, AEA-TRS-1043, February 1991.
- 51) Trapp, J.A. and V.H. Ransom, "A Choked-Flow Calculation Criterion for Nonhomogeneous, Nonequilibrium Two-Phase Flows," *International Journal of Multiphase Flow*, Volume 8, pp. 669-681, 1992.
- 52) "Upper Plenum Test Facility – UPTF – Test No. 10: Tie Plate Countercurrent Flow Test," U9 316/88/3, March 1988.
- 53) "Upper Plenum Test Facility – UPTF – Test No. 29: Entrainment/Deentrainment Test," E314/90/19, November 1990.
- 54) "Pump Two-Phase Performance Program," EPRI NP-1556, Volumes 1 through 8, September 1980.
- 55) "Mixing of ECC Water with Steam: 1/3 Scale Test and Summary," EPRI Report EPRI-294-2, June, 1975.
- 56) Carpenter, E.F. and A.P. Colburn, "The Effect of Vapor Velocity on Condensation Inside Tubes," *Proceedings of General Discussion on Heat Transfer, Institute of Mechanical Engineering/American Society of Mechanical Engineers*, pp. 20-26, 1951.
- 57) Collier, J.G., *Convective Boiling and Condensation*, 2nd Edition, McGraw-Hill, New York, 1981.
- 58) "Quick Look Report - UPTF - Test No. 6, Downcomer Countercurrent Flow Test," U9 316/89/2, Siemens AG UB KWU, March 1989.
- 59) "Experimental Data Report - UPTF - Test No. 6, Downcomer Countercurrent Flow Test," U9 316/88/18, Siemens AG UB KWU, March 1989.
- 60) "Quick Look Report - UPTF - Test No. 7, Downcomer Countercurrent Flow Test," E314/90/003, Siemens AG KWU, March 1990.
- 61) "Experimental Data Report - UPTF - Test No. 7, Downcomer Countercurrent Flow Test," U9 316/89/14, Siemens AG UB KWU, July 1989.
- 62) "Upper Plenum Test Facility, Test No. 8 Cold/Hot Leg Flow Pattern Test Quick Look Report," U9 316/88/11, Siemens AG, Erlangen Germany, September 1988.
- 63) "Upper Plenum Test Facility, Test No. 8 Cold/Hot Leg Flow Pattern Test Experimental Data Report," U9 316/88/12, Siemens AG, Erlangen Germany, September 1988.
- 64) XN-75-27(A), "Exxon Nuclear Neutronic Design Methods for Pressurized Water Reactors," Exxon Nuclear Company

- 65) EMF-96-029(P)(A), Reactor Analysis System for PWRs, January 1997.
- 66) Wilks, S.S., "Determination of Sample Sizes for Setting Tolerance Limits," Ann. Math. Stat., Vol. 12, pp. 91-96, 1941.
- 67) Somerville, P.N., "Tables for Obtaining Non-Parametric Tolerance Limits," Ann. Math. Stat., Vol. 29, No. 2, pp 599-601, June 1958.
- 68) "An Acceptable Model and Related Statistical Methods for the Analysis of Fuel
Densification," Regulatory Guide 1.126, Revision 1, U.S. Nuclear Regulatory
Commission, March 1978.
- 69) Abramowitz, M. and I. Stegun, "Handbook of Mathematical Functions with Formulas,
Graphs, and Mathematical Tables," National Bureau of Standards, Applied Mathematics
Series 55, 1966.
- 70) Box, G.E.P, M.E. Muller, "A note on the generation of random normal deviates," Annals
Math. Stat, V. 29, pp. 610-611 (1958).

Appendix A Overview of Base Case and Sensitivity Studies

A.1 Base Case Analyses Description

To demonstrate the range of applicability of the models used in the various sensitivity studies, four base case analyses are characterized in this Appendix. These are:

- 3-loop PWR, worst break, worst single failure, nominal (100%) core power, and plant technical specifications on rod power, and cosine power shape, no RODEX3A.
- 3-loop PWR, worst break, worst single failure, nominal (100%) core power, and plant technical specifications on rod power, and cosine power shape, no RODEX3A, no accumulator N₂.
- 3-loop PWR, worst break, worst single failure, high core power, and plant technical specifications on rod power, and top skewed power shape, no RODEX3A, no accumulator N₂.
- 4-loop PWR, worst break, worst single failure, high core power, and plant technical specifications on rod power, and top skewed power shape, no RODEX3A, no accumulator N₂.

The 3-loop PWR is an operating plant owned by a FRA-ANP customer with a 15x15 fuel design. The 4-loop PWR does not represent any particular 4-loop plant; however, it has the general dimensions typical of 4-loop PWRs. Those code models which may disguise the phenomena of interest for a given sensitivity study or add a computational burden to the problem have been removed for sensitivity study purposes only. These include the RODEX3A fuel model and accumulator nitrogen. With regard to RODEX3A, incorporation of the fuel model significantly increases calculation run times. A special suite of fuel rod studies was performed using the RODEX3A code. The key findings of these calculations are discussed in some detail in Appendix B. Accumulator nitrogen is neglected by using a valve at the accumulator exit that shuts off nitrogen flow as the accumulator completes discharging. The transport of the nitrogen has been shown to amplify code variability during late reflood, possibly disguising the effect of certain parameters expected to influence late reflood PCTs.

For these four base case input models, the plant and containment nodalization follow the governing guidelines issued at the time of model development (see References 15 and 16). Based on sensitivity studies using these input models only a few minor details have changed in the most recent revision of the guidelines.

A.2 LBLOCA Calculation and Event Description

From earlier sensitivity studies, the worst break size and worst single failure were identified. These parameters have been carried through most of the sensitivity studies performed during methodology development. The base case transients are well characterized by the event summary given in Table A.1. Figures A.1 through A.4 show the PCT trends for the 3-loop nominal power case with nitrogen and a 3-loop nominal power, 3-loop high power, and 4-loop high power case modeled without accumulator nitrogen release. The plots identify two cases: "Base" and "Case 7". In the suite of sensitivity studies, case 7 was designed to be identical to the base case so that the results from these two calculations would overlay. This provided a check on the sensitivity study process.

In general, the four base cases have very similar trends. The LBLOCA is initiated at time 0.0 s by a postulated large rupture of the reactor coolant system (RCS) primary piping. The worst break size for the 3-loop model is the 70% DEGB and for the 4-loop model, it is the 100% DEG. Based on deterministic studies, the worst break location was identified as being in the cold leg piping between the reactor coolant pump and the reactor vessel for the RCS loop containing the pressurizer. The break initiates a rapid depressurization of the RCS. A reactor trip signal is issued at about 0.7 s when the low pressurizer pressure trip setpoint is reached; however, reactor trip and scram are conservatively neglected in the analysis. The reactor initially shutdowns by coolant voiding in the core region.

For these break sizes, a rapid depressurization occurs, along with a core flow stagnation and reversal. This causes the fuel rods to experience departure from nucleate boiling (DNB) within a few seconds of the break. Subsequently, the limiting fuel rods dissipate heat via the film and transition boiling heat transfer regimes. The coolant voiding presents a strong negative reactivity contribution to the nuclear reaction and core fission ends. As heat transfer from the fuel rods is reduced, the cladding temperature rises.

Within the first few seconds, coolant in all regions of the RCS begins to flash. At the break plane, the loss of subcooling in the coolant results in substantially reduced break flow. This reduces the depressurization rate, and for the 4-loop leads to a period of positive core flow. The 3-loop result shows reduced downflow as the reactor coolant pumps in the intact loops continue to supply water to the vessel. Cladding temperatures are reduced from this blowdown cooling period in the 4-loop calculation; while, the 3-loop only shows a reduction in the rate of heatup.

This positive core flow or reduced downflow period ends as two-phase conditions occur in the reactor coolant pumps, reducing their effectiveness. Once again, the core flow reverses as most of the vessel mass flows out through the broken cold leg.

The mitigation of the LBLOCA begins when the safety injection actuation signal (SIAS) is issued. This occurs from high containment pressure. A worst single failure be considered for ECCS safety analysis. This single failure is assumed to be the loss of one low-pressure safety injection pump. The on-time start of containment spray and fan coolers is also assumed.

The RCS pressure falls below the accumulator pressure within 13 s. When this happens, fluid from the accumulators is injected into the cold legs. In the early delivery of accumulator water, high pressure and high break flow drive some of this fluid to bypass the core. Core heat transfer remains poor and the fuel rod cladding temperatures increased. As RCS and containment pressures equilibrate (around 25 s), ECCS water begins to fill the lower plenum and eventually lower portions of the core; thus, core heat transfer improves and cladding temperatures decrease.

Around 55 s, the relatively large volume of accumulator water is exhausted and core recovery must rely only on LPSI pump delivery of coolant. At this time (shown only for the case given in Figure A.1), the nitrogen gas used to pressurize the accumulator is transported out of the ECCS and RCS through the break. This may result in a short period of improved core heat transfer as the nitrogen gas displaces water in the downcomer into the core. After the accumulators have been exhausted, the LPSI coolant may (3-loop, nominal power cases) or may not (high power cases) be able to sustain cooling given the core decay heat and higher steam temperatures created by quenching of the lower portions of the core. The peak fuel rod cladding temperatures may increase for a short period until more energy is removed from the core from LPSI pump delivery and decay heat is reduced. Steam generated from fuel rod rewet entrains liquid and passes through the vessel upper plenum, the hot legs, the steam generator, and the

reactor coolant pump before it is vented out the break. The resistance of this flow path to the steam flow is balanced by the driving force of water filling the downcomer. This resistance acts to retard the progression of the core reflood and postpones core wide cooling. Eventually (within a couple of minutes of the accident), the core reflood progresses sufficiently to ensure core wide cooling. Full core quench will come in a matter of minutes after core wide cooling. Long-term cooling is then sustained with the residual heat removal system.

A.3. Sensitivity Studies Overview

Many sensitivity studies were performed in the development of the FRA-ANP RLBLOCA methodology. A detailed discussion of each study is not practical. It is important to present the evolution of these studies in order to demonstrate a pedigree for the methodology and to define ranges of applicability for these sensitivity studies. Table A.2 outlines classes of sensitivity studies that have been performed, explains the objective of these calculations, and presents general conclusions drawn from these calculations.

The basic philosophy in performing the earliest sensitivity studies was to first identify a best-estimate, "worst" case model. These models were characterized by a worst break size, worst single failure and plant technical specifications for hot rod power. Power distributions resembled a cosine shape. The 3-loop, nominal power cases conform to this description. This approach was considered to provide a bounding result to a "nominal" LBLOCA. It was later recognized that some of these assumptions may not extrapolate to even more limiting conditions. In consideration of this possibility, studies were performed at high powers and with top skewed power profiles to examine sensitivities near the criterion on peak clad temperature. For this reason, the high powered, 3- and 4-loop models were prepared and executed.

The results from the sensitivity studies sometimes deviated from the descriptions given in Section A.2. Underlining each of these studies are various assumptions about nodalization, the modeling of particular phenomena, runtime sequence, and plant state (nominal vs. "limiting" conditions). As the methodology developed, such issues evolved and are now reflected in the guidelines for performing RLBLOCA analyses (References 15 and 16). In general, quantitative results only represent one component of what may be defined as a "good" or "bad" result. In evaluating results, qualitative trends and deviations from the base cases have also been considered,

- "Is the expected sensitivity present?"
 - "If not, is this important?"
 - "If so, how do I capture this in a guideline?"

To answer this and other questions, the CSAU methodology recommends that the PIRT be considered. This has been followed during the methodology development.

Table A.1 Base Case Large Break LOCA Approximate Sequence of Events Table

Event	<u>W</u> 3-loop Times, sec	<u>W</u> 3-loop HP Times, sec	<u>W</u> 4-loop HP Times, sec
Analysis Initiated	0.00	0.00	0.00
Break Opened	0.0	0.0	0.0
Safety Injection Signal	<1	<1	<1
Broken Loop Accumulator/ SIT Flow Initiated	8	8	8
Intact Loop Accumulator/ SIT Flow Initiated	13	13	13
End of Bypass/Beginning of Refill	25	25	25
Broken Loop Accumulator/ SIT Empties	55	55	55
Beginning of Reflood	30	30	30
Intact Accumulator/ SIT Empties	55, 57	55, 57	55, 57
PCT Occurred	28	140	111

Table A.2 Sensitivity Studies Performed for Methodology



Table A.2 Sensitivity Studies Performed for Methodology

Table A.2 Sensitivity Studies Performed for Methodology

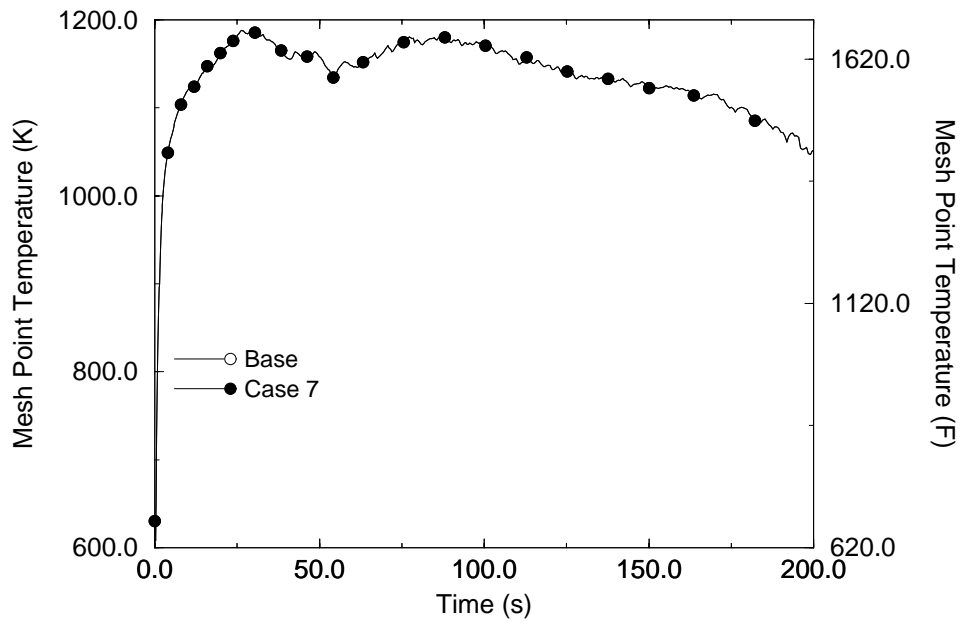


Figure A.1 PCT independent of elevation for 3-loop plant at nominal power with accumulator nitrogen effects

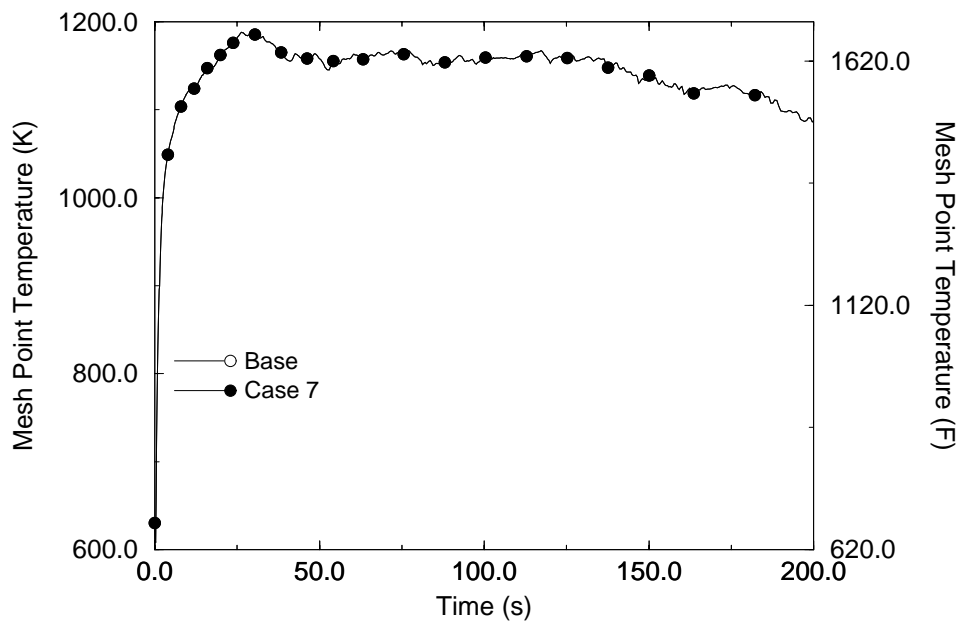


Figure A.2 PCT independent of elevation for the 3-loop plant at nominal power with accumulator nitrogen effects

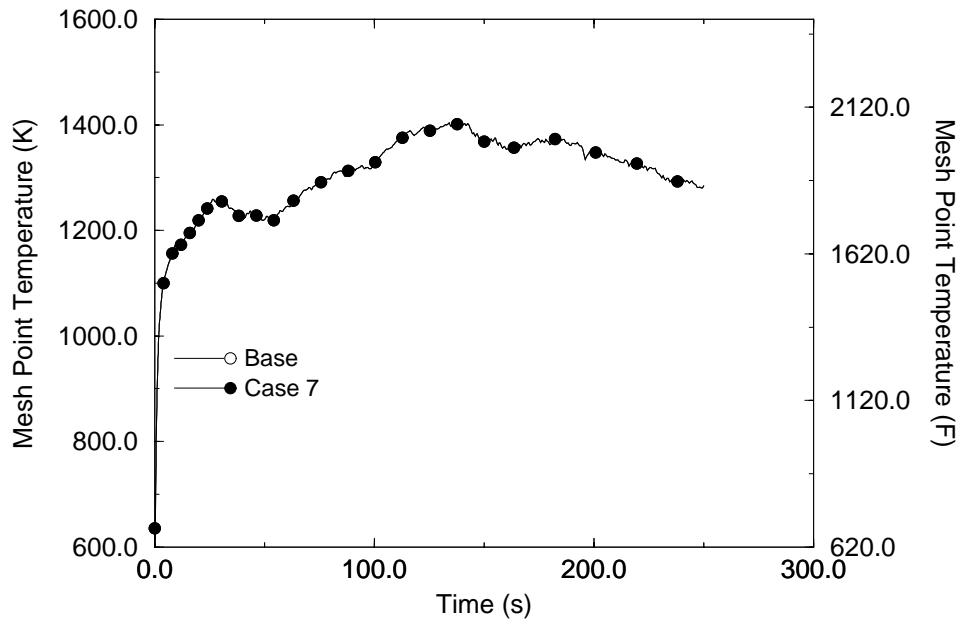


Figure A.3 PCT independent of elevation for the 3-loop plant at high power without accumulator nitrogen effects

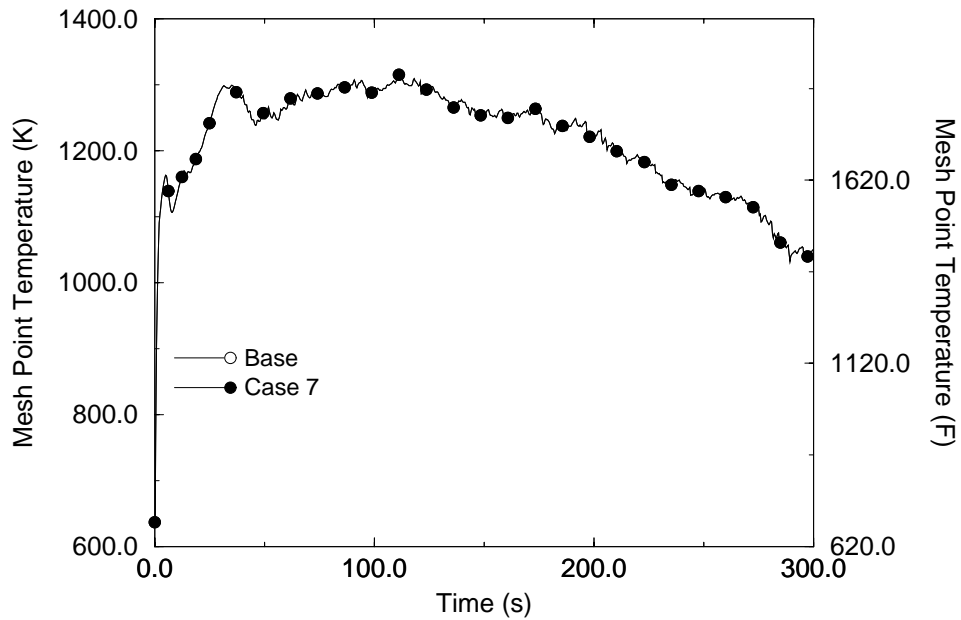


Figure A.4 PCT Independent of Elevation for the 4-loop Plant at High Power Without Accumulator Nitrogen Effects

Appendix B Conservatism

Among the major assumptions stated for the FRA-ANP RLBLOCA methodology are declarations of adopted conservatism. Such declarations are not always physically intuitive. In these instances, sensitivity studies have been performed to arrive at the stated conclusions. In this appendix, selections of calculations are presented to support some of the statements of conservatism presented in this methodology document.

B.1 Analysis for Fresh Fuel Assemblies Only

Only fresh fuel assemblies are specifically analyzed in the RLBLOCA methodology. By considering “Time-in-Cycle” as an uncertainty parameter, identification of a limiting hot rod and hot assembly is required. The motivation for this limitation is the necessity for a strategy that demonstrates that the methodology realistically supports the limiting conditions during an operation cycle. Core loading experience supports the premise that fresh fuel assemblies tend to give limiting peak assembly powers during a cycle. Cycle-to-cycle burnup will have two effects on PCT: reduced power and stored energy. Both of these factors are highly-ranked phenomena based on the PIRT given in Table 3.4 and their reduction will contribute to lower PCTs. However, the criterion for identifying the hot rod is based on the maximum core peaking factor F_q . F_q will fluctuate during a cycle creating the opportunity for burned or gadolinia bearing fuel assemblies to become limiting. This sensitivity study examined the question of whether this fluctuation in F_q creates the possibility that second or third cycle fuel could be limiting.

To evaluate the position that fresh fuel is limiting, a series of deterministic sensitivity studies was performed using models representing 3- and 4-Loop PWRs with 15x15 and 17x17 fuel designs, respectively. The validation strategy was to examine PCT sensitivity at BOC, MOC, and EOC for fresh and once burnt fuel for a 3-loop and 4-loop PWR. The analysis presented in this section was performed similar to the RLBLOCA methodology that sets the limiting rod at the technical specification limit for radial power peaking ($F\Delta h$) including uncertainties.

Following the methodology as described in Section 5.1.3.2, RODEX3A and S-RELAP5 input was created describing the fuel conditions and power distributions at various times in life. To eliminate the contribution of radial power dependency on burnup, all calculations were performed with the same radial power distribution used in the base cases (see Appendix A).

Assembly lifetime was assumed to extend to two operational cycles. The calculations were performed as described in Section A.2. with the addition of the RODEX3A fuel rod models. Tables B.1. and B.2 show the results from the studies for the 3- and 4-loop PWRs, respectively. Figures B.1. and B.2. show the PCT traces comparing the results of cycle 1 BOC (BOC1) vs. cycle 2 BOC, MOC, and EOC for the two plant types. As shown in the tables and figures, the PCT calculations using fresh fuel, cycle 1 fuel, generally bounds the once burnt, cycle 2 results.

By using the same radial power distribution in each case, the only two differences between the calculations are fuel rod material properties and axial shape. Examination of the power shapes show that case-to-case differences are subtle for the BOC and MOC cases; thus, supporting the conclusion that the material property differences have the most influence the results. The material property changes reduce stored energy. This effect on stored energy is best observed during the blowdown and refill phases of the LBLOCA as can be observed in Figures B.1 and B.2. The axial shapes for the EOC cases show some differences in the PCT location. The EOC2 case has a higher power peak in the top portion of the core. This explains why the PCT calculated in the EOC2 cases in the 3- and 4-loop calculations is greater than the EOC1. The small differences shown in PCT is inconsequential, because the once burned fuel at EOC is not likely to be near the $F\Delta h$ technical specification limits. Thus, the higher PCTs for the EOC2 fuel compared to the EOC1 fuel, clearly are driven by unrealistic increasing the EOC2 fuel power.

The conclusion drawn from this study is that because of the reduction in power and stored energy with burnup, fuel assemblies residing in the core for more than one cycle will not be limiting. For this reason, the FRA-ANP RLBLOCA methodology has chosen to only analyze fresh fuel assemblies.

B.2 Analysis without Clad Swelling and Rupture

Cladding swelling and rupture is a possibility whenever fuel temperatures are highly elevated. Before rod failure, the cladding is expected to swell like a balloon. At some point, the material stresses within the cladding will yield to the internal pressure and the fuel rod will fail. Cladding temperatures will be influenced by three additional conditions as a result of swelling and rupture. These are increased cladding surface area, increased gap size, and reduced assembly flow area or blockage. With regard to PCT, these are competing effects. The larger surface area and gap size will act to reduce cladding temperatures; however, flow blockage may prevent rod

locations above the rupture point from receiving coolant and increase temperatures above the rupture location.

Cladding swelling and rupture is a required model for 10CFR50 Appendix K analysis. NUREG-630, "Cladding Swelling and Rupture Models," outlines acceptable models for describing swelling and rupture. The S-RELAP5 code used within the FRA-ANP RLBLOCA methodology has the same cladding swelling and rupture model used in existing FRA-ANP Appendix K licensing methodologies (model based on those described in NUREG-630). Experience with Appendix K methodologies has shown that the use of swelling and rupture models produce less conservative PCTs than when neglecting this phenomenon. To assess how this model performs with the FRA-ANP RLBLOCA methodology, a sensitivity study was performed for both a 3- and 4-loop PWR with 15x15 and 17x17 fuel designs, respectively.

Figures B.3 and B.4 show the PCT sensitivity to fuel rupture. In both instances, the case modeling fuel rupture shows a significant decrease in rod temperature. This is evidence that despite the blockage effect, the increased fuel rod surface area and the increased thermal resistance across the fuel-cladding gap resulting from swelling provides the dominant influence on the temperature transient. By the RLBLOCA methodology not treating rod swelling and rupture, the phenomena is conservatively bounded.

B.3. Radial Power Distributions

[

]

- []
- []
- []
- []

[

]

A set of ten radial power cases were designed for this study. These cases were analyzed using the 3-loop plant model. This same study was also performed for the 4-loop plant; however, results from that study showed little sensitivity since the transient in the 4-loop plants experiences quicker mitigation. The ten cases are summarized in the table below. The abbreviation HA identifies the hot assembly, SA identifies the surrounding assemblies, AA identifies the average assemblies, and CA identifies the cold assemblies. Those cases identified as "High" power had the core powers raised so that predicted peak cladding temperature results would be near the criterion. Given the original base case (HA>SA>AA>CA), averaging the peaking factors as defined in the table was all that was necessary to derive the other cases. The one exception is the HA>SA = AA>>CA. In this case the cold assembly power was assumed to be 20% less than the base case value.

Radial Configuration	Power
HA>SA>AA>CA (base)	Nominal
HA>SA=AA=CA	Nominal
HA>SA=AA>CA	Nominal
HA>SA=AA>>CA	Nominal
HA>SA>AA=CA	Nominal
HA>SA>AA>CA	High
HA>SA=AA=CA	High
HA>SA=AA>CA	High
HA>SA=AA>>CA	High
HA>SA>AA=CA	High

Figures B.5 and B.6 show the results from this study for the high power cases and the nominal power cases, respectively. In a separate study examining the effect of accumulator nitrogen on code variability, this same set of ten cases was redone. Figures B.7 and B.8 show the results. For the two plots showing the high power results, the case HA>SA=AA=CA stands out as having the highest PCT. While the most peaked case, HA>SA>AA>CA, does not show a second reflood peak in either case. At the nominal power, the trends are less pronounced.

[

]

B.4. Pump Two-Phase Degradation

During a LOCA event in a PWR, the reactor coolant will reach saturation conditions and a two-phase mixture of steam and water will circulate through the coolant loops and through the reactor coolant pumps (RCPs). The LOCA will result in pump operation far from rated conditions for single-phase fluid flow and may induce reverse flow and a negative pressure differential. In a large break LOCA, this period occurs for a brief time shortly after the break opens. The head generated by RCPs during this period can significantly enhance heat transfer in the core and may limit the rise in cladding temperature and, in some cases, actually reduce cladding temperatures during this period. Most safety analysis conservatively assumes RCP trip to reduce the effectiveness of the pumps to enhance heat transfer during blowdown.

The LBLOCA PIRT developed for the FRA-ANP RLBLOCA methodology ranks pump two-phase degradation as high. For this reason, sensitivity studies were performed examining the effect of a more severe degradation model on PCTs. As shown in Figures B.9 and B.10, the two-phase degradation of the Semiscale pump bound the two-phase characteristic of other well known pump experimental programs (figures come from NUREG-1230, "Compendium of ECCS Research for Realistic LOCA Analysis," Reference 2).

The Semiscale pump model can be defined for an S-RELAP5 RLBLOCA calculation through input. The S-RELAP5 pump model describes pump behavior by single-phase homologous curves, two-phase, fully degraded homologous curves, and void-dependent degradation multipliers for head and torque. The head across the pump is computed as:

$$H_{2\phi} = H_{1\phi} + M(\alpha)[H_{DEGRAD} - H_{1\phi}]$$

where $H_{2\phi}$, $H_{1\phi}$, H_{DEGRAD} and $M(\alpha)$ are two phase head, single-phase head, fully degraded head and degradation multiplier (a function of void fraction), respectively. A similar description is used for predicting the hydraulic torque for the pump.

In the sensitivity studies the single-phase homologous curves ($H_{1\phi}$) used for all cases are supplied by the default Westinghouse pump data that is coded in S-RELAP5. The model describing two-phase degradation (H_{DEGRAD} and $M(\alpha)$) is entered as tabular input to S-RELAP5. For the base case, the default EPRI-CE data (Reference 59) for two-phase degradation is specified. The sensitivity study examined replacing the EPRI-CE degradation model with the Semiscale degradation model. The degradation model is only applied when two-phase conditions are present in the pump. During the rapid blowdown resulting from a LBLOCA, this period lasts about 10-15s following the break.

The PCT results, relative to the three base cases without accumulator nitrogen, are shown in Figures B.11 - B.13 (extracted for the time period of interest). For the 3-loop plant cases, no sensitivity is evident. This is the expected result, since the break size chosen was selected to minimize the enhanced blowdown heat transfer provided by the pumps. The 4-loop plant case does show an increase in the blowdown peak PCT of about 18 °F (10 K).

The PCT change of 18 °F well within the expected variability of the results which is about 30 °F (see Appendix C). In hindsight the pump degradation does not appear to be as significant of a parameter as originally anticipated. This result is consistent with the original work performed on the CSAU methodology (Reference 4). Since it has been demonstrated that increased pump degradation is slightly conservative, the Semiscale two-phase degradation has been adopted for FRA-ANP RLBLOCA analyses.

Table B.1 Key results for burnup studies for a 3-loop PWR at tech-spec radial power

Case #	Case	PCT Temp (F)	Delta Temp	Calc F _Q
1	BOC1 (base case)	1662.8	0.0	2.091
2	MOC1	1676.5	13.7	2.180
3	EOC1	1533.7	-129.1	2.086
4	BOC2	1500.3	-162.5	2.144
5	MOC2	1580.4	-82.4	2.106
6	EOC2	1564.4	-98.4	2.088

Table B.2 Key results for burnup studies for a 4-loop PWR at tech-spec radial power

Case #	Case	PCT Temp (F)	Delta Temp	Calc F _Q
1	BOC1 (base case)	1469.9	0.0	1.982
2	MOC1	1466.1	-3.8	2.122
3	EOC1	1318.1	-151.8	2.054
4	BOC2	1415.8	-54.1	2.029
5	MOC2	1351.7	-118.2	2.016
6	EOC2	1334.5	-135.4	1.998

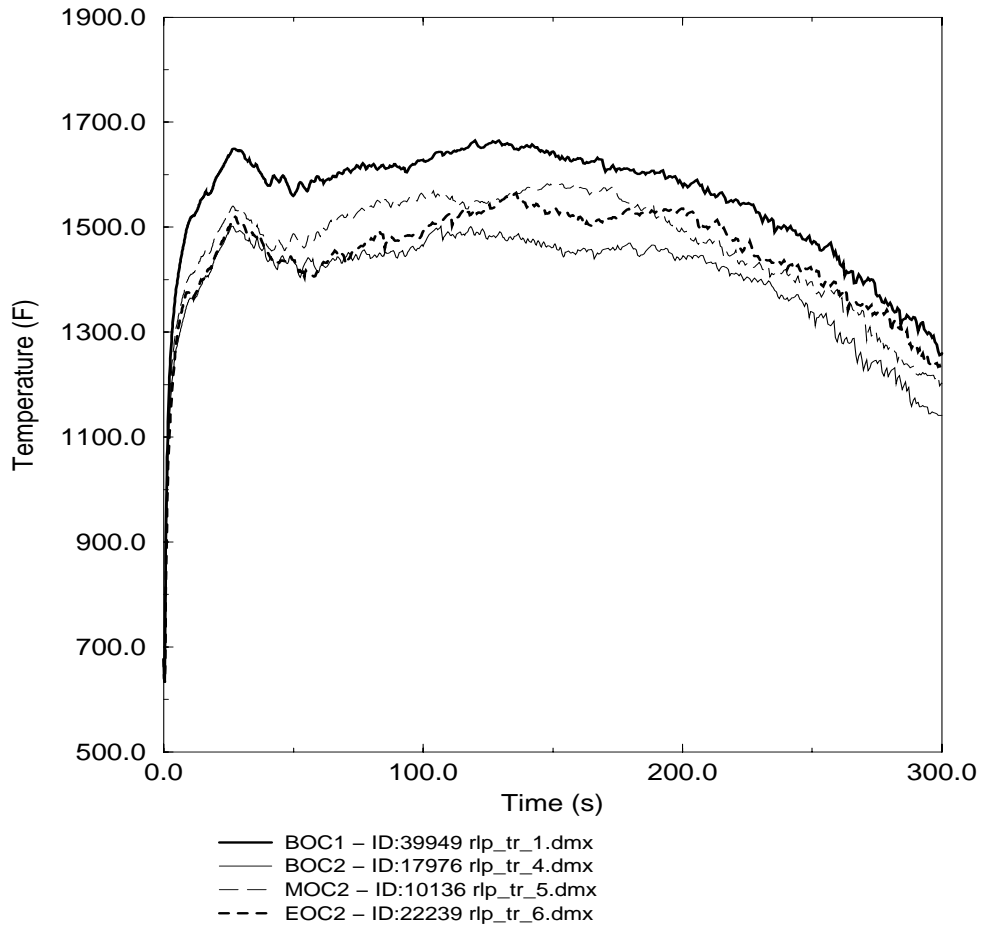


Figure B.1 PCT traces comparing a fresh fuel assembly at BOC to once burnt fuel at BOC, MOC, and EOC (3-loop, tech-spec power).

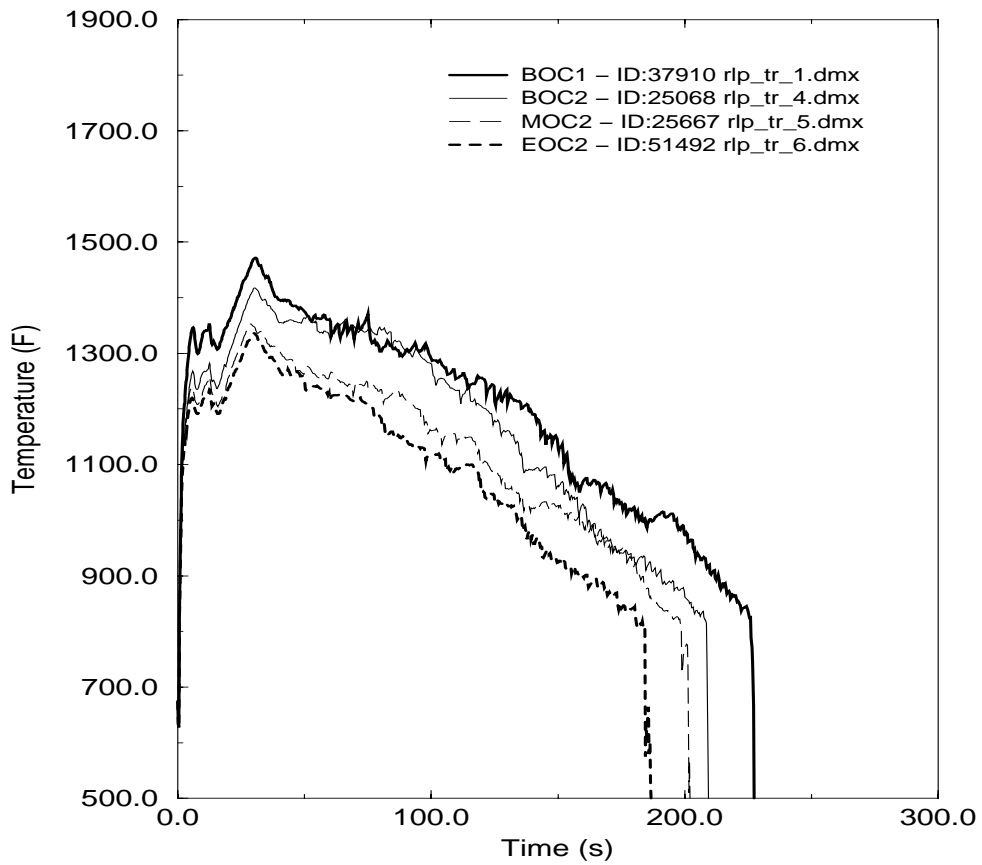


Figure B.2 PCT traces comparing a fresh fuel assembly at BOC to once burnt fuel at BOC, MOC, and EOC (4-loop, tech-spec power).

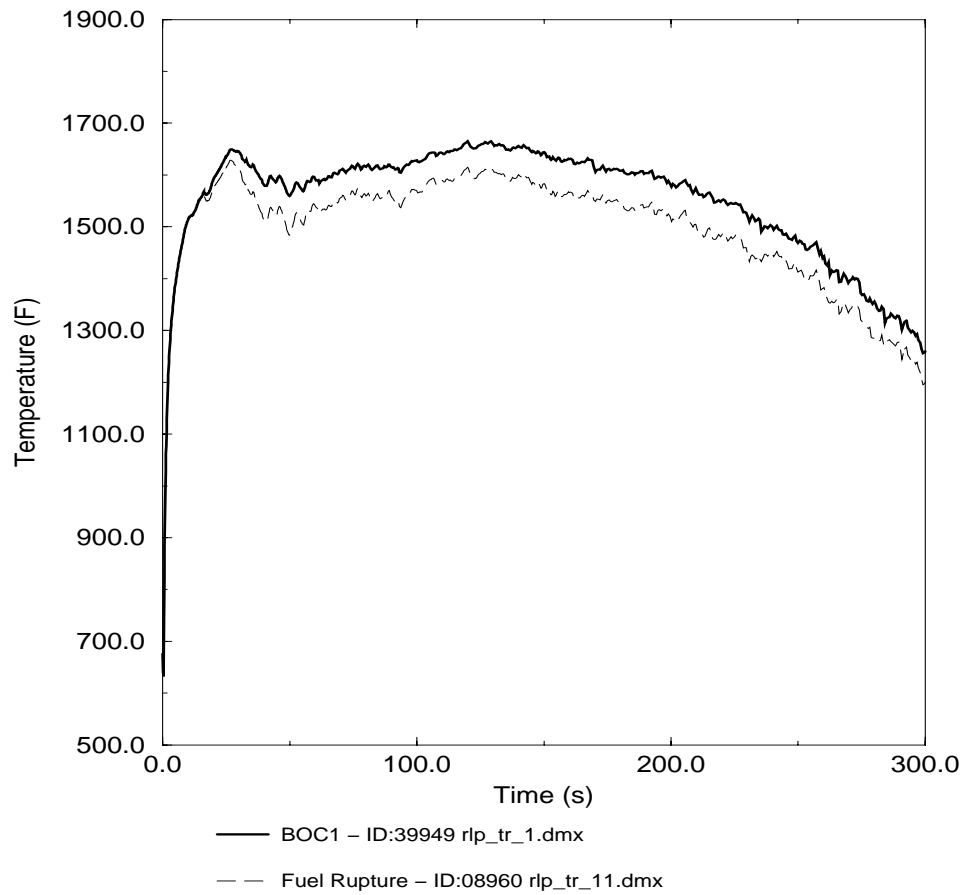


Figure B.3 Influence of fuel rupture on PCT (3-loop, tech-spec power)

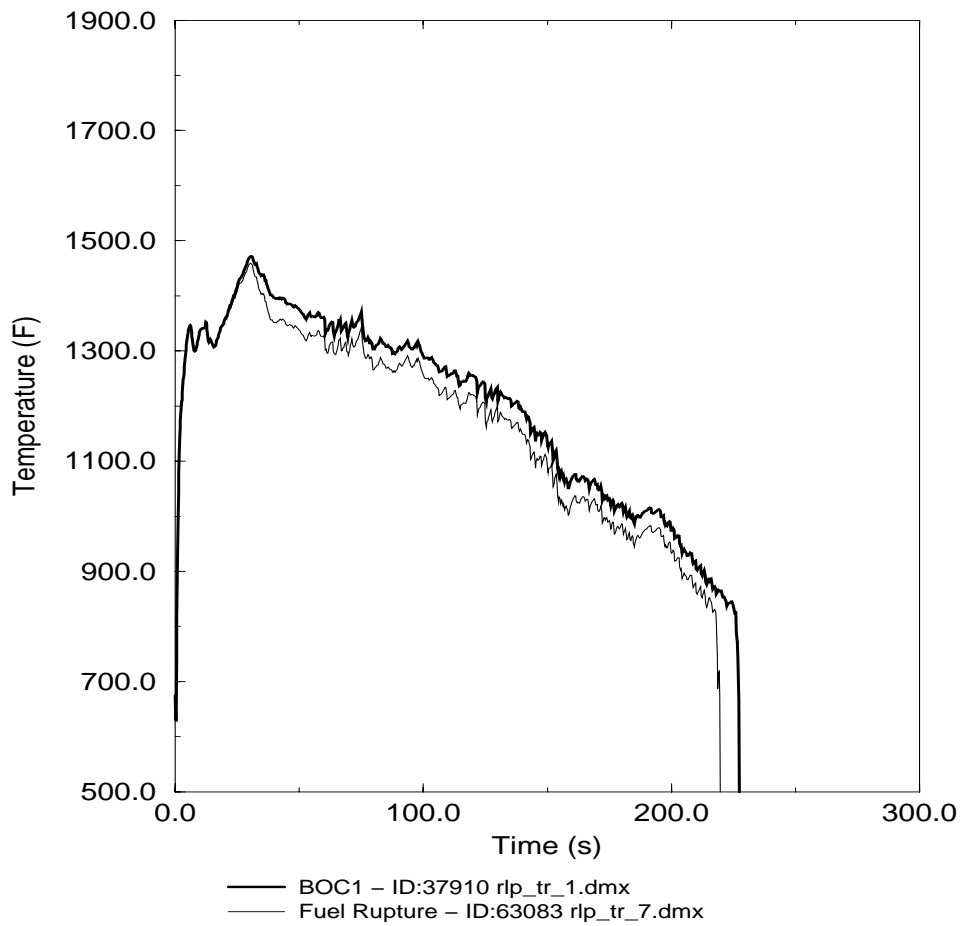


Figure B.4 Influence of fuel rupture on PCT (4-loop, tech-spec power)

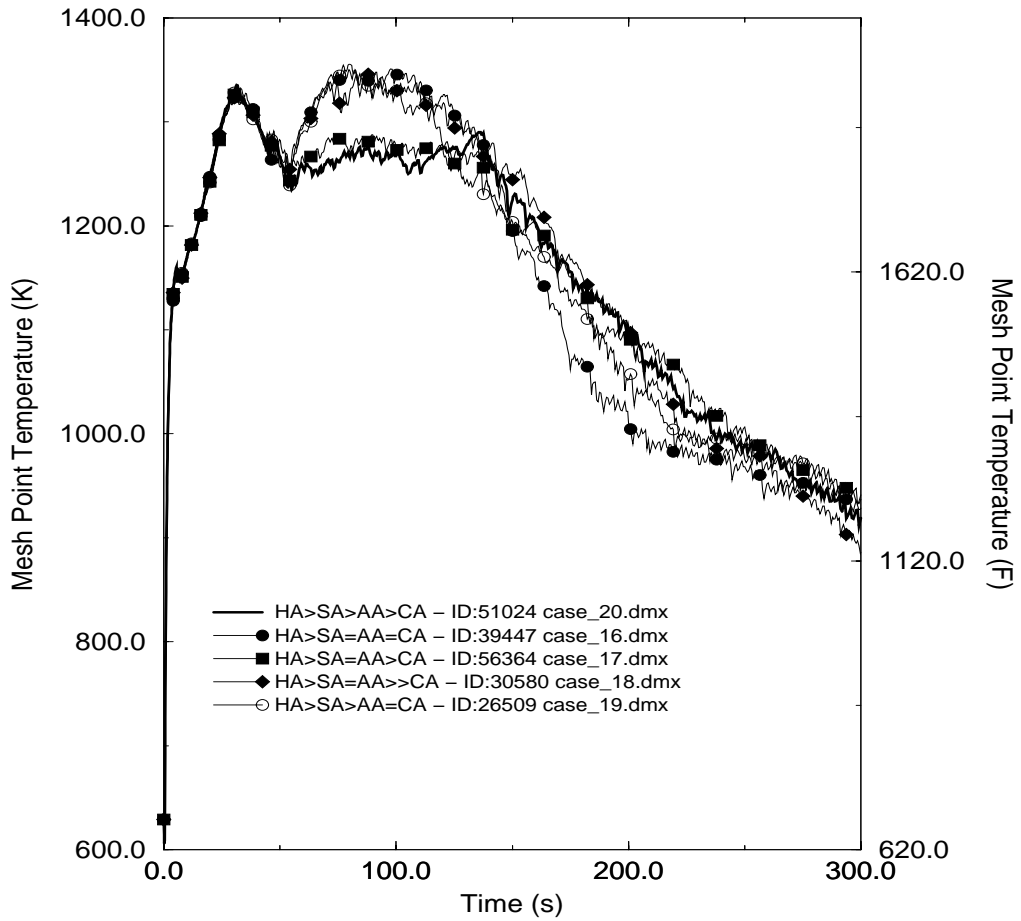


Figure B.5 PCTs from radial power sensitivity studies at high power

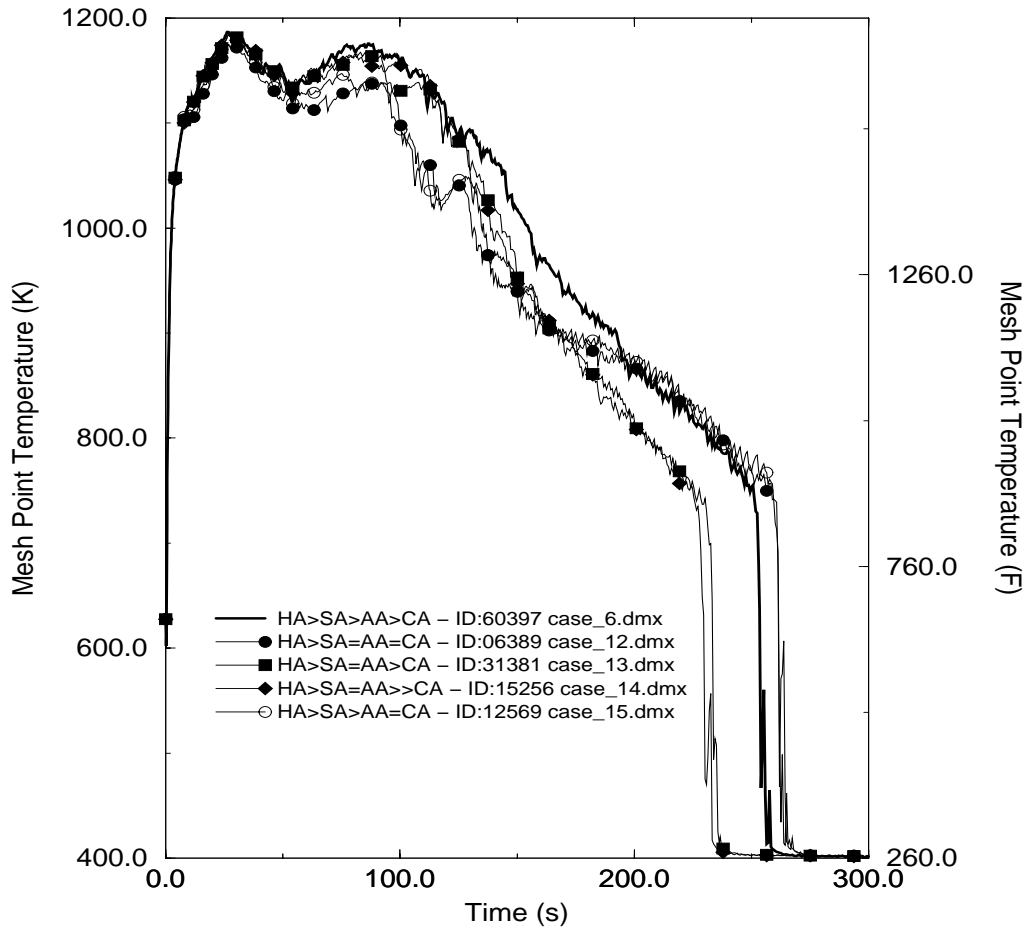


Figure B.6 PCTs from radial power sensitivity studies at nominal power

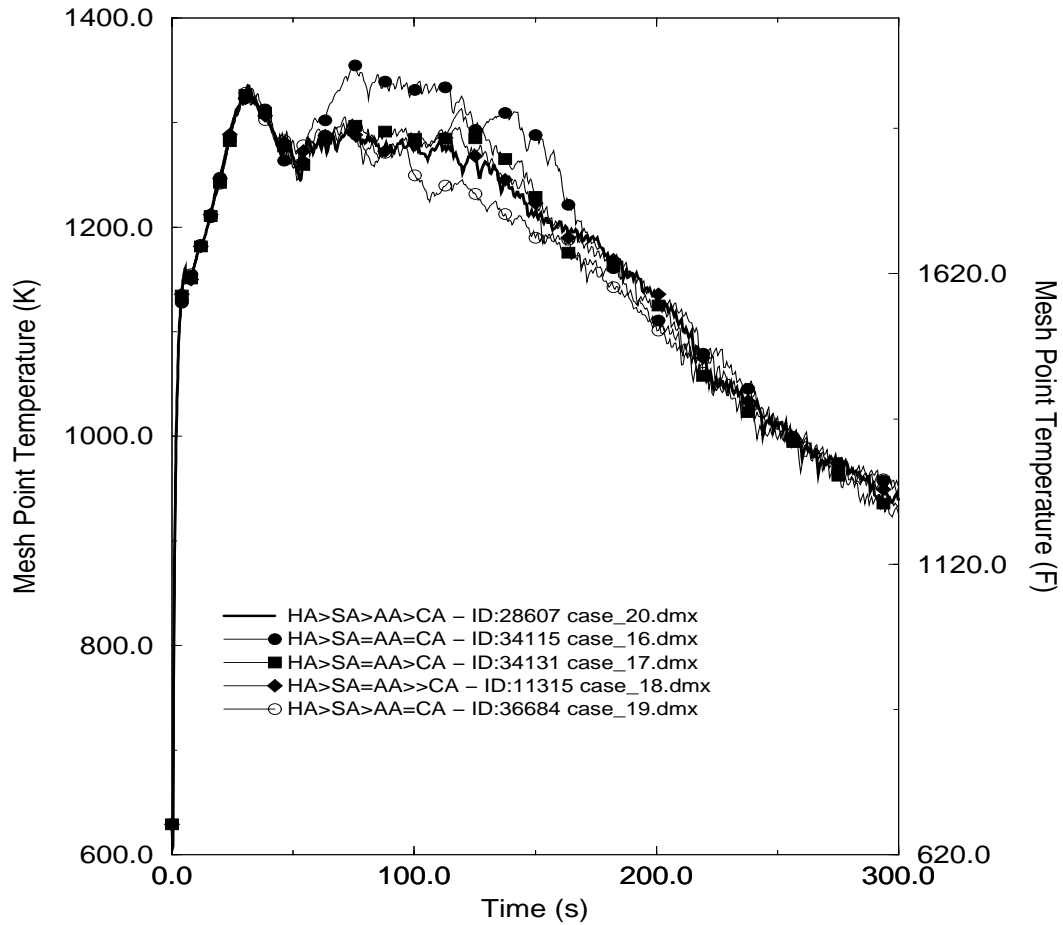
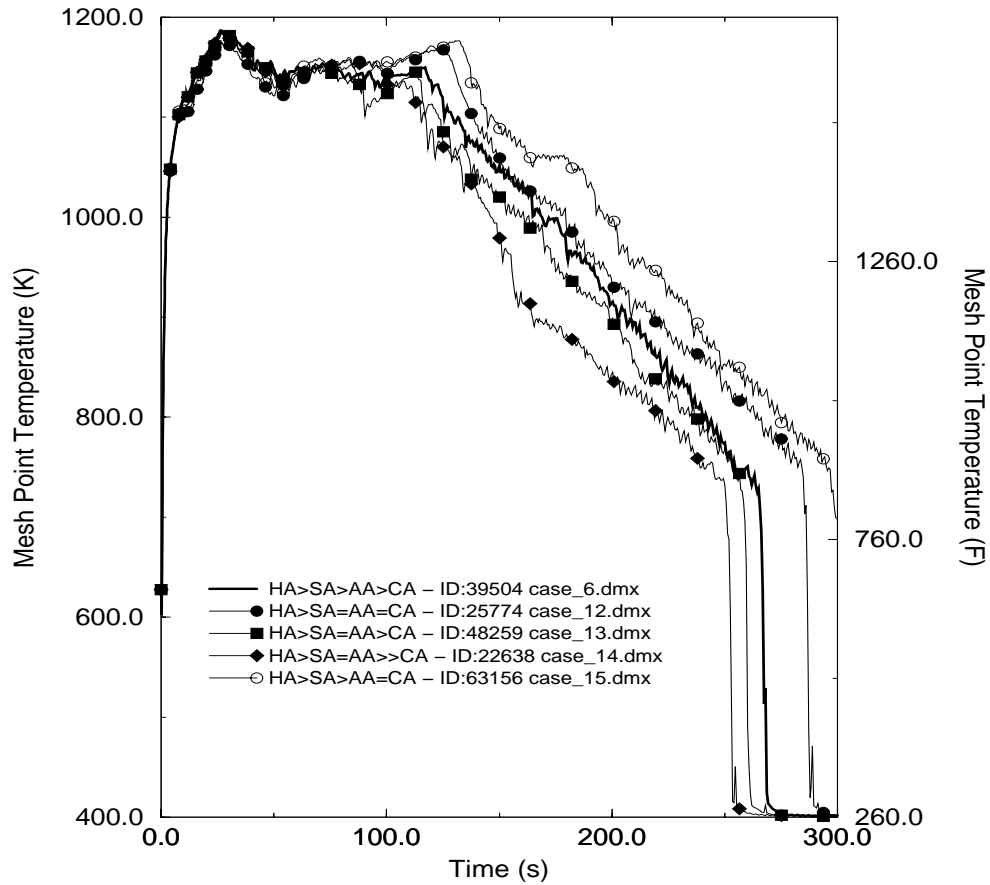


Figure B.7 PCTs from radial power sensitivity studies at high power (accumulators valved out)



**Figure B.8 PCTs from radial power sensitivity studies at nominal power
(accumulators valved out)**

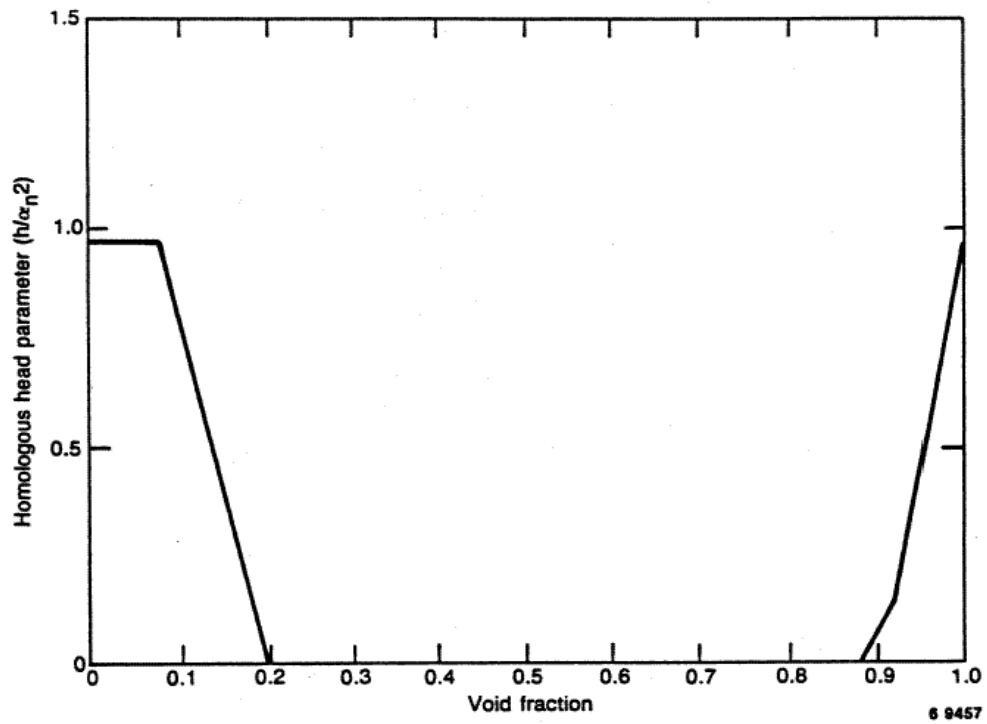


Figure B.9 Two-phase head multiplier for Semiscale pump model

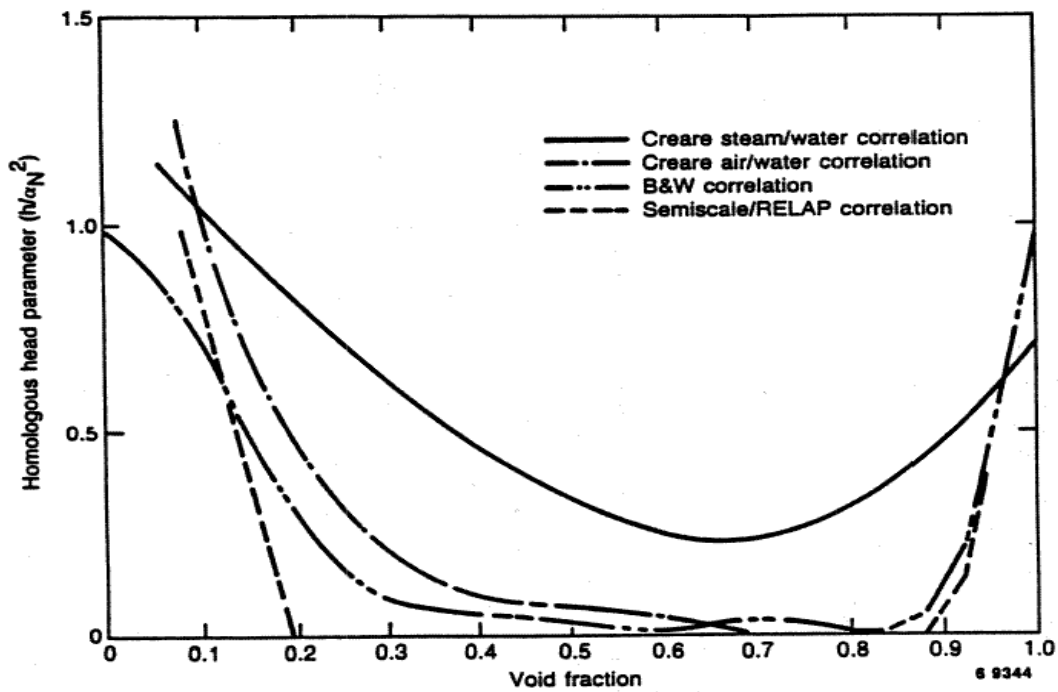


Figure B.10 Two-phase head multiplier for Semiscale pump model compared to other pump models

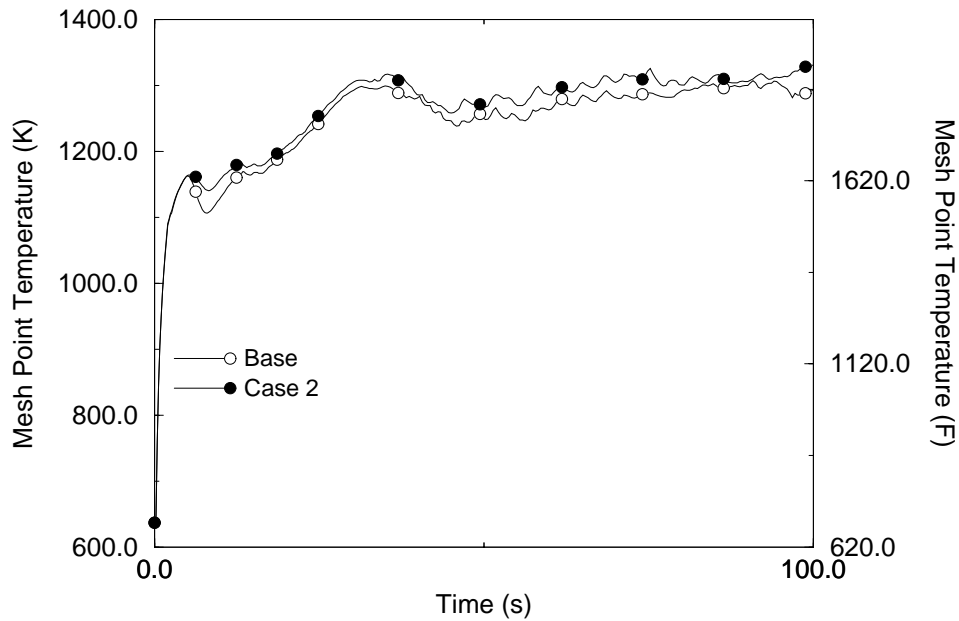


Figure B.11 Effect of Semiscale pump two-phase degradation model on PCT for 4-loop plant at high power

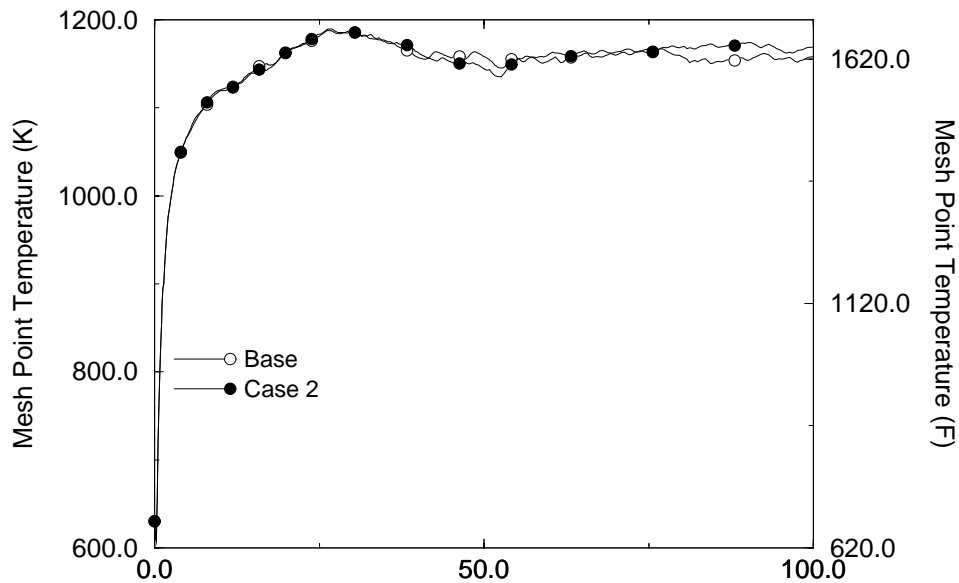


Figure B.12 Effect of Semiscale pump two-phase degradation model on PCT for 3-loop plant at nominal power

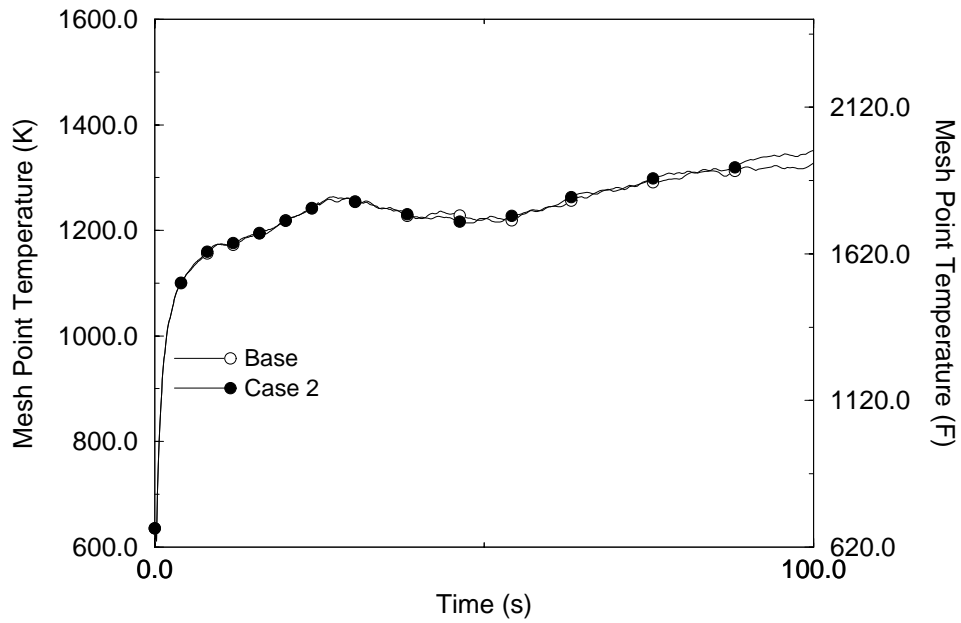


Figure B.13 Effect of Semiscale pump two-phase degradation model on PCT for 3-loop plant at high power

Appendix C Time Step Sensitivity

Appendix K methodologies require that computer program solution convergence be demonstrated by studies of system modeling or noding and calculation time steps. [

]

This sensitivity study was performed by randomly varying time steps over a range from the base case time step set to about 20% larger. Four time step ranges were used to cover the main phases of the LBLOCA: blowdown (0-25 s), early reflood (25-60 s), late reflood (60-160 s), and cool down (>160 s). Each time step range was varied independently. Figure B.16 shows the results from these 14 calculations. Early in the event, S-RELAP5 shows very good agreement for all 14 cases. As the accumulators discharge, there is some noticeable divergence in the results. This is the result of downcomer boiling which can be exacerbated by the accumulator nitrogen passing through the system.

[

]

The cause of the variability, downcomer boiling, has been investigated. Downcomer boiling along the sector adjacent to the broken loop contributes to liquid holdup. This liquid holdup is vulnerable to entrainment out the break from pressure oscillations driven by condensation or the transport of the accumulator nitrogen bubble. The amount of mass held up does vary significantly and a large amount of coolant may be unphysically lost when a pressure spike occurs.

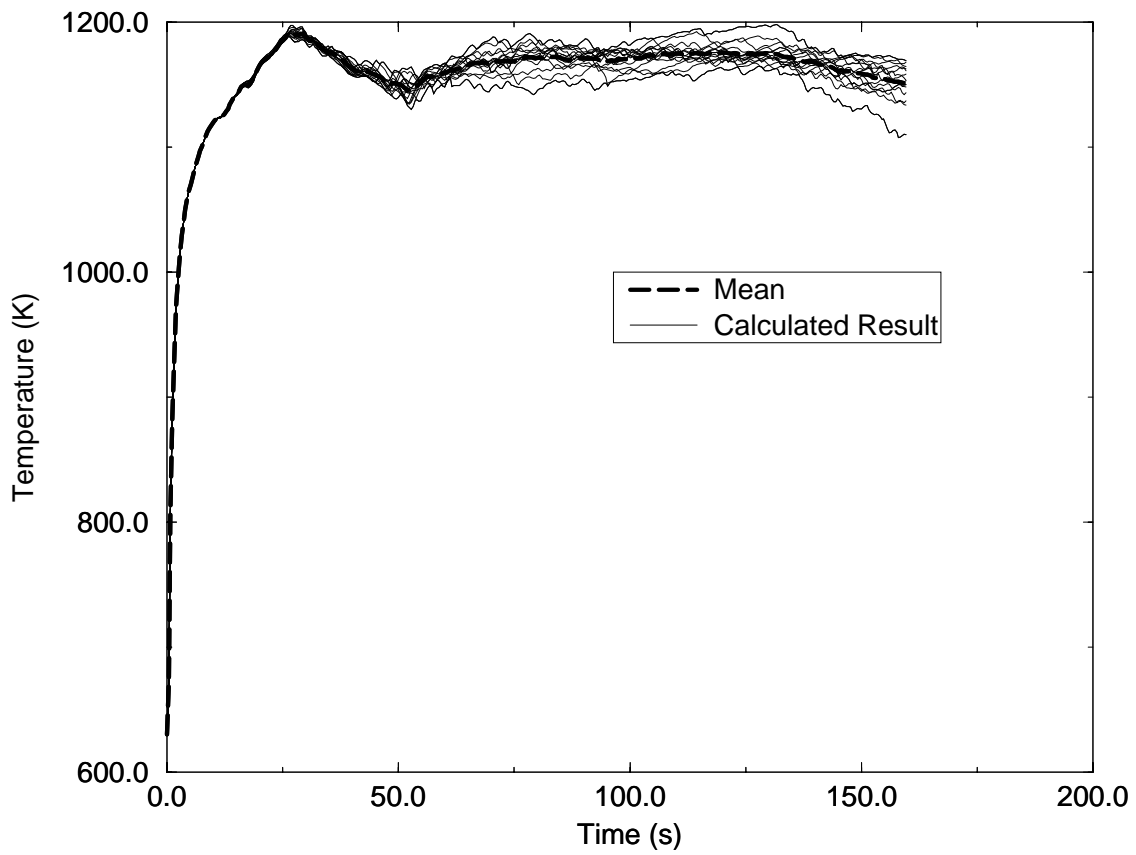


Figure C.1 PCT results from time step sensitivities performed for base case LBLOCA on 3-loop plant at nominal power

Distribution

Richland (E-mail):

R. E. Collingham
J. S. Holm
J. F. Mallay

BWR Safety Analysis

M. E. Garrett
D. J. Braun
D. G. Carr
T. P. Currie
T. W. Eichenberg
A. N. Ham
C. E. Hendrix
J. C. Hibbard
J. G. Hwang
J. G. Ingham
S. S. Luo
D. B. McBurney
S. C. Mellinger
J. M. Moose
L. G. Riniker
R. R. Schnepf
D. C. Serell
S. A. Tylinski
A. W. Will

PWR Safety Analysis

R. C. Gottula
T. H. Chen
N. F. Fausz
T. R. Lindquist
G. B. Peeler
B. A. Reeves
S. M. Sloan
B. D. Stitt
E. L. Tolman

Safety Analysis Methods

D. W. Pruitt
M. T. Bunker
K. E. Carlson
J. C. Chandler
H. Chow
S. C. Franz
K. R. Greene
M. J. Hibbard
S. E. Jensen
T. H. Keheley
L. J. Lommers
R. B. Macduff
R. P. Martin
A. B. Meginnis
W. T. Nutt
R. J. Veklotz

Richland (hard copy):

H. Chow
R. P. Martin
A. B. Meginnis
L. D. O'Dell

Erlangen (hard copy):

F. Depisch, NDS1
K. Schneider, NDS1
G.-J. Seeberger, NDS1

Lynchburg

J. J. Cudlin
J. D. Gale
R. A. Shaw